

**SYNTHESES AND BIOCHEMICAL ASSESSMENTS OF  
MODIFIED NUCLEOSIDES, NUCLEIC ACIDS AND  
PEPTIDES CONTAINING TROPOLONE SURROGATES**

*By*  
**SAGARIKA MEHER**  
**CHEM11201604026**

**National Institute of Science Education and Research (NISER)**  
**Bhubaneswar**

*A thesis submitted to the*  
*Board of Studies in Chemical Sciences*  
*In partial fulfillment of requirements*  
*for the Degree of*  
**DOCTOR OF PHILOSOPHY**  
*of*  
**HOMI BHABHA NATIONAL INSTITUTE**




**May, 2023**

# Homi Bhabha National Institute<sup>1</sup>

## Recommendations of the Viva Voce Committee

As members of the Viva Voce Committee, we certify that we have read the dissertation prepared by SAGARIKA MEHER entitled: "Syntheses and Biochemical Assesments of Modified Nucleosides, Nucleic Acid and Peptides Containing Tropolone Surrogates" and recommend that it may be accepted as fulfilling the thesis requirement for the award of Degree of Doctor of Philosophy.

Chairman – Prof. A. Srinivasan

 07.07.23

Guide / Convener – Dr. Nagendra K. Sharma

 07.07.23

Examiner – Prof. Surajit Sinha

 7.7.2023

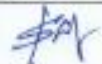
Member 1- Prof. C. Gunanathan

 7-7-2023

Member 2- Dr. Chandra S. Purohit

 07/07/23

Member 3- Dr. Shantanu Pal

 9/7/23

Final approval and acceptance of this thesis is contingent upon the candidate's submission of the final copies of the thesis to HBNI.

I/We hereby certify that I/we have read this thesis prepared under my/our direction and recommend that it may be accepted as fulfilling the thesis requirement.

Date: 07.07.23

Place: NER  
Bhubaneswar

Signature

Co-guide (if any)

  
Signature

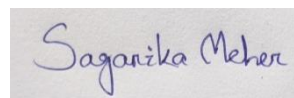
Guide

<sup>1</sup> This page is to be included only for final submission after successful completion of viva voce.

## **STATEMENT BY AUTHOR**

This dissertation has been submitted in partial fulfillment of requirements for an advanced degree at Homi Bhabha National Institute (HBNI) and is deposited in the Library to be made available to borrowers under rules of the HBNI.

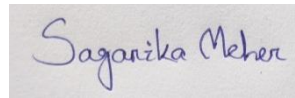
Brief quotations from this dissertation are allowable without special permission, provided that accurate acknowledgement of source is made. Requests for permission for extended quotation from or reproduction of this manuscript in whole or in part may be granted by the Competent Authority of HBNI when in his or her judgment the proposed use of the material is in the interests of scholarship. In all other instances, however, permission must be obtained from the author.

A rectangular box containing a handwritten signature in blue ink that reads "Sagarika Meher".

**SAGARIKA MEHER**

## **DECLARATION**

I, hereby declare that the investigation presented in the thesis has been carried out by me. The work is original and has not been submitted earlier as a whole or in part for a degree / diploma at this or any other Institution / University.



**SAGARIKA MEHER**



## List of Publications arising from the thesis

### Journal

#### Published

- 1) **Meher, S.**; Gade, C. R.; Sharma, N. K. Tropolone-Conjugated DNA: A Fluorescent Thymidine Analogue Exhibits Solvatochromism, Enzymatic Incorporation into DNA and HeLa Cell Internalization. *ChemBioChem* **2023**, 24 (4), e202200732.
- 2) **Meher, S.**; Kumari, S.; Dixit, M.; Sharma, N. K. Cu-Catalyzed Synthesis of Alkylaminotroponyl Sulfones as Pseudomonas Aeruginosa Quorum Sensing Inhibitors Targeting LasI/R QS Circuitry. *Chem. Asian J.* **2022**, 17 (23), e202200866.
- 3) **Meher, S.**; Sharma, N. K. Azulene Tethered N-Aryl Nucleobases: Synthesis, Morphology and Biochemical Evaluations. *New J. Chem.* **2023**, 47, 5593-5597
- 4) Dalabehera, N. R.; **Meher, S.**; Bhusana Palai, B.; Sharma, N. K. Instability of Amide Bond with Trifluoroacetic Acid (20%): Synthesis, Conformational Analysis, and Mechanistic Insights into Cleavable Amide Bond Comprising  $\beta$ -Troponylhydrazino Acid. *ACS omega* **2020**, 5 (40), 26141–26152.

#### Under preparation

- 1) **Meher, S.**; Sharma, N. K. Fluorescent Nucleoside: Synthesis of Aminotroponyl sulfonyl-dT (<sup>ATS</sup>dT) Analogs That Exhibit Solvatochromic Fluorescence and localize at HeLa Cell Nucleus. (*Manuscript under revision*)
- 2) **Meher, S.**; Gade, C. R.; Sharma, N. K. Tropolone-Clicked DNA: A Fluorescent Thymidine Analogue Exhibits Solvatochromism, Enzymatic Incorporation into DNA and HeLa Cell Internalization. (*Manuscript under preparation*)

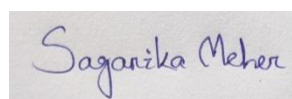
- 3) **Meher, S.;** Sharma, N. K. Azulene Tethered C-nucleoside: Synthesis and Template Independent Enzymatic Incorporation into DNA. (*Manuscript under preparation*)
- 4) **Meher, S.;** Sharma, N. K., Tropolonylbodipy-Cisplatin complex: Synthesis, Photophysical Studies and HeLa cell Imaging. (*Manuscript under preparation*)

### **Conferences**

- 1) Oral and Poster presentation in International Society of Nucleosides, Nucleotides, and Nucleic Acids, IS3NA- Virtual Symposium- 2021, 26- 27<sup>th</sup> Aug, 2021
- 2) Poster presentation in National Bioorganic Chemistry Conference- 2018, NBCC- 2018, 22-24<sup>th</sup> December 2018, NISER, Bhubaneswar, India
- 3) Poster presentation in 7<sup>th</sup> National Conference on Recent Advancement in Material Sciences (RAIMS- 2022), and Odisha Chemical Society (OCS), 18- 19<sup>th</sup> Nov, 2022, VSSUT, Burla, India.
- 4) Participant: ACS on Campus, 23<sup>rd</sup> Jul, 2018, NISER, Bhubaneswar, India.
- 5) Participant: Webinar on Latest Research on Catalytic & Structural Study of Organometallic Compounds and Nanomaterials, Educare Taiwan, 3<sup>rd</sup> Jul, 2022.

### **Others (Workshop)**

- 1) Participant: Hands-on Methodology in Clinical Cancer Research, 18- 20<sup>th</sup> Jul, 2019, NISER, Bhubaneswar, India



**SAGARIKA MEHER**

**Dedicated to....**  
My Beloved Family  
&  
Teachers

## ACKNOWLEDGEMENTS

First and foremost, I would like to thank my parents, Mr. Jaya Chandra Meher & Mrs. Bhubaneswari Meher, and my family members for their unlimited support, sacrifices, encouragement, unconditional love, and affection throughout my life.

I express my deep and sincere gratitude to my research supervisor, Dr. Nagendra Kumar Sharma, for giving me the opportunity to do research and providing invaluable guidance throughout this journey. His scholarly and insightful conversations about many topics in science and life have made an inspirational experience for me in NISER. I learned a lot of new things under his mentorship, which inspired me to push my limitations and conduct better-quality research. I also extend my heartfelt thanks to his wife and collaborator, Dr. Manjusha Dixit, and family for their help during the research.

I would like to thank Prof. A. Srinivasan, Director, NISER, Prof. S. Panda, Prof. V. Chandrashekar, and Prof. T. K. Chandrashekar, Ex-Directors, NISER, for helping us with all the laboratory and instrumental facilities. I sincerely thank all the Deans, especially Prof. Panay K. Swain and academic staff members for their generous assistance. I also like to acknowledge NISER for providing infrastructure and fellowship. It is my privilege to be a part of this esteemed institution.

I sincerely thank my thesis monitoring committee members, Prof. A. Srinivasan, Dr. C. Gunanathan, Dr. C. S. Purohit, and Dr. S. Pal (IIT, Bhubaneswar), for their enormous help and support throughout my research time. I am immensely thankful to the thesis reviewers for their valuable input in the present thesis.

I want to convey my sincere thanks to the School of Chemical Science (SCS) faculty and staff members. I am extremely grateful to Dr. Mriganka, Mr. Mirza, Mr. Deepak, Mr. Sanjaya, Mr. Prakash, Mr. Amit, and Mrs. Anuradha for their help.

I express my sincere gratitude to my teacher, the late Prof. S. Chinda. I sincerely thank all my school teachers, graduation teachers, and post-graduation professors.

I have been fortunate enough to work with an incredible group of people. I would like to thank my current and past lab members, Dr. S. Mohanlal, Dr. S. K. Pandit, Dr. S. L. Bhakta, Dr. R. Bag, Dr. C. S. Reddy, Dr. C. Balachandra, Dr. A. N. Bollu, Dr. B. B. Palai, Chinmay, Manish, Subhashree, Ankita, Malobika, Ramu, Nihar, Saideep, Tushar, Mintu, Rohit, Gajendra, Shiba, Asmita, Bhagya, Subhasish, Adesh, Maria, Pritha, Sangeeta, and Abhinandan.

I have been fortunate enough to make close friends, and I am thankful to Dr. Syama, Dr. Sruti, and Dr. Kasturi for an enjoyable and memorable stay at NISER. I also thank all my friends Dr. Milan, Dr. Biplab, Dr. Shalini, Dr. Kiran, Ms. Bratati, Ms. Prerana, Ms. Somlata, Ms. Namrata, Ms. Priyanka, Mr. Tanmoy, and all my batchmates for the beautiful times we have spent. I also thank my childhood friends Sonia and Monika for the bond we share.

I would not miss this opportunity to thank my sisters, Niharika, Swagatika, and brother, Braja Mohan, who are my strength, happiness, and lifeline. I also thank all my students and the people of Bheunria & Padampur for their boundless respect and love.

I am grateful to the Almighty for his enormous blessings and guidance in every step of my life to overcome all the challenges with confidence and honesty.

Finally, I would like to thank everybody important to the successful realization of this thesis.

## SYNOPSIS

### Introduction

Nucleosides and amino acids as building blocks of nucleic acids (DNA/RNA) and peptides constitute necessary components of the foundation of life. They have stimulated interest in researchers due to their unique properties, such as structural diversity, multiplex binding sites, self-assembly ability, stability, biocompatibility, etc. What aids to make these molecular scaffolds so intriguing is the wealth of supramolecular bonds that molecules use to interact with each other and their refined interplay.<sup>1</sup> Recently modified nucleosides, nucleic acids, and peptides have been the subject of research due to their pivotal role in understanding different biochemical pathways, pharmaceutical applications, designing nanodevices, etc.<sup>2</sup> Indeed the results reflect on fulfilling demands of drugs like recombinant insulin (synthetic peptide) or a pandemic saviour- remdesivir (modified nucleoside). Additionally, fluorescent nucleosides have emerged as an extraordinarily useful category of chemical and biological tools for the molecular-level understanding of nucleic acid structures, activities, locations and interactions.<sup>3</sup> Modifications in these biomolecular structures generally include incorporation of benzenoid or heterocyclic moieties. Tropolone is a seven-membered, non-benzenoid aromatic compound present in many bioactive natural products.<sup>4</sup> This chromophoric molecule has unique hydrogen bonding properties and excellent metal chelating abilities. Tropolone and its derivatives possess anti-inflammatory, antibacterial, antitumor, antiviral and anticancer properties. However, its potential has not yet been fully explored, providing us the research opportunity, including synthetic design, characterization, and biological evaluation in nucleic acids and peptides.

This thesis comprises six chapters including introductions. Chapter-1 describes the general introduction of DNA, modified nucleosides, cleavable amide bonds and tropolonyl

derivatives. Chapter-2 (part A and B) encompasses syntheses, photophysical studies and biochemical evaluations of two tropolonyl modified nucleosides. Chapter-3 (part A and B) describes the syntheses of Alkylaminotroponyl Sulfone (ATS) derivatives as bacterial quorum sensing inhibitors along with the syntheses of ATS mediated modified nucleosides. Chapter-4 elaborates the synthesis and applications of tropolone derived Azulene tethered nucleobases and C-nucleoside (part A and B). Chapter-5 focuses on synthesis and photophysical properties of a troponylbodipy-cisplatin complex and troponylbodipy-C-nucleoside analogue. The final chapter-6 describes the synthesis and mechanistic insights of cleavable amide bond comprising  $\beta$ -troponylhydrazino acid.

## **Chapter 1. Introduction**

This chapter describes the brief introduction of modified nucleobases, fluorescent DNA/RNA analogues, cleavable amide bonds and tropolone derivatives. Generally most of chromophores/fluorophores are derived from benzenoid aromatic scaffolds. However, non-benzenoid chromophores are also available in nature as troponoid natural products which contain Tropolone scaffolds. Tropolone is a seven-membered, non-benzenoid aromatic molecule having therapeutic potential. Recently tropolone has been introduced into the nucleoside and amino acids for studying structural and functional properties of DNA/RNA and peptides.

## **Chapter 2A. Synthesis, Photophysical Studies and Biochemical Evaluations of Tropolone Conjugated DNA**

Tropolone-Conjugated DNA: A Fluorescent Thymidine Analogue Exhibits Solvatochromism, Enzymatic Incorporation into DNA and HeLa Cell Internalization. (S. Meher<sup>‡</sup>, C. R. Gade<sup>‡</sup>, N. K. Sharma\*, *ChemBioChem*, **2023**, e202200732)

The non-benzenoid aromatic scaffold tropolone has unique photophysical and metal-chelating qualities. It has recently been conjugated with DNA, and its photophysical characteristics have been studied. In this chapter we have discussed about synthesis of following tropolonyl modified nucleoside derivatives.

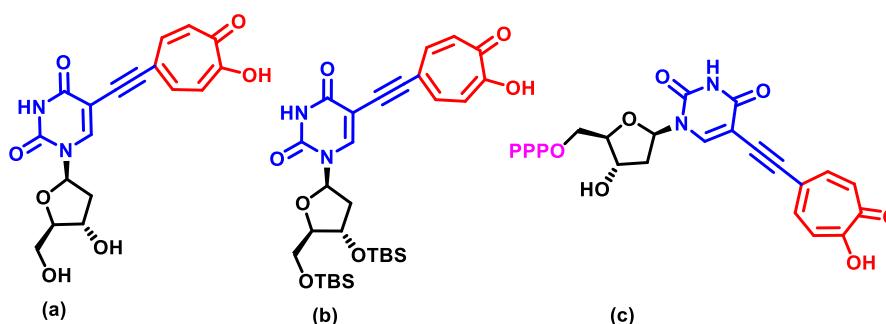


**Figure 1.** Chemical structure of (a) tr-dU, (b) tr-<sup>TBS</sup>dU and (c) tr-dUTP/tr-dTTP.

TBS-protected derivative of fluorescent nucleoside tr-dU i.e tr-<sup>TBS</sup>dU is synthesized for studying its solvent-dependent fluorescence behavior. The tr-<sup>TBS</sup>dU derivative exhibit maximum quantum yield in aprotic nonpolar solvents while maximum Stokes shift in DMF/Toluene. Thus tr-<sup>TBS</sup>dU has an environmentally sensitive fluorescence (ESF) character.

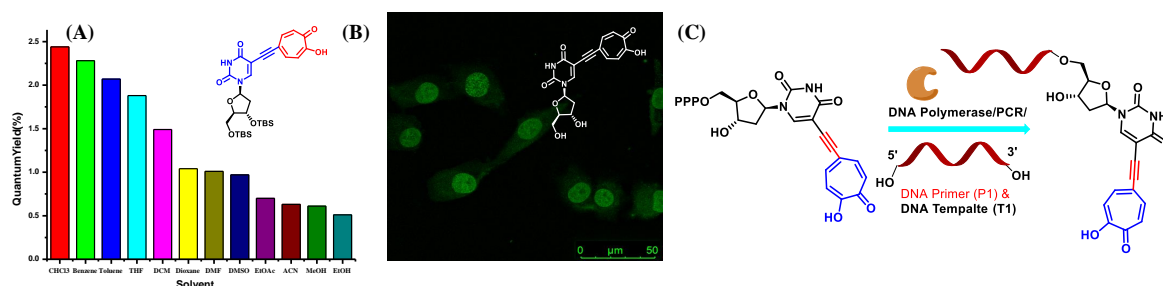


**Figure 2.** Quantum yield of tr-<sup>TBS</sup>dU in different Solvents (A), HeLa cell internalization of tr-dU (Image in FITC channel), Enzymatic incorporation of tr-dUTP into DNA (C).

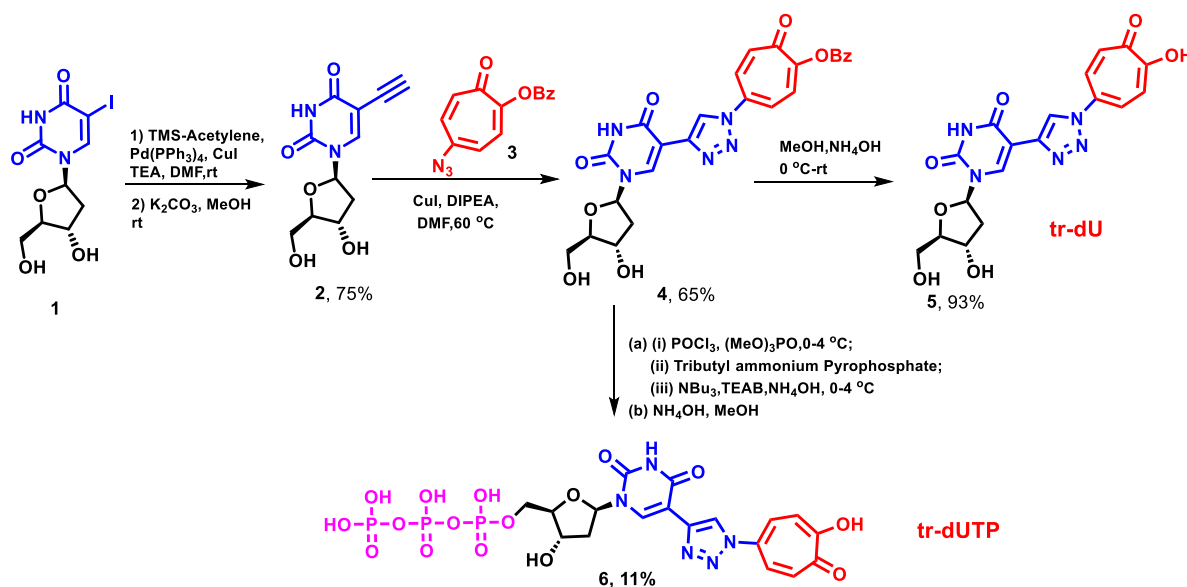


The triphosphate analogue (tr-dUTP/tr-dTTP) is also synthesized and enzymatically incorporated into DNA primer in presence of DNA polymerase and DNA template. For practical utility, cell permeability and viability of free tr-dU nucleoside are examined which reveals that tr-dU is cell permeable and fluorescently localizes over the cell nucleus. Importantly, this nucleoside has no significant cytotoxicity effect on both normal and cancerous cells. Hence, tr-dU is a promising fluorescent nucleoside analogue for labelling the DNA.

## Chapter 2B. Synthesis, Photophysical Studies and Biochemical Evaluations of Triazolyl-tropolonyled DNA

(S. Meher, C. R. Gade, N. K. Sharma\*, *Manuscript under preparation*)

This chapter describes the synthesis of topolonyl modified nucleoside by click chemistry and enzymatic incorporation of its triphosphate derivative in to DNA.



**Scheme 1.** Synthesis of tr-dU and tr-dUTP.

We studied the photophysical properties of tr-dU in different solvents and found that it shows solvatochromism. tr-dU is cell permeable and fluorescently localizes over the cell nucleus. Importantly, this nucleoside has no significant cytotoxicity effect on both normal and cancerous cells. Hence, tr-dU is a promising fluorescent nucleoside analogue for labelling the DNA.

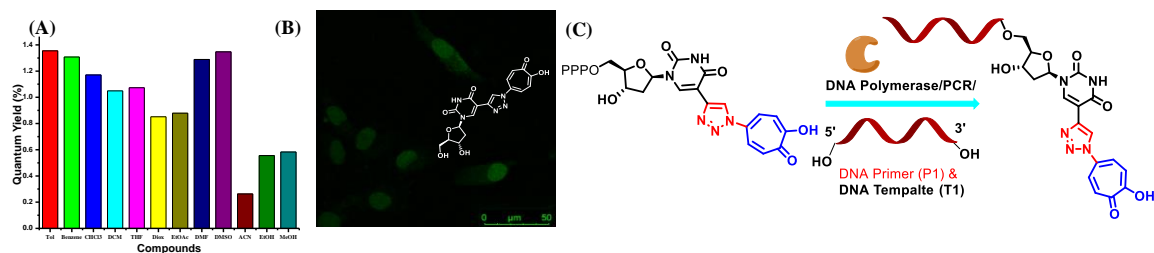


**Figure 3.** Quantum yield of tr-dU in different Solvents (A), Hela cell internalization of tr-dU (Image in FITC channel), Enzymatic incorporation of tr-dUTP in to DNA (C).

### Chapter 3A. Alkylaminotroponyl Sulfones as *Pseudomonas aeruginosa* Quorum Sensing Inhibitors

Cu-Catalyzed Synthesis of Alkylaminotroponyl Sulfones as *Pseudomonas aeruginosa* Quorum Sensing Inhibitors Targeting *lasI/R* QS Circuitry. S. Meher, S. Kumari, M. Dixit\*, N. K. Sharma\*, *Chem Asian J.*, **2022**, 17, e202200866.

The scarcity of novel bioactive molecules against multidrug-resistant (MDR) bacterial strains is alarming. The antibiotic crisis is associated with multidrug-resistant pathogens such as *Pseudomonas aeruginosa* and others. This bacterial virulence is regulated via Quorum sensing (QS), a cell-cell communication process. Disabling QS circuits (*las*, *pqs*, *rhl*) with small molecules has been recommended as a potential strategy to prevent bacterial pathogenicity. This strategy focuses on interruption of bacterial virulence, rather than killing them to tackle the drug resistance problem. Herein, we describe the synthesis of

rationally designed Alkylamionotroponyl Sulfone (ATS) derivatives by Cu-catalyzed C(sp<sup>2</sup>)-H functionalization at troponone ring and the screening of their anti-QS activity against *P. aeruginosa*. Importantly, only two sulfones (**5c/7b**, ~20 μM) remarkably exhibit the down regulation of the *lasI/R* QS genes. These two molecules also inhibit swarming motility, biofilm formation and pyocyanin production which reduce *P. aeruginosa* virulence in cells. Hence ATS derivatives could be considered as potential therapeutic candidates for the treatment of *P. aeruginosa* infections.

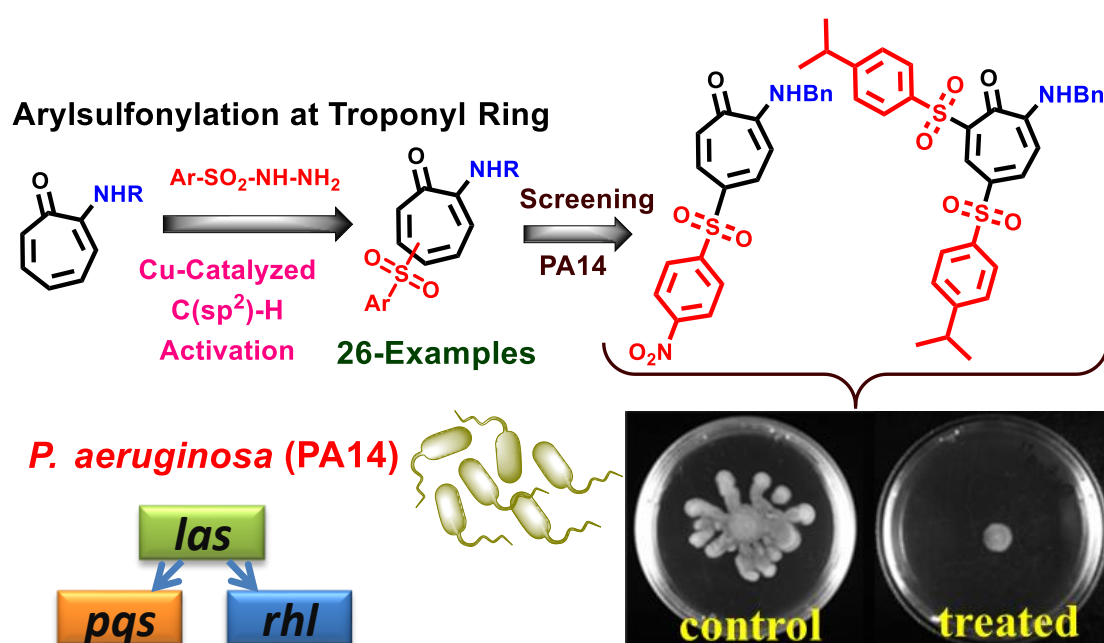


**Figure 4.** New Inhibitors of Bacteria's Quorum Sensing System: Synthesis of novel ATS derivatives and their anti-QS activity against PA14.

### Chapter 3B. Troponylsulfone Conjugated Nucleosides: Synthesis, Photophysics and Confocal Microscopy Studies

(S. Meher and N. K. Sharma\*, *Manuscript under preparation*)

ATS derivatives exhibited fluorescence properties. Hence two ATS derivatives were used for the synthesis of two new modified nucleosides. We performed their photophysical studies and found that these two nucleosides are sensitive to polarity of solvents and showed solvatochromism. These are non-toxic towards HEK293T and HeLa cell lines and fluorescently localize over the nucleus. In the contrast only ATS derivative resides in cytoplasm.

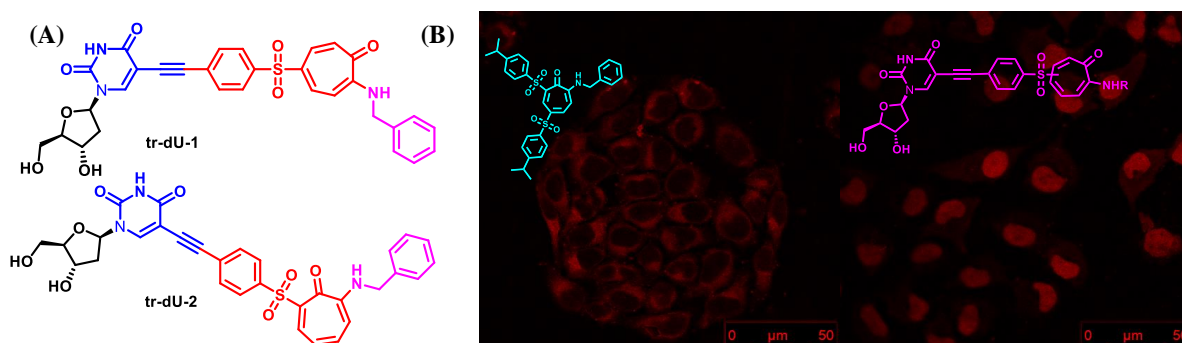


**Figure 5.** Chemical structure of ATS-mediated modified nucleosides (A), HeLa cell internalization of ATS derivative and tr-dU (Image in TRITC channel).

#### Chapter 4A. Azulene tethered *N*-aryl Nucleobases: Synthesis, Morphology and Biochemical Evaluations

Azulene Tethered *N*-Aryl Nucleobases: Synthesis, Morphology and Biochemical Evaluations, S. Meher, N. K. Sharma\*, *New J. Chem.*, **2023**, DOI: 10.1039/D2NJ06272K.

Azulene is a non-benzenoid aromatic molecule comprising unique structural and functional properties. Herein, we report four new azulene based *N*-aryl nucleobases via nucleophilic aromatic substitution ( $S_NAr$ ) exhibiting distinct morphologies with no cytotoxic effect toward HEK293T cell line. Silver complex of the cytosine derivative i.e. Silver nanocomposite (Az-C-Ag complex) has also been synthesized, showing antibacterial

property against *Pseudomonas aeruginosa* (PA14) with a minimum inhibitory concentration of 20  $\mu\text{M}$ .

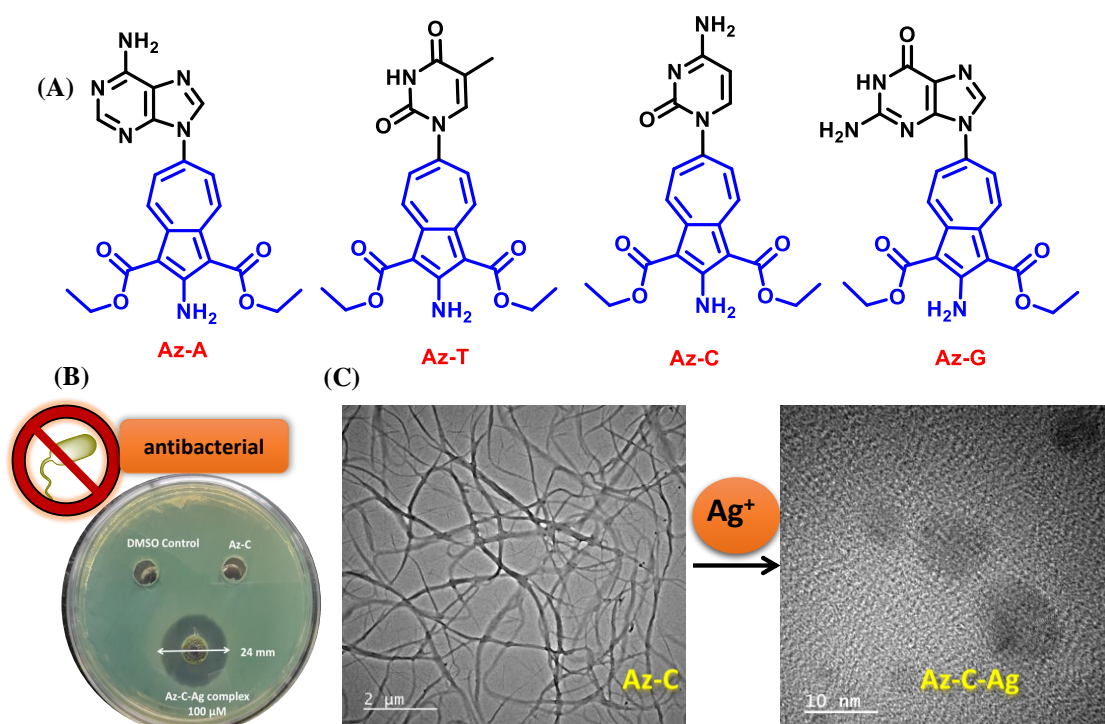


**Figure 6.** Structure of azulene tethered nucleobases (A), antibacterial activity of Az-C-Ag complex (B), breaking the networking structure of Az-C by incorporating silver ions (C).

#### Chapter 4B. Azulene Tethered C-nucleoside: Synthesis and Template Independent Enzymatic Incorporation into DNA

(S. Meher and N. K. Sharma\*, *Manuscript under preparation*)

This chapter deals with a modified C-nucleoside containing azulene moiety. This product was synthesized by performing heck coupling reaction between glycal and Bromo-azulenyl derivative followed by TBS-deprotection and reduction steps. The crystal packing diagram shows  $\pi$ - $\pi$  stacking between azulene rings. SEM/ TEM images also depict unique morphologies. For practical utility Cell viability assay was performed and no significant cytotoxicity was observed towards HEK293T or HeLa cell line.

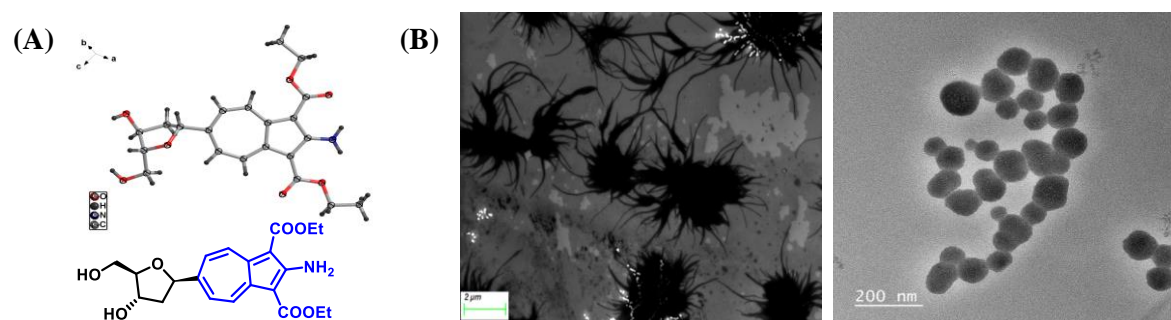


**Figure 7.** Single crystal and chemical structure of azulenyl nucleoside (A), SEM/ TEM images (B).

## Chapter 5. Troponylbodipy-Cisplatin complex and C-nucleoside analogues: Synthesis and Biochemical Evaluations

(S. Meher and N. K. Sharma\*, *Manuscript under preparation*)

BODIPY analogues are generally known for their fluorescence properties and applications in cellular imaging. Bodipy nucleosides are very useful in molecular biology. In the other hand BODIPY labeled Pt complexes are of great interest for studying their cellular uptake and distribution in cancer cells. In this chapter we have designed and synthesized a troponylbodipy-cisplatin complex and troponylbodipy-C-nucleoside. The photophysical property of troponylbodipy-cisplatin complex was conducted and we noticed that it possesses 5 fold less quantum yield than its parent bodipy unit. It is non-cytotoxic towards HeLa and KEK293T cell lines and localizes over cell nucleus. The troponylbodipy-C-nucleoside could also show fluorescent behaviors. It will also be interesting to evaluate its photophysical properties and biochemical applications.



peptides is cleavable with TFA (~20%) through the formation of a new heterocyclic molecule N-troponylpyrazolidinone or troponylpyrazolidinone.

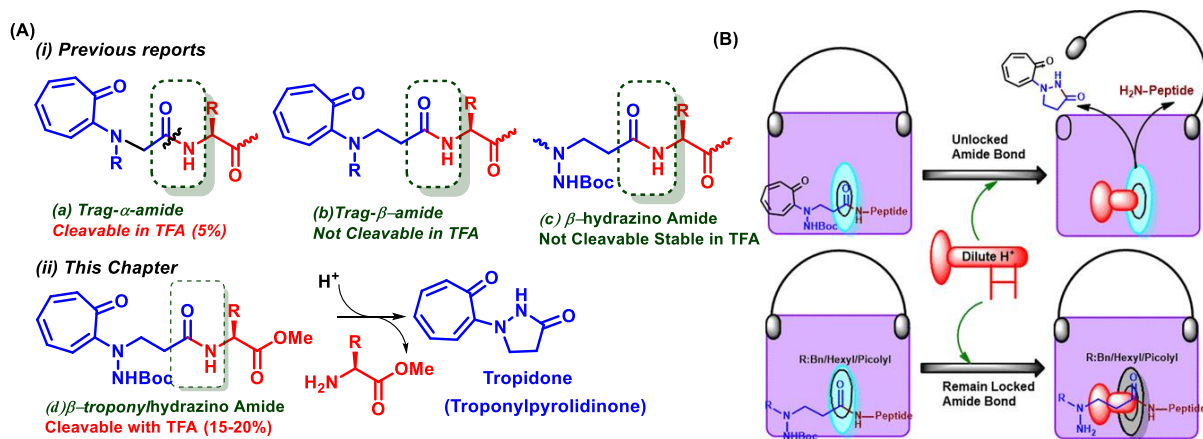


**Figure 8.** Previously reported troponyl-/hydrazine-containing amides (A-i) and rationally designed  $\beta$ -troponylhydrazinyl peptides and their instability under acidic conditions (A-ii), Schematic representation of amide bond cleavage in  $\beta$ -troponylhydrazinyl peptides.

## References

- 1 F. Pu, J. Ren and X. Qu, *Chem. Soc. Rev.*, 2018, **47**, 1285–1306.
- 2 S. Sivakova and S. J. Rowan, *Chem. Soc. Rev.*, 2005, **34**, 9–21.
- 3 W. Xu, K. M. Chan and E. T. Kool, *Nat. Chem.*, 2017, **9**, 1043–1055.
- 4 H. Guo, D. Roman and C. Beemelmanns, *Nat. Prod. Rep.*, 2019, **36**, 1137–1155.



## List of Figures

<b>Figure 1.1.</b>	Components of nucleoside and nucleotide	3
<b>Figure 1.2</b>	DNA double helix and hydrogen bonding between nucleobases	4
<b>Figure 1.3</b>	Reaction mechanism of polymerase-catalyzed phosphodiester bond formation	5
<b>Figure 1.4</b>	Scope of modifications in nucleosides	8
<b>Figure 1.5</b>	Synthesis of base modified nucleoside analogs	11
<b>Figure 1.6</b>	Types of FNAs based on their structural relationship with the natural nucleobases	12
<b>Figure 1.7</b>	Selected examples of fluorescent base modified nucleosides	13
<b>Figure 1.8</b>	Selected examples of fluorescent nucleosides having alkynyl linkage	14
<b>Figure 1.9</b>	Incorporation of fluorescent nucleosides into DNA having alkynyl linkage	15
<b>Figure 1.10</b>	Post synthetic modification by click chemistry and selected examples of fluorescent nucleosides having triazolyl linkage	16
<b>Figure 1.11</b>	Selected examples of Bodipy containing nucleosides	17
<b>Figure 1.12</b>	Selected examples of C-nucleosides and metal mediated base pairs	18
<b>Figure 1.13</b>	Selected examples of biologically active modified nucleosides	19
<b>Figure 1.14</b>	Progress and applications of nucleic acid chemistry	20
<b>Figure 1.15</b>	Mechanism of action of nucleoside analogs	21
<b>Figure 1.16</b>	Stability of peptide bond (A), Hydrolyzable amide bonds (B)	23
<b>Figure 1.17</b>	Tropone and tropolone chemical structures (A) and tautomers (B).	24
<b>Figure 1.18</b>	Selected examples of troponoid natural products	25

<b>Figure 2A.1</b>	Previously reported troponyl/ aminotroponyl-thymidine analogs and this report.	40
<b>Figure 2A.2</b>	Absorption (A), emission spectra (B, C), and quantum yield (D) of tr- <sup>TBS</sup> dU ( <b>7</b> ) in various solvents (20 μM)	44
<b>Figure 2A.3</b>	Solvatochromism (A) and a plot of Stokes shift vs. E <sub>T</sub> (30) (B) for tr- <sup>TBS</sup> dU ( <b>7</b> )	44
<b>Figure 2A.4</b>	PAGE Analysis of primer extension reactions of tr-dTTP ( <b>9</b> ) with different DNA polymerases	46
<b>Figure 2A.5</b>	Confocal microscopic images for tr-dU ( <b>7</b> ) treated HeLa Cells with DAPI staining (12 h incubation (A-F), 24 h incubation (G-L))	48
<b>Figure 2A.6</b>	Cell proliferation assays of compound tr-dU ( <b>10</b> ) in HEK293T and HeLa cells	49
<b>Figure 2B.1</b>	Troponyl nucleosides in previous and this chapter	75
<b>Figure 2B.2</b>	Primer extension reactions of tt-dTTP ( <b>6</b> ) with DNA polymerase (Therminator)	77
<b>Figure 2B.3</b>	Absorption (A), emission spectra (B, C), and quantum yield (D) of tt-dU ( <b>5</b> ) in various solvents (20 μM)	79
<b>Figure 2B.4.</b>	Cell proliferation assays of compound tt-dU ( <b>5</b> ) in HEK293T and HeLa cells	80
<b>Figure 2B.5</b>	Confocal microscopic images for tt-dU ( <b>5</b> ) treated HeLa Cells with DAPI staining (12 h incubation (A-F), 24 h incubation (G-L))	81

<b>Figure 3A.1</b>	Antibiotic and anti-quorum sensing compounds (reported and this report); (a-c) previous reports, (d) this report, (e) <i>Pseudomonas aeruginosa</i> and QS system	106
<b>Figure 3A.2</b>	Plausible reaction mechanism of ATS formation	110
<b>Figure 3A.3</b>	Swarming assays of <i>P. aeruginosa</i> (PA14) in DMSO control and in presence of ATS derivatives ( <b>3a/b/c</b> - <b>11a/b/c</b> ) at 100 $\mu$ M concentration	112
<b>Figure 3A.4</b>	Concentration-dependent swarming assays of <i>P. aeruginosa</i> (PA14) in presence of ATS derivatives ( <b>3b</b> , <b>4b</b> , <b>7b</b> , <b>11b</b> , <b>5c</b> and <b>9c</b> ) at different concentrations (20-100 $\mu$ M)	113
<b>Figure 3A.5</b>	Effect of ATS derivatives on biofilm formation (qualitative analysis)	114
<b>Figure 3A.6.</b>	Effect of ATS derivatives on biofilm formation; (A) Quantitative analysis of <i>P. aeruginosa</i> biofilm formation in the absence (control) or presence of ATS derivatives, (B) Concentration dependent biofilm assay	115
<b>Figure 3A.7</b>	Effect of ATS derivatives on pyocyanin production; (A) Quantitative analysis of <i>P. aeruginosa</i> pyocyanin production in the absence (control) or presence of ATS derivatives, (B) Concentration dependent pyocyanin assay	116
<b>Figure 3A.8</b>	Schematic diagram of the interconnected <i>lasI/R</i> and <i>LasI/R</i>	117

systems.

<b>Figure 3A.9</b>	Schematic workflow for qRT-PCR experiment	119
<b>Figure 3A.10</b>	Effects of ATS treatment on expression of QS-related genes; Quantitative real-time PCR analysis showing the transcript levels of (A) <i>lasR</i> genes and (B) <i>lasI</i> genes and (C) <i>lasB</i> genes in presence of ATS derivatives ( <b>3b</b> , <b>4b</b> , <b>7b</b> , <b>11b</b> , <b>5c</b> and <b>9c</b> )	119
<b>Figure 3A.11</b>	Cell proliferation assays of ATS derivatives ( <b>3b</b> , <b>4b</b> , <b>7b</b> , <b>11b</b> , <b>5c</b> and <b>9c</b> )	120
<b>Figure 3A.12</b>	ATS-mediated attenuation of <i>P. aeruginosa</i> cytotoxicity towards HEK293T cells; Plot showing Cell survivality (A), Microscopic images of HEK293T cells treated with PA14 (B), 7b treated PA14 (C), and 5c treated PA14 (D)	121
<b>Figure 3B.1</b>	(A) Alkylaminotroponyl sulfone (ATS) derivatives as <i>Pseudomonas aeruginosa</i> Quorum Sensing (QS) inhibitors, (B) Previously reported troponyl thymidine analogues, (C) This report- synthesis and biochemical evaluations of <sup>ATS</sup> dT analogs	208
<b>Figure 3B.2</b>	(A) Absorption, (B) Emission, (C) Normalized emission spectra, (D) Quantum yield of compound <b>3a</b> in different solvents at 10 <sup>-5</sup> M concentration	211
<b>Figure 3B.3</b>	(A) Normalized absorptions and emissions of compound <b>3a</b> , <b>3b</b> and <b>3c</b> in DMSO solvent, (B) Quantum yield of all ATS derivatives ( <b>3a/b/c</b> - <b>11a/b/c</b> ) in DMSO solvent	214

<b>Figure 3B.4</b>	Absorption (A), Emission spectra (B, C) and Quantum yield (D) of <sup>ATS</sup> dT-1 ( <b>14</b> ); Absorption (E), Emission spectra (F, G) and Quantum yield (H) of <sup>ATS</sup> dT-2 ( <b>15</b> ) in different solvents	216
<b>Figure 3B.5</b>	Geometrically optimized structure HOMO-LUMO diagrams and their energy differences using DFT calculation: (A) <sup>ATS</sup> dT-1 ( <b>14</b> ) and (B) <sup>ATS</sup> dT-1 ( <b>15</b> )	217
<b>Figure 3B.6</b>	Cell proliferation assays of <sup>ATS</sup> dT-1 ( <b>14</b> ) and <sup>ATS</sup> dT-1 ( <b>15</b> )	218
<b>Figure 3B.7</b>	Confocal microscopic images of HeLa cells incubated with compound <b>5c</b> (A-C, 12 h incubation time; D-F, 24 h incubation time) along with BODIPY dye staining	219
<b>Figure 3B.8</b>	Confocal microscopic images of HeLa cells incubated with <sup>ATS</sup> dT-1 ( <b>14</b> ) (A-F) and <sup>ATS</sup> dT-2 ( <b>15</b> ) (G-L) along with DAPI staining for colocalization (12 h incubation time)	221
<b>Figure 3B.9</b>	Confocal microscopic images of HeLa cells incubated with <sup>ATS</sup> dT-1 ( <b>14</b> ) (A-F) and <sup>ATS</sup> dT-2 ( <b>15</b> ) (G-L) along with DAPI staining for colocalization (24 h incubation time)	222
<b>Figure 4A.1</b>	Previously reported <i>N</i> -aryl nucleobases, amino-azulene derivatives and this report	239
<b>Figure 4A.2</b>	Crystal structure and packing diagram of Az-C ( <b>4</b> )	241
<b>Figure 4A.3</b>	Crystal structure and packing diagram of Az-T ( <b>3</b> )	242
<b>Figure 4A.4</b>	Optimized structures of Az-A/T/G/C ( <b>3-6</b> ) nucleobases	243

<b>Figure 4A.5</b>	(A, B) HRTEM and (C, D) FESEM images of Az-C ( <b>4</b> ); (E) HRTEM and (F, G) FESEM images of Az-T ( <b>3</b> ), (H) an image of boat lily plant	244
<b>Figure 4A.6</b>	(A) UV-Vis spectra of Az-C ( <b>4</b> ) and Az-C-Ag complex ( <b>8</b> ), (B) Graphical representation of the synthesis of compound <b>8</b>	245
<b>Figure 4A.7</b>	(A, B) HRTEM and (C) FESEM images of Az-C-Ag complex ( <b>8</b> )	245
<b>Figure 4A.8</b>	(A) Plot for concentration-dependent antimicrobial activity of silver nanoparticles (Az-C-silver complex) ( <b>8</b> ) against PA14 by disc diffusion assay, (B) Image of LB plate showing zone of clearance for compound <b>8</b> at 100 $\mu$ M concentration	246
<b>Figure 4A.9</b>	(A) Plots for Cell viability assay of compounds Az-T ( <b>3</b> ), Az-C ( <b>4</b> ), Az-A ( <b>5</b> ), Az-G ( <b>6</b> ) and (B) Az-C-Ag complex ( <b>8</b> ) for HEK293T cell line	247
<b>Figure. 4B.1</b>	(A) Previously reported C-nucleosides and (B) this report	283
<b>Figure 4B.2</b>	D <sub>2</sub> O exchange NMR experiment of C-nucleoside ( <b>10</b> )	285
<b>Figure 4B.3</b>	Crystal structure and packing diagram of azulenyl C-nucleoside ( <b>10</b> )	286
<b>Figure 4B.4</b>	.UV-Vis spectrum of C-nucleoside ( <b>10</b> ) in acetonitrile at 10 $\mu$ M concentration	287
<b>Figure 4B.5</b>	(A, B) HRTEM, (C, D) FESEM images at different magnifications and (E) EDAX analysis of azulenyl C-nucleoside	288

(10)

<b>Figure 4B.6</b>	Cell proliferation assay of compound <b>10</b> in HEK293 and HeLa cells	289
<b>Figure 5.1.</b>	Previous and this reports on bodipy cisplatin and tropinylbodipy nucleoside analogs	317
<b>Figure 5.2</b>	<sup>1</sup> H NMR spectra comparison of compounds <b>3</b> and <b>4</b>	318
<b>Figure 5.3</b>	Normalized absorption and emission spectra of compounds <b>3</b> and <b>4</b> in PBS buffer at 10 <sup>-5</sup> M concentration	319
<b>Figure 5.4</b>	Cell proliferation assay of compound <b>4</b>	320
<b>Figure 5.5</b>	Confocal microscopic images of HeLa cells incubated with compound <b>4</b> (stained with DAPI) for 24 h at a concentration of 100 μM	321
<b>Figure 6.1</b>	(A) Previously reported troponyl/hydrazine containing amides; (B) Rationally designed β-troponylhydrazinyl peptides & their instability under acidic conditions	355
<b>Figure 6.2.</b>	<sup>1</sup> H-NMR DMSO-d <sub>6</sub> titration plot for BocNH (A) and Amide NH (B), Proposed conformation of β-troponylhydrazino peptides/control peptide (C)	359
<b>Figure 6.3</b>	Conformational analyses of crystal peptide <b>5a*</b> in solid state: analysis of crystal <b>5a*</b> : (A) ORTEP diagram; (B) Unit Cell packing; (C) Packing arrangement; (D) Helical supramolecular	360

self-assembly structure. (\*Tertiary Butyl ester of **5a**)

- Figure 6.4** Conformational analyses of crystal **5h** in solid state: (A) ORTEP diagram; (B) Unit Cell; (C) Hydrogen bonding pattern; (D) Helical supramolecular assembly 361
- Figure 6.5** Conformational analyses of control peptide crystal (**6a**) in solid state: (A) ORTEP diagram; (B) Unit cell; (C) Packing arrangement; (D) Intermolecular hydrogenbondinng; (E) Supramolecular self-assembly helical structure 362
- Figure 6.6** Conformational analyses of Troponylpyrazolidinone crystal (**9**): (A) ORTEP diagram; (B) unit cell packing; and (C) Intramolecular hydrogen bonding 364
- Figure 6.7** Time-dependent <sup>1</sup>H-NMR kinetic plot-Mole Fraction vs. Time (min) with hybrid peptide **5a** (A) and its exponential plot for half-life calculation (B) 366
- Figure 6.8** Time dependent UV-Spectra of dipeptide **6a** under acidic conditions (20% TFA in ACN) 367
- Figure 6.9** The proposed mechanism of  $\beta$ -troponylhydrazinyl peptides propenamide cleavage under mild acidic conditions 368



## List of Schemes

<b>Scheme 1.1</b>	Standard methods for synthesis of nucleoside triphosphates (B= modified or natural nucleobase; R= H, OH, or modification)	6
<b>Scheme 2A.1</b>	Synthesis of TBS-protected nucleoside tr- <sup>TBS</sup> dU.	41
<b>Scheme 2A.2</b>	Synthesis of troponyl-dUTP (tr-dUTP) and tr-dU	45
<b>Scheme 2B.1</b>	Synthesis of troponyl-dU (tt-dU, <b>5</b> ) and its triphosphate analog (tt-dUTP, <b>6</b> )	76
<b>Scheme 3A.1</b>	Synthesis of ATS derivatives <i>via</i> C(sp <sup>2</sup> )-H activation	107
<b>Scheme 3A.2</b>	The substrate scope of Arylsulfonation at alkylaminotropone	109
<b>Scheme 3B.1</b>	Cu-catalyzed arylsulfonation of <i>N</i> -benzylaminotropone <i>via</i> C(sp <sup>2</sup> )-H activation	209
<b>Scheme 3B.2</b>	Synthesis of troponyl sulfone conjugated nucleoside <sup>ATS</sup> dT-1 ( <b>14</b> ) and <sup>ATS</sup> dT-2 ( <b>15</b> )	210
<b>Scheme 4A.1</b>	Synthesis of <i>N</i> -azulenyl Nucleobases	240
<b>Scheme 4B.1</b>	Synthesis of diethyl 2-amino-6-bromoazulene-1, 3-dicarboxylate ( <b>3</b> )	283
<b>Scheme 4B.2</b>	Synthesis of azulenyl C-nucleoside ( <b>10</b> )	284
<b>Scheme 5.1</b>	Synthesis of the platinum complex [Pt(NH <sub>3</sub> ) <sub>2</sub> (PTB)Cl](NO <sub>3</sub> ) ( <b>4</b> )	318
<b>Scheme 5.2</b>	Synthesis and crystal structure of bromotroponimine difluoro boron complex ( <b>8</b> )	322

<b>Scheme 5.3</b>	Synthesis of troponylbodipy 3'-keto C- nucleoside derivative ( <b>12</b> )	323
<b>Scheme 6.1.</b>	Synthesis of <i>N</i> -troponylated- $\beta$ -hydrazino acid/peptides	356
<b>Scheme 6.2</b>	Synthesis of control <i>N</i> -alkylated- $\beta$ -hydrazino acid/peptides	357
<b>Scheme 6.3</b>	Reaction of $\beta$ -troponylhydrazino peptides/non-tropoyl- $\beta$ -hydrazino peptides with TFA	364

## List of Tables

<b>Table 2A.1</b>	Summary table of Fluorescence properties of tr- <sup>TBS</sup> dU ( <b>7</b> )	43
<b>Table 2B.1</b>	Summary table of Fluorescence properties of tt-dU ( <b>5</b> )	79
<b>Table 3A.1.</b>	Optimization studies of ATS <b>3a/3b/3c</b>	108
<b>Table 3A.2</b>	Primers used for quantitative RT-PCR experiment	118
<b>Table 3B.1</b>	Summary table of photophysical properties of compound <b>3a</b> in different solvents	211
<b>Table 3B.2</b>	Summary table of photophysical properties of the compound <b>3a/b/c-11a/b/c</b> in DMSO	213
<b>Table 3B.3</b>	Summary table of photophysical properties of the compound <sup>ATS</sup> dT-1( <b>14</b> ) and <sup>ATS</sup> dT-2 ( <b>15</b> ) in different solvents	215
<b>Table 5.1</b>	Summary table of photophysical properties of compounds <b>3</b> and <b>4</b> in PBS buffer	319

# CONTENTS

Summary	Page No.
SYNOPSIS	x
LIST OF FIGURES	xxi
LIST OF SCHEMES	xxix
LIST OF TABLES	xxx

## CHAPTER-1

### CHAPTER 1. Introduction to Modified Nucleosides, Nucleic Acids, Peptides and Tropolone

1.1 Introduction	2
1.2 Objective of the present thesis	25
1.3 References	26

## CHAPTER-2

### CHAPTER 2A. Synthesis, Photophysical Studies and Biochemical Evaluations of Tropolone Conjugated DNA

2A.1 Introduction	38
2A.2 Objective	40
2A.3 Results and Discussion	40
2A.4 Conclusion	49
2A.5 Experimental Section	50
2A.6 References and Notes	56
2A.7 Appendix	63

### CHAPTER 2B. Tropolone Clicked DNA: Synthesis, Photophysical Studies and Biochemical Evaluations

2B.1 Introduction	73
2B.2 Objective	75
2B.3 Results and Discussion	76
2B.4 Conclusion	82
2B.5 Experimental Section	82
2B.6 References and Notes	86
2B.7 Appendix	93

## **CHAPTER-3**

### **CHAPTER 3A. Alkylaminotroponyl Sulfones as *Pseudomonas aeruginosa* Quorum**

#### **Sensing Inhibitors**

3A.1 Introduction	104
3A.2 Objective	105
3A.3 Results and Discussion	106
3A.4 Conclusion	121
3A.5 Experimental Section	122
3A.6 References and Notes	138
3A.7 Appendix	145

### **CHAPTER 3B. Troponylsulfone Conjugated Nucleosides: Synthesis, Photophysics and HeLa cell Imaging**

3B.1 Introduction	206
3B.2 Objective	207
3B.3 Results and Discussion	208
3B.4 Conclusion	223
3B.5 Experimental Section	223

3B.6 References and Notes	226
3B.7 Appendix	231

## CHAPTER-4

### CHAPTER 4A. Azulene tethered *N*-aryl Nucleobases: Synthesis, Morphology and Biochemical Evaluations

4A.1 Introduction	237
4A.2 Objective	238
4A.3 Results and Discussion	239
4A.4 Conclusion	247
4A.5 Experimental Section	248
4A.6 References and Notes	252
4A.7 Appendix	255

### CHAPTER 4B. Azulene Tethered C-nucleoside: Synthesis and Morphological studies

4B.1 Introduction	281
4B.2 Objective	282
4B.3 Results and Discussion	283
4B.4 Conclusion	289
4B.5 Experimental Section	289
4B.6 References and Notes	294
4B.7 Appendix	299

## CHAPTER-5

### CHAPTER 5. Troponylbodipy Cisplatin and C-nucleoside Analogs: Synthesis and Biochemical Evaluation

5.1 Introduction	315
------------------	-----

5.2 Objective	317
5.3 Results and Discussion	317
5.4 Conclusion	323
5.5 Experimental Section	323
5.6 References and Notes	328
5.7 Appendix	334

## CHAPTER-6

### CHAPTER 6. Synthesis and Mechanistic Insights of Cleavable Amide Bond

#### Comprising $\beta$ -Troponylhydrazino Acid

6.1 Introduction	353
6.2 Objective	355
6.3 Results and Discussion	239
6.4 Conclusion	368
6.5 Experimental Section	369
6.6 References and Notes	379
6.7 Appendix	382
<b>Thesis Summary</b>	456

#### List of abbreviations

A	Adenine
Å	Angstrom
Aa/AA	Amino acid
AMR	Antimicrobial resistance
aq.	Aqueous
ATS	Alkylaminotroponyl Sulfone

Az	Azulene
Bn	Benzyl
Boc	Tert-butyloxycarbonyl
BODIPY	boron-dipyrromethane
br	Broad
C	Cytosine
°C	Degrees Celsius
CCDC	Cambridge Crystallographic Data Centre
d	Doublet
DNA	Deoxy ribose nucleic acid
DMF	N,N-dimethylformamide
DCM	Dichloromethane
DMSO	Dimethyl sulfoxide
DIPEA	Diisopropylethylamine
dU	Deoxy Uridine
EDC.HCl	N-(3-Dimethylaminopropyl)-N'-ethylcarbodiimide hydrochloride
equiv.	Equivalent
ESI-MS	Electrospray ionization Mass Spectrometry
ESF	Environment Sensitive Fluorescence
Et	Ethyl

EtOAc	Ethylacetate
FDA	Food and Drug Administration
G	Guanine
g	Gram(s)
h	Hour(s)
HCL	Hydrochloric acid
HIV	Human Immunodeficiency Virus
HOMO	Highest Occupied Molecular Orbital
HRMS	High Resolution Mass Spectrometry
Hz	Hertz
IR	Infrared (spectroscopy)
$\lambda$	Wavelength
LiOH	Lithium Hydroxide
LUMO	Lowest unoccupied Molecular Orbital
m/z	Mass to charge ratio
$\mu$	Micro
MeOH	Methanol
mg	Milli gram
MHz	Megahertz
$\mu$ L	Micro litre
mp	Melting point
NMR	Nuclear Magnetic Resonance



nm	Nanometers
NTP	Nucleoside Tri-phosphate
p	Para
PA	Pseudomonas aeruginosa
PCR	Polymerase Chain Reaction
PEX	Primer Extension Reaction
Ph	Phenyl
Phe	Phenyl alanine
pH	Hydrogen ion concentration in aqueous solution
ppm	Parts per million
q	Quartet
QS	Quorum Sensing
rt	Room temperature
s	Singlet
t	Triplet
T	Thymine
TEA	Triethylamine
TFA	Trifluoroacetic acid
THF	Tetrahydrofuran
TLC	Thin layer chromatography
Ts	<i>p</i> -toluenesulfonyl (tosyl)
UV	Ultraviolet

## **CHAPTER 1**

---

### **Introduction to Modified Nucleosides, Nucleic Acids, Peptides and Tropolone**

---

#### **1.1 Introduction**

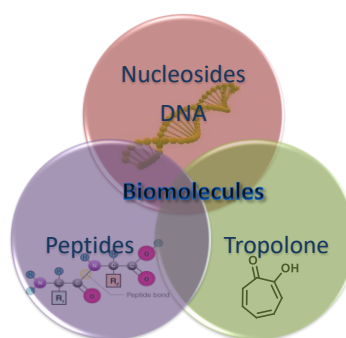
#### **1.2 Objective of the present thesis**

#### **1.3 References and Notes**

## 1.1 Introduction

This thesis entitled "Syntheses and Biochemical Assessments of Modified Nucleosides, Nucleic Acids, and Peptides Containing Tropolone Surrogates" is an embodiment of research intended towards the synthesis and studies on various nucleosides, DNA, and cleavable peptides comprising troponyl scaffolds. Before diving into the thesis, it is necessary to get acquainted with the core biomolecules. Their brief overview is provided in the following segments-

- a) DNA and Nucleosides
- b) Peptides- Cleavable amide bonds
- c) Tropolone and Troponoids



### 1.1a. DNA and Nucleosides

#### *Structure of Nucleic Acids*

Nucleic acids are the fundamental molecules of life, containing the genetic blueprints for all living species on the planet. They have been refined over billions of years of evolution to attain an optimal balance of complexity and elegance, an ideal combination of design and function. In living cells, there are two kinds of nucleic acids, i.e., deoxyribonucleic acid (DNA) and ribonucleic acid (RNA). Two types of sugar units are found in nucleic acids: deoxyribose (only found in DNA) and ribose (only found in RNA). As a result, the two nucleic acids have been named accordingly. The essential building elements of nucleic acids are natural nucleosides, composed of a nucleobase and a sugar ring. A nucleoside and at least one phosphate group constitute nucleotides. The nucleobases found in nucleic acids resemble either a purine or a pyrimidine ring structure and are referred to as purines or pyrimidines. Adenine (A), guanine (G), cytosine (C), and thymine (T) are the four natural bases found in

DNA. The first two are purine derivatives, while the other two are pyrimidine derivatives. The first three nucleobases of RNA are the same as in DNA, but instead of thymine, another pyrimidine derivative, uracil (U), is present as a fourth nucleobase (Figure 1.1).<sup>1,2</sup> Aside from these major bases, many other nucleobases occur in nature. RNAs have a wide range of changed nucleobases, whereas eukaryotic DNA has only modified nucleobases, including the methylation of the C5-position of cytosine or the exocyclic amino group of adenine. In eukaryotes, these changes support a system for regulating and expressing specific genes at the DNA level.<sup>3</sup>

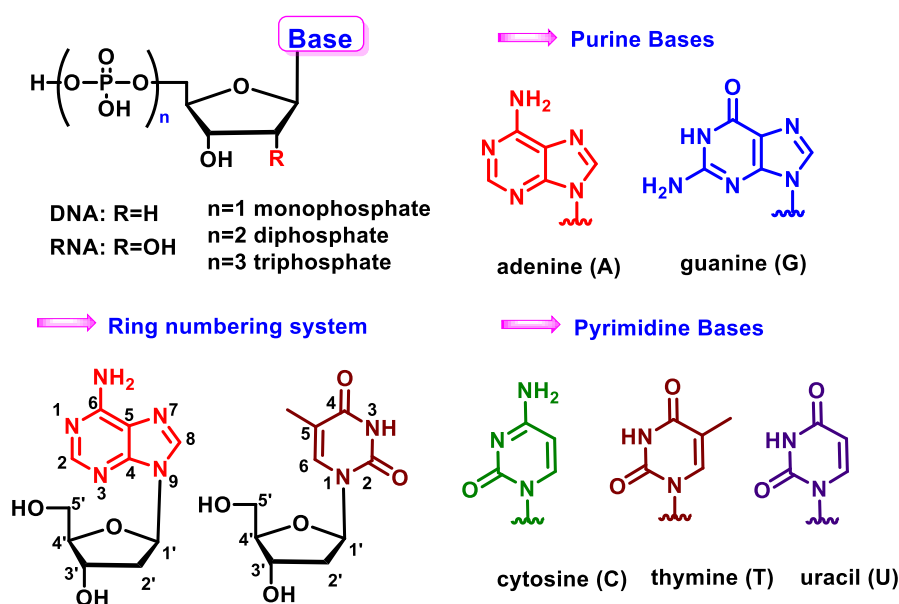


**Figure 1.1.** Components of nucleoside and nucleotide.

Franklin, Wilkins, Watson, and Crick discovered the structural foundation of DNA in 1953, highlighting the double helix structure of DNA. Hydrophobic and stacking forces and well-defined hydrogen bonding patterns keep DNA in this classic double-stranded helical structure. The DNA helical structure is constructed from complementary single strands oriented in an anti-parallel fashion (one strand 5'-3', another 3'-5'). These nucleobase pairs of nucleic acids interact via two or three hydrogen bonds (Figure 1.2, PC-microbiologynotes.org). While the Watson-Crick base pairing is dominant in nucleic acids, it

is important to note that nucleobases do not have exclusive binding behavior. There are 28 base-pairing motifs, which can involve at least two hydrogen bonds produced between the four common nucleobases. These include reverse Watson–Crick, Hoogsteen, and 'wobble' (or mismatched) base pairs.<sup>1,4</sup> These and other nucleobase binding modes can play important roles in any nucleobase self-assembly process governed by hydrogen bonding, particularly when the geometry of the double helix does not constrain the interaction.

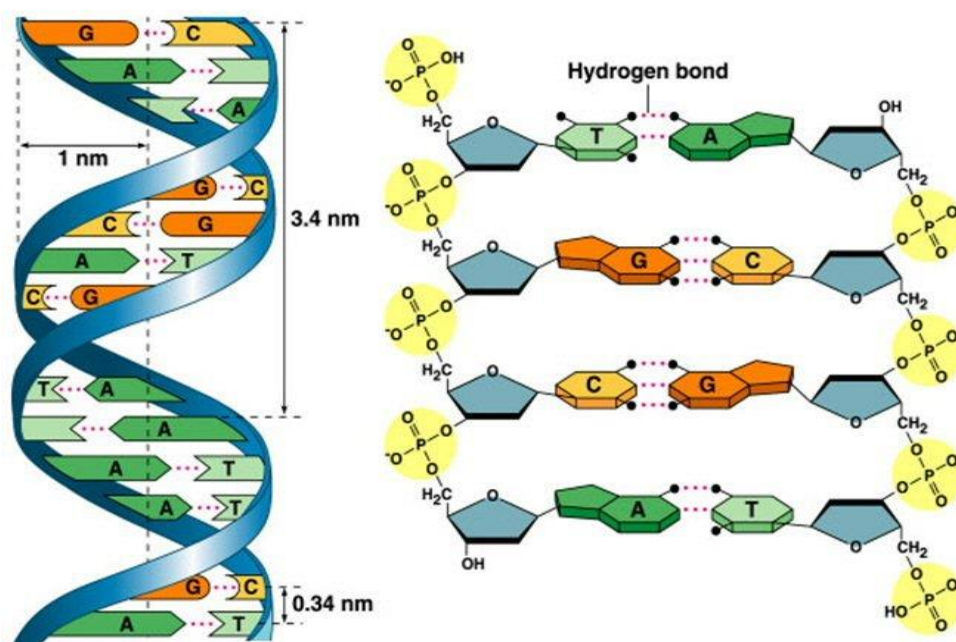


**Figure 1.2.** DNA double helix and hydrogen bonding between nucleobases.

### *Synthesis of DNA*

The biosynthesis of nucleic acids is achieved by polymerase enzymes using nucleoside triphosphate as the building block. Nucleic acids can be synthesized using two methods, each with advantages and downsides.<sup>5</sup> First is the chemical method that employs solid support/phosphoramidite chemistry in a DNA synthesizer machine, with phosphoramidite derivatives of nucleosides as the building blocks. Large-scale synthesis is possible using this approach. However, the chain length is limited and necessitates a huge volume of chemicals and reagents, making small-scale synthesis problematic. The second one

is the enzymatic method, which follows the biosynthesis principle and requires nucleoside triphosphate (NTP) derivatives as a building block. Except for the scalability issue, oligomers with long chain lengths can be synthesized here. In this case, small amounts of starting materials are required compared to the first method. NTP's primary purpose is to serve as a substrate for polymerase. The addition of NTPs to primer is catalyzed by polymerase in the 3' direction, which is complementary to the template. The crystal structure of polymerase with duplex DNA and NTP explains the reaction mechanism of this process. The mechanism is defined by the widely accepted two metal ions model (Figure 1.3, © 2018 PNAS).<sup>6,7</sup> Three carboxylates of asparates bind two magnesium metal ions (**A** and **B**). Metal ion **A** interacts with the primer's 3'-OH group, lowering its *pK<sub>a</sub>* value and facilitating attack on incoming NTP. Metal **A** also binds with the entering nucleotide's alpha phosphates, which helps to stabilize its negative charge. Metal ion **B** interacts with the incoming NTP's beta and gamma phosphates, stabilizing the negative charge and leaving the pyrophosphate group. The 3'-OH of primer attacks alpha phosphate and produces a new phosphodiester bond. The same concept also works for nucleic acid synthesis using modified triphosphates.<sup>8</sup>

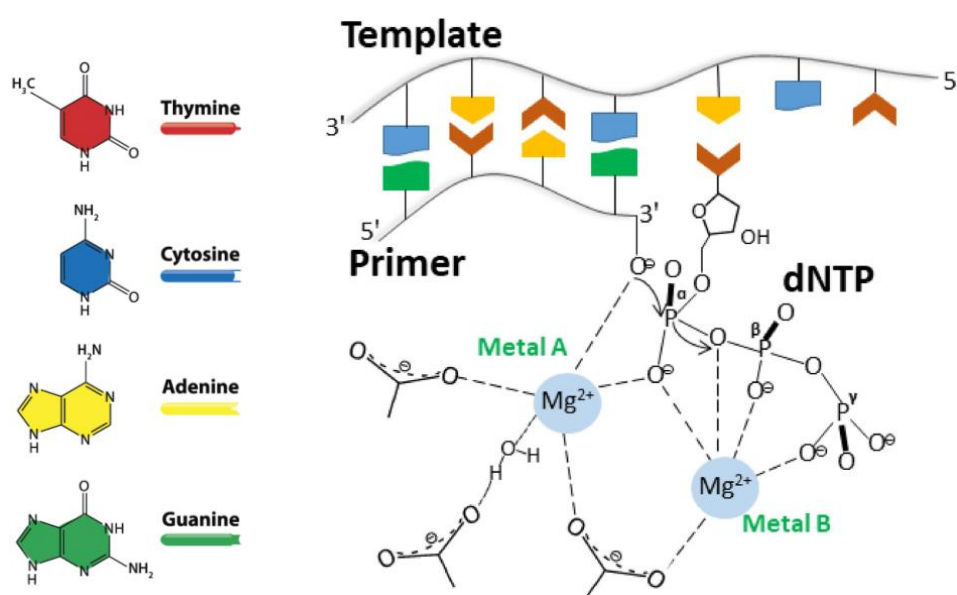
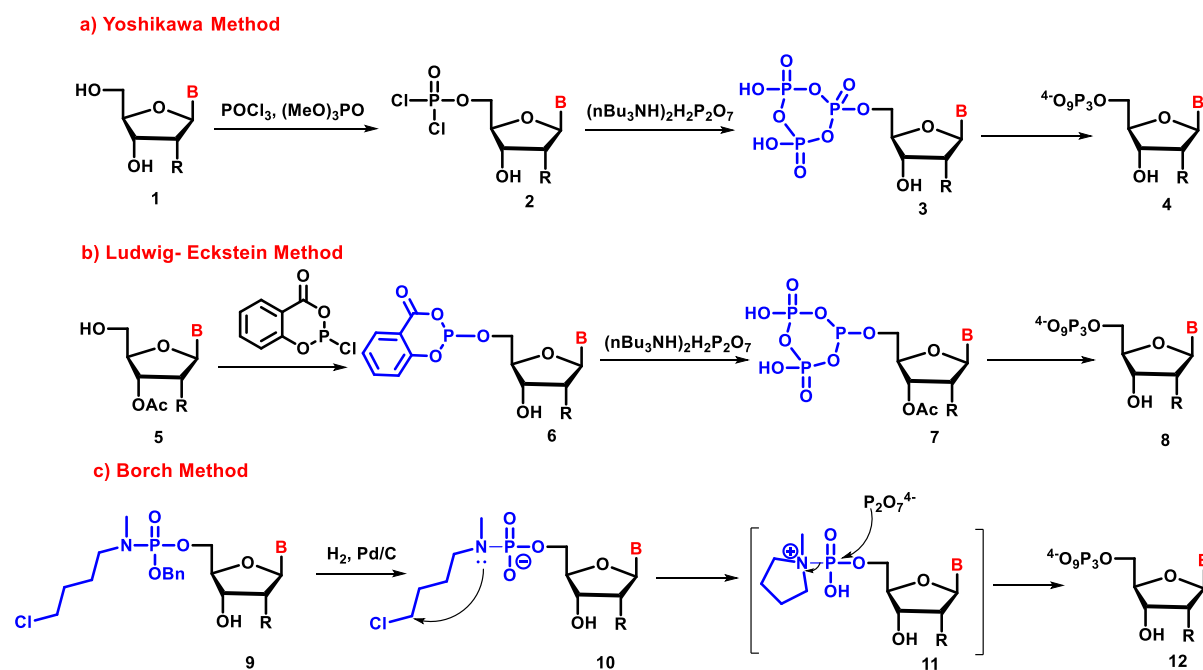


**Figure 1.3.** Reaction mechanism of polymerase-catalyzed phosphodiester bond formation.

*Synthesis of Nucleoside Triphosphates*

Numerous synthetic campaigns have focused on modified triphosphates. Still, a broadly applicable and high-yielding approach for synthesizing NYPs/ dNTPs remains unclear. Despite the laborious purification required for these reactive species, recent improvements have improved access to modified nucleoside triphosphates. Some of the standard methods for nucleoside triphosphate synthesis are explained in Scheme 1.1.



**Scheme 1.1.** Standard methods for synthesis of nucleoside triphosphates (B= modified or natural nucleobase; R= H, OH, or modification).

The Yoshikawa method is one of the first and still most used methods for synthesizing nucleoside triphosphates (Scheme 1.1-a).<sup>9,10</sup> The highly reactive phosphorodichlorate intermediate (**2**) is produced by selective 5'-monophosphorylation of an unprotected nucleoside precursor (**1**) with the electrophilic phosphorous oxychloride ( $\text{POCl}_3$ ). This intermediate (**2**) is then treated in situ with pyrophosphate to produce cyclic triphosphate (**3**), which is then hydrolyzed to produce the desired compound (**4**). The advantages of this

approach stem from its simplicity. There is no need for a protecting groups, and the use of trialkylphosphate solvents primarily guides phosphorylation to the 5'-regioisomer.<sup>11,12</sup> However, not all nucleosides are compatible with the use of a strong electrophilic phosphorous reagent, and modern analytical techniques have revealed the formation of many undesirable by-products.<sup>13,14</sup>

Ludwig and Eckstein's "one-pot, three-steps" approach, established in the late 1980s, is another most dependable and popular procedure for synthesizing modified triphosphates.<sup>15</sup> In brief, the modified nucleoside precursor (**5**) is treated with salicyl phosphorochlorite, which specifically reacts with the free 5'-hydroxyl group to generate the activated phosphite intermediate (**6**) (Scheme 1.1-b). The bifunctional phosphite (**6**) then experiences two nucleophilic substitution reactions driven by tris(tetra-nbutylammonium) hydrogen pyrophosphate, resulting in salicylic acid displacement and the production of the cyclic intermediate (**7**). In the end, iodine-mediated oxidation of derivative (**7**) results in the formation of modified (d)NTP (**8**) through a cyclic nucleoside triphosphate. This protocol has the advantage of lowering the number of unwanted by-products (e.g., regioisomers, mono-, di-, and oligo-phosphates) produced in the Yoshikawa methodology, simplifying the subsequent HPLC purification. Furthermore, the formation of all the intermediates during the reaction can be easily monitored by <sup>31</sup>P-NMR. The sole disadvantage of this procedure is that it takes a slightly longer synthetic route than the Yoshikawa method.<sup>16,17</sup> Despite this minor disadvantage, the Ludwig-Eckstein method yielded an impressive palette of modified dNTPs.

Other methods encounter problems such as the formation of side products, low yields, and the incompatibility of functional groups with strong electrophilic phosphorous reagents. Thus, a different approach employing a highly reactive zwitterionic intermediate (Scheme 1.1-c) has been developed to avoid these drawbacks.<sup>18</sup> The O-benzyl-protected phosphoramidate ester (**9**) is activated by removing the protecting group, forming the reactive



pyrrolidinium phosphoramidate zwitterion (**11**). This intermediate is susceptible to react in situ with pyrophosphate resulting triphosphate derivative. This approach has been successfully applied in synthesizing farnesyltransferase inhibitors and phosphoramidate prodrugs.<sup>19</sup>

### *Need and scope of modifications in nucleosides*

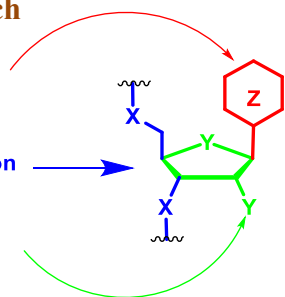
Nucleic acids and nucleosides have found their utility in novel materials, catalysis, and data storage in the technological field and potential targeted treatment and diagnostic modalities in the medical field. Despite these advantages, the efficiency of nucleic acids in natural settings and in various practical (in vivo) applications is frequently hampered by inherent limitations. These include easy degradation by endo- and exo-nucleases, rapid renal clearance and poor pharmacokinetic properties, restricted access to more complex functional patterns, and a lack of functional groups capable of mediating binding or catalysis. Nature corrects some of these flaws by inserting further chemical alterations into the scaffold of nucleic acids, primarily at the nucleobase level.<sup>20,21</sup> This finding inspired chemists to tailor nucleosides, in which chemical modifications can be introduced at any point in the sugar moiety, phosphodiester backbone, nucleobase, or any combinations thereof (Figure 1.4). It brought remarkable progress in DNA nanotechnology, and even the trojan horse concept was applied to deliver modified nucleosides as drug candidates.<sup>22,23</sup>

#### Synthetic Approach

Base modification

Backbone modification

Sugar modification



#### Trojanhorse Concept

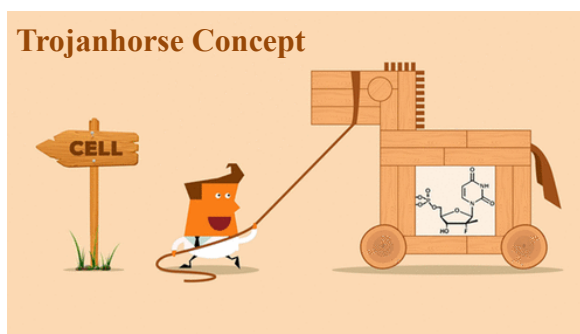


**Figure 1.4.** Scope of modifications in nucleosides.

Different types of nucleic acids were produced as a result of sugar ring modifications, including Locked nucleic acid (LNA), Peptide nucleic acid (PNA), Bridged nucleic acid (BNA), Glycol nucleic acid (GNA), Ethylene-bridged nucleic acid (ENA), and Phosphordiamidate morpholino oligomers (PMO).<sup>24-26</sup> Backbone-modified nucleic acids with Phosphorothioate, Boranophosphate, Phosphonoacetate, and Amide linkage have also been thoroughly investigated.<sup>22</sup> In the synthetic oligonucleotide research area, the synthesis of modified nucleosides is probably the most common. Natural pyrimidine nucleobases can be modified by substituting the C2, C4, N3, C5, and C6 positions. C5-substituted compounds have received the most attention for their potential applications in medicine and biochemistry.<sup>27</sup> Similarly, substitutions at the C2, C6, and C8 positions are prevalent in natural purine nucleobases.

#### *Synthesis of base modified nucleosides*

Transition metals have played an important role in drug development, as the formation of carbon-carbon bond is essential for synthesizing novel structures. These reactions are typically challenging to carry out using conventional synthesis techniques. Still, with transition metal-catalyzed cross-coupling development, chemists seeking the next active molecule in the drug discovery process now have access to new horizons. Pd-mediated cross-coupling reactions are likely the most successful and widely used chemical for the synthesis of new compounds among various transition metals.<sup>28,29</sup> This cross-coupling reaction was recognised with a Nobel Prize shared by Richard Heck, Ei-ichi Negishi, and Akira Suzuki in 2010. Their seminal work has resulted in a number of Pd-mediated protocols for highly efficient C-C, C-N, and C-O bond formation. Pd-catalyzed cross-coupling (Sonogashira coupling, Stille coupling, Suzuki-Miyaura coupling, Heck coupling, etc.) is currently the most efficient method of generating a library of diverse structures required for drug discovery activities (Figure 1.5). Many C5 or C6 modified pyrimidine nucleosides and C2 or C8

modified purine nucleosides have been synthesized using transition-metal assisted cross-coupling processes. However, late-stage functional diversity in a molecule is frequently required to determine the ideal structure-activity relationship. Transition metals have been used to provide a wide range of functional groups via carbon-carbon and carbon-hetero atom bond formation, providing rapid access to novel chemical entities that are critical for drug discovery. Recently, transition metal-catalyzed cross-coupling reactions based on direct C-H functionalization have been advanced.<sup>30</sup> These methods don't require organometallic substrates and compete with classic Pd-catalyzed cross-couplings in developing new carbon-carbon bonding strategies. The reactions require only one activated substrate (C-H activation); in some cases, even no activation is required for either substrate (double C-H activation). They are atom efficient, avoiding the synthesis of often unstable activated substrates. The primary difficulties associated with C-H functionalization reactions include: (i) the need to develop regioselective activation of specific C-H bonds in the presence of other C-H bonds; (ii) low chemoselectivity, which means sensitive functional groups must be protected before coupling; and (iii) the need to work at high temperatures to activate C-H bonds with intrinsic low activity, which frequently causes substrate decomposition. Syntheses of the modified nucleosides by direct C-H bond activations have been substantially employed because of improved coupling efficiency and the availability of milder reaction conditions applicable to less stable nucleosides. However, it is still necessary to develop conditions that are compatible with both the solvent requirements for water-soluble nucleotides and the phosphate ester stability.

The above methods were employed for modifications on nucleosides which inclined towards the design of functional DNA and drug molecules. Nucleosides possessing emissive properties gained more attention as they are helpful in monitoring biochemical processes using fluorescence techniques.

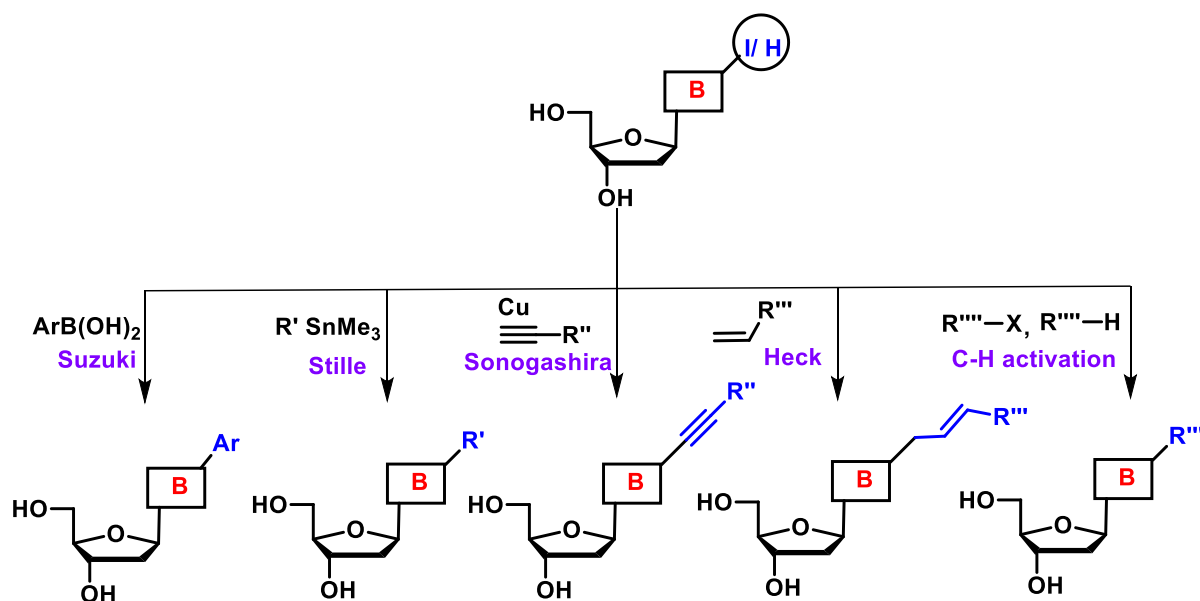


**Figure 1.5.** Synthesis of base modified nucleoside analogs.

### *Fluorescent nucleobases*

Studying various dynamic structures and activities of DNA and RNA in biology demands technologies that can investigate these biomolecules selectively and deeply. Modified fluorescent nucleobases that can be incorporated into nucleic acids along with their natural counterparts have emerged as a potent class of molecular reporters, as natural nucleobases in nucleic acids are virtually non-fluorescent under ambient conditions. In 1969, Stryer reported the emissive compounds formycin and 2-aminopurine (2AP), which started the journey of Fluorescent Nucleic Acid (FNA) analogs.<sup>31</sup> FNAs are classified as isomorphous, enlarged, extended, and chromophoric base analogs based on their chemical structure and relationships to natural nucleobases (Figure 1.6).<sup>32,33</sup> The presence of small substituents or the quantity and position of heteroatoms in the heterocyclic core distinguishes isomorphous nucleoside analogs from natural nucleosides. Additional aromatic rings are annealed to the purine or pyrimidine core in expanded nucleosides. A fluorophore is attached to the nucleobase through a linker in extended nucleoside analogs. Finally, in chromophoric

nucleoside derivatives, the whole nucleobase is replaced by a structurally unique, often bulky, aromatic chromophore.

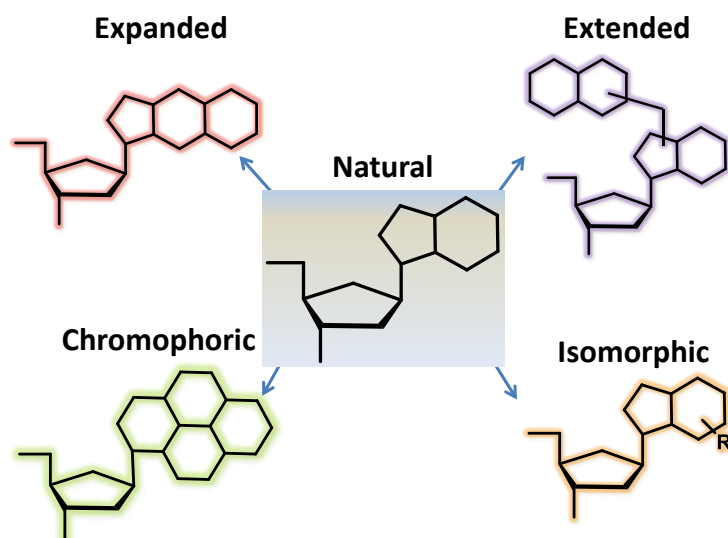


**Figure 1.6.** Types of FNAs based on their structural relationship with the natural nucleobases.

Several groups around the world are involved in tailoring modified nucleosides. Some examples are given in Figure 1.7. Saito and coworkers demonstrated a novel approach in the construction of base-discriminating fluorescent (BDF) nucleosides, which can identify the type of base opposite the BDF base by a fluorescence change. The fluorescence intensity of the probe DNA containing BDF nucleosides changes dramatically only when it hybridizes with a specific target sequence. This evident change in fluorescence is used for gene SNP typing. The homogeneous SNP typing approach based on BDF probes would effectively replace traditional SNP typing methods.<sup>34,35</sup> Various Microenvironment sensitive fluorescent nucleosides were reported by Tor and coworkers, Srivatsan and coworkers.<sup>36,37</sup> Wilhelmson and coworkers made tricyclic cytidine analogs exhibiting fluorescence.<sup>38</sup> Bag and coworkers synthesized many fluorescent nucleosides containing triazole moiety and studied their binding ability with BSA protein.<sup>39</sup> Nucleosides modified by Kool and coworkers, Hock and

coworkers, and Purse and coworkers are well known.<sup>40,41</sup> The molecular rotor introduced by Leudtke and coworkers is the brightest fluorescent nucleoside reported to date.<sup>42</sup>

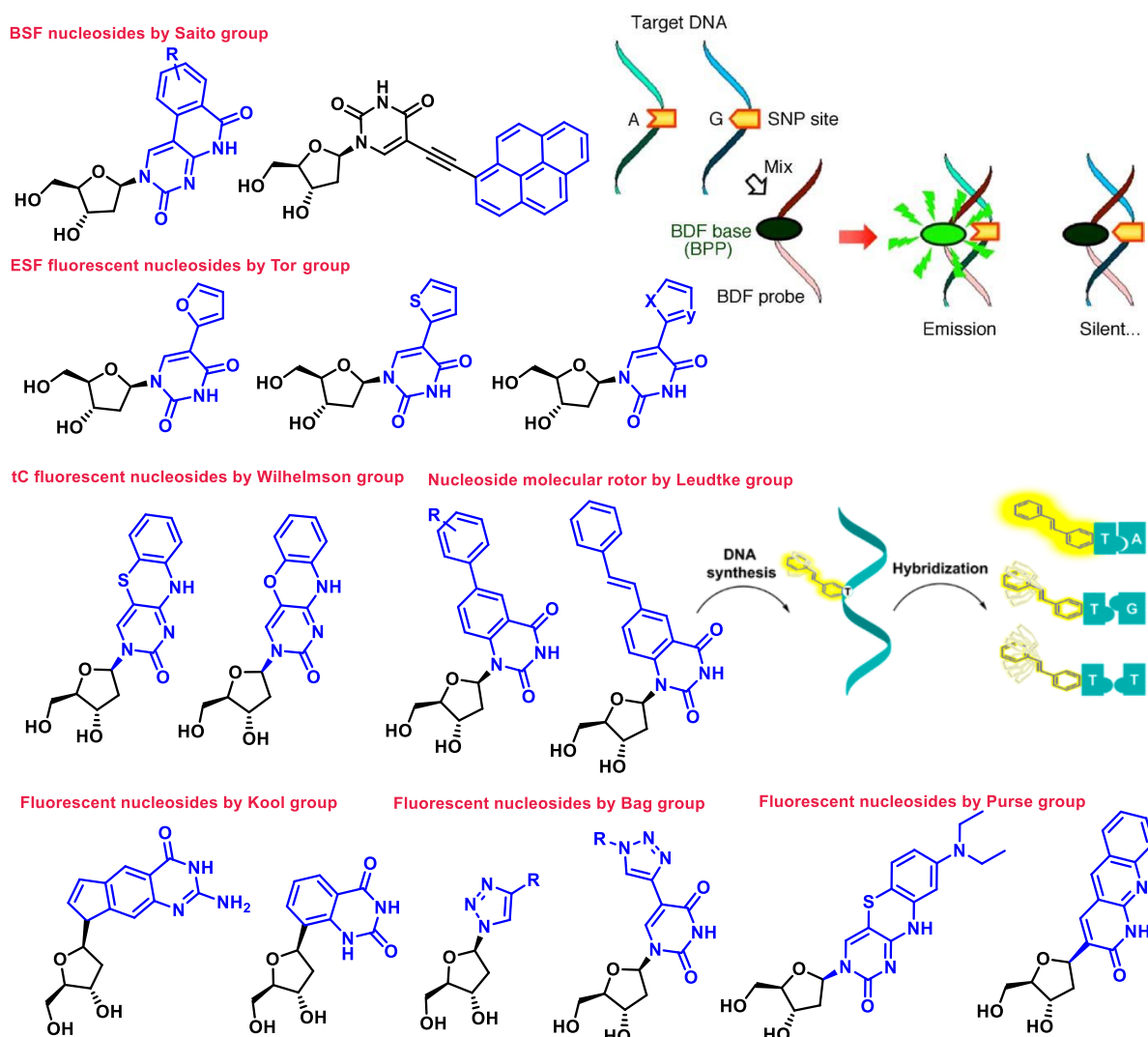


**Figure 1.7.** Selected examples of fluorescent base modified nucleosides.

#### *Fluorescent nucleosides having alkynyl linkage*

The attachment of an alkynyl linker is one of the most studied C5 modifications in pyrimidine nucleosides. The capacity of acetylenes and their highly conjugated homologs to create significant electrical transmission between consecutive subunits is well recognized. The linear *sp*-hybridized carbon chain can offer solid structures that should allow for the precise position of the substituents attached with alkynyl functionalized oligonucleotide

probes, allowing for a better knowledge of substituent-nucleotide interaction. Oligonucleotides containing such extended fluorescent nucleosides have found essential uses in the research of SNP detection, nucleic acid lesion, and the electron transfer process in DNA. Fluorophores can be connected to nucleobases via a single C-C bond, extending the  $\pi$ -conjugation and introducing modified optical properties into the nucleoside. Fused benzene rings, heterocycles (furan, thiophene, oxazole, and thiazole, etc.), pyrene, bodipy, and other fluorescent dyes have been attached using alkynyl linkage (Figure 1.8) by many research groups. When incorporated into oligonucleotides, several of these analogs generate stable base pairs and exhibit microenvironment sensitivity.

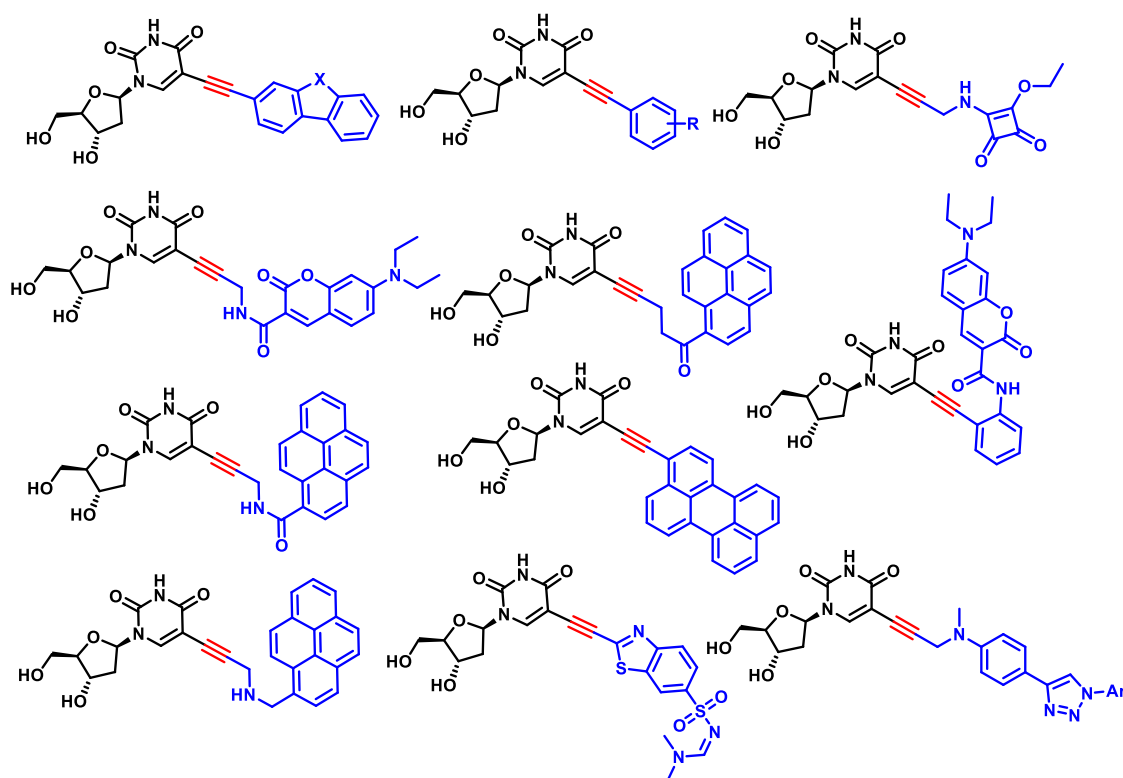


**Figure 1.8.** Selected examples of fluorescent nucleosides having alkynyl linkage.

Hocek and coworkers have synthesized numerous environment-sensitive fluorophores (ESF) showing microenvironment sensitivity. They incorporated them into DNA enzymatically to study DNA-Protein interaction and cell imaging (Figure 1.9).<sup>43,44</sup>

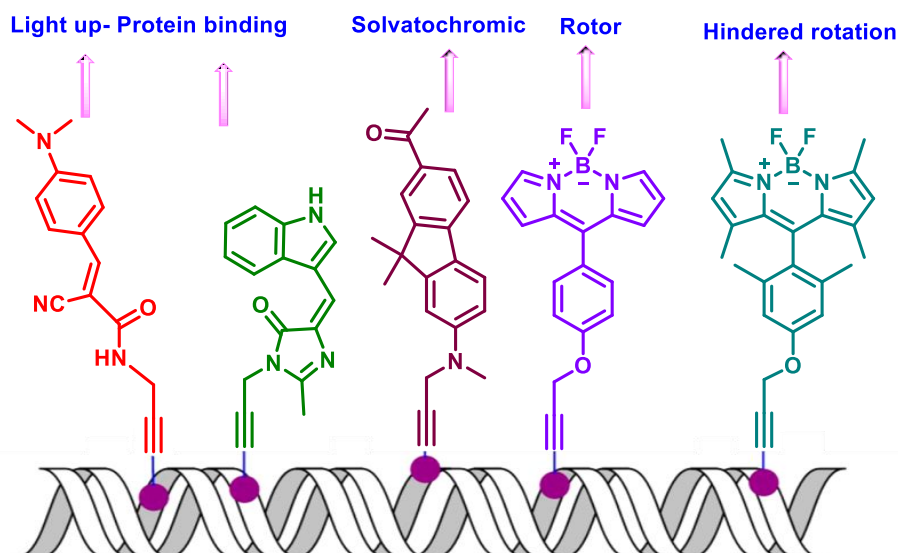


**Figure 1.9.** Incorporation of fluorescent nucleosides into DNA having alkyne linkage.

#### *Fluorescent nucleosides having triazolyl linkage*

For a long time, nucleosides, nucleotides, and oligonucleotides have been investigated as substrates for click chemistry (Figure 1.10).<sup>45</sup> The bioconjugation of nucleosides and oligonucleotides containing alkyne-modified nucleobases with azide-modified fluorescent dyes, sugars, and peptides are extensively described. These coupling processes frequently required Cu(I), a ligand, and heating or overnight stirring. Click chemistry has also been investigated for nucleosides and oligodeoxynucleotides (ODNs) with modified sugars containing terminal alkyne groups.<sup>46</sup> The fluorescent properties of nucleosides with triazolyl modifications were influenced primarily by (i) the location of nucleobases to which a triazolyl unit is attached, (ii) the site of triazolyl attachment to the nucleobase (N1 vs. C4), and (iii) additional substitutions at nucleobase or triazolyl units. Post-synthetic alterations are one of the most significant advantages of click chemistry.<sup>47</sup> It has become a standard tool for drug discovery, bioconjugation, proteomic profiling, and possible cellular target identification. Bertozzi, Meldal, and Sharpless were bestowed with the Nobel Prize for the introduction and development of click chemistry.



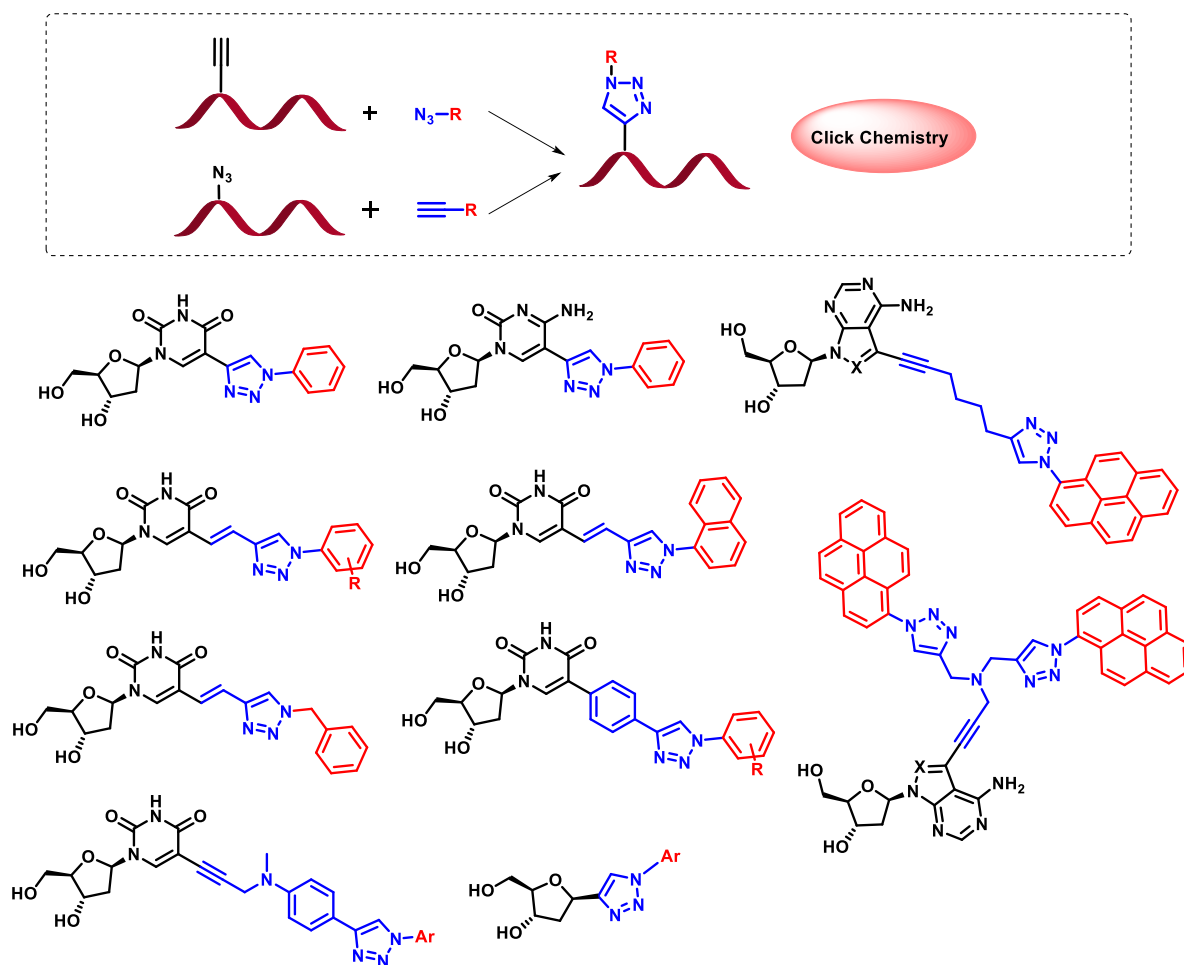


**Figure 1.10.** Post synthetic modification by click chemistry and selected examples of fluorescent nucleosides having triazolyl linkage.

#### *Fluorescent nucleosides containing Bodipy analogs*

Dyes with a Bodipy core are a type of fluorescent molecule with appealing features that can be utilized as fluorescent tags. The key benefits of these dyes are their remarkable photostability, high brightness, and low susceptibility to environmental polarity and pH.<sup>48</sup> Recently, fluorescent deoxyuridine analogs have been investigated based on the Bodipy fluorophore and its incorporation into DNA.<sup>49</sup> They possess exceptional fluorescence characteristics and have been effectively used to probe local viscosity in various systems. The use of fluorescence techniques and the probe's ability to be incorporated into DNA can provide novel information on interactions of DNA with proteins and lipids, which can lead to

the characterization of the DNA microenvironment in a cellular context (Figure 1.11, Figure 1. 11-A, ©2023 American Chemical Society ).<sup>50–52</sup>

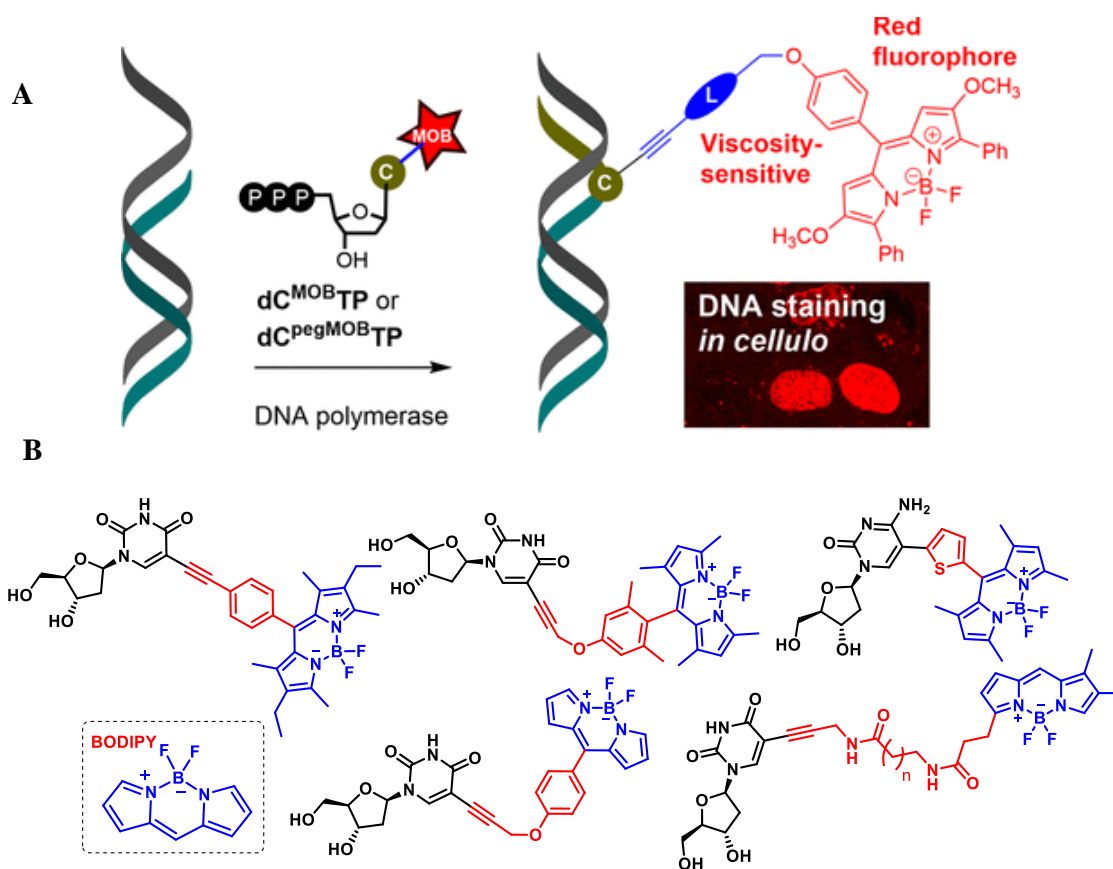


**Figure 1.11.** Selected examples of Bodipy containing nucleosides.

### *C-nucleoside analogs*

C-Nucleosides are a significant class of compounds distinguished by the substitution of a stable, hardly degradable C-C bond by a labile glycosidic C-N bond. C-Nucleosides with hydrophobic aryl groups as nucleobase surrogates have received a lot of attention due to their utility in expanding the genetic alphabet. They selectively pair with the same or another hydrophobic nucleobase in oligonucleotide duplexes due to enhanced packing and favorable desolvation energy compared to canonical hydrophilic nucleobases. Various C-nucleoside analogs have been described as anticancer and antiviral agents.<sup>53,54</sup> Some examples of C-nucleosides are provided in Figure 1.12.

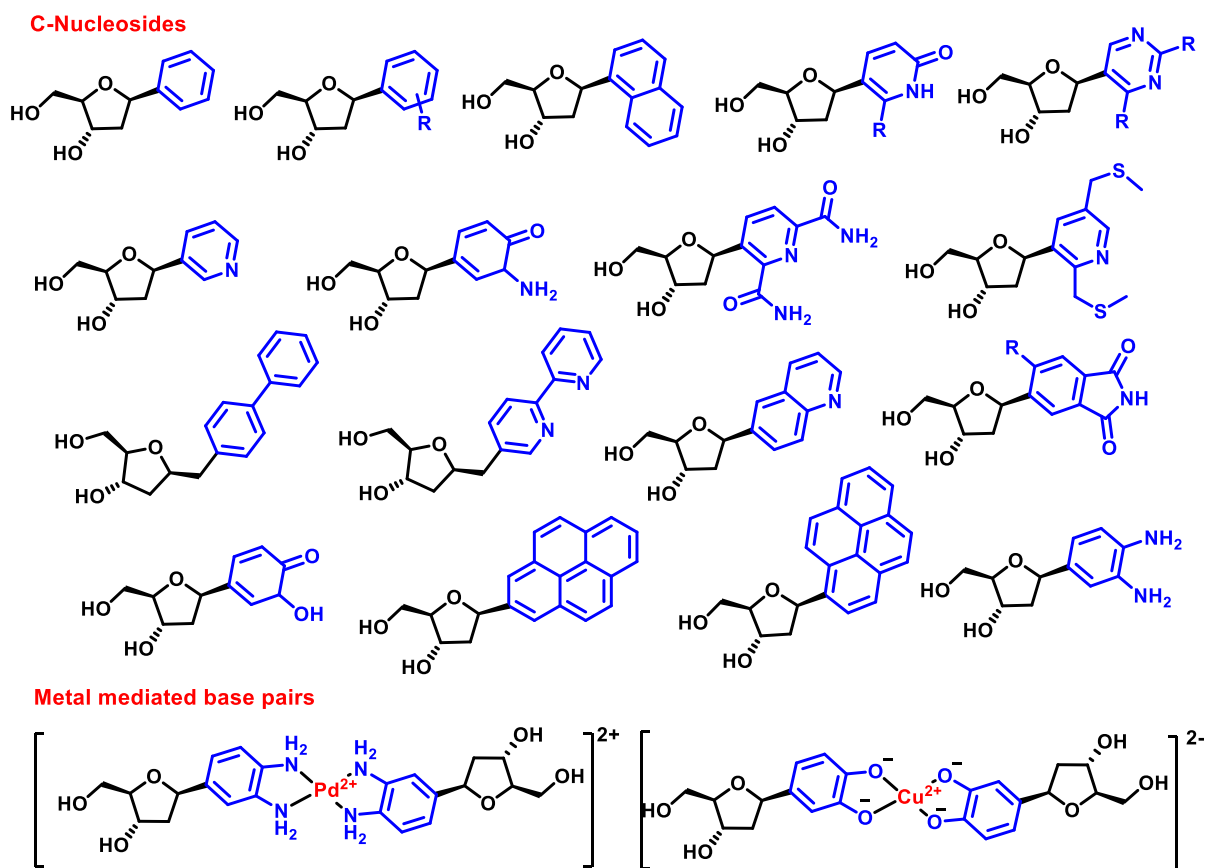


**Figure 1.12.** Selected examples of C-nucleosides and metal mediated base pairs.

C-nucleosides can be developed into metal-mediated base pairs with potential applications. The Metallo-base pairs were created by selecting optimal combinations of ligand-bearing nucleosides and metal ions based on their binding affinity and intrinsic structure. The majority of them were synthetically inserted into DNA strands without significant structural disruption, resulting in duplex stabilization. This property would be used to truncate functional DNAs like aptamers and DNazymes and design DNA-based switchable devices and machines. Other properties of metallo-base pairs, such as redox activity and kinetic behaviour, should be investigated for future biological applications.<sup>55</sup>

#### *Applications of modified nucleobases/ nucleic acid chemistry*

Nucleoside modifications have been used in various applications after decades of research. They have been incorporated into noncanonical DNA structures for structural elucidation,

modification, and stabilization and for different therapeutic and diagnostic uses (Figure 1.13, 1.14). Furthermore, without the introduction of nucleoside modifications, the field of oligonucleotide therapeutics, particularly antisense, RNAi, and aptamer-based candidates, would not have gained popularity. In addition, nucleic acid therapies have emerged as intriguing alternatives to traditional vaccination techniques. mRNA vaccines against SARS-CoV-2 are already accessible, and others are being explored for different infectious agents or used in cancer clinical trials.<sup>56</sup> With several oligonucleotide-based medicines on the market and over a hundred candidates in early to late-stage clinical trials, recent progress has been swift, broad, and exciting. Such advancements have been made possible partly because of the capacity to rationally design and easily manufacture nucleic acid analogs, which allows for targeted modifications to many of the inherent features that determine their biological activity and potency. The field of oligonucleotide therapies is now concentrating on creating effective delivery systems as well as the foundations for determining fruitful pharmacokinetic and pharmacodynamic correlations for chemically modified nucleic acids. These include strategies for delivering promising clinical candidates to the liver, muscle, and central nervous system.<sup>23,29,57</sup>

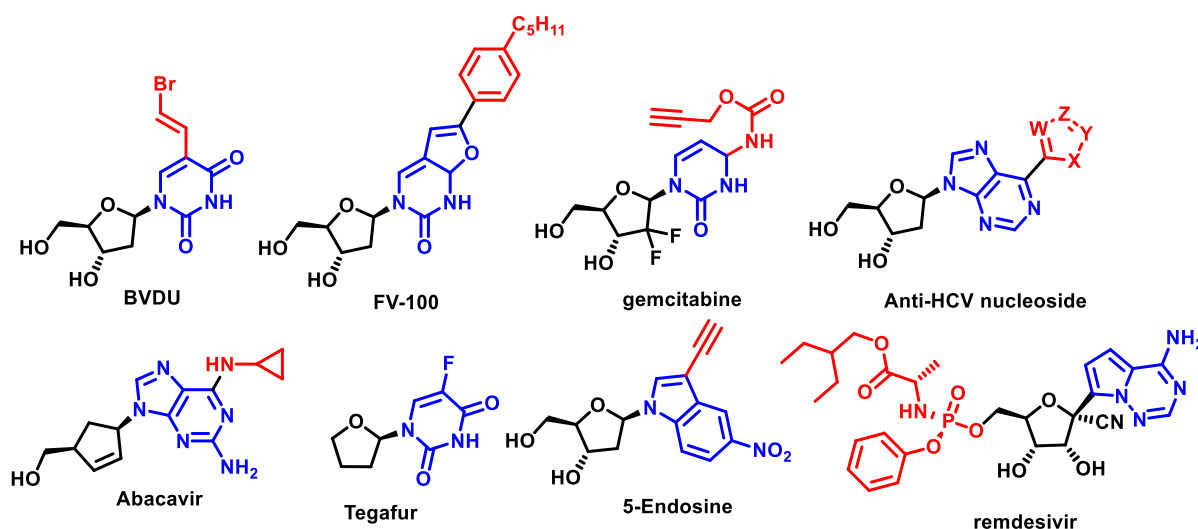


**Figure 1.13.** Selected examples of biologically active modified nucleosides.

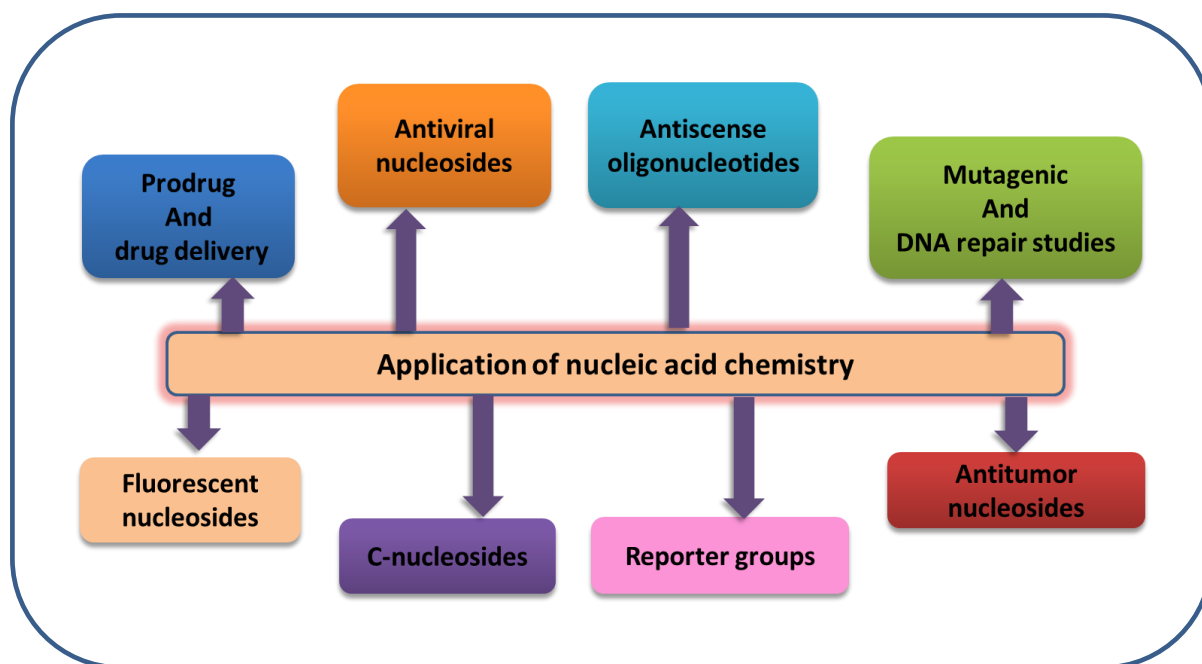


**Figure 1.14.** Progress and applications of nucleic acid chemistry.

#### *Mechanism for action of nucleoside analogs*

Therapeutic nucleoside and nucleotide analogs currently in use utilize the same metabolic pathways as endogenous nucleosides or nucleotides (Figure 1.15, ©2013 Macmillan Publishers Limited).<sup>58</sup> Nucleoside and nucleotide analogs enter cells by particular nucleoside transporters. There is increasing evidence that organic anion or cation transporters and peptide transporters have a role in cellular uptake. Cellular uptake of nucleosides is an active process (requires energy) that involves both equilibrative nucleoside transporters (ENTs) and concentrative nucleoside transporters (CNTs). In humans, three CNTs and four ENTs have been identified. Once within the cell, the nucleoside analog encounters an initial rate-limiting phosphorylation step by a nucleoside kinase, forming a monophosphate metabolite. Nucleoside monophosphate kinase then performs a second phosphorylation step, while nucleoside diphosphate kinase performs the third phosphorylation step. Triphosphates can either be incorporated into nucleic acids and compete with their natural equivalents or hinder nucleic acid production by inhibiting key enzymes such as polymerases.

Ribonucleotide reductase M1 (RRM1), a crucial enzyme involved in nucleotide metabolism, can be inhibited by both diphosphorylated and triphosphorylated analogs. Catabolic enzymes, such as deaminases and 5' nucleotidases, can reduce the number of active metabolites. Once the active phosphorylated metabolites of nucleoside analogs have been produced in cells, they may induce the termination of chain elongation, accumulation of mutations, and apoptosis depending upon their modification purposes. Antiviral and anticancer nucleoside analogs widely follow this mechanism.<sup>58,59</sup>

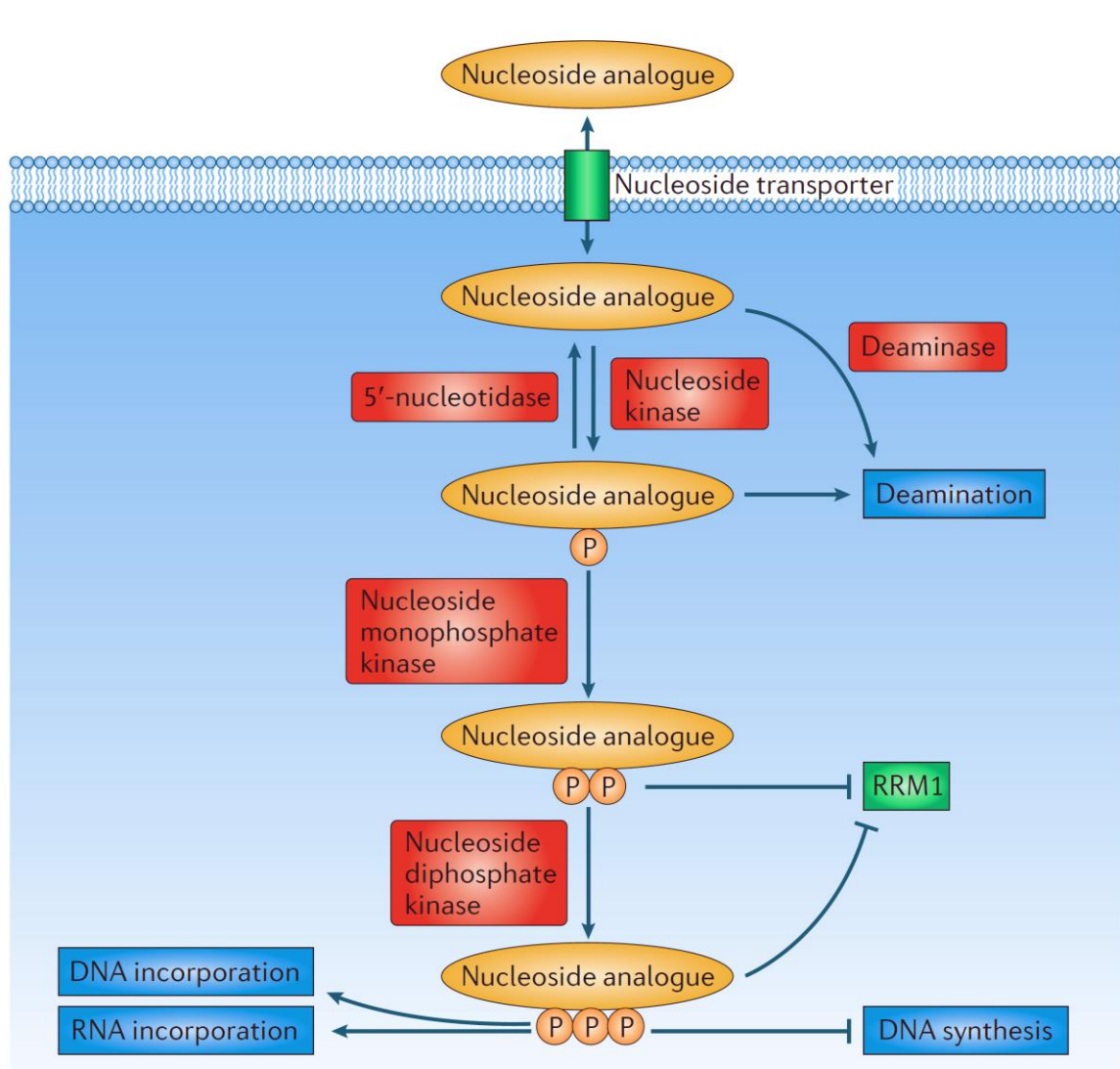


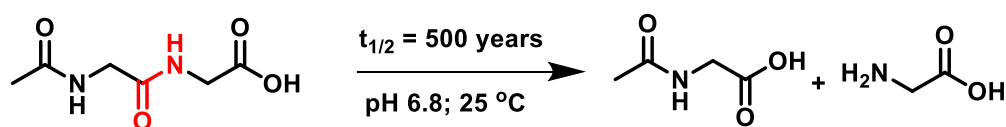
**Figure 1.15.** Mechanism of action of nucleoside analogs.

### 1.1b. Peptides- Cleavable amide bonds

The transfer of genetic information from DNA to RNA and finally to a protein is famous as the central dogma of life, which Francis Crick proposed. The enzyme RNA polymerase uses DNA as a template to generate a pre-mRNA transcript during transcription. The pre-mRNA is processed to produce a mature mRNA molecule that is translated to produce the protein molecule. Proteins are nothing but polypeptide chains that govern a variety of biological activities. Amino acids are the peptides' building blocks linked together by an amide bond. Natural amides are highly stable, with an estimated half-life of 350-600 years for spontaneous hydrolysis at neutral pH and ambient temperature.<sup>60-62</sup> Although amides are easily cleaved/ hydrolyzed by enzymes such as proteases, it is difficult to selectively cleave an amide's C-N bond using synthetic chemistry. Generally, it requires heating under strongly acidic or basic conditions to cleave an amide bond. Several groups have attempted to cleave amide bonds chemically (Figure 1.6).<sup>63,64</sup> In case of ring-strained cyclic amides, the constituent atoms of the amide bond deviate from planarity, resulting in poor electron delocalization and a significant loss in the amide bond's partial double bond character. Thus, several highly strained cyclic lactams are synthesized, and their amide bonds are discovered to be cleavable under mild conditions.<sup>65,66</sup> Because of resonance decoupling via N-C=O torsion, the C=O bond of reactive lactams amide is emerging to the strong electrophile as ketonic carbonyl. Brown and coworkers demonstrated mechanistically that resonance decoupling causes a significant increase in hydrolysis rate by direct nucleophilic attack at the carbonyl of strained amide.<sup>67,68</sup> The most twisted amide is trimethylazatricyclodecanone, a highly strained lactam with significant resonance decoupling via the N-C bond and is readily hydrolyzable. This twisted lactam likewise exhibits amide's dual reactivity, namely the nucleophilic character of amine and the electrophilic nature of carbonyl. Kostic and colleagues prepared an artificial peptidase that cleaves sequence-

specific amide bonds as Pro-Met/Pro-His peptide segments under mild conditions with a Pd catalyst.<sup>69</sup> Few natural amide bonds are precisely demonstrated in the literature through the formation of thiazolinone derivatives (via Edman degradation), oxazolinium intermediates, and chemical modification of the amide backbone.<sup>70–72</sup> Most notably, Edman degradation for amide bond cleavage is the basis for protein sequencing technology. The presence of zinc species in the active sites of metalloproteases has prompted synthetic chemists to use  $\text{Zn}^{2+}$  to cleave amide bonds. Mashima and coworkers reported the cleavage of amides bearing a  $\alpha$ -hydroxyethyl group under mild conditions with Lewis acid  $\text{Zn}(\text{OTf})_2$ .<sup>73</sup> Garg and coworkers established the conversion of amide functional group into ester group by cleaving amide C-N bond employing Ni catalyst in the repertoire of creating reactive amide group.<sup>74–76</sup> Transamidation is a vital chemical transformation reaction for ligating or removing amino-functionalized chemical moieties at carboxylate-functionalized compounds. Gellman, Stahl, and colleagues investigated the amide groups for transamidation reactions between secondary and tertiary amines using a Zr/Hf-catalyst.<sup>77–80</sup> There are also ample reports on other metal-catalyzed and metal-free transamidation reactions.

**A) Peptide bonds are stable**



**B) Hydrolyzable amide bonds**

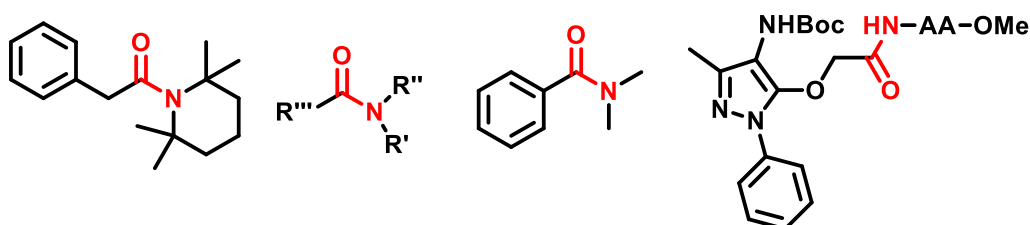


**Figure 1.16.** Stability of peptide bond (A), Hydrolyzable amide bonds (B).



### 1.1c. Tropolone and Troponoids

Tropolone, a chemical with a nonbenzenoid aromatic seven-membered ring, was initially presented by Dewar in 1945, which was further confirmed by Alexander Todd and coworkers.<sup>81,82</sup> The carbonyl functional group on the tropolone ring is more polarised. The partial positive charge at the carbonyl carbon is more stabilized compared to aliphatic ketones and aldehydes, and also stabilized due to aromaticity in tropolone.<sup>83</sup> The positively charged carbon allows electrons to be delocalized over the seven-membered ring. Notably, the hydroxyl proton in tropolone rigorously shifts between the carbonyl and hydroxyl functional groups, resulting in tropolone existing in two highly mobile tautomeric forms (Figure 1.17). However, in case of isomers 3-hydroxytropone and 4-hydroxytropone proton transfer isn't possible as they are separated by more than one bond.

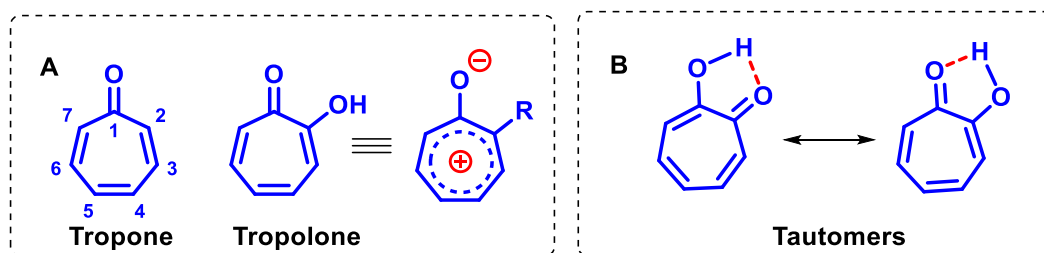


**Figure 1.17.** Tropone and tropolone chemical structures (A) and tautomers (B).

Tropolones and natural compounds with a tropolonoid/ troponoid motif have various bioactivities, including antimicrobial, antiviral, and anticancer properties.<sup>84–87</sup> Some examples of troponoid natural products exhibiting biological properties are provided in Figure 1.8. These molecules possess unique hydrogen bonding patterns and metal-chelating abilities with divalent ions, such as  $\text{Ni}^{2+}$ ,  $\text{Mg}^{2+}$ ,  $\text{Zn}^{2+}$ , and  $\text{Cu}^{2+}$ .<sup>88,89</sup> Such properties allow troponoids to interact with the active site of metalloenzymes. Additionally, substituted tropolones are a powerful unique chemotype for the synthesis of inhibitors of metalloenzyme drug targets.<sup>90</sup>

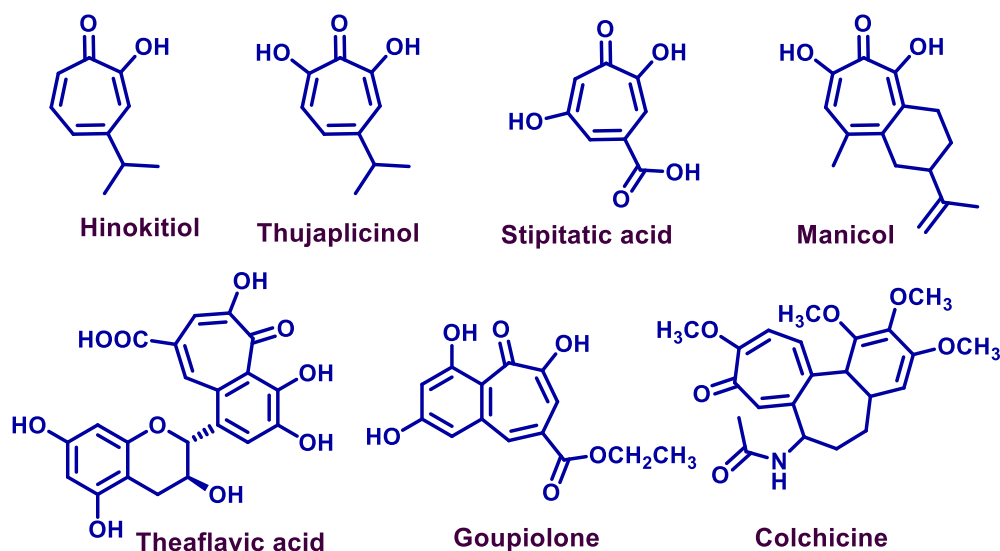


**Figure 1.18.** Selected examples of troponoid natural products.

## 1.2 Objective of the present thesis

This era has witnessed the development of many drug molecules which clinically served humankind. As a result, synthetic biology/ biochemistry is a developing interdisciplinary field with the overarching goal of creating systems in which artificial chemical processes replicate high-level behaviors of organic matter. In the above discussions, we can comprehend the importance of nucleosides, nucleic acids, and peptides. Natural nucleic acids and peptides possess various therapeutic values, but their modified analogs can behold target-specific and enhanced sensitivity properties. The new-age synthetic strategies have captivated scientists to synthesize these designer molecules and explore their biochemical utility. Most of the modifications include benzenoid and heterocyclic moieties. But in this thesis, we have employed a non-benzenoid aromatic scaffold, tropolone, and its derivatives for making modified nucleosides, nucleic acid, and peptide analogs. We have also evaluated some of its bioactivity and got exciting results. The synopsis part provides a brief idea, and the following chapters (Chapters- 2 to 6) comprise all the details regarding the syntheses and biochemical assessments.

### 1.3 References and Notes

- (1) Sivakova, S.; Rowan, S. J. Nucleobases as Supramolecular Motifs. *Chem. Soc. Rev.* **2005**, *34* (1), 9–21.
- (2) Pu, F.; Ren, J.; Qu, X. Nucleobases, Nucleosides, and Nucleotides: Versatile Biomolecules for Generating Functional Nanomaterials. *Chem. Soc. Rev.* **2018**, *47* (4), 1285–1306.
- (3) Hong, Y.; Lam, J. W. Y.; Tang, B. Z. Aggregation-Induced Emission. *Chem. Soc. Rev.* **2011**, *40* (11), 5361–5388.
- (4) Jaenisch, R.; Bird, A. Epigenetic Regulation of Gene Expression: How the Genome Integrates Intrinsic and Environmental Signals. *Nat. Genet.* **2003**, *33* (3), 245–254.
- (5) Hoose, A.; Vellacott, R.; Storch, M.; Freemont, P. S.; Ryadnov, M. G. DNA Synthesis Technologies to Close the Gene Writing Gap. *Nat. Rev. Chem.* **2023**, *7* (3), 144–161.
- (6) Doublie, S.; Tabor, S.; Long, A. M.; Richardson, C. C.; Ellenberger, T. Crystal Structure of a Bacteriophage T7 DNA Replication Complex at 2.2 Å Resolution. *Nature* **1998**, *391* (6664), 251–258.
- (7) Kim, S. C.; O’Flaherty, D. K.; Zhou, L.; Lelyveld, V. S.; Szostak, J. W. Inosine, but None of the 8-Oxo-Purines, Is a Plausible Component of a Primordial Version of RNA. *Proc. Natl. Acad. Sci.* **2018**, *115* (52), 13318–13323.
- (8) Hottin, A.; Marx, A. Structural Insights into the Processing of Nucleobase-Modified Nucleotides by DNA Polymerases. *Acc. Chem. Res.* **2016**, *49* (3), 418–427.
- (9) Yoshikawa, M.; Kato, T.; Takenishi, T. A Novel Method for Phosphorylation of Nucleosides to 5'-Nucleotides. *Tetrahedron Lett.* **1967**, *8* (50), 5065–5068.

- (10) Yoshikawa, M.; Kato, T.; Takenishi, T. Studies of Phosphorylation. III. Selective Phosphorylation of Unprotected Nucleosides. *Bull. Chem. Soc. Jpn.* **1969**, 42 (12), 3505–3508.
- (11) Gillerman, I.; Fischer, B. An Improved One-Pot Synthesis of Nucleoside 5'-Triphosphate Analogues. *Nucleosides, Nucleotides and Nucleic Acids* **2010**, 29 (3), 245–256.
- (12) Burgess, K.; Cook, D. Syntheses of Nucleoside Triphosphates. *Chem. Rev.* **2000**, 100 (6), 2047–2060.
- (13) Wu, W.; Bergstrom, D. E.; Davisson, V. J. A Combination Chemical and Enzymatic Approach for the Preparation of Azole Carboxamide Nucleoside Triphosphate. *J. Org. Chem.* **2003**, 68 (10), 3860–3865.
- (14) Borsenberger, V.; Kukwikila, M.; Howorka, S. Synthesis and Enzymatic Incorporation of Modified Deoxyuridine Triphosphates. *Org. Biomol. Chem.* **2009**, 7 (18), 3826–3835.
- (15) Ludwig, J.; Eckstein, F. Rapid and Efficient Synthesis of Nucleoside 5'-O-(1-Thiotriphosphates), 5'-Triphosphates and 2', 3'-Cyclophosphorothioates Using 2-Chloro-4H-1, 3, 2-Benzodioxaphosphorin-4-One. *J. Org. Chem.* **1989**, 54 (3), 631–635.
- (16) Lam, C.; Hipolito, C.; Perrin, D. M. Synthesis and Enzymatic Incorporation of Modified Deoxyadenosine Triphosphates. Wiley Online Library 2008.
- (17) Caton-Williams, J.; Smith, M.; Carrasco, N.; Huang, Z. Protection-Free One-Pot Synthesis of 2'-Deoxynucleoside 5'-Triphosphates and DNA Polymerization. *Org. Lett.* **2011**, 13 (16), 4156–4159.

- (18) Wu, W.; Freel Meyers, C. L.; Borch, R. F. A Novel Method for the Preparation of Nucleoside Triphosphates from Activated Nucleoside Phosphoramidates. *Org. Lett.* **2004**, *6* (13), 2257–2260.
- (19) Wu, W.; Sigmond, J.; Peters, G. J.; Borch, R. F. Synthesis and Biological Activity of a Gemcitabine Phosphoramidate Prodrug. *J. Med. Chem.* **2007**, *50* (15), 3743–3746.
- (20) Flamme, M.; McKenzie, L. K.; Sarac, I.; Hollenstein, M. Chemical Methods for the Modification of RNA. *Methods* **2019**, *161*, 64–82.
- (21) Xu, W.; Chan, K. M.; Kool, E. T. Fluorescent Nucleobases as Tools for Studying DNA and RNA. *Nat. Chem.* **2017**, *9* (11), 1043–1055.
- (22) McKenzie, L. K.; El-Khoury, R.; Thorpe, J. D.; Damha, M. J.; Hollenstein, M. Recent Progress in Non-Native Nucleic Acid Modifications. *Chem. Soc. Rev.* **2021**, *50* (8), 5126–5164.
- (23) Pradere, U.; Garnier-Amblard, E. C.; Coats, S. J.; Amblard, F.; Schinazi, R. F. Synthesis of Nucleoside Phosphate and Phosphonate Prodrugs. *Chem. Rev.* **2014**, *114* (18), 9154–9218.
- (24) Ghosh, U.; Gupta, S.; Sinha, S. Synthesis of 5'-Thiol Functionalized Morpholino Oligo-Nucleotide and Subsequent Conjugation with IGT to Improve Delivery and Antisense Efficacy In Vitro. *Bioconjug. Chem.* **2022**.
- (25) Yamaguchi, T.; Horiba, M.; Obika, S. Synthesis and Properties of 2'-O, 4'-C-Spirocyclopropylene Bridged Nucleic Acid (ScpBNA), an Analogue of 2', 4'-BNA/LNA Bearing a Cyclopropane Ring. *Chem. Commun.* **2015**, *51* (47), 9737–9740.
- (26) Gaynor, J. W.; Campbell, B. J.; Cosstick, R. RNA Interference: A Chemist's

- Perspective. *Chem. Soc. Rev.* **2010**, 39 (11), 4169–4184.
- (27) R Kore, A.; Charles, I. Recent Developments in the Synthesis and Applications of C5-Substituted Pyrimidine Nucleosides and Nucleotides. *Curr. Org. Chem.* **2012**, 16 (17), 1996–2013.
- (28) Liang, Y.; Wnuk, S. F. Modification of Purine and Pyrimidine Nucleosides by Direct CH Bond Activation. *Molecules* **2015**, 20 (3), 4874–4901.
- (29) Kapdi, A. R.; Maiti, D.; Sanghvi, Y. S. *Palladium-Catalyzed Modification of Nucleosides, Nucleotides and Oligonucleotides*; Elsevier, 2018.
- (30) Ackermann, L.; Vicente, R.; Kapdi, A. R. Transition-metal-catalyzed Direct Arylation of (Hetero) Arenes by C–H Bond Cleavage. *Angew. Chemie Int. Ed.* **2009**, 48 (52), 9792–9826.
- (31) Ward, D. C.; Reich, E.; Stryer, L. Fluorescence Studies of Nucleotides and Polynucleotides: I. Formycin, 2-Aminopurine Riboside, 2, 6-Diaminopurine Riboside, and Their Derivatives. *J. Biol. Chem.* **1969**, 244 (5), 1228–1237.
- (32) Dziuba, D.; Didier, P.; Ciaco, S.; Barth, A.; Seidel, C. A. M.; Mély, Y. Fundamental Photophysics of Isomorphic and Expanded Fluorescent Nucleoside Analogues. *Chem. Soc. Rev.* **2021**, 50 (12), 7062–7107.
- (33) Sinkeldam, R. W.; Greco, N. J.; Tor, Y. Fluorescent Analogs of Biomolecular Building Blocks: Design, Properties, and Applications. *Chem. Rev.* **2010**, 110 (5), 2579–2619.
- (34) Okamoto, A.; Tanaka, K.; Fukuta, T.; Saito, I. Design of Base-Discriminating Fluorescent Nucleoside and Its Application to T/C SNP Typing. *J. Am. Chem. Soc.* **2003**, 125 (31), 9296–9297.

- (35) Okamoto, A.; Saito, Y.; Saito, I. Design of Base-Discriminating Fluorescent Nucleosides. *J. Photochem. Photobiol. C Photochem. Rev.* **2005**, *6* (2–3), 108–122.
- (36) Noé, M. S.; Ríos, A. C.; Tor, Y. Design, Synthesis, and Spectroscopic Properties of Extended and Fused Pyrrolo-DC and Pyrrolo-C Analogs. *Org. Lett.* **2012**, *14* (12), 3150–3153.
- (37) Tanpure, A. A.; Pawar, M. G.; Srivatsan, S. G. Fluorescent Nucleoside Analogs: Probes for Investigating Nucleic Acid Structure and Function. *Isr. J. Chem.* **2013**, *53* (6-7), 366–378.
- (38) Wilhelmsson, L. M.; Sandin, P.; Holmén, A.; Albinsson, B.; Lincoln, P.; Nordén, B. Photophysical Characterization of Fluorescent DNA Base Analogue, TC. *J. Phys. Chem. B* **2003**, *107* (34), 9094–9101.
- (39) Bag, S. S.; Gogoi, H. Design of “Click” Fluorescent Labeled 2'-Deoxyuridines via C5-[4-(2-Propynyl (Methyl) Amino)] Phenyl Acetylene as a Universal Linker: Synthesis, Photophysical Properties, and Interaction with BSA. *J. Org. Chem.* **2018**, *83* (15), 7606–7621.
- (40) Samaan, G. N.; Wyllie, M. K.; Cizmiciu, J. M.; Needham, L.-M.; Nobis, D.; Ngo, K.; Andersen, S.; Magennis, S. W.; Lee, S. F.; Purse, B. W. Single-Molecule Fluorescence Detection of a Tricyclic Nucleoside Analogue. *Chem. Sci.* **2021**, *12* (7), 2623–2628.
- (41) Krueger, A. T.; Kool, E. T. Fluorescence of Size-Expanded DNA Bases: Reporting on DNA Sequence and Structure with an Unnatural Genetic Set. *J. Am. Chem. Soc.* **2008**, *130* (12), 3989–3999.
- (42) Karimi, A.; Börner, R.; Mata, G.; Luedtke, N. W. A Highly Fluorescent Nucleobase Molecular Rotor. *J. Am. Chem. Soc.* **2020**, *142* (34), 14422–14426.

- (43) Hocek, M. Enzymatic Synthesis of Base-Functionalized Nucleic Acids for Sensing, Cross-Linking, and Modulation of Protein–DNA Binding and Transcription. *Acc. Chem. Res.* **2019**, *52* (6), 1730–1737.
- (44) Dadová, J.; Orság, P.; Pohl, R.; Brázdová, M.; Fojta, M.; Hocek, M. Vinylsulfonamide and Acrylamide Modification of DNA for Cross-linking with Proteins. *Angew. Chemie* **2013**, *125* (40), 10709–10712.
- (45) Devaraj, N. K.; Finn, M. G. Introduction: Click Chemistry. *Chemical Reviews*. ACS Publications 2021, pp 6697–6698.
- (46) Müggenburg, F.; Müller, S. Azide-Modified Nucleosides as Versatile Tools for Bioorthogonal Labeling and Functionalization. *Chem. Rec.* **2022**, *22* (5), e202100322.
- (47) Fantoni, N. Z.; El-Sagheer, A. H.; Brown, T. A Hitchhiker’s Guide to Click-Chemistry with Nucleic Acids. *Chem. Rev.* **2021**, *121* (12), 7122–7154.
- (48) Loudet, A.; Burgess, K. BODIPY Dyes and Their Derivatives: Syntheses and Spectroscopic Properties. *Chem. Rev.* **2007**, *107* (11), 4891–4932.
- (49) Ehrenschwender, T.; Wagenknecht, H.-A. 4, 4-Difluoro-4-Bora-3a, 4a-Diaza-s-Indacene as a Bright Fluorescent Label for DNA. *J. Org. Chem.* **2011**, *76* (7), 2301–2304.
- (50) Dziuba, D.; Pohl, R.; Hocek, M. Bodipy-Labeled Nucleoside Triphosphates for Polymerase Synthesis of Fluorescent DNA. *Bioconjug. Chem.* **2014**, *25* (11), 1984–1995.
- (51) Güixens-Gallardo, P.; Zawada, Z.; Matyašovský, J.; Dziuba, D.; Pohl, R.; Kraus, T.; Hocek, M. Brightly Fluorescent 2'-Deoxyribonucleoside Triphosphates Bearing



- Methylated Bodipy Fluorophore for in Cellulo Incorporation to DNA, Imaging, and Flow Cytometry. *Bioconjug. Chem.* **2018**, 29 (11), 3906–3912.
- (52) Kuba, M.; Pohl, R.; Kraus, T.; Hocek, M. Nucleotides Bearing Red Viscosity-Sensitive Dimethoxy-Bodipy Fluorophore for Enzymatic Incorporation and DNA Labeling. *Bioconjug. Chem.* **2022**.
- (53) De Clercq, E. C-Nucleosides to Be Revisited: Miniperspective. *J. Med. Chem.* **2016**, 59 (6), 2301–2311.
- (54) Li, Q.; Groaz, E.; Persoons, L.; Daelemans, D.; Herdewijn, P. Synthesis and Antitumor Activity of C-7-Alkynylated and Arylated Pyrrolotriazine C-Ribonucleosides. *ACS Med. Chem. Lett.* **2020**, 11 (8), 1605–1610.
- (55) Takezawa, Y.; Shionoya, M. Metal-Mediated DNA Base Pairing: Alternatives to Hydrogen-Bonded Watson–Crick Base Pairs. *Acc. Chem. Res.* **2012**, 45 (12), 2066–2076.
- (56) Pardi, N.; Hogan, M. J.; Porter, F. W.; Weissman, D. mRNA Vaccines—a New Era in Vaccinology. *Nat. Rev. Drug Discov.* **2018**, 17 (4), 261–279.
- (57) Anastasi, C.; Quéléver, G.; Burlet, S.; Garino, C.; Souard, F.; Kraus, J.-L. New Antiviral Nucleoside Prodrugs Await Application. *Curr. Med. Chem.* **2003**, 10 (18), 1825–1843.
- (58) Jordheim, L. P.; Durantel, D.; Zoulim, F.; Dumontet, C. Advances in the Development of Nucleoside and Nucleotide Analogues for Cancer and Viral Diseases. *Nat. Rev. Drug Discov.* **2013**, 12 (6), 447–464.
- (59) Cano-Soldado, P.; Pastor-Anglada, M. Transporters That Translocate Nucleosides and

- Structural Similar Drugs: Structural Requirements for Substrate Recognition. *Med. Res. Rev.* **2012**, 32 (2), 428–457.
- (60) Radzicka, A.; Wolfenden, R. Rates of Uncatalyzed Peptide Bond Hydrolysis in Neutral Solution and the Transition State Affinities of Proteases. *J. Am. Chem. Soc.* **1996**, 118 (26), 6105–6109.
- (61) Smith, R. M.; Hansen, D. E. The PH-Rate Profile for the Hydrolysis of a Peptide Bond. *J. Am. Chem. Soc.* **1998**, 120 (35), 8910–8913.
- (62) Barrett, A.; Woessner, J.; Rawlings, N. D. Enzymes Can of Course Efficiently Orchestrate Amide Cleavage under Physiological Conditions. *Handb. Proteolytic Enzym.* **2004**, 2, 1–30.
- (63) Balachandra, C.; Sharma, N. K. Instability of Amide Bond Comprising the 2-Aminotropone Moiety: Cleavable under Mild Acidic Conditions. *Org. Lett.* **2015**, 17 (16), 3948–3951.
- (64) Dalabehera, N. R.; Meher, S.; Bhusana Palai, B.; Sharma, N. K. Instability of Amide Bond with Trifluoroacetic Acid (20%): Synthesis, Conformational Analysis, and Mechanistic Insights into Cleavable Amide Bond Comprising  $\beta$ -Troponylhydrazino Acid. *ACS omega* **2020**, 5 (40), 26141–26152.
- (65) Clayden, J.; Moran, W. J. The Twisted Amide 2-Quinuclidone: 60 Years in the Making. *Angew. Chemie Int. Ed.* **2006**, 45 (43), 7118–7120.
- (66) Szostak, M.; Aubé, J. Medium-Bridged Lactams: A New Class of Non-Planar Amides. *Org. Biomol. Chem.* **2011**, 9 (1), 27–35.
- (67) Somayaji, V.; Brown, R. S. Distorted Amides as Models for Activated Peptide NC: O

- Units Produced during Enzyme-Catalyzed Acyl Transfer Reactions. 1. The Mechanism of Hydrolysis of 3, 4-Dihydro-2-Oxo-1, 4-Ethanoquinoline and 2, 3, 4, 5-Tetrahydro-2-Oxo-1, 5-Ethanobenzazepine. *J. Org. Chem.* **1986**, *51* (14), 2676–2686.
- (68) Bennet, A. J.; Somayaji, V.; Brown, R. S.; Santarsiero, B. D. The Influence of Altered Amidic Resonance on the Infrared and Carbon-13 and Nitrogen-15 NMR Spectroscopic Characteristics and Barriers to Rotation about the NC (O) Bond in Some Anilides and Toluamides. *J. Am. Chem. Soc.* **1991**, *113* (20), 7563–7571.
- (69) Parac, T. N.; Kostić, N. M. Effects of Linkage Isomerism and of Acid– Base Equilibria on Reactivity and Catalytic Turnover in Hydrolytic Cleavage of Histidyl Peptides Coordinated to Palladium (II). Identification of the Active Complex between Palladium (II) and the Histidyl Residue. *J. Am. Chem. Soc.* **1996**, *118* (25), 5946–5951.
- (70) Edman, P. Mechanism of the Phenyl Iso Thiocyanate Degradation of Peptides. *Nature* **1956**, *177*, 667–668.
- (71) Mahesh, S.; Tang, K.-C.; Raj, M. Amide Bond Activation of Biological Molecules. *Molecules* **2018**, *23* (10), 2615.
- (72) Samaritoni, J. G.; Copes, A. T.; Crews, D. K.; Glos, C.; Thompson, A. L.; Wilson, C.; O'Donnell, M. J.; Scott, W. L. Unexpected Hydrolytic Instability of N-Acylated Amino Acid Amides and Peptides. *J. Org. Chem.* **2014**, *79* (7), 3140–3151.
- (73) Kita, Y.; Nishii, Y.; Onoue, A.; Mashima, K. Combined Catalytic System of Scandium Triflate and Boronic Ester for Amide Bond Cleavage. *Adv. Synth. Catal.* **2013**, *355* (17), 3391–3395.
- (74) Hie, L.; Fine Nathel, N. F.; Shah, T. K.; Baker, E. L.; Hong, X.; Yang, Y.-F.; Liu, P.;

- Houk, K. N.; Garg, N. K. Conversion of Amides to Esters by the Nickel-Catalysed Activation of Amide C–N Bonds. *Nature* **2015**, 524 (7563), 79–83.
- (75) Simmons, B. J.; Weires, N. A.; Dander, J. E.; Garg, N. K. Nickel-Catalyzed Alkylation of Amide Derivatives. *ACS Catal.* **2016**, 6 (5), 3176–3179.
- (76) Tobisu, M.; Nakamura, K.; Chatani, N. Nickel-Catalyzed Reductive and Borylative Cleavage of Aromatic Carbon–Nitrogen Bonds in N-Aryl Amides and Carbamates. *J. Am. Chem. Soc.* **2014**, 136 (15), 5587–5590.
- (77) Tamura, M.; Tonomura, T.; Shimizu, K.; Satsuma, A. Transamidation of Amides with Amines under Solvent-Free Conditions Using a CeO<sub>2</sub> Catalyst. *Green Chem.* **2012**, 14 (3), 717–724.
- (78) Stephenson, N. A.; Zhu, J.; Gellman, S. H.; Stahl, S. S. Catalytic Transamidation Reactions Compatible with Tertiary Amide Metathesis under Ambient Conditions. *J. Am. Chem. Soc.* **2009**, 131 (29), 10003–10008.
- (79) Baker, E. L.; Yamano, M. M.; Zhou, Y.; Anthony, S. M.; Garg, N. K. A Two-Step Approach to Achieve Secondary Amide Transamidation Enabled by Nickel Catalysis. *Nat. Commun.* **2016**, 7 (1), 11554.
- (80) Acosta-Guzmán, P.; Mateus-Gómez, A.; Gamba-Sánchez, D. Direct Transamidation Reactions: Mechanism and Recent Advances. *Molecules* **2018**, 23 (9), 2382.
- (81) Dewar, M. J. S. Structure of Stipitatic Acid. *Nature* **1945**, 155 (3924), 50–51.
- (82) Corbett, R. E.; Johnson, A. W.; Todd, A. R. 31. The Structure of Stipitatic Acid. *J. Chem. Soc.* **1950**, 147–149.
- (83) Pauson, P. L. Tropones and Tropolones. *Chem. Rev.* **1955**, 55 (1), 9–136.

- (84) Tavis, J. E.; Lomonosova, E. The Hepatitis B Virus Ribonuclease H as a Drug Target. *Antiviral Res.* **2015**, *118*, 132–138.
- (85) Cao, F.; Orth, C.; Donlin, M. J.; Adegboyega, P.; Meyers, M. J.; Murelli, R. P.; Elagawany, M.; Elgendy, B.; Tavis, J. E. Synthesis and Evaluation of Troponoids as a New Class of Antibiotics. *ACS omega* **2018**, *3* (11), 15125–15133.
- (86) Morita, Y.; Matsumura, E.; Okabe, T.; Shibata, M.; Sugiura, M.; Ohe, T.; Tsujibo, H.; Ishida, N.; Inamori, Y. Biological Activity of Tropolone. *Biol. Pharm. Bull.* **2003**, *26* (10), 1487–1490.
- (87) Saleh, N. A.; Zwiefak, A.; Mordarski, M.; Pulverer, G. Antibacterial Activity of Selected Tropones and Tropolones. *Zentralblatt für Bakteriologie. Mikrobiologie und Hygiene. Ser. A Med. Microbiol. Infect. Dis. Virol. Parasitol.* **1988**, *270* (1–2), 160–170.
- (88) Meyer, N.; Löhnwitz, K.; Zulys, A.; Roesky, P. W.; Dochnahl, M.; Blechert, S. Aminotroponate Zinc Complexes as Catalysts for the Intramolecular Hydroamination of Alkenes and Alkynes. *Organometallics* **2006**, *25* (15), 3730–3734.
- (89) Dochnahl, M.; Löhnwitz, K.; Lühl, A.; Pissarek, J.-W.; Biyikal, M.; Roesky, P. W.; Blechert, S. Functionalized Aminotroponimate Zinc Complexes as Catalysts for the Intramolecular Hydroamination of Alkenes. *Organometallics* **2010**, *29* (12), 2637–2645.
- (90) Ononye, S. N.; VanHeyst, M. D.; Oblak, E. Z.; Zhou, W.; Ammar, M.; Anderson, A. C.; Wright, D. L. Tropolones as Lead-like Natural Products: The Development of Potent and Selective Histone Deacetylase Inhibitors. *ACS Med. Chem. Lett.* **2013**, *4* (8), 757–761.

## **CHAPTER 2**

### **PART-A**

---

## **Synthesis, Photophysical Studies and Biochemical Evaluations of Tropolone Conjugated DNA**

---

### **2A.1 Introduction**

### **2A.2 Objective**

### **2A.3 Results and Discussion**

### **2A.4 Conclusion**

### **2A.5 Experimental Section**

### **2A.6 References and Notes**

### **2A.7 Appendix**

## 2A.1 Introduction

Deoxyribonucleic acid (DNA) is the biomolecule communicating genetic information for an organism's development and functioning. It is synthesized through polymerase chain reactions using the building block deoxyribonucleoside triphosphate (dNTP).<sup>1-3</sup> Recently, structurally modified DNA has been synthesized to meet desired functional properties, including fluorescence properties.<sup>4,5</sup> Native DNA is a nonfluorescent molecule, but it can become fluorescent by the extension of  $\pi$ - conjugation at nucleobases or by the chemical ligation of selective chromophores/ fluorescent dyes at nucleobases.<sup>6,7</sup> There are two major sites of DNA for attaching the chromophores/ dyes/ fluorophores: the sugar unit and nucleobase rings. The fluorophore-conjugated nucleobases have emerged as powerful synthetic tools to improve fluorescence efficiency.<sup>8,9</sup> The attachment of chromophores/ fluorophores through the linker at the DNA with a functional group (amine/azide/alkyne) has become an attractive and economical method for labeling DNA.<sup>10-12</sup> Fluorescent nucleoside analogs are commonly classified as isomorphic nucleosides, pteridines, size-expanded nucleosides, and extended nucleosides based on their molecular structure and relationships to natural nucleobases.<sup>13</sup> The introduction of the appropriate electron-withdrawing group (EWG) on a purine ring and electron-donating groups (EDG) on a pyrimidine ring induces the fluorescence character of nucleobases with the W-C hydrogen bonding.<sup>13,14</sup> Recently, Hocek and co-workers have prepared functional DNA by appending an alkyne linker at nucleobase for sensing and cross-linking, which are helpful for studying the protein-DNA binding modulation and transcription.<sup>15-19</sup> Saito and co-workers have coupled an aryl residue at deoxyguanosine through an ethynyl linker for exploring the base-discriminating fluorescent (BDF) and environmentally sensitive fluorescent (ESF) probes.<sup>20,21</sup> Bag and co-workers have attached different aromatic scaffolds at the nucleobases, which shows microenvironment-sensitive fluorescence.<sup>22</sup> Tor and co-workers have reported the fluorescent

ring fused cytosine analogs such as pyrrole fused cytosine (pC) and thiophenyl-pC.<sup>23</sup> Wilhelmson and co-workers have appended a phenyl scaffold at the cytidine pyrimidine ring through a sulfur-containing six-membered heterocyclic ring to make fluorescent analogs.<sup>24,25</sup> Srivatsan and co-workers have developed microenvironment-sensitive hetero bicyclic pyrimidine fluorescent RNA analogs.<sup>26–28</sup> Kool and co-workers have synthesized various fluorescent DNA analogs using different organic fluorophores directly at sugar rings for labeling the DNA.<sup>8</sup> Most chromophores are derived from the benzenoid aromatic scaffolds. In the repertoire of functional DNA synthesis, the non-benzenoid moiety-conjugated DNA analogs are not well explored. Tropolone is a non-benzenoid aromatic scaffold and its related derivatives are constituents of troponoid natural products. Tropolone and its naturally occurring derivatives (troponoids) exhibit broad spectrum of biological activities.<sup>29–31</sup> Tropolone has unique intramolecular hydrogen bonding, photophysical properties, and strong metal chelating ability with  $\text{Cu}^{2+}/\text{Ni}^{2+}/\text{Zn}^{2+}$  ions.<sup>32–34</sup> Recently, tropolone has been considered a novel scaffold for tuning the structural and functional properties of peptides and DNA. Troponyl deoxyuridine (tr-dU) nucleoside analog exhibits pH-dependent fluorescence. The tr-dU containing DNA strand significantly enhances fluorescence after forming a duplex with a complementary DNA strand.<sup>35,36</sup> However, tr-dU nucleoside is insoluble in most organic solvents. For practical use, exploring the solvent-dependent fluorescence properties and enzymatic incorporation into DNA primer would be interesting. Additionally, various nucleosides are used as therapeutic drugs for their bioactivity, like antibacterial, antifungal, anticancer, and antitumor properties.<sup>37</sup> Thus we opted to evaluate its cytotoxicity and cell permeability. Herein, we have derivatized the tr-dU and demonstrated its solvent-dependent fluorescence, enzymatic incorporation into DNA primer, HeLa cell-internalization, and cell proliferation through various assays.



## 2A.2 Objective

Tropolone conjugated DNA was previously reported from our group, which was chemically synthesized using phosphoramidite derivatives and it exhibited pH-dependent UV-Fluorescence properties. We realized that this intriguing scaffold had a lot of potentials and required more investigation. In this chapter, we have derivatized different tr-dU analogs and demonstrated the solvent-dependent fluorescence property, enzymatic incorporation into DNA primer, HeLa cell-internalization, and cell proliferation assays.

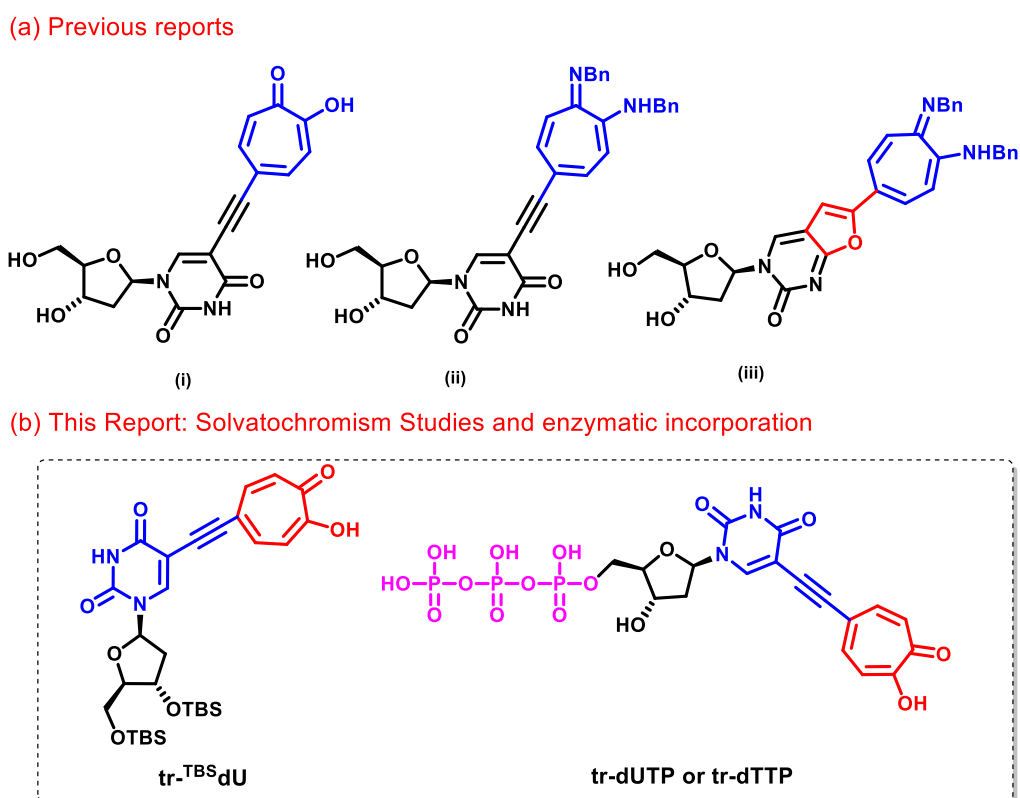
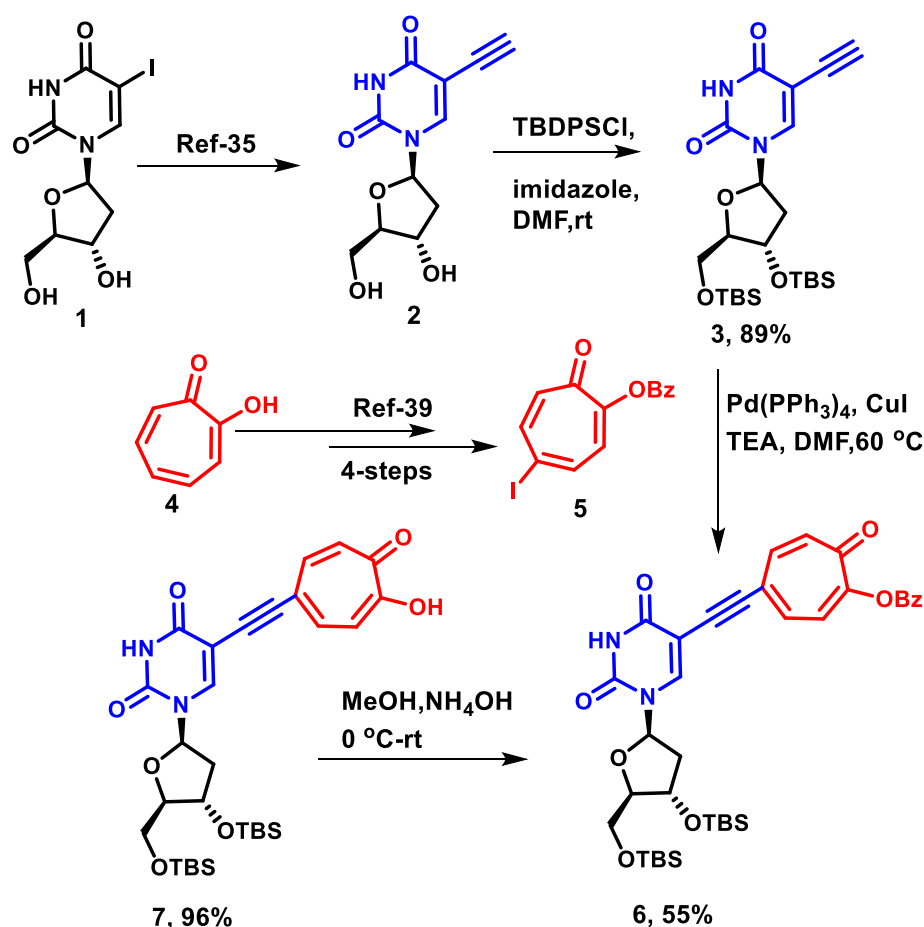


**Figure 2A.1.** Previously reported troponyl/ aminotroponyl-thymidine analogs and this report.

## 2A.3 Results and Discussion

As unprotected tr-dU nucleoside is insoluble in most organic solvents, we synthesized TBS-protected tr-dU derivative tr-TBSdU by following the synthetic route (Scheme 2A.1). 5-

Iododeoxyuridine (**1**) was converted into 5-ethynyl deoxyuridine derivative (**2**) following the previous reports.<sup>35,38</sup> Its hydroxyl groups (3'-OH and 5'-OH) were protected with TBDPS-Cl under mild basic conditions that produced functionalized nucleoside (**3**). Next, commercially available Tropolone (**4**) was converted into 5-Iodotropolone by following the previous report.<sup>39</sup> For examining the role of chromophore tropolone in the photophysical properties of troponyl nucleoside, we prepared tr-<sup>TBS</sup>dU modified nucleoside (**7**). The characterization data of new derivatives are provided in the Appendix.



**Scheme 2A.1.** Synthesis of TBS-protected nucleoside tr-<sup>TBS</sup>dU.

In the literature, fluorescent nucleosides are synthesized by conjugating non-emissive nucleobases with aromatic fluorophores via a  $\pi$ -bond that induces an internal charge transfer (ICT) state. Their fluorescent behavior strongly depends on microenvironments such as

polarity, hydrogen bonding, viscosity, and pH.<sup>40,41</sup> Tropolone is a weak fluorescent molecule mainly owing to the  $\pi$ - $\pi^*$ ,  $n$ - $\pi^*$ , and intramolecular charge transfer.<sup>42</sup> Tropolone-conjugated deoxyuridinyI DNA exhibits pH-dependent fluorescence. However, its nucleoside was insoluble in organic solvents. Thus we converted tr-dU into TBS derivative (tr-<sup>TBS</sup>dU, **7**), which was soluble in most of the organic solvents. We recorded the UV-Vis fluorescence spectra of compound **7** in different organic solvents such as chloroform, benzene, toluene, THF, DCM, dioxane, *N,N*-dimethylformamide (DMF), dimethylsulfoxide (DMSO), ethylacetate, acetonitrile (ACN), methanol, and ethanol. Their UV-vis and fluorescence spectra are provided in (Figure 2A.2). We measured its relative quantum yield in the different solvents by using quinine sulfate (0.5M H<sub>2</sub>SO<sub>4</sub>) as a reference (Table 2A.1). For comparative studies, we generated a bar diagram of quantum yield vs. solvents (Figure 2A.2-D). This bar diagram clearly shows the solvent-dependent fluorescence properties of tr-<sup>TBS</sup>dU (**7**), such as high in nonpolar solvents (~ 2.4% in chloroform) and low in polar solvents (~ 0.5% ethanol). We noticed that the quantum yield of tr-<sup>TBS</sup>dU (**7**) was nearly the same in aromatic solvent (benzene/toluene) but slightly lower than chloroform; The quantum yield of nucleoside (**7**) was relatively higher in THF than DCM, while almost the same for solvents dioxane, DMF and DMSO. But the quantum yields are low in higher protic/polar solvents (MeOH and EtOH). The normalized emission spectra of nucleoside (tr-<sup>TBS</sup>dU, **7**) were generated, which shows the characteristic red shift by increasing the polarity of solvents (Figure 2A.2-C). The maximum difference in the emission wavelength ( $\Delta\lambda_{em}$ ) is ~25 nm, ( $\lambda_{em}$  DMF-  $\lambda_{em}$  CHCl<sub>3</sub>). It is also reported that tropolone is weakly fluorescent in nonpolar solvent (hexane) and acidic pH, while nonfluorescent in neutral and alkaline pH conditions. These results strongly support the induction of ICT system in the tr-<sup>TBS</sup>dU fluorescent nucleoside analog owing to the tropolone donor and uridine acceptor that exerts a push-pull effect. Next, we propose the possible tautomeric structures of tr-<sup>TBS</sup>dU (**7**) as **7-i** and **7-ii** (Figure 2A.3-A) owing to the

nature of intramolecular hydrogen bonding at the tropolone ring in the conjugated system. We assume the tautomeric structure of  $\text{tr-}^{\text{TBS}}\text{dU}$  (**7-i**) is favorable in nonpolar solvents, while  $\text{tr-}^{\text{TBS}}\text{dU}$  (**7-ii**) in polar solvents. The intramolecular hydrogen bond's strength diminishes with ACN, DMF, DMSO, EtOH, and MeOH polar solvents. It perturbs the intramolecular hydrogen-bonded tautomer (**7-i**) and lowers the push-pull effect and hence decreasing fluorescence efficiency. Thus, in a polar protic solvent, diminished emission was observed, possibly due to the fluorescence quenching event mediated via dipolar/H-bonding interaction. In the literature, the solvent polarity parameter  $E_T(30)$  exhibits a linear correlation graph with the quantum yield of solvatochromism possessing fluorophores.<sup>43,44</sup> We also plotted the quantum yield of  $\text{tr-}^{\text{TBS}}\text{dU}$  (**7**) vs. quantum yield in different solvents (Figure 2A.3-B). This plot exhibits a linear relationship with the solvents' polarity, revealing the solvatochromism of  $\text{tr-}^{\text{TBS}}\text{dU}$  (**7**). However,  $\text{tr-}^{\text{TBS}}\text{dU}$  (**7**) does not show the linear graph of its quantum yield vs. solvent viscosity. Thus fluorescent  $\text{tr-}^{\text{TBS}}\text{dU}$  (**7**) is an environmentally sensitive fluorescent (ESF) nucleoside molecule.

**Table 2A.1.** Summary table of Fluorescence properties of  $\text{tr-}^{\text{TBS}}\text{dU}$  (**7**)

Entry	Solvent	$\lambda_{\text{abs}}(\text{nm})$	$\lambda_{\text{em}}(\text{nm})$	Stokes shift (nm)	$\Phi_f$	OD (nm)
1	<b>CHCl<sub>3</sub></b>	364	441.00	77.00	0.0244	354
2	<b>Benzene</b>	366	441.96	75.96	0.0228	361
3	<b>Toluene</b>	366	443.93	77.93	0.0207	354
4	<b>THF</b>	365	448.93	83.93	0.0188	356
5	<b>DCM</b>	364	441.00	77.00	0.0149	352
6	<b>Dioxane</b>	365	443.93	78.93	0.0104	354
7	<b>DMF</b>	391, 415	464.92, 465.97	73.92, 50.97	0.0101	363
8	<b>DMSO</b>	388	461.94	73.94	0.0097	367
9	<b>EtOAc</b>	365	448.93	83.93	0.0070	352
10	<b>Acetonitrile</b>	362	453.03	91.03	0.0063	342
11	<b>MeOH</b>	377	459.84	82.84	0.0061	358
12	<b>EtOH</b>	378	451.96	73.96	0.0051	360

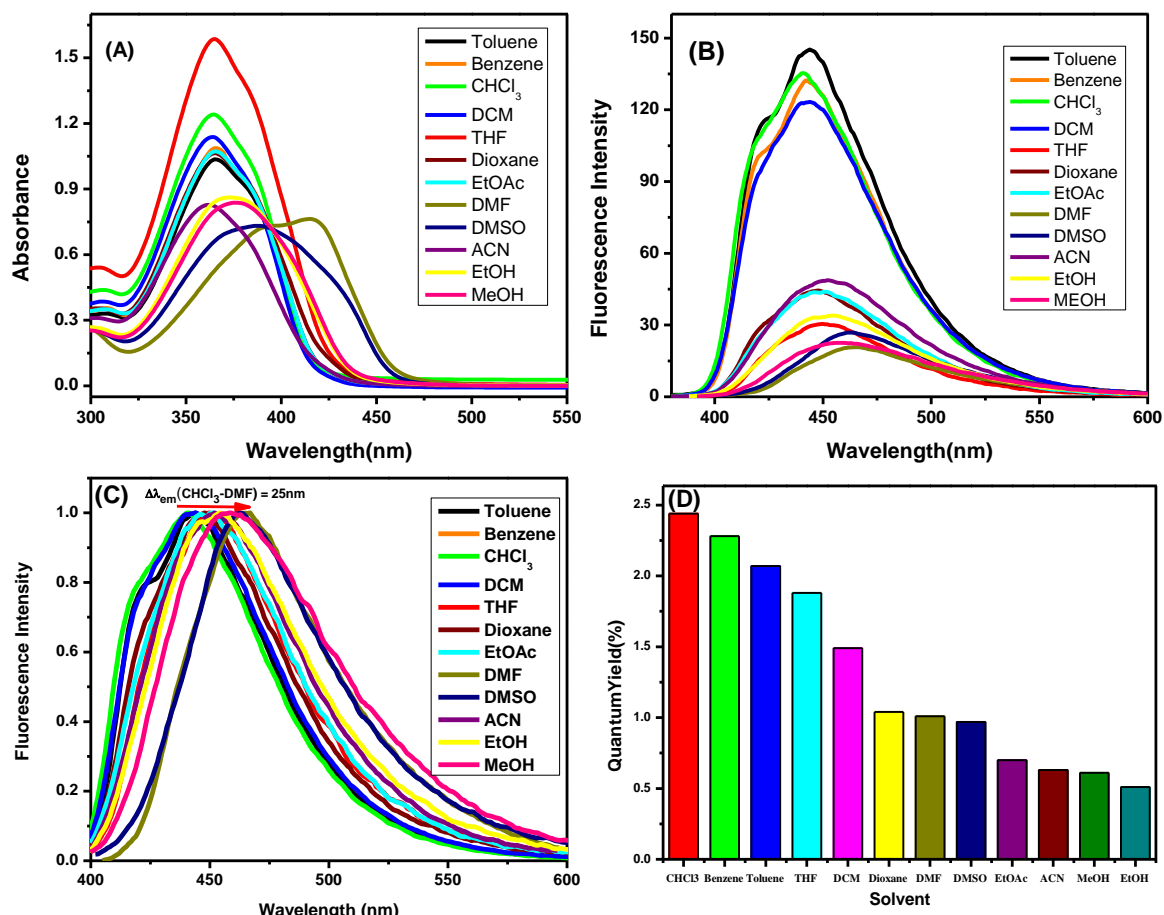


**Figure 2A.2.** Absorption (A), emission spectra (B, C), and quantum yield (D) of  $\text{tr-TBS dU (7)}$  in various solvents (20  $\mu\text{M}$ ).

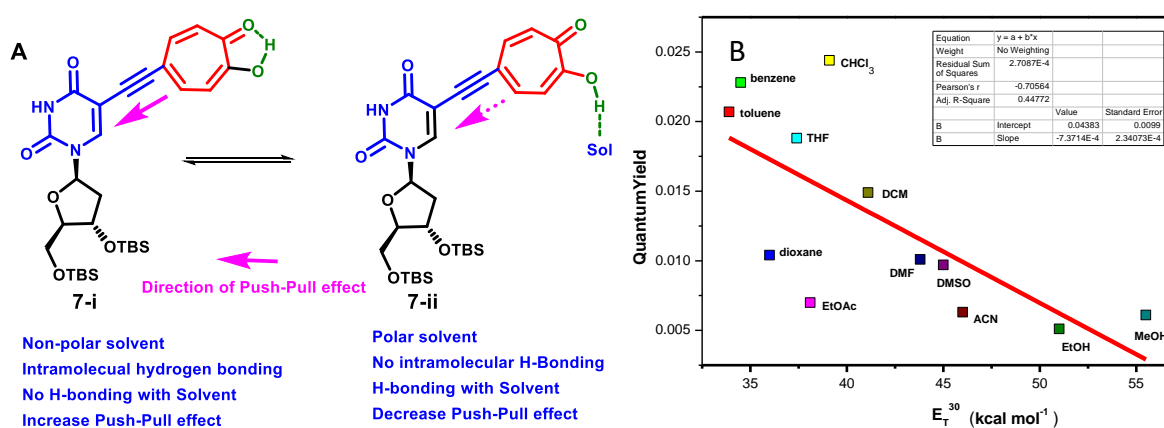
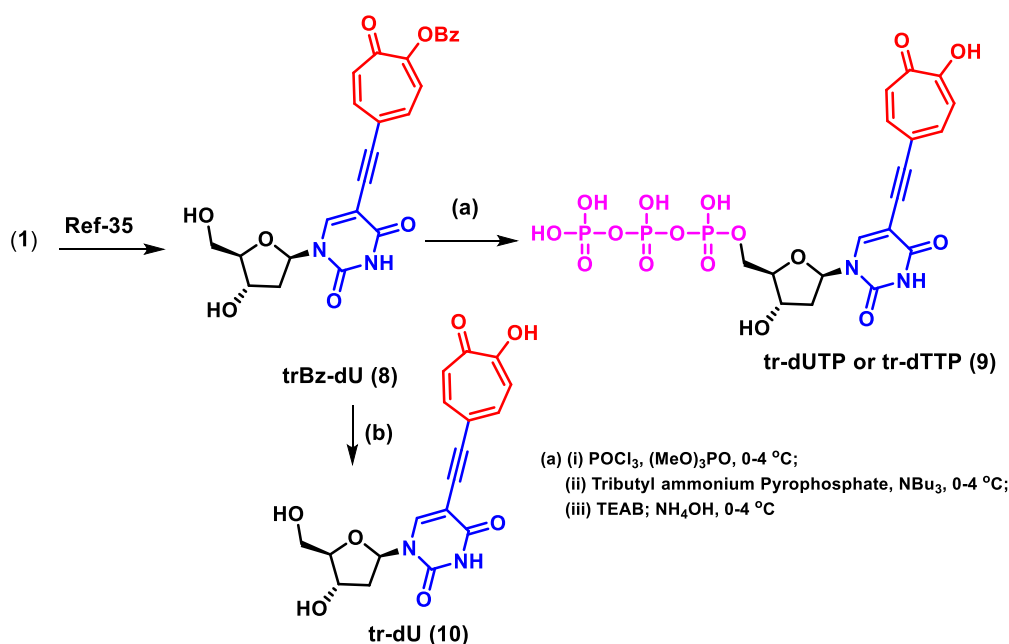


**Figure 2A.3.** Solvatochromism (A) and a plot of Stokes shift vs.  $E_T(30)$  (B) for  $\text{tr-TBS dU (7)}$ .



**Scheme 2A.2.** Synthesis of troponyl-dUTP (tr-dUTP) and tr-dU.

For the enzymatic incorporation, we synthesized tr-dUTP or tr-dTTP from the previously synthesized nucleoside (tr-dU, **8**) by treating it with  $\text{POCl}_3$ , followed by a reaction with pyrophosphate. The synthesis of triphosphate is a laborious procedure and needs special care.<sup>45,46</sup> During phosphorylation, the Bz group was deprotected with ammonium hydroxide solution. After HPLC purification, we isolated troponyl deoxyuridynyl triphosphate (tr-dUTP or trdTTP, **9**) in moderate yield. This tr-dTTP (**9**) was characterized by NMR and ESI-MASS.

For the enzymatic synthesis of troponylated DNA, we investigated the incorporation of tr-dUTP (**9**) into FAM labeled DNA primer (P1) guided by template DNA (T1) in presence of DNA polymerases (Figure 2A.4).

The sequence of P1 and T1 are following:

**P1:** FAM-5'-TGTAACGACGGCCAGT-3'

**T1:** 3'-ACATTTTGCTGCCGGTCA $\Delta$ \*GTCGAGGCAT 5'

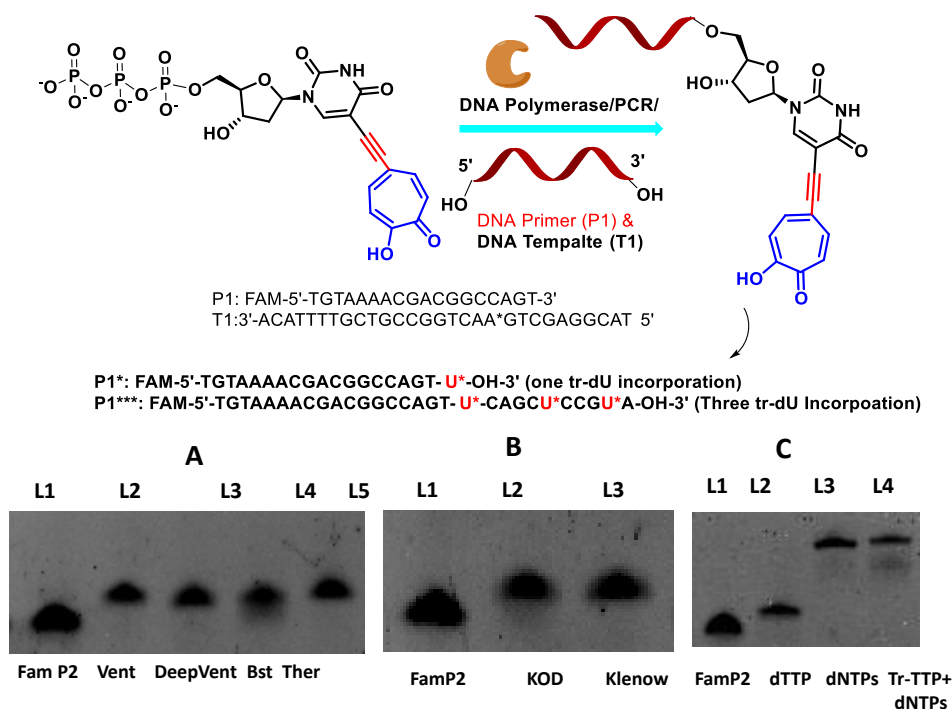


**Figure 2A.4.** PAGE Analysis of primer extension reactions of tr-dTTP (9) with different DNA polymerases.

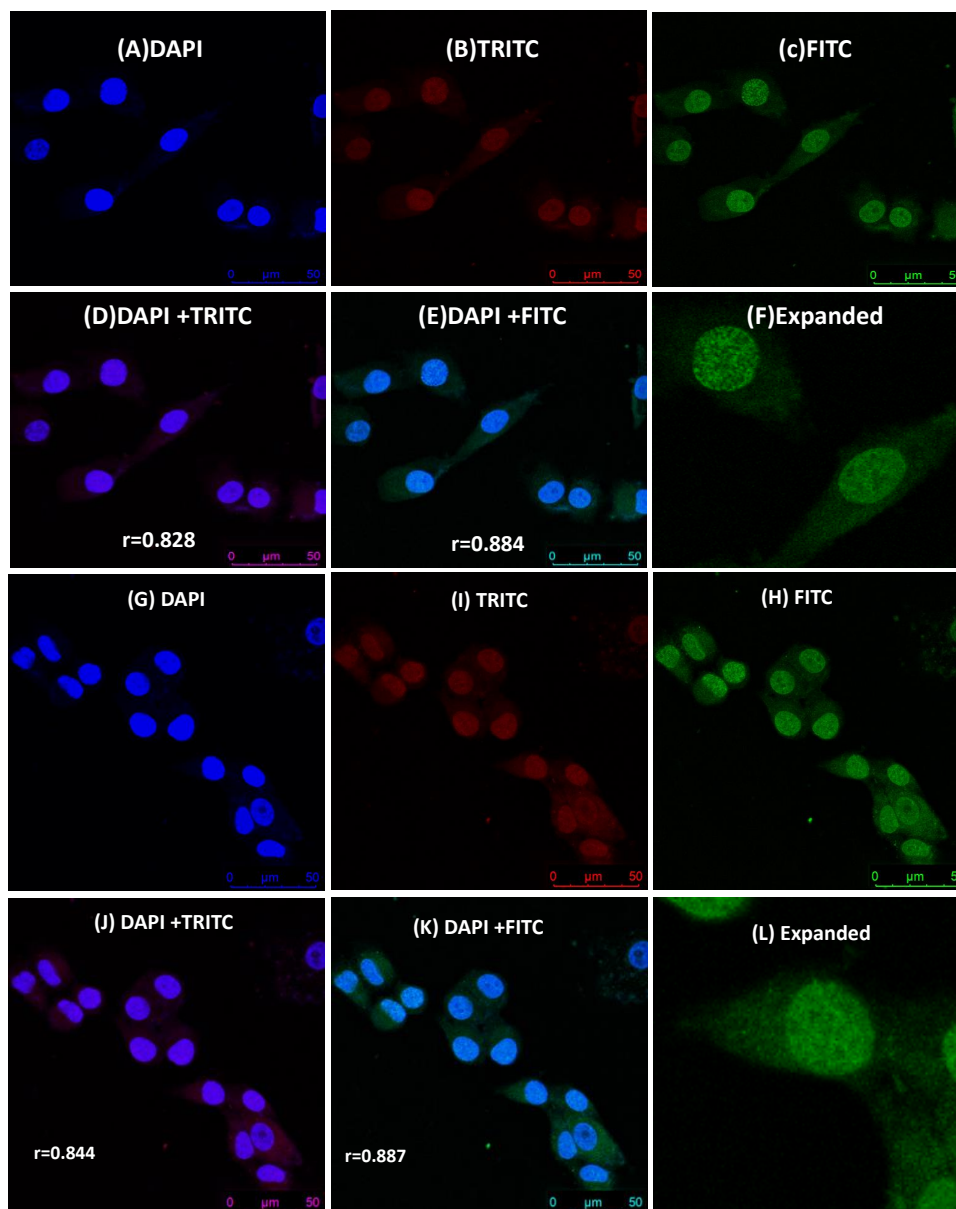
We performed the primer extension reaction using PCR with the following commercially available enzymes: Vent, DeepVent, Bst, Therminator, KOD, and Klenow. We used known substrate dNTP (dTTP/dATP/dGTP/dCTP) for a control experiment in primer extension reaction. The extension of primer (P1) was analyzed by gel-electrophoretic technique. Their gel-shift images are illustrated in Figure 2A.4. The remarkable gel shifts of FAM-primer (P1) are noticed after primer extension reaction with tr-dUTP/trdTTP (9) in presence of DNA polymerases vent/ DeepVent/ Bst/ Therminator/ KOD/ Klenow using PCR (Figure 2A.4-A, B). For control studies, similar results are noticed with natural substrate dTTP with primer extension experiments (Figure 2A.4-C) with Therminator polymerase. For the investigation of full-length extension of primer, a mixture of tr-dUTP and other dNTP (dATP/dGTP/dCTP) were employed for primer extension reaction and compared with the control experiment using all four dNTPs (dATP/dTTP/dGTP/ dCTP) in presence of Therminator DNA polymerase. The gel-shift images of those experiments are depicted in

Figure 2A.4-C, which strongly support the full-length extension of the primer. Similar results were noticed with native dNTP. These results strongly support the enzymatic incorporation of tr-dUTP/trdTTP (**9**) into DNA by releasing diphosphate ion during the primer extension reaction. Hence, compound **9** was proved to be a substrate of DNA polymerases.

In the literature, native triphosphate nucleosides exhibit poor cell permeability. Recently, Hocek et al. reported the transfection of modified dNTP using a unique synthetic nucleoside triphosphate transporter (SNTT).<sup>47,48</sup> However, nucleosides and related molecules are prodrugs for various diseases, including antiviral, anticancer, and antibiotic drugs.<sup>49</sup> Lately, fluorescent nucleoside analogs exhibit improved cell permeability and are applied for labeling of biomolecules in vitro/vivo conditions.<sup>10</sup> Herein, we examined the cell permeability of unprotected fluorescent tr-dU (**10**) analog into HeLa cell lines. tr-dU (**10**) was incubated with HeLa cells by following the standard protocol and studied by confocal microscope. HeLa cells were visualized under bright light and different channels such as DAPI (blue channel,  $\lambda_{\text{ex}} = 358 \text{ nm}$ ), FITC (green channel,  $\lambda_{\text{ex}} = 490 \text{ nm}$ ) and TRITC (red channel,  $\lambda_{\text{ex}} = 570 \text{ nm}$ ). The cells treated with tr-dU and stained with DAPI were visualized (Figure 2A.5) where tr-dU is majorly found to be located in nucleus. In Figure 2A.5-A, DAPI stained, tr-dU treated cells clearly show the localization of DAPI at cellular nucleus. Under FITC (green) channel, confocal images of tr-dU treated cells show cell-internalization without any transfecting reagents. Similar observations were noticed under TRITC (red) channel. The colocalization studies of trdU with DAPI were performed in both channels (green/red). Pearson's coefficients ( $r$ ) values were estimated by using JACoP plugin in Fiji: ImageJ.<sup>50</sup> For red and green channels Pearson's coefficient values ( $r$ ) are 0.83 and 0.88, respectively. We also examined the incorporation of tr-dU into the genomic DNA but we could not find it by gel electrophoretic techniques probably due to lack of intracellular phosphorylation. These results strongly support the localization of tr-dU nucleoside in



nucleus of HeLa cells. In the literature, tropolone is a known natural scaffold for forming metal complexes, strongly with  $\text{Cu}^{2+}$ . Thus tr-dU could bind with free  $\text{Cu}^{2+}$  ions of intracellular environments and affect other related biochemical process. Our works are in progress to explore the metal binding studies with tr-dU-DNA analogues in vitro/vivo conditions. Hence tr-dU is an emerging and promising fluorescent nucleoside.



**Figure 2A.5.** Confocal microscopic images for tr-dU (7) treated HeLa Cells with DAPI staining (12 h incubation (A-F), 24 h incubation (G-L)).

For practical applicability, we examined the cytotoxicity of unprotected nucleoside tr-dU (**10**) for both normal (HEK239T) and cancerous (HeLa) cell lines by MTS assay. Their concentration dependent cell viability data are provided in Figure 2A.6. We found no significant cell cytotoxicity with tr-dU in both cell lines. Thus this nucleoside can be used for labeling DNA in situ.

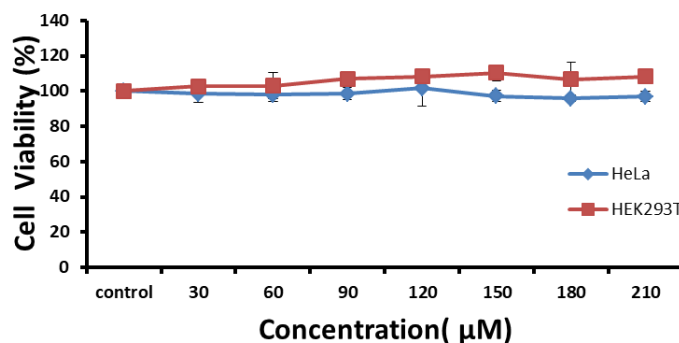


**Figure 2A.6.** Cell proliferation assays of compound tr-dU (**10**) in HEK293T and HeLa cells.

## 2A.4 Conclusion

A TBS-protected derivative of fluorescent nucleoside tr-dU, tr-<sup>TBS</sup>dU, has been synthesized to examine its solvent-dependent fluorescence behavior. The tr-<sup>TBS</sup>dU derivative exhibited maximum quantum yield in aprotic nonpolar solvents and maximum Stokes shift in DMF/toluene. Thus tr-<sup>TBS</sup>dU has an environmentally sensitive fluorescence (ESF) character. Its triphosphate analog (tr-dUTP/tr-dTTP) was also synthesized and enzymatically incorporated into a DNA primer in the presence of DNA polymerase and DNA template. Importantly, tr-dTTP exhibited pH-responsive fluorescence properties. For practical use, the cell permeability and viability of free tr-dU nucleoside were examined; this revealed that tr-dU is cell permeable and fluorescently localized over the nucleus. Importantly, this nucleoside has no significant cytotoxic effect on either normal or cancerous cells. Tr-dU could strongly bind with the free Cu<sup>2+</sup> of the intracellular environment owing to the troponyl unit's metal chelating ability, which could be helpful for designing metal-ion-based probes for

binding target-specific biochemical activity. Hence, tr-dU is a promising fluorescent nucleoside analog for labeling DNA.

### 2A.5 Experimental Section

*General Information:* Unless otherwise mentioned, materials obtained from commercial suppliers were used without further purification. DMF and DCM were distilled over  $\text{CaH}_2$  and stored over 4Å molecular sieves. Tributyl amine was distilled over potassium hydroxide and stored over 4Å molecular sieves. DNA oligos and FAM labeled primers were purchased from IDT. All enzymes and buffers for primer extension reactions were purchased from New England Bio labs. Mass spectra were obtained from Bruker micrOTOF-Q II Spectrometer and the samples were prepared in methanol and injected in methanol and water mixture. All NMR spectra were recorded on Bruker AV- 400 at room temperature and processed using Mnova software from Mestrelab Research. Absorption spectra were obtained using Jasco V-730 spectrometer and Fluorescence spectra were obtained from Agilent spectrophotometer and Perkin-Elmer LS-55 using Xenon lamp. Reactions were monitored by thin layer chromatography, visualized by UV and Ninhydrin. Column chromatography was performed in 230-400 mesh silica except Triphosphate product (purified by DEAE Sephadex-A25). Polymerase Chain Reactions were performed in Bio-rad T100 Thermal Cycler. HPLC was done in Waters 2998. Confocal Images were taken in Leica Microscope.

*Primer extension experiments for PAGE analysis:* For all enzymatic reactions 5' FAM labelled primer (FAM-P1, 1.0  $\mu\text{M}$ ), Template T1 (2.0  $\mu\text{M}$ ), tr-dTTP (100  $\mu\text{M}$ ), and dNTPs (100  $\mu\text{M}$ ) (for control experiments) were treated in a total reaction mixture of 10.0  $\mu\text{l}$  with respective DNA polymerase under optimized conditions.

*Ventexo- DNA polymerase:* 5' FAM labeled primer (FAM-P1, 1.0  $\mu$ M), Template T1 ( 2.0  $\mu$ M), tr-dTTP (100  $\mu$ M) 10 x Thermopol buffer ( 1.0  $\mu$ l) and Vent exo DNA polymerase (1.0 unit) were treated in a total reaction mixture of 10.0  $\mu$ l at 55°C for 60 minutes.

*Deep Ventexo- DNA polymerase:* 5' FAM labeled primer (FAM-P1, 1.0  $\mu$ M), Template T1 (2.0  $\mu$ M), Tr-TTP (100  $\mu$ M) 10 x Thermopol buffer (1.0  $\mu$ l) and DeepVentexo DNA polymerase (1.0 unit) were treated in a total reaction mixture of 10.0  $\mu$ l at 55°C for 60 minutes.

*Klenowexo- DNA polymerase:* 5' FAM labelled primer (FAM-P1, 1.0  $\mu$ M), Template T1 (2.0  $\mu$ M), tr-dTTP (100  $\mu$ M) 10 x NEB buffer 2 (1.0  $\mu$ l) and Klenowexo- DNA polymerase (10.0 unit) were treated in a total reaction mixture of 10.0  $\mu$ l at 37°C for 60 minutes.

*Bst DNA polymerase:* 5' FAM labeled primer (FAM-P1, 1.0  $\mu$ M), Template T1 (2.0  $\mu$ M), tr-dTTP (100  $\mu$ M) 10 x Thermopol buffer (1.0  $\mu$ l), and Bst DNA polymerase (1.0 unit) were treated in a total reaction mixture of 10.0  $\mu$ l at 55°C for 60 minutes.

*Therminator DNA polymerase:* 5' FAM labeled primer (FAM-P1, 1.0  $\mu$ M), Template T1 (2.0  $\mu$ M), tr-dTTP (100  $\mu$ M) 10 x Thermopol buffer (1.0  $\mu$ l) and Therminator DNA polymerase (1.0 unit) were treated in a total reaction mixture of 10.0  $\mu$ l at 55°C for 60 minutes.

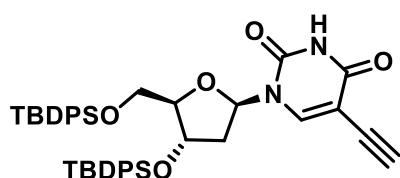
*KOD Dash DNA polymerase:* 5' FAM labeled primer (FAM-P1, 1.0  $\mu$ M), Template T1 (2.0  $\mu$ M), tr-dTTP (100  $\mu$ M) 10 x KOD reaction buffer (1.0  $\mu$ l), and KOD Dash DNA polymerase (1.0 unit) were treated in a total reaction mixture of 10.0  $\mu$ l at 55°C for 60 minutes.

*Primer extension experiments for full length synthesis of DNA using tr-dTTP:* 5' FAM labelled primer (FAM-P1, 1.0  $\mu$ M), Template T1 (2.0  $\mu$ M), tr-dTTP (100  $\mu$ M) , dATP (100  $\mu$ M), dCTP (100  $\mu$ M), dGTP (100  $\mu$ M), 10x Thermopol reaction buffer (1.0  $\mu$ l) and Therminator DNA polymerase (1.0 unit) were treated in a total reaction mixture of 10.0  $\mu$ l at

55°C for 60 minutes. Control experiments were performed with dTTP (100  $\mu$ M) and four dNTPs (dATP,dTTP,dCTP and dGTP each 100  $\mu$ M) under similar conditions. After primer extension reaction the reactions were quenched with 10.0  $\mu$ l of 2x loading dye (it contains 90% formamide; 0.5% EDTA; 0.1% xylene cyanol and 0.1% bromphenol blue) by heating at 85°C for 5 minutes followed by cooling at 4°C. Primer extension reactions were analyzed by 20% denaturing urea PAGE. Gels prepared and run in 1x TBE (TrisBoric acid EDTA, pH 8.0) buffer followed by visualization using Bio-rad gel doc system.

### *Characterization data of products*

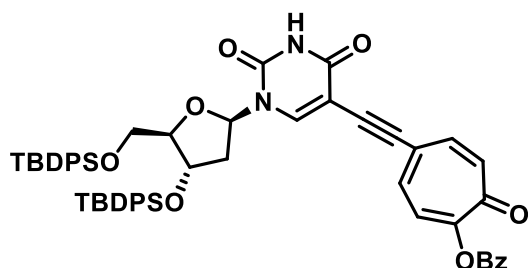
3',5-Bis-O-(tert-butyldiphenylsilyl)-5-ethynyl-2'-deoxyuridine (**3**): 5-ethynyl 2-deoxy uridine



(**2**) (100 mg, 0.397 mmol) was dissolved in DMF (2.0 mL) and tert-butyldiphenylchlorosilane (0.31 mL, 1.19 mmol) and imidazole (134 mg, 1.98 mmol) were added. The mixture

was allowed to stir at ambient temperature for 18 h and throughout the reaction, an inert atmosphere was maintained. After the reaction mixture was evaporated under reduced pressure after completion, diluted with water and extracted with ethyl acetate. The collected organic layers were washed with brine and dried over Na<sub>2</sub>SO<sub>4</sub>. After evaporation in a rotavap, the crude product was purified by column chromatography (Si-gel, 0.5% MeOH/CH<sub>2</sub>Cl<sub>2</sub>) to give 257mg (89%) of **3** as a white foamy solid. TLC - 1% MeOH/CH<sub>2</sub>Cl<sub>2</sub>  $R_f$  = 0.6; <sup>1</sup>H NMR (400 MHz, CDCl<sub>3</sub>):  $\delta$  9.04 (s, 1H), 8.09 (s, 1H), 7.66 - 7.27 (m, 20H), 6.46 (dd,  $J$  = 8.7, 5.3 Hz, 1H), 4.51 (d,  $J$  = 5.1 Hz, 1H), 4.01 (s, 1H), 3.76 – 3.68 (m, 1H), 3.30 (dd,  $J$  = 11.7, 2.2 Hz, 1H), 2.97 (s, 1H), 2.51 – 2.42 (m, 1H), 2.02 – 1.94 (m, 1H), 1.10 (s, 9H), 0.98 (s, 9H), <sup>13</sup>C NMR (101 MHz, CDCl<sub>3</sub>)  $\delta$  162.60, 161.18, 148.95, 143.53, 135.67, 135.60, 135.57, 135.47, 133.08, 132.97, 132.35, 132.14, 130.08, 130.03, 130.00, 129.93, 127.91, 127.90, 127.87, 99.23, 88.39, 86.03, 82.20, 74.27, 74.19, 63.97, 42.05, 36.51, 31.47, 19.14, 18.95, 0.01., HRMS ESI-Tof Calcd for (C<sub>43</sub>H<sub>48</sub>N<sub>2</sub>O<sub>5</sub>Si<sub>2</sub>+Na) 751.2958, Found 751.2994.

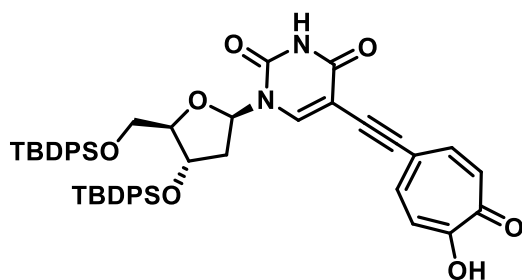
3',5-Bis-O-(tert-butyldiphenylsilyl)-5-(2-benzoyloxy troponyl) ethynyl- 2'-deoxyuridine (**6**):



3',5'-Bis-O-tert-butyldimethylsilyl-5-ethynyl 2'-deoxy uridine(**3**) (125 mg, 0.171 mmol) , 5-Iodo-2-benzoyloxytropone(**4**) (72mg, 0.205 mmol) , Tetrakis(triphenylphosphine)palladium (20 mg,

0.017 mmol ), copper (I) iodide (1.3 mg, 0.034 mmol) and triethylamine ( 0.1 ml, 0.514 mmol ) were dissolved in dry DMF (2 ml) and stirred overnight under argon atmosphere. The solvents were evaporated in a rotavap and the reaction mixture was purified on silica gel by EtOAc/Hexane to obtain 90 mg of pale yellow solid in 55 % yield. TLC 2% MeOH/CH<sub>2</sub>Cl<sub>2</sub>R<sub>f</sub> =0.32, <sup>1</sup>H NMR (400 MHz, CDCl<sub>3</sub>) δ 9.70 (s, 1H), 8.22 (s, 1H), 8.18 – 8.10 (m, 2H), 7.67 – 7.28 (m, 23H), 7.01 (d, *J* = 11.4 Hz, 2H), 6.74 (d, *J* = 11.8 Hz, 2H), 6.55 (dd, *J* = 8.9, 5.2 Hz, 1H), 4.56 (d, *J* = 5.2 Hz, 1H), 4.04 (s, 1H), 3.81 (d, *J* = 10.5 Hz, 1H), 3.27 (d, *J* = 9.8 Hz, 1H), 2.54 – 2.42 (m, *J* = 12.9, 5.1 Hz, 1H), 2.09 – 2.00 (m, 1H), 1.09 (s, 9H), 0.95 (s, 9H), <sup>13</sup>C NMR (101 MHz, CDCl<sub>3</sub>) δ 163.86, 161.34, 149.19, 143.26, 135.72, 135.64, 135.51, 135.20, 133.85, 133.08, 132.97, 132.64, 131.94, 130.54, 130.24, 130.21, 130.17, 130.11, 128.75, 128.72, 128.59, 128.17, 128.10, 127.99, 127.97, 99.61, 94.98, 88.53, 86.05, 85.28, 74.38, 64.12, 42.38, 27.04, 26.92, 19.26, 19.00, HRMS ESI-TofCalcd for(C<sub>57</sub>H<sub>56</sub>N<sub>2</sub>O<sub>8</sub>Si<sub>2</sub>+H) 953.3648, Found 953.3628.

3',5-Bis-O-(tert-butyldiphenylsilyl)-5-( tropolonyl) ethynyl- 2'-deoxyuridine (**7**): Compound

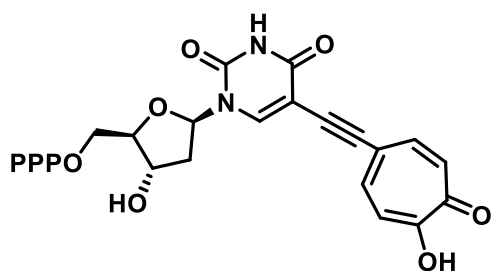


**6** (50 mg, 0.05 mmol) was dissolved in 3 ml MeOH and two drops of benzene were added to get a clear solution. To the stirring solution, ammonia solution (1 ml) was added slowly at 0

°C. After addition reaction was removed from the ice bath and allowed to stir at room temperature for about 1.5 hours. Solvents were evaporated under reduced pressure after

completion of the reaction. The compound was co-evaporated with DCM and Hexane. Product was precipitated using methanol and dried to get yellow solid in 96% yield (43 mg. TLC 5% MeOH/DCM.  $R_f=0.47$ ,  $^1\text{H}$  NMR (400 MHz,  $\text{CDCl}_3$ )  $\delta$  8.65 (s, 1H), 8.17 (s, 1H), 7.66–7.28 (m, 20H), 7.14–6.93 (m, 4H), 6.55 (dd,  $J = 9.0, 5.1$  Hz, 1H), 4.56 (d,  $J = 5.1$  Hz, 1H), 4.03 (s, 1H), 3.85–3.74 (m, 1H), 3.27 (dd,  $J = 11.7, 1.9$  Hz, 1H), 2.53–2.41 (m,  $J = 13.0, 5.1$  Hz, 1H), 2.09–2.00 (m, 1H), 1.10 (s, 9H), 0.95 (s, 9H),  $^{13}\text{C}$  NMR (101 MHz,  $\text{CDCl}_3$ )  $\delta$  171.27, 160.83, 148.92, 142.52, 140.38, 135.68, 135.61, 135.49, 135.18, 133.06, 132.96, 132.61, 131.92, 130.17, 130.12, 130.07, 128.07, 128.05, 127.94, 127.92, 123.42, 123.15, 99.97, 95.21, 88.45, 85.92, 82.56, 74.33, 64.09, 42.22, 26.99, 26.87, 19.20, 18.98, HRMS ESI-TofCalcd for ( $\text{C}_{50}\text{H}_{52}\text{N}_2\text{O}_7\text{Si}_2+\text{H}$ ) 849.3386, Found 849.3392.

3',5-Bis-O-(tert-butyldiphenylsilyl)-5-( tropolonyl) ethynyl- 2'-deoxyuridinetriphosphate (**9**):



To a solution of 5-(2-benzyloxy tropolonyl) ethynyl-2'-deoxyuridine (**8**) (70 mg, 0.073 mmol, 1.0 equiv) in trimethyl phosphate, freshly distilled  $\text{POCl}_3$  (17  $\mu\text{L}$ , 0.184 mmol, 2.5 equiv) was added in ice-cold condition under argon atmosphere. The solution was stirred for 24 h at  $\sim 4^\circ\text{C}$ . After 24 h, it was observed that the starting material wasn't completely consumed. Bis(tributylammonium) pyrophosphate (202 mg, 0.368 mmol, 5.0 equiv.) solution in DMF and tributylamine (0.2 ml, mmol, 11.0 equiv.) were simultaneously added to the reaction mixture in ice-cold condition. The reaction mixture was continued for 30 min at  $4^\circ\text{C}$  and quenched with 1 M triethyl ammonium bicarbonate buffer (TEAB, 15 ml), and washed with ethyl acetate. The aqueous layer was evaporated to dryness and purified using a DEAE Sephadex-A25 anion exchange column (0.1M–1M TEAB buffer, pH 7.5) followed by HPLC (TEAB buffer and acetonitrile solvent system). Evaporation of the appropriate fraction resulted in the desired triphosphate in 15% yield (13 mg) as a triethyl ammonium salt.  $^1\text{H}$  NMR (400 MHz,  $\text{D}_2\text{O}$ )  $\delta$  8.68 (s, 1H),

7.62 (d,  $J = 9.5$  Hz, 2H), 7.05 (d,  $J = 8.1$  Hz, 2H), 6.90 (s, 1H), 6.15 (s, 1H), 4.47 (s, 1H), 4.20 (s, 1H), 4.09 (d,  $J = 9.6$  Hz, 1H), 4.01 (t,  $J = 9.4$  Hz, 1H), 2.56 (d,  $J = 12.4$  Hz, 1H), 2.26 (d,  $J = 12.5$  Hz, 1H).  $^{31}\text{P}$  NMR (162 MHz,  $\text{D}_2\text{O}$ )  $\delta$  4.93(br,P), -10.57 (br, P), -22.87 (br, P), HRMS ESI-ToF Calculated for  $(\text{C}_{18}\text{H}_{19}\text{N}_2\text{O}_{16}\text{P}_3\text{-H})$  610.9864, Found 611.1028.

*Photophysical studies of tr-<sup>TBS</sup>dU (7):* All the Absorption and Emission spectra of the compound **7** (10  $\mu\text{M}$ ) were measured in different solvents using their respective spectrophotometer with a cell of 1 cm path length. Relative Quantum yield of nucleoside **7** in different solvents was determined relative to quinine sulfate as the standard. Following equation was used to calculate the quantum yield.

$$\Phi_{\text{F(x)}} = (\text{A}_\text{s}/\text{A}_\text{x})(\text{F}_\text{x}/\text{F}_\text{s})(\text{n}_\text{x}/\text{n}_\text{s})^2 \Phi_{\text{f(s)}}$$

Where s is the standard, x is the modified nucleoside, A is the absorbance at excitation wavelength, F is the area under the emission curve, n is the refractive index of the solvent, and  $\Phi_\text{F}$  is the quantum yield. Quantum yield of quinine sulfate in 0.1 M  $\text{H}_2\text{SO}_4$  is 0.54.

*Cell Internalization studies by confocal microscope:* HeLa Cells were treated with tr-dU (100  $\mu\text{M}$ ) under incubation period 12/24 hr before fixing the cells for imaging. Also cells were stained with DAPI for studying colocalization. All images are taken at same magnification (63 x).

*Cell viability/ Cytotoxicity studies:* In order to analyse the effect of tr-dU on cell viability, cell proliferation assay was conducted. Human embryonic kidney derived cell line HEK293T and human cervical carcinoma derived cell line HeLa cells were used for the assay.  $2 \times 10^4$  cells/mL in 10% DMEM were seeded in 96 well microtitre plate and incubated for 10 h. After incubation cells were observed for its shape and confluency and media as carefully aspirated. Different concentrations of respective compounds (**10**) were prepared in DMEM medium and



each concentration was added in triplicate along with only media and DMSO (exact concentration used for making the compound solution) control. The 96 well plate was incubated under standard conditions (humidified incubator with 5% CO<sub>2</sub> under 37°C) for 24 h. The CellTiter 96® AQueous One Solution as used to analyse the cell proliferation ability in presence of different compounds. 10 µl of CellTiter 96® AQueous One Solution Reagent was mixed into each well of the 96-well assay plate containing the samples in 190 µl of culture medium followed by incubation for 1 h at standard condition. After incubation absorbance was recorded using Varioscan at 490 nm.

## 2A.6 References and Notes

- (1) Hofer, A.; Crona, M.; Logan, D. T.; Sjöberg, B.-M. DNA Building Blocks: Keeping Control of Manufacture. *Crit. Rev. Biochem. Mol. Biol.* **2012**, *47* (1), 50–63.
- (2) Nick McElhinny, S. A.; Ramsden, D. A. Polymerase Mu Is a DNA-Directed DNA/RNA Polymerase. *Mol. Cell. Biol.* **2003**, *23* (7), 2309–2315.
- (3) Baranovskiy, A. G.; Babayeva, N. D.; Lisova, A. E.; Morstadt, L. M.; Tahirov, T. H. Structural and Functional Insight into Mismatch Extension by Human DNA Polymerase  $\alpha$ . *Proc. Natl. Acad. Sci.* **2022**, *119* (17), e2111744119.
- (4) Santorelli, A.; Gothelf, K. V. Conjugation of Chemical Handles and Functional Moieties to DNA during Solid Phase Synthesis with Sulfonyl Azides. *Nucleic Acids Res.* **2022**, *50* (13), 7235–7246.
- (5) Lehner, M.; Rieth, S.; Höllmüller, E.; Spliesgar, D.; Mertes, B.; Stengel, F.; Marx, A. Profiling of the ADP-ribosylome in Living Cells. *Angew. Chemie* **2022**, *134* (18), e202200977.
- (6) Porter, A.; Wang, L.; Han, L.; Lu, X. L. Bio-Orthogonal Click Chemistry Methods to

- Evaluate the Metabolism of Inflammatory Challenged Cartilage after Traumatic Overloading. *ACS Biomater. Sci. Eng.* **2022**, 8 (6), 2564–2573.
- (7) Liu, X.; Chang, Y.-T. Fluorescent Probe Strategy for Live Cell Distinction. *Chem. Soc. Rev.* **2022**.
  - (8) Xu, W.; Chan, K. M.; Kool, E. T. Fluorescent Nucleobases as Tools for Studying DNA and RNA. *Nat. Chem.* **2017**, 9 (11), 1043–1055.
  - (9) Karimi, A.; Börner, R.; Mata, G.; Luedtke, N. W. A Highly Fluorescent Nucleobase Molecular Rotor. *J. Am. Chem. Soc.* **2020**, 142 (34), 14422–14426.
  - (10) Sinkeldam, R. W.; Greco, N. J.; Tor, Y. Fluorescent Analogs of Biomolecular Building Blocks: Design, Properties, and Applications. *Chem. Rev.* **2010**, 110 (5), 2579–2619.
  - (11) Samaan, G. N.; Wyllie, M. K.; Cizmic, J. M.; Needham, L.-M.; Nobis, D.; Ngo, K.; Andersen, S.; Magennis, S. W.; Lee, S. F.; Purse, B. W. Single-Molecule Fluorescence Detection of a Tricyclic Nucleoside Analogue. *Chem. Sci.* **2021**, 12 (7), 2623–2628.
  - (12) Ward, D. C.; Reich, E.; Stryer, L. Fluorescence Studies of Nucleotides and Polynucleotides: I. Formycin, 2-Aminopurine Riboside, 2, 6-Diaminopurine Riboside, and Their Derivatives. *J. Biol. Chem.* **1969**, 244 (5), 1228–1237.
  - (13) Saito, Y.; Hudson, R. H. E. Base-Modified Fluorescent Purine Nucleosides and Nucleotides for Use in Oligonucleotide Probes. *J. Photochem. Photobiol. C Photochem. Rev.* **2018**, 36, 48–73.
  - (14) Hocek, M. Enzymatic Synthesis of Base-Functionalized Nucleic Acids for Sensing, Cross-Linking, and Modulation of Protein–DNA Binding and Transcription. *Acc. Chem. Res.* **2019**, 52 (6), 1730–1737.

- (15) Matyašovský, J.; Tack, L.; Palágyi, A.; Kuba, M.; Pohl, R.; Kraus, T.; Güixens-Gallardo, P.; Hocek, M. Nucleotides Bearing Aminophenyl-or Aminonaphthyl-3-Methoxychromone Solvatochromic Fluorophores for the Enzymatic Construction of DNA Probes for the Detection of Protein–DNA Binding. *Org. Biomol. Chem.* **2021**, *19* (45), 9966–9974.
- (16) Güixens-Gallardo, P.; Hocek, M. Acetophenyl-thienyl-aniline-linked Nucleotide for Construction of Solvatochromic Fluorescence Light-up DNA Probes Sensing Protein–DNA Interactions. *Chem. Eur. J.* **2021**, *27* (24), 7090–7093.
- (17) Kuba, M.; Pohl, R.; Kraus, T.; Hocek, M. Nucleotides Bearing Red Viscosity-Sensitive Dimethoxy-Bodipy Fluorophore for Enzymatic Incorporation and DNA Labeling. *Bioconjug. Chem.* **2022**.
- (18) Dziuba, D.; Jurkiewicz, P.; Cebecauer, M.; Hof, M.; Hocek, M. A Rotational BODIPY Nucleotide: An Environment-Sensitive Fluorescence-Lifetime Probe for DNA Interactions and Applications in Live-Cell Microscopy. *Angew. Chemie* **2016**, *128* (1), 182–186.
- (19) Dadová, J.; Orság, P.; Pohl, R.; Brázdová, M.; Fojta, M.; Hocek, M. Vinylsulfonamide and Acrylamide Modification of DNA for Cross-linking with Proteins. *Angew. Chemie* **2013**, *125* (40), 10709–10712.
- (20) Yanagi, M.; Suzuki, A.; Hudson, R. H. E.; Saito, Y. A Fluorescent 3, 7-Bis-(Naphthalen-1-Ylethynylated)-2'-Deoxyadenosine Analogue Reports Thymidine in Complementary DNA by a Large Emission Stokes Shift. *Org. Biomol. Chem.* **2018**, *16* (9), 1496–1507.
- (21) Okamoto, A.; Tanaka, K.; Fukuta, T.; Saito, I. Design of Base-Discriminating

- Fluorescent Nucleoside and Its Application to T/C SNP Typing. *J. Am. Chem. Soc.* **2003**, *125* (31), 9296–9297.
- (22) Bag, S. S.; Gogoi, H. Design of “Click” Fluorescent Labeled 2'-Deoxyuridines via C5-[4-(2-Propynyl (Methyl) Amino)] Phenyl Acetylene as a Universal Linker: Synthesis, Photophysical Properties, and Interaction with BSA. *J. Org. Chem.* **2018**, *83* (15), 7606–7621.
- (23) Noé, M. S.; Ríos, A. C.; Tor, Y. Design, Synthesis, and Spectroscopic Properties of Extended and Fused Pyrrolo-DC and Pyrrolo-C Analogs. *Org. Lett.* **2012**, *14* (12), 3150–3153.
- (24) Wilhelmsson, L. M.; Sandin, P.; Holmén, A.; Albinsson, B.; Lincoln, P.; Nordén, B. Photophysical Characterization of Fluorescent DNA Base Analogue, TC. *J. Phys. Chem. B* **2003**, *107* (34), 9094–9101.
- (25) Dyrager, C.; Börjesson, K.; Dinér, P.; Elf, A.; Albinsson, B.; Wilhelmsson, L. M.; Grøtli, M. Synthesis and Photophysical Characterisation of Fluorescent 8-(1H-1, 2, 3-Triazol-4-yl) Adenosine Derivatives. Wiley Online Library 2009.
- (26) Manna, S.; Sarkar, D.; Srivatsan, S. G. A Dual-App Nucleoside Probe Provides Structural Insights into the Human Telomeric Overhang in Live Cells. *J. Am. Chem. Soc.* **2018**, *140* (39), 12622–12633.
- (27) Ghosh, P.; Kropp, H. M.; Betz, K.; Ludmann, S.; Diederichs, K.; Marx, A.; Srivatsan, S. G. Microenvironment-Sensitive Fluorescent Nucleotide Probes from Benzofuran, Benzothiophene, and Selenophene as Substrates for DNA Polymerases. *J. Am. Chem. Soc.* **2022**, *144* (23), 10556–10569.
- (28) Tanpure, A. A.; Pawar, M. G.; Srivatsan, S. G. Fluorescent Nucleoside Analogs:

- Probes for Investigating Nucleic Acid Structure and Function. *Isr. J. Chem.* **2013**, *53* (6-7), 366–378.
- (29) Guo, H.; Roman, D.; Beemelmans, C. Tropolone Natural Products. *Nat. Prod. Rep.* **2019**, *36* (8), 1137–1155.
- (30) Bentley, R. A Fresh Look at Natural Tropolonoids. *Nat. Prod. Rep.* **2008**, *25* (1), 118–138.
- (31) Dochnahl, M.; Löhnwitz, K.; Lühl, A.; Pissarek, J.-W.; Biyikal, M.; Roesky, P. W.; Blechert, S. Functionalized Aminotroponimate Zinc Complexes as Catalysts for the Intramolecular Hydroamination of Alkenes. *Organometallics* **2010**, *29* (12), 2637–2645.
- (32) Muetterties, E. L.; Roesky, H.; Wright, C. M. Chelate Chemistry. V. Metal Chelates Based on Tropolone and Its Derivatives. *J. Am. Chem. Soc.* **1966**, *88* (21), 4856–4861.
- (33) Breheret, E. F.; Martin, M. M. Electronic Relaxation of Troponoids: Tropolone Fluorescence. *J. Lumin.* **1978**, *17* (1), 49–60.
- (34) Hojo, M.; Hasegawa, H.; Yoneda, H. Role of Triple Ion Formation in the Acid–Base Reaction between Tropolone and Triethylamine in Acetonitrile. *J. Chem. Soc. Perkin Trans. 2* **1994**, No. 8, 1855–1859.
- (35) Bollu, A.; Sharma, N. K. Tropolone-Conjugated DNA: Fluorescence Enhancement in the Duplex. *ChemBioChem* **2019**, *20* (11), 1467–1475.
- (36) Bollu, A.; Panda, S. S.; Sharma, N. K. Fluorescent DNA Analog: 2-Aminotroponyl-Pyrrolyl-2'-Deoxyuridiny DNA Oligo Enhance Fluorescence in DNA-Duplex as Compared to 2-Aminotroponyl-Ethynyl-2'-Deoxyuridiny DNA Oligo. *Nucleosides*.

*Nucleotides Nucleic Acids* **2022**, 1–15.

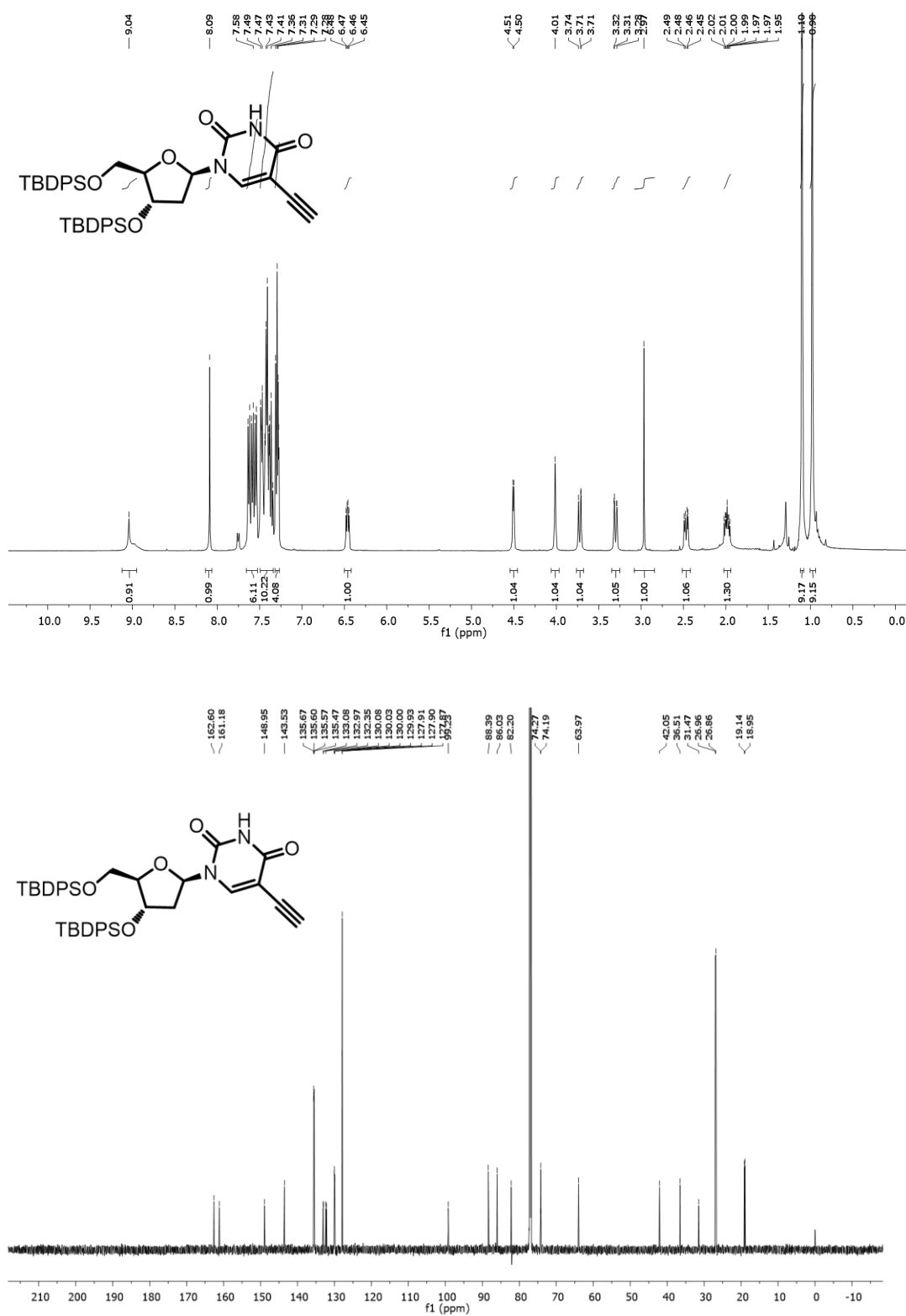
- (37) Pradere, U.; Garnier-Amblard, E. C.; Coats, S. J.; Amblard, F.; Schinazi, R. F. Synthesis of Nucleoside Phosphate and Phosphonate Prodrugs. *Chem. Rev.* **2014**, *114* (18), 9154–9218.
- (38) Palai, B. B.; Panda, S. S.; Sharma, N. K. Synthesis of Aminotroponyl-/Difluoroboronyl Aminotroponyl Deoxyuridine Phosphoramidites. *Curr. Protoc.* **2022**, *2* (12), e609.
- (39) Potenziano, J.; Spitale, R.; Janik, M. E. Improved and Highly Versatile Synthesis of 5-Aryltropones. *Synth. Commun.* **2005**, *35* (15), 2005–2016.
- (40) Seio, K.; Kanamori, T.; Masaki, Y. Solvent- and Environment-Dependent Fluorescence of Modified Nucleobases. *Tetrahedron Lett.* **2018**, *59* (21), 1977–1985.
- (41) Wang, X.; Martínez-Fernández, L.; Zhang, Y.; Zhang, K.; Improta, R.; Kohler, B.; Xu, J.; Chen, J. Solvent-Dependent Stabilization of a Charge Transfer State Is the Key to Ultrafast Triplet State Formation in an Epigenetic DNA Nucleoside. *Chem. Eur. J.* **2021**, *27* (42), 10932–10940.
- (42) Palai, B. B.; Soren, R.; Sharma, N. K. BODIPY Analogues: Synthesis and Photophysical Studies of Difluoro Boron Complexes from 2-Aminotropone Scaffolds through N, O-Chelation. *Org. Biomol. Chem.* **2019**, *17* (26), 6497–6505.
- (43) Cerón-Carrasco, J. P.; Jacquemin, D.; Laurence, C.; Planchat, A.; Reichardt, C.; Sraïdi, K. Solvent Polarity Scales: Determination of New ET (30) Values for 84 Organic Solvents. *J. Phys. Org. Chem.* **2014**, *27* (6), 512–518.
- (44) Dziuba, D.; Pospíšil, P.; Matyášovský, J.; Brynda, J.; Nachtigallová, D.; Rulíšek, L.;

- Pohl, R.; Hof, M.; Hocek, M. Solvatochromic Fluorene-Linked Nucleoside and DNA as Color-Changing Fluorescent Probes for Sensing Interactions. *Chem. Sci.* **2016**, 7 (9), 5775–5785.
- (45) Mishra, N. C.; Broom, A. D. A Novel Synthesis of Nucleoside 5'-Triphosphates. *J. Chem. Soc. Chem. Commun.* **1991**, No. 18, 1276–1277.
- (46) Caton-Williams, J.; Smith, M.; Carrasco, N.; Huang, Z. Protection-Free One-Pot Synthesis of 2'-Deoxynucleoside 5'-Triphosphates and DNA Polymerization. *Org. Lett.* **2011**, 13 (16), 4156–4159.
- (47) Güixens-Gallardo, P.; Zawada, Z.; Matyašovský, J.; Dziuba, D.; Pohl, R.; Kraus, T.; Hocek, M. Brightly Fluorescent 2'-Deoxyribonucleoside Triphosphates Bearing Methylated Bodipy Fluorophore for in Cellulo Incorporation to DNA, Imaging, and Flow Cytometry. *Bioconjug. Chem.* **2018**, 29 (11), 3906–3912.
- (48) Zawada, Z.; Tatar, A.; Mocilac, P.; Buděšínský, M.; Kraus, T. Transport of Nucleoside Triphosphates into Cells by Artificial Molecular Transporters. *Angew. Chemie Int. Ed.* **2018**, 57 (31), 9891–9895.
- (49) Anastasi, C.; Quéléver, G.; Burlet, S.; Garino, C.; Souard, F.; Kraus, J.-L. New Antiviral Nucleoside Prodrugs Await Application. *Curr. Med. Chem.* **2003**, 10 (18), 1825–1843.
- (50) Dunn, K. W.; Kamocka, M. M.; McDonald, J. H. A Practical Guide to Evaluating Colocalization in Biological Microscopy. *Am. J. Physiol. Physiol.* **2011**, 300 (4), C723–C742.

**2A.7 Appendix**

1. $^1\text{H}$ , $^{13}\text{C}$ NMR (400MHz, $\text{CDCl}_3$ ) and HRMS of <b>3</b> .....	64
2. $^1\text{H}$ , $^{13}\text{C}$ NMR (400MHz, $\text{CDCl}_3$ ) and HRMS of <b>6</b> .....	66
3. $^1\text{H}$ , $^{13}\text{C}$ NMR (400 MHz , $\text{CDCl}_3$ ) and HRMS of <b>7</b> .....	68
4. $^1\text{H}$ , $^{31}\text{P}$ NMR (400 MHz , $\text{D}_2\text{O}$ ) and HRMS of <b>9</b> .....	70



1.  $^1\text{H}$ ,  $^{13}\text{C}$  NMR (400MHz,  $\text{CDCl}_3$ ) and HRMS of **3**Figure A1.  $^1\text{H}/^{13}\text{C}$  NMR of Compound **3** in  $\text{CDCl}_3$ .

## Generic Display Report

## Analysis Info

Analysis Name D:\Data\JULY-2018\NKS\11072018\_NKS-SNM-188.d  
Method pos tune\_wide.m  
Sample Name  
Comment

Acquisition Date 7/11/2018 7:41:50 PM

Operator MRIGANKA  
Instrument microTOF-Q II

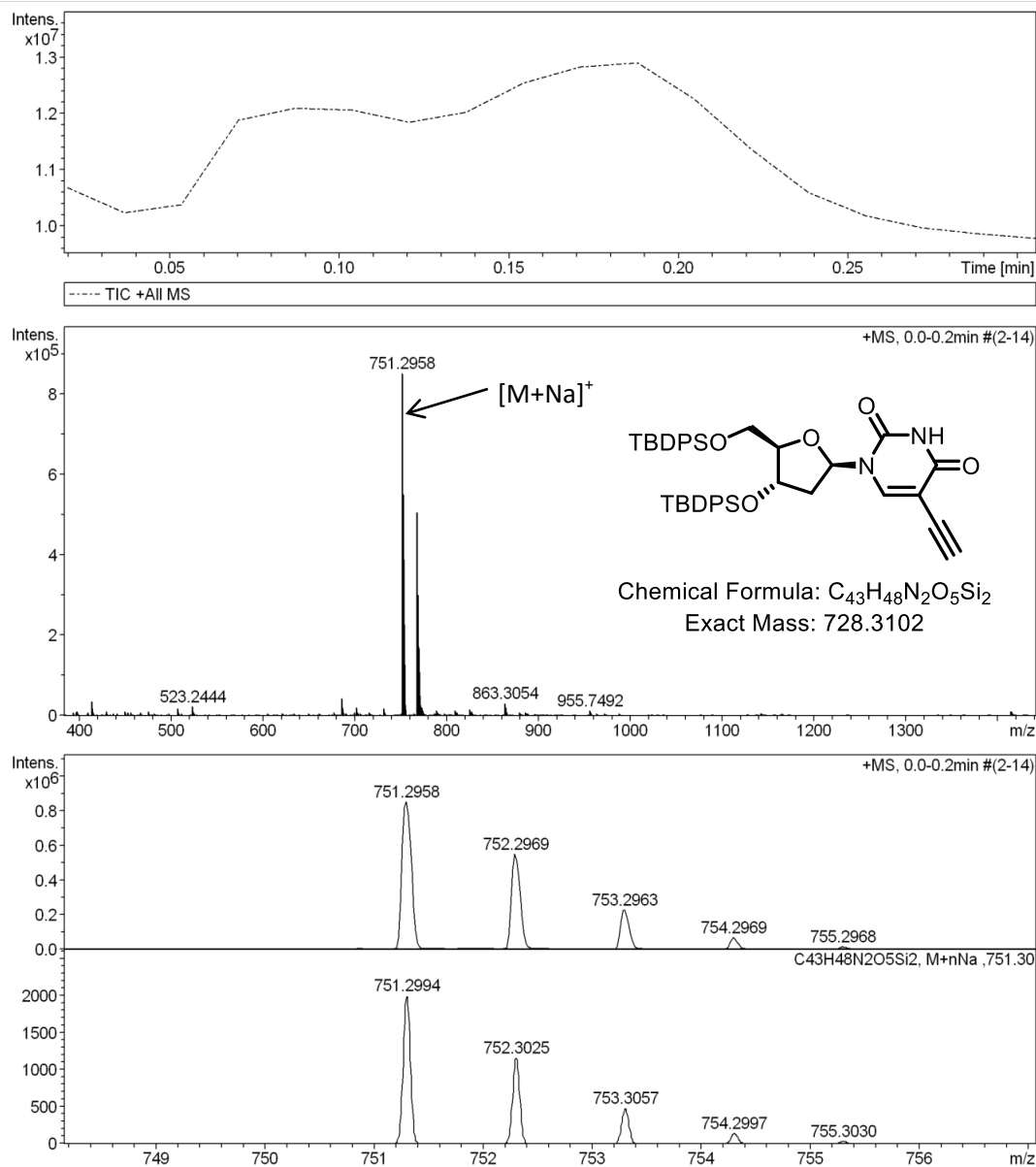
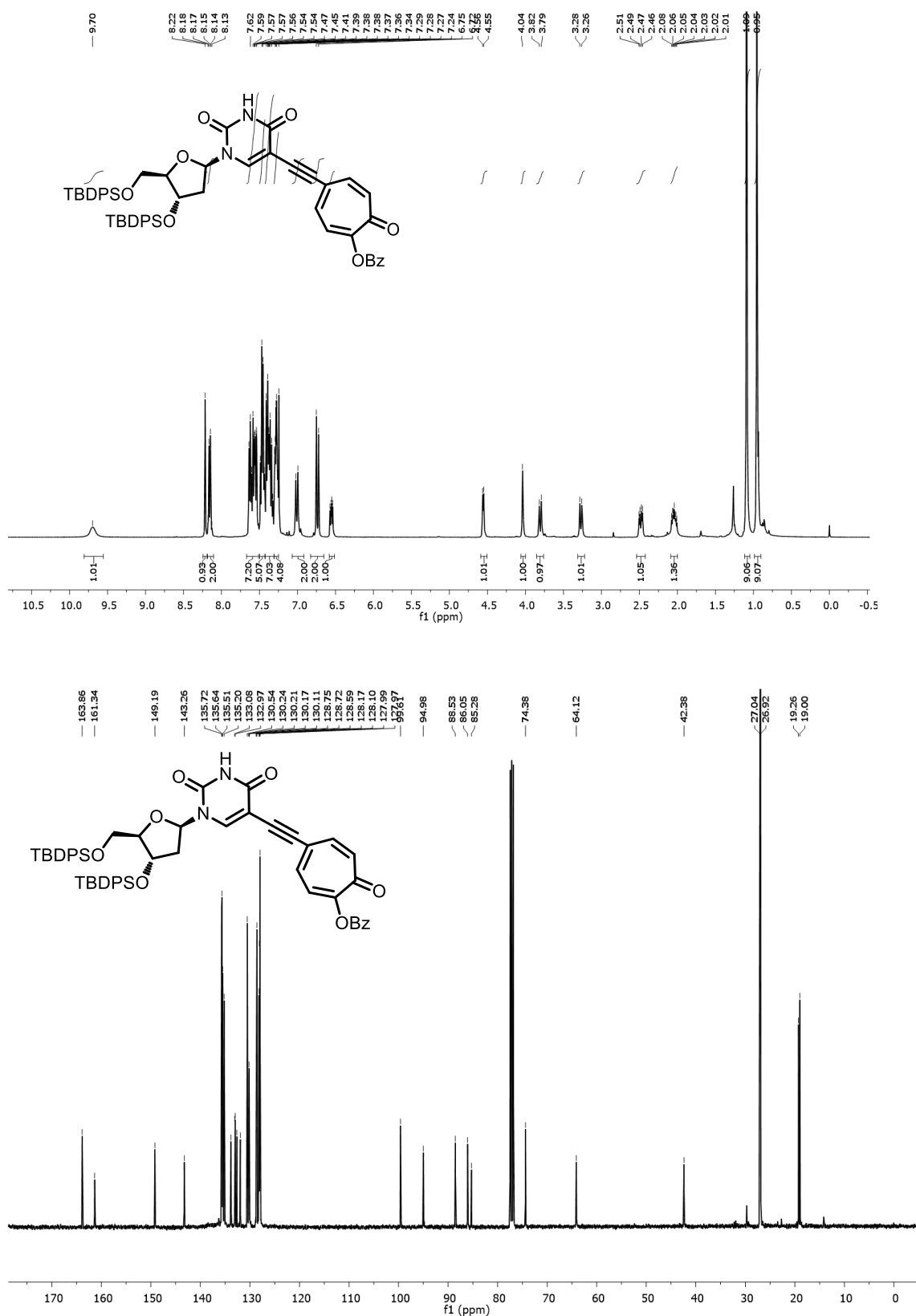


Figure A2. ESI-MS/HRMS spectra of compound 3.

2.  $^1\text{H}$ ,  $^{13}\text{C}$  NMR (400MHz,  $\text{CDCl}_3$ ) and HRMS of **6**Figure A3.  $^1\text{H}/^{13}\text{C}$  NMR of Compound **6** in  $\text{CDCl}_3$ .

## Generic Display Report

## Analysis Info

Analysis Name D:\Data\JULY-2018\NKS\18072018\_NKS\_SNM-187.d

Method pos tune\_wide.m

Sample Name Tmix-200418

Comment

Acquisition Date 7/18/2018 5:47:15 PM

Operator Amit S.Sahu

Instrument micrOTOF-Q II

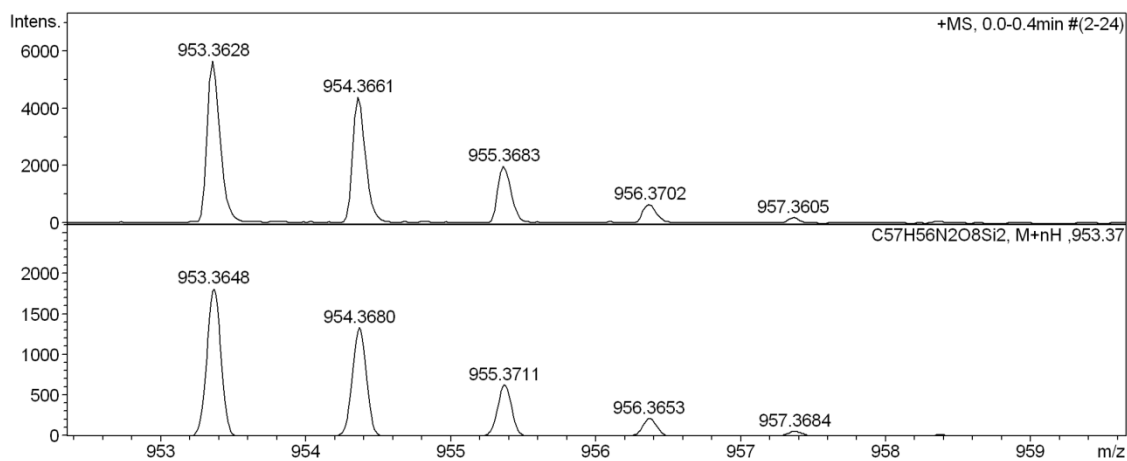
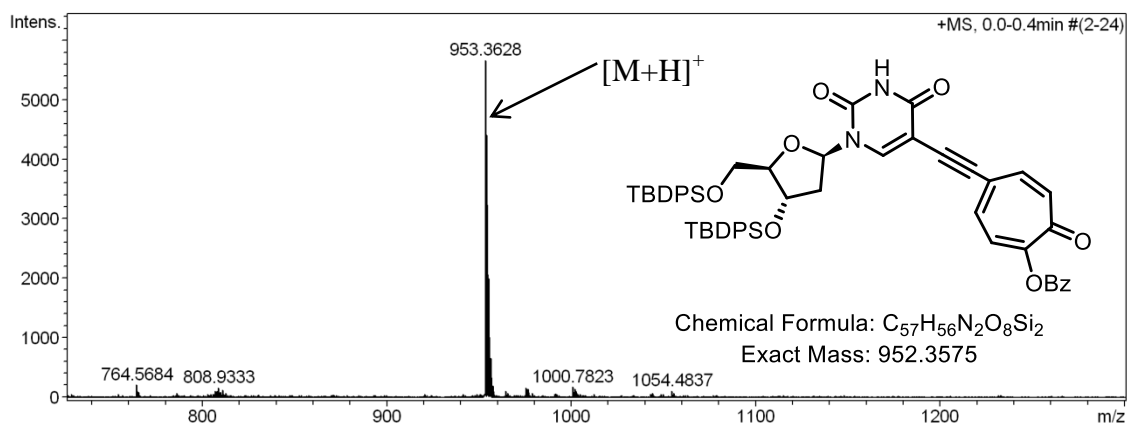
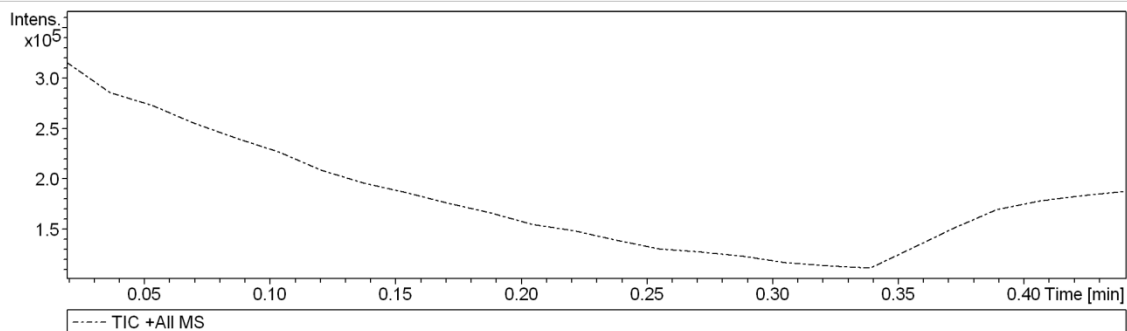
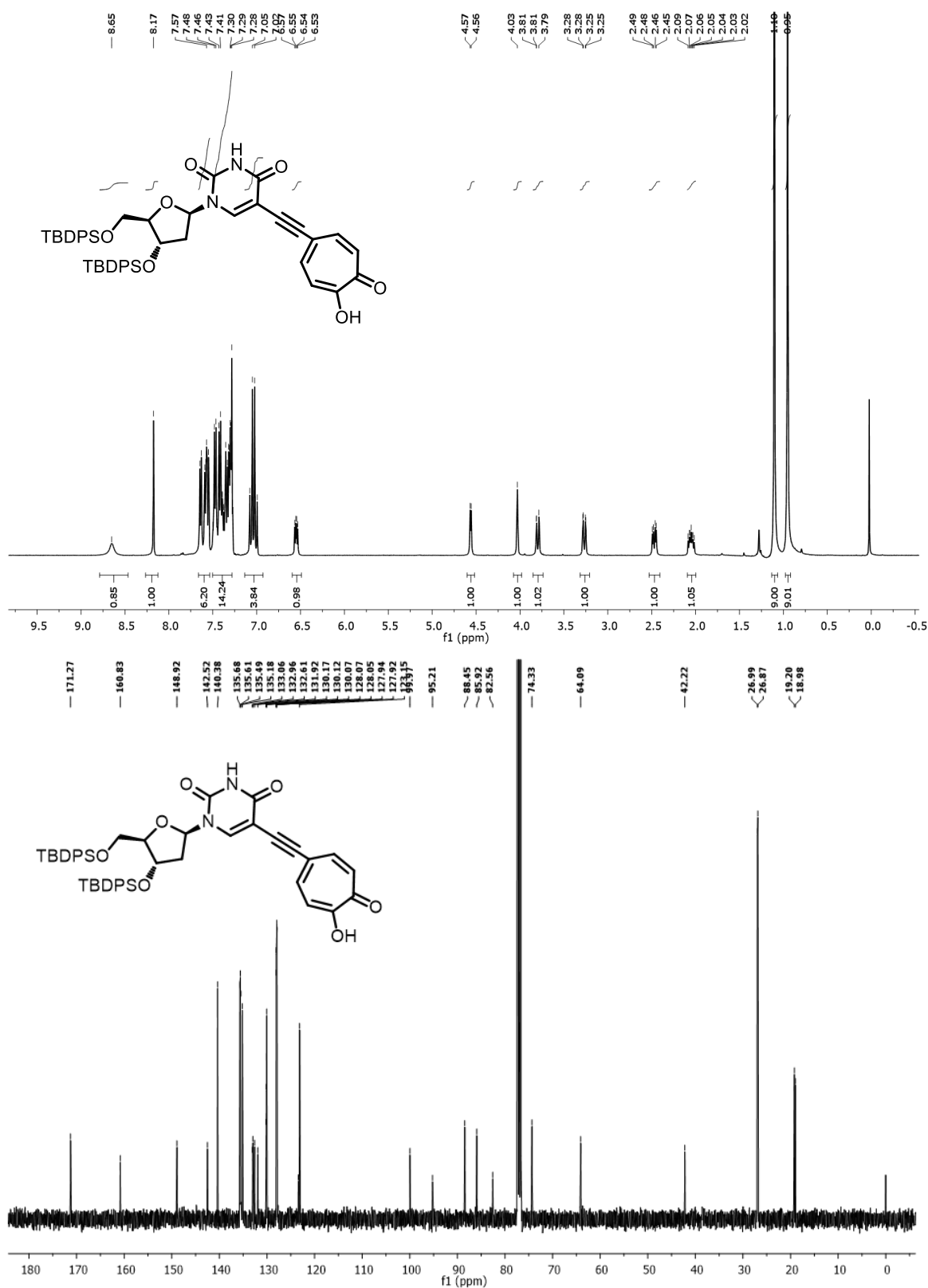


Figure A4. ESI-MS/HRMS spectra of compound 6.

3.  $^1\text{H}$ ,  $^{13}\text{C}$  NMR (400 MHz,  $\text{CDCl}_3$ ) and HRMS of **7**Figure A5.  $^1\text{H}/^{13}\text{C}$  NMR of Compound **7** in  $\text{CDCl}_3$ .

## Display Report

## Analysis Info

Analysis Name D:\Data\NOV-2018\NKS\29112018\_NKS\_SNM\_848\_RE.d  
Method pos tune high.m  
Sample Name Tmix-131118  
Comment

Acquisition Date 11/29/2018 2:49:42 PM

Operator Amit S.Sahu  
Instrument micrOTOF-Q II 10337

## Acquisition Parameter

Source Type	ESI	Ion Polarity	Positive	Set Nebulizer	0.4 Bar
Focus	Not active	Set Capillary	4500 V	Set Dry Heater	180 °C
Scan Begin	50 m/z	Set End Plate Offset	-500 V	Set Dry Gas	4.0 l/min
Scan End	3000 m/z	Set Collision Cell RF	1600.0 Vpp	Set Divert Valve	Waste

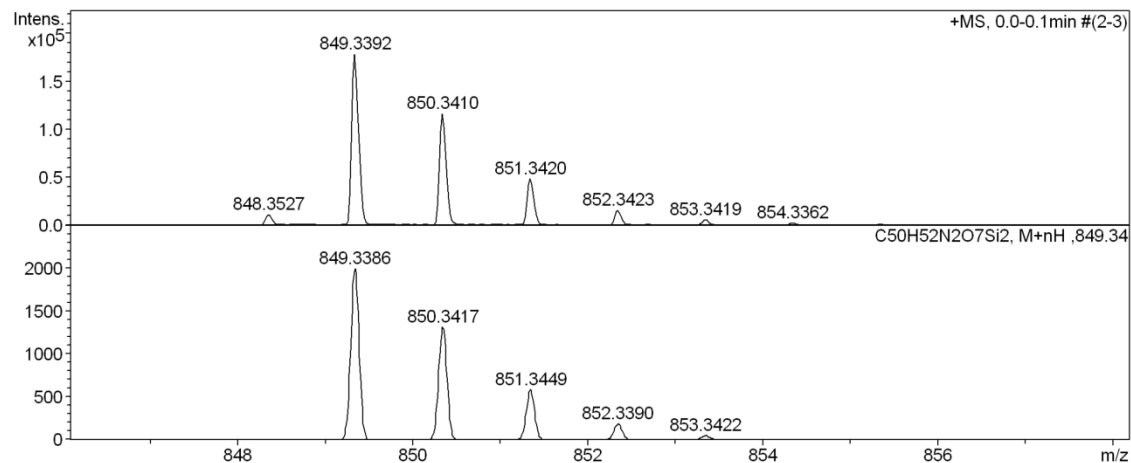
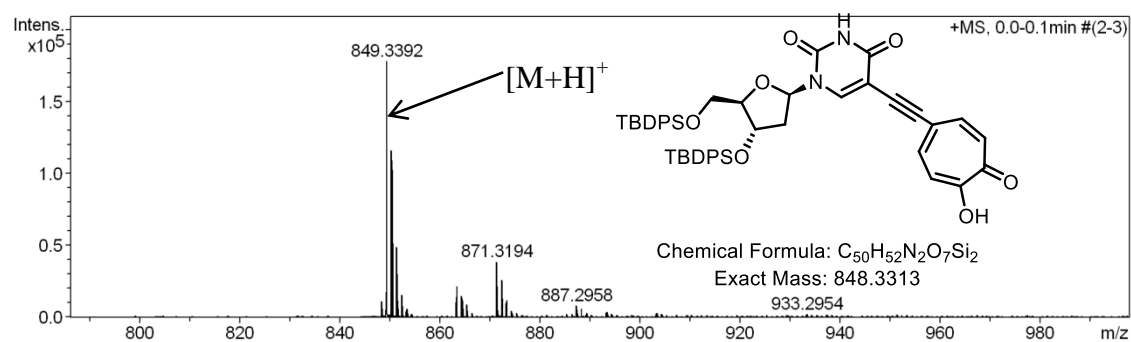
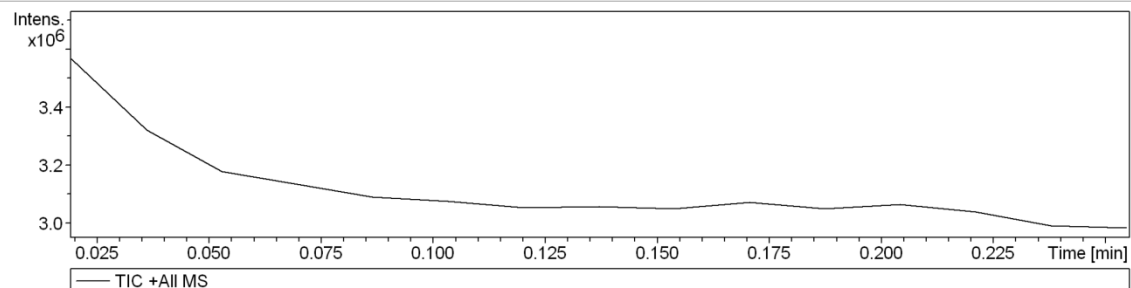
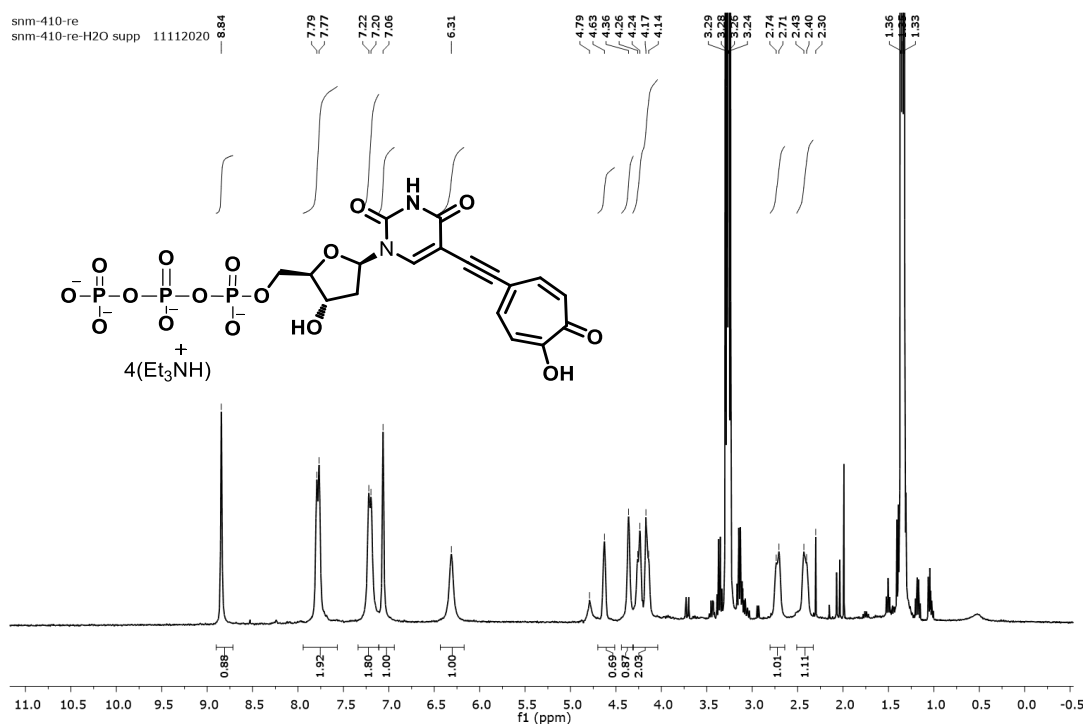
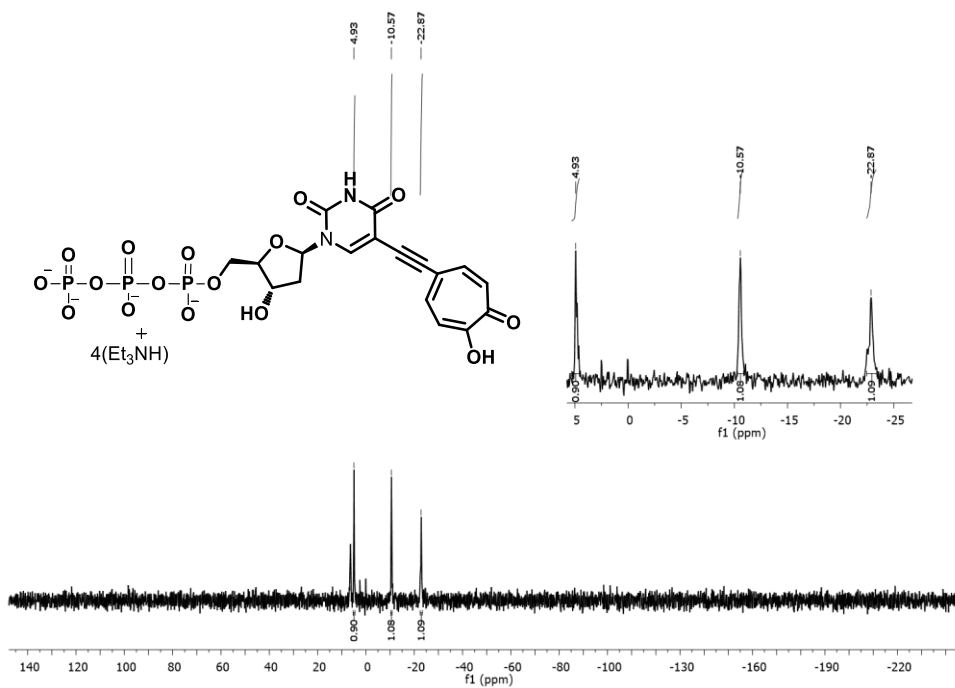


Figure A6. ESI-MS/HRMS spectra of compound 7

4.  $^1\text{H}$ ,  $^{31}\text{P}$  NMR (400 MHz,  $\text{D}_2\text{O}$ ) and HRMS of **9**Figure A7.  $^1\text{H}$  NMR of Compound **9** in  $\text{D}_2\text{O}$  after water suppression.Figure A8.  $^{31}\text{P}$  NMR of Compound **9** in  $\text{D}_2\text{O}$ .

## Display Report

## Analysis Info

Analysis Name D:\Data\NOV-2020\NKS\24112020\_NKS\_SNM-610-8.d  
Method NEG tune\_wide.m  
Sample Name Tmix-131118  
Comment

Acquisition Date 11/26/2020 6:07:13 AM

Operator Amit S.Sahu  
Instrument micrOTOF-Q II 10337

## Acquisition Parameter

Source Type	ESI	Ion Polarity	Negative	Set Nebulizer	0.4 Bar
Focus	Not active	Set Capillary	2500 V	Set Dry Heater	180 °C
Scan Begin	50 m/z	Set End Plate Offset	-500 V	Set Dry Gas	4.0 l/min
Scan End	3000 m/z	Set Collision Cell RF	650.0 Vpp	Set Divert Valve	Waste

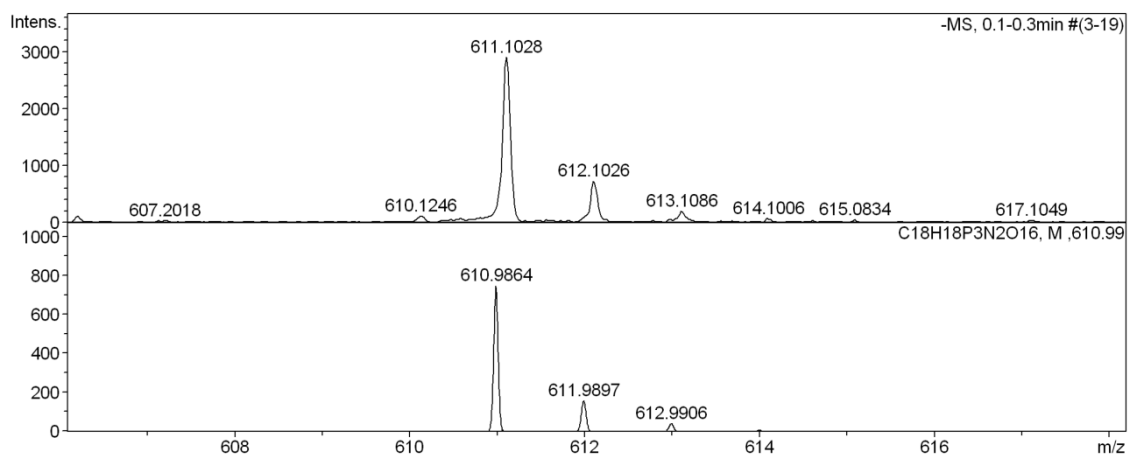
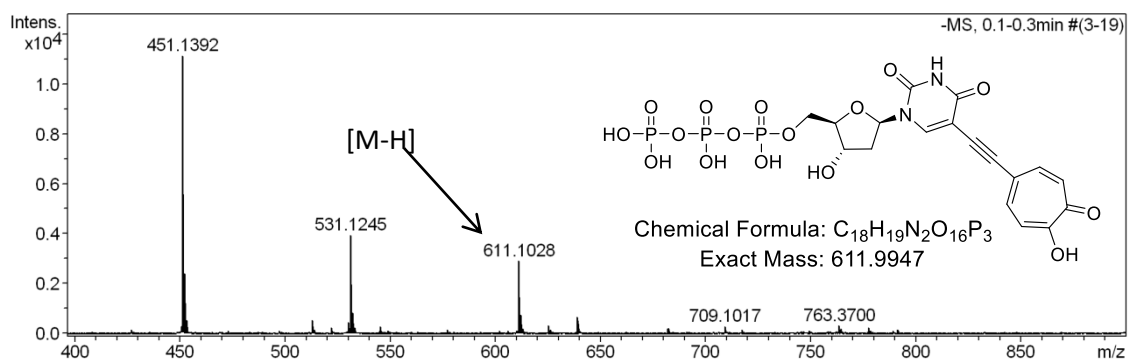
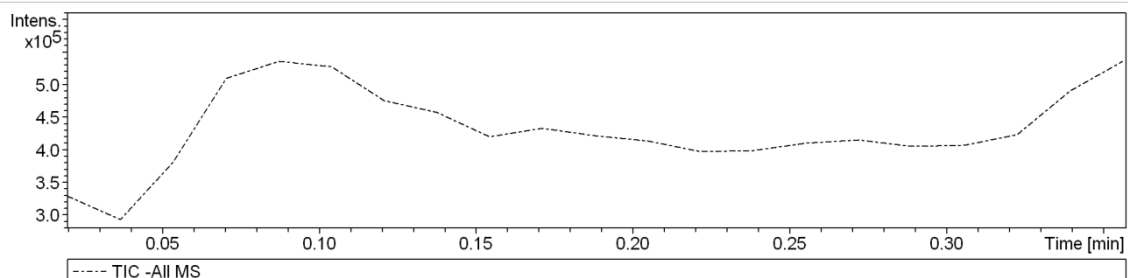


Figure A9. ESI-MS/HRMS spectra of compound 9



## **CHAPTER 2**

### **PART-B**

---

## **Tropolone Clicked DNA: Synthesis, Photophysical Studies and Biochemical Evaluations**

---

### **2B.1 Introduction**

### **2B.2 Objective**

### **2B.3 Results and Discussion**

### **2B.4 Conclusion**

### **2B.5 Experimental Section**

### **2B.6 References and Notes**

### **2B.7 Appendix**

## 2B.1 Introduction

Nucleic acids (DNA/RNA) are commonly involved in all biological operations of cellular life, such as metabolic control, catalysis, and energy transmission.<sup>1</sup> The composition of nucleic acids has been widely examined and analyzed, leading to the discovery of modified nucleosides alongside the primary constituent units (A/T/G/C/U).<sup>2</sup> Recent years have witnessed increasing development and exploitation of modified nucleosides, increasing interest in nucleic acid chemistry. Moreover, fluorescent nucleic acid (FNA) analogs are of a distinct category where simple chemical modifications can formulate novel products. The synthesis of FNAs has provided powerful tools for monitoring biochemical phenomena in real time.<sup>3–5</sup> Its nucleosides are classified into isomorphous, enlarged, extended, and chromophoric base analogs based on their chemical structure and relationships to natural nucleobases.<sup>6</sup> Isomorphous nucleoside analogs differ from natural nucleosides by the presence of small substituents or the number and position of heteroatoms in the heterocyclic core. Expanded nucleosides have additional aromatic rings annealed to the purine or pyrimidine core. A fluorophore is linked to the nucleobase in extended nucleoside analogs. Finally, in chromophoric nucleoside analogs, the whole nucleobase is replaced by a structurally different and frequently bulky aromatic chromophore.<sup>7</sup> Additionally, environment-sensitive fluorophores (ESF) can sense changes in the microenvironment (polarity/ viscosity/ pH), secondary structures, or intramolecular interactions. The response represents useful photophysical features such as changes in absorption or emission wavelengths (solvatochromism), fluorescence lifetime, quantum yield, color, and so on.<sup>8–10</sup> Microenvironment-sensitive fluorescent molecules are ubiquitous for sensing of biomolecules and studying inter-biomolecular interactions inside a cell.<sup>11–16</sup> These synthetic nucleoside mimics are also important candidates for antiviral, antimicrobial, antitumor, and anticancer drugs. In the search for new biologically active nucleoside analogs, structural variations

involving changes to the nucleosides have been achieved using different synthetic methodologies.<sup>17–22</sup> Metal-mediated cross-coupling reactions (Sonogashira coupling, Stille coupling, Suzuki-Miyaura coupling, Heck coupling, etc.) are perhaps the most successful and widely used chemistry today for the synthesis of novel nucleosides.<sup>23,24</sup> The copper(I)-catalyzed azide-alkyne cycloaddition (CuAAC or click reaction) is also one of the most important bioorthogonal reactions and has been widely utilized to modify oligonucleotides (ONs) and DNA. The copper (I)-catalyzed Huisgen 1,3-dipolar cycloaddition of azides with terminal alkynes has high specificity and efficiency in connecting two different molecular entities. It was independently introduced by Sharpless and Meldal in 2001 to provide regioselectively 1,2,3-triazole moieties.<sup>25–27</sup> Click chemistry bagged the Nobel Prize in 2022 and is undoubtedly a widely used concept in medicinal chemistry and drug discovery. Click reactions are very appealing for biological applications since they are by definition fast, stereospecific (although not necessarily enantioselective), and can be conducted in aqueous solutions with high yield.<sup>28–32</sup> These properties help for biomolecular conjugation in vitro or if the reaction is non-toxic, even in cells or in vivo, where the concentration of targeted biomolecules is typically low.<sup>33</sup> Recently, many triazole-modified nucleosides have been reported and reviewed by several groups, like Brown and co-workers, Rentmeister and co-workers. These are used as photoswitchable DNA interstrand crosslinking agents for thermal stability study and DNA fluorescence mismatch sensing by various groups.<sup>34,35</sup> Nielsen and co-workers have reported the effect of triazole-modified 2 - deoxyuridines on the stability of DNA: DNA and DNA: RNA duplexes.<sup>36,37</sup> Hocek and co-workers have introduced Azidophenyl to label DNA using click chemistry for electrochemical detection of DNA–protein interactions.<sup>38</sup> Fujimoto and co-workers have synthesized sensitive DNA Probes for Photochemical Ligation.<sup>39</sup> However, the majority of the alterations in nucleosides include benzenoid and heterocyclic aromatic scaffolds. In the repertoire of functional DNA synthesis,

the non-benzenoid moiety-conjugated DNA analogs are not well explored. Tropolone is a non-benzenoid aromatic scaffold whose derivatives constitute troponoid natural products.<sup>40,41</sup> Tropolone has unique intramolecular hydrogen bonding, metal chelating, and therapeutic properties.<sup>42–46</sup> Recently, tropolone has been employed as a novel scaffold for tuning the structural and functional properties of peptides and DNA. The conjugation of tropolone at nucleobase was achieved by a Pd-catalyzed Sonogashira coupling reaction.<sup>47</sup> Troponyl deoxyuridine (tr-dU) nucleoside analog exhibits pH-dependent fluorescence.<sup>48,49</sup> Herein, we have conjugated azido tropolone unit at modified nucleoside, ethynyl-dU, in the presence of Cu(I) ions through click chemistry and commenced its biochemical evaluations.

## 2B.2 Objective

In the previous chapter, we synthesized fluorescent troponyl thymidine/ uridine analogs via a Pd-catalyzed Sonogashira coupling reaction. We studied their solvent-dependent fluorescence characters, cell permeability, and enzymatic incorporation into DNA. In this chapter, we described the conjugation of tropolone at uridine via triazole ring through Click chemistry. We also explored its fluorescence properties, cytotoxicity, and cell permeability. Its triphosphate derivative was synthesized for incorporation into DNA primer by the primer extension reaction using DNA polymerase.

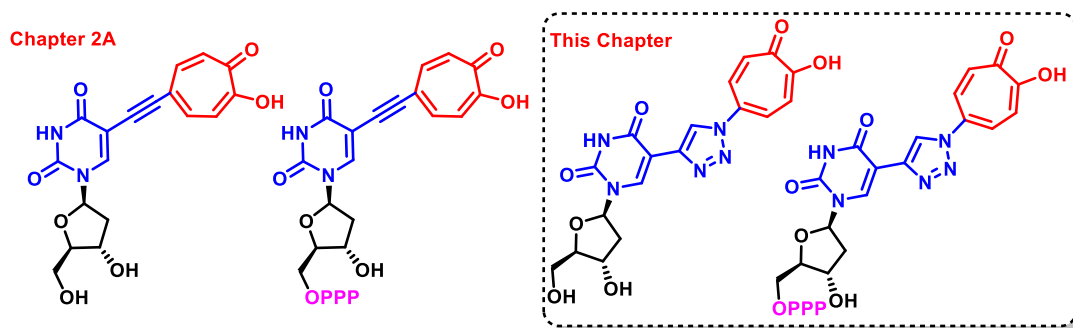
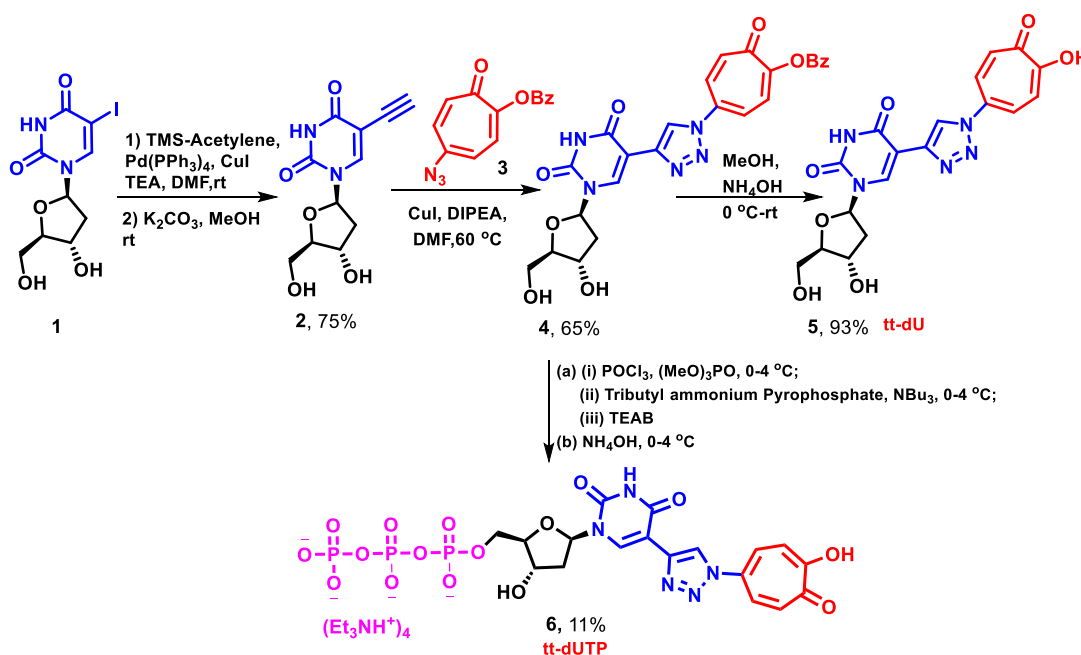


**Figure 2B.1.** Troponyl nucleosides in previous and this chapter.

### 2B.3 Results and Discussion

5-iodo-2'-deoxyuridine was modified into 5-ethynyl-2'-deoxyuridine (**2**) by following the reported procedure.<sup>47</sup> Tropolone was derivatized into azide functionalized tropolone i. e. 5-azido-tropolonyl benzoate (**3**) in 5 steps and the details are provided in the experimental section. This azide derivative (**3**) was coupled with 5-ethynyl-2'-deoxyuridine (**2**) with Cu-catalyzed [3+2] cycloaddition reactions (Click chemistry) that produced desired Bz- protected thymidine nucleoside, tt-<sup>bz</sup>dU (**4**) (Scheme 2B.1). We synthesized the triphosphate analog, tt-dUTP or tt-dTTP (**6**) from the previously synthesized nucleoside (**4**) by treating it with POCl<sub>3</sub>, followed by a reaction with pyrophosphate. The synthesis of triphosphate is an extensive procedure that requires great care. After phosphorylation, the Bz group was deprotected with ammonium hydroxide solution. We obtained tropolonyl deoxyuridinyI triphosphate (tt-dUTP, **6**) in considerable yield after HPLC purification. Compound **5** was synthesized from compound **4** by deprotecting the Bz group for fluorescence and biochemical studies. All the compounds were characterized by NMR and ESI-HRMS analysis.



**Scheme 2B.1.** Synthesis of troponyl-dU (tt-dU, **5**) and its triphosphate analog (tt-dUTP, **6**).

We investigated the incorporation of tt-dUTP (**6**) into DNA primer (P1) guided by template DNA (T1) in the presence of DNA polymerases enzyme (Therimator) for the enzymatic synthesis of tropolonylated DNA (Figure 2B.2). The sequence of P1 and T1 are following:

**P1:** 5'-TGTAACGACGGCCAGT-3'

**T1:** 3'-ACATTTTGCTGCCGGTCA<sup>A\*</sup>GTCGAGGCAT 5'

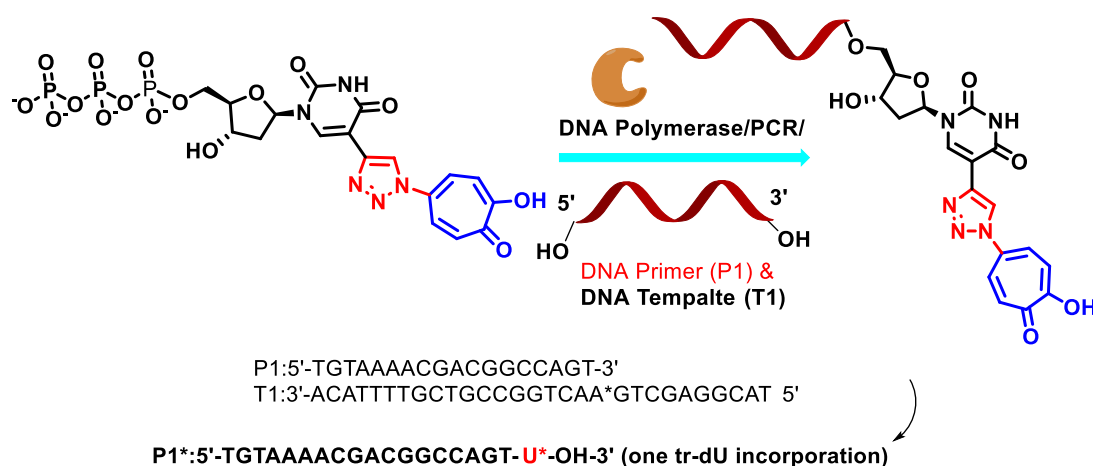


**Figure 2B.2.** Primer extension reactions of tt-dTTP (**6**) with DNA polymerase (Therminator).

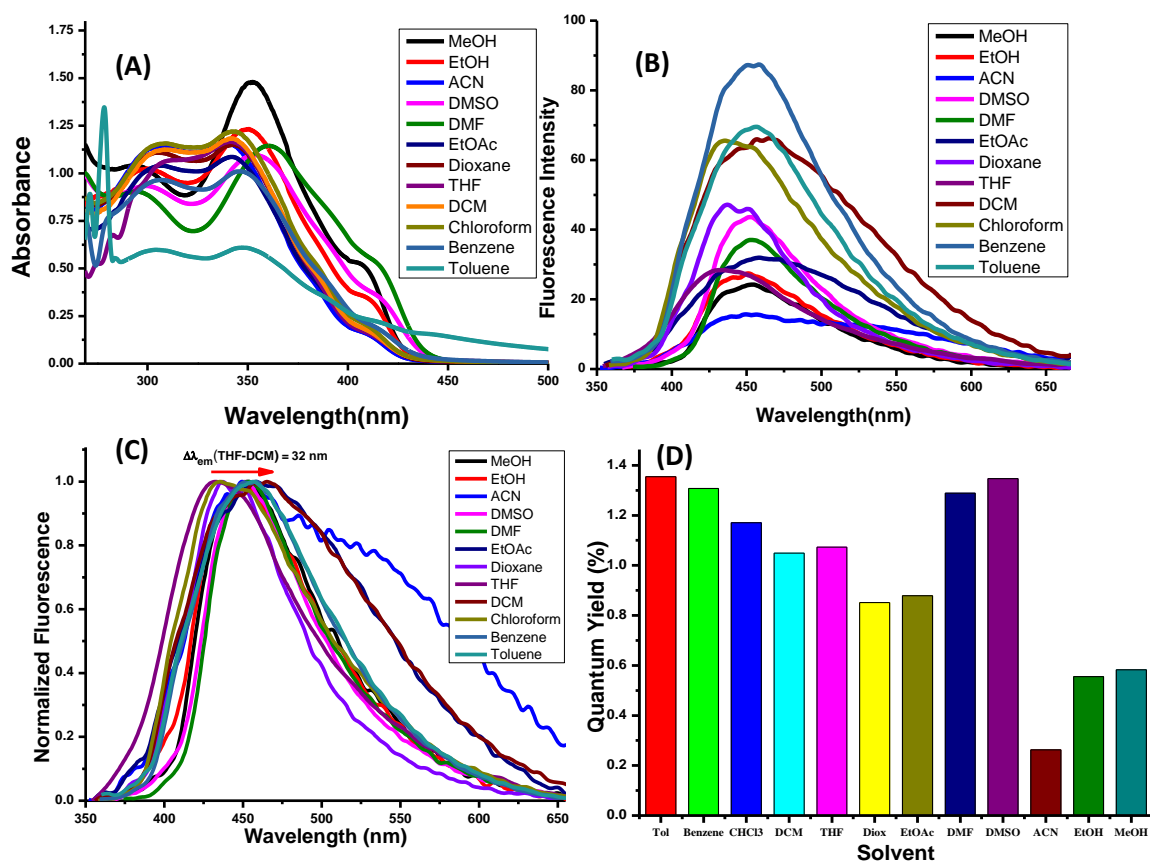
The incorporation of tt-dUTP (**6**) into oligonucleotide using Therminator by polymerase extension (PEX) reaction was verified by LCMS analysis. Calculated mass for extended primer (single extension) =  $6009 + 54 (3 \text{ NH}_4) = 6063 / 4 = 1515.75$ , observed = 1515.32. Hence tt-dUTP (**6**) is a substrate of DNA polymerase enzyme.

Our previous works showed that tropolonyl nucleoside exhibited solvent-dependent fluorescence behavior. Tropolone exhibits the electronic transitions  $\pi$ - $\pi^*$ ,  $n$ - $\pi^*$ , and intramolecular charge transfer.<sup>50</sup> It contributes to the photophysical properties of the nucleoside. Here we performed the photophysical studies of tt-dU (**5**) to examine the effect of triazole and tropolone ring in its absorption and emission properties. We recorded the

absorption and emission spectra of modified nucleoside tt-dU (**5**) in different solvents- MeOH, EtOH, DMSO, DMF, EtOAc, Dioxane, ACN, THF, DCM, CHCl<sub>3</sub>, Benzene, and Toluene. The spectral properties are provided in Table 2B.1 and Figure 2B.3. The absorption peaks of tt-dU (**5**) appeared relatively at shorter wavelengths in the non-hydrogen bonding solvents compared to hydrogen bonding solvents. We observed two absorption maxima ( $\lambda_{\text{abs}}$  = 305, 445 nm) in case of nonpolar solvents (Table 2B.1, Entry 1-7), whereas it showed approximately 2- 5 nm bathochromic shift in polar/ protic solvents (Figure 2B.3-A). In the fluorescence spectra the emission maxima range from 432 nm- 464 nm (Figure 2B.3-B/C). The nucleoside, tt-dU (**5**), exhibited solvatochromism, but the trend is not continuous from the nonpolar to polar solvents. We extracted the quantum yields of tt-dU (**5**) in different solvent systems taking aq. quinine sulfate in H<sub>2</sub>SO<sub>4</sub> as a reference, which is summarized in Figure 2B.3-D. Importantly, tt-dU (**5**) exhibits the highest fluorescence quantum yield (~1.3%) in aromatic solvents (toluene & benzene) and DMF and DMSO, while the lowest in non-hydrogen bonding polar solvent ACN (0.3%) and the protic polar solvents. We assume that  $\pi$ - $\pi$  interaction of tt-dU (**5**) with aromatic solvent lowered the HOMO-LUMO energy band in comparison to other given solvents. The hydrogen bond acceptor solvents DMF/DMSO encapsulate the tt-dU (**5**), lower the HOMO-LUMO energy band and enhance fluorescence significantly. The protic solvents disrupt the intramolecular hydrogen bonding and decrease the quantum yield. The optimized structure from DFT studies also showed the coplanar organization of the triazole uracil with the triazole-CH pointing toward O4 (of C4 carbonyl in pyrimidine ring) of the uracil probably through a CH-O hydrogen bonding interaction and a N/O lone pair repulsion. This structural preference is well documented in the literature.<sup>51</sup> From the above studies, it is evident that tt-dU (**5**) is an environment-sensitive fluorophore though it doesn't possess a large quantum yield. It can be used as a probe for further biochemical evaluations.

**Table 2B.1.** Summary table of Fluorescence properties of tt-dU (5)

S.N.	Solvent	$\lambda_{\text{abs}}$ (nm)	Absorbance	$\lambda_{\text{em}}$ (nm)	stokes shift	$\epsilon_{\text{max}}$ (M cm <sup>-1</sup> )	$\Phi_f$ (%)
1	Tol	305, 345	0.61	455	110	61000	1.35
2	Benzene	305, 345	1.01	455	110	101000	1.30
3	CHCl <sub>3</sub>	305, 345	1.224	436	91	122400	1.17
4	DCM	305, 345	1.184	464	119	118400	1.05
5	THF	305, 345	1.17	432	87	117000	1.07
6	Diox	305, 345	1.152	437	92	115200	0.85
7	EtOAc	305, 345	1.088	458	113	108800	0.88
8	DMF	294, 360	1.144	455	95	114400	1.29
9	DMSO	299, 353	1.095	455	102	109500	1.35
10	ACN	305, 345	1.161	449	104	116100	0.26
11	EtOH	300, 350	1.232	451	101	123200	0.55
12	MeOH	295, 352	1.478	453	101	147800	0.58

**Figure 2B.3.** Absorption (A), emission spectra (B, C), and quantum yield (D) of tt-dU (5) in various solvents (20 μM).



We executed the MTS assay to evaluate the cytotoxicity of nucleoside tt-dU (**5**) for both normal (HEK293T) and malignant (HeLa) cell lines (Figure 2B.4). The findings on their concentration-dependent cell viability showed no substantial cytotoxicity with tr-dU in any cell line. As a result, this nucleoside can be utilized for further studies.

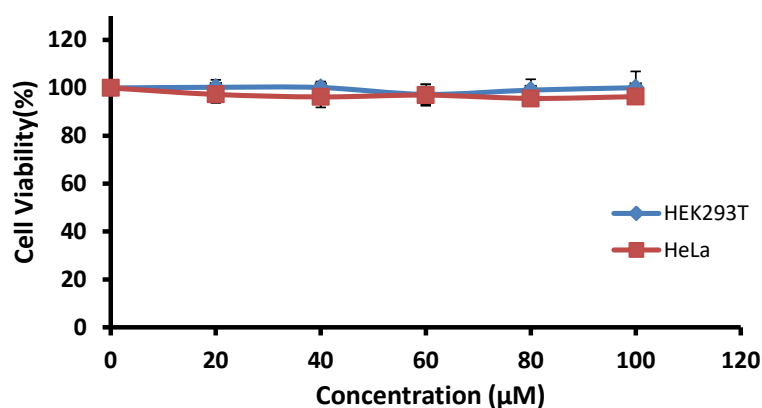


**Figure 2B.4.** Cell proliferation assays of compound tt-dU (**5**) in HEK293T and HeLa cells.

Nucleosides and similar compounds are prodrugs for a wide range of diseases, including antiviral, anticancer, and antibiotic drugs. Fluorescent nucleoside analogs have recently demonstrated better cell permeability and are being used for labeling biomolecules in vitro/vivo.<sup>52,53</sup> Thus, The cell permeability of fluorescent tt-dU (**5**) into HeLa cell lines was investigated. HeLa cells were incubated with tt-dU (**5**) for 12/ 24 h and stained with DAPI following the standard protocol and observed under a confocal microscope. Images were captured in bright light and various channels, i.e., DAPI (blue channel,  $\lambda_{\text{ex}}$  358 nm), FITC (green channel,  $\lambda_{\text{ex}}$  490 nm), and TRITC (red channel,  $\lambda_{\text{ex}}$  570 nm). The tt-dU (**5**) was primarily identified in the nucleus region of cell (Figure 2B.5). DAPI stained, tt-dU treated cells in Figure 2B.5-A/G reveal DAPI localization at the cellular nucleus. For this study, no transfecting reagents were used. Colocalization tests of tt-dU (**5**) with DAPI were carried out in both channels (green/red). Pearson's coefficient values ( $r$ ) for the red and green channels are 0.76 and 0.75, respectively ( for 12 h incubation time). These values were computed in

Fiji: ImageJ using the JACoP plugin.<sup>54</sup> Results are the same for both 12 h and 24 h incubation time.

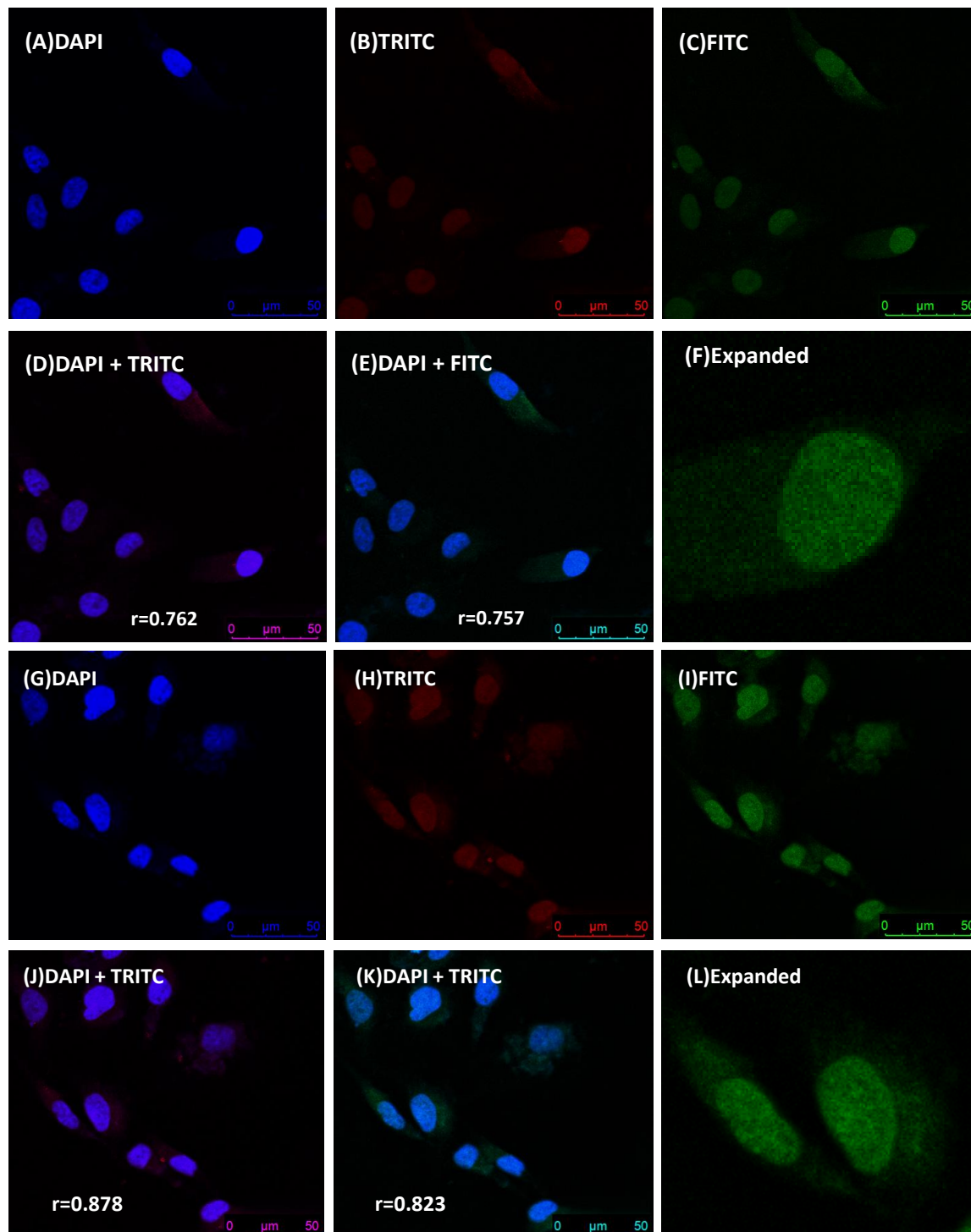


**Figure 2B.5.** Confocal microscopic images for tt-dU (5) treated HeLa Cells with DAPI staining (12 h incubation (A-F), 24 h incubation (G-L)).

## 2B.4 Conclusion

We accomplished the synthesis of tropolonyl triazolyl deoxyuridine (tt-dU, **5**) nucleoside, its triphosphate (tt-dUTP, **6**), and DNA. Our photophysical studies strongly support that tt-dU nucleoside exhibit fluorescence ( $\Phi_f \sim 1.3\%$  in toluene). Its fluorescence character also depends upon the solvent polarity, i.e., higher in nonpolar solvents and lower in polar/protic solvents. Importantly, its triphosphate analog (tt-dUTP, **6**) was enzymatically incorporate into DNA through primer extension reaction with DNA polymerases (Therminator). This nucleoside (tt-dU, **5**) was permeable in cell-line (HeLa cells) and exhibited fluorescence. It was mainly localized at the cellular nucleus. It had no significant cytotoxicity against HEK293T or HeLa cell lines. Hence, tt-dU (**5**) is a promising fluorescent nucleoside analog and could be applicable for designing DNA-based fluorescence probes. It may bind with metal ions ( $\text{Cu}^{2+}$ ) and regulate the metal-dependent biochemical process owing to the metal-chelating properties of tropolone residue.

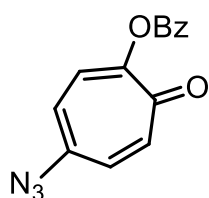
## 2B.5 Experimental Section

*General information:* All the materials were obtained from commercial suppliers and used without further purification. DMF and DCM were distilled over  $\text{CaH}_2$  and stored over 4Å molecular sieves. Tributyl amine was distilled over potassium hydroxide and stored over 4Å molecular sieves. Reactions were monitored by thin layer chromatography, visualized by UV and Ninhydrin. Column chromatography was performed in 230-400 mesh silica except Triphosphate product (purified by DEAE Sephadex-A25). Polymerase Chain Reactions were performed in Bio-rad T100 Thermal Cycler. HPLC was done in Waters 2998. DNA oligos and FAM labelled primers were purchased from IDT. All enzymes and buffers for primer extension reactions were bought from New England Bio labs. Mass spectra were obtained from Bruker micrOTOF-Q II Spectrometer and the samples were prepared in

methanol and injected in methanol:water mixture. All NMR spectra were recorded on Bruker AV-400 at room temperature and processed using Mnova software from Mestrelab Research. HRMS data of compounds were obtained from Bruker and Waters mass spectrometer. Absorption spectra were obtained using Jasco V-730 spectrometer and Fluorescence spectra were obtained from Agilent spectrophotometer and Perkin-Elmer LS-55 using Xenon lamp. Confocal Images were taken in Leica Microscope.

#### *Characterization data of products*

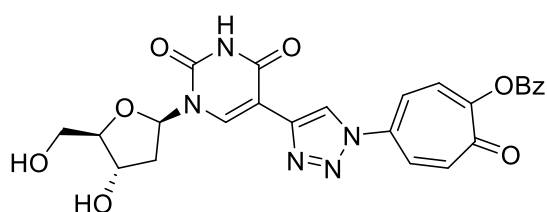
4-azido-7-oxocyclohepta-1,3,5-trien-1-yl benzoate (**3**): 5-amino tropolone was synthesized



starting from tropolone by following reported literature procedure.<sup>55</sup> 5-amino tropolone (0.2 g, 1.45 mmol), was dissolved in 2.5 ml conc. HCl and 5 ml distilled water was added to the reaction mixture. The resulting solution was stirred at -20 °C. Sodium nitrate (0.148 g, 1.72 mmol) dissolved in 5 ml distilled water was added to it slowly in 30 min and stirred for 20 min. Then Sodium azide (0.114 g, 1.72 mmol) dissolved in 5 ml distilled water was added slowly over 30 min. The reaction mixture was heated for one hour at 55 °C. Then it was cooled down to rt and extracted with dichloromethane. The aqueous layer was neutralized with sodium hydroxide solution and extracted with dichloromethane. The organic layers were washed with brine solution and dried with anhydrous sodium sulfate. The solution was concentrated and purified by column chromatography to obtain 5-Azido tropolone as brown colour compound (0.156 g, 40% yield). To 5-Azido tropolone (0.5 g 3.06 mmol) dissolved in dry dichloromethane (6 ml), triethyl amine (1.7 ml, 12.3 mmol) was added and stirred at room temperature under nitrogen atmosphere for 2- 5 minutes. Benzoyl chloride (0.71 ml, 6.1 mmol) was added to it and reaction mixture was stirred at rt for 2 to 4 hour. DCM (50 ml) was added to the reaction and extracted with water after completion of the reaction. The organic layer was washed with NaHCO<sub>3</sub> and brine solutions followed by drying on anhydrous sodium sulfate and

concentrated to obtain 0.78 g of 5-azido-2-benzoyloxy tropone as beige colour solid in 95% yield.  $^1\text{H}$  NMR (400 MHz,  $\text{CDCl}_3$ )  $\delta$  8.17 (d,  $J = 7.1$  Hz, 2H), 7.63 (t,  $J = 7.5$  Hz, 1H), 7.50 (t,  $J = 7.8$  Hz, 2H), 7.28 (d,  $J = 9.7$  Hz, 2H), 6.80 (d,  $J = 167.0$  Hz, 2H),  $^{13}\text{C}$  NMR (101 MHz,  $\text{CDCl}_3$ )  $\delta$  ppm 164.12, 145.61, 133.96, 133.75, 130.62, 130.28, 128.84, 128.69, 128.58, HRMS ESI-Tof Calcd for ( $\text{C}_{14}\text{H}_9\text{N}_3\text{O}_3 + \text{Na}$ ) 290.0536, Found 290.0531.

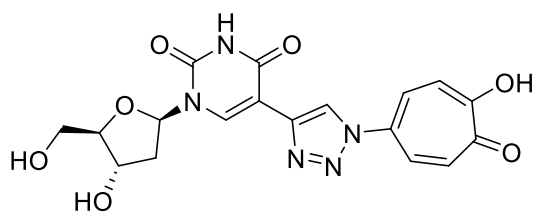
4-(4-(1-((2R,4S,5R)-4-hydroxy-5-(hydroxymethyl)tetrahydrofuran-2-yl)-2,4-dioxo-1,2,3,4-



tetrahydropyrimidin-5-yl)-1H-1,2,3-triazol-1-yl)-7-oxocyclohepta-1,3,5-trien-1-yl benzoate

(4): 5-ethynyl 2-deoxy uridine (0.25 g, 1 mmol), 5-azido 2-benzoyloxy tropolone (0.241 g, 1 mmol), copper iodide (0.194 g, 1 mmol), di-isopropylethylamine (0.355 ml, 2 mmol) dissolved in anhydrous dimethylformamide (5 ml) and stirred at  $70^\circ\text{C}$  for 24 h under nitrogen atmosphere. The reaction mixture was evaporated in a rotavapor followed by column chromatography (MeOH:DCM) to get 0.334 g of yellow colour solid in 65% yield.  $^1\text{H}$  NMR (400 MHz, DMSO)  $\delta$  11.80 (s, 1H), 8.99 (s, 1H), 8.73 (s, 1H), 8.11 (t,  $J = 22.9$  Hz, 4H), 7.77 (t,  $J = 6.9$  Hz, 1H), 7.63 (t,  $J = 6.9$  Hz, 4H), 6.25 (s, 1H), 5.32 (s, 1H), 5.09 (s, 1H), 4.30 (s, 1H), 3.88 (s, 1H), 3.63 (s, 2H), 2.22 (s, 2H),  $^{13}\text{C}$  NMR (101 MHz, DMSO)  $\delta$  163.76, 161.53, 150.11, 141.05, 140.16, 137.68, 134.83, 130.47, 129.54, 128.68, 121.26, 104.77, 88.22, 85.47, 71.08, 61.82, HRMS ESI-Tof Calcd for ( $\text{C}_{25}\text{H}_{21}\text{N}_5\text{O}_8 + \text{Na}$ ) 542.1282, Found 542.1260.

1-((2R,4S,5R)-4-hydroxy-5-(hydroxymethyl)tetrahydrofuran-2-yl)-5-(1-(4-hydroxy-5-



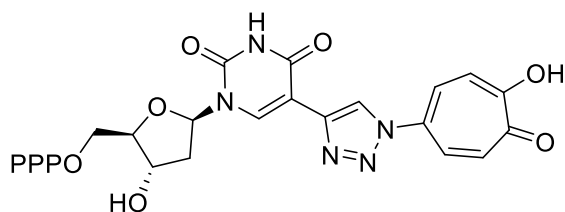
oxocyclohepta-1,3,6-trien-1-yl)-1H-1,2,3-

triazol-4-ylpyrimidine-2,4(1H,3H)-dione (5):

Compound 4 (50 mg, 0.05 mmol) was dissolved in 3 ml MeOH and two drops of benzene. To the stirring solution, ammonia solution (1 ml) was added slowly at  $0^\circ\text{C}$ . After addition reaction was removed from the ice bath and allowed

to stir at room temperature for about 1.5 hours. After completion of the reaction, solvents were evaporated under reduced pressure. The compound was co-evaporated with DCM and Hexane. The product was precipitated using methanol/Diethyl ether and dried to get a yellow solid (37 mg, 93% yield).  $^1\text{H}$  NMR (400 MHz, DMSO)  $\delta$  8.63 (s, 1H), 7.96 (s, 1H), 7.87 (d,  $J$  = 7.6 Hz, 2H), 7.51 (d,  $J$  = 7.0 Hz, 1H), 7.45 (t,  $J$  = 7.3 Hz, 1H), 7.35 (s, 1H), 6.25 (t,  $J$  = 6.6 Hz, 1H), 5.31 (s, 1H), 5.06 (s, 1H), 4.30 (s, 1H), 3.87 (s, 1H), 3.62 (s, 2H), 2.21 (d,  $J$  = 5.3 Hz, 2H),  $^{13}\text{C}$  NMR (101 MHz, DMSO)  $\delta$  161.58, 150.15, 140.21, 137.03, 121.32, 105.33, 88.14, 85.30, 71.10, 61.85, HRMS ESI-Tof Calcd for ( $\text{C}_{18}\text{H}_{17}\text{N}_5\text{O}_7+\text{Na}$ ) 439.1104, Found 439.2038.

((2R,3S,5R)-3-hydroxy-5-(5-(1-(4-hydroxy-5-oxocyclohepta-1,3,6-trien-1-yl)-1H-1,2,3-triazol-4-yl)-2,4-dioxo-3,4-dihydropyrimidin-1(2H)-yl)tetrahydrofuran-2-yl)methyl



tetrahydrogen triphosphate (**6**): To a solution of compound (**4**) (70 mg, 0.134 mmol, 1.0 equiv) in trimethyl phosphate, freshly distilled  $\text{POCl}_3$  (31  $\mu\text{L}$ , 0.337 mmol, 2.5 equiv) was

added in ice-cold condition under argon atmosphere. The solution was stirred for 24 hr at  $\sim 4^\circ\text{C}$ . After 24 h, it was observed that the starting material wasn't completely consumed. Bis(tributylammonium) pyrophosphate (370 mg, 0.674 mmol, 5.0 equiv.) in DMF and tributylamine (0.351 ml, 1.48 mmol, 11.0 equiv.) were simultaneously added to the reaction mixture in ice-cold condition. The reaction was continued for 30 min at  $4^\circ\text{C}$  and quenched with 1 M triethyl ammonium bicarbonate buffer (TEAB, 15 ml), and washed with ethyl acetate. The aqueous layer was evaporated and purified using a DEAE Sephadex-A25 anion exchange column (0.1M– 1M TEAB buffer, pH 7.5) followed by HPLC (TEAB buffer and acetonitrile solvent system). Evaporation of the appropriate fraction resulted in the desired triphosphate in 11% yield (10 mg) as a triethyl ammonium salt.  $^1\text{H}$  NMR (400 MHz,  $\text{D}_2\text{O}$ )  $\delta$

8.38 (s, 2H), 7.55 (s, 1H), 7.51 (d,  $J = 13.1$  Hz, 1H), 6.68 (d,  $J = 31.2$  Hz, 1H), 6.37 – 6.21 (m, 1H), 5.92 (d,  $J = 20.6$  Hz, 1H), 4.05 (s, 1H), 2.90 (d,  $J = 8.5$  Hz, 2H), 2.54 (s, 3H),  $^{31}\text{P}$  NMR (162 MHz,  $\text{D}_2\text{O}$ )  $\delta$  6.36 (d,  $J = 10.0$  Hz), -10.43 (d,  $J = 25.7$  Hz), -22.9 (t), HRMS ESI-Tof Calcd for ( $\text{C}_{18}\text{H}_{20}\text{N}_5\text{O}_{16}\text{P}_3\text{-H}$ ) 652.9956, Found 652.9969.

*Photophysical studies of tt-dU (5)*: All the Absorption and Emission spectra of the compound **5** (10  $\mu\text{M}$ ) were measured in different solvents using their respective spectrophotometer with a cell of 1 cm path length. Spectroscopy samples were prepared from concentrated DMSO stock solutions; hence, all samples contain 0.4 v% or 0.2 v% DMSO. Relative Quantum yield of nucleoside **5** in different solvents was determined relative to quinine sulfate as the standard. Following equation was used to calculate the quantum yield.

$$\Phi_{\text{F(x)}} = (A_{\text{s}}/A_{\text{x}})(F_{\text{x}}/F_{\text{s}})(n_{\text{x}}/n_{\text{s}})^2 \Phi_{\text{f(s)}}$$

Where s is the standard, x is the modified nucleoside, A is the absorbance at excitation wavelength, F is the area under the emission curve, n is the refractive index of the solvent, and  $\Phi_{\text{F}}$  is the quantum yield. Quantum yield of quinine sulfate in 0.1 M  $\text{H}_2\text{SO}_4$  is 0.54.

## 2B.6 References and Notes

- (1) Pu, F.; Ren, J.; Qu, X. Nucleobases, Nucleosides, and Nucleotides: Versatile Biomolecules for Generating Functional Nanomaterials. *Chem. Soc. Rev.* **2018**, 47 (4), 1285–1306.
- (2) Jaaenisch, R.; Bird, A.; Epigenetic Regulation of Gene Expressions: How the Genome Integrates Intrinsic and Environmental Signals. *Nat. Genet.* **2003**, 33 (3), 245–254.
- (3) Cohen, B. E.; McAnaney, T. B.; Park, E. S.; Jan, Y. N.; Boxer, S. G.; Jan, L. Y. Probing Protein Electrostatics with a Synthetic Fluorescent Amino Acid. *Science* (80-. ). **2002**, 296 (5573), 1700–1703.

- (4) Lee, H. S.; Guo, J.; Lemke, E. A.; Dimla, R. D.; Schultz, P. G. Genetic Incorporation of a Small, Environmentally Sensitive, Fluorescent Probe into Proteins in *Saccharomyces Cerevisiae*. *J. Am. Chem. Soc.* **2009**, *131* (36), 12921–12923.
- (5) Lavis, L. D.; Raines, R. T. Bright Building Blocks for Chemical Biology. *ACS Chem. Biol.* **2014**, *9* (4), 855–866.
- (6) Saito, Y.; Hudson, R. H. E. Base-Modified Fluorescent Purine Nucleosides and Nucleotides for Use in Oligonucleotide Probes. *J. Photochem. Photobiol. C Photochem. Rev.* **2018**, *36*, 48–73.
- (7) Dziuba, D.; Didier, P.; Ciaco, S.; Barth, A.; Seidel, C. A. M.; Mély, Y. Fundamental Photophysics of Isomorphic and Expanded Fluorescent Nucleoside Analogues. *Chem. Soc. Rev.* **2021**, *50* (12), 7062–7107.
- (8) Ghosh, P.; Kropp, H. M.; Betz, K.; Ludmann, S.; Diederichs, K.; Marx, A.; Srivatsan, S. G. Microenvironment-Sensitive Fluorescent Nucleotide Probes from Benzofuran, Benzothiophene, and Selenophene as Substrates for DNA Polymerases. *J. Am. Chem. Soc.* **2022**, *144* (23), 10556–10569.
- (9) Dziuba, D.; Pospíšil, P.; Matyašovský, J.; Brynda, J.; Nachtigallová, D.; Rulíšek, L.; Pohl, R.; Hof, M.; Hocek, M. Solvatochromic Fluorene-Linked Nucleoside and DNA as Color-Changing Fluorescent Probes for Sensing Interactions. *Chem. Sci.* **2016**, *7* (9), 5775–5785.
- (10) Güixens-Gallardo, P.; Hocek, M. Acetophenyl-thienyl-aniline-linked Nucleotide for Construction of Solvatochromic Fluorescence Light-up DNA Probes Sensing Protein-DNA Interactions. *Chem. Eur. J.* **2021**, *27* (24), 7090–7093.
- (11) Loving, G. S.; Sainlos, M.; Imperiali, B. Monitoring Protein Interactions and



- Dynamics with Solvatochromic Fluorophores. *Trends Biotechnol.* **2010**, 28 (2), 73–83.
- (12) Amaro, M.; Šachl, R.; Jurkiewicz, P.; Coutinho, A.; Prieto, M.; Hof, M. Time-Resolved Fluorescence in Lipid Bilayers: Selected Applications and Advantages over Steady State. *Biophys. J.* **2014**, 107 (12), 2751–2760.
- (13) Wu, F.-Y.; Xiang, Y.-L.; Wu, Y.-M.; Xie, F.-Y. Study of Interaction of a Fluorescent Probe with DNA. *J. Lumin.* **2009**, 129 (11), 1286–1291.
- (14) Dadová, J.; Orság, P.; Pohl, R.; Brázdová, M.; Fojta, M.; Hocek, M. Vinylsulfonamide and Acrylamide Modification of DNA for Cross-linking with Proteins. *Angew. Chemie* **2013**, 125 (40), 10709–10712.
- (15) Hocek, M. Enzymatic Synthesis of Base-Functionalized Nucleic Acids for Sensing, Cross-Linking, and Modulation of Protein–DNA Binding and Transcription. *Acc. Chem. Res.* **2019**, 52 (6), 1730–1737.
- (16) Dziuba, D.; Jurkiewicz, P.; Cebecauer, M.; Hof, M.; Hocek, M. A Rotational BODIPY Nucleotide: An Environment-Sensitive Fluorescence-Lifetime Probe for DNA Interactions and Applications in Live-Cell Microscopy. *Angew. Chemie* **2016**, 128 (1), 182–186.
- (17) Ferrero, M.; Gotor, V. Biocatalytic Selective Modifications of Conventional Nucleosides, Carbocyclic Nucleosides, and C-Nucleosides. *Chem. Rev.* **2000**, 100 (12), 4319–4348.
- (18) Ichikawa, E.; Kato, K. Sugar-Modified Nucleosides in Past 10 Years, a Review. *Curr. Med. Chem.* **2001**, 8 (4), 385–423.
- (19) Pathak, T. Azidonucleosides: Synthesis, Reactions, and Biological Properties. *Chem.*

- Rev.* **2002**, *102* (5), 1623–1668.
- (20) De Clercq, E. Strategies in the Design of Antiviral Drugs. *Nat. Rev. drug Discov.* **2002**, *1* (1), 13–25.
  - (21) Clercq, E. De. Antivirals and Antiviral Strategies. *Nat. Rev. Microbiol.* **2004**, *2* (9), 704–720.
  - (22) Joubert, N.; Pohl, R.; Klepetářová, B.; Hocek, M. Modular and Practical Synthesis of 6-Substituted Pyridin-3-Yl C-Nucleosides. *J. Org. Chem.* **2007**, *72* (18), 6797–6805.
  - (23) Kapdi, A. R.; Maiti, D.; Sanghvi, Y. S. *Palladium-Catalyzed Modification of Nucleosides, Nucleotides and Oligonucleotides*; Elsevier, 2018.
  - (24) Kapdi, A. R.; Sanghvi, Y. S. The Future of Drug Discovery: The Importance of Modified Nucleosides, Nucleotides, and Oligonucleotides. In *Palladium-catalyzed modification of nucleosides, nucleotides and oligonucleotides*; Elsevier, 2018; pp 1–18.
  - (25) Perrone, D.; Marchesi, E.; Preti, L.; Navacchia, M. L. Modified Nucleosides, Nucleotides and Nucleic Acids via Click Azide-Alkyne Cycloaddition for Pharmacological Applications. *Molecules* **2021**, *26* (11), 3100.
  - (26) Fantoni, N. Z.; El-Sagheer, A. H.; Brown, T. A Hitchhiker's Guide to Click-Chemistry with Nucleic Acids. *Chem. Rev.* **2021**, *121* (12), 7122–7154.
  - (27) Agrahari, A. K.; Bose, P.; Jaiswal, M. K.; Rajkhowa, S.; Singh, A. S.; Hotha, S.; Mishra, N.; Tiwari, V. K. Cu (I)-Catalyzed Click Chemistry in Glycoscience and Their Diverse Applications. *Chem. Rev.* **2021**, *121* (13), 7638–7956.
  - (28) El-Sagheer, A. H.; Brown, T. Efficient RNA Synthesis by in Vitro Transcription of a

- Triazole-Modified DNA Template. *Chem. Commun.* **2011**, 47 (44), 12057–12058.
- (29) Devaraj, N. K.; Finn, M. G. Introduction: Click Chemistry. *Chemical Reviews*. ACS Publications 2021, pp 6697–6698.
- (30) Kolb, H. C.; Sharpless, K. B. ;The Growing Impact of Click Chemistry on Drug Discovery. *Drug Discov. Today* **2003**, 8 (24), 1128–1137.
- (31) Finn, M. G.; Kolb, H. C.; Sharpless, K. B. Click Chemistry Connections for Functional Discovery. *Nat. Synth.* **2022**, 1 (1), 8–10.
- (32) Klöcker, N.; Weissenboeck, F. P.; Rentmeister, A. Covalent Labeling of Nucleic Acids. *Chem. Soc. Rev.* **2020**, 49 (23), 8749–8773.
- (33) Chandrasekaran, K. S.; Rentmeister, A. Clicking a Fish: Click Chemistry of Different Biomolecules in Danio Rerio. *Biochemistry* **2018**, 58 (1), 24–30.
- (34) Haque, M. M.; Sun, H.; Liu, S.; Wang, Y.; Peng, X. Photoswitchable Formation of a DNA Interstrand Cross-Link by a Coumarin-Modified Nucleotide. *Angew. Chemie Int. Ed.* **2014**, 53 (27), 7001–7005.
- (35) Ming, X.; Seela, F. A Nucleobase-discriminating Pyrrolo-dC Click Adduct Designed for DNA Fluorescence Mismatch Sensing. *Chem. Eur. J.* **2012**, 18 (31), 9590–9600.
- (36) Hornum, M.; Kumar, P.; Podsiadly, P.; Nielsen, P. Increasing the Stability of DNA: RNA Duplexes by Introducing Stacking Phenyl-Substituted Pyrazole, Furan, and Triazole Moieties in the Major Groove. *J. Org. Chem.* **2015**, 80 (19), 9592–9602.
- (37) Kumar, P.; Hornum, M.; Nielsen, L. J.; Enderlin, G.; Andersen, N. K.; Len, C.; Hervé, G.; Sartori, G.; Nielsen, P. ;High-Affinity RNA Targeting by Oligonucleotides Displaying Aromatic Stacking and Amino Groups in the Major Groove. Comparison

- of Triazoles and Phenyl Substituents. *J. Org. Chem.* **2014**, 79 (7), 2854–2863.
- (38) Balintová, J.; Špaček, J.; Pohl, R.; Brázdová, M.; Havran, L.; Fojta, M.; Hocek, M. Azidophenyl as a Click-Transformable Redox Label of DNA Suitable for Electrochemical Detection of DNA–Protein Interactions. *Chem. Sci.* **2015**, 6 (1), 575–587.
- (39) Ami, T.; Fujimoto, K. Click Chemistry as an Efficient Method for Preparing a Sensitive DNA Probe for Photochemical Ligation. *ChemBioChem* **2008**, 9 (13), 2071–2074.
- (40) Guo, H.; Roman, D.; Beemelmans, C. Tropolone Natural Products. *Nat. Prod. Rep.* **2019**, 36 (8), 1137–1155.
- (41) Ononye, S. N.; VanHeyst, M. D.; Oblak, E. Z.; Zhou, W.; Ammar, M.; Anderson, A. C.; Wright, D. L. Tropolones as Lead-like Natural Products: The Development of Potent and Selective Histone Deacetylase Inhibitors. *ACS Med. Chem. Lett.* **2013**, 4 (8), 757–761.
- (42) Meher, S.; Kumari, S.; Dixit, M.; Sharma, N. K. Cu-Catalyzed Synthesis of Alkylaminotroponyl Sulfones as Pseudomonas Aeruginosa Quorum Sensing Inhibitors Targeting LasI/R QS Circuitry. *Chem. Asian J.* **2022**, 17 (23), e202200866.
- (43) Breheret, E. F.; Martin, M. M. Electronic Relaxation of Troponoids: Tropolone Fluorescence. *J. Lumin.* **1978**, 17 (1), 49–60.
- (44) Muetterties, E. L.; Roesky, H.; Wright, C. M. Chelate Chemistry. V. Metal Chelates Based on Tropolone and Its Derivatives. *J. Am. Chem. Soc.* **1966**, 88 (21), 4856–4861.
- (45) Dochnahl, M.; Löhnwitz, K.; Lühl, A.; Pissarek, J.-W.; Biyikal, M.; Roesky, P. W.;

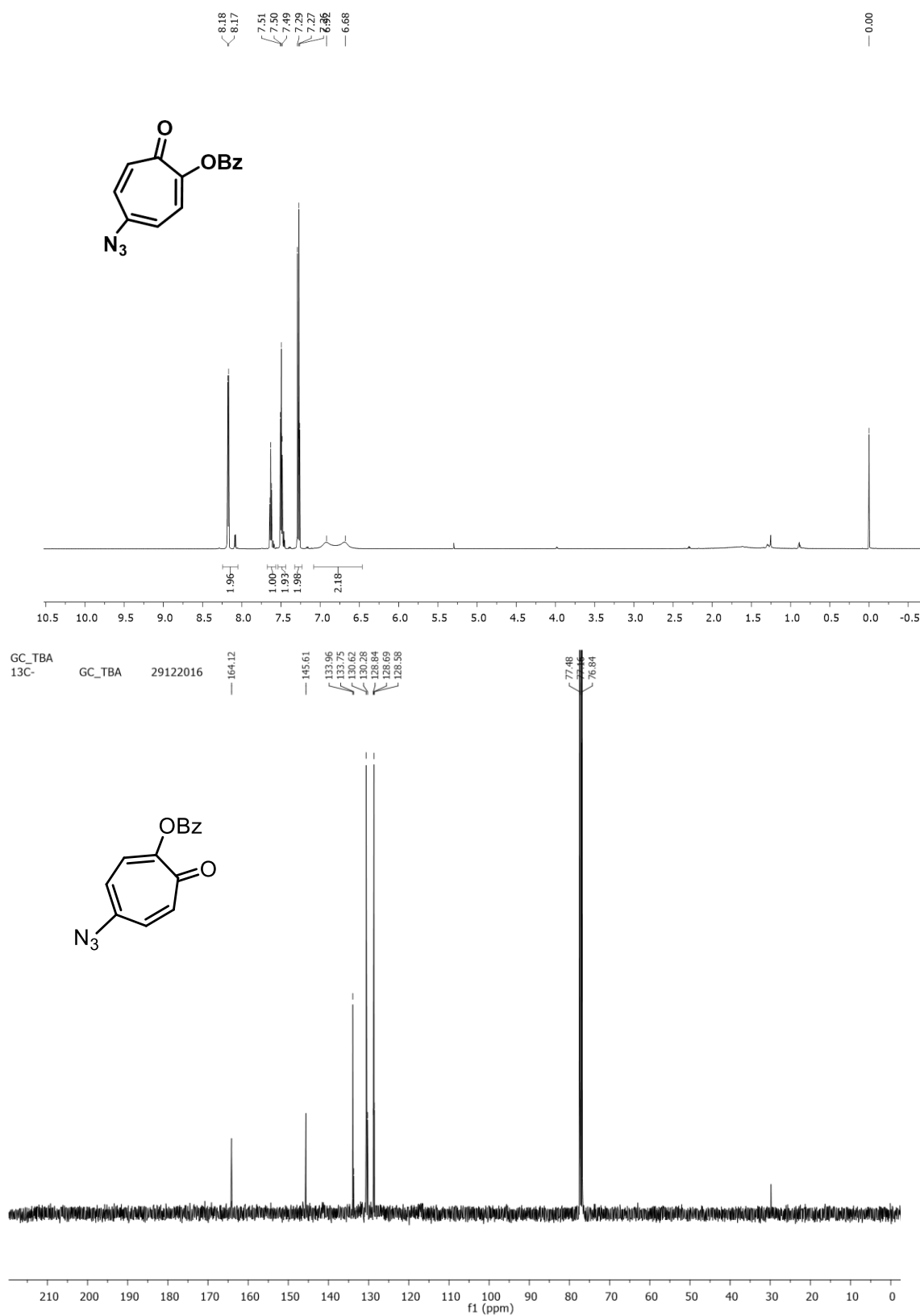
- Blechert, S. Functionalized Aminotroponimate Zinc Complexes as Catalysts for the Intramolecular Hydroamination of Alkenes. *Organometallics* **2010**, 29 (12), 2637–2645.
- (46) Meyer, N.; Löhnwitz, K.; Zulys, A.; Roesky, P. W.; Dochnahl, M.; Blechert, S. ;Aminotroponate Zinc Complexes as Catalysts for the Intramolecular Hydroamination of Alkenes and Alkynes. *Organometallics* **2006**, 25 (15), 3730–3734.
- (47) Meher, S.; Gade, C. R.; Sharma, N. K. Tropolone-Conjugated DNA: A Fluorescent Thymidine Analogue Exhibits Solvatochromism, Enzymatic Incorporation into DNA and HeLa Cell Internalization. *ChemBioChem* **2022**, e202200732.
- (48) Bollu, A.; Sharma, N. K. Tropolone-Conjugated DNA: Fluorescence Enhancement in the Duplex. *ChemBioChem* **2019**, 20 (11), 1467–1475.
- (49) Bollu, A.; Panda, S. S.; Sharma, N. K. Fluorescent DNA Analog: 2-Aminotroponyl-Pyrrolyl-2'-Deoxyuridiny DNA Oligo Enhance Fluorescence in DNA-Duplex as Compared to 2-Aminotroponyl-Ethynyl-2'-Deoxyuridiny DNA Oligo. *Nucleosides. Nucleotides Nucleic Acids* **2022**, 1–15.
- (50) Palai, B. B.; Soren, R.; Sharma, N. K. ;BODIPY Analogues: Synthesis and Photophysical Studies of Difluoro Boron Complexes from 2-Aminotropone Scaffolds through N, O-Chelation. *Org. Biomol. Chem.* **2019**, 17 (26), 6497–6505.
- (51) Andersen, N. K.; Døssing, H.; Jensen, F.; Vester, B.; Nielsen, P. ;Duplex and Triplex Formation of Mixed Pyrimidine Oligonucleotides with Stacking of Phenyl-Triazole Moieties in the Major Groove. *J. Org. Chem.* **2011**, 76 (15), 6177–6187.
- (52) Anastasi, C.; Quéléver, G.; Burlet, S.; Garino, C.; Souard, F.; Kraus, J.-L. New Antiviral Nucleoside Prodrugs Await Application. *Curr. Med. Chem.* **2003**, 10 (18),

1825–1843.

- (53) Sinkeldam, R. W.; Greco, N. J.; Tor, Y. Fluorescent Analogs of Biomolecular Building Blocks: Design, Properties, and Applications. *Chem. Rev.* **2010**, *110* (5), 2579–2619.
- (54) Dunn, K. W.; Kamocka, M. M.; McDonald, J. H. A Practical Guide to Evaluating Colocalization in Biological Microscopy. *Am. J. Physiol. Physiol.* **2011**, *300* (4), C723–C742.
- (55) Potenziano, J.; Spitale, R.; Janik, M. E. Improved and Highly Versatile Synthesis of 5-Aryltropones. *Synth. Commun.* **2005**, *35* (15), 2005–2016.

## 2B.7 Appendix

1. $^1\text{H}$ , $^{13}\text{C}$ NMR (400MHz, $\text{CDCl}_3$ ) and HRMS of <b>3</b> .....	94
2. $^1\text{H}$ , $^{13}\text{C}$ NMR (400 MHz, DMSO) and HRMS of <b>4</b> .....	96
3. $^1\text{H}$ , $^{13}\text{C}$ NMR (400 MHz , DMSO) and HRMS of <b>5</b> .....	98
4. $^1\text{H}$ , $^{31}\text{P}$ NMR (400 MHz , $\text{D}_2\text{O}$ ) and HRMS of <b>6</b> .....	100

1.  $^1\text{H}$ ,  $^{13}\text{C}$  NMR (400MHz,  $\text{CDCl}_3$ ) and HRMS of **3**Figure A1.  $^1\text{H}/^{13}\text{C}$  NMR of Compound **3** in  $\text{CDCl}_3$ .

## Display Report

## Analysis Info

Analysis Name D:\Data\DEC-2016\NKS\GC\11102017\_NKS\_GC-TBA.d  
Method Wash.pos tune\_low\_22092017.m  
Sample Name ESI-MS  
Comment

Acquisition Date 10/13/2017 8:13:34 PM

Operator G.CREDDY  
Instrument microTOF-Q II 10337

## Acquisition Parameter

Source Type	ESI	Ion Polarity	Positive	Set Nebulizer	0.4 Bar
Focus	Active	Set Capillary	4500 V	Set Dry Heater	180 °C
Scan Begin	50 m/z	Set End Plate Offset	-500 V	Set Dry Gas	4.0 l/min
Scan End	3000 m/z	Set Collision Cell RF	200.0 Vpp	Set Divert Valve	Source

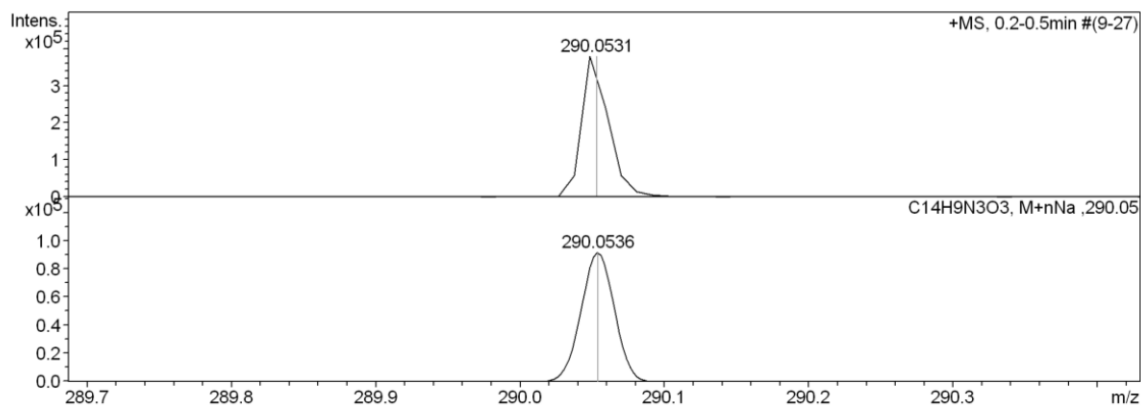
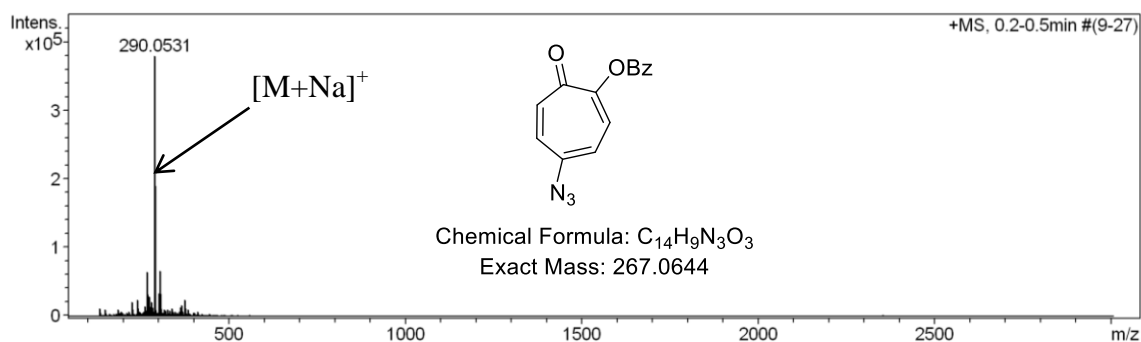
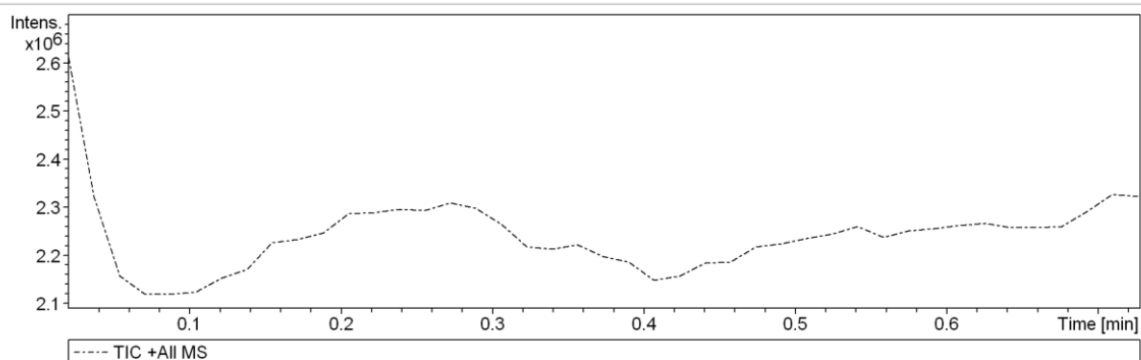
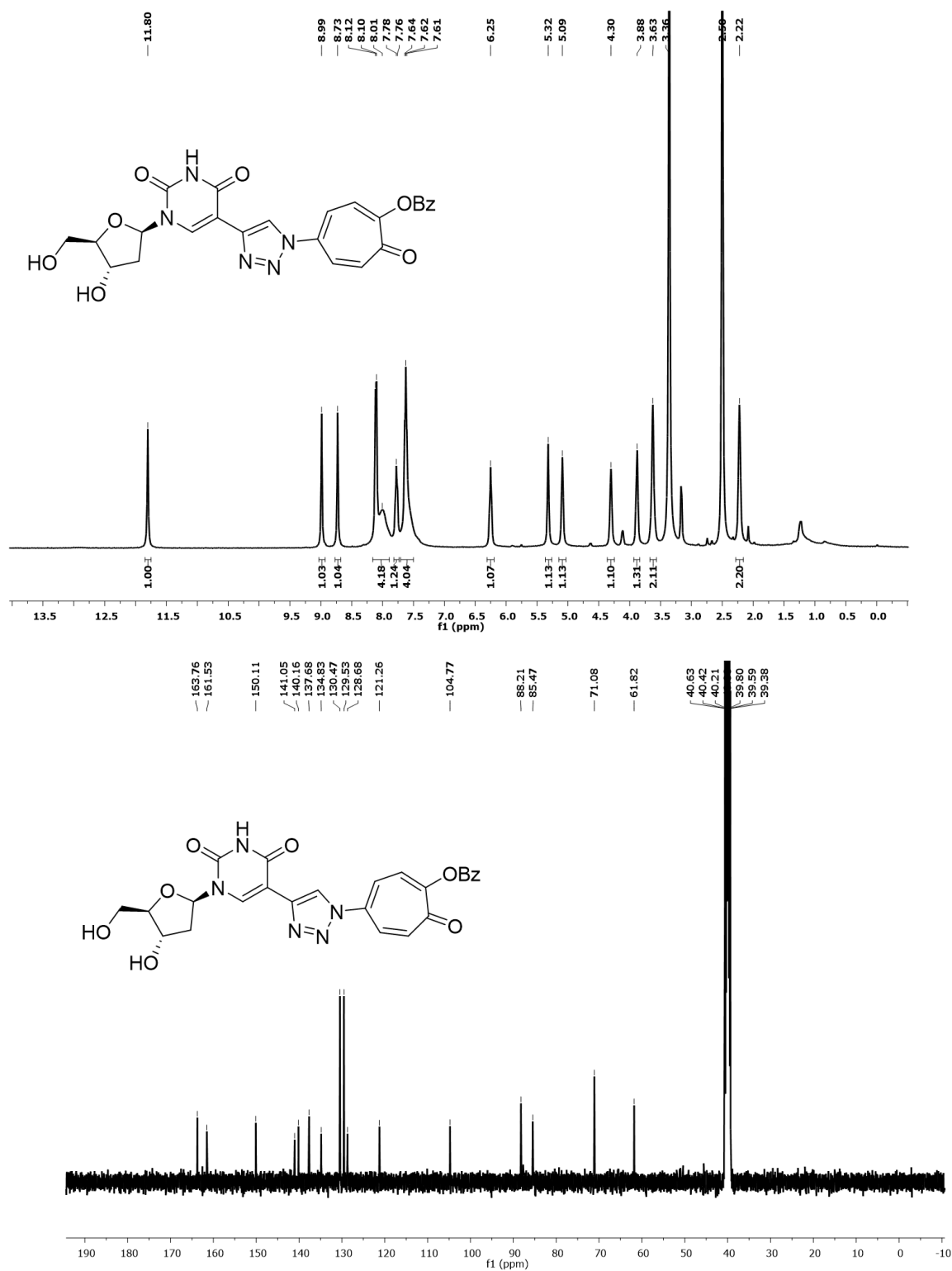
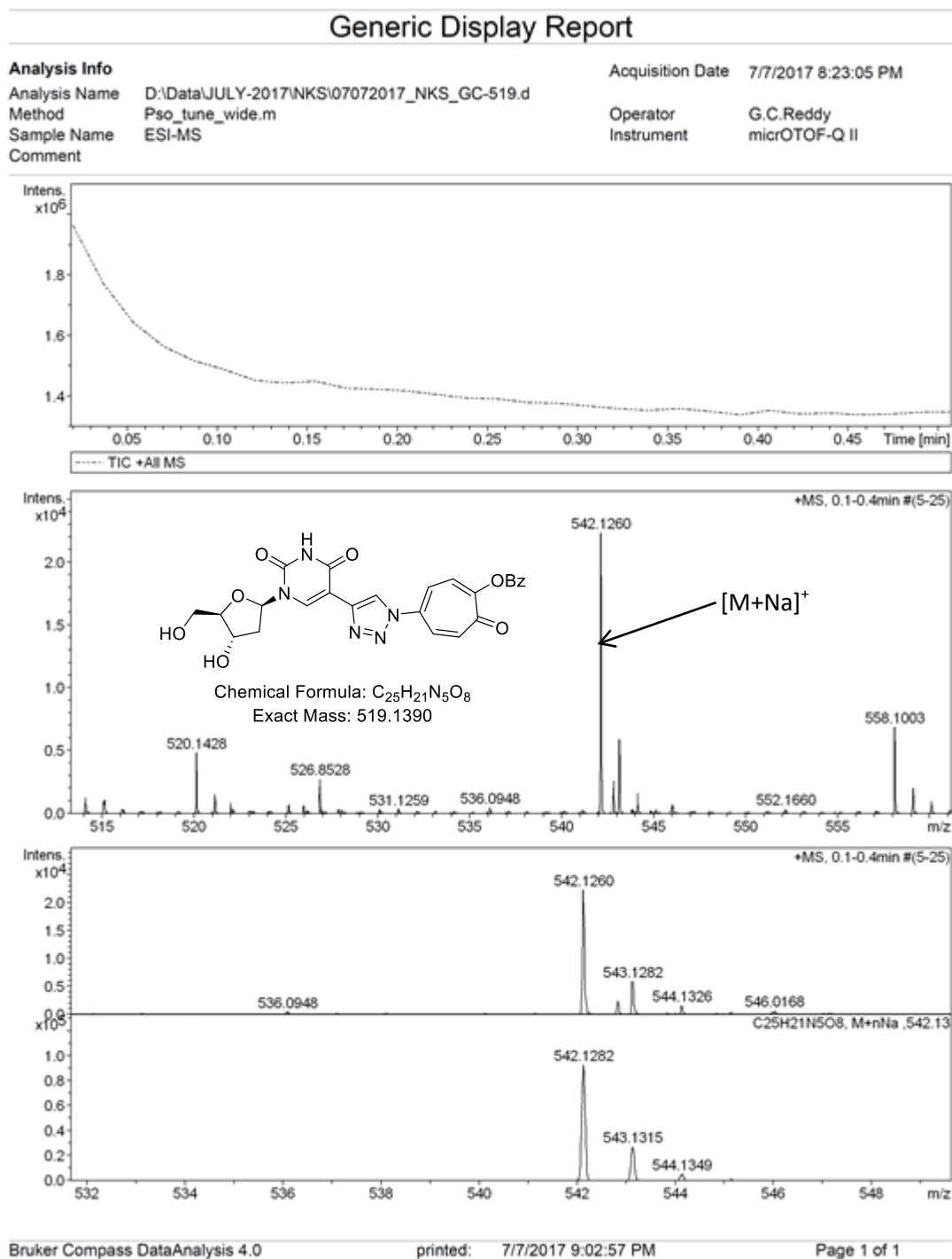
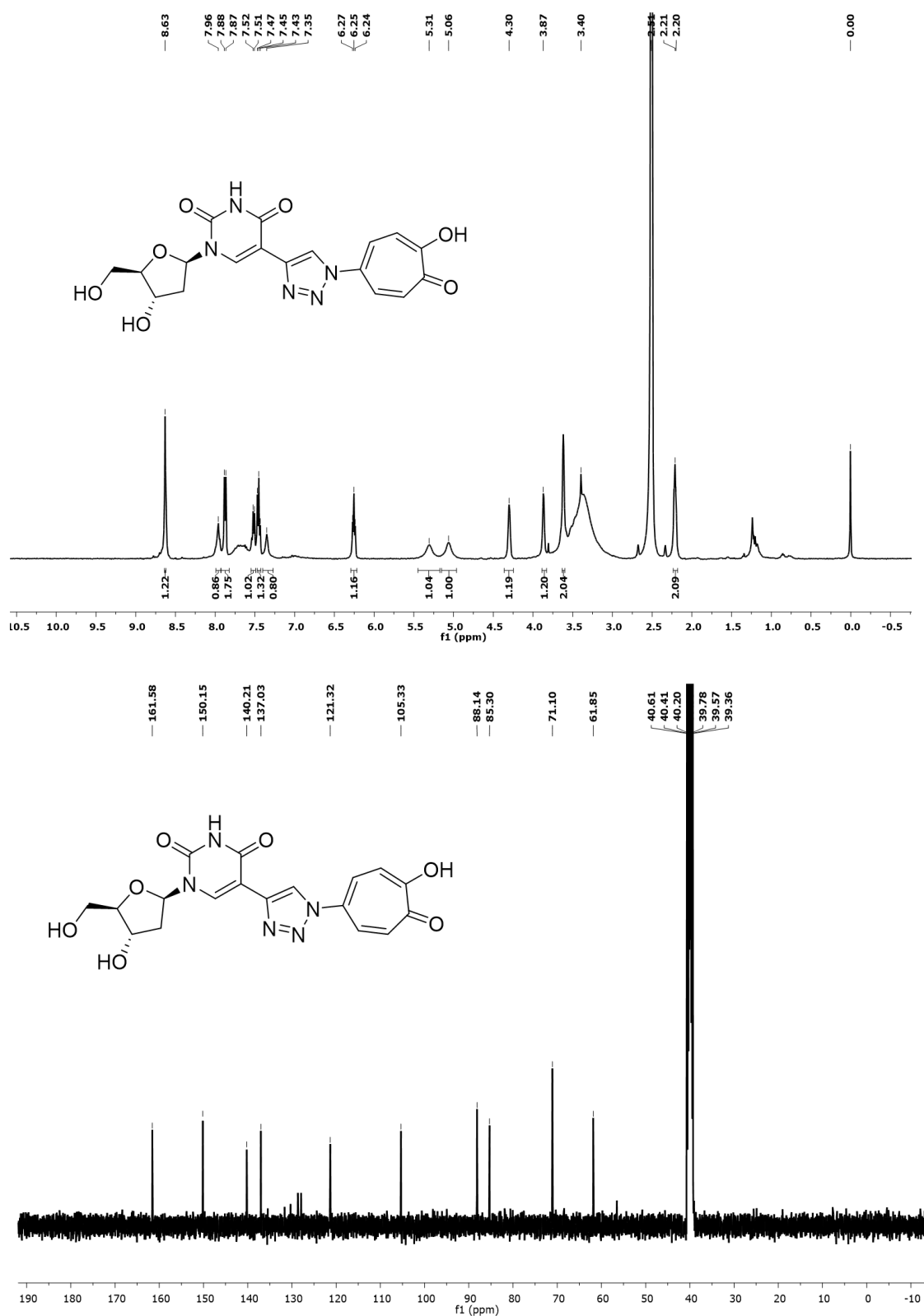


Figure A2. ESI-MS/HRMS spectra of compound 3.



2.  $^1\text{H}$ ,  $^{13}\text{C}$  NMR (400 MHz, DMSO) and HRMS of **4**Figure A3.  $^1\text{H}/^{13}\text{C}$  NMR of Compound **4** in DMSO- $d_6$ .

**Figure A4.** ESI-MS/HRMS spectra of compound **4**.

3.  $^1\text{H}$ ,  $^{13}\text{C}$  NMR (400 MHz, DMSO) and HRMS of **5**Figure A5.  $^1\text{H}/^{13}\text{C}$  NMR of Compound **5** in DMSO- $d_6$ .

NKS\_SNM\_TTS\_OH

15-Dec-2022

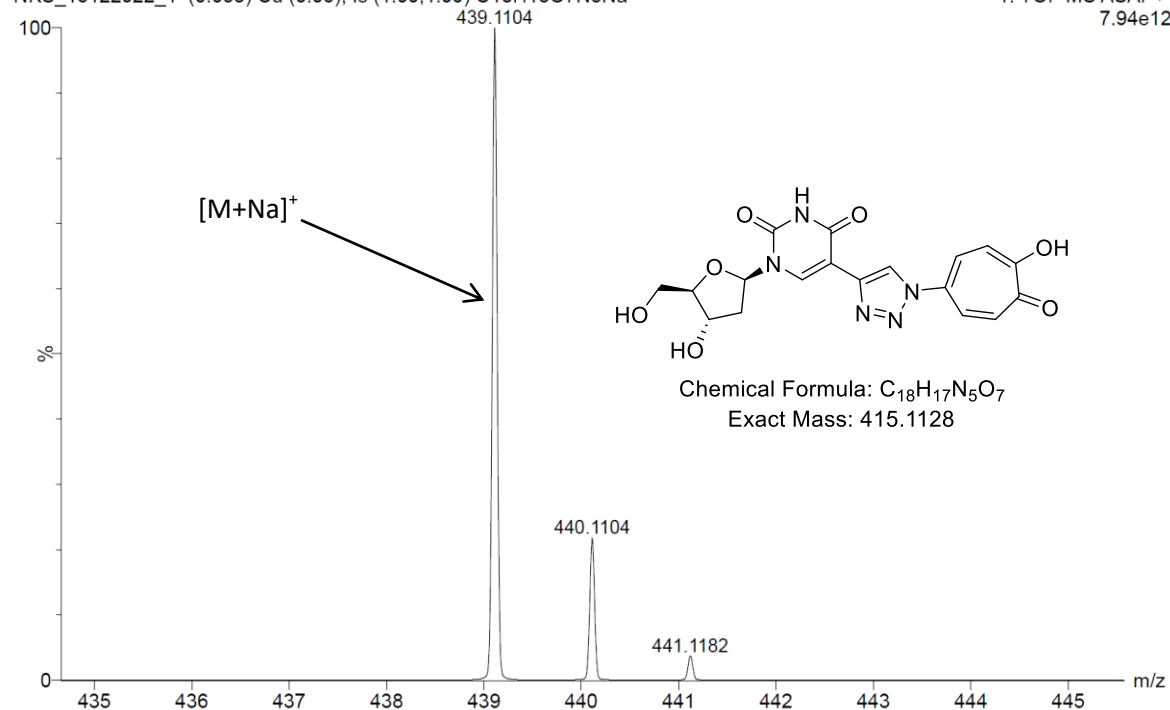
10:21:23

XEVO-G2XSQTOF#YFA1739

NKS\_15122022\_1 (0.053) Cu (0.05); Is (1.00,1.00) C<sub>18</sub>H<sub>18</sub>O<sub>7</sub>N<sub>5</sub>Na

1: TOF MS ASAP+

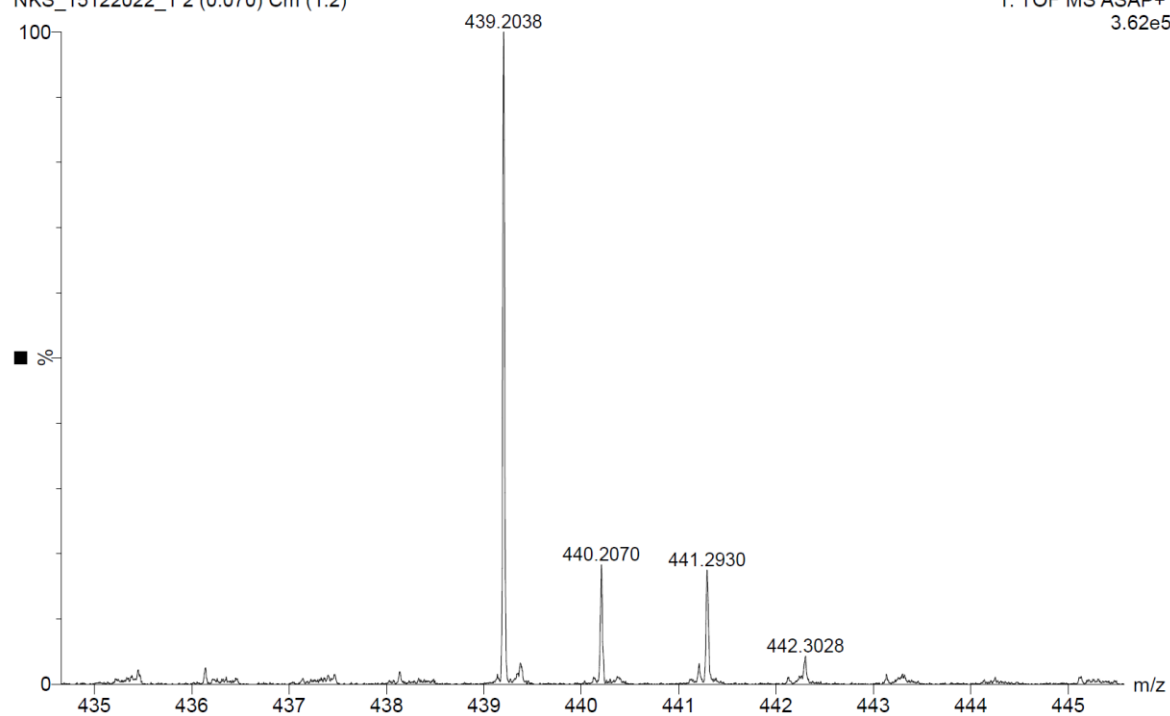
7.94e12

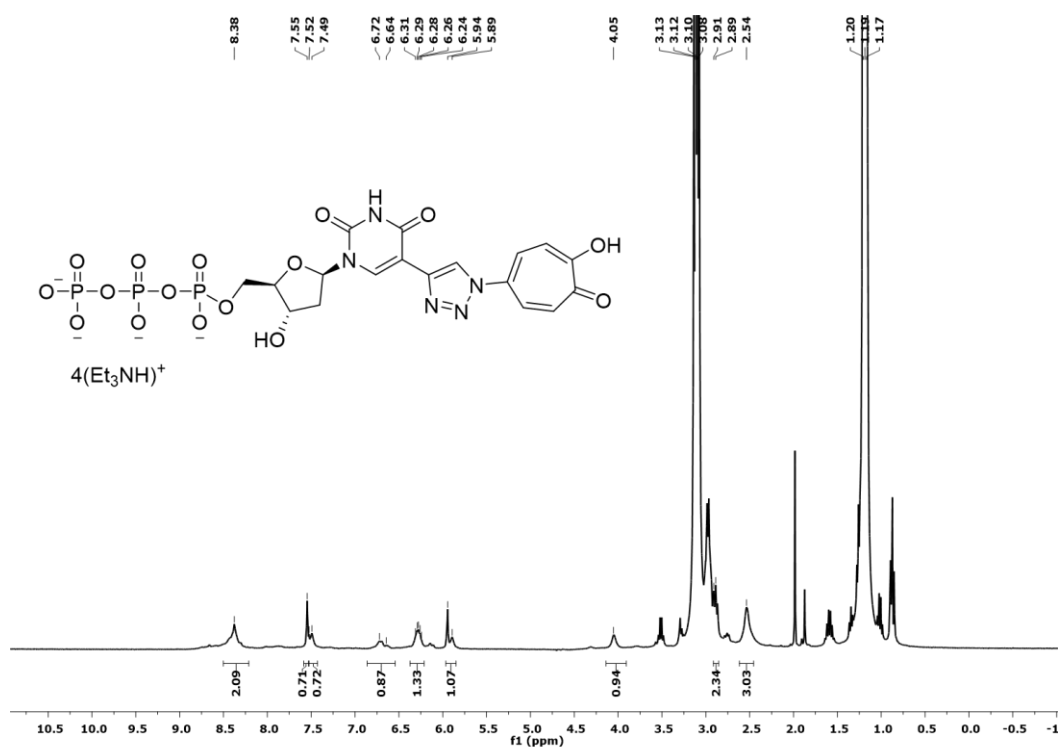
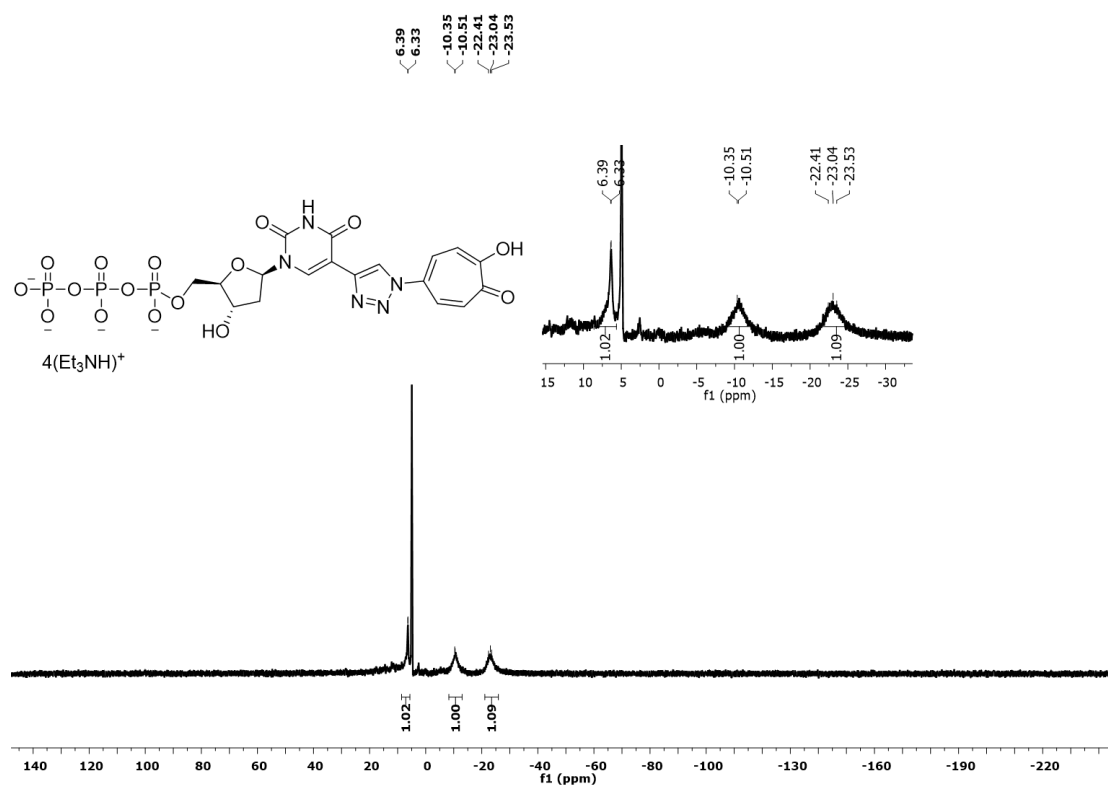


NKS\_15122022\_1 2 (0.070) Cm (1:2)

1: TOF MS ASAP+

3.62e5

**Figure A6.** ESI-MS/HRMS spectra of compound **5**.

4.  $^1\text{H}$ ,  $^{31}\text{P}$  NMR (400 MHz,  $\text{D}_2\text{O}$ ) and HRMS of **6**Figure A7.  $^1\text{H}$  NMR of Compound **6** after water suppression.Figure A8.  $^{31}\text{P}$  NMR of Compound **6** in  $\text{D}_2\text{O}$ .

## Generic Display Report

## Analysis Info

Analysis Name D:\Data\MAR-2017\NKS\22032017\_NKS\_GC\_519-HPLC-2-10.3.d  
Method neg\_tune\_low.m  
Sample Name Bruker micro TOF -Q II  
Comment

Acquisition Date 3/22/2017 7:56:06 PM

Operator Amit S.Sahu

Instrument microTOF-Q II

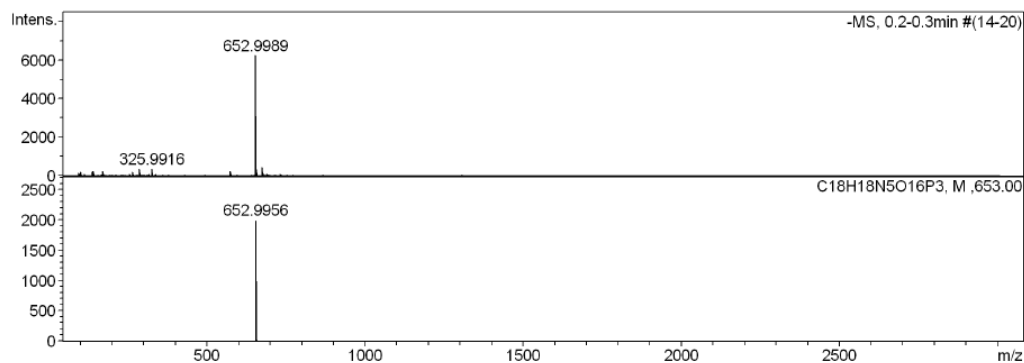
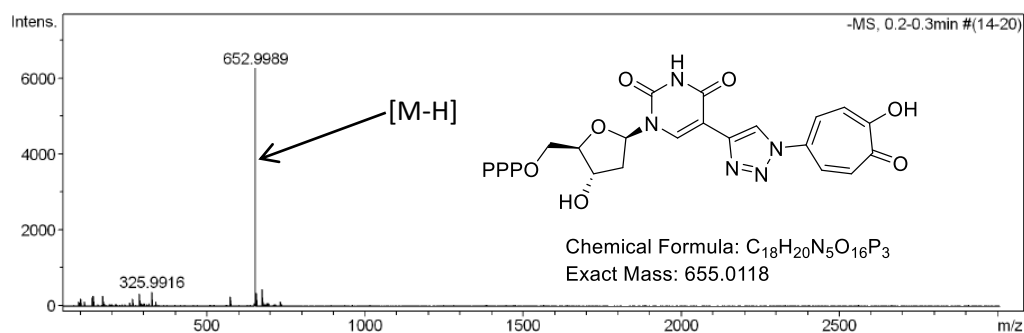
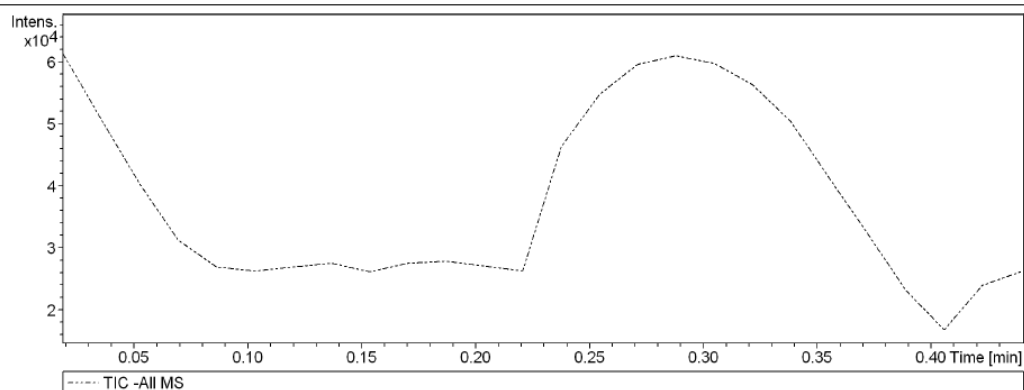


Figure A9. ESI-MS/HRMS spectra of compound 6.

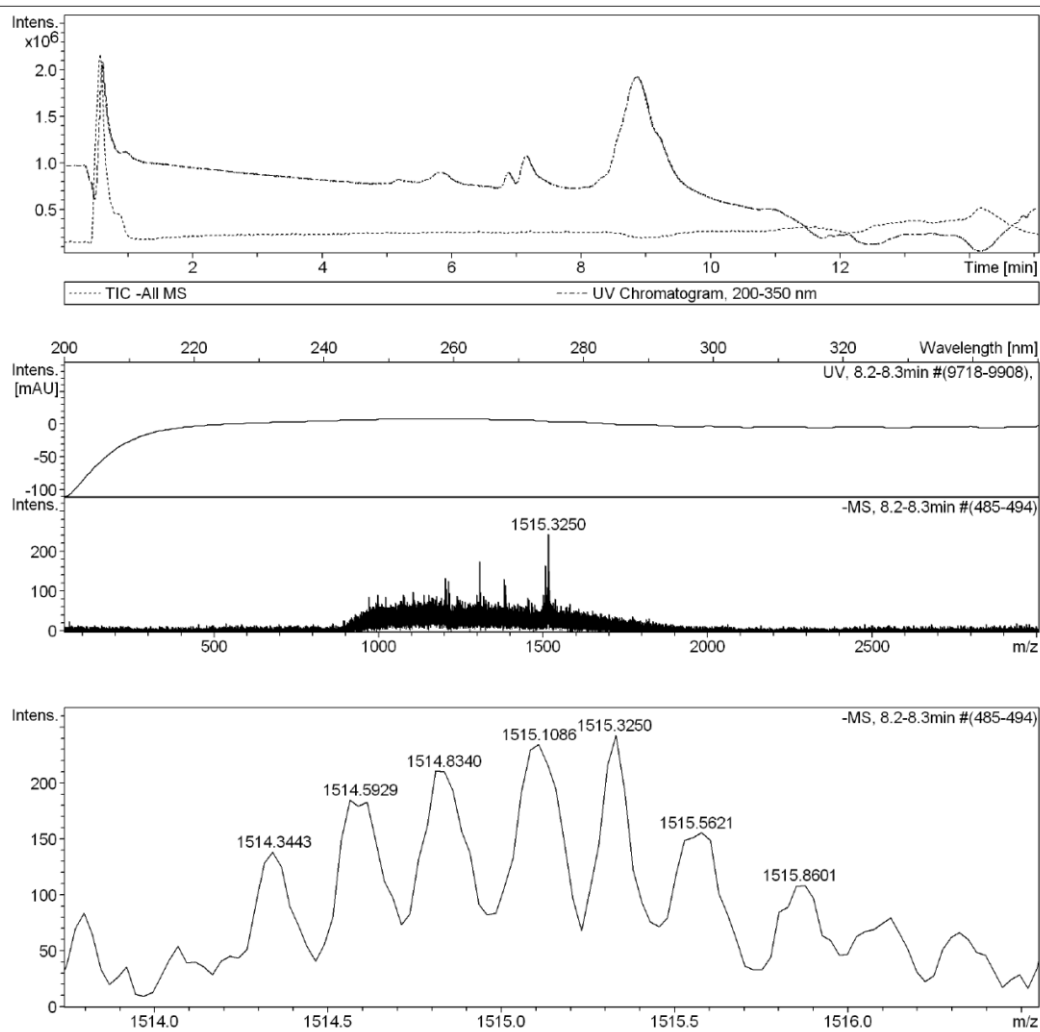
## Display Report

**Analysis Info**

Analysis Name	D:\Data\AUG-2016\NKS\GC\01042017_NKS_GC_P2-655_2-D_5_01_652.d
Method	cafeine-no-uv.m
Sample Name	01042017_NKS_GC_P2-655
Comment	
Acquisition Date	4/3/2017 8:46:25 PM
Operator	G.C.SREDDY
Instrument	microTOF-Q II 10337

**Acquisition Parameter**

Source Type	ESI	Ion Polarity	Negative	Set Nebulizer	1.7 Bar
Focus	Not active	Set Capillary	2800 V	Set Dry Heater	220 °C
Scan Begin	50 m/z	Set End Plate Offset	-500 V	Set Dry Gas	7.0 l/min
Scan End	3000 m/z	Set Collision Cell RF	2100.0 Vpp	Set Divert Valve	Waste



Calculated mass for extended primer =  $6009 + 54 \text{ (3 NH}_4\text{)} = 6063 / 4 = 1515.75$ , observed = 1515.32

**Figure A10.** LC-MS of primer extension reaction of DNA with compound 6.

## CHAPTER 3

### PART-A

---

### **Alkylaminotroponyl Sulfones as *Pseudomonas aeruginosa* Quorum Sensing Inhibitors**

---

#### **3A.1 Introduction**

#### **3A.2 Objective**

#### **3A.3 Results and Discussion**

#### **3A.4 Conclusion**

#### **3A.5 Experimental Section**

#### **3A.6 References and Notes**

#### **3A.7 Appendix**



### 3A.1 Introduction

Bacterial infections have remained a primary cause of concern throughout history.<sup>1</sup> Persistent use of antibiotics as monotherapy or in combination has definitely reduced mortality but at the same time is the leading cause of redundant emergence of antibiotic-resistant bacterial pathogenic strains.<sup>2</sup> Drug designing strategies must be changed in order to find a sustainable solution to counteract the emerging multidrug resistance issue.<sup>3</sup> One such multidrug-resistant and highly adaptable bacterium responsible for nosocomial infections is *Pseudomonas aeruginosa* (PA).<sup>4</sup> The bacterium is a well-known causative agent of cystic fibrosis and airway infections. Various reports suggest that the emergence of multidrug-resistant PA is higher than that of novel antibiotics produced for treating the same. It has been reported as the prime reason for hospital-acquired infection in European countries.<sup>5</sup> Biofilm formation, Pyocyanin secretion, and protease production are a few important virulent factors possessed by the bacterium.<sup>6</sup> Ability to form biofilm is an added advantage for this bacterium that reduces the efficacy of any drug by limiting its penetration potential inside the cell. These virulent factors, as well as their capacity to conquer antibiotics, are controlled by the complex cell to cell chemical signaling system known as quorum sensing (QS).<sup>7,8</sup> The *lasI/R* QS circuit regulates the expression of virulent factors.<sup>9</sup> Elastase, a protease encoded by *lasB* gene under QS regulon is the most virulent factor. It is responsible for disrupting the tight junctions between host epithelial cells. Pyocyanin production increases oxidative stress and alters the mitochondrial electron transport system of the host.<sup>10</sup> Therefore, drug-designing strategies should be advanced to control bacterial infections, aiming to inhibit the virulence factors against designing the complete bactericidal drugs. However, the development process might be a reason for concern owing to its safety issues against human uses. In the literature, sulfone derivatives are bioactive molecules that serve not only popular antibiotics but also potential drug candidates for the treatment of AIDS/HIV infection and Alzheimer's disease

(Figure 3A.1-a).<sup>11</sup> Tropolone, a non-benzenoid aromatic molecule, is a constituent of many troponoid natural products, which exhibit diverse biological activities such as antibacterial, anti-inflammatory, antitumor, and antiviral activity.<sup>12,13</sup> For example, the naturally occurring Thujaplicin and synthetic analog tropolonyl-naphthalenyl urea are potent antibiotics (Figure 3A.1-b/c). Thus we rationally designed troponyl-sulfones by synergizing sulfones and troponyl moieties in a single scaffold to explore their efficacy on PA (Figure 3A.1-d). Herein, we planned to synthesize troponyl-sulfone derivatives by modern metal catalyzed C-H activation methods because tropolone derivatives have metal-chelating properties.<sup>14</sup> Recently, the synthesis of sulfones has attracted more and more attention and direct sulfonylation of C–H bonds projects a new vision for sulfone synthesis leading to low atom and step economy.<sup>15,16</sup> Several groups such as Dong et al., Wei et al., Tan et al., and a group of We, Wu, Zeng, Manolikakes, and Zhang have reported the direct C-H sulfonylation of arenes based on Cu, Pd, Rh and Ru metals by the assistance of a directing group.<sup>17,18</sup> Additionally, sulfones could act as useful synthons for C–C bond formation via fragment coupling, Julia olefination and the Ramberg–Backlund rearrangement in synthetic chemistry.<sup>19–21</sup> This is the very first report which describes the synthesis of alkylaminotroponyl sulfone (ATS) derivatives through the Cu-catalyzed C(sp<sup>2</sup>)-H activation at tropone ring. This report also describes their biological activities as anti-quorum sensing agents against PA (PA14).

### 3A.2 Objective

The scarcity of novel bioactive molecules against multidrug-resistant (MDR) bacterial strains like *Pseudomonas aeruginosa* is alarming. This bacterial virulence is regulated via Quorum sensing (QS), a cell-cell communication process. Disabling QS circuits (*las*, *pqs*, *rhl*) with small molecules has been proposed as a potential strategy to prevent bacterial pathogenicity. This strategy focuses on the interruption of bacterial virulence, rather than killing them to tackle the drug resistance problem. In this chapter, we have rationally

designed troponyl sulfones and tested their bioactivity toward the PA14 strain. This is the first report describing the synthesis of alkylaminotroponyl sulfone (ATS) derivatives through the Cu-catalyzed C(sp<sup>2</sup>)-H activation at troponone ring.

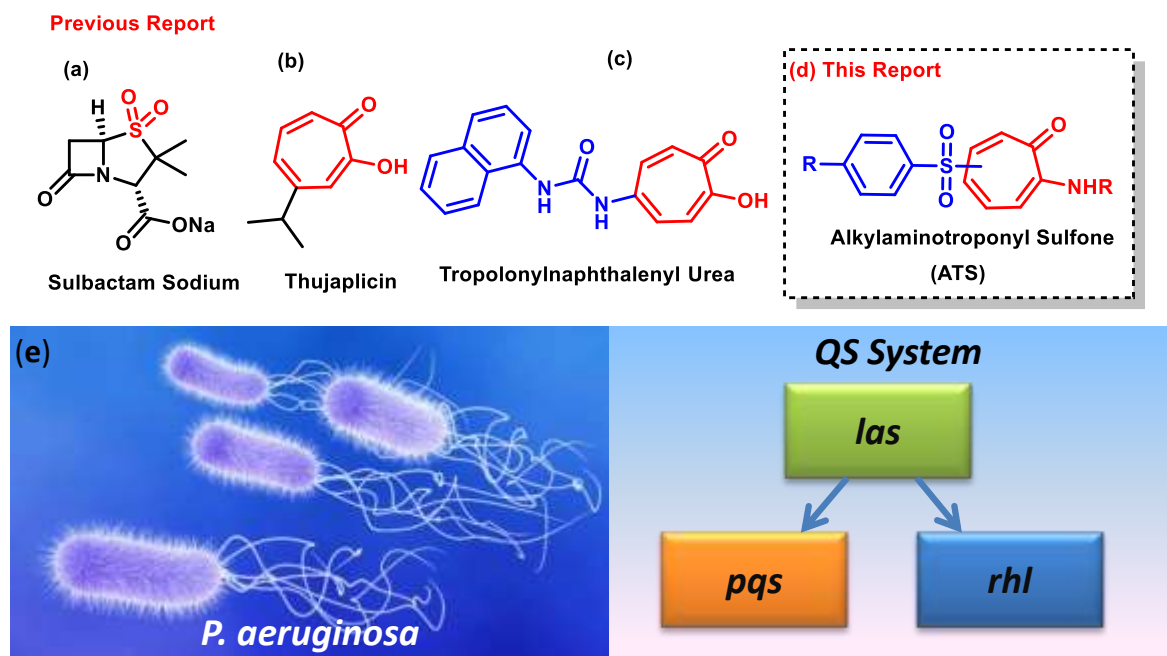
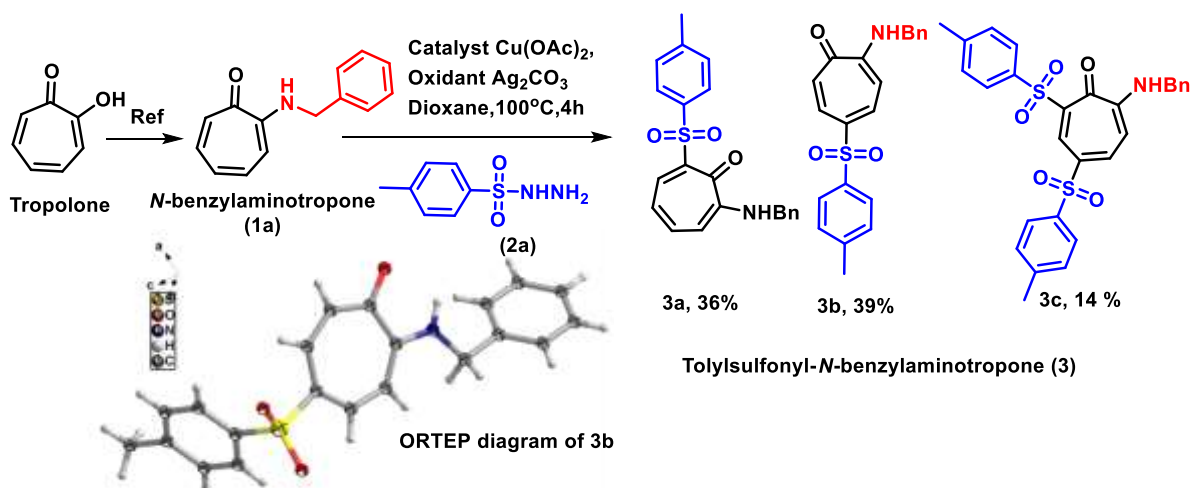


**Figure 3A.1.** Antibiotic and anti-quorum sensing compounds (reported and this report); (a-c) previous reports, (d) this report, (e) *Pseudomonas aeruginosa* and QS system.

### 3A.3 Results and Discussion

We began the synthesis of alkylaminotroponyl sulfone (ATS) derivatives from the commercially available Tropolone molecule. Tropolone was converted into *N*-alkylaminotroponone derivatives (**1**) by following the previously reported procedure.<sup>22</sup> Herein we synthesized three derivatives of aminotropones such as *N*-Benzylaminotroponone (**1a**), *N*-Isopropyl aminotroponone (**1b**) and *N*-Octylaminotroponone (**1c**). In Scheme 3A.1, the aminotroponone (**1a**) was treated with *p*-tolylsulfonyl hydrazide (**2a**) in presence of the Cu-catalyst Cu(OAc)<sub>2</sub> (10 mol %) and an oxidant Ag<sub>2</sub>CO<sub>3</sub> at 100 °C in solvent dioxane. After completion of the reaction, we isolated three types of ATS derivatives (**3a/3b/3c**) such as C-7

sulfonylated (**3a**), C-5 sulfonylated (**3b**) and C-5,7 disulfonylated (**3c**) with overall yield ca. 89%. We noticed that the C-7 sulfonylated (**3a**) and C-5 sulfonylated (**3b**) were major products with an approximate yield ratio (1:1) and a minor product C-5,7 disulfonylated (**3c**). However, the yield of C-5 derivative is slightly higher than the C-7. Their characterization data ( $^1\text{H}$ -/ $^{13}\text{C}$ -NMR/ESI-HRMS) are provided in the Appendix. Pleasantly, we obtained the single crystal of C-5 ATS derivative (**3b**) and studied it by X-ray diffractometer. Its solved X-ray data is submitted to the Cambridge crystallographic data centre (CCDC) with reference number 2169438. The ORTEP diagram of ATS (**3b**) is depicted in Scheme 3A.1, while other x-ray parameters are provided in the Appendix.



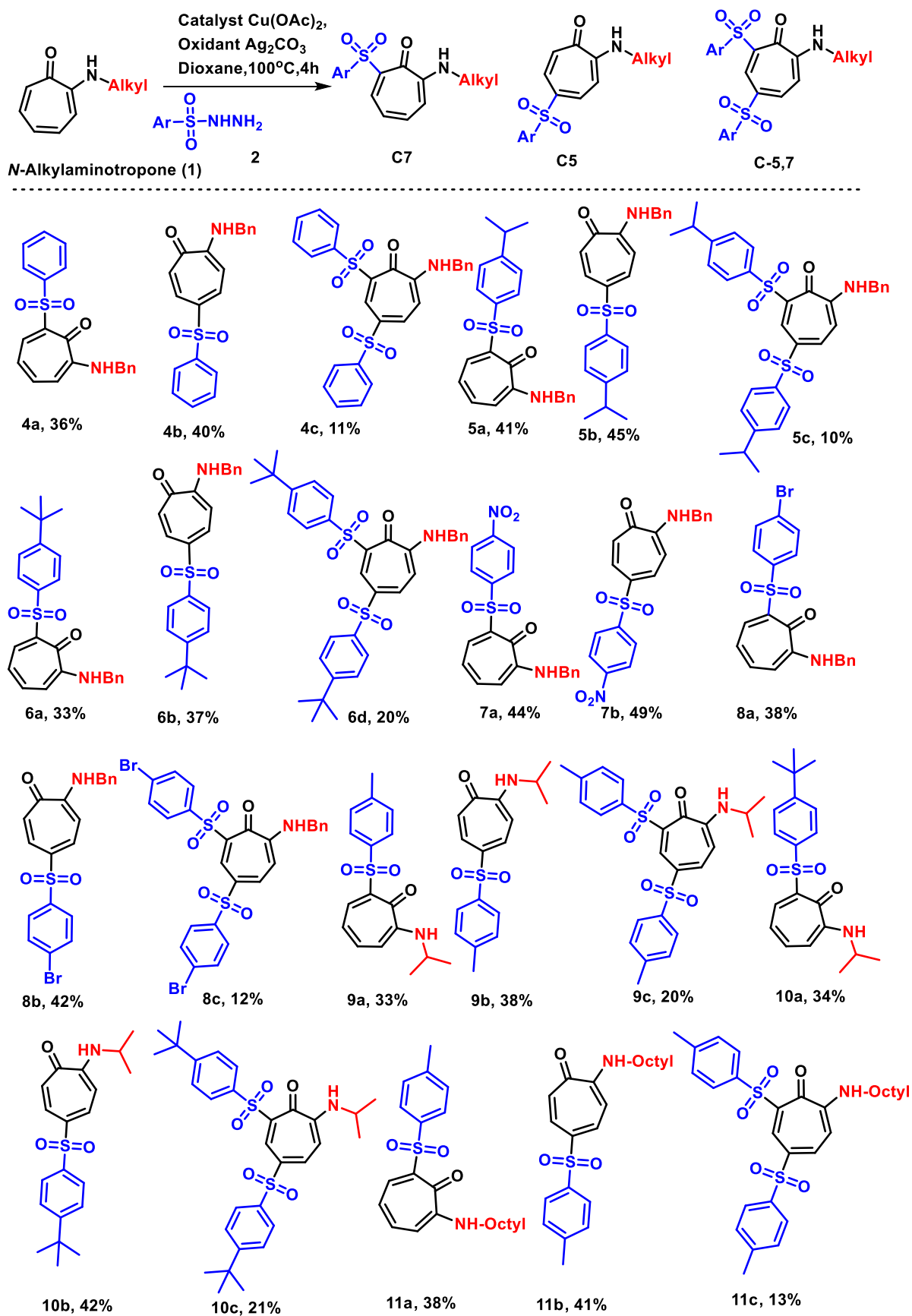
**Scheme 3A.1.** Synthesis of ATS derivatives *via* C(sp<sup>2</sup>)-H activation.

We optimized the reaction conditions for the synthesis of ATS derivatives by altering the catalyst, oxidant, solvent and temperature conditions. The optimization table is provided bellow (Table 3A.1). Our results show that the catalyst Cu(OAc)<sub>2</sub>, oxidant Ag<sub>2</sub>CO<sub>3</sub>, solvent 1,4-dioxane and temperature 100 °C are the optimized conditions for the synthesis of alkylaminotroponyl sulfone derivatives.

**Table 3A.1.** Optimization studies of ATS **3a/3b/3c**

Entry	Cu Salt	Oxidant	Solvent	Total yield
1	Cu(OAc) <sub>2</sub>	Ag <sub>2</sub> CO <sub>3</sub>	Dioxane	89%
2	Cu(OAc) <sub>2</sub>	Ag <sub>2</sub> CO <sub>3</sub>	DMF	17%
3	Cu(OAc) <sub>2</sub>	Ag <sub>2</sub> CO <sub>3</sub>	ACN	70%
4	Cu(OAc) <sub>2</sub>	Ag <sub>2</sub> CO <sub>3</sub>	DCE	46%
5	Cu(OAc) <sub>2</sub>	AgOAc	Dioxane	30%
6	Cu(OAc) <sub>2</sub>	AgNO <sub>3</sub>	Dioxane	23%
7	Cu(OTf) <sub>2</sub>	Ag <sub>2</sub> CO <sub>3</sub>	Dioxane	trace
8	CuBr	Ag <sub>2</sub> CO <sub>3</sub>	Dioxane	43%
9	CuI	Ag <sub>2</sub> CO <sub>3</sub>	Dioxane	35%
10	---	Ag <sub>2</sub> CO <sub>3</sub>	Dioxane	nd

We performed the similar experiment with other alkylaminotropones (**1**) and arylsulfonyl hydrazides (**2**) that produced respective alkylaminotroponyl sulfones **4<sub>a/b/c</sub>**-**11<sub>a/b/c</sub>** (Scheme 3A.2). These derivatives are also characterized by NMR and ESI-HRMS. Their characterization data are provided in the Appendix. However, we could not notice the formation of disulfonylated product from *p*-nitroaryl sulfonyl hydrazide and *N*-benzylaminotropone possibly owing to the electron withdrawing NO<sub>2</sub>-group which may exert electrostatic repulsion between two nitro groups. We also noticed that the bulky 2,4,6-triisopropylsulfonyl hydrazide did not give sulfonylated products due to the steric congestion. Herein, we did not apply aliphatic sulfonyl hydrazides for sulfonylation of alkylaminotropone because of the relative instability of the sulfonyl radicals, generated in situ from aliphatic sulfonyl hydrazides under the reaction conditions. We also executed a gram scale synthesis for scheme 3A.1 demonstrating the good scalability of our method and it followed quite the same trend in terms of yield distribution.



Scheme 3A.2. The substrate scope of Arylsulfonation at alkylaminotropone.

The plausible catalytic cycle is described in Figure 3A.2. Initially, aminotropone (**1**) forms a complex (A-B) with  $\text{Cu}(\text{OAc})_2$  through the ligand exchange. This complex reacts with the sulfonyl radical to afford Cu(I) complex (C) via single electron transfer process (SET) with three probable products. The sulfonyl radical has been generated from the arylsulfonyl hydrazide by SET through the deprotonations and  $\text{N}_2$ -elimination with copper catalyst. In the literature, generation of such sulfonyl radical is also reported.<sup>23</sup> In next, the Cu(I)-complex (C-1/2) give Cu(II)-complex (D-1/2) via  $\text{Cu}(\text{OAc})_2$ -promoted oxidation. Meanwhile,  $\text{CuOAc}$  is oxidized by  $\text{Ag}_2\text{CO}_3$  to regenerate  $\text{Cu}(\text{OAc})_2$ . Finally, this sulfonyl Cu(II) complex (D-1/2) produce Cu(II) complex (E-1/2) through proton transfer process which leads to the desired aminotroponyl sulfonylated products **3a/3b** via the ligand dissociation, accompanying the regeneration of the  $\text{Cu}(\text{OAc})_2$  to complete the catalytic cycle.

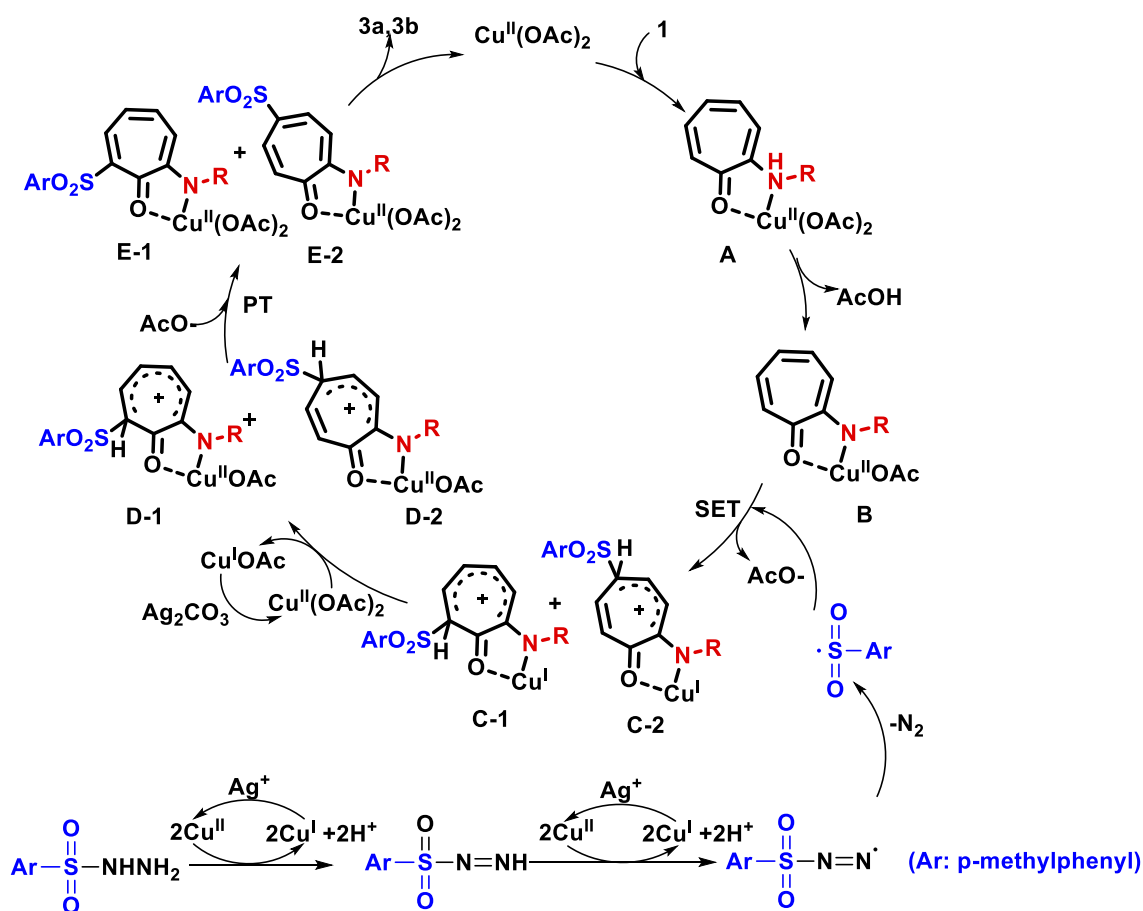


**Figure 3A.2.** Plausible reaction mechanism of ATS formation.

To ensure the radical mechanism, we performed a similar sulfonylation reaction with the radical inhibitor reagent, 2,2,6,6-tetramethylpiperidine-*N*-oxyl (TEMPO). Herein, we couldn't isolate any ATS derivatives that strongly support the proposed radical mechanism. Hence we can conclude that a free sulfonyl radical process may be involved in our reaction system.

The swarming motility pattern is an important asset in PA, contributing to its antibiotic resistance potential.<sup>24</sup> This motility pattern is a group-mediated movement on hard/semi-solid surfaces. The swarmer cells are often elongated in size and have a unique way of moving together in bunches.<sup>25</sup> Swarming motility is a surfactant-induced pattern whose synthesis is regulated by quorum-sensing (QS) in PA14.<sup>26,27</sup> In the literature, nonbenzenoid troponyl derivatives (tropolone-based metalloprotein inhibitors) have shown anti-QS properties and inhibited bacterial cells swarming.<sup>28</sup> Thus, we examined the role of twenty-six ATS derivatives in bacterial cell swarming. Importantly, we noticed remarkable inhibition of bacterial cell swarming without inhibiting the growth of the bacterium by six ATS derivatives (**3b**, **4b**, **7b**, **11b**, **5c** and **9c**). The swarming pattern was observed in control after 24h of incubation in the control medium, whereas only the grown colony of the bacterium was observed in the center, in the swarm media treated with 100  $\mu$ M of sulfonyl compounds (Figure 3A.3). The six ATS derivatives (**3b**, **4b**, **7b**, **11b**, **5c** and **9c**) inhibiting swarming are either C-5 or C-5,7 derivatives. None of the C-7 ATS derivatives showed antismarming properties. The dose-dependent studies indicated that *di*-(*p*-isopropyl)-phenyl ATS (**5c**) and *p*-nitrophenyl ATS derivative (**7b**) most effectively inhibited swarming at a deficient concentration of 20  $\mu$ M while the other four compounds (**3b**, **4b**, **11b** and **9c**) showed anti-swarming activity at a concentration of 60  $\mu$ M (Figure 3A.4).



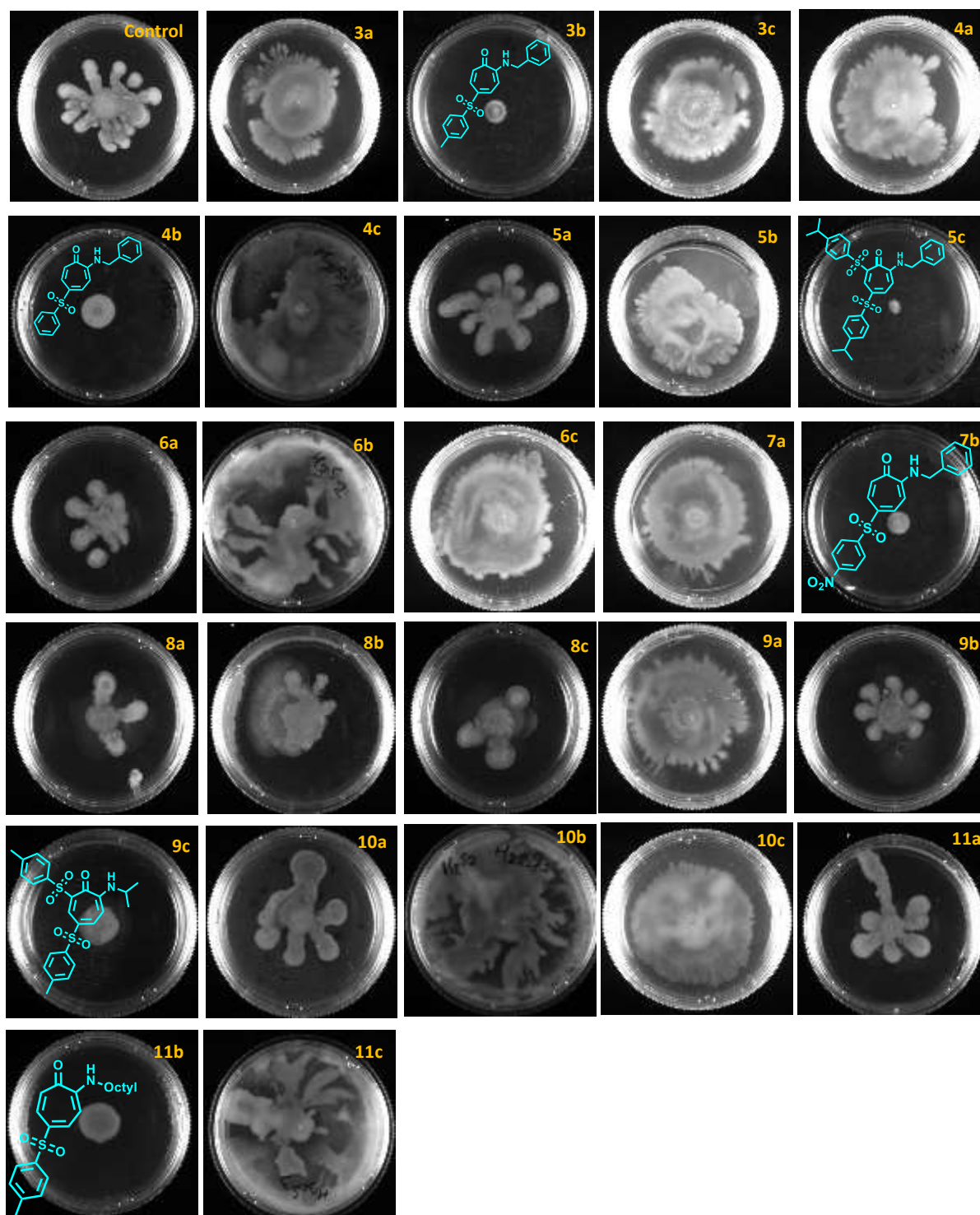


**Figure 3A.3.** Swarming assays of *P. aeruginosa* (PA14) in DMSO control and in presence of ATS derivatives (**3<sub>a/b/c</sub>**-**11<sub>a/b/c</sub>**) at 100  $\mu$ M concentration.

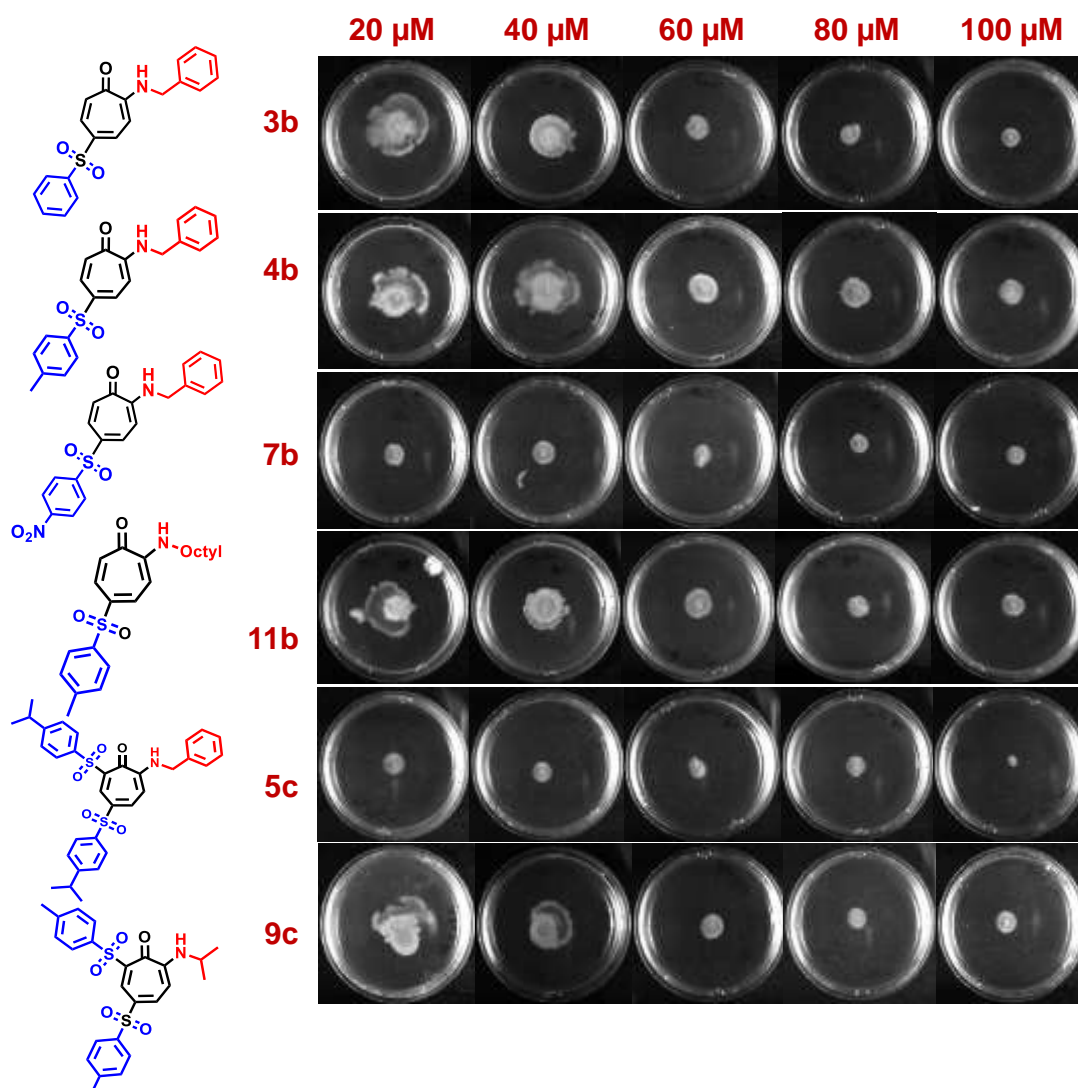


**Figure 3A.4.** Concentration-dependent swarming assays of *P. aeruginosa* (PA14) in presence of ATS derivatives (**3b**, **4b**, **7b**, **11b**, **5c** and **9c**) at different concentrations (20-100  $\mu$ M).

Biofilm formation is again an essential trait enhancing the pathogenicity and virulence potential of PA14. Biofilm is a matrix of cells encased inside self-secreted hydrated extracellular polymeric substances (EPS). This shows collective behavior and often protects cells by acting as a barrier against different hostile conditions such as antibiotics along with other harsh environmental conditions (salinity, pH, temperature fluctuations).<sup>29</sup> The quorum-sensing (QS) system is the key regulator of biofilm formation in PA resulting in enhanced virulence and antibiotic resistance.<sup>30</sup> To evaluate the anti-biofilm activity of the ATS

derivatives, we performed an initial screening of all 26 ATS derivatives at a high concentration of 100  $\mu$ M (Figure 3A.5, Figure 3A.6-A). In quantitative analysis, we noticed that only eight compounds (**3b**, **4b**, **7b**, **8b**, **9b**, **10b**, **11b** and **5c**) showed remarkably high reduction ( $> 50\%$ ) in biofilm formation, whereas six other compounds (**3a**, **5b**, **6c**, **9c**, **10a** and **10b**) also affected the biofilm formation significantly by more than 30%. To analyze the effective anti-biofilm dose of the selected six compounds, we measured the anti-biofilm activity at different concentrations i.e 20, 40, 60, 80, and 100  $\mu$ M (Figure 3A.6-B). These studies showed that all the selected compounds significantly inhibited the biofilm formation of PA (PA14) in a dose-dependent manner. The *di*-(*p*-isopropyl phenyl) ATS derivative (**5c**) significantly reduced biofilm formation by 54% even at 40  $\mu$ M concentration, followed by (*p*-nitrophenyl) ATS derivative (**7b**), which effectively rendered biofilm formation by 46% at the mentioned concentration ( $p < 0.0001$ ).

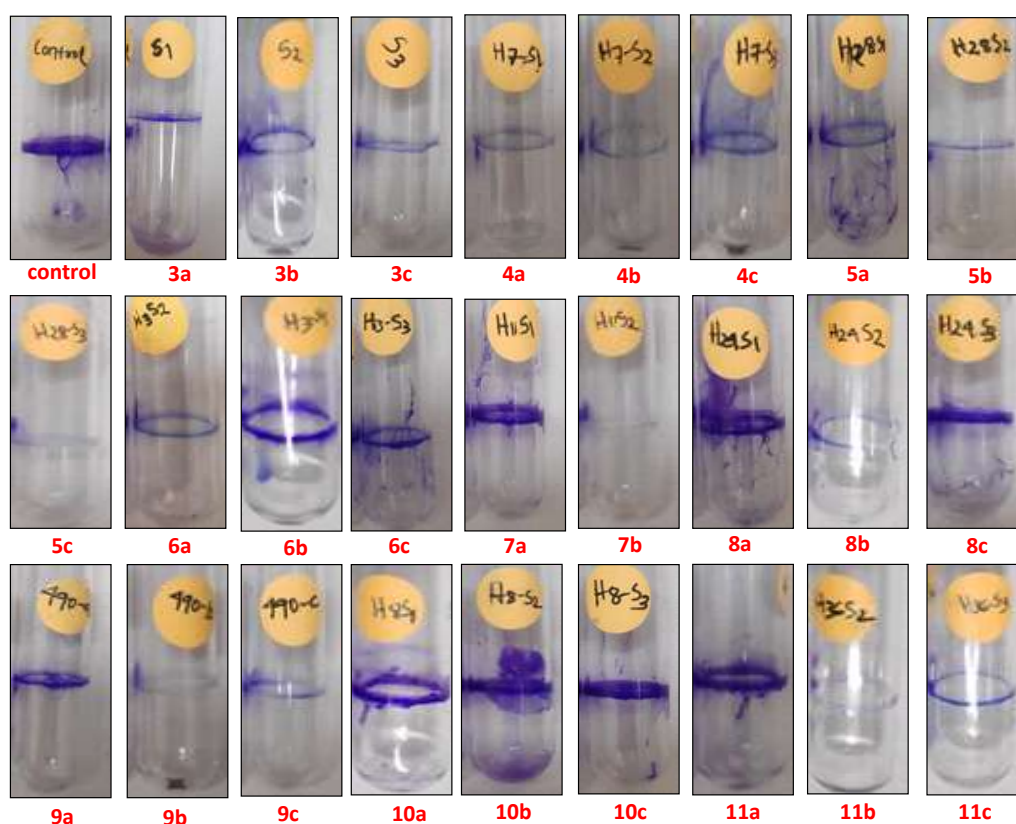


**Figure 3A.5.** Effect of ATS derivatives on biofilm formation (qualitative analysis).

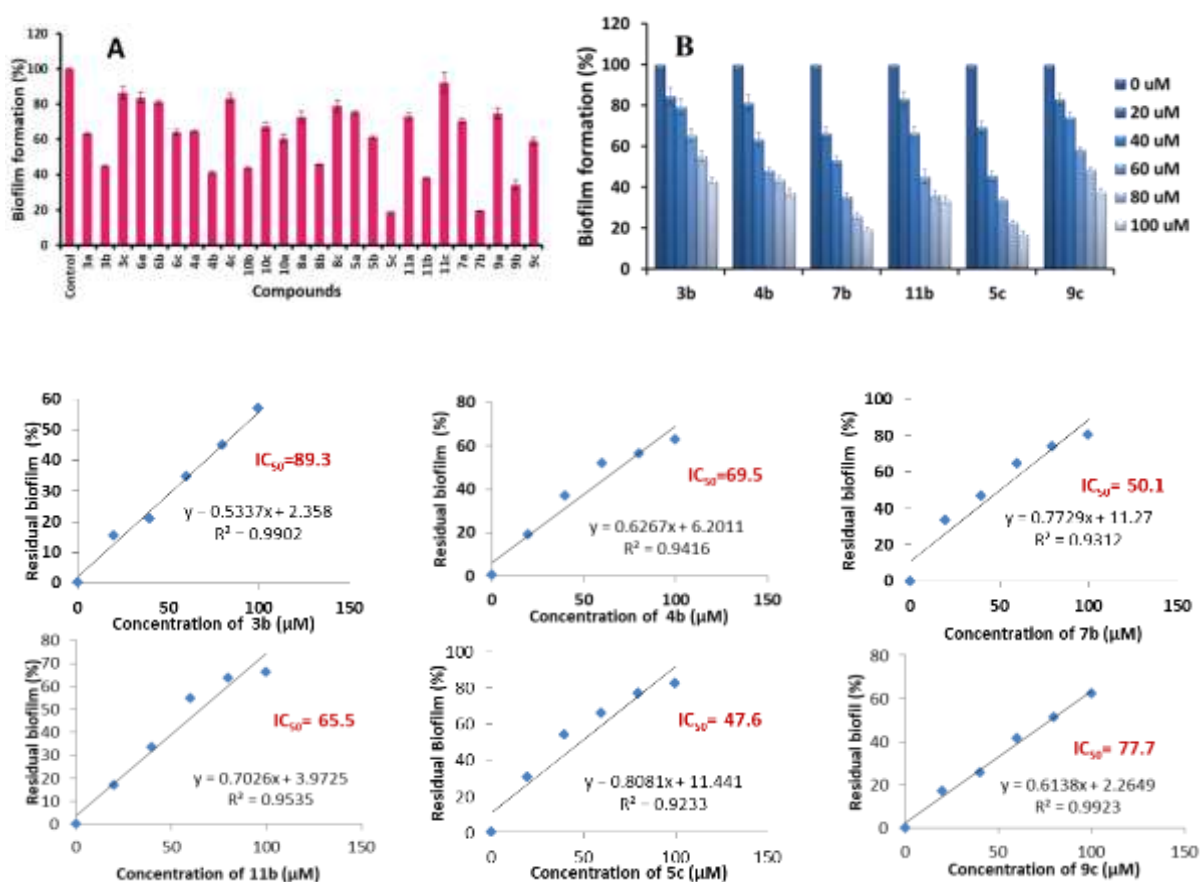


**Figure 3A.6.** Effect of ATS derivatives on biofilm formation; (A) Quantitative analysis of *P. aeruginosa* biofilm formation in the absence (control) or presence of ATS derivatives, (B) Concentration dependent biofilm assay.

The clinical isolates of PA are known for the production of pyocyanin, a phenazine known for its toxicity. Pyocyanin, a redox-active secondary metabolite, plays a crucial role in the generation of reactive oxygen species.<sup>31</sup> Pyocyanin production is under QS regulon and helps bacterium in coping with oxidative stress. QS defective mutants are highly susceptible to oxidative stress due to the decreased levels of *cyclopropanation* along with decreased levels of fatty acid saturation.<sup>32</sup> Owing to the role of pyocyanin in PA pathogenicity and in maintaining its fitness during competitive surroundings, we analyzed the effect of synthesized ATS derivatives on pyocyanin synthesis. Herein, only six sulfone derivatives (**3b**, **4b**, **7b**, **11b**, **5c** and **9c**), out of 26, significantly inhibited the pyocyanin synthesis ( $p < 0.001$ ) at



concentration of 100  $\mu\text{M}$  (Figure 3A.7-A). Next, we evaluated pyocyanin synthesis with increasing concentrations of ATS compounds by pyocyanin assay. Their concentration range was the same for evaluating anti-swarming and anti-biofilm concentrations. We noticed the inhibition of Pyocyanin production by all the selected compounds in a dose-dependent manner (Figure 3A.7-B). Importantly, ATS derivative (**5c**) was the most potent pyocyanin synthesis inhibitor that inhibited the pyocyanin synthesis by 34% at only 20  $\mu\text{M}$  concentration. The pyocyanin synthesis was further inhibited to 76 % on increasing the concentration from 20  $\mu\text{M}$  to 100  $\mu\text{M}$ . We found that all six selected derivatives showed anti-swarming activity and anti-pyocyanin activity in a dose-dependent manner.

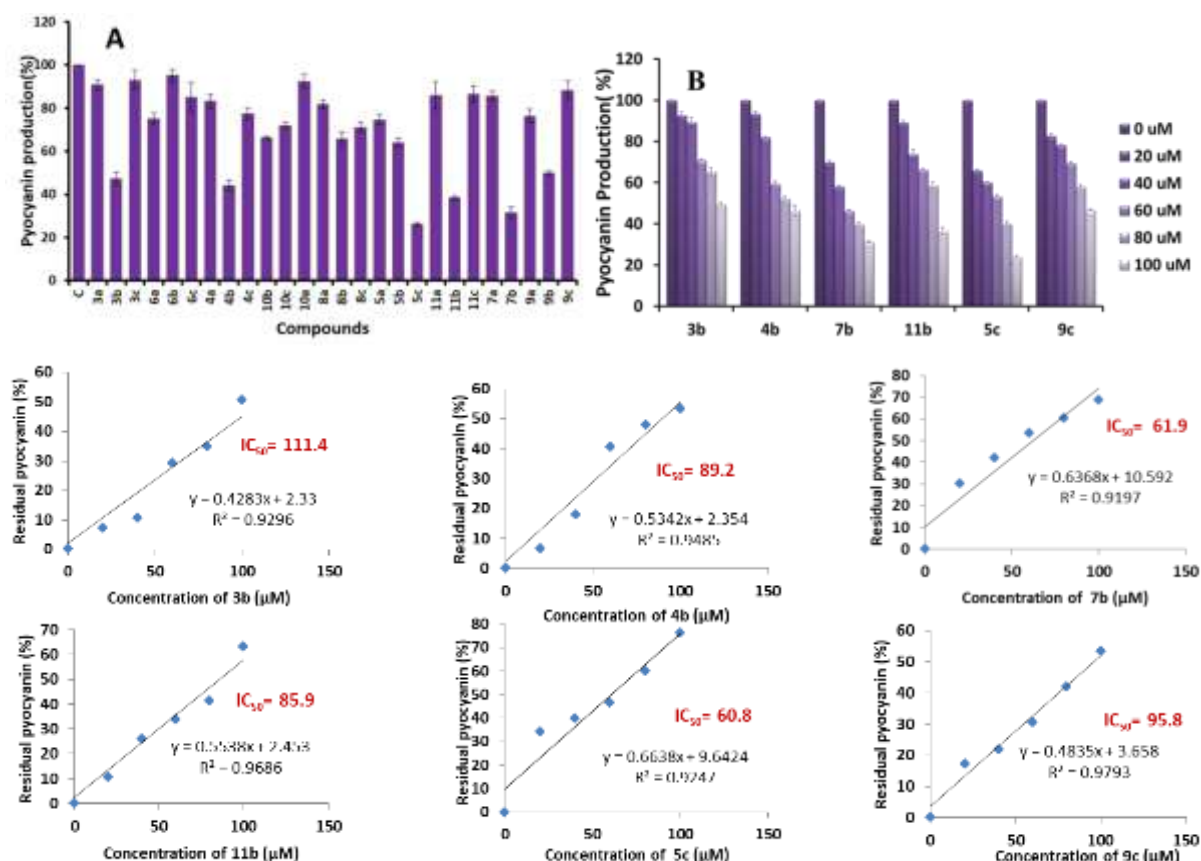


**Figure 3A.7.** Effect of ATS derivatives on pyocyanin production; (A) Quantitative analysis of *P. aeruginosa* pyocyanin production in the absence (control) or presence of ATS derivatives, (B) Concentration dependent pyocyanin assay.

In PA (PA14), LuxI/R quorum-sensing systems regulates the synchronous synthesis of various virulence factors like pyocyanin and elastase along with crucial involvement in biofilm formation.<sup>33</sup> The *lasI* gene synthesizes autoinducer 3-oxo-c12-homoserine lactone (3OC12–HSL) and *lasR* gene gets activated on binding with the autoinducer (Figure 3A.8). The complex formed between LasR and 3OC12–HSL further orchestrates the transcription of various genes including *lasB* and *rhl* (a second quorum-sensing receptor).<sup>34, 35</sup> *lasB* encodes for elastase B, a multifunctional enzyme which synchronously regulates various physio-pathological phenomena occurring during bacteria-host interaction.<sup>36</sup> Elastase production, one of the most virulent traits of PA is the main reason behind PA mediated mortality in hospitals. Elastase specifically hydrolyzes internal peptide bonds present on the amino portion of hydrophobic amino acid residues and thus has the potential to cleave a wide range of proteinaceous substrates.<sup>37</sup>

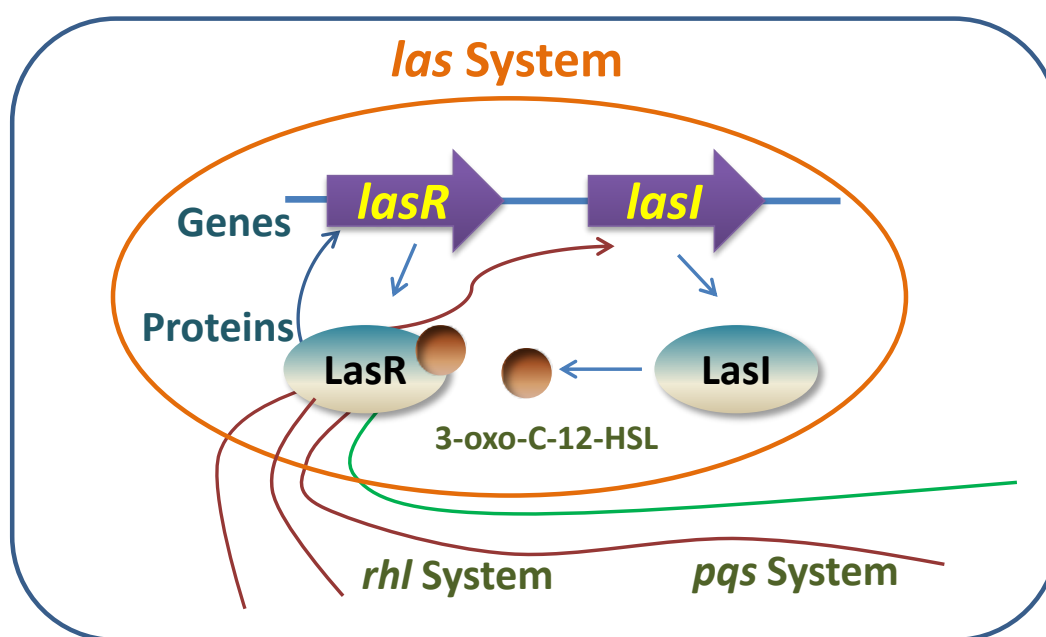


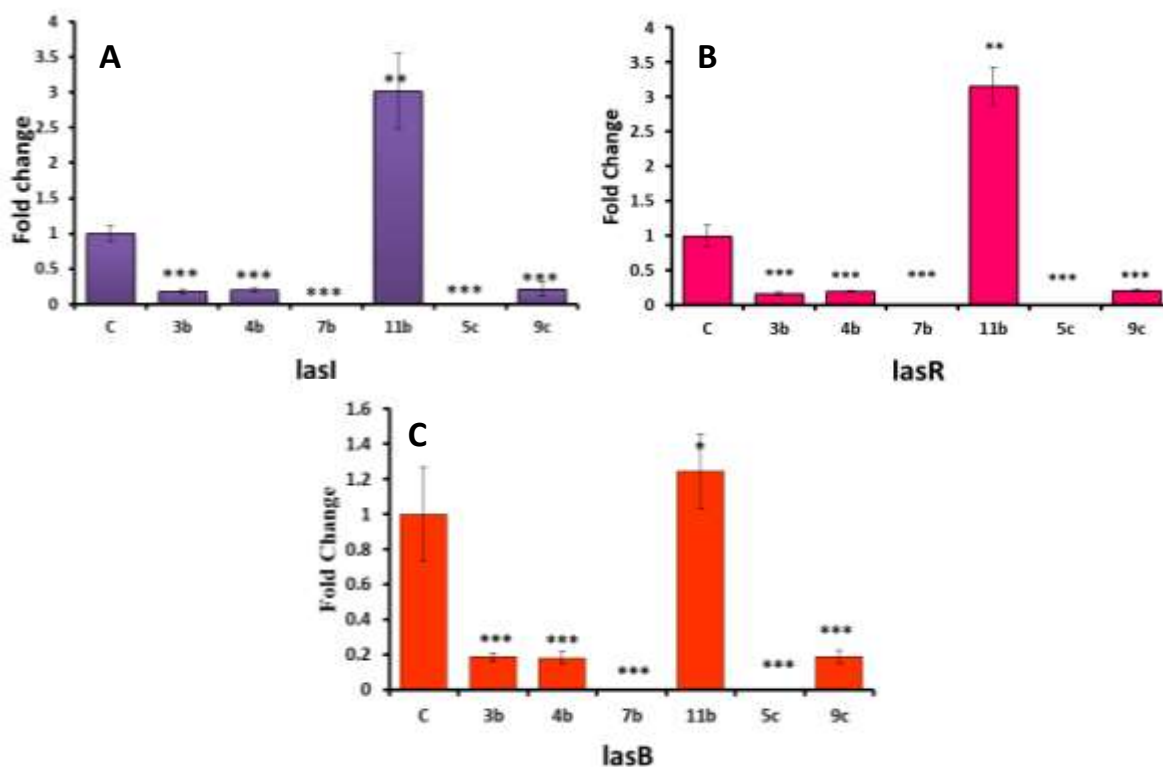
**Figure 3A.8.** Schematic diagram of the interconnected *lasI/R* and LasI/R systems.

Thus we performed qRT-PCR experiment to determine the efficacy of synthesized ATS derivatives at gene level (Table 3A.2, Figure 3A.9). Bacterium PA was treated with

selected ATS derivatives (**3b**, **4b**, **7b**, **11b**, **5c** and **9c**) at anti-swarming concentration for 18h. We studied the expression of both *lasI* and *lasR* genes. The transcript levels of the *16S* RNA gene were similar in control (cells grown in LB medium) or in LB medium supplemented with the mentioned compounds; hence it was used for normalization. The sulfonyl compounds **5c** and **7b** downregulated *lasI* and *lasR* significantly by 99.9 % and 99.7 % at 20  $\mu$ M concentration (Figure 3A.10-A/B). Surprisingly, sulfonyl derivative (**11b**) did not show any down regulating effect on both selected genes (*lasI* and *lasR*) though it effectively reduced biofilm formation, pyocyanin synthesis, and swarming motility. The same expression pattern was observed in *lasB* in presence of sulfonyl compounds (Figure 3A.10-C). Our results indicate that two isopropylbenzenesulfonyl groups of **5c** and one nitrobenzenesulfonyl group of **7b** greatly contribute to the remarkable anti-QS activity. In the literature, tropolone/tropone comprising isopropyl, nitro and sulfur substituents has also shown a higher antibacterial activity than its parental moiety.<sup>38</sup> However, in our case, the major difference was nitro and isopropyl moieties were not directly attached to the tropone ring; instead, we embedded them with the help of sulfonyl units.

**Table 3A.2.** Primers used for quantitative RT-PCR experiment

Gene	PCR primer sequence (5' to 3')
<i>lasI</i>	Fw: GGTTATGACGCACTCAGTCC
	Rv: TTCAGCATGTAGGGGCCAGT
<i>lasR</i>	Fw: GTGGAAAATTGGAGTGGAGC
	Rv: ACGATGAAGGCGTTCTCGTA
<i>lasB</i>	Fw: GACCTGATCGACGTGTCCAA
	Rv: ATCGCTTTCAGTTCGTCGGC
<i>16s</i>	Fw: TAAGCACCGGCTAACTTCGT
	Rv: AACCACCTACGCGCGCTTTA





of the compounds was evaluated in HEK293T cell lines (Figure 3A.11). None of the tested six compounds (**3b**, **4b**, **7b**, **11b**, **5c** and **9c**) showed toxicity at the studied concentrations, which were much higher than that of their anti-QS concentration.

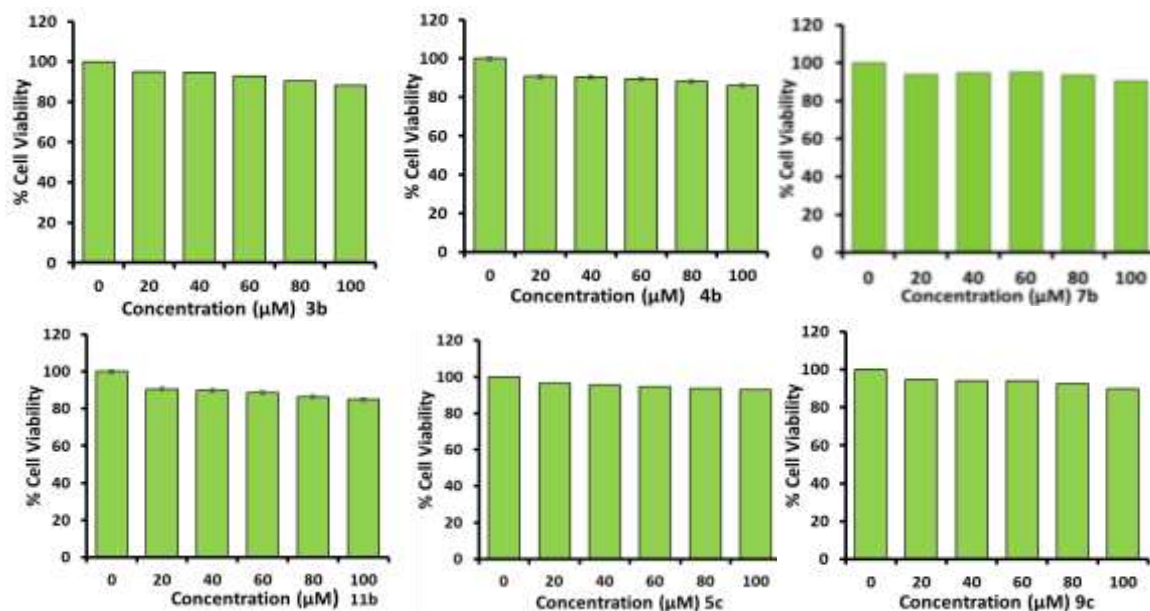


**Figure 3A.11.** Cell proliferation assays of ATS derivatives (**3b**, **4b**, **7b**, **11b**, **5c** and **9c**).

Considering the use of our synthesized six ATS derivatives as a therapeutic agent against PA14, cytotoxicity assay was performed. To this end, cell viability of HEK293T cell lines was measured post 12 hours of infection with treated and untreated PA14. As expected, PA strain PA14 was found to be cytotoxic against HEK293T cell line, decreasing the viability significantly as compared to the DMSO control. Our results depicted that compounds **5c** and **7b** treatment significantly reduced PA virulence-mediated cytotoxicity toward HEK293T cells and dramatically increased the viability (Figure 3A.12-A-D). Around 89% ( $p < 0.0001$ ) and 80% ( $p < 0.0001$ ) of PA14-infected cells survived in the presence of compounds **5c** and **7b**, respectively, while only 37% ( $p < 0.0001$ ) of cells were viable in the blank group. Thus, these results indicated that compounds **5c** (20μM) and **7b** (20μM) can be potential biofilm, swarming, pyocyanin, and virulence inhibitors in acute PA infections.

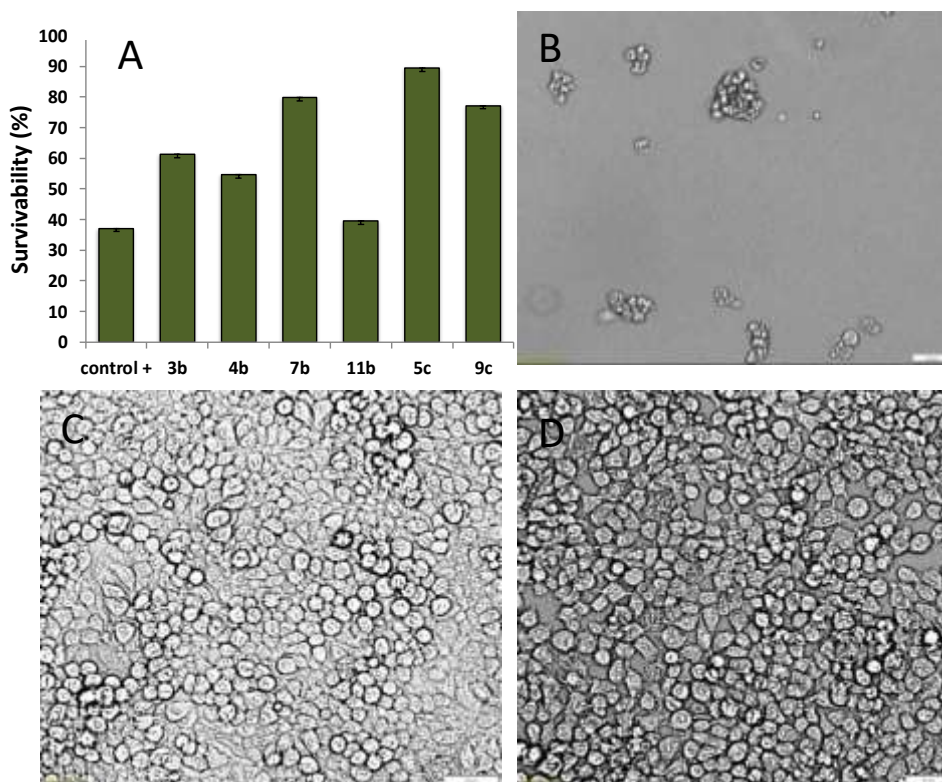


**Figure 3A.12.** ATS-mediated attenuation of *P. aeruginosa* cytotoxicity towards HEK293T cells; Plot showing Cell survivality (A), Microscopic images of HEK293T cells treated with PA14 (B), 7b treated PA14 (C), and 5c treated PA14 (D).

### 3A.4 Conclusion

In summary, we have successfully introduced aryl sulfonyl moiety at alkylaminotropone derivatives through Cu-catalyzed C-H activation. So far, there is no such report on arylsulfonation at non-benzenoid aromatic tropone ring. We have explored their antagonism against the multidrug resistant bacteria PA (PA14) by performing the following assays: biofilm inhibition, pyocyanin inhibition, and anti-swarming activities. Our result strongly supports that six compounds (**3b**, **4b**, **7b**, **11b**, **5c** and **9c**) showed remarkable inhibitory potential. The ATS derivative **5c** is the most effective, followed by **7b**, in rendering biofilm formation and pyocyanin production. Both ATS (**5c/7b**) have effectively limited the swarming motility at 20  $\mu$ M concentration. These two ATS (**5c/7b**) inhibit the

*lasI/R* systems of PA by significantly down regulating the expression of *lasI/R* genes (~ 99%, ( $p < .0001$ )). We also notice that these two ATS (**5c/7b**) are non-toxic towards HEK293T cell lines. Thus we have tested for the virulent effect of PA infection. Our results show that the survival of HEK293T cells is increased by ~89% and ~80% when treated with PA grown in the presence of compound **5c** and **7b**, respectively, as compared to untreated PA control (~37%). Overall, both ATS (**5c/7b**) are potentially novel QS inhibitors and anti-biofilm, anti-swarming agents, which could be considered as therapeutic drugs for the treatment of PA infection.

### 3A.5 Experimental Section

*General information:* Unless otherwise noted, materials were purchased from commercial suppliers and were used as received. Reactions were monitored by thin layer chromatography, visualized by UV and Ninhydrin. Column chromatography was performed in 230-400 mesh silica. Mass spectra (HRMS) were obtained from Bruker microTOF-Q II Spectrometer and the samples were prepared in methanol and injected in methanol and water mixture. NMR spectra were recorded on Bruker 400 MHz and Bruker 700 MHz NMR spectrometer at room temperature and processed using Mnova software from Mestrelab Research. The crystal data were collected on a Rigaku Oxford diffractometer.

*Typical procedure for the preparation of aminotropones:* All the alkylaminotropones were synthesized by following the reported procedure.<sup>22</sup> 2-Tosyloxytropone and amines (1.2 equiv.) were dissolved in ethanol, and to this Et<sub>3</sub>N (3.0) was added. The reaction mixture was allowed to reflux, monitored by TLC. The general reaction time observed for all the reactions was 24–36 h. All the volatiles were evaporated under reduced pressure after reaction completion. To the crude product, 1.0 N HCl was added and extracted with dichloromethane (three times), and then the combined organic layers were dried over Na<sub>2</sub>SO<sub>4</sub> and evaporated

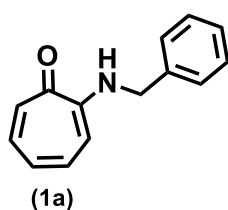
under reduced pressure. The obtained crude product was purified by silica gel column chromatography by using an ethyl acetate and hexane mixture as the mobile phase.

*Typical procedure for the preparation of sulfonyl hydrazides:* Sulfonyl hydrazides were prepared according to the literature procedure.<sup>39</sup> The hydrazine monohydrate (80%) (30 mmol) was added drop wise into the solution of sulfonyl chloride (10 mmol) in THF (50 mL) under nitrogen at 0 °C. Subsequently, the mixture was further stirred at 0 °C for 30 minutes. After the completion of the reaction, the solvent was removed by evaporation, and the residue was extracted with dichloromethane (3 x 20 mL), and the combined organic layer was washed with water, brine, and dried over Na<sub>2</sub>SO<sub>4</sub>. Concentration in vacuum followed by silica gel column purification with petroleum ether/ethyl acetate eluent gave the desired product **2** in yields range from 70-95%.

*General procedure for copper-catalyzed C-H sulfonylation:* Aminotropone **1** (0.2 mmol), sulfonyl hydrazide **2** (0.3 mmol), anhydrous Cu(OAc)<sub>2</sub> (0.02 mmol), silver carbonate (0.6 mmol), and anhydrous 1,4-dioxane (3mL) were added to a round bottom flask under argon and stirred at 100 °C for 4 h. After the completion of the reaction, the reaction mixture was passed through celite and the filtrate was evaporated under reduced pressure. The residue was purified by column chromatography using dichloromethane (also ethyl acetate/hexane in some cases) as eluent to get the desired products.

#### *Characterization data of products*

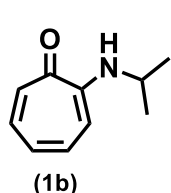
2-(benzylamino)cyclohepta-2,4,6-trien-1-one (**1a**): <sup>1</sup>H NMR (700 MHz, CDCl<sub>3</sub>) δ 7.59 (s,



1H), 7.38 – 7.26 (m, 6H), 7.20 – 7.13 (m, 2H), 6.68 (t, *J* = 9.4 Hz, 1H), 6.53 (d, *J* = 10.3 Hz, 1H), 4.55 (d, *J* = 5.8 Hz, 2H), <sup>13</sup>C NMR (176 MHz, CDCl<sub>3</sub>) δ 177.00, 155.39, 137.37, 136.43, 136.25, 129.22,

128.93, 127.81, 127.30, 122.70, 109.18, 47.02, HRMS (ESI) calcd for  $C_{14}H_{13}NO$ :  $[M+Na]^+$  234.0889, found: 234.0885.

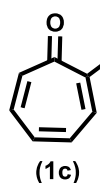
2-(isopropylamino)cyclohepta-2,4,6-trien-1-one (**1b**):  $^1H$  NMR (400 MHz,  $CDCl_3$ )  $\delta$  7.34 –



7.13 (m, 3H), 6.69 (t, 1H), 6.60 (d,  $J = 10.6$  Hz, 1H), 3.94 – 3.80 (m, 1H), 1.36(d,  $J = 6.4$  Hz, 6H),  $^{13}C$  NMR (101 MHz,  $CDCl_3$ )  $\delta$  176.57, 154.68, 137.19, 136.29, 128.24, 121.83, 108.89, 43.80, 22.01, , HRMS (ESI) calcd for

$C_{10}H_{13}NO$ :  $[M+Na]^+$  186.0889, found 186.0875.

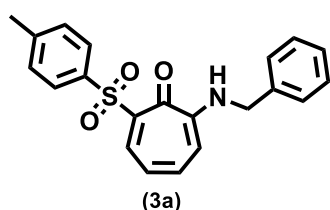
2-(octylamino)cyclohepta-2,4,6-trien-1-one (**1c**):  $^1H$  NMR (700 MHz,  $CDCl_3$ )  $\delta$  7.26 – 7.14



(m, 3H), 7.12 (d,  $J = 11.5$  Hz, 1H), 6.63 (t,  $J = 9.5$  Hz, 1H), 6.50 (d,  $J = 10.4$  Hz, 1H), 3.27 (dd,  $J = 13.1$ , 6.5 Hz, 2H), 1.71 (dt,  $J = 14.4$ , 7.2 Hz, 2H), 1.41 (dt,  $J = 14.7$ , 7.3

Hz, 2H), 1.33 – 1.21 (m, 8H), 0.86 (t,  $J = 6.8$  Hz, 3H),  $^{13}C$  NMR (176 MHz,  $CDCl_3$ )  $\delta$  176.57, 155.68, 137.22, 136.31, 128.26, 121.93, 108.61, 42.89, 31.76, 29.25, 29.16, 28.45, 27.14, 22.62, 14.08, HRMS (ESI) calcd for  $C_{15}H_{23}NO$ :  $[M+Na]^+$  256.1672, found 256.1671.

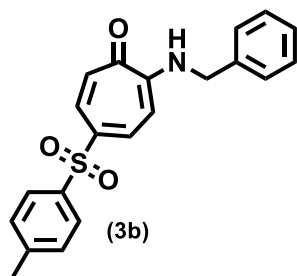
2-(benzylamino)-7-tosylcyclohepta-2,4,6-trien-1-one(**3a**): Following the general procedure



the title compound was isolated by column chromatography (eluent: dichloromethane) as a yellow solid in 36% yield (28 mg).  $^1H$  NMR (700 MHz,  $CDCl_3$ )  $\delta$  8.61 (d,  $J = 10.0$  Hz, 1H),

7.99 (s, 1H), 7.92 (d,  $J = 8.0$  Hz, 2H), 7.42 (t,  $J = 10.1$  Hz, 1H), 7.35 – 7.30 (m, 3H), 7.27 (d,  $J = 8.0$  Hz, 2H), 7.23 (d,  $J = 7.0$  Hz, 2H), 6.84 (t,  $J = 9.9$  Hz, 1H), 6.58 (d,  $J = 10.5$  Hz, 1H), 4.49 (d,  $J = 5.6$  Hz, 2H), 2.38 (s, 3H).  $^{13}C$  NMR (176 MHz,  $CDCl_3$ )  $\delta$  170.48, 157.72, 143.59, 142.08, 138.30, 138.04, 136.36, 134.92, 129.09, 129.07, 128.61, 128.32, 127.63, 119.34, 109.10, 47.50, 21.64, HRMS (ESI) calcd for  $C_{21}H_{19}NO_3S$ :  $[M+Na]^+$  388.0978, found 388.1001.

2-(benzylamino)-5-tosylcyclohepta-2,4,6-trien-1-one (**3b**): Following the general procedure

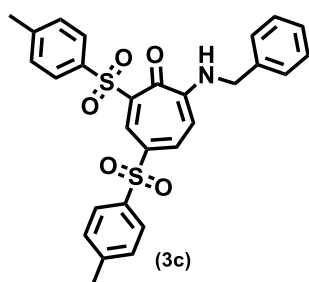


the title compound was isolated by column chromatography (eluent: dichloromethane) as a pale yellow solid in 39% yield (30 mg).

$^1\text{H}$  NMR (700 MHz,  $\text{CDCl}_3$ )  $\delta$  8.03 (d,  $J$  = 10.8 Hz, 2H), 7.80 (d,  $J$  = 12.3 Hz, 1H), 7.76 (d,  $J$  = 8.0 Hz, 2H), 7.40 – 7.32 (m, 3H),

7.30 – 7.26 (m, 4H), 7.08 (d,  $J$  = 12.2 Hz, 1H), 6.53 (d,  $J$  = 11.0 Hz, 1H), 4.59 (d,  $J$  = 5.9 Hz, 2H), 2.39 (s, 3H),  $^{13}\text{C}$  NMR (176 MHz,  $\text{CDCl}_3$ )  $\delta$  176.43, 156.93, 144.00, 138.97, 136.91, 135.00, 134.35, 133.30, 130.01, 129.19, 128.36, 127.43, 127.43, 127.22, 105.99, 47.34, 21.56, , HRMS (ESI) calcd for  $\text{C}_{21}\text{H}_{19}\text{NO}_3\text{S}$ :  $[\text{M}+\text{Na}]^+$  388.0978, found 388.1007.

7-(benzylamino)-2,4-ditosylcyclohepta-2,4,6-trien-1-one (**3c**): Following the general

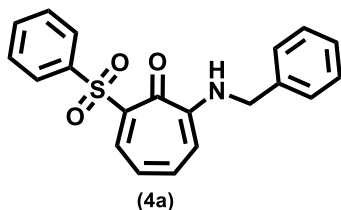


procedure the title compound was isolated by column chromatography (eluent: dichloromethane) as a yellow solid in

15% yield (14 mg).  $^1\text{H}$  NMR (700 MHz,  $\text{CDCl}_3$ )  $\delta$  9.22 (s, 1H), 8.38 (s, 1H), 8.22 (d,  $J$  = 11.2 Hz, 1H), 7.90 (d,  $J$  = 7.9 Hz, 2H),

7.85 (d,  $J$  = 7.9 Hz, 2H), 7.38 – 7.32 (m, 5H), 7.28 (d,  $J$  = 7.9 Hz, 2H), 7.21 (d,  $J$  = 6.3 Hz, 2H), 6.62 (d,  $J$  = 11.2 Hz, 1H), 4.55 (d,  $J$  = 5.7 Hz, 2H), 2.42 (s, 3H), 2.39 (s, 3H),  $^{13}\text{C}$  NMR (176 MHz,  $\text{CDCl}_3$ )  $\delta$  170.18, 158.68, 144.52, 144.23, 141.07, 138.37, 137.34, 136.59, 135.16, 133.69, 131.45, 130.29, 129.34, 129.21, 129.00, 128.84, 127.73, 127.67, 106.80, 47.98, 21.66, 21.62, HRMS (ESI) calcd for  $\text{C}_{28}\text{H}_{25}\text{NO}_5\text{S}_2$ :  $[\text{M}+\text{Na}]^+$  542.1066, found 542.1103.

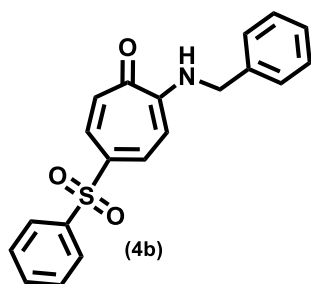
2-(benzylamino)-7-(phenylsulfonyl)cyclohepta-2,4,6-trien-1-one (**4a**): Following the general procedure the title compound was isolated by column chromatography (eluent: dichloromethane) as a yellow solid in 36% yield (27 mg).  $^1\text{H}$  NMR (700 MHz,  $\text{CDCl}_3$ )  $\delta$  8.62 (d,  $J$  = 10.1 Hz, 1H), 8.04 (d,  $J$  = 7.8 Hz, 2H), 7.98 (s, 1H), 7.55 (t,  $J$  = 7.3 Hz, 1H), 7.48 (t,  $J$  = 7.6 Hz, 2H), 7.43 (t,  $J$  = 10.2 Hz, 1H), 7.38 – 7.27 (m, 3H), 7.23 (d,  $J$  = 7.2 Hz, 2H), 6.85



(t,  $J = 10.0$  Hz, 1H), 6.59 (d,  $J = 10.6$  Hz, 1H), 4.50 (d,  $J = 5.8$  Hz, 2H),  $^{13}\text{C}$  NMR (176 MHz,  $\text{CDCl}_3$ )  $\delta$  170.45, 157.74, 142.18, 141.30, 138.16, 136.09, 134.86, 132.75, 129.11, 128.53, 128.39, 128.35, 127.61, 119.32, 109.10, 47.52,

HRMS (ESI) calcd for  $\text{C}_{20}\text{H}_{17}\text{NO}_3\text{S}$ :  $[\text{M}+\text{Na}]^+$  374.0821, found 374.0842.

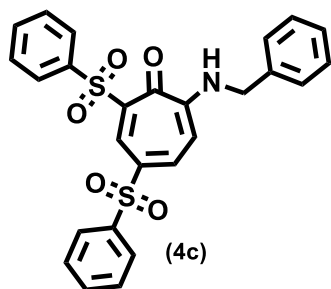
2-(benzylamino)-5-(phenylsulfonyl)cyclohepta-2,4,6-trien-1-one (**4b**): Following the general



procedure the title compound was isolated by column chromatography (eluent: dichloromethane) as a yellow solid in 40% yield (30 mg).  $^1\text{H}$  NMR (400 MHz,  $\text{CDCl}_3$ )  $\delta$  8.04 (dd,  $J = 11.0, 2.0$  Hz, 2H), 7.93 – 7.85 (m, 2H), 7.81 (dd,  $J = 12.2, 2.0$  Hz, 1H), 7.59 – 7.44 (m, 3H), 7.43 – 7.30 (m, 3H), 7.30 – 7.26 (m,

2H), 7.08 (d,  $J = 12.2$  Hz, 1H), 6.54 (d,  $J = 11.1$  Hz, 1H), 4.59 (d,  $J = 5.9$  Hz, 2H),  $^{13}\text{C}$  NMR (101 MHz,  $\text{CDCl}_3$ )  $\delta$  176.42, 157.03, 142.06, 137.12, 134.98, 134.33, 132.95, 132.89, 129.33, 129.19, 128.37, 127.42, 127.36, 127.18, 105.83, 47.38, HRMS (ESI) calcd for  $\text{C}_{20}\text{H}_{17}\text{NO}_3\text{S}$ :  $[\text{M}+\text{Na}]^+$  374.0821, found 374.0842.

7-(benzylamino)-2,4-bis(phenylsulfonyl)cyclohepta-2,4,6-trien-1-one (**4c**): Following the

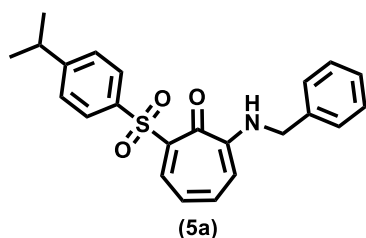


general procedure the title compound was isolated by column chromatography (eluent: dichloromethane) as a yellow solid in 11% yield (8 mg).  $^1\text{H}$  NMR (700 MHz,  $\text{CDCl}_3$ )  $\delta$  9.24 (d,  $J = 1.6$  Hz, 1H), 8.43 (s, 1H), 8.24 (d,  $J = 11.2$  Hz, 1H), 8.01 (d,

$J = 7.6$  Hz, 2H), 7.97 (d,  $J = 7.6$  Hz, 2H), 7.60 (t,  $J = 7.4$  Hz, 1H), 7.57 – 7.53 (m, 3H), 7.47 (t,  $J = 7.8$  Hz, 2H), 7.36 – 7.31 (m, 3H), 7.22 – 7.18 (m, 2H), 6.65 (d,  $J = 11.3$  Hz, 1H), 4.57 (d,  $J = 5.8$  Hz, 2H),  $^{13}\text{C}$  NMR (176 MHz,  $\text{CDCl}_3$ )  $\delta$  170.11, 158.82, 141.43, 141.39, 140.31, 136.69, 134.70, 133.63, 133.47, 133.26, 130.91, 129.68, 129.36, 128.92, 128.85, 128.55,

127.74, 127.59, 106.95, 48.01, HRMS (ESI) calcd for  $C_{26}H_{21}NO_5S_2$ :  $[M+Na]^+$  514.0753, found 514.0772.

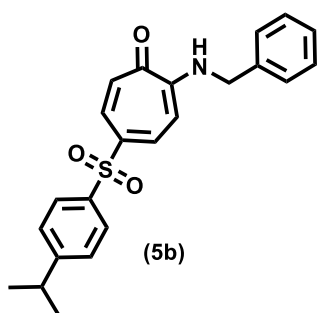
2-(benzylamino)-7-((4-isopropylphenyl)sulfonyl)cyclohepta-2,4,6-trien-1-one (5a):



Following the general procedure the title compound was isolated by column chromatography (eluent: dichloromethane) as a yellow solid in 41% yield (50 mg).

$^1H$  NMR (700 MHz,  $CDCl_3$ )  $\delta$  8.61 (d,  $J$  = 10.1 Hz, 1H), 7.99 (s, 1H), 7.97 (d,  $J$  = 8.3 Hz, 2H), 7.41 (t,  $J$  = 10.1 Hz, 1H), 7.35 – 7.29 (m, 5H), 7.24 (d,  $J$  = 7.2 Hz, 2H), 6.84 (t,  $J$  = 9.9 Hz, 1H), 6.58 (d,  $J$  = 10.5 Hz, 1H), 4.50 (d,  $J$  = 5.8 Hz, 2H), 2.97 – 2.88 (m, 1H), 1.24 (s, 3H), 1.23 (s, 3H),  $^{13}C$  NMR (176 MHz,  $CDCl_3$ )  $\delta$  170.51, 157.73, 154.18, 142.01, 138.51, 138.12, 136.40, 134.93, 129.09, 128.78, 128.32, 127.63, 126.56, 119.33, 109.04, 47.51, 34.19, 23.62, HRMS (ESI) calcd for  $C_{23}H_{23}NO_3S$ :  $[M+Na]^+$  416.1291, found 416.1291.

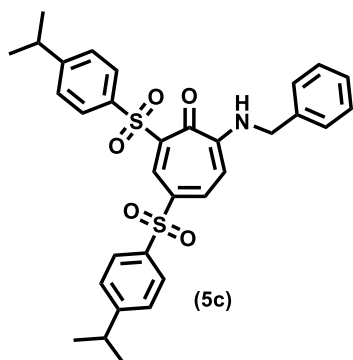
2-(benzylamino)-5-((4-isopropylphenyl)sulfonyl)cyclohepta-2,4,6-trien-1-one (5b):



Following the general procedure the title compound was isolated by column chromatography (eluent: dichloromethane) as a yellow solid in 45% yield (55 mg).  $^1H$  NMR (700 MHz,  $CDCl_3$ )

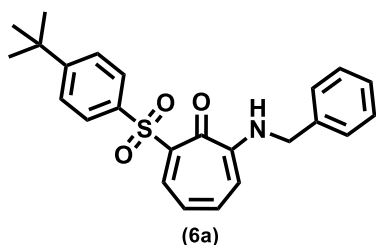
$\delta$  8.06 (s, 1H), 8.04 (d,  $J$  = 11.2 Hz, 1H), 7.82 (d,  $J$  = 12.3 Hz, 1H), 7.79 (d,  $J$  = 8.0 Hz, 2H), 7.37 (t,  $J$  = 7.3 Hz, 2H), 7.34 (d,  $J$  = 7.7 Hz, 3H), 7.29 – 7.26 (m, 2H), 7.08 (d,  $J$  = 12.2 Hz, 1H), 6.54 (d,  $J$  = 11.0 Hz, 1H), 4.59 (d,  $J$  = 5.8 Hz, 2H), 2.98 – 2.90 (m, 1H), 1.23 (d,  $J$  = 6.9 Hz, 6H),  $^{13}C$  NMR (176 MHz,  $CDCl_3$ )  $\delta$  176.44, 156.96, 154.65, 139.21, 136.99, 135.04, 134.43, 133.29, 129.18, 128.35, 127.54, 128.52, 128.44, 127.19, 106.06, 47.33, 34.20, 23.60, HRMS (ESI) calcd for  $C_{23}H_{23}NO_3S$ :  $[M+Na]^+$  416.1291, found 416.1299.



7-(benzylamino)-2,4-bis((4-isopropylphenyl)sulfonyl)cyclohepta-2,4,6-trien-1-one **(5c)**:

Following the general procedure the title compound was isolated by column chromatography (eluent: dichloromethane) as a yellow solid in 10% yield (12 mg).  $^1\text{H}$  NMR (700 MHz,  $\text{CDCl}_3$ )  $\delta$  9.25 (s, 1H), 8.41 (s, 1H), 8.26 (d,  $J = 11.2$  Hz, 1H), 7.97 (d,  $J = 8.2$  Hz, 2H), 7.90 (d,  $J = 8.2$  Hz, 2H), 7.41 (d,  $J = 8.2$  Hz, 2H), 7.38 – 7.33 (m, 5H), 7.23

(d,  $J = 6.0$  Hz, 2H), 6.64 (d,  $J = 11.3$  Hz, 1H), 4.58 (d,  $J = 5.8$  Hz, 2H), 3.01 – 2.94 (m, 2H), 1.28 (d,  $J = 6.9$  Hz, 6H), 1.26 (d,  $J = 6.9$  Hz, 6H),  $^{13}\text{C}$  NMR (176 MHz,  $\text{CDCl}_3$ )  $\delta$  170.21, 158.70, 155.13, 154.83, 141.10, 138.66, 137.53, 136.73, 135.22, 133.71, 131.49, 129.35, 129.20, 128.84, 127.80, 127.78, 127.73, 126.70, 106.73, 47.98, 34.27, 34.23, 23.60, HRMS (ESI) calcd for  $\text{C}_{32}\text{H}_{33}\text{NO}_5\text{S}_2$ :  $[\text{M}+\text{Na}]^+$  598.1692, found 598.1729.

2-(benzylamino)-7-((4-(tert-butyl)phenyl)sulfonyl)cyclohepta-2,4,6-trien-1-one **(6a)**:

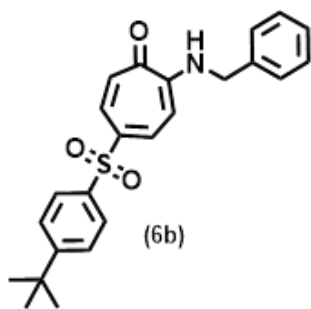
Following the general procedure the title compound was isolated by column chromatography (eluent: dichloromethane) as a yellow solid in 33% yield (32 mg).  $^1\text{H}$  NMR (700 MHz,  $\text{CDCl}_3$ )  $\delta$  8.64 (d,  $J = 10.0$  Hz, 1H), 8.03 (s,

1H), 7.99 (d,  $J = 8.0$  Hz, 2H), 7.51 (d,  $J = 8.0$  Hz, 2H), 7.44 (t,  $J = 10.0$  Hz, 1H), 7.35 (m, 3H), 7.26 (d,  $J = 6.7$  Hz, 2H), 6.86 (t,  $J = 9.8$  Hz, 1H), 6.60 (d,  $J = 10.4$  Hz, 1H), 4.52 (d,  $J = 5.0$  Hz, 2H), 1.33 (s, 9H).  $^{13}\text{C}$  NMR (176 MHz,  $\text{CDCl}_3$ )  $\delta$  170.52, 157.74, 156.45, 142.02, 138.16, 138.14, 136.37, 134.94, 129.10, 128.50, 128.33, 127.63, 125.48, 119.35, 109.06, 47.51, 35.15, 31.09, HRMS (ESI) calcd for  $\text{C}_{24}\text{H}_{25}\text{NO}_3\text{S}$ :  $[\text{M}+\text{H}]^+$  408.1628, found 408.1660.

2-(benzylamino)-5-((4-(tert-butyl)phenyl)sulfonyl)cyclohepta-2,4,6-trien-1-one **(6b)**:

Following the general procedure the title compound was isolated by column chromatography (eluent: dichloromethane) as a yellow solid in 37% yield (28 mg).  $^1\text{H}$  NMR (400 MHz,

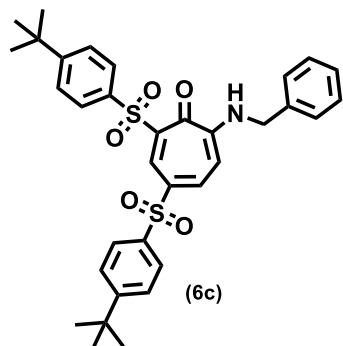
$\text{CDCl}_3$ )  $\delta$  8.04 (dd,  $J = 10.9, 1.9$  Hz, 2H), 7.83 (dd,  $J = 12.3, 2.0$  Hz, 1H), 7.79 (d,  $J = 8.6$  Hz,



2H), 7.50 (d,  $J = 8.6$  Hz, 2H), 7.40 – 7.32 (m, 3H), 7.30 – 7.26 (m, 2H), 7.09 (d,  $J = 12.2$  Hz, 1H), 6.54 (d,  $J = 11.1$  Hz, 1H), 4.59 (d,  $J = 5.9$  Hz, 2H), 1.31 (s, 9H),  $^{13}\text{C}$  NMR (101 MHz,  $\text{CDCl}_3$ )  $\delta$  176.45, 156.94, 138.84, 136.99, 135.00, 134.46, 133.31, 129.19, 128.37, 127.44, 127.24, 126.41, 106.03, 47.35,

35.19, 31.03, HRMS (ESI) calcd for  $\text{C}_{24}\text{H}_{25}\text{NO}_3\text{S}$ :  $[\text{M}+\text{Na}]^+$  430.1447, found 430.1462.

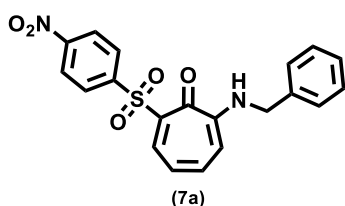
7-(benzylamino)-2,4-bis((4-(tert-butyl)phenyl)sulfonyl)cyclohepta-2,4,6-trien-1-one (6c):



Following the general procedure the title compound was isolated by column chromatography (eluent: dichloromethane) as a yellow solid in 20% yield (26 mg).  $^1\text{H}$  NMR (400 MHz,  $\text{CDCl}_3$ )  $\delta$  9.24 (d,  $J = 1.9$  Hz, 1H), 8.40 (t,  $J = 5.3$  Hz, 1H), 8.24 (dd,  $J = 11.2, 1.9$  Hz, 1H), 7.95 (d,  $J = 8.6$  Hz, 2H), 7.88 (d,  $J = 8.6$  Hz, 2H), 7.55 (d,  $J = 8.6$  Hz, 2H), 7.49 (d,  $J = 8.6$

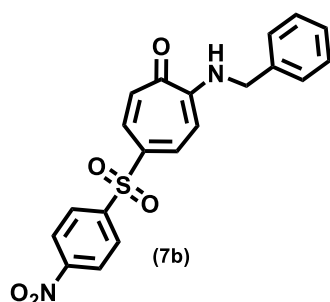
Hz, 2H), 7.36 (d,  $J = 1.7$  Hz, 1H), 7.34 (d,  $J = 1.9$  Hz, 2H), 7.21 (dd,  $J = 6.8, 2.5$  Hz, 2H), 6.62 (d,  $J = 11.3$  Hz, 1H), 4.55 (d,  $J = 5.8$  Hz, 2H), 1.33 (s, 9H), 1.31 (s, 9H),  $^{13}\text{C}$  NMR (101 MHz,  $\text{CDCl}_3$ )  $\delta$  170.23, 158.72, 157.39, 157.10, 141.11, 138.32, 137.19, 136.77, 135.19, 133.73, 131.47, 129.35, 128.90, 128.83, 127.73, 127.47, 126.70, 125.60, 106.74, 47.98, 35.26, 35.21, 31.06, 31.04, HRMS (ESI) calcd for  $\text{C}_{34}\text{H}_{37}\text{NO}_5\text{S}_2$ :  $[\text{M}+\text{Na}]^+$  626.2005, found 626.2035.

2-(benzylamino)-7-((4-nitrophenyl)sulfonyl)cyclohepta-2,4,6-trien-1-one (7a):



Following the general procedure the title compound was isolated by column chromatography (eluent: dichloromethane) as a yellow solid in 44% yield (37 mg).  $^1\text{H}$  NMR (700 MHz,

CDCl<sub>3</sub>)  $\delta$  8.57 (d,  $J$  = 10.1 Hz, 1H), 8.31 (d,  $J$  = 8.6 Hz, 2H), 8.21 (d,  $J$  = 8.6 Hz, 2H), 7.98 (s, 1H), 7.50 (t,  $J$  = 10.2 Hz, 1H), 7.41 – 7.29 (m, 3H), 7.23 (d,  $J$  = 7.0 Hz, 2H), 6.90 (t,  $J$  = 10.0 Hz, 1H), 6.66 (d,  $J$  = 10.6 Hz, 1H), 4.53 (d,  $J$  = 5.7 Hz, 2H), <sup>13</sup>C NMR (176 MHz, CDCl<sub>3</sub>)  $\delta$  170.20, 157.89, 150.09, 147.22, 142.99, 138.21, 134.77, 134.53, 129.85, 129.21, 128.53, 127.60, 123.60, 119.49, 109.57, 47.62. HRMS (ESI) calcd for C<sub>20</sub>H<sub>16</sub>N<sub>2</sub>O<sub>5</sub>S: [M+Na]<sup>+</sup> 419.0672, found 419.0666.

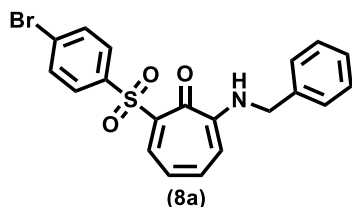


2-(benzylamino)-5-((4-nitrophenyl)sulfonyl)cyclohepta-2,4,6-

trien-1-one (**7b**): Following the general procedure the title compound was isolated by column chromatography (eluent: dichloromethane) as a yellow solid in 49% yield (41 mg). <sup>1</sup>H NMR (400 MHz, CDCl<sub>3</sub>)  $\delta$  8.33 (d,  $J$  = 8.8 Hz, 2H), 8.16 (s, 1H), 8.10 – 7.99 (m, 3H), 7.80 (dd,  $J$  = 12.3, 2.1 Hz, 1H),

7.45 – 7.31 (m, 3H), 7.30 – 7.26 (m, 2H), 7.09 (d,  $J$  = 12.3 Hz, 1H), 6.56 (d,  $J$  = 11.1 Hz, 1H), 4.61 (d,  $J$  = 5.9 Hz, 2H), <sup>13</sup>C NMR (101 MHz, CDCl<sub>3</sub>)  $\delta$  176.29, 157.33, 150.18, 147.76, 137.81, 134.61, 134.11, 130.73, 129.28, 128.63, 128.54, 127.44, 127.13, 124.63, 105.77, 47.48, HRMS (ESI) calcd for C<sub>20</sub>H<sub>16</sub>N<sub>2</sub>O<sub>5</sub>S: [M+Na]<sup>+</sup> 419.0672, found 419.0694.

2-(benzylamino)-7-((4-bromophenyl)sulfonyl)cyclohepta-2,4,6-trien-1-one (**8a**):

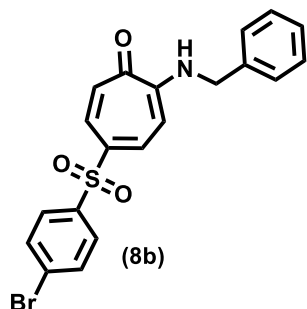


Following the general procedure the title compound was isolated by column chromatography (eluent: dichloromethane) as a yellow solid in 38% yield (52 mg). <sup>1</sup>H NMR (700 MHz, CDCl<sub>3</sub>)  $\delta$  8.60 (d,  $J$  = 10.0 Hz, 1H), 8.02

(s, 1H), 7.93 (d,  $J$  = 7.9 Hz, 2H), 7.63 (d,  $J$  = 8.0 Hz, 2H), 7.47 (t,  $J$  = 10.0 Hz, 1H), 7.41 – 7.33 (m, 3H), 7.28 (d,  $J$  = 7.7 Hz, 2H), 6.88 (t,  $J$  = 9.8 Hz, 1H), 6.64 (d,  $J$  = 10.4 Hz, 1H), 4.54 (d,  $J$  = 4.8 Hz, 2H), <sup>13</sup>C NMR (176 MHz, CDCl<sub>3</sub>)  $\delta$  170.31, 157.80, 142.44, 140.28,

138.09, 135.70, 134.76, 131.65, 130.31, 129.15, 128.42, 127.93, 127.61, 119.38, 109.28, 47.56, HRMS (ESI) calcd for  $C_{20}H_{16}NO_3SBr$ :  $[M+Na]^+$  451.9926, found 451.9912.

2-(benzylamino)-5-((4-bromophenyl)sulfonyl)cyclohepta-2,4,6-trien-1-one **(8b)**:



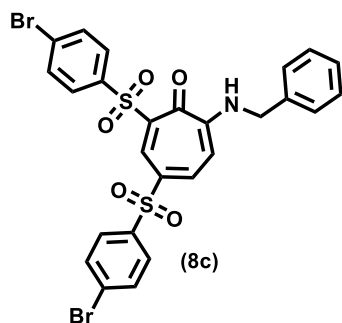
Following the general procedure the title compound was isolated

by column chromatography (eluent: dichloromethane) as a yellow solid in 42% yield (58 mg).  $^1H$  NMR (700 MHz,  $CDCl_3$ )  $\delta$

8.09 (s, 1H), 8.00 (dd,  $J = 11.0, 1.5$  Hz, 1H), 7.78 (dd,  $J = 12.3, 1.7$  Hz, 1H), 7.73 (d,  $J = 8.5$  Hz, 2H), 7.63 (d,  $J = 8.5$  Hz, 2H),

7.42 – 7.30 (m, 3H), 7.28 (d,  $J = 7.3$  Hz, 2H), 7.08 (d,  $J = 12.3$  Hz, 1H), 6.53 (d,  $J = 11.1$  Hz, 1H), 4.60 (d,  $J = 5.9$  Hz, 2H),  $^{13}C$  NMR (176 MHz,  $CDCl_3$ )  $\delta$  176.36, 157.10, 141.03, 137.22, 134.84, 134.17, 132.69, 132.18, 129.23, 128.89, 128.44, 128.23, 127.44, 127.17, 105.88, 47.40, HRMS (ESI) calcd for  $C_{20}H_{16}NO_3SBr$ :  $[M+Na]^+$  451.9926, found 451.9912.

7-(benzylamino)-2,4-bis((4-bromophenyl)sulfonyl)cyclohepta-2,4,6-trien-1-one **(8c)**:



Following the general procedure the title compound was

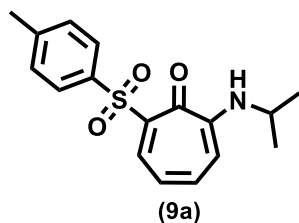
isolated by column chromatography (eluent: dichloromethane) as a yellow solid in 12% yield (16 mg).  $^1H$

NMR (700 MHz,  $CDCl_3$ )  $\delta$  9.16 (d,  $J = 13.2$  Hz, 1H), 8.44 (s, 1H), 8.20 (t,  $J = 11.9$  Hz, 1H), 7.88 (t,  $J = 11.1$  Hz, 2H), 7.82

(d,  $J = 8.4$  Hz, 2H), 7.69 (t,  $J = 11.3$  Hz, 2H), 7.63 (d,  $J = 8.5$  Hz, 2H), 7.37 (s, 2H), 7.26 – 7.19 (m, 3H), 6.64 (d,  $J = 11.3$  Hz, 1H), 4.58 (d,  $J = 5.7$  Hz, 2H),  $^{13}C$  NMR (176 MHz,  $CDCl_3$ )  $\delta$  169.99, 158.84, 141.51, 140.34, 139.15, 136.59, 134.49, 133.37, 133.00, 131.86, 130.67, 130.52, 129.45, 129.11, 129.01, 128.87, 128.66, 127.70, 106.98, 48.12, HRMS (ESI) calcd for  $C_{26}H_{19}NO_5S_2Br_2$ :  $[M+Na]^+$  671.8944, found 671.8963.

2-(isopropylamino)-7-tosylcyclohepta-2,4,6-trien-1-one (**9a**): Following the general procedure the title compound was isolated by column chromatography (eluent:

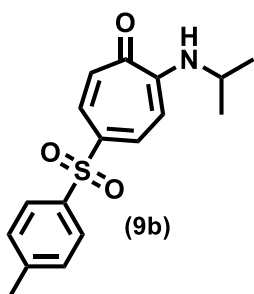
ethylacetate/hexane) as a yellow semi-solid in 33% yield (23 mg).



$^1\text{H}$  NMR (700 MHz,  $\text{CDCl}_3$ )  $\delta$  8.57 (d,  $J = 10.2$  Hz, 1H), 7.93 (d,  $J = 8.3$  Hz, 2H), 7.70 (d,  $J = 6.7$  Hz, 1H), 7.45 (t,  $J = 10.2$  Hz, 1H), 7.29 (d,  $J = 8.1$  Hz, 2H), 6.79 (t,  $J = 9.9$  Hz, 1H), 6.58 (d,  $J$

$= 10.7$  Hz, 1H), 3.89 – 3.80 (m, 1H), 2.40 (s, 3H), 1.28 (d,  $J = 6.4$  Hz, 6H),  $^{13}\text{C}$  NMR (176 MHz,  $\text{CDCl}_3$ )  $\delta$  170.14, 156.99, 143.44, 142.01, 138.59, 137.70, 135.26, 129.08, 128.47, 118.45, 108.89, 44.66, 21.75, 21.65, HRMS (ESI) calcd for  $\text{C}_{17}\text{H}_{19}\text{NO}_3\text{S}$ :  $[\text{M}+\text{Na}]^+$  340.0978, found 340.1003.

2-(isopropylamino)-5-tosylcyclohepta-2,4,6-trien-1-one (**9b**): Following the general procedure the title compound was isolated by column



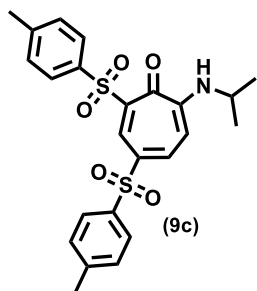
chromatography (eluent: ethylacetate/hexane) as a yellow semi-solid in 38% yield (26 mg).  $^1\text{H}$  NMR (700 MHz,  $\text{CDCl}_3$ )  $\delta$  8.06 (dd,  $J =$

11.2, 2.0 Hz, 1H), 7.80 (dd,  $J = 12.2$ , 2.1 Hz, 1H), 7.77 (d,  $J = 8.3$  Hz, 2H), 7.68 (d,  $J = 6.8$  Hz, 1H), 7.29 (d,  $J = 8.2$  Hz, 2H), 7.03 (d,  $J$

$= 12.2$  Hz, 1H), 6.54 (d,  $J = 11.3$  Hz, 1H), 3.95 – 3.87 (m, 1H), 2.39 (s, 3H), 1.34 (d,  $J = 6.5$  Hz, 6H),  $^{13}\text{C}$  NMR (176 MHz,  $\text{CDCl}_3$ )  $\delta$  176.12, 156.08, 143.88, 139.19, 136.84, 134.39, 132.24, 129.99, 127.33, 126.07, 105.81, 44.60, 21.81, 21.55, , HRMS (ESI) calcd for  $\text{C}_{17}\text{H}_{19}\text{NO}_3\text{S}$ :  $[\text{M}+\text{Na}]^+$  340.0978, found 340.1001.

7-(isopropylamino)-2,4-ditosylcyclohepta-2,4,6-trien-1-one (**9c**): Following the general procedure the title compound was isolated by column chromatography (eluent:

ethylacetate/hexane) as a yellow solid in 20% yield (20 mg).  $^1\text{H}$  NMR (700 MHz,  $\text{CDCl}_3$ )  $\delta$  9.20 (d,  $J = 1.9$  Hz, 1H), 8.23 – 8.18 (m, 1H), 8.11 (s, 1H), 7.92 (d,  $J = 8.2$  Hz, 2H), 7.86 (d,  $J = 8.3$  Hz, 2H), 7.34 (d,  $J = 8.1$  Hz, 2H), 7.30 (d,  $J = 8.1$  Hz, 2H), 6.58 (d,  $J = 11.5$  Hz, 1H),

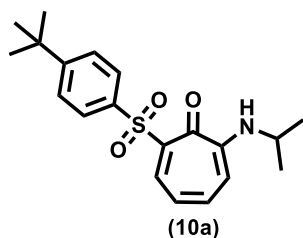


3.96 – 3.87 (m,  $J = 12.7, 6.3$  Hz, 1H), 2.42 (s, 3H), 2.40 (s, 3H), 1.30 (d,  $J = 6.4$  Hz, 6H),  $^{13}\text{C}$  NMR (101 MHz,  $\text{CDCl}_3$ )  $\delta$  169.94, 157.83, 144.40, 144.11, 140.84, 138.57, 137.59, 136.55, 134.02, 130.52, 130.25, 129.21, 128.90, 127.60, 106.69, 45.60, 29.70, 21.67, 21.64, HRMS (ESI) calcd for  $\text{C}_{24}\text{H}_{25}\text{NO}_5\text{S}_2$ :  $[\text{M}+\text{Na}]^+$  472.1247, found

472.1254.

2-((4-(tert-butyl)phenyl)sulfonyl)-7-(isopropylamino)cyclohepta-2,4,6-trien-1-one (**10a**):

Following the general procedure the title compound was isolated by column chromatography

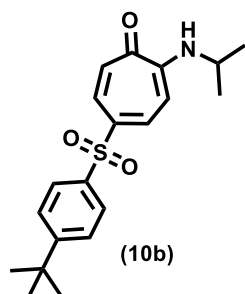


(eluent: dichloromethane) as a yellow solid in 34% yield (26 mg).

$^1\text{H}$  NMR (400 MHz,  $\text{CDCl}_3$ )  $\delta$  8.57 (dd,  $J = 10.1, 0.9$  Hz, 1H), 7.97 (d,  $J = 8.6$  Hz, 2H), 7.71 (d,  $J = 7.1$  Hz, 1H), 7.50 (d,  $J = 8.6$  Hz, 2H), 7.44 (t,  $J = 10.2$  Hz, 1H), 6.79 (t,  $J = 9.9$  Hz, 1H), 6.57

(d,  $J = 10.7$  Hz, 1H), 3.91 – 3.78 (m,  $J = 13.1, 6.5$  Hz, 1H), 1.31 (s, 9H), 1.29 (d,  $J = 6.4$  Hz, 6H).  $^{13}\text{C}$  NMR (101 MHz,  $\text{CDCl}_3$ )  $\delta$  170.19, 157.03, 156.27, 141.92, 138.47, 137.82, 135.31, 128.35, 125.47, 118.45, 108.79, 44.67, 35.14, 31.10, 21.78, HRMS (ESI) calcd for  $\text{C}_{20}\text{H}_{25}\text{NO}_3\text{S}$ :  $[\text{M}+\text{Na}]^+$  382.1447, found 382.1463.

5-((4-(tert-butyl)phenyl)sulfonyl)-2-(isopropylamino)cyclohepta-2,4,6-trien-1-one (**10b**):

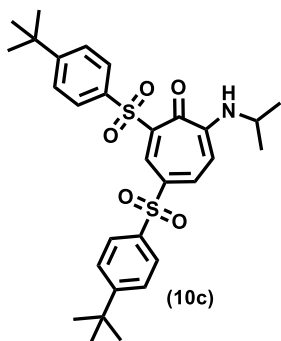


Following the general procedure the title compound was isolated by column chromatography (eluent: dichloromethane) as a yellow solid in 42% yield (32 mg).  $^1\text{H}$  NMR (400 MHz,  $\text{CDCl}_3$ )  $\delta$  8.06 (dd,  $J = 11.2, 2.0$  Hz, 1H), 7.85 – 7.75 (m, 3H), 7.66 (d,  $J = 7.4$  Hz, 1H), 7.48 (d,  $J = 8.5$  Hz, 2H), 7.01 (d,  $J = 12.2$  Hz, 1H), 6.53 (d,  $J = 11.3$  Hz, 1H),

3.95 – 3.82 (m, 1H), 1.32 (d,  $J = 6.4$  Hz, 6H), 1.28 (s, 9H),  $^{13}\text{C}$  NMR (101 MHz,  $\text{CDCl}_3$ )  $\delta$  176.13, 156.79, 156.11, 139.09, 136.92, 134.49, 132.25, 127.15, 126.37, 126.06, 105.85,

44.60, 35.15, 31.03, 21.81, HRMS (ESI) calcd for  $C_{20}H_{25}NO_3S$ :  $[M+Na]^+$  382.1447, found 382.1459.

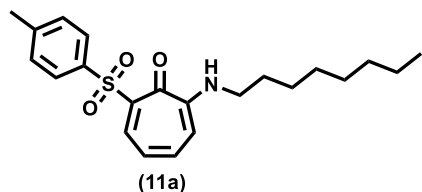
2,4-bis((4-(tert-butyl)phenyl)sulfonyl)-7-(isopropylamino)cyclohepta-2,4,6-trien-1-one (**10c**):



Following the general procedure the title compound was isolated by column chromatography (eluent: dichloromethane) as a yellow solid in 21% yield (25 mg).  $^1H$  NMR (700 MHz,  $CDCl_3$ )  $\delta$  9.21 (s, 1H), 8.24 (d,  $J$  = 11.3 Hz, 1H), 8.14 (d,  $J$  = 7.9 Hz, 1H), 7.96 (d,  $J$  = 8.4 Hz, 2H), 7.89 (d,  $J$  = 8.4 Hz, 2H), 7.55 (d,  $J$  = 8.4 Hz, 2H), 7.50 (d,  $J$  = 8.4 Hz, 2H), 6.59 (d,  $J$  = 11.5 Hz, 1H), 3.97 – 3.88 (m,

1H), 1.32 (s, 9H), 1.31 (s, 12H), 1.29 (s, 3H),  $^{13}C$  NMR (176 MHz,  $CDCl_3$ )  $\delta$  169.96, 157.84, 157.28, 157.00, 140.93, 138.44, 137.31, 136.72, 133.88, 130.45, 128.79, 127.39, 126.73, 125.65, 106.76, 45.63, 35.28, 35.24, 31.09, 31.06, 21.69. HRMS (ESI) calcd for  $C_{30}H_{37}NO_5S_2$ :  $[M+Na]^+$  578.2005, found 578.2039.

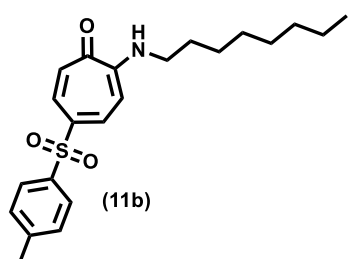
2-(octylamino)-7-tosylcyclohepta-2,4,6-trien-1-one (**11a**): Following the general procedure



the title compound was isolated by column chromatography (eluent: dichloromethane) as a brownish-yellow dense liquid in 38% yield (30 mg).  $^1H$  NMR (700 MHz,  $CDCl_3$ )  $\delta$  8.57 (d,  $J$  = 10.1 Hz, 1H),

7.93 (d,  $J$  = 8.3 Hz, 2H), 7.75 (s, 1H), 7.45 (t,  $J$  = 10.1 Hz, 1H), 7.28 (d,  $J$  = 8.2 Hz, 2H), 6.80 (t,  $J$  = 9.9 Hz, 1H), 6.54 (d,  $J$  = 10.7 Hz, 1H), 3.28 (dd,  $J$  = 13.2, 6.9 Hz, 2H), 2.39 (s, 3H), 1.69 – 1.66 (m, 2H), 1.39 – 1.36 (m, 2H), 1.31 – 1.27 (m,  $J$  = 8.3, 5.2 Hz, 8H), 0.88 (t,  $J$  = 6.9 Hz, 3H).  $^{13}C$  NMR (176 MHz,  $CDCl_3$ )  $\delta$  170.15, 158.04, 143.45, 142.00, 138.48, 137.76, 135.41, 129.04, 128.54, 118.60, 108.66, 43.35, 31.72, 29.14, 29.07, 28.22, 27.03, 22.60, 21.63, 14.06, HRMS (ESI) calcd for  $C_{22}H_{29}NO_3S$ :  $[M+Na]^+$  410.1760, found 410.1760.

2-(octylamino)-5-tosylcyclohepta-2,4,6-trien-1-one (**11b**): Following the general procedure

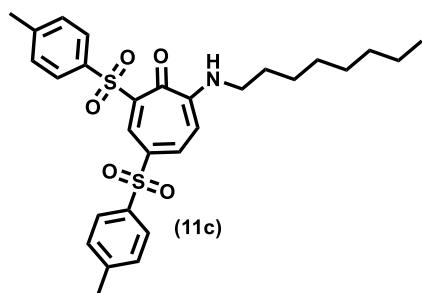


the title compound was isolated by column chromatography (eluent: dichloromethane) as a yellow solid in 41% yield (32 mg).

$^1\text{H}$  NMR (400 MHz,  $\text{CDCl}_3$ )  $\delta$  8.07 (dd,  $J = 11.0, 1.3$  Hz, 1H), 7.86 – 7.69 (m, 4H), 7.29 (d,  $J = 8.1$  Hz, 2H), 7.03 (d,  $J = 12.2$  Hz, 1H), 6.51 (d,  $J = 11.2$  Hz, 1H), 3.37 (dd,  $J = 13.0, 6.7$  Hz, 2H), 2.39 (s, 3H), 1.74 (dt,  $J = 14.7, 7.2$  Hz, 2H), 1.46 – 1.38 (m, 2H), 1.36 – 1.26 (m, 8H), 0.88 (t,  $J = 6.4$  Hz, 3H),

$^{13}\text{C}$  NMR (101 MHz,  $\text{CDCl}_3$ )  $\delta$  176.15, 157.14, 143.91, 139.14, 136.86, 134.46, 132.39, 130.00, 127.34, 126.18, 105.64, 43.25, 31.73, 29.15, 29.11, 28.20, 27.02, 22.62, 21.57, 14.09, HRMS (ESI) calcd for  $\text{C}_{22}\text{H}_{29}\text{NO}_3\text{S}$ :  $[\text{M}+\text{Na}]^+$  410.1760, found 410.1779.

7-(octylamino)-2,4-ditosylcyclohepta-2,4,6-trien-1-one (**11c**): Following the general



procedure the title compound was isolated by column chromatography (eluent: dichloromethane) as a yellow solid in 13% yield (14 mg).

$^1\text{H}$  NMR (700 MHz,  $\text{CDCl}_3$ )  $\delta$  9.20 (s, 1H), 8.23 (d,  $J = 10.6$  Hz, 2H), 7.88 (dd,  $J = 38.5, 7.9$  Hz, 4H), 7.33 (d,  $J = 7.8$  Hz, 2H), 7.28 (d,  $J = 7.6$  Hz, 2H), 6.58 (d,  $J = 11.3$  Hz, 1H), 3.37 (d,  $J = 6.2$  Hz, 2H), 2.42 (s, 3H), 2.39 (s, 3H), 1.69 – 1.65 (m, 2H), 1.38 – 1.33 (m,  $J = 7.0$  Hz, 2H), 1.28 – 1.25 (m, 8H), 0.87 (t,  $J = 6.9$  Hz, 3H),

$^{13}\text{C}$  NMR (176 MHz,  $\text{CDCl}_3$ )  $\delta$  169.90, 158.97, 144.40, 144.12, 140.92, 138.59, 137.49, 136.43, 130.53, 130.25, 129.18, 128.93, 127.57, 106.70, 43.88, 31.67, 29.04, 29.00, 28.0, 26.89, 22.57, 21.65, 21.60, 14.05, . HRMS (ESI) calcd for  $\text{C}_{29}\text{H}_{35}\text{NO}_5\text{S}_2$ :  $[\text{M}+\text{Na}]^+$  564.1849, found 564.1866.

*Swarming Assay:* Swarming motility assays were performed in M9 medium (Himedia) amended with 0.5% Bacto™ casamino acids (BD) and solidified with 0.6% Bacto™ agar (BD). 10 ml of swarm media supplemented with 100  $\mu\text{M}$  of different Alkylaminotroponyl



sulphone (**ATS**) derivatives were poured on petridishes (60 mm diameter) and were allowed to dry for 30 min. The plates were spot inoculated at the centre with one isolated colony grown on LB with the help of a straight wire loop. The plates were incubated in upright position at 37°C for 24 hours<sup>40</sup>. The plates were carefully taken out and observed for tendril formation. Images were taken in Gel Doc™ XR+ and processed by using Image lab™ software.

*Biofilm Assay:* Biofilm formation ability in presence of various synthesized Alkylaminotroponyl sulfone (**ATS**) derivatives was studied qualitatively and quantitatively by glass tube and microtitre plate assay. Briefly for qualitative analysis, 20 µL of overnight grown culture (OD<sub>595</sub> adjusted to 0.5) of PA14 was inoculated into 2 ml LB broth supplemented with 100 µM of different **ATS** derivatives and incubated at 37°C for 48 h. After incubation the culture was carefully decanted and the tube was rinsed twice by milli-Q water followed by staining with 0.1% aqueous solution of crystal violet for 30 min at room temperature. The crystal violet stain was carefully decanted and the tubes were washed with milli-Q water thrice followed by air drying and crystal violet ring observation.<sup>41</sup>

For quantitative analysis, 10 µL of overnight grown culture (OD<sub>595</sub> adjusted to 0.5) of PA14 was inoculated into 100 µL LB broth supplemented with 100 µg/ ml of different tropolone compounds taken in a micro-titre plate and incubated at 37°C for 48 h under moist condition. After incubation the supernatant were carefully taken off and unattached cells in the supernatant were carefully removed followed by washing with milliQ water twice. 125 µL of 0.1% crystal violet solution was added and micro-titre plate was incubated for 30 min followed by washing with milli-Q water thrice. The plates were air-dried and de-stained with 200 µL of 30% acetic acid and biofilm formation was indirectly quantified in terms of optical density of dissolved crystal violet at 595nm.<sup>42</sup> Compounds showing significant biofilm reduction were further tested for their anti-biofilm activity in dose dependent manner taking

concentration range from 20  $\mu\text{M}$  to 100  $\mu\text{M}$  and their  $\text{IC}_{50}$  values for biofilm formation were obtained.

**Pyocyanin Assay:** In order to assess the effect of synthesized Alkylaminotroponylsulfone (**ATS**) derivatives on pyocyanin production, *Pseudomonas aeruginosa* (PA14) were grown overnight in 5 mL minimal media (Himedia) in presence of 100  $\mu\text{M}$  of all the 26 **ATS** derivatives (**3a-11c**) under shaking condition<sup>43</sup>. After incubation, supernatant was collected from the 5 mL culture by centrifugation of the entire culture at 5000 rpm for 15 min at room temperature. The pyocyanin fraction was further extracted by adding 3 mL chloroform in the supernatant. Pyocyanin was then re-extracted into 1 mL of acidified water (0.2 mol/L HCl) which gave a pink–red solution. For the quantitation of the pyocyanin within the solution, the absorbance was measured at 520 nm. Pyocyanin inhibition was also performed at variable concentration to analyze their  $\text{IC}_{50}$  values for pyocyanin production.

**QRT-PCR (quantitative real-time polymerase chain reaction) analysis:** RNA was extracted from overnight grown 2 mL culture of PA14 treated with Alkylaminotroponyl sulfonone (**ATS**) derivatives (**3b**, **4b**, **7b**, **11b**, **5c** and **9c**) using the RiboPure™ kit (Ambion) according to the manufacturer's instruction. RNA purity was assessed by spectrophotometer (NanoDrop ND-1000). Samples showing ratios of  $A_{260}/A_{280}$  close to 2.0 were selected. First strand cDNA was synthesized from 1  $\mu\text{g}$  of treated RNA using the Verso cDNA synthesis kit (Thermo Scientific) as per manufacture's guidelines. Primers were designed for *lasI*, *lasB*, *lasR* genes using the sequences obtained from pseudomonas database (<https://www.pseudomonas.com/>) (Table S2). cDNA was diluted 10-fold and combined with primer pairs and PowerUp™ SYBR® Green Master Mix (Thermo Scientific) on an Applied Biosystems real-time PCR system (QuantStudio 6 and 7 Flex Real-Time PCR System) according to the following protocol: 95 °C for 2 min; 40 cycles of 95 °C for 3 sec, 60 °C for 30 sec; followed by a melt curve cycle. The housekeeping gene 16S ribosomal RNA (rRNA) was used as an internal

standard for quantification of the total RNA<sup>44</sup>. For each gene, a common threshold setting applied to each of the three biological replicates determined the threshold cycle ( $C_T$ ). Relative abundance of each gene was determined by the  $2^{-\Delta\Delta C_t}$  method.<sup>45</sup>

*HEK293T cell viability assay:* 20000 HEK293T cells were plated in triplicate in a 96-well plate. The plates were incubated for 18 h under normal culture conditions (37°C and 5% CO<sub>2</sub>). Cells were washed thrice with PBS followed by addition of 200uL of DMEM supplemented with 10 µL of OD<sub>600</sub>=2 of PA14 grown in presence and absence of anti-swarm concentrations of compounds. The plates were incubated for 12 hour followed by viability analysis through MTS assay<sup>46,47</sup>.

*Cell proliferation assay:* The cytotoxicity analysis of selected six compounds (**3b**, **4b**, **7b**, **11b**, **5c** and **9c**) on HEK293T cells derived from human embryonic kidney was performed using MTS CellTiter 96® AQueous One Solution Reagent (Promega, WI, USA) as per the manufacturer's protocol. 20000 cells/ well were seeded in a 96 well plate for 16h followed by treatment with defined range of concentrations (0 to 100 µM) of selected compounds for 18 h. After incubation cell cytotoxicity was measured in terms of cell viability by addition of MTS reagent. The final absorbance was taken at 490nm using Varioskan Flash multimode reader (Thermo Scientific).

### 3A.6 References and Notes

- (1) Behera, P.; Kumar Singh, K.; Kumar Saini, D.; De, M. Rapid Discrimination of Bacterial Drug Resistivity by Array-Based Cross-Validation Using 2D MoS<sub>2</sub>. *Chem. Eur. J.* **2022**, e202201386.
- (2) Choi, H.; Ham, S.-Y.; Cha, E.; Shin, Y.; Kim, H.-S.; Bang, J. K.; Son, S.-H.; Park, H.-D.; Byun, Y. Structure–Activity Relationships of 6-and 8-Gingerol Analogs as Anti-

- Biofilm Agents. *J. Med. Chem.* **2017**, *60* (23), 9821–9837.
- (3) Privalsky, T. M.; Soohoo, A. M.; Wang, J.; Walsh, C. T.; Wright, G. D.; Gordon, E. M.; Gray, N. S.; Khosla, C. Prospects for Antibacterial Discovery and Development. *J. Am. Chem. Soc.* **2021**, *143* (50), 21127–21142.
  - (4) Rosenthal, V. D.; Al-Abdely, H. M.; El-Kholy, A. A.; AlKhawaja, S. A. A.; Leblebicioglu, H.; Mehta, Y.; Rai, V.; Hung, N. V.; Kanj, S. S.; Salama, M. F. International Nosocomial Infection Control Consortium Report, Data Summary of 50 Countries for 2010-2015: Device-Associated Module. *Am. J. Infect. Control* **2016**, *44* (12), 1495–1504.
  - (5) Lambert, M.-L.; Suetens, C.; Savey, A.; Palomar, M.; Hiesmayr, M.; Morales, I.; Agodi, A.; Frank, U.; Mertens, K.; Schumacher, M. Clinical Outcomes of Health-Care-Associated Infections and Antimicrobial Resistance in Patients Admitted to European Intensive-Care Units: A Cohort Study. *Lancet Infect. Dis.* **2011**, *11* (1), 30–38.
  - (6) Alonso, B.; Fernández-Barat, L.; Di Domenico, E. G.; Marín, M.; Cercenado, E.; Merino, I.; de Pablos, M.; Muñoz, P.; Guembe, M. Characterization of the Virulence of *Pseudomonas Aeruginosa* Strains Causing Ventilator-Associated Pneumonia. *BMC Infect. Dis.* **2020**, *20* (1), 1–8.
  - (7) Kearns, D. B. A Field Guide to Bacterial Swarming Motility. *Nat. Rev. Microbiol.* **2010**, *8* (9), 634–644.
  - (8) Chuang, S. K.; Vrla, G. D.; Fröhlich, K. S.; Gitai, Z. Surface Association Sensitizes *Pseudomonas Aeruginosa* to Quorum Sensing. *Nat Commun* **10**: 4118. 2019.
  - (9) Hurley, M. N.; Cámara, M.; Smyth, A. R. Novel Approaches to the Treatment of

- Pseudomonas Aeruginosa* Infections in Cystic Fibrosis. *Eur. Respir. J.* **2012**, *40* (4), 1014–1023.
- (10) Aykac, K.; Ozsurekci, Y.; Tanir Basaranoglu, S. Future Directions and Molecular Basis of Ventilator Associated Pneumonia. *Can. Respir. J.* **2017**, *2017*.
- (11) Liang, H.-W.; Jiang, K.; Ding, W.; Yuan, Y.; Shuai, L.; Chen, Y.-C.; Wei, Y. Selective Remote C–H Sulfonylation of Aminoquinolines with Arylsulfonyl Chlorides via Copper Catalysis. *Chem. Commun.* **2015**, *51* (95), 16928–16931.
- (12) Guo, H.; Roman, D.; Beemelmans, C. Tropolone Natural Products. *Nat. Prod. Rep.* **2019**, *36* (8), 1137–1155.
- (13) Ononye, S. N.; VanHeyst, M. D.; Oblak, E. Z.; Zhou, W.; Ammar, M.; Anderson, A. C.; Wright, D. L. Tropolones as Lead-like Natural Products: The Development of Potent and Selective Histone Deacetylase Inhibitors. *ACS Med. Chem. Lett.* **2013**, *4* (8), 757–761.
- (14) Muetterties, E. L.; Roesky, H.; Wright, C. M. Chelate Chemistry. V. Metal Chelates Based on Tropolone and Its Derivatives. *J. Am. Chem. Soc.* **1966**, *88* (21), 4856–4861.
- (15) Shen, C.; Zhang, P.; Sun, Q.; Bai, S.; Hor, T. S. A.; Liu, X. Recent Advances in C–S Bond Formation via C–H Bond Functionalization and Decarboxylation. *Chem. Soc. Rev.* **2015**, *44* (1), 291–314.
- (16) Zhao, X.; Dong, V. M. Carbon–Sulfur Reductive Elimination from Palladium (IV) Sulfinate Complexes. *Angew. Chemie* **2011**, *123* (4), 962–964.
- (17) Zhao, X.; Dimitrijevic, E.; Dong, V. M. Palladium-Catalyzed C–H Bond Functionalization with Arylsulfonyl Chlorides. *J. Am. Chem. Soc.* **2009**, *131* (10),

- 3466–3467.
- (18) Qiao, H.; Sun, S.; Yang, F.; Zhu, Y.; Zhu, W.; Dong, Y.; Wu, Y.; Kong, X.; Jiang, L.; Wu, Y. Copper (I)-Catalyzed Sulfonylation of 8-Aminoquinoline Amides with Sulfonyl Chlorides in Air. *Org. Lett.* **2015**, *17* (24), 6086–6089.
- (19) El-Awa, A.; Noshi, M. N.; du Jourdin, X. M.; Fuchs, P. L. Evolving Organic Synthesis Fostered by the Pluripotent Phenylsulfone Moiety. *Chem. Rev.* **2009**, *109* (6), 2315–2349.
- (20) Blakemore, P. R. The Modified Julia Olefination: Alkene Synthesis via the Condensation of Metallated Heteroarylalkylsulfones with Carbonyl Compounds. *J. Chem. Soc. Perkin Trans. 1* **2002**, No. 23, 2563–2585.
- (21) Söderman, S. C.; Schwan, A. L. 1, 2-Dibromotetrachloroethane: An Ozone-Friendly Reagent for the in Situ Ramberg-Bäcklund Rearrangement and Its Use in the Formal Synthesis of E-Resveratrol. *J. Org. Chem.* **2012**, *77* (23), 10978–10984.
- (22) Palai, B. B.; Soren, R.; Sharma, N. K. BODIPY Analogues: Synthesis and Photophysical Studies of Difluoro Boron Complexes from 2-Aminotropone Scaffolds through N, O-Chelation. *Org. Biomol. Chem.* **2019**, *17* (26), 6497–6505.
- (23) Chen, G.; Zhang, X.; Zeng, Z.; Peng, W.; Liang, Q.; Liu, J. Copper-Catalyzed Remote C-H Sulfonylation of 8-Aminoquinoline Amides with Arylsulfonyl Hydrazides. *ChemistrySelect* **2017**, *2* (5), 1979–1982.
- (24) Verstraeten, N.; Braeken, K.; Debkumari, B.; Fauvart, M.; Fransaer, J.; Vermant, J.; Michiels, J. Living on a Surface: Swarming and Biofilm Formation. *Trends Microbiol.* **2008**, *16* (10), 496–506.

- (25) Rütchlin, S.; Böttcher, T. Inhibitors of Bacterial Swarming Behavior. *Chem. Eur. J.* **2020**, *26* (5), 964–979.
- (26) Caiazza, N. C.; Shanks, R. M. Q.; O'toole, G. A. Rhamnolipids Modulate Swarming Motility Patterns of *Pseudomonas Aeruginosa*. *J. Bacteriol.* **2005**, *187* (21), 7351–7361.
- (27) Mangwani, N.; Kumari, S.; Das, S. Effect of Synthetic N-Acylhomoserine Lactones on Cell–Cell Interactions in Marine *Pseudomonas* and Biofilm Mediated Degradation of Polycyclic Aromatic Hydrocarbons. *Chem. Eng. J.* **2016**, *302*, 172–186.
- (28) Fullagar, J. L.; Garner, A. L.; Struss, A. K.; Day, J. A.; Martin, D. P.; Yu, J.; Cai, X.; Janda, K. D.; Cohen, S. M. Antagonism of a Zinc Metalloprotease Using a Unique Metal-Chelating Scaffold: Tropolones as Inhibitors of *P. Aeruginosa* Elastase. *Chem. Commun.* **2013**, *49* (31), 3197–3199.
- (29) Hall, C. W.; Mah, T.-F. Molecular Mechanisms of Biofilm-Based Antibiotic Resistance and Tolerance in Pathogenic Bacteria. *FEMS Microbiol. Rev.* **2017**, *41* (3), 276–301.
- (30) Lee, J.; Zhang, L. The Hierarchy Quorum Sensing Network in *Pseudomonas Aeruginosa*. *Protein Cell* **2015**, *6* (1), 26–41.
- (31) Guendouze, A.; Plener, L.; Bzdrenga, J.; Jacquet, P.; Rémy, B.; Elias, M.; Lavigne, J.-P.; Daudé, D.; Chabrière, E. Effect of Quorum Quenching Lactonase in Clinical Isolates of *Pseudomonas Aeruginosa* and Comparison with Quorum Sensing Inhibitors. *Front. Microbiol.* **2017**, *8*, 227.
- (32) Davenport, P. W.; Griffin, J. L.; Welch, M. Quorum Sensing Is Accompanied by Global Metabolic Changes in the Opportunistic Human Pathogen *Pseudomonas*

- Aeruginosa*. *J. Bacteriol.* **2015**, 197 (12), 2072–2082.
- (33) Tan, M.-W.; Rahme, L. G.; Sternberg, J. A.; Tompkins, R. G.; Ausubel, F. M. *Pseudomonas Aeruginosa* Killing of *Caenorhabditis Elegans* Used to Identify *P. Aeruginosa* Virulence Factors. *Proc. Natl. Acad. Sci.* **1999**, 96 (5), 2408–2413.
- (34) Parsek, M. R.; Greenberg, E. P. Acyl-Homoserine Lactone Quorum Sensing in Gram-Negative Bacteria: A Signaling Mechanism Involved in Associations with Higher Organisms. *Proc. Natl. Acad. Sci.* **2000**, 97 (16), 8789–8793.
- (35) Liu, J.; Hou, J.-S.; Chang, Y.-Q.; Peng, L.-J.; Zhang, X.-Y.; Miao, Z.-Y.; Sun, P.-H.; Lin, J.; Chen, W.-M. New Pqs Quorum Sensing System Inhibitor as an Antibacterial Synergist against Multidrug-Resistant *Pseudomonas Aeruginosa*. *J. Med. Chem.* **2021**.
- (36) Galdino, A. C. M.; Viganor, L.; De Castro, A. A.; Da Cunha, E. F. F.; Mello, T. P.; Mattos, L. M.; Pereira, M. D.; Hunt, M. C.; O'Shaughnessy, M.; Howe, O. Disarming *Pseudomonas Aeruginosa* Virulence by the Inhibitory Action of 1, 10-Phenanthroline-5, 6-Dione-Based Compounds: Elastase B (LasB) as a Chemotherapeutic Target. *Front. Microbiol.* **2019**, 1701.
- (37) Miyoshi, S.; Shinoda, S. Microbial Metalloproteases and Pathogenesis. *Microbes Infect.* **2000**, 2 (1), 91–98.
- (38) Trust, T. J. Antibacterial Activity of Tropolone. *Antimicrob. Agents Chemother.* **1975**, 7 (5), 500–506.
- (39) Yu, X.; Li, X.; Wan, B. Palladium-Catalyzed Desulfitative Arylation of Azoles with Arylsulfonyl Hydrazides. *Org. Biomol. Chem.* **2012**, 10 (37), 7479–7482.
- (40) Overhage, J.; Lewenza, S.; Marr, A. K.; Hancock, R. E. W. Identification of Genes

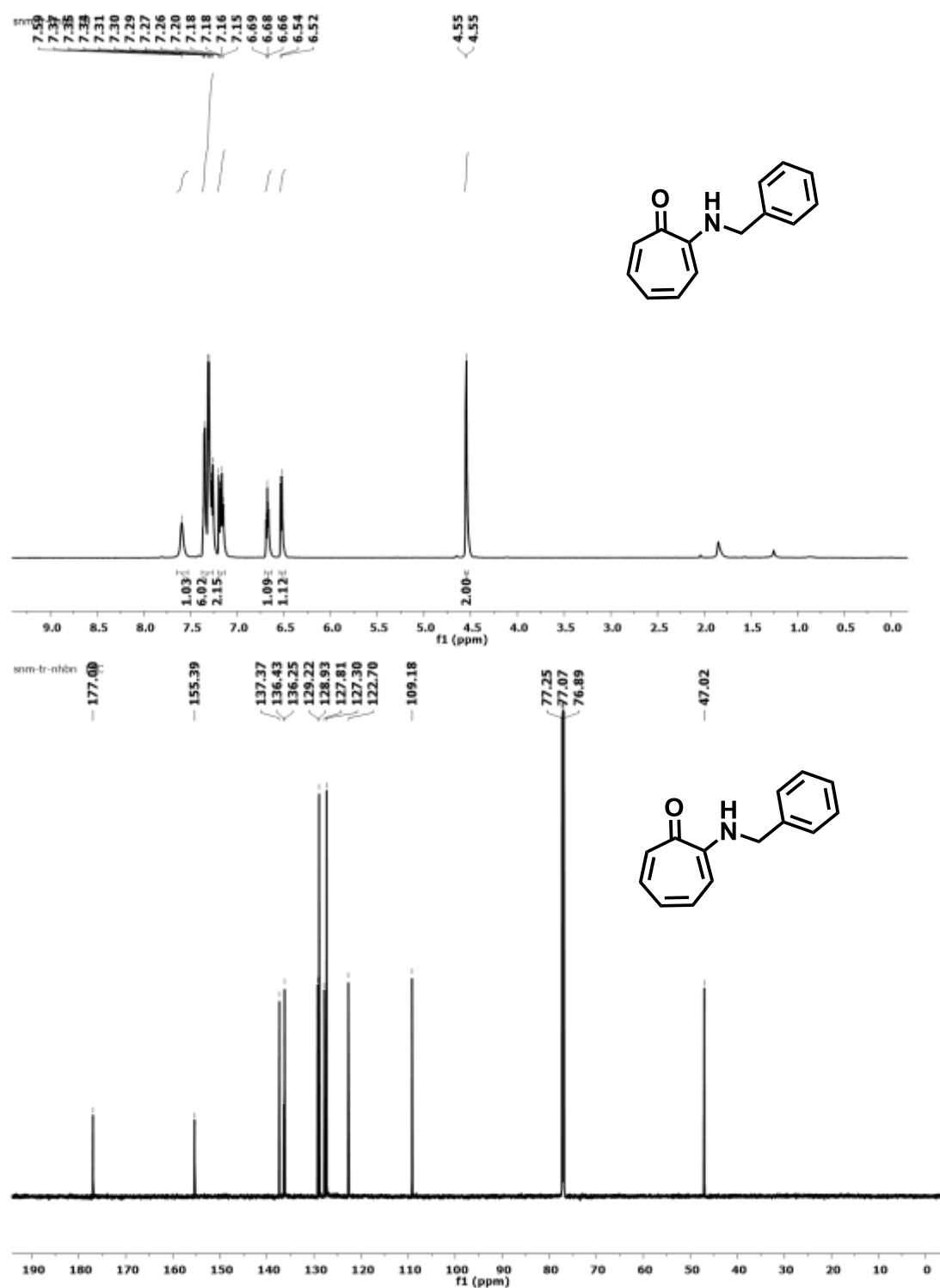


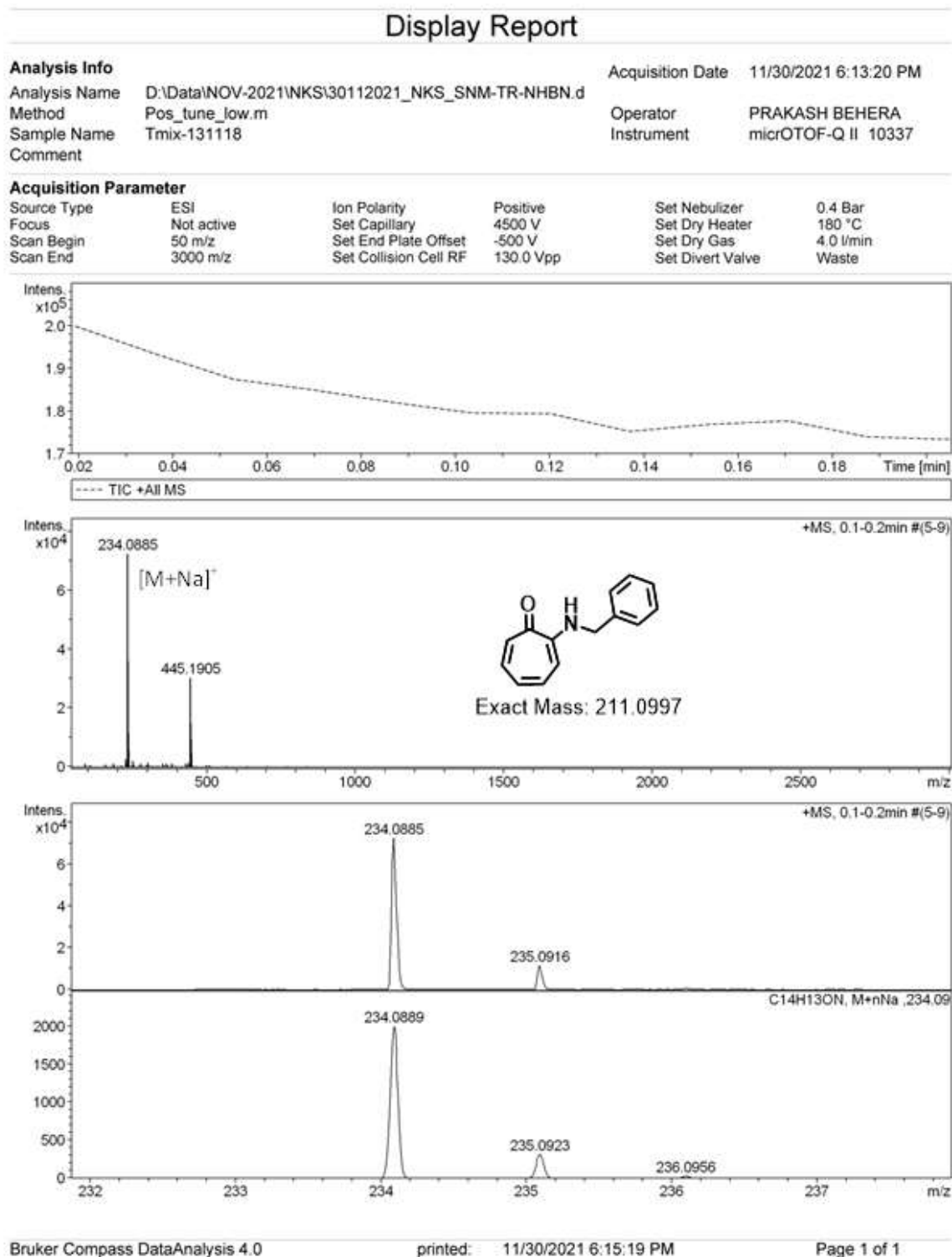
- Involved in Swarming Motility Using a *Pseudomonas Aeruginosa* PAO1 Mini-Tn 5-Lux Mutant Library. *J. Bacteriol.* **2007**, 189 (5), 2164–2169.
- (41) Haney, E. F.; Trimble, M. J.; Cheng, J. T.; Vallé, Q.; Hancock, R. E. W. Critical Assessment of Methods to Quantify Biofilm Growth and Evaluate Antibiofilm Activity of Host Defence Peptides. *Biomolecules* **2018**, 8 (2), 29.
- (42) Judith, H. M.; Daniel, E. K.; George, A. O. Growing and Analyzing Static Biofilms. *Curre Proto in Microbiol* **2005**.
- (43) Ugurlu, A.; Yagci, A. K.; Ulusoy, S.; Aksu, B.; Bosgelmez-Tinaz, G. Phenolic Compounds Affect Production of Pyocyanin, Swarming Motility and Biofilm Formation of *Pseudomonas Aeruginosa*. *Asian Pac. J. Trop. Biomed.* **2016**, 6 (8), 698–701.
- (44) Uchiya, K.; Sugita, A.; Nikai, T. Involvement of SPI-2-Encoded SpiC in Flagellum Synthesis in *Salmonella Enterica* Serovar Typhimurium. *BMC Microbiol.* **2009**, 9 (1), 1–10.
- (45) Livak, K. J.; Schmittgen, T. D. Analysis of Relative Gene Expression Data Using Real-Time Quantitative PCR and the 2<sup>−</sup> ΔΔCT Method. *methods* **2001**, 25 (4), 402–408.
- (46) Gi, M.; Jeong, J.; Lee, K.; Lee, K.-M.; Toyofuku, M.; Yong, D. E.; Yoon, S. S.; Choi, J. Y. A Drug-Repositioning Screening Identifies Pentetic Acid as a Potential Therapeutic Agent for Suppressing the Elastase-Mediated Virulence of *Pseudomonas Aeruginosa*. *Antimicrob. Agents Chemother.* **2014**, 58 (12), 7205–7214.
- (47) O’Loughlin, C. T.; Miller, L. C.; Siryaporn, A.; Drescher, K.; Semmelhack, M. F.; Bassler, B. L. A Quorum-Sensing Inhibitor Blocks *Pseudomonas Aeruginosa*

Virulence and Biofilm Formation. *Proc. Natl. Acad. Sci.* **2013**, *110* (44), 17981–17986.

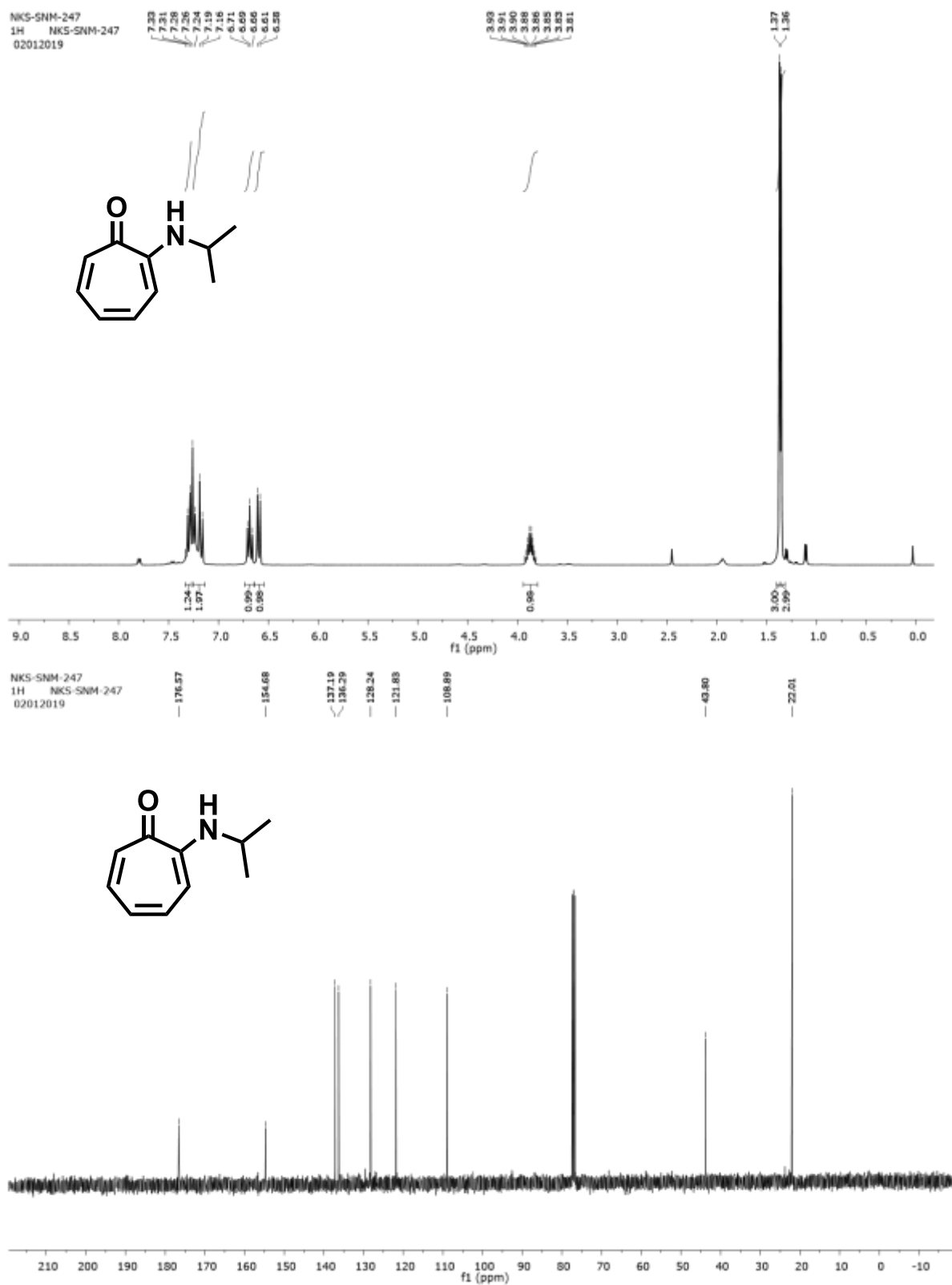
### 3A.7 Appendix

1. $^1\text{H}$ , $^{13}\text{C}$ Spectra and HRMS.....	146
2. Crystal data of compound 3b.....	204

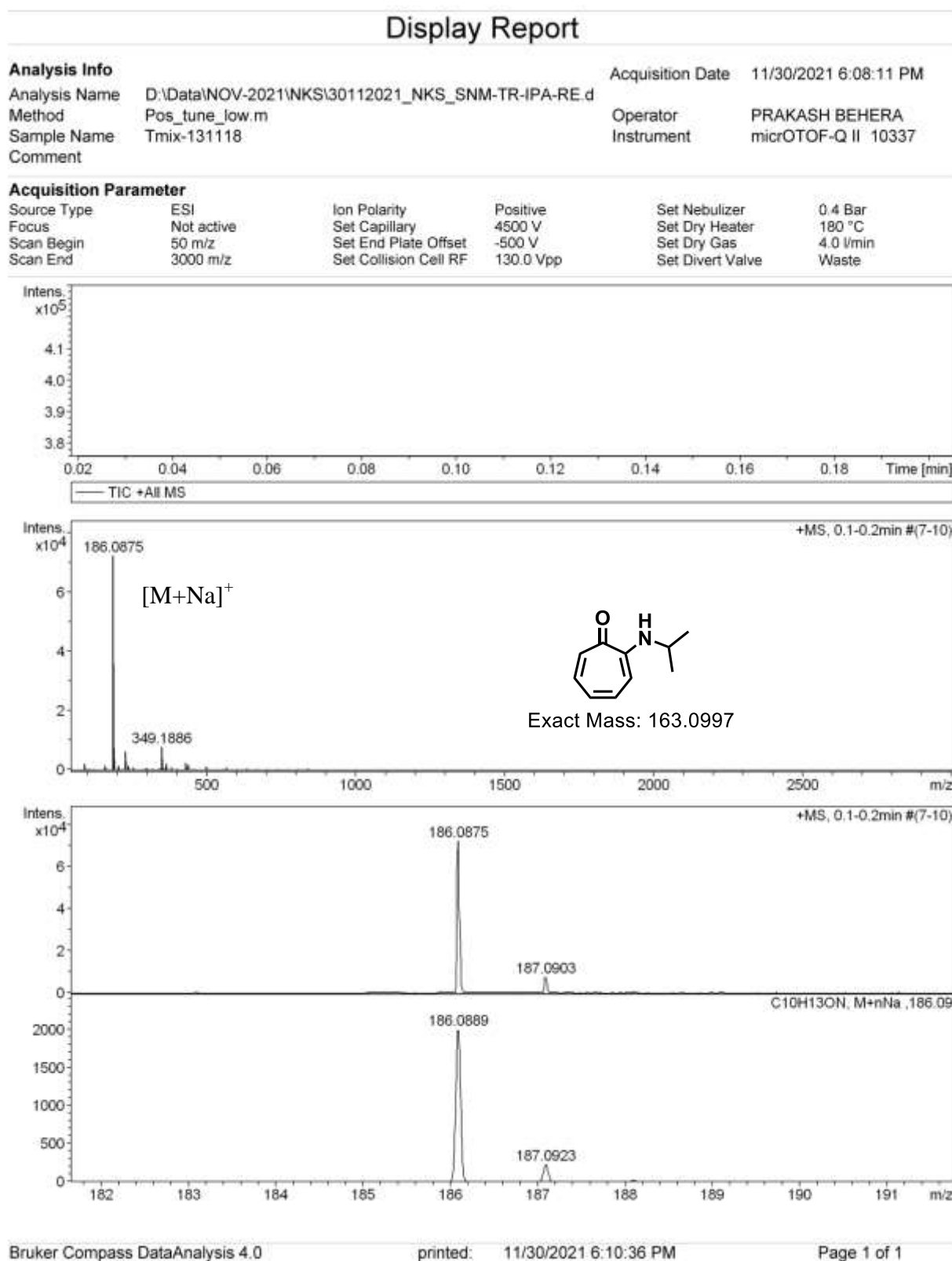
1.  $^1\text{H}$ ,  $^{13}\text{C}$  Spectra and HRMS $^1\text{H}$ ,  $^{13}\text{C}$  NMR (700MHz,  $\text{CDCl}_3$ ) and HRMS of **1a****Figure A1.**  $^1\text{H}/^{13}\text{C}$  NMR (700MHz,  $\text{CDCl}_3$ ) spectra of compound **1a** in  $\text{CDCl}_3$

**Figure A2.** ESI-MS/HRMS spectra of compound **1a**

$^1\text{H}$ ,  $^{13}\text{C}$  NMR (400MHz,  $\text{CDCl}_3$ ) and HRMS of **1b**

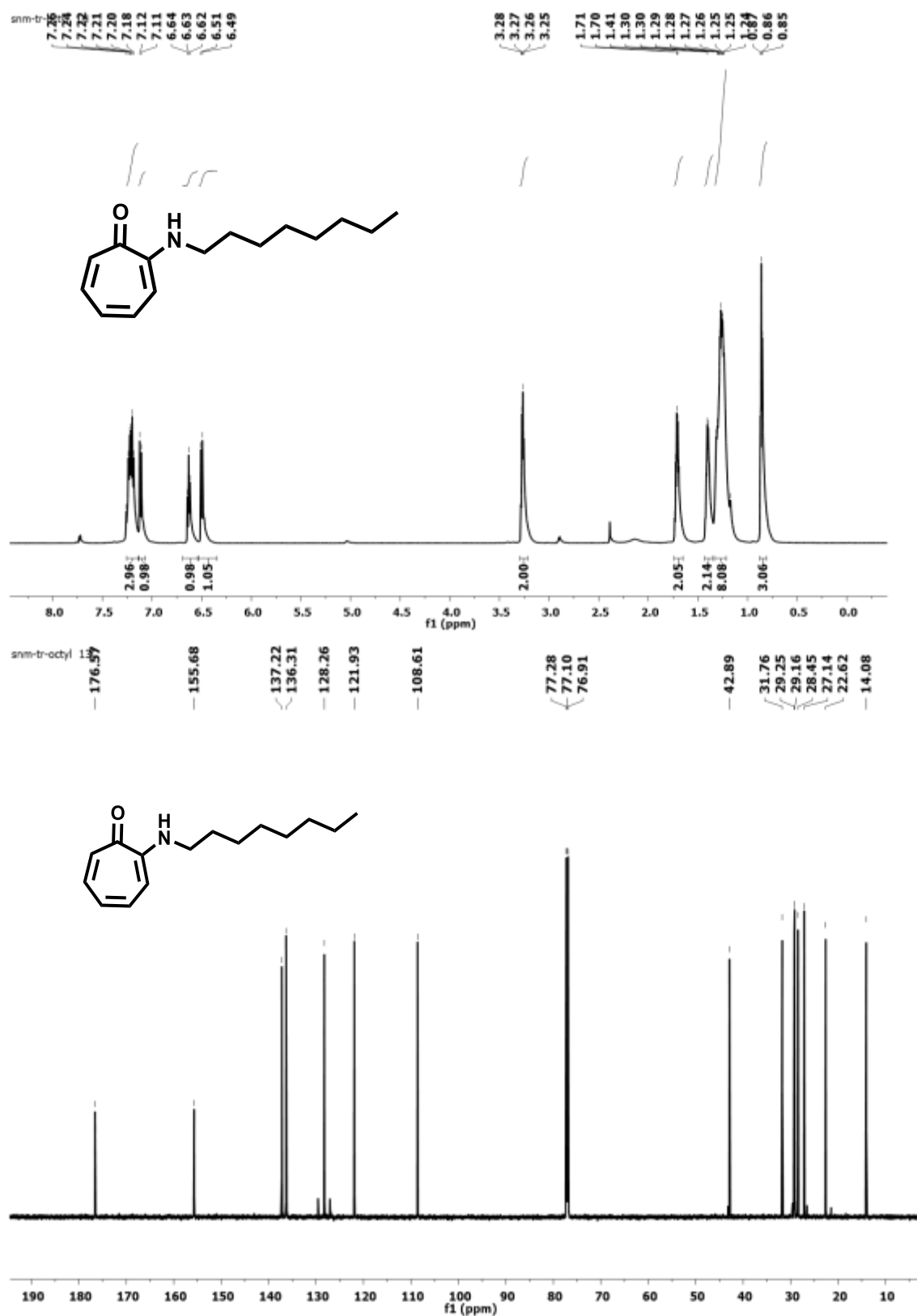


**Figure A3.**  $^1\text{H}/^{13}\text{C}$  NMR (400MHz,  $\text{CDCl}_3$ ) spectra of compound **1b** in  $\text{CDCl}_3$

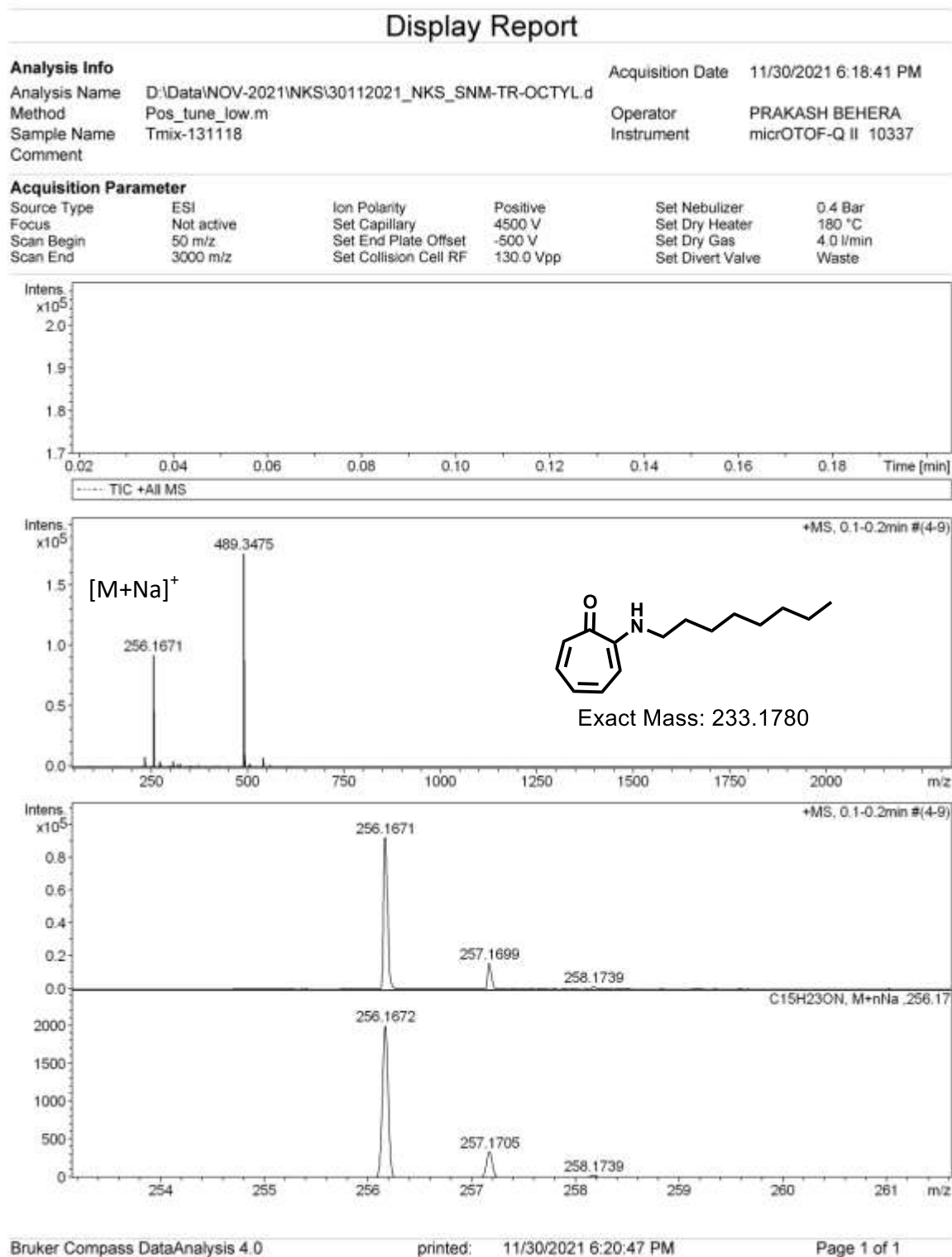


**Figure A4.** ESI-MS/HRMS spectra of compound **1b**

$^1\text{H}$ ,  $^{13}\text{C}$  NMR (700MHz,  $\text{CDCl}_3$ ) and HRMS of **1c**

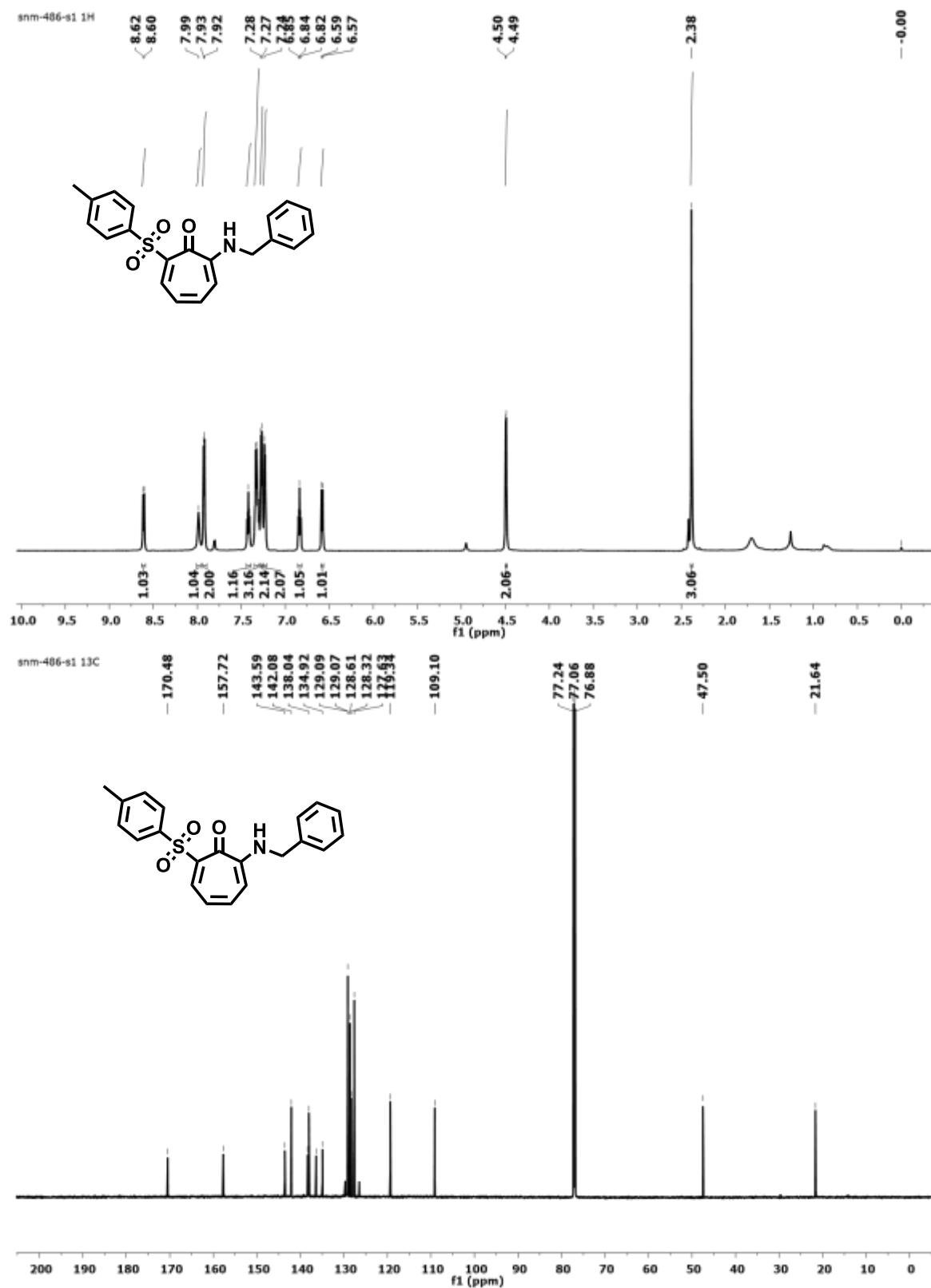


**Figure A5.**  $^1\text{H}/^{13}\text{C}$  NMR (700MHz,  $\text{CDCl}_3$ ) spectra of compound **1c** in  $\text{CDCl}_3$

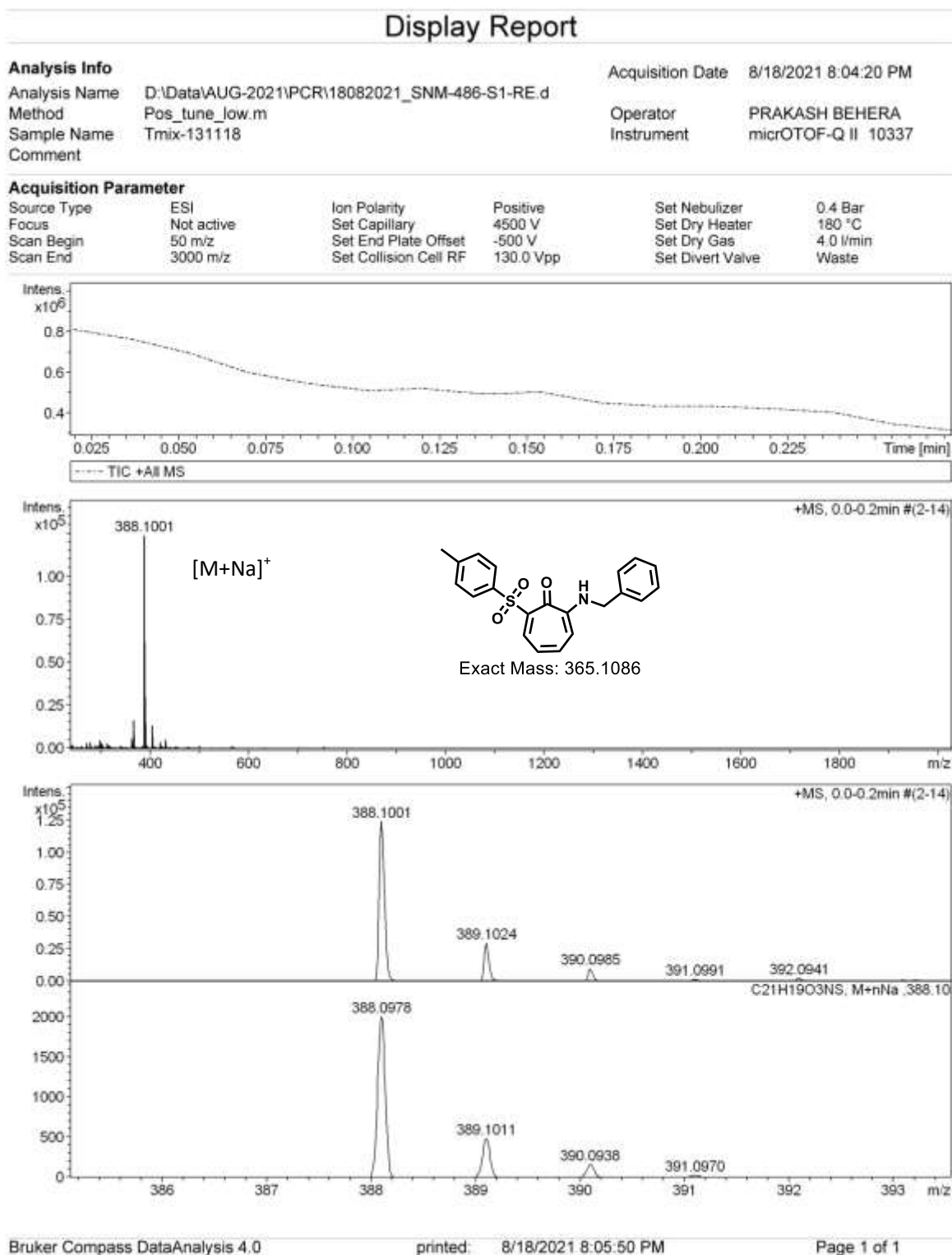
**Figure A6.** ESI-MS/HRMS spectra of compound **1c**



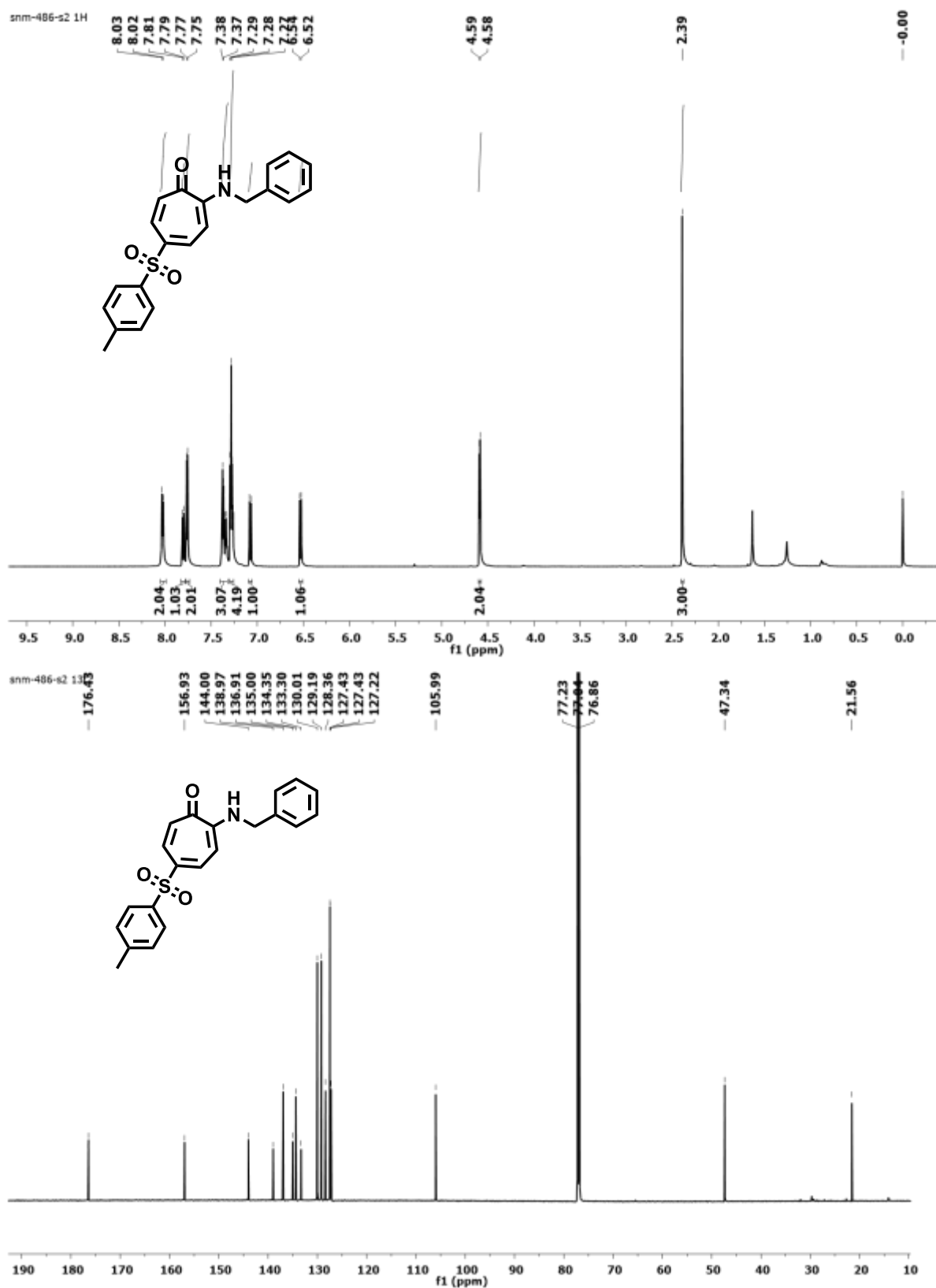
$^1\text{H}$ ,  $^{13}\text{C}$  NMR (700MHz,  $\text{CDCl}_3$ ) and HRMS of **3a**



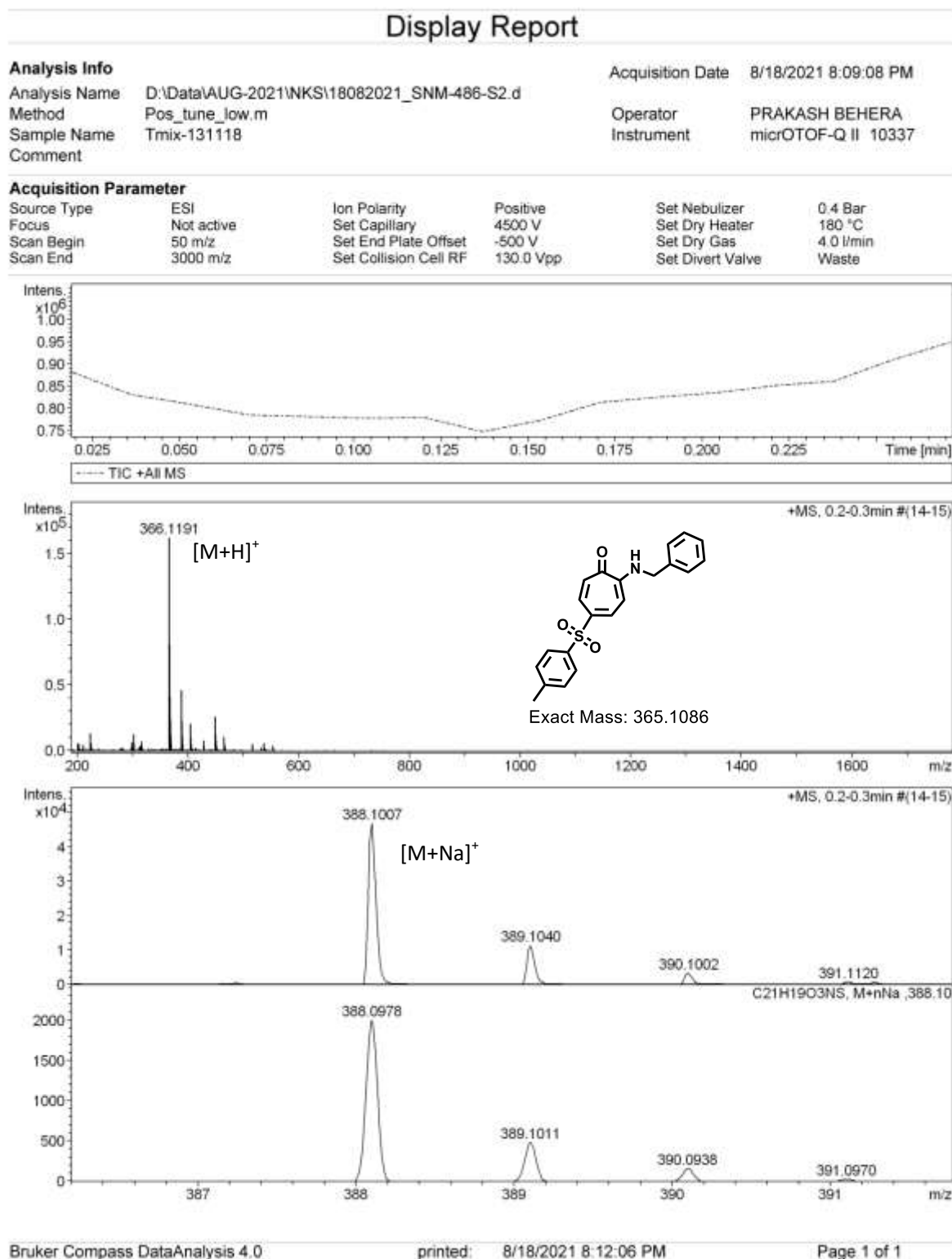
**Figure A7.**  $^1\text{H}/^{13}\text{C}$  NMR (700MHz,  $\text{CDCl}_3$ ) spectra of compound **3a** in  $\text{CDCl}_3$

**Figure A8.** ESI-MS/HRMS spectra of compound **3a**

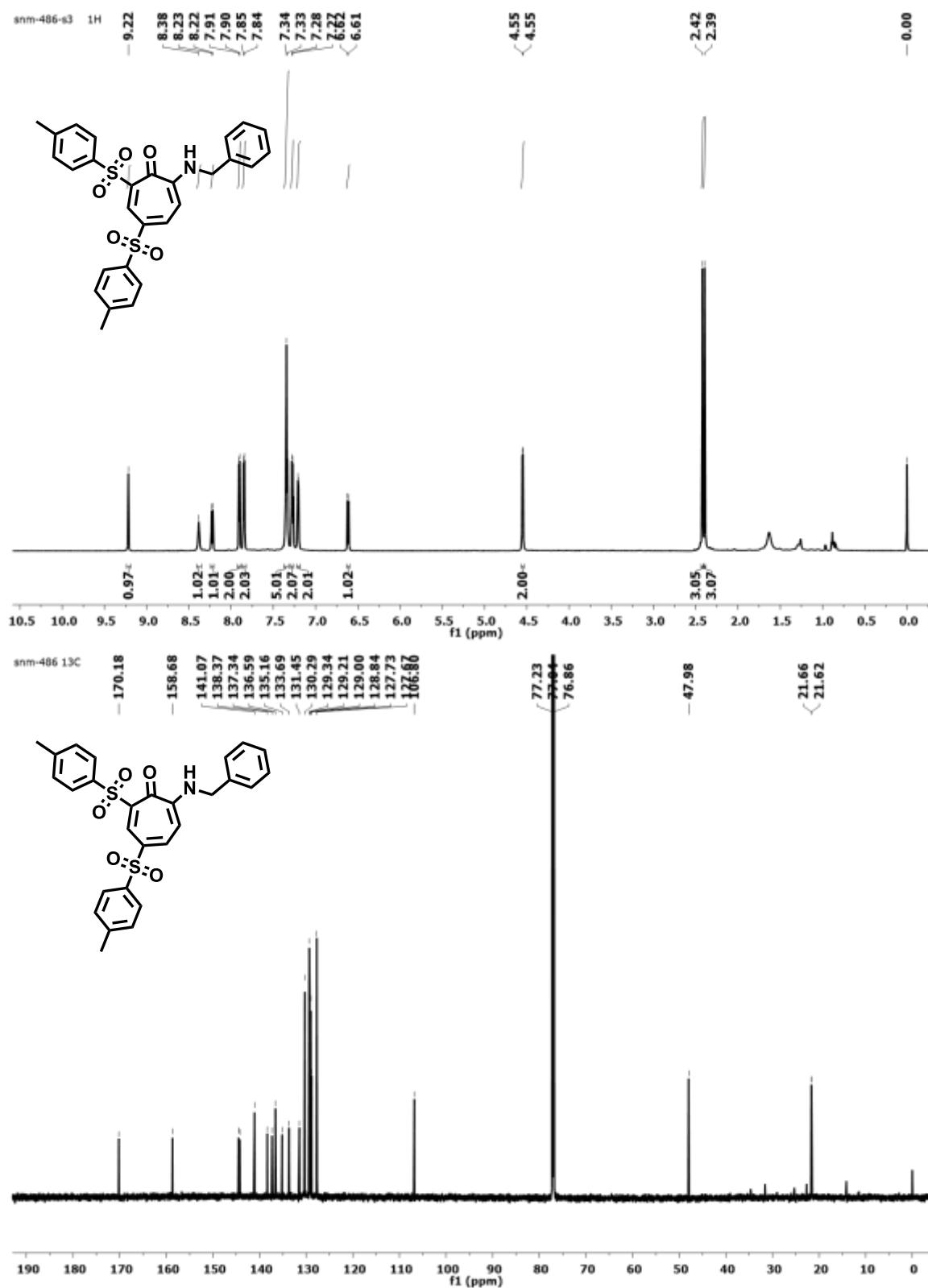
$^1\text{H}$ ,  $^{13}\text{C}$  NMR (700MHz,  $\text{CDCl}_3$ ) and HRMS of **3b**



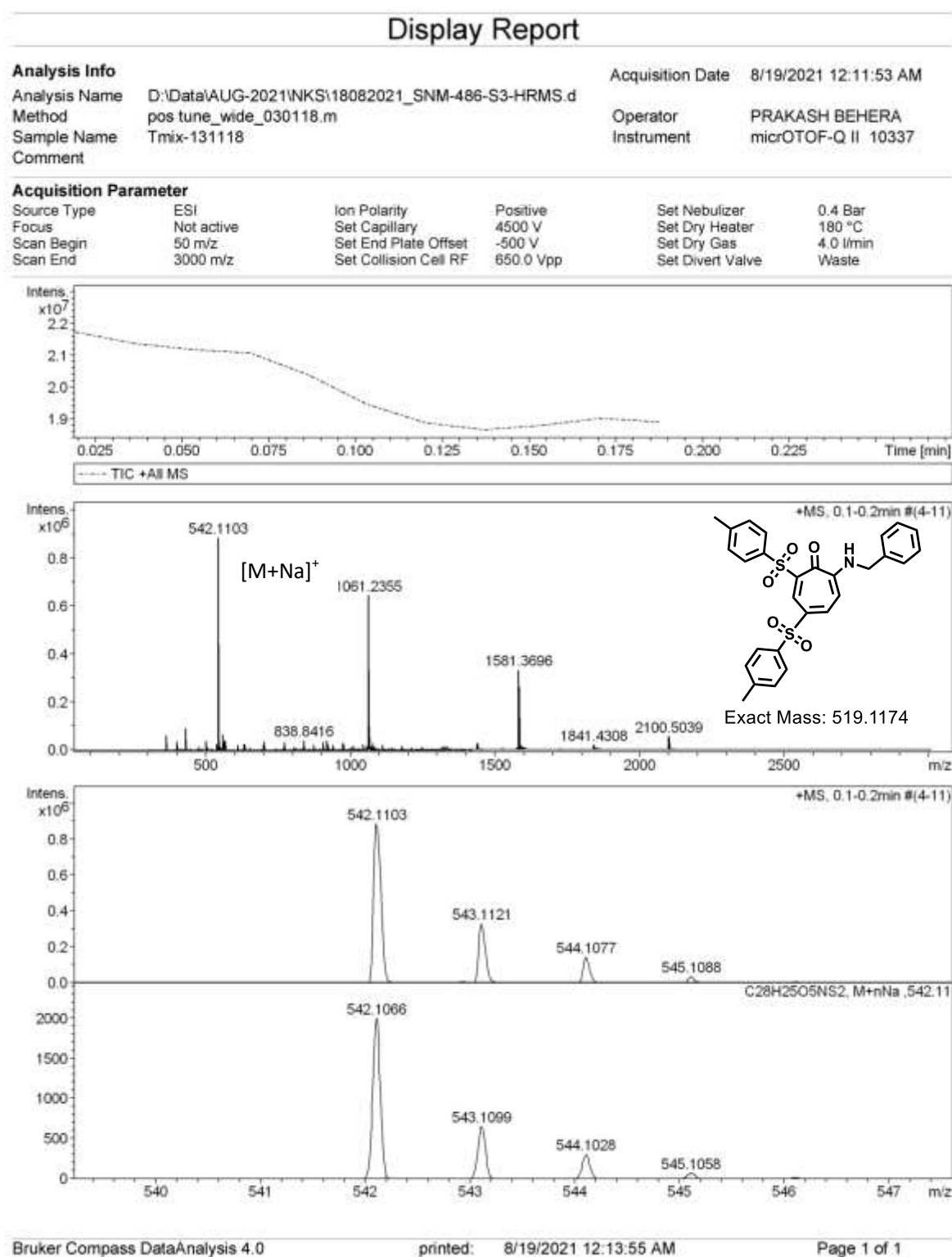
**Figure A9.**  $^1\text{H}/^{13}\text{C}$  NMR (700MHz,  $\text{CDCl}_3$ ) spectra of compound **3b** in  $\text{CDCl}_3$



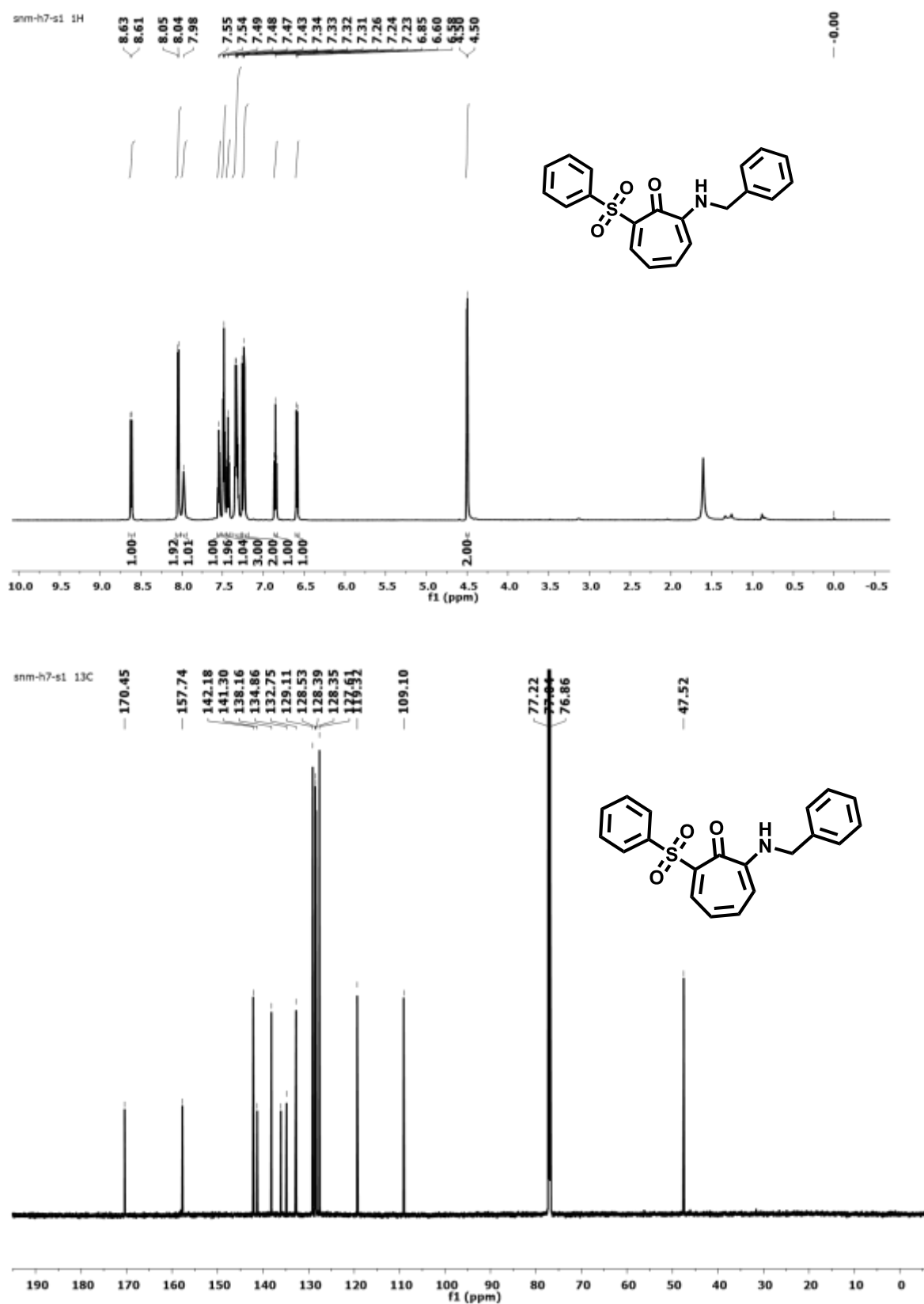
$^1\text{H}$ ,  $^{13}\text{C}$  NMR (700MHz,  $\text{CDCl}_3$ ) and HRMS of **3c**



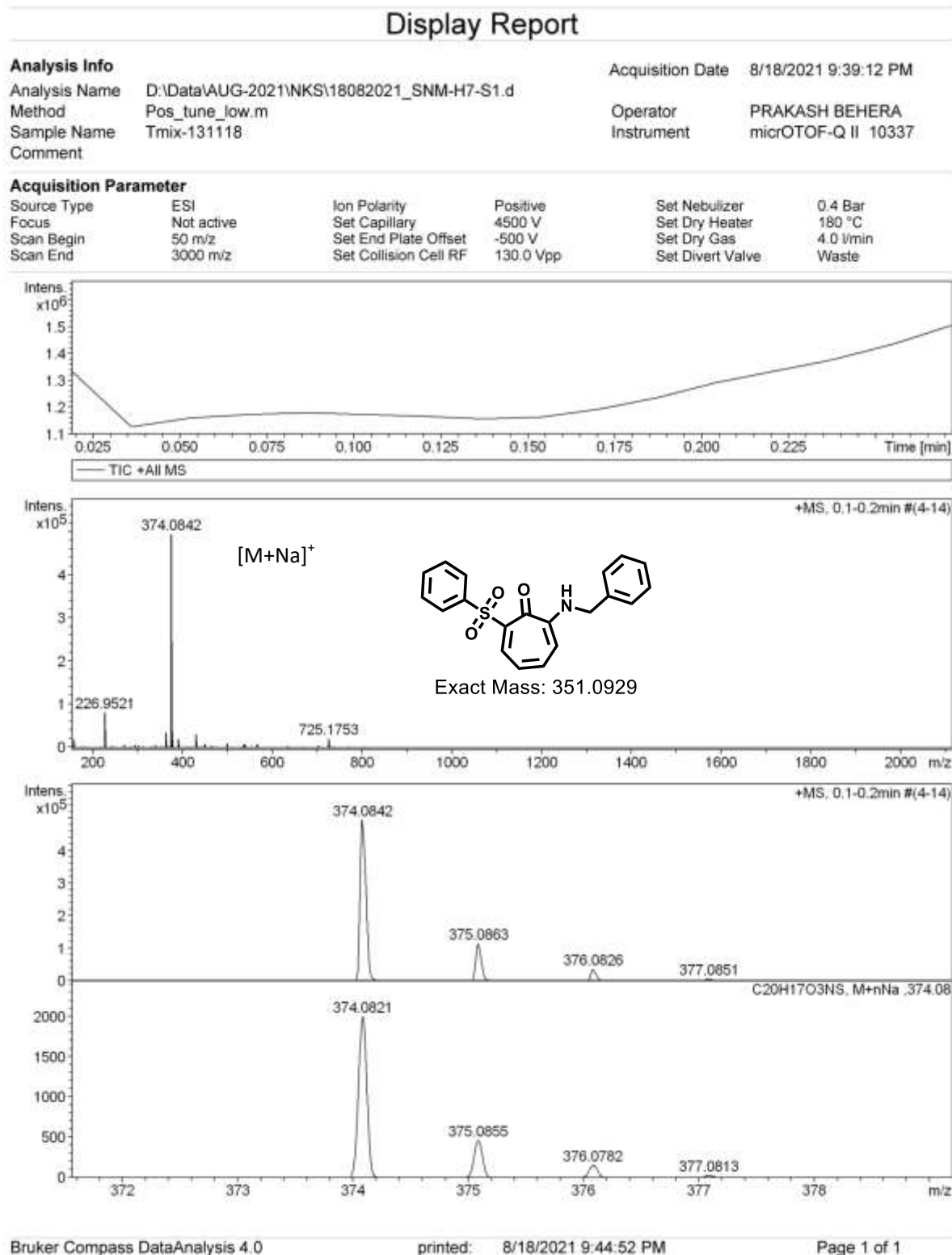
**Figure A11.**  $^1\text{H}/^{13}\text{C}$  NMR (700MHz,  $\text{CDCl}_3$ ) spectra of compound **3c** in  $\text{CDCl}_3$

Figure A12. ESI-MS/HRMS spectra of compound **3c**

$^1\text{H}$ ,  $^{13}\text{C}$  NMR (700MHz,  $\text{CDCl}_3$ ) and HRMS of **4a**



**Figure A13.**  $^1\text{H}/^{13}\text{C}$  NMR (700MHz,  $\text{CDCl}_3$ ) spectra of compound **4a** in  $\text{CDCl}_3$

**Figure A14.** ESI-MS/HRMS spectra of compound **4a**



$^1\text{H}$ ,  $^{13}\text{C}$  NMR (400MHz,  $\text{CDCl}_3$ ) and HRMS of **4b**

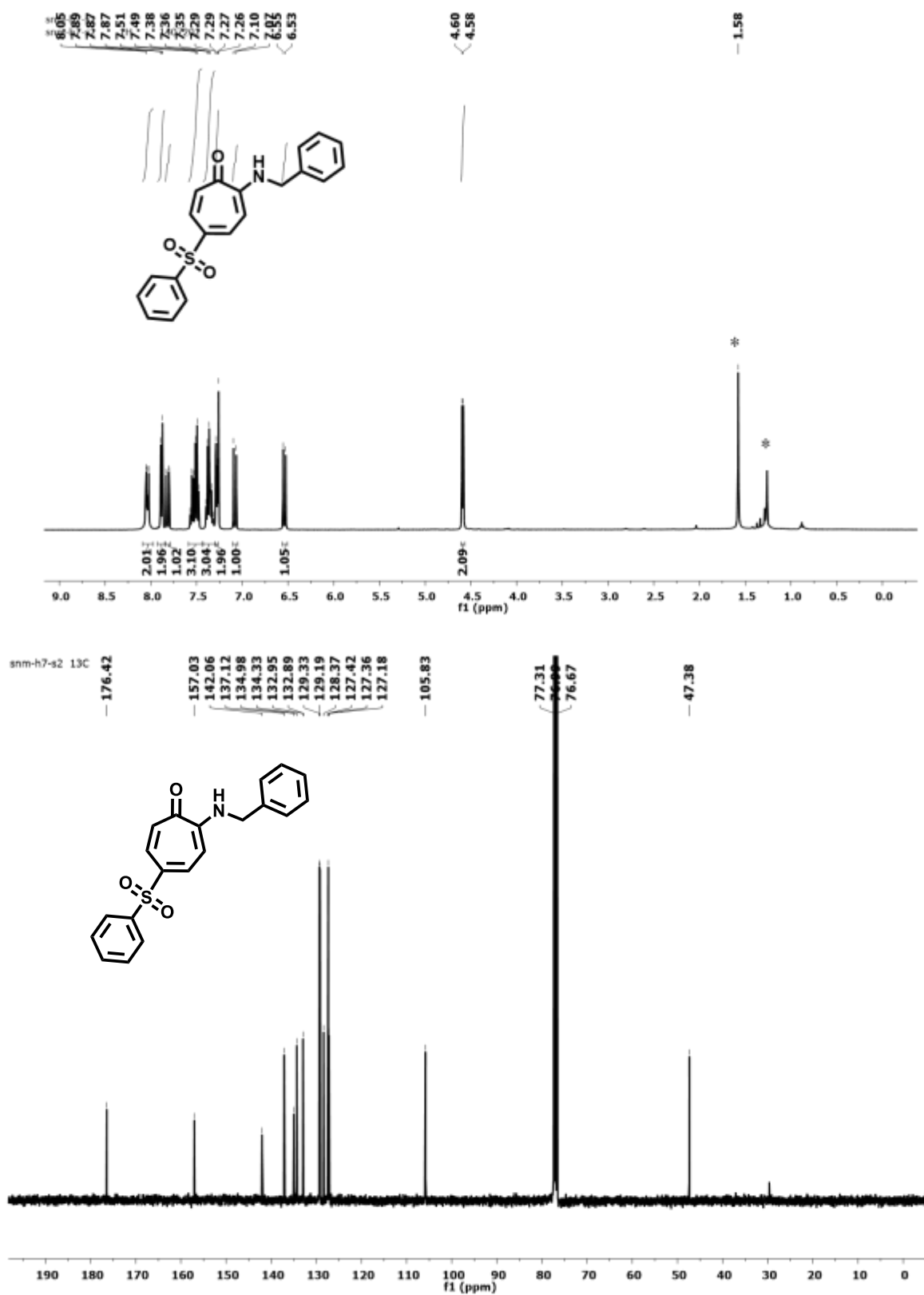


**Figure A15.**  $^1\text{H}/^{13}\text{C}$  NMR (400MHz,  $\text{CDCl}_3$ ) spectra of compound **4b** in  $\text{CDCl}_3$

## Display Report

## Analysis Info

Analysis Name D:\Data\AUG-2021\NKS\18082021\_SNM-H7-S2.d  
Method Pos\_tune\_low.m  
Sample Name Tmix-131118  
Comment

Acquisition Date 8/18/2021 9:41:11 PM

Operator PRAKASH BEHERA  
Instrument micrOTOF-Q II 10337

## Acquisition Parameter

Source Type	ESI	Ion Polarity	Positive	Set Nebulizer	0.4 Bar
Focus	Not active	Set Capillary	4500 V	Set Dry Heater	180 °C
Scan Begin	50 m/z	Set End Plate Offset	-500 V	Set Dry Gas	4.0 l/min
Scan End	3000 m/z	Set Collision Cell RF	130.0 Vpp	Set Divert Valve	Waste

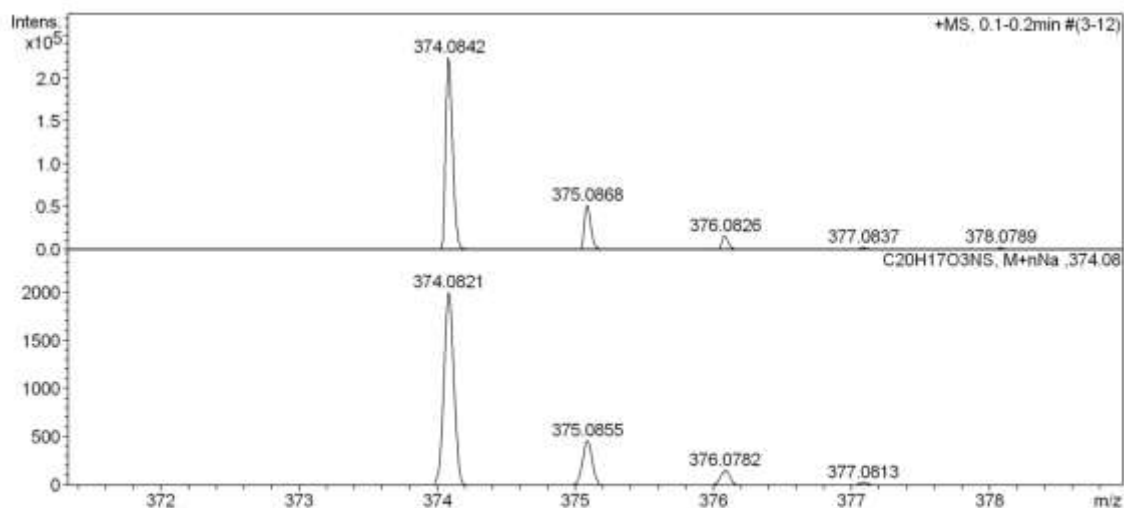
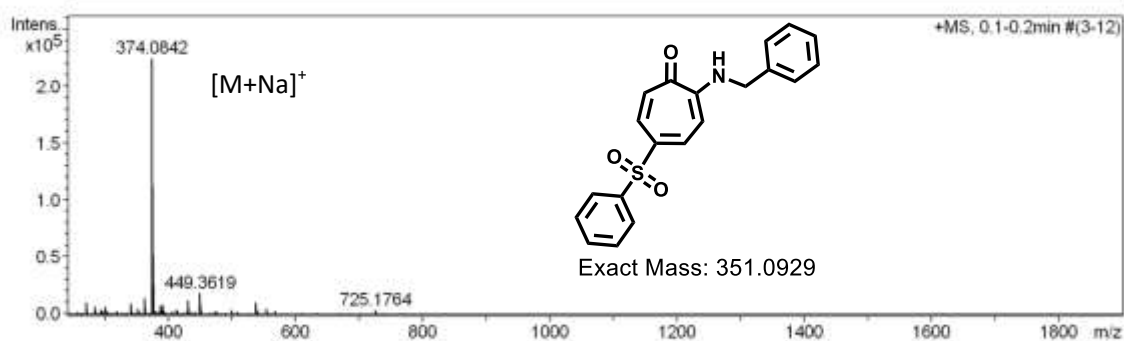
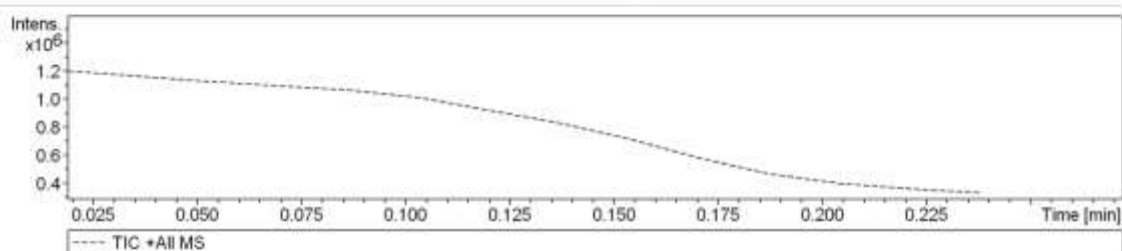
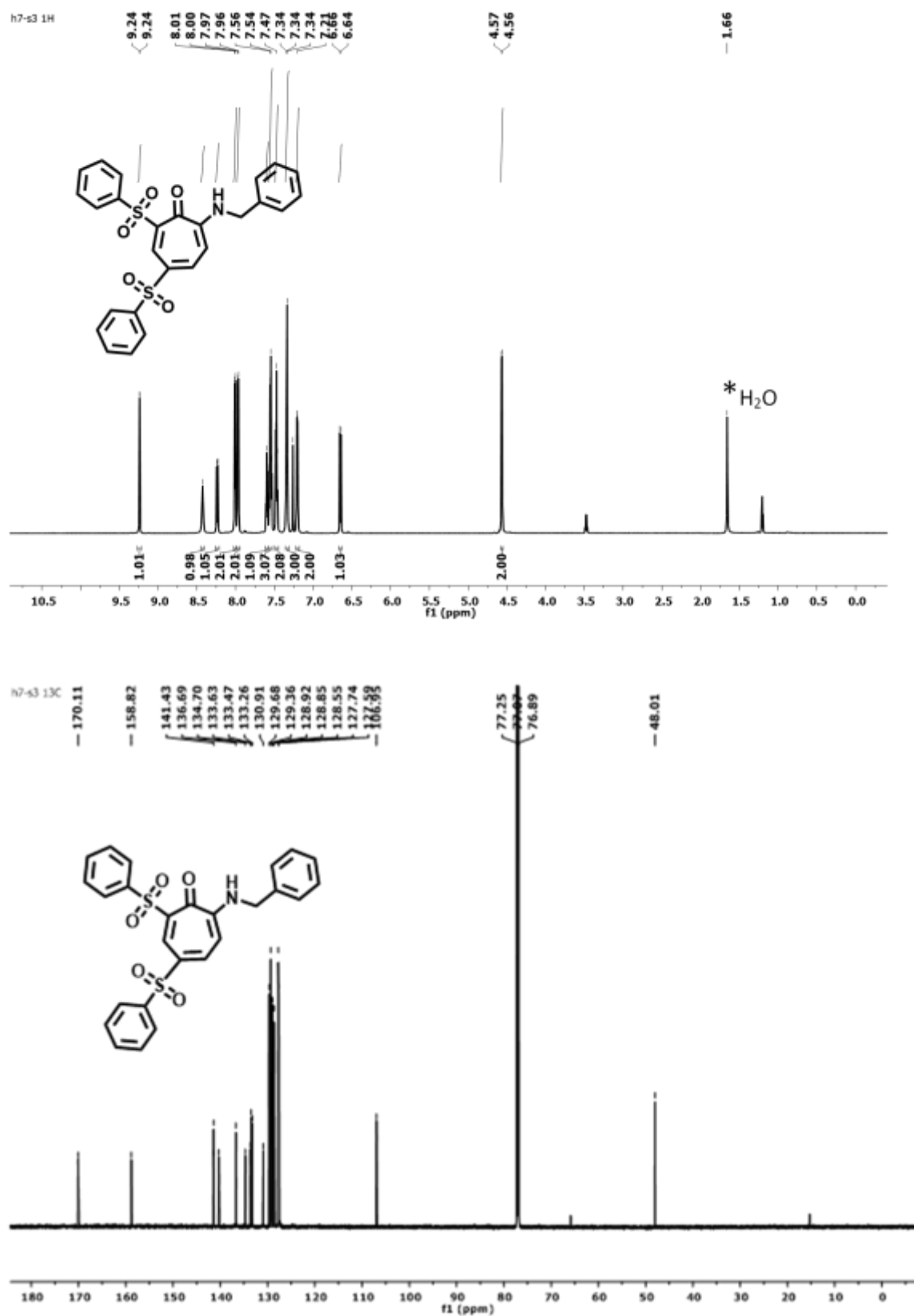
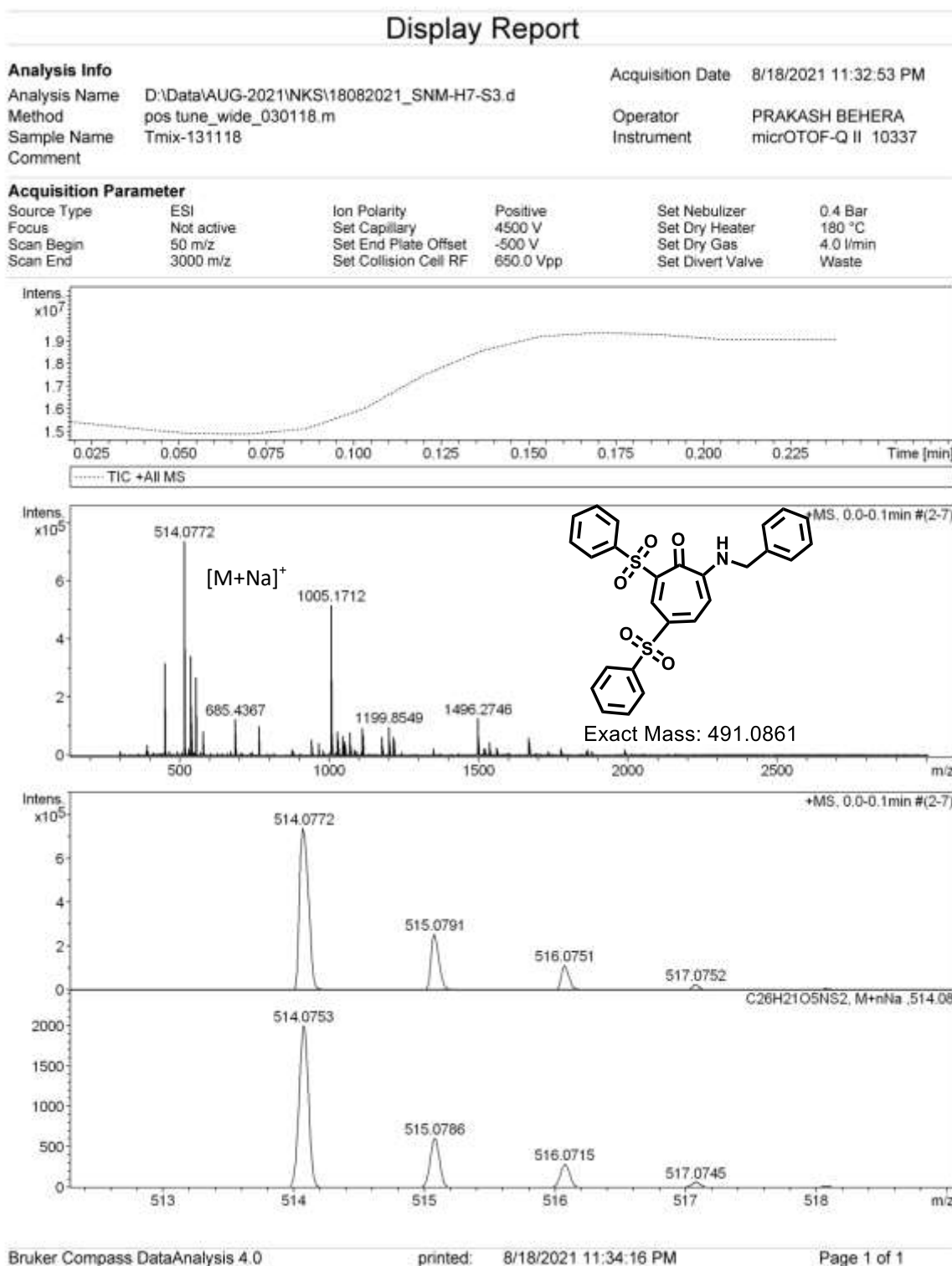


Figure A16. ESI-MS/HRMS spectra of compound 4b

$^1\text{H}$ ,  $^{13}\text{C}$  NMR (700MHz,  $\text{CDCl}_3$ ) and HRMS of **4c**

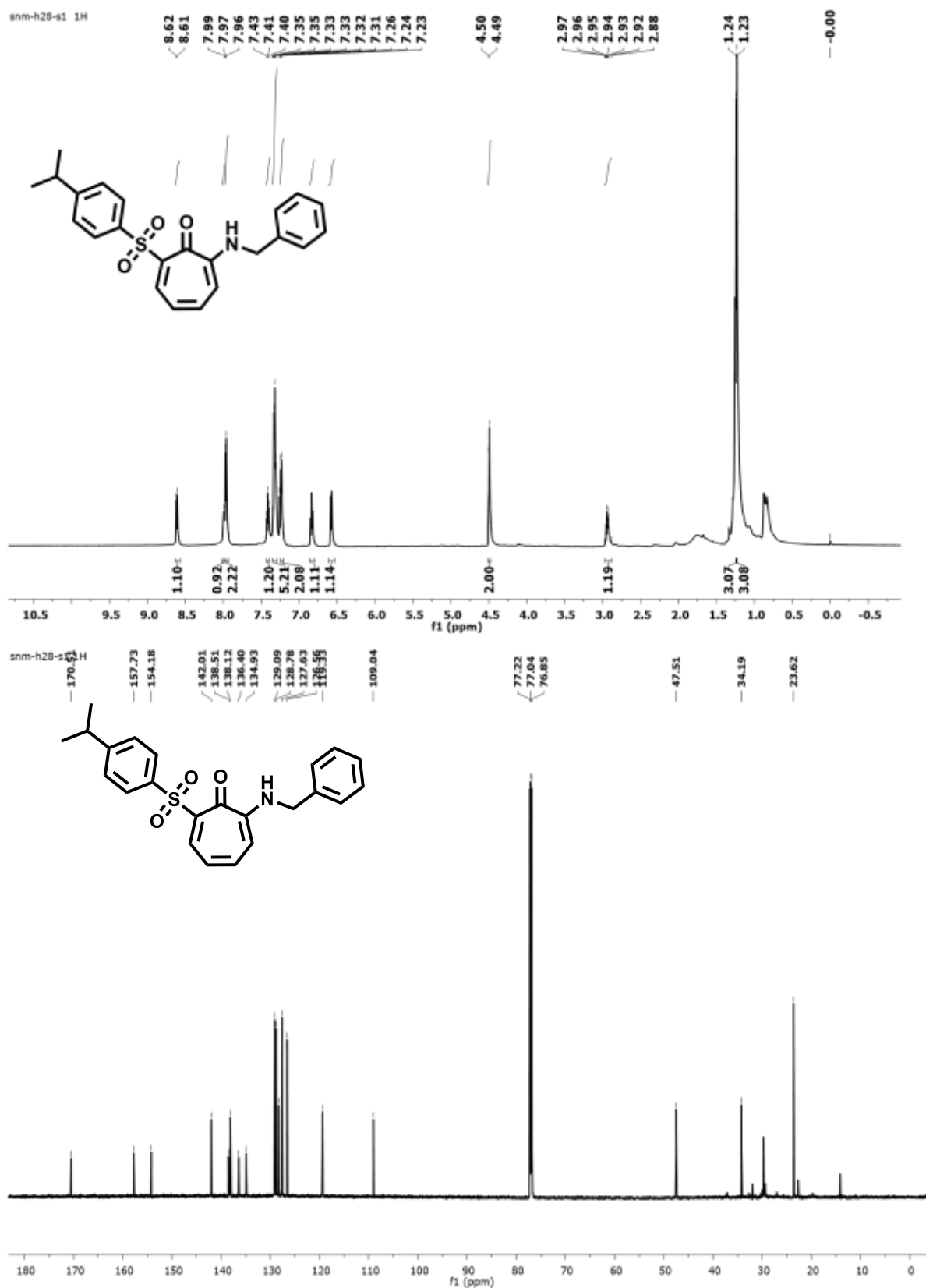


**Figure A17.**  $^1\text{H}/^{13}\text{C}$  NMR (700MHz,  $\text{CDCl}_3$ ) spectra of compound **4c** in  $\text{CDCl}_3$

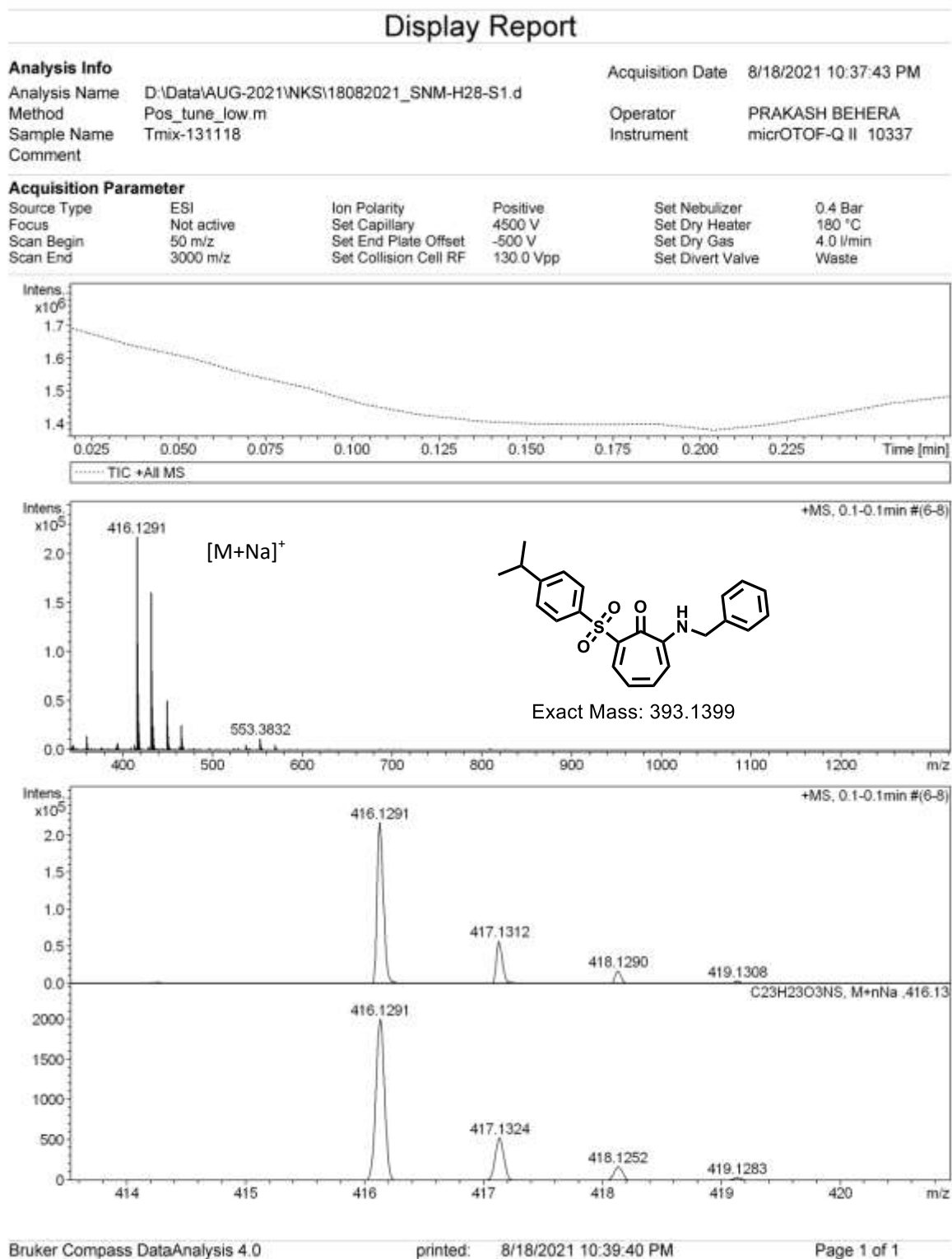


**Figure A18.** ESI-MS/HRMS spectra of compound **4c**

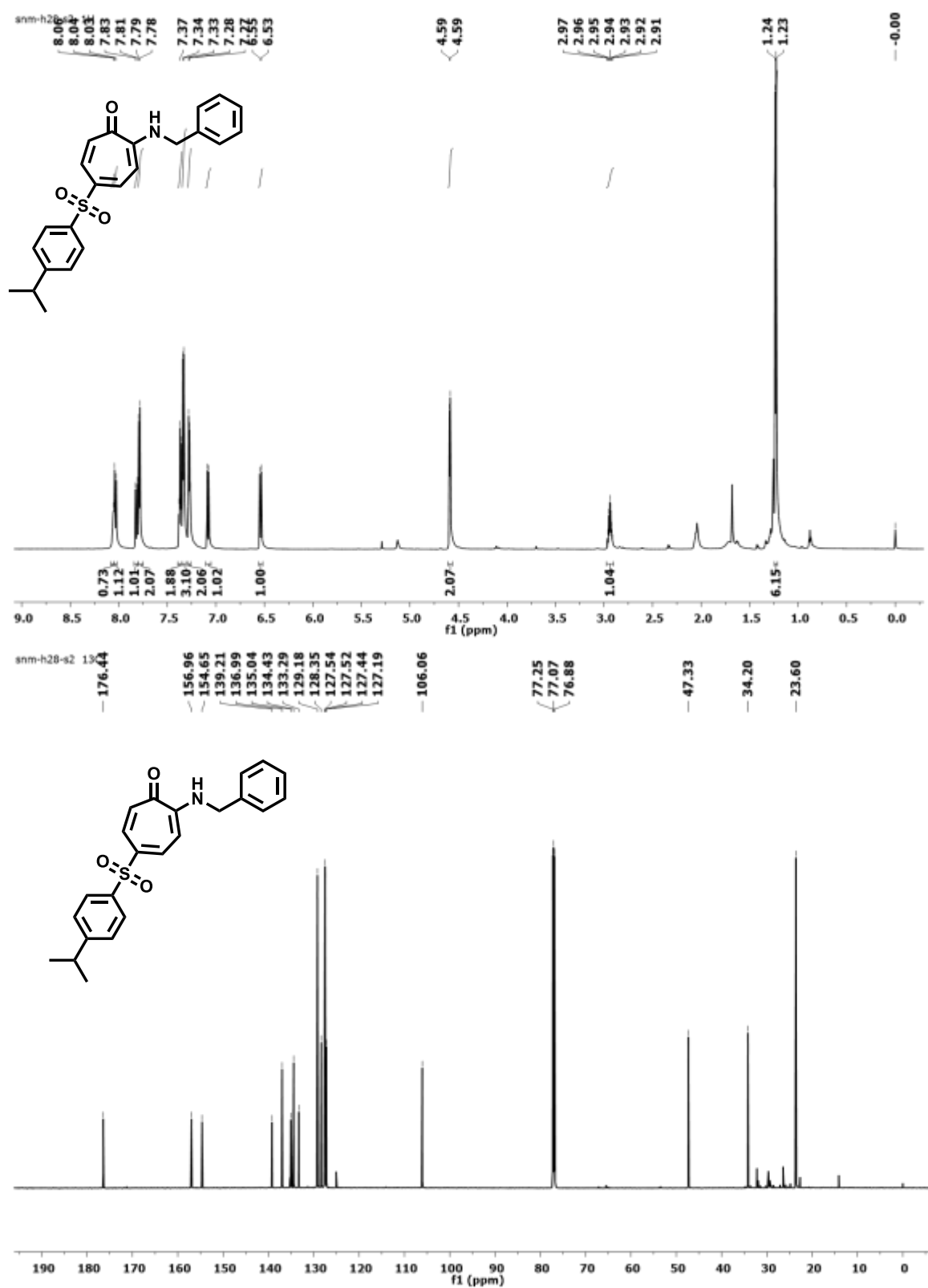
$^1\text{H}$ ,  $^{13}\text{C}$  NMR (700MHz,  $\text{CDCl}_3$ ) and HRMS of **5a**



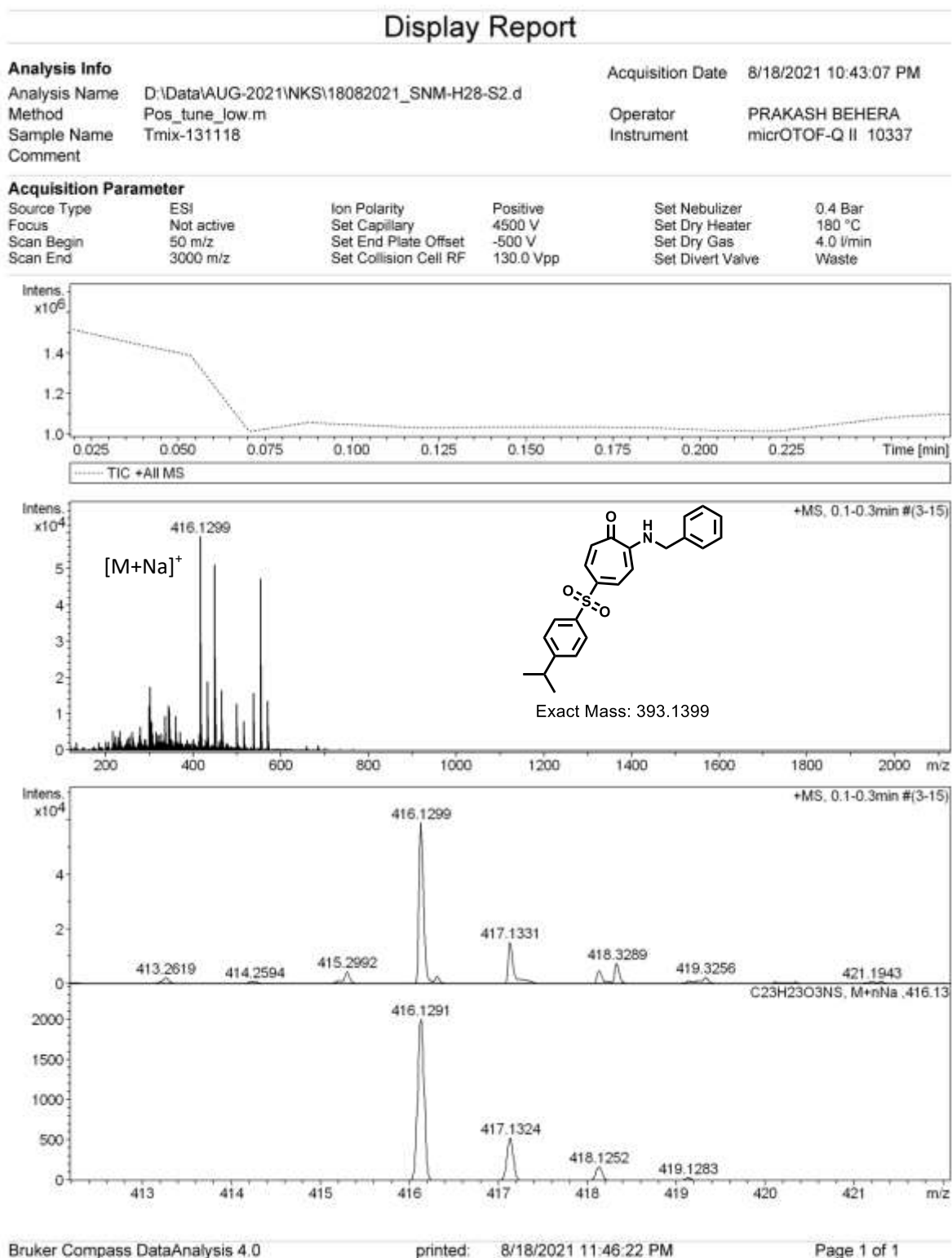
**Figure A19.**  $^1\text{H}/^{13}\text{C}$  NMR (700MHz,  $\text{CDCl}_3$ ) spectra of compound **5a** in  $\text{CDCl}_3$

**Figure A20.** ESI-MS/HRMS spectra of compound **5a**

$^1\text{H}$ ,  $^{13}\text{C}$  NMR (700MHz,  $\text{CDCl}_3$ ) and HRMS of **5b**

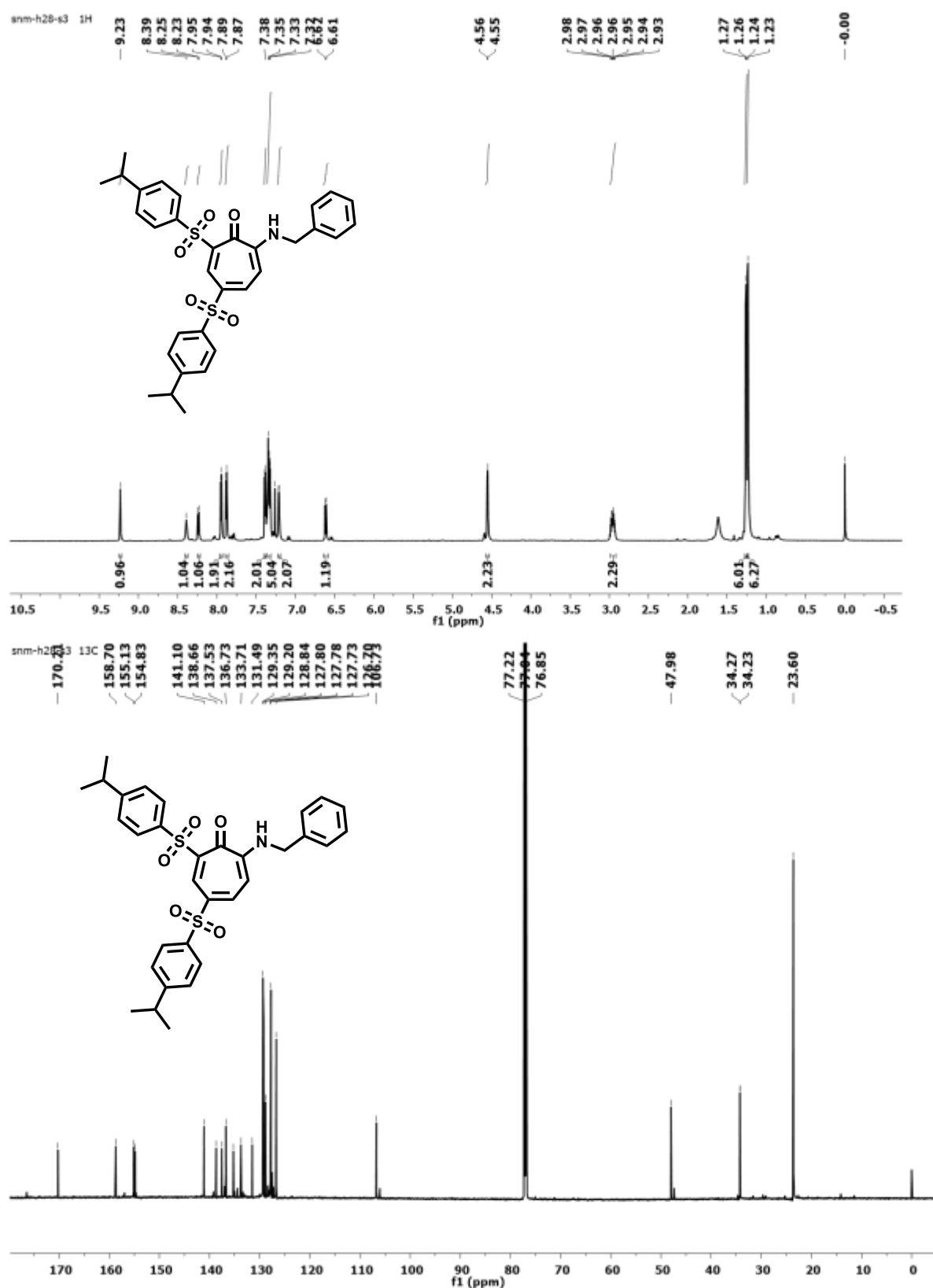


**Figure A21.**  $^1\text{H}/^{13}\text{C}$  NMR (700MHz,  $\text{CDCl}_3$ ) spectra of compound **5b** in  $\text{CDCl}_3$

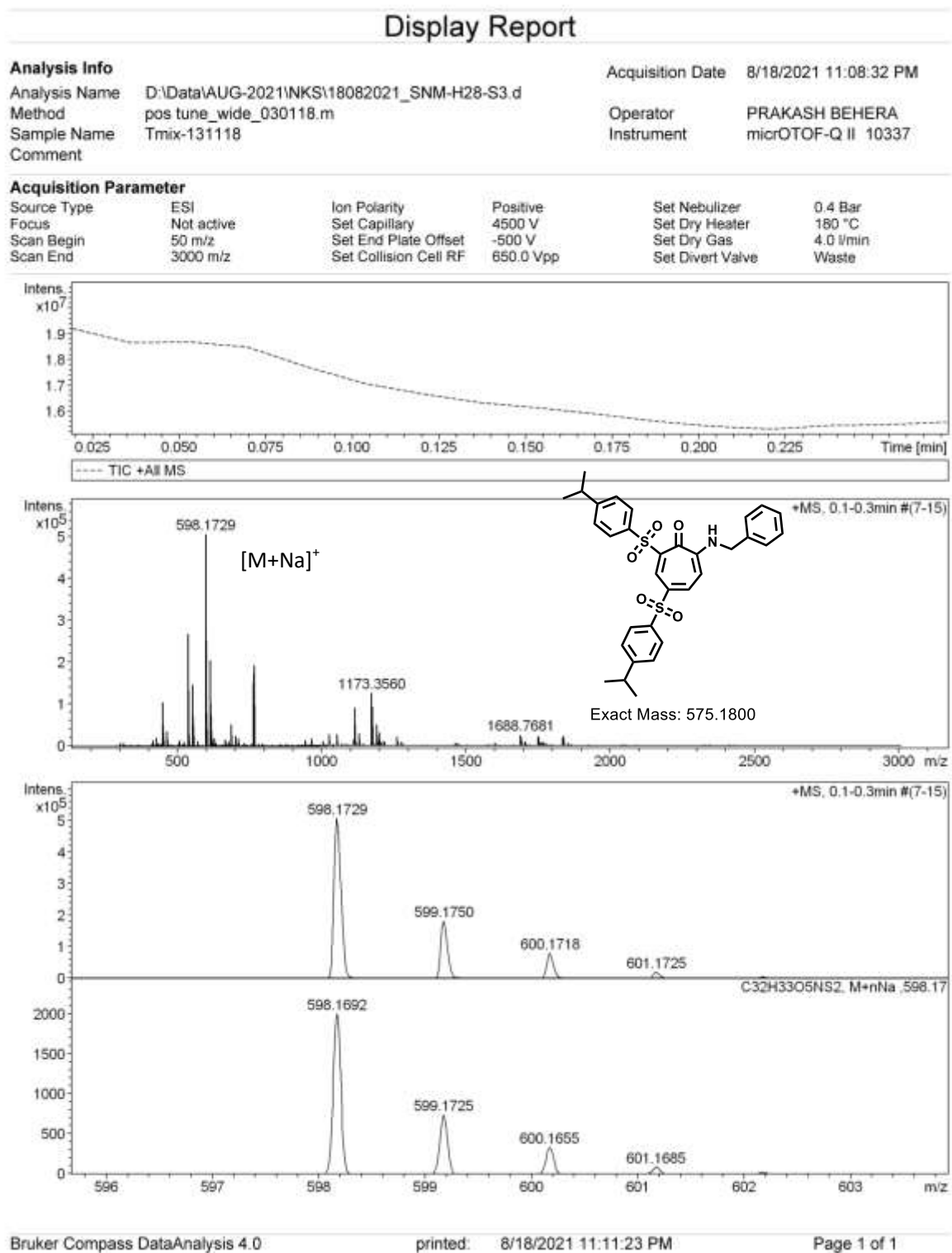
**Figure A22.** ESI-MS/HRMS spectra of compound **5b**



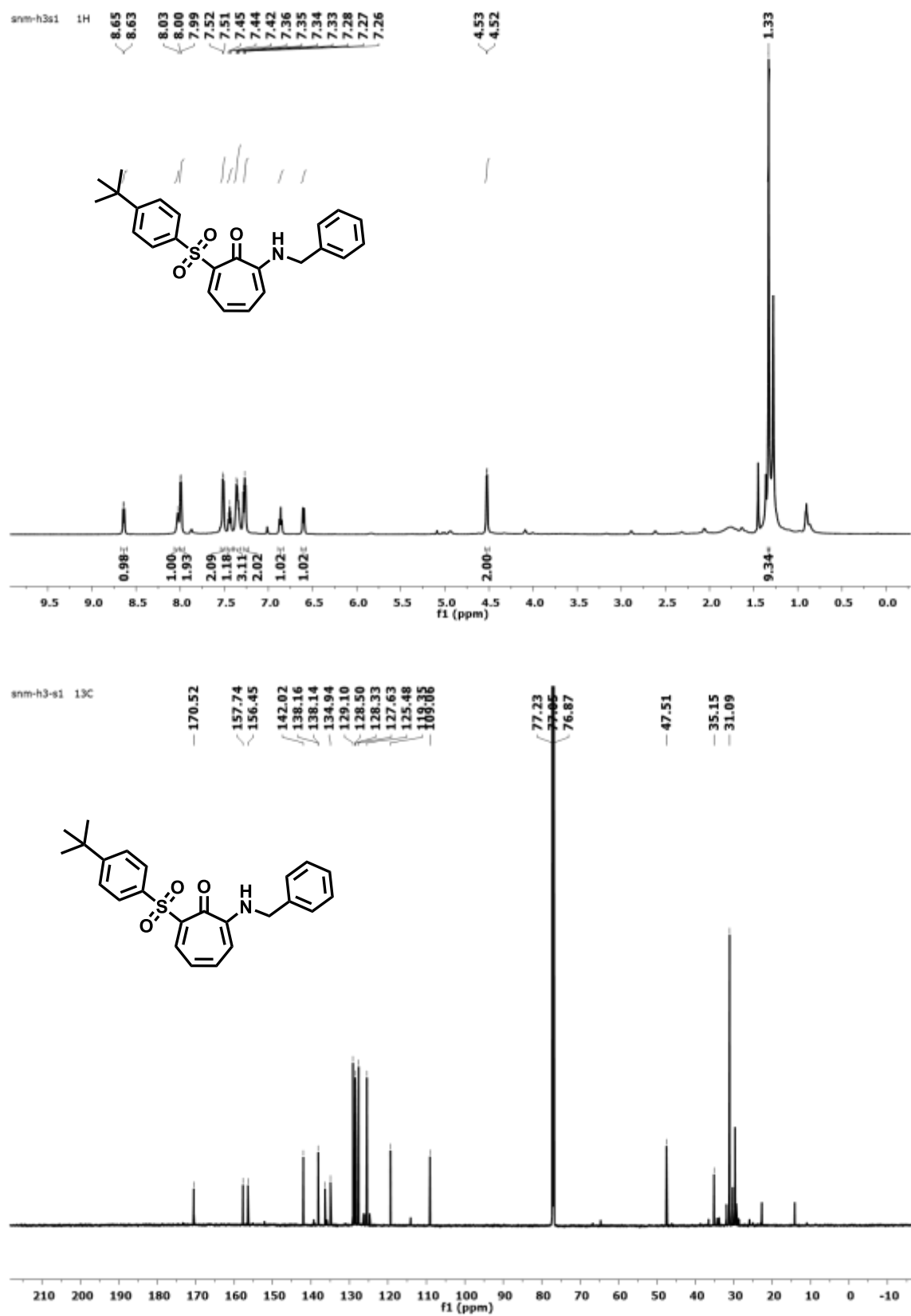
$^1\text{H}$ ,  $^{13}\text{C}$  NMR (700MHz,  $\text{CDCl}_3$ ) and HRMS of **5c**



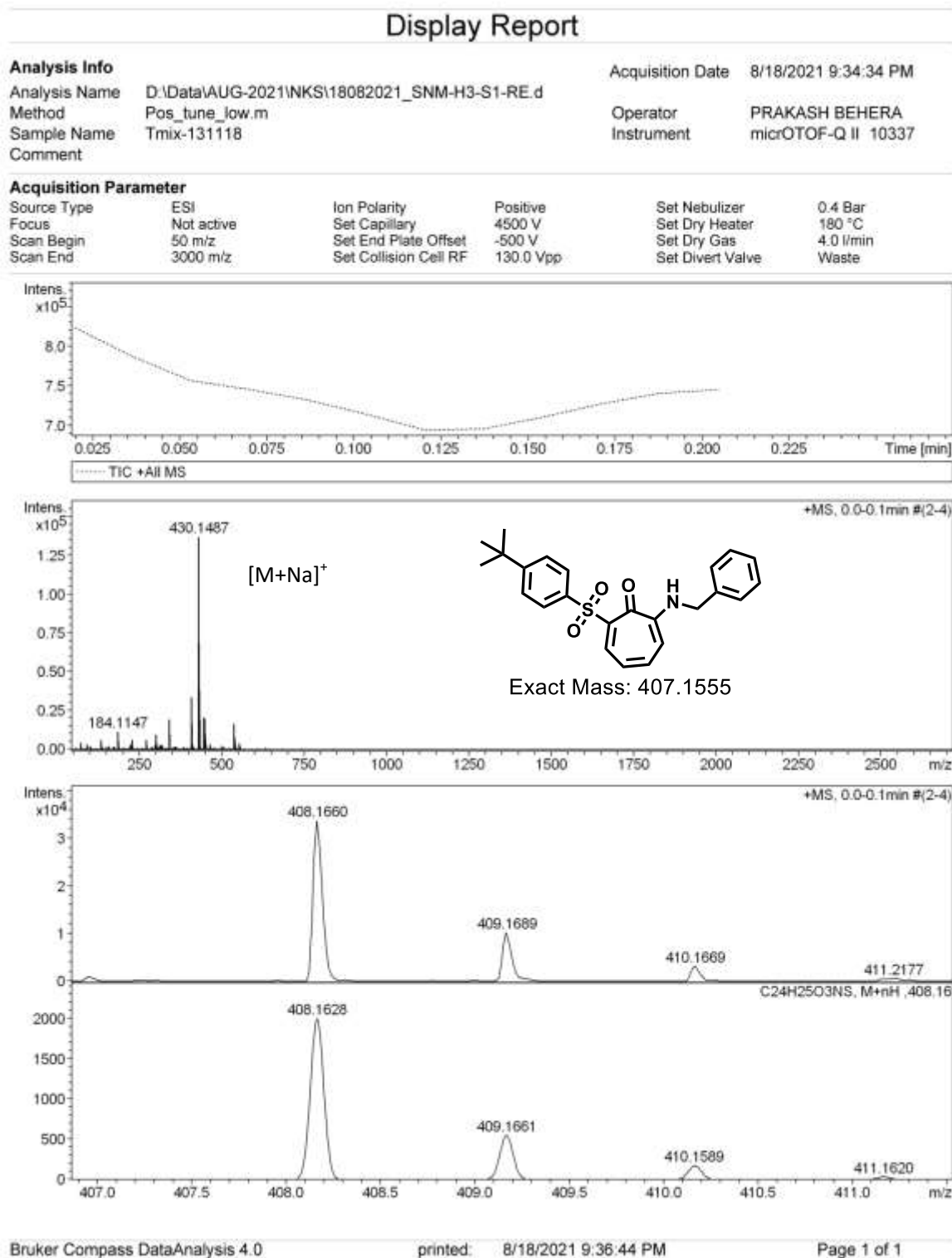
**Figure A23.**  $^1\text{H}/^{13}\text{C}$  NMR (700MHz,  $\text{CDCl}_3$ ) spectra of compound **5c** in  $\text{CDCl}_3$

Figure A24. ESI-MS/HRMS spectra of compound **5c**

$^1\text{H}$ ,  $^{13}\text{C}$  NMR (700MHz,  $\text{CDCl}_3$ ) and HRMS of **6a**



**Figure A25.**  $^1\text{H}/^{13}\text{C}$  NMR (700MHz,  $\text{CDCl}_3$ ) spectra of compound **6a** in  $\text{CDCl}_3$



**Figure A26.** ESI-MS/HRMS spectra of compound **6a**

$^1\text{H}$ ,  $^{13}\text{C}$  NMR (400MHz,  $\text{CDCl}_3$ ) and HRMS of **6b**

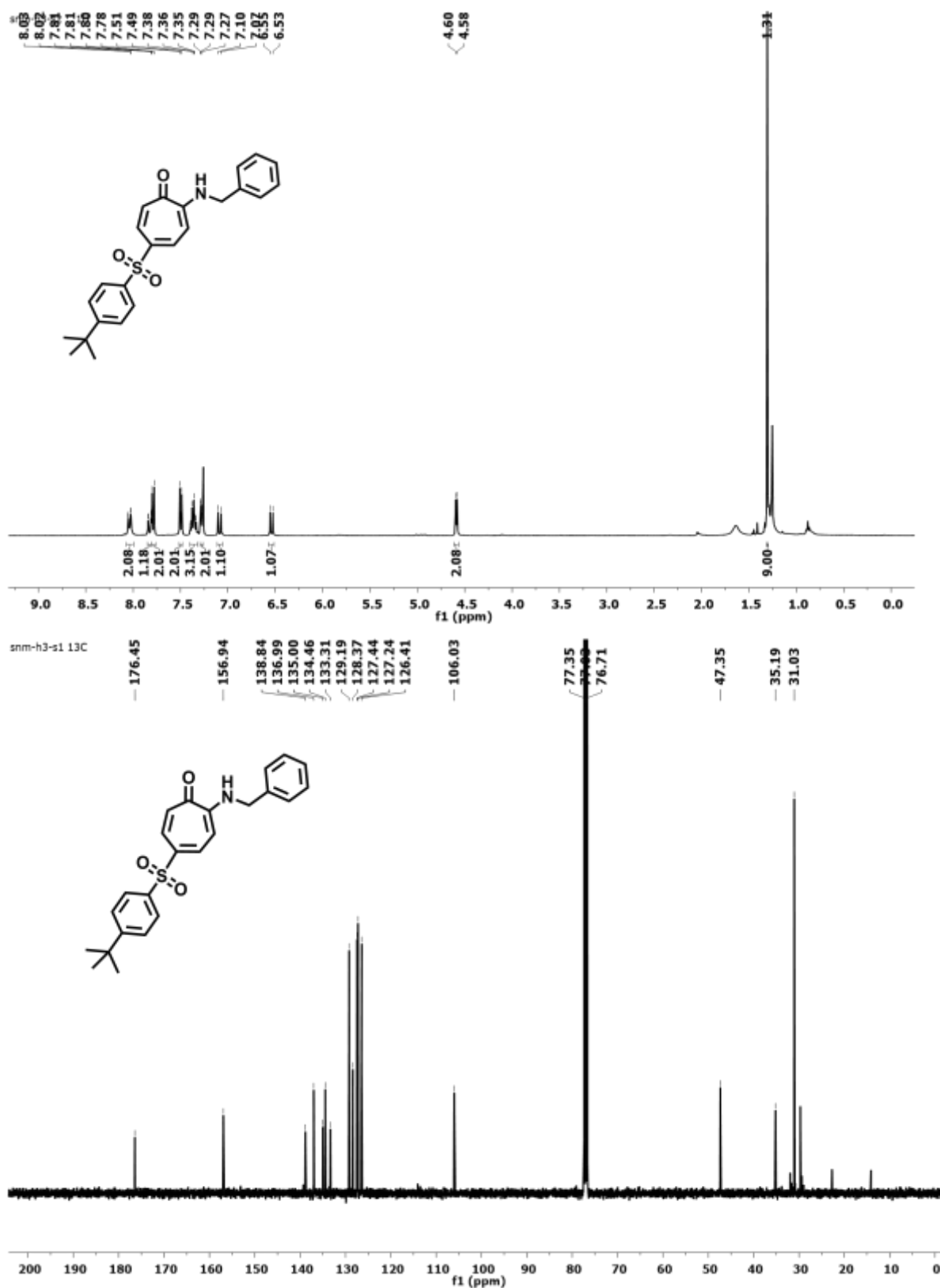
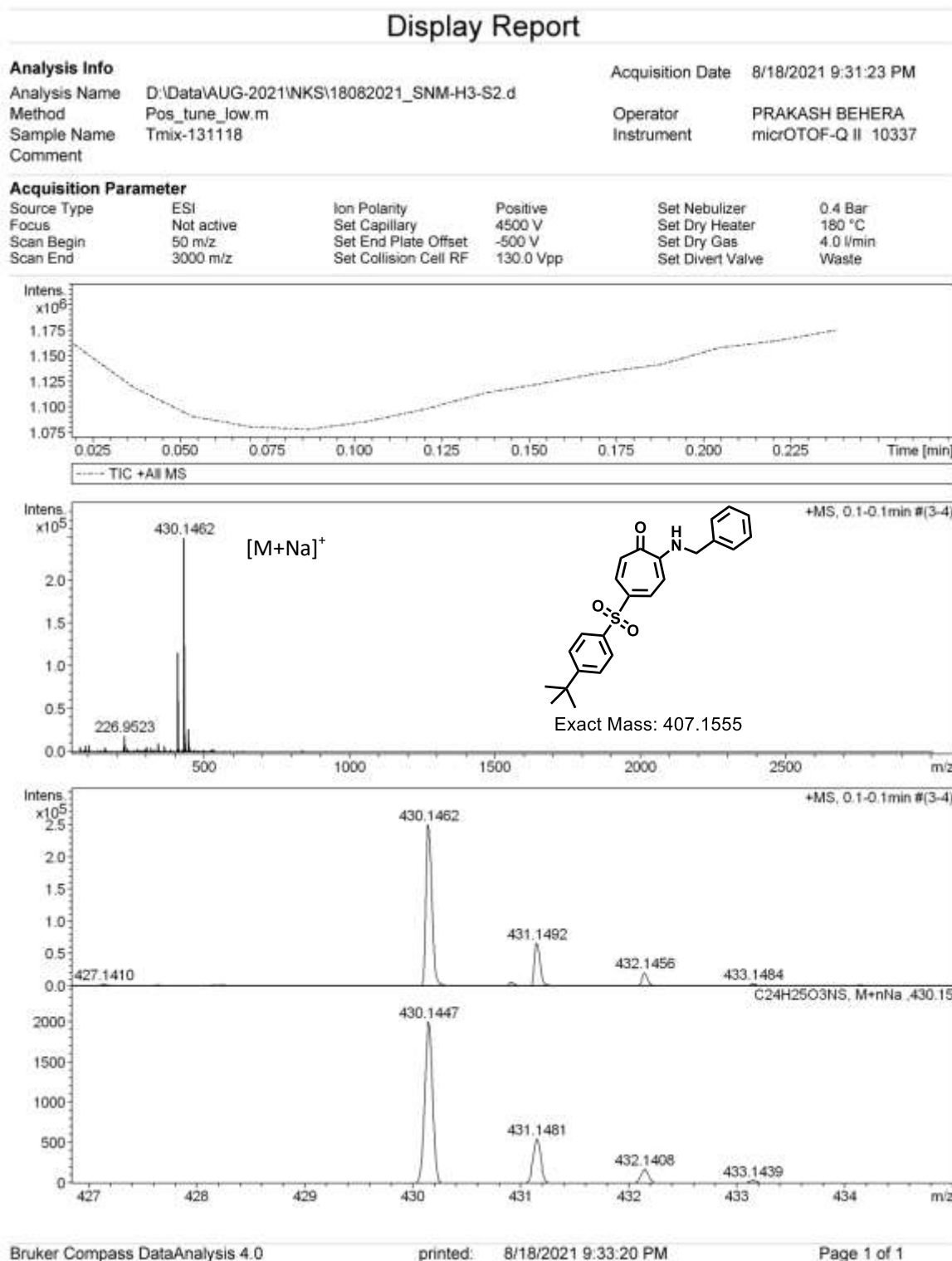
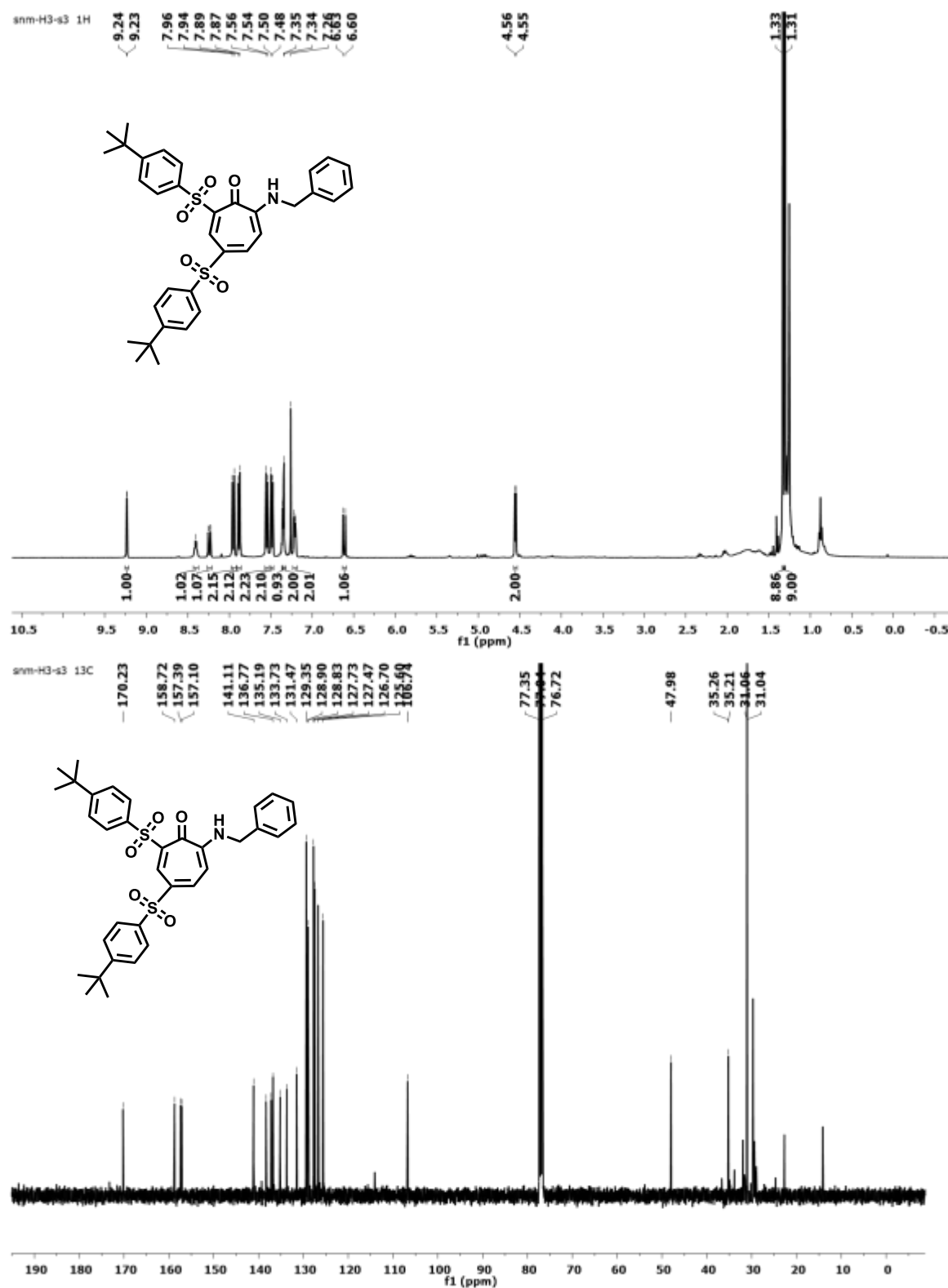


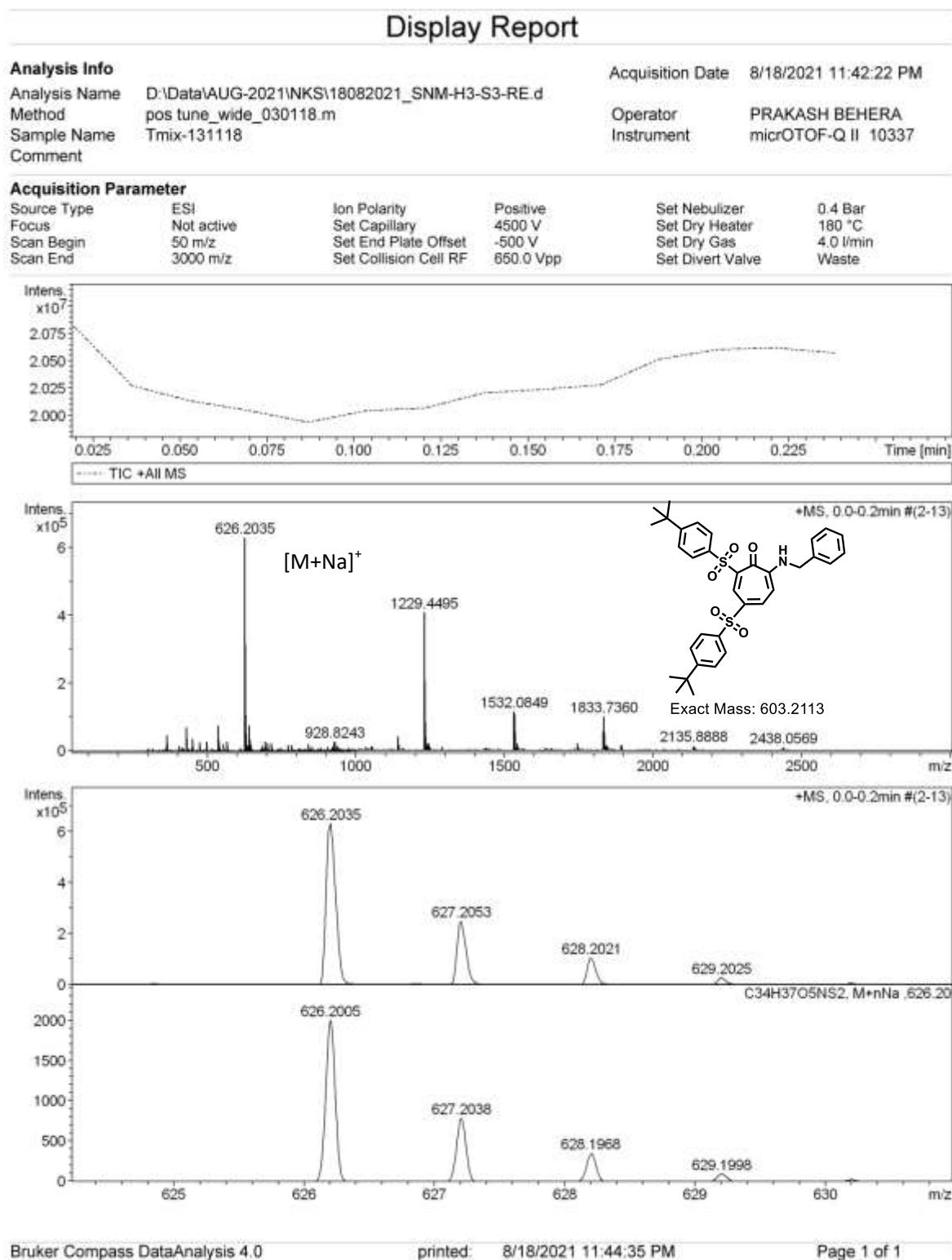
Figure A27.  $^1\text{H}/^{13}\text{C}$  NMR (400MHz,  $\text{CDCl}_3$ ) spectra of compound **6b** in  $\text{CDCl}_3$

**Figure A28.** ESI-MS/HRMS spectra of compound **6b**

$^1\text{H}$ ,  $^{13}\text{C}$  NMR (400MHz,  $\text{CDCl}_3$ ) and HRMS of **6c**

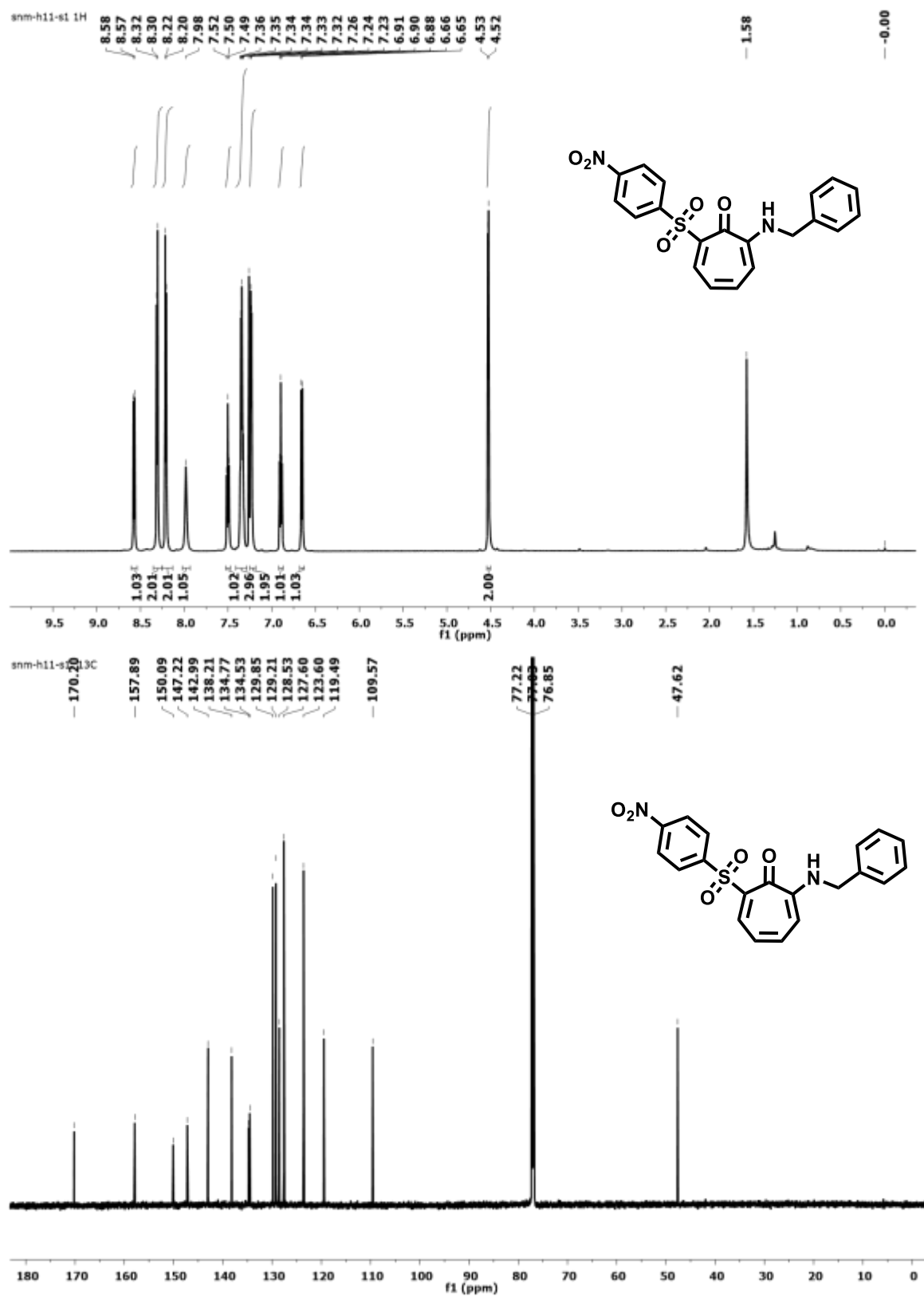


**Figure A29.**  $^1\text{H}/^{13}\text{C}$  NMR (400MHz,  $\text{CDCl}_3$ ) spectra of compound **6c** in  $\text{CDCl}_3$

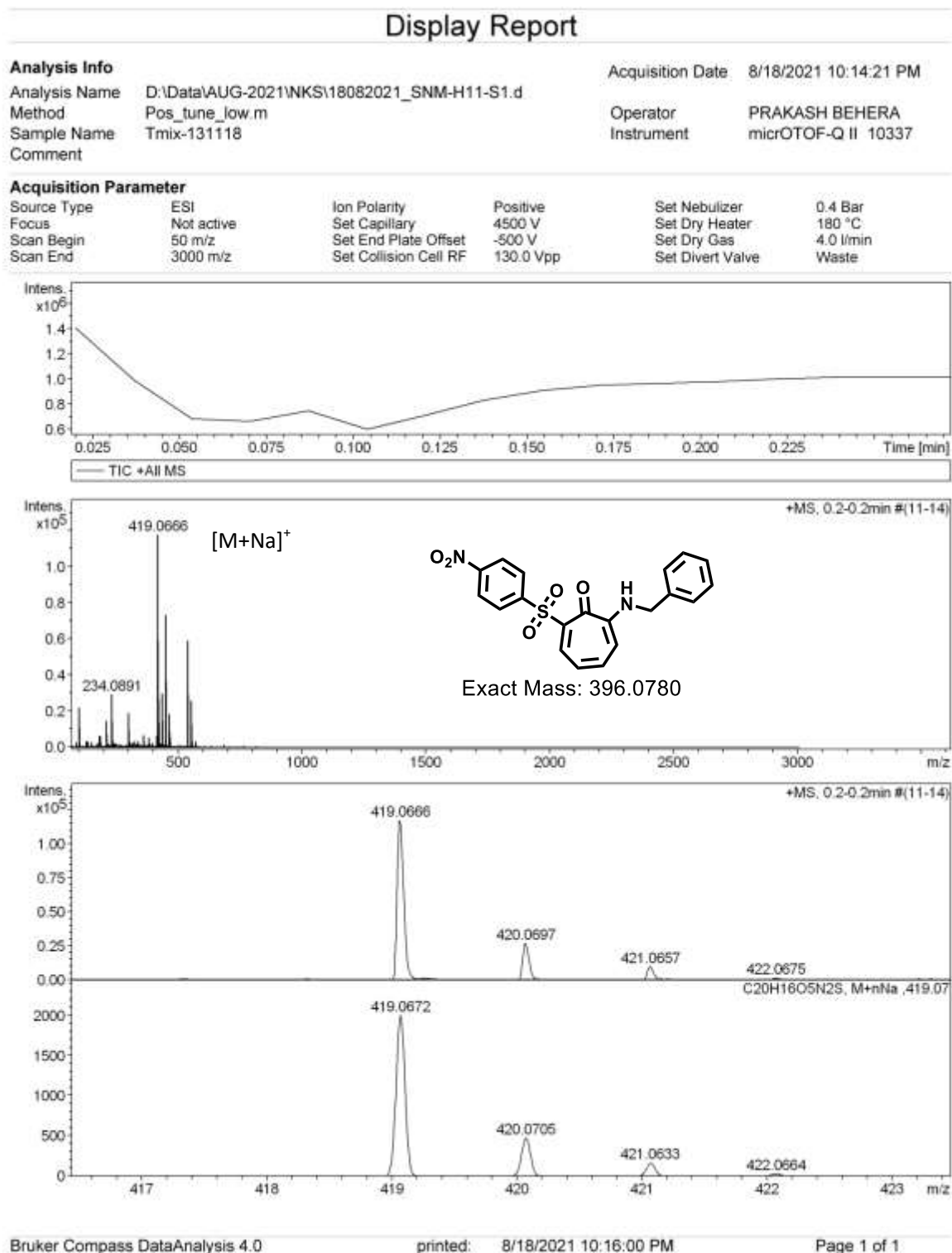
Figure A30. ESI-MS/HRMS spectra of compound **6c**



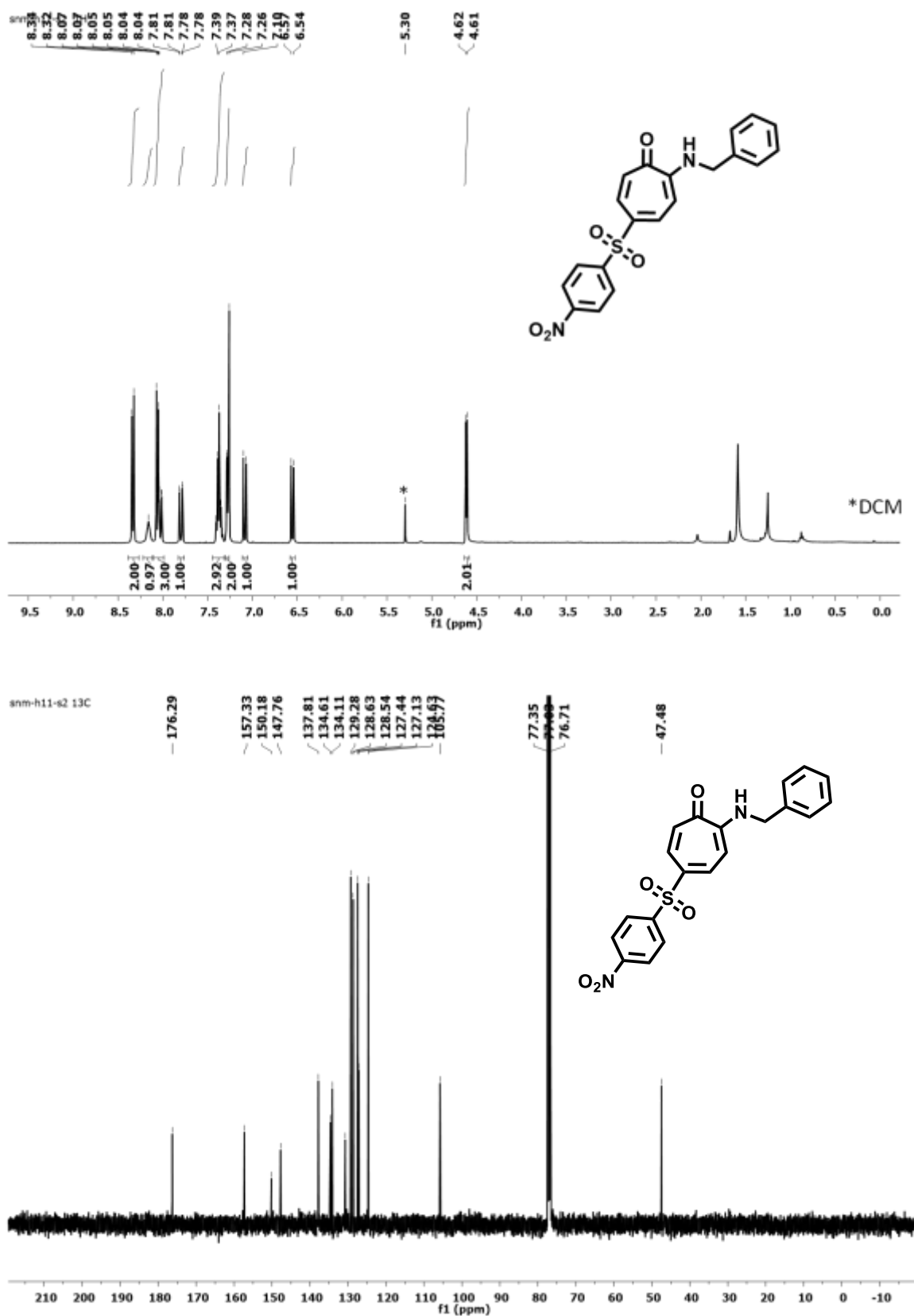
$^1\text{H}$ ,  $^{13}\text{C}$  NMR (700MHz,  $\text{CDCl}_3$ ) and HRMS of **7a**



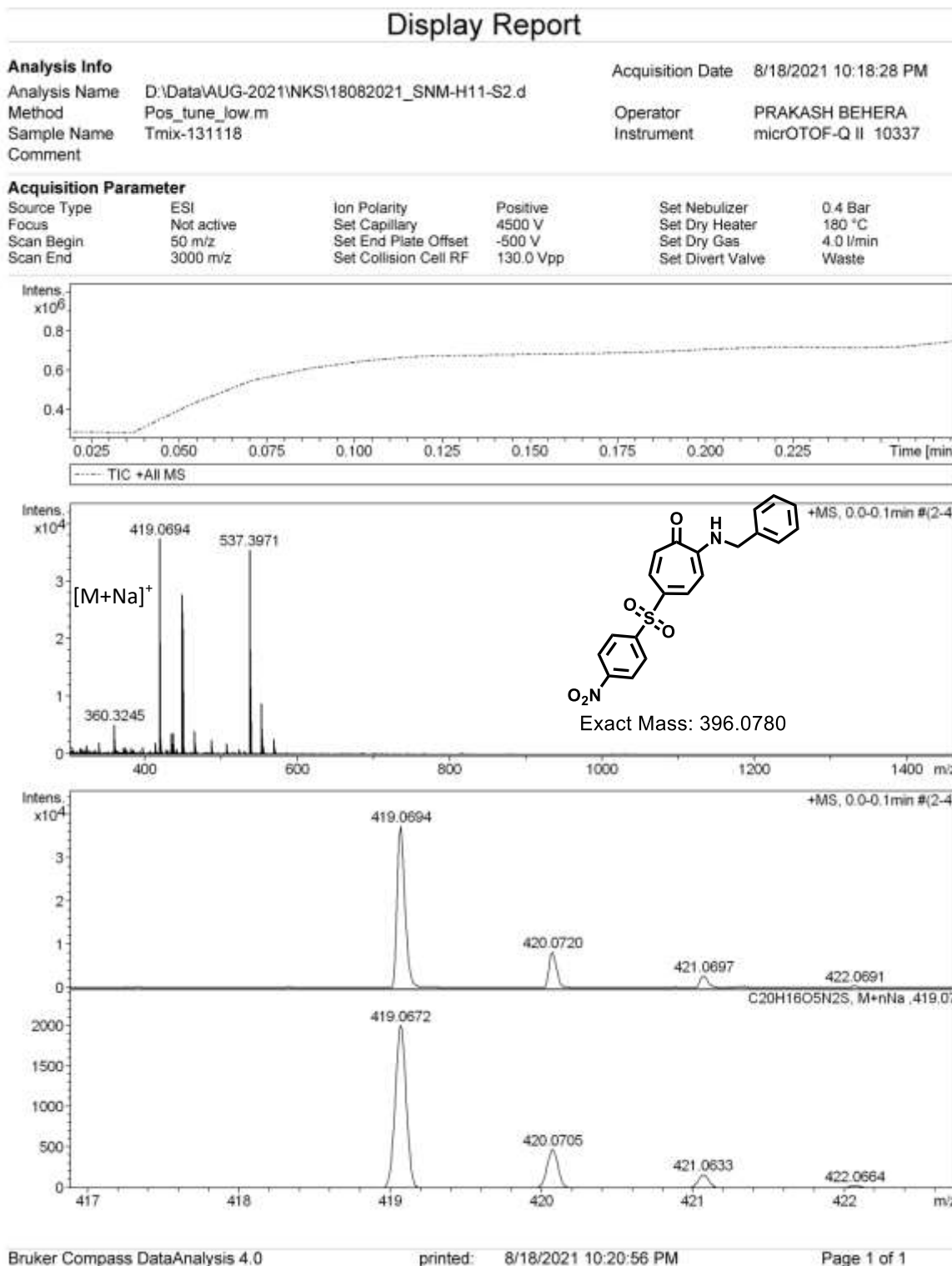
**Figure A31.**  $^1\text{H}/^{13}\text{C}$  NMR (700MHz,  $\text{CDCl}_3$ ) spectra of compound **7a** in  $\text{CDCl}_3$

Figure A32. ESI-MS/HRMS spectra of compound **7a**

$^1\text{H}$ ,  $^{13}\text{C}$  NMR (400MHz,  $\text{CDCl}_3$ ) and HRMS of **7b**



**Figure A33.**  $^1\text{H}/^{13}\text{C}$  NMR (400MHz,  $\text{CDCl}_3$ ) spectra of compound **7b** in  $\text{CDCl}_3$



**Figure A34.** ESI-MS/HRMS spectra of compound **7b**

$^1\text{H}$ ,  $^{13}\text{C}$  NMR (700MHz,  $\text{CDCl}_3$ ) and HRMS of **8a**

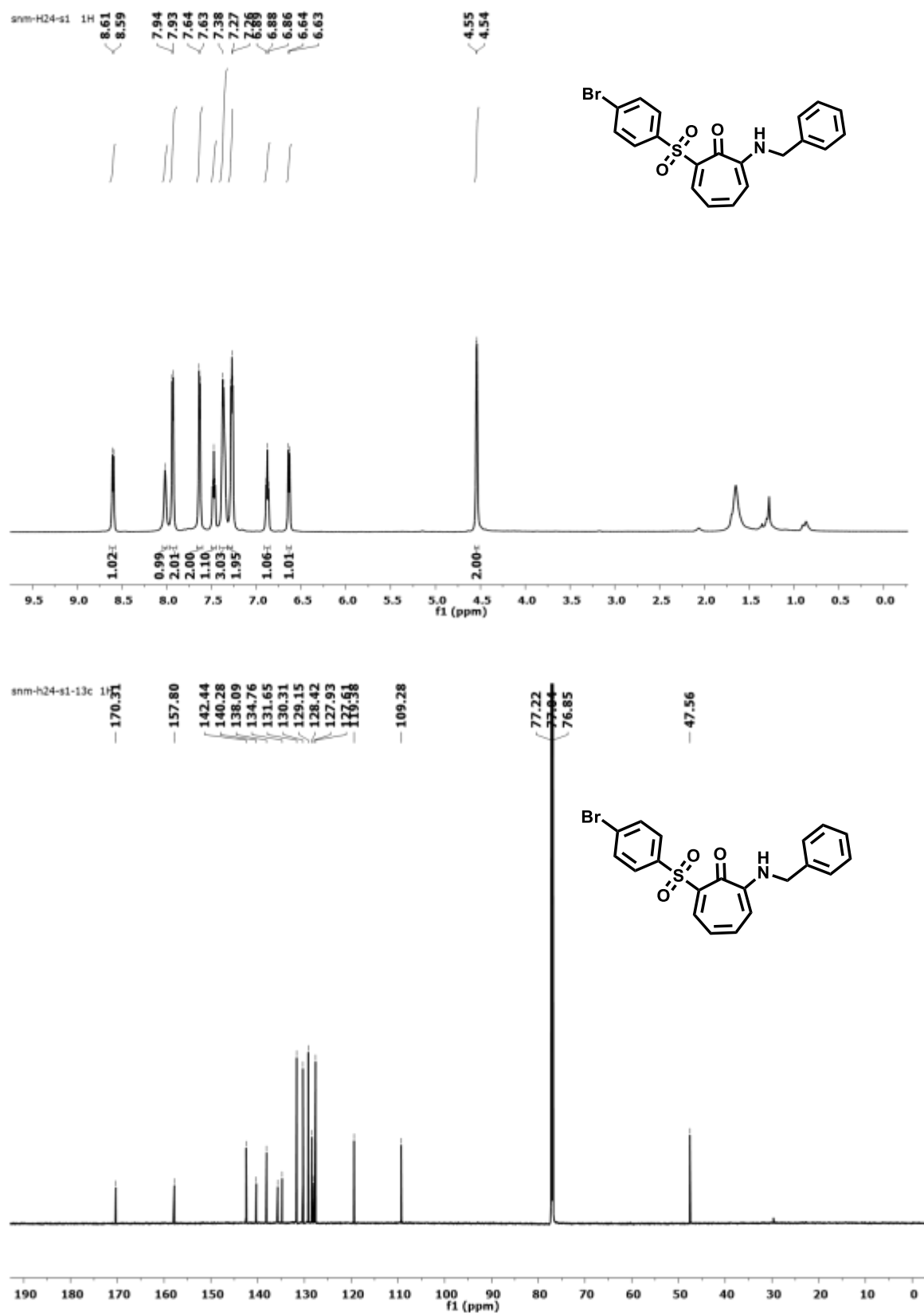


**Figure A35.**  $^1\text{H}/^{13}\text{C}$  NMR (700MHz,  $\text{CDCl}_3$ ) spectra of compound **8a** in  $\text{CDCl}_3$

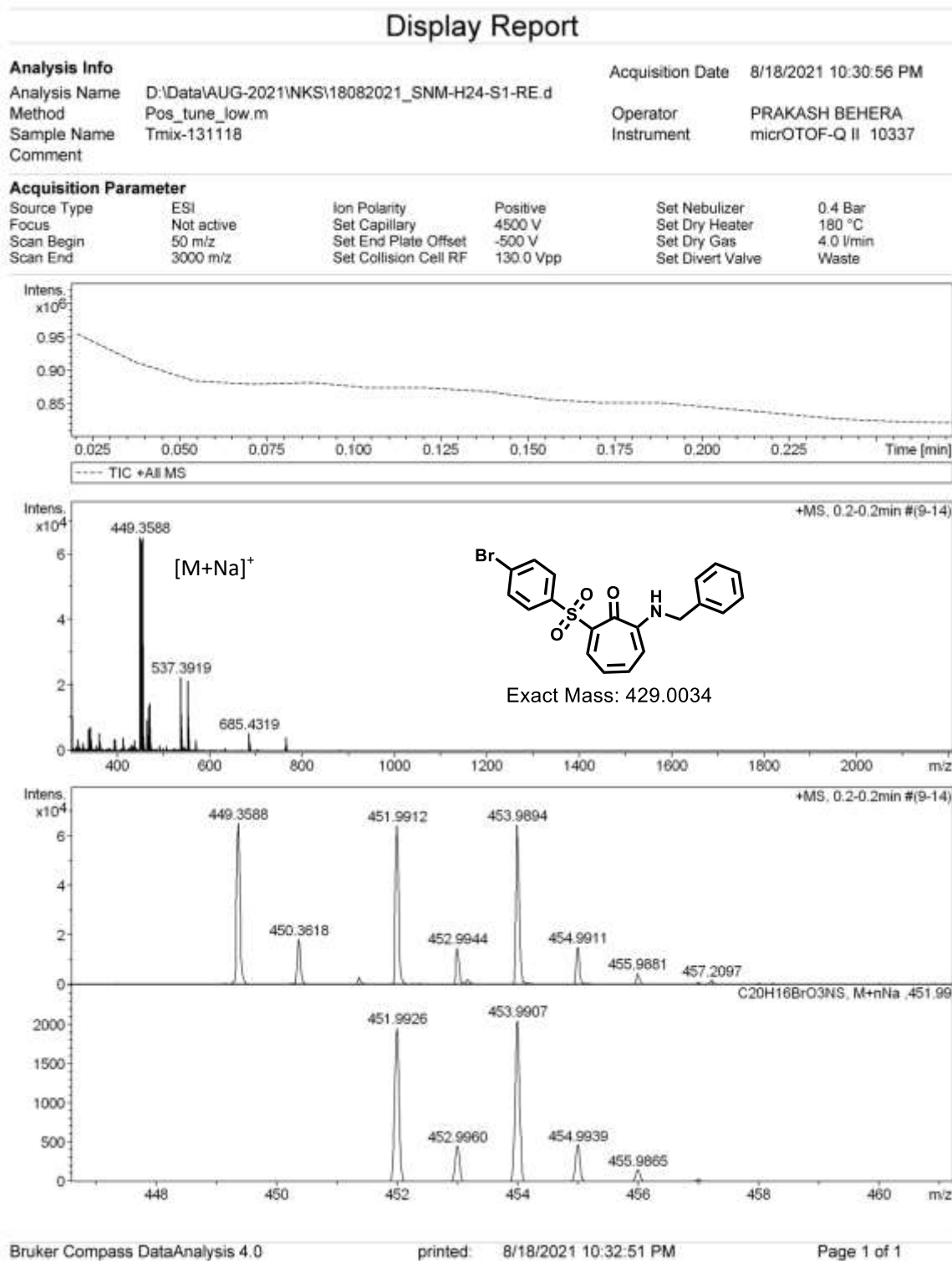
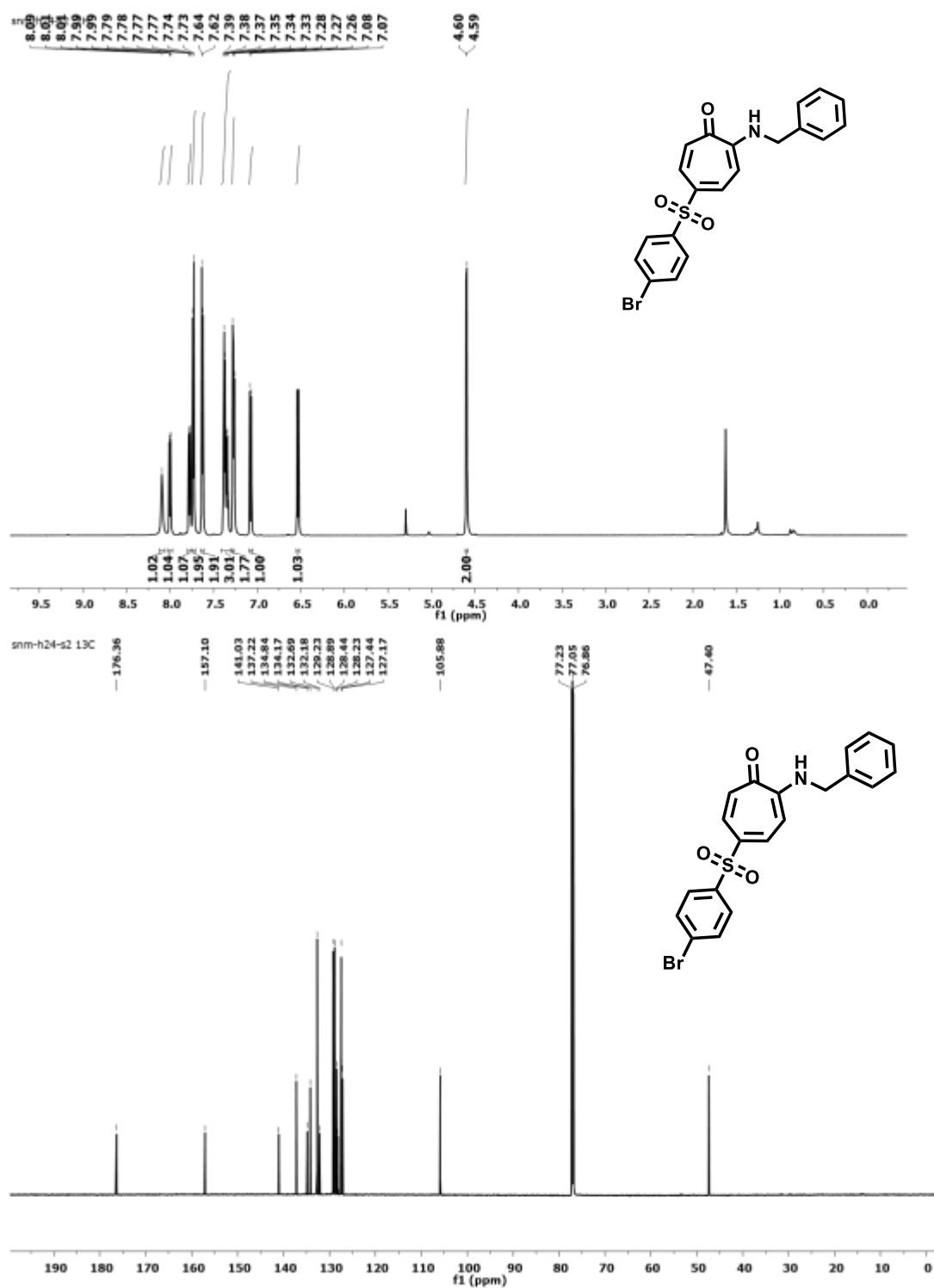
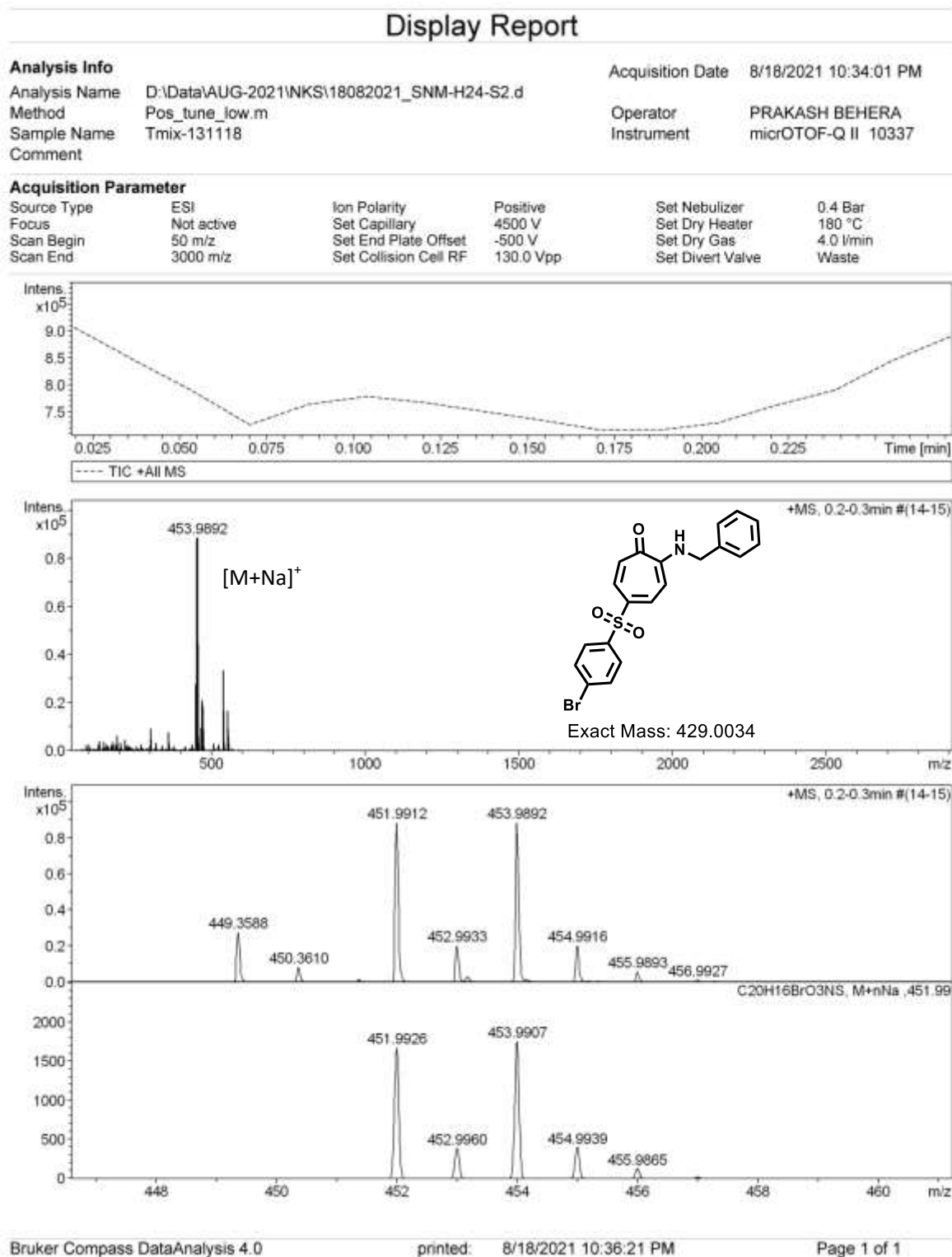


Figure A36. ESI-MS/HRMS spectra of compound 8a

$^1\text{H}$ ,  $^{13}\text{C}$  NMR (700MHz,  $\text{CDCl}_3$ ) and HRMS of **8b**

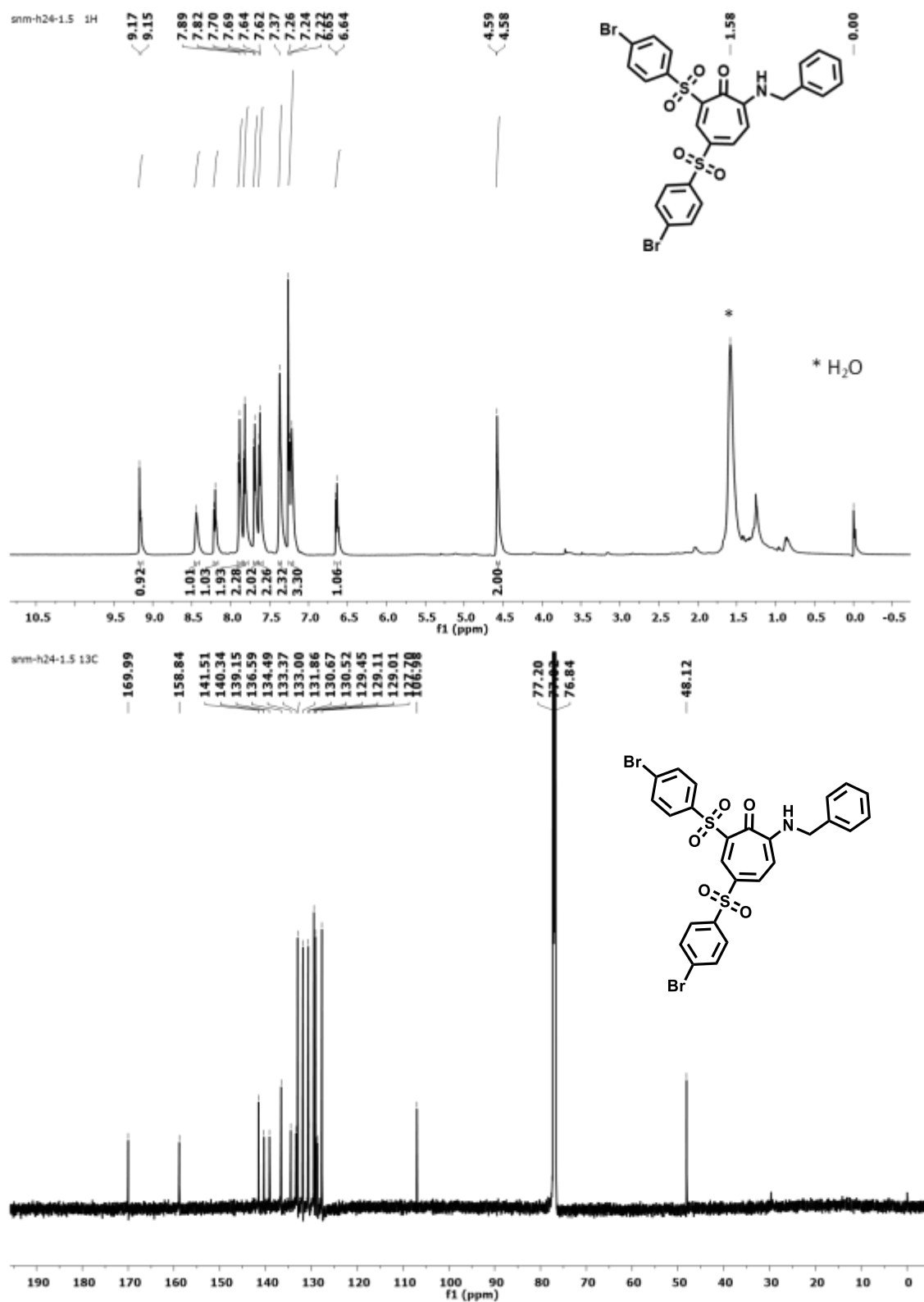


**Figure A37.**  $^1\text{H}/^{13}\text{C}$  NMR (700MHz,  $\text{CDCl}_3$ ) spectra of compound **8b** in  $\text{CDCl}_3$

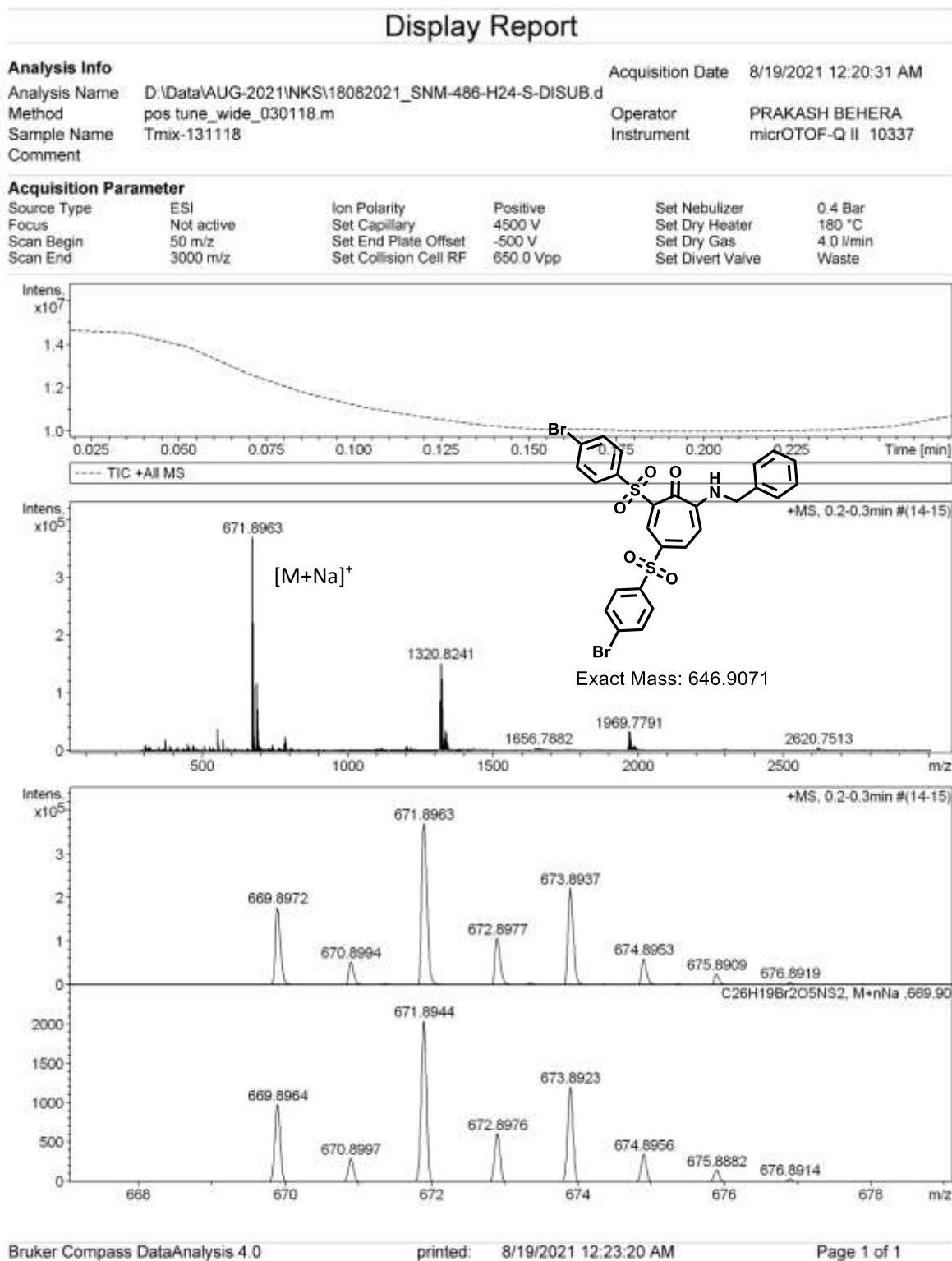
**Figure A38.** ESI-MS/HRMS spectra of compound **8b**



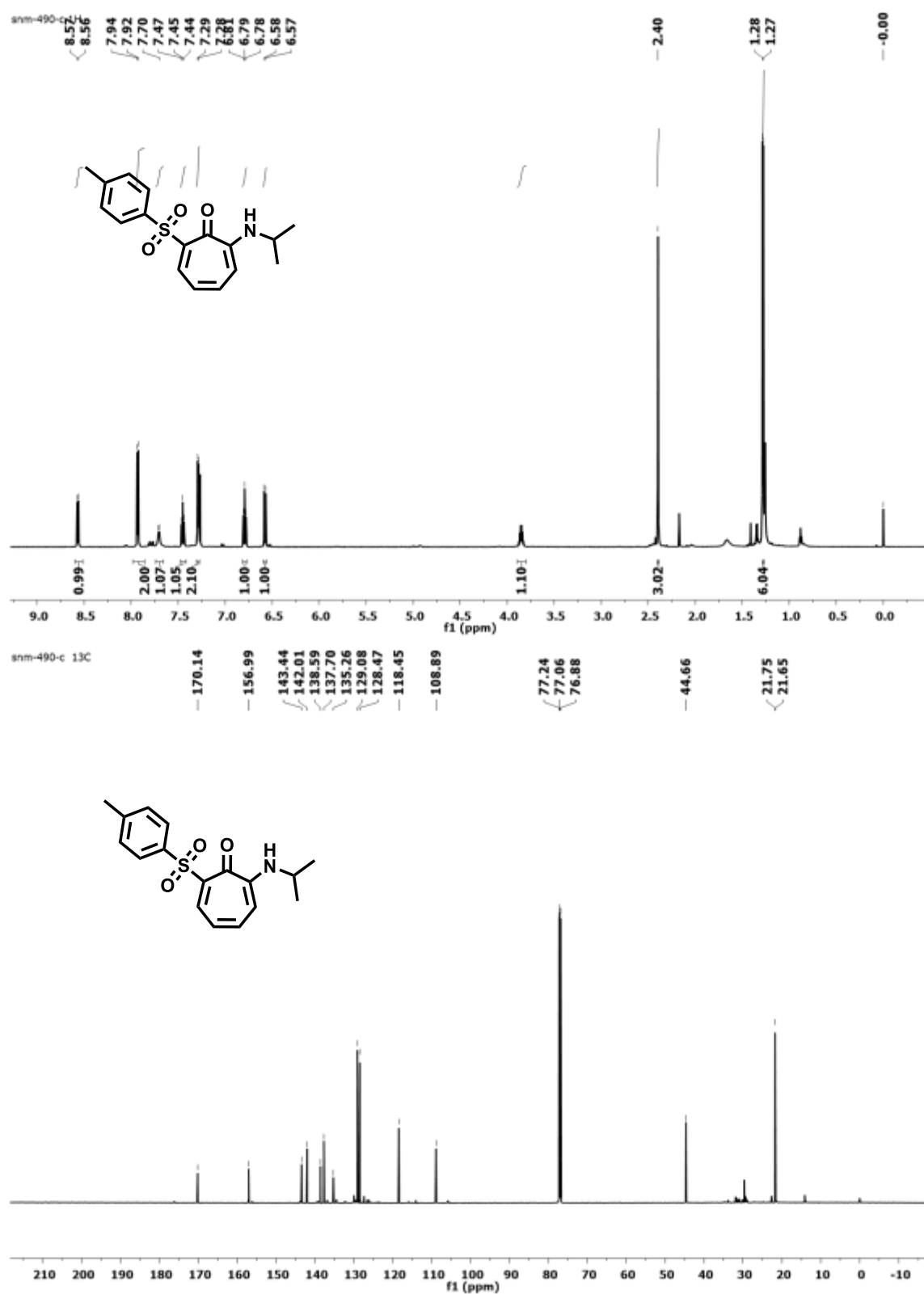
$^1\text{H}$ ,  $^{13}\text{C}$  NMR (700MHz,  $\text{CDCl}_3$ ) and HRMS of **8c**



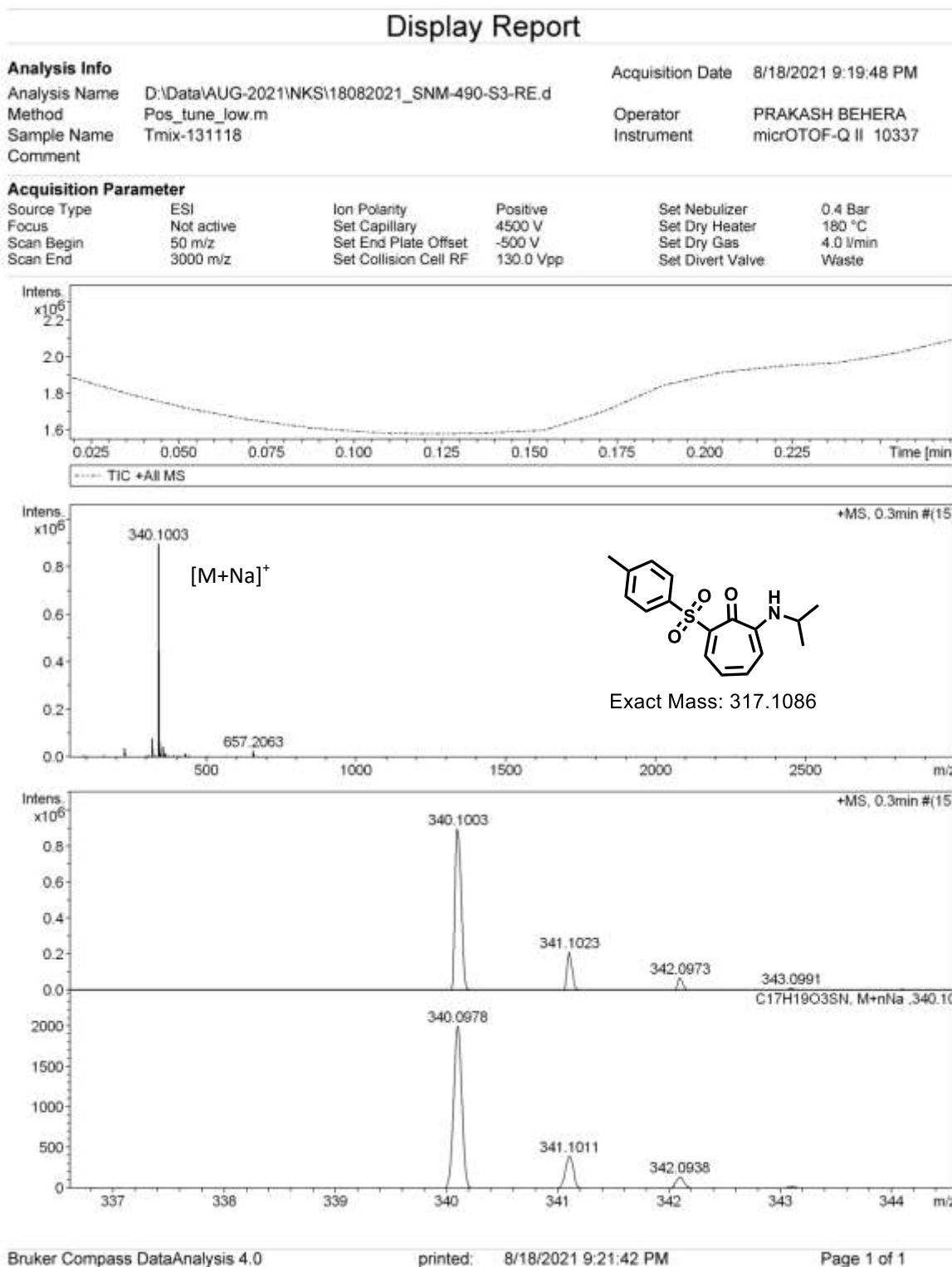
**Figure A39.**  $^1\text{H}/^{13}\text{C}$  NMR (700MHz,  $\text{CDCl}_3$ ) spectra of compound **8c** in  $\text{CDCl}_3$

**Figure A40.** ESI-MS/HRMS spectra of compound **8c**

$^1\text{H}$ ,  $^{13}\text{C}$  NMR (700MHz,  $\text{CDCl}_3$ ) and HRMS of **9a**

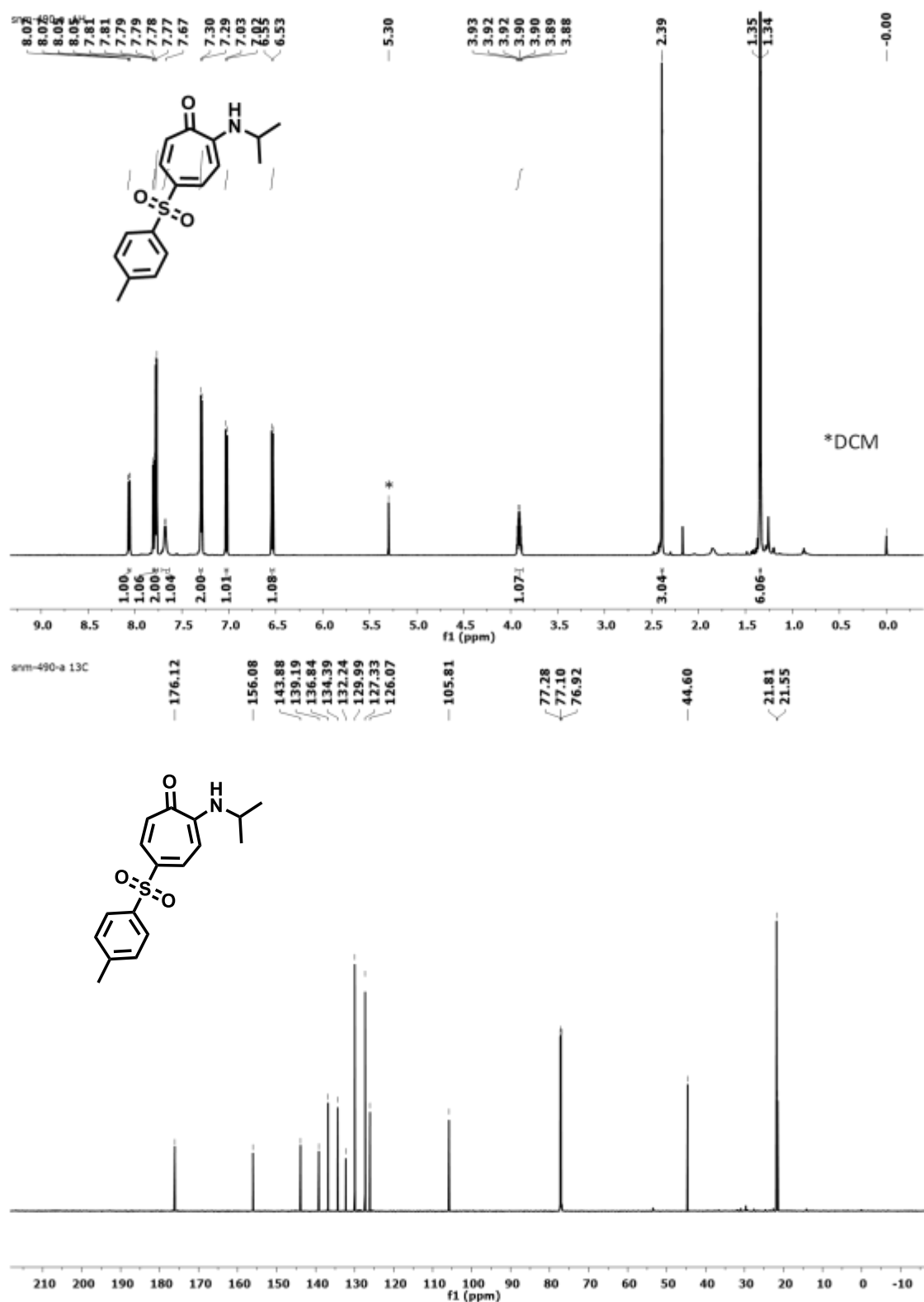


**Figure S41.**  $^1\text{H}/^{13}\text{C}$  NMR (700MHz,  $\text{CDCl}_3$ ) spectra of compound **9a** in  $\text{CDCl}_3$

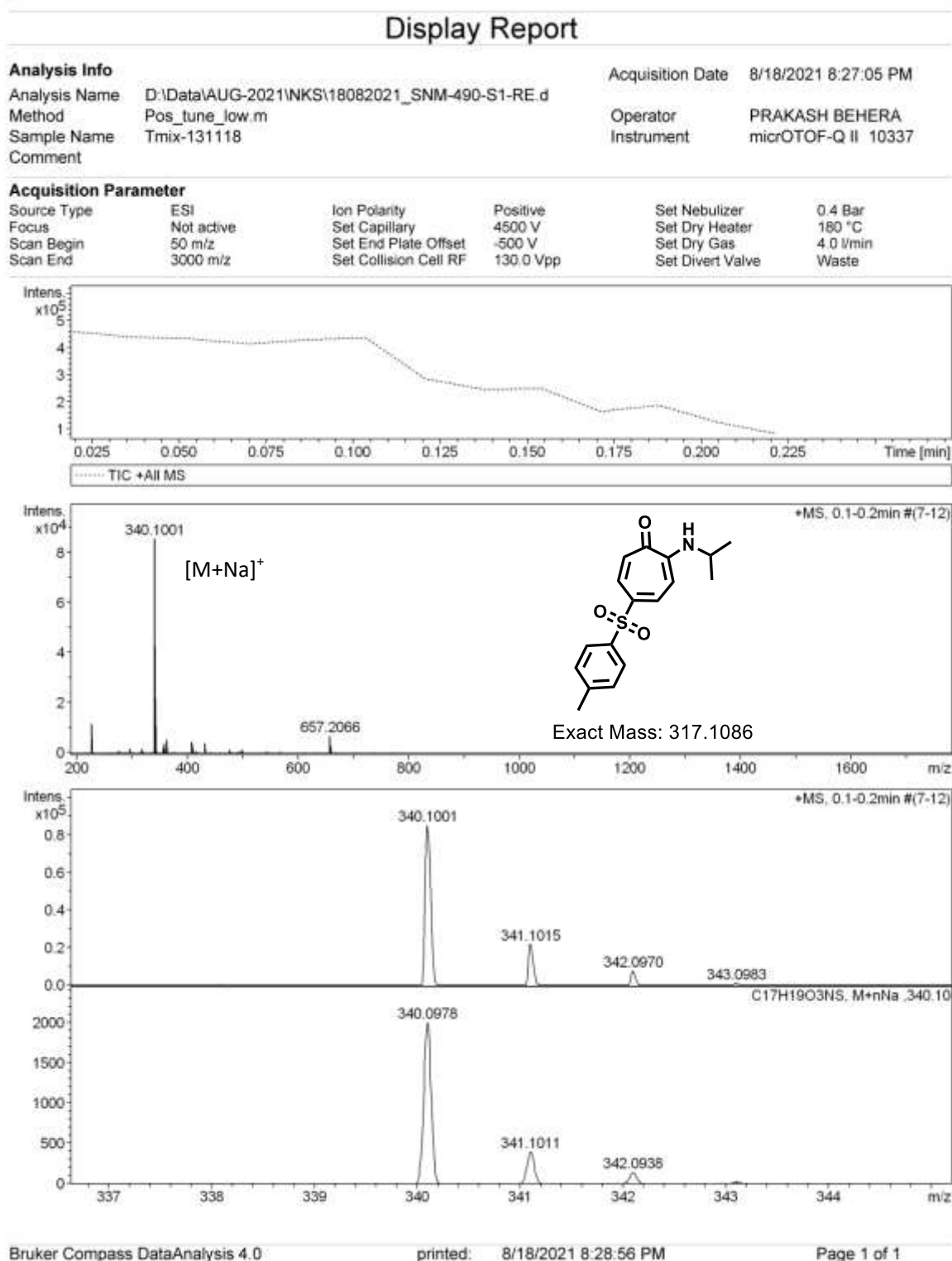


**Figure A42.** ESI-MS/HRMS spectra of compound **9a**

$^1\text{H}$ ,  $^{13}\text{C}$  NMR (700MHz,  $\text{CDCl}_3$ ) and HRMS of **9b**



**Figure A43.**  $^1\text{H}/^{13}\text{C}$  NMR (700MHz,  $\text{CDCl}_3$ ) spectra of compound **9b** in  $\text{CDCl}_3$

**Figure A44.** ESI-MS/HRMS spectra of compound **9b**

$^1\text{H}$ ,  $^{13}\text{C}$  NMR (700MHz,  $\text{CDCl}_3$ ) and HRMS of **9c**

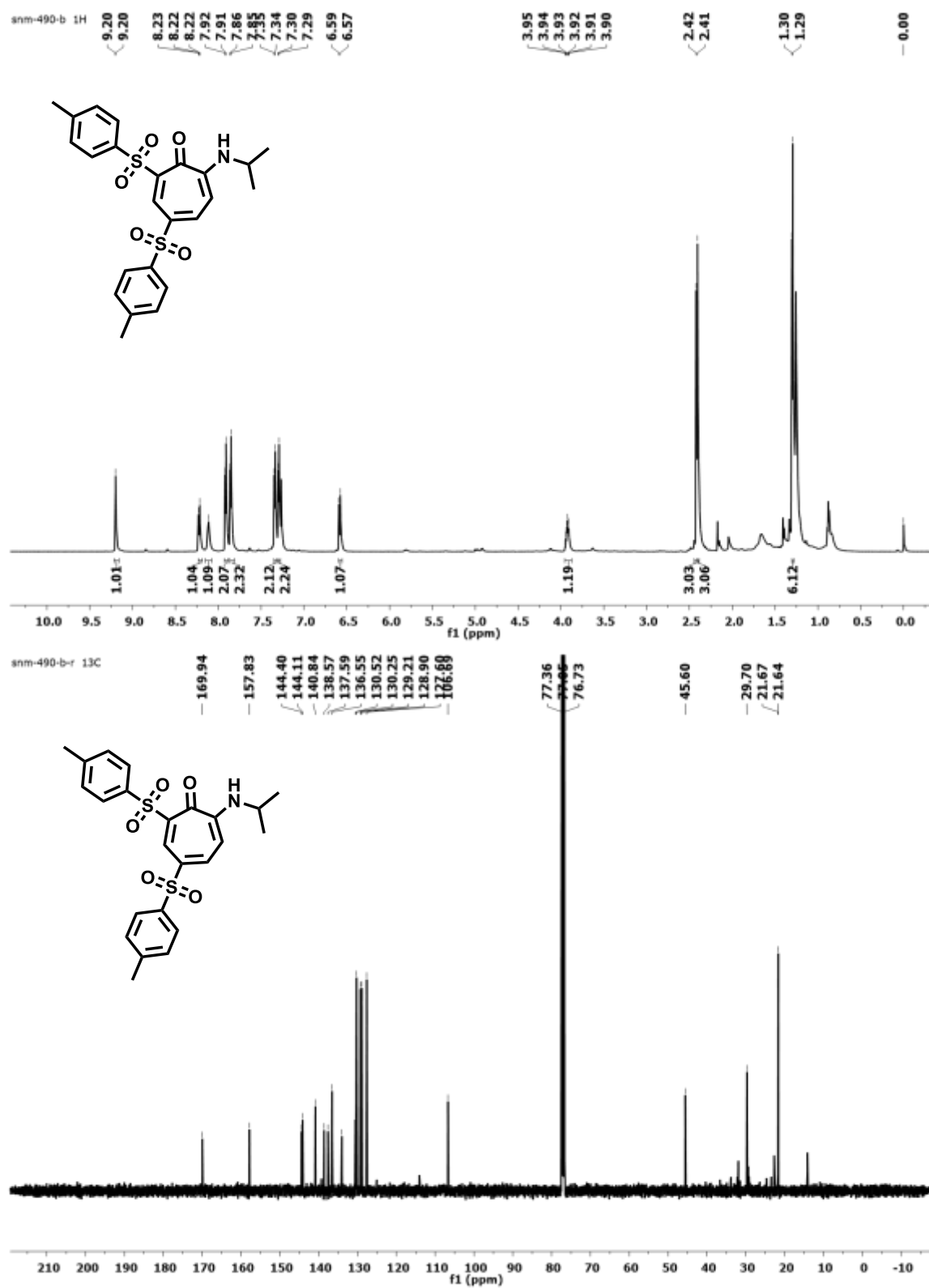


**Figure A45.**  $^1\text{H}/^{13}\text{C}$  NMR (700MHz,  $\text{CDCl}_3$ ) spectra of compound **9c** in  $\text{CDCl}_3$

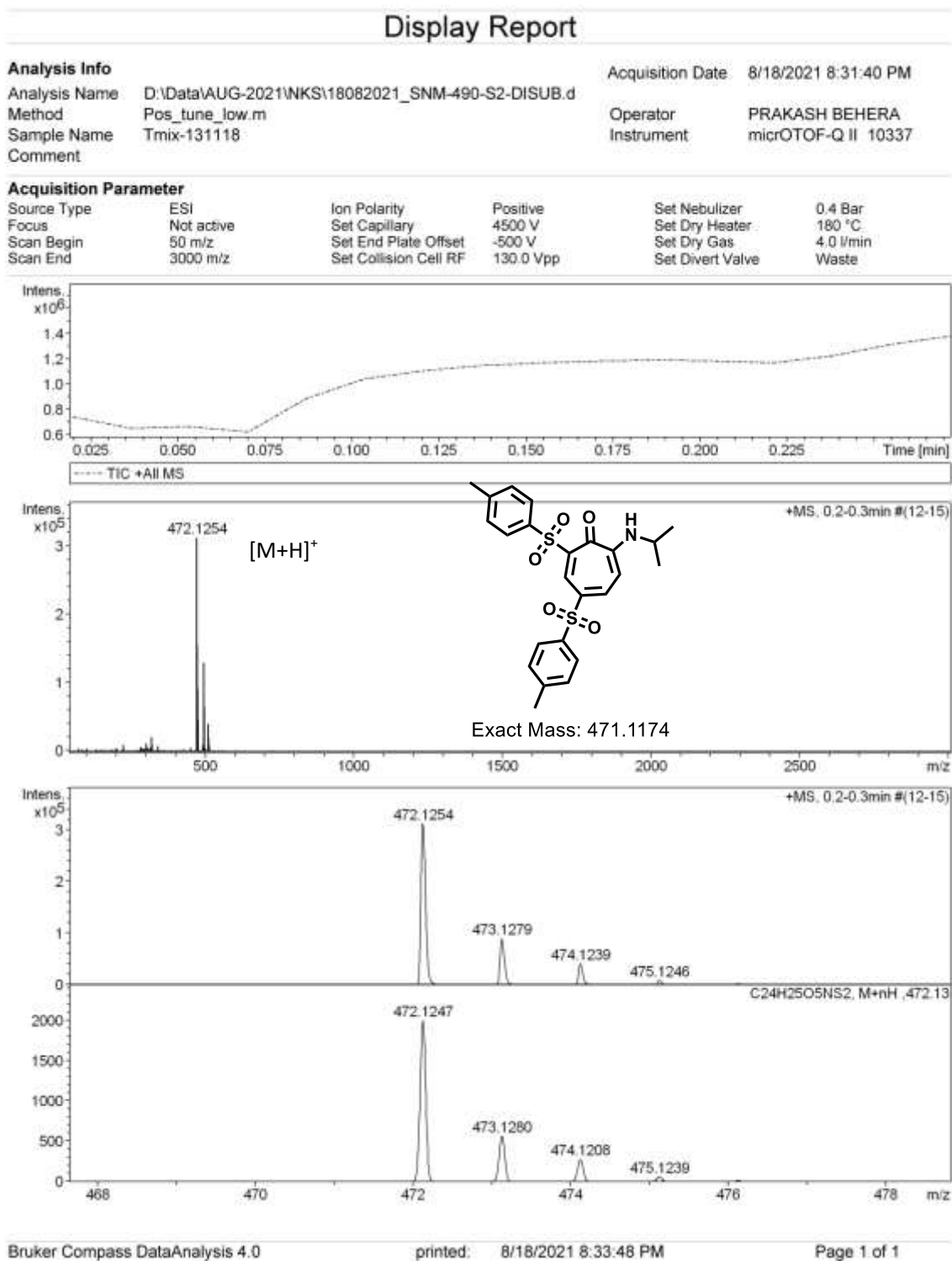
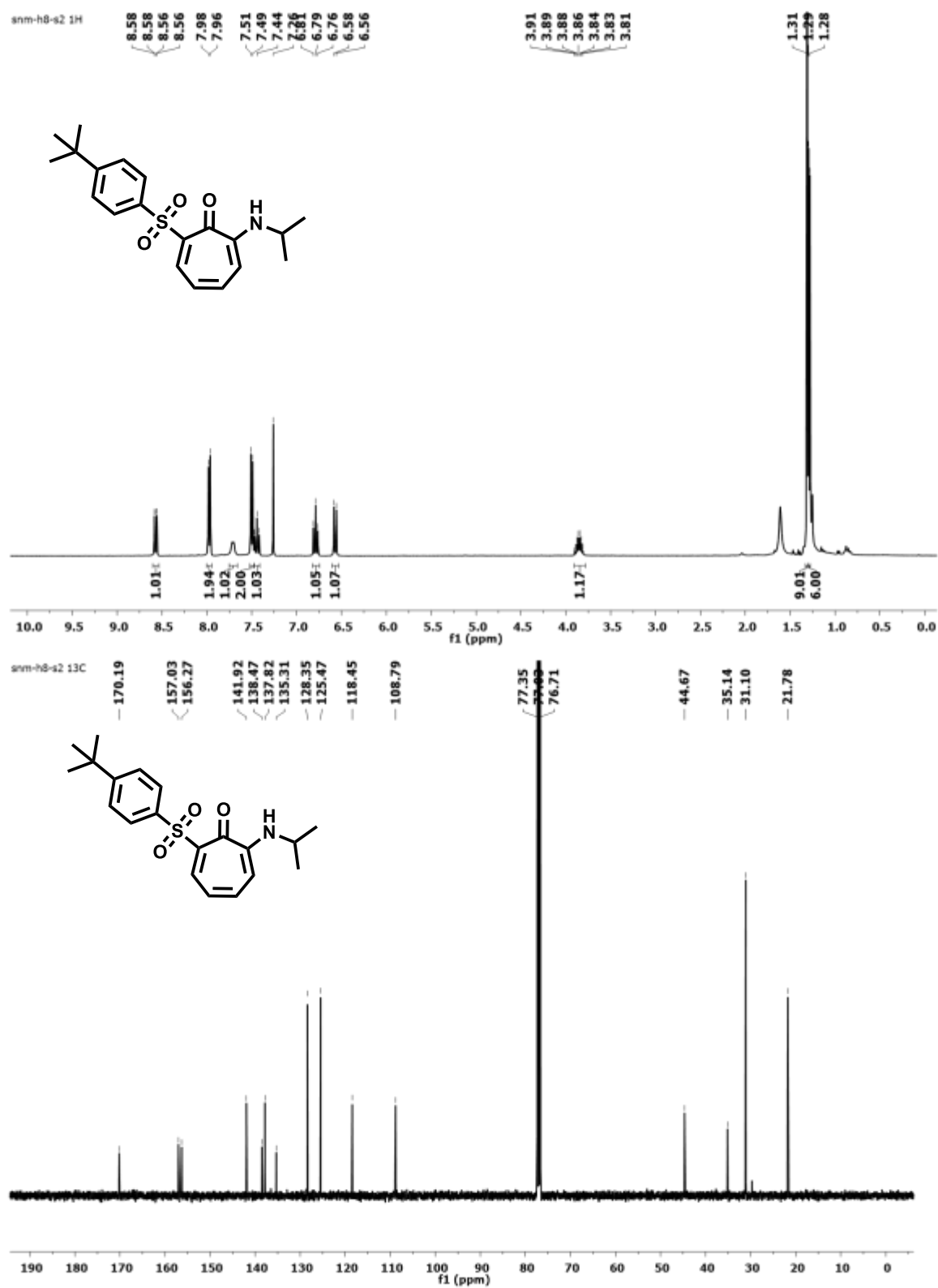


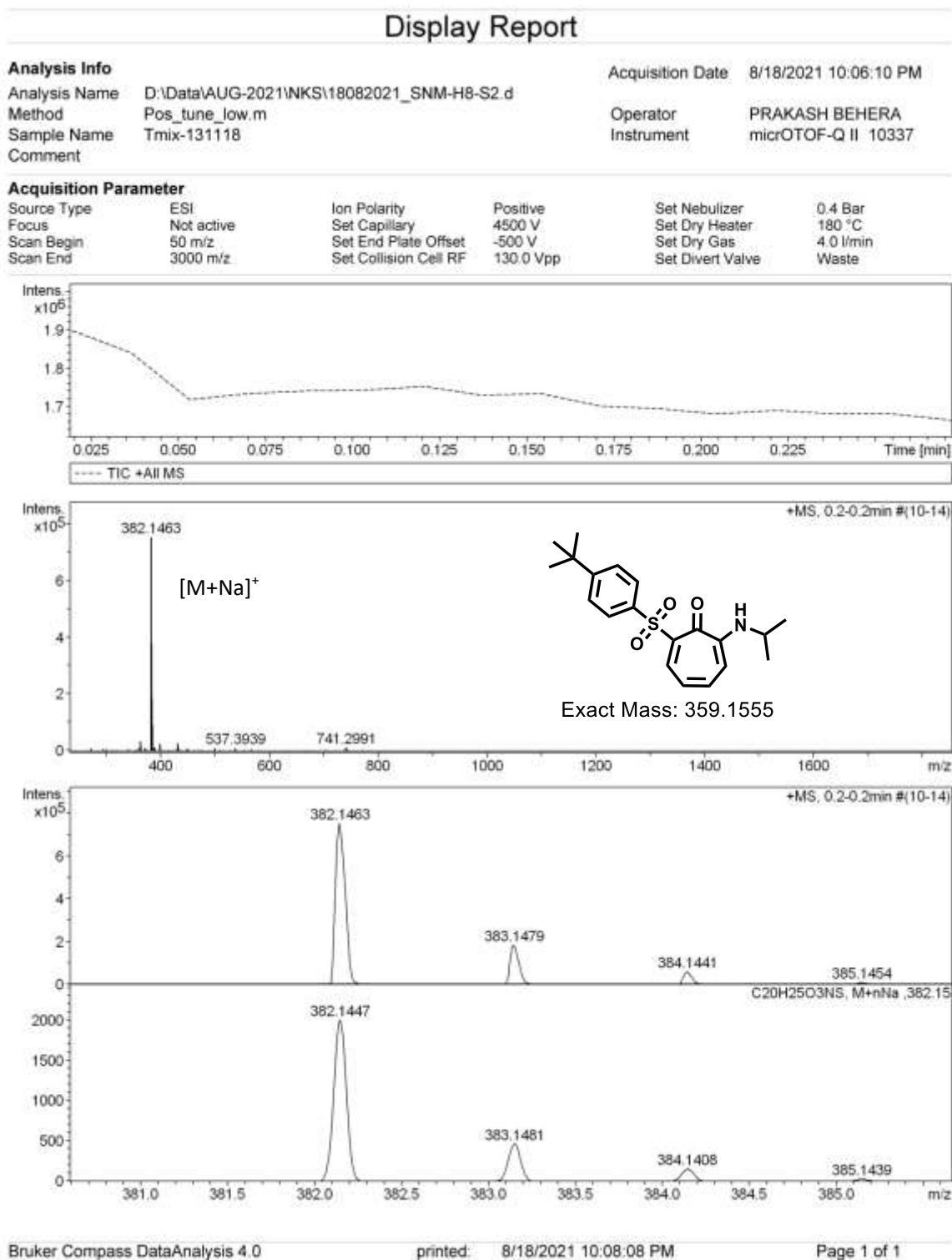
Figure A46. ESI-MS/HRMS spectra of compound 9c



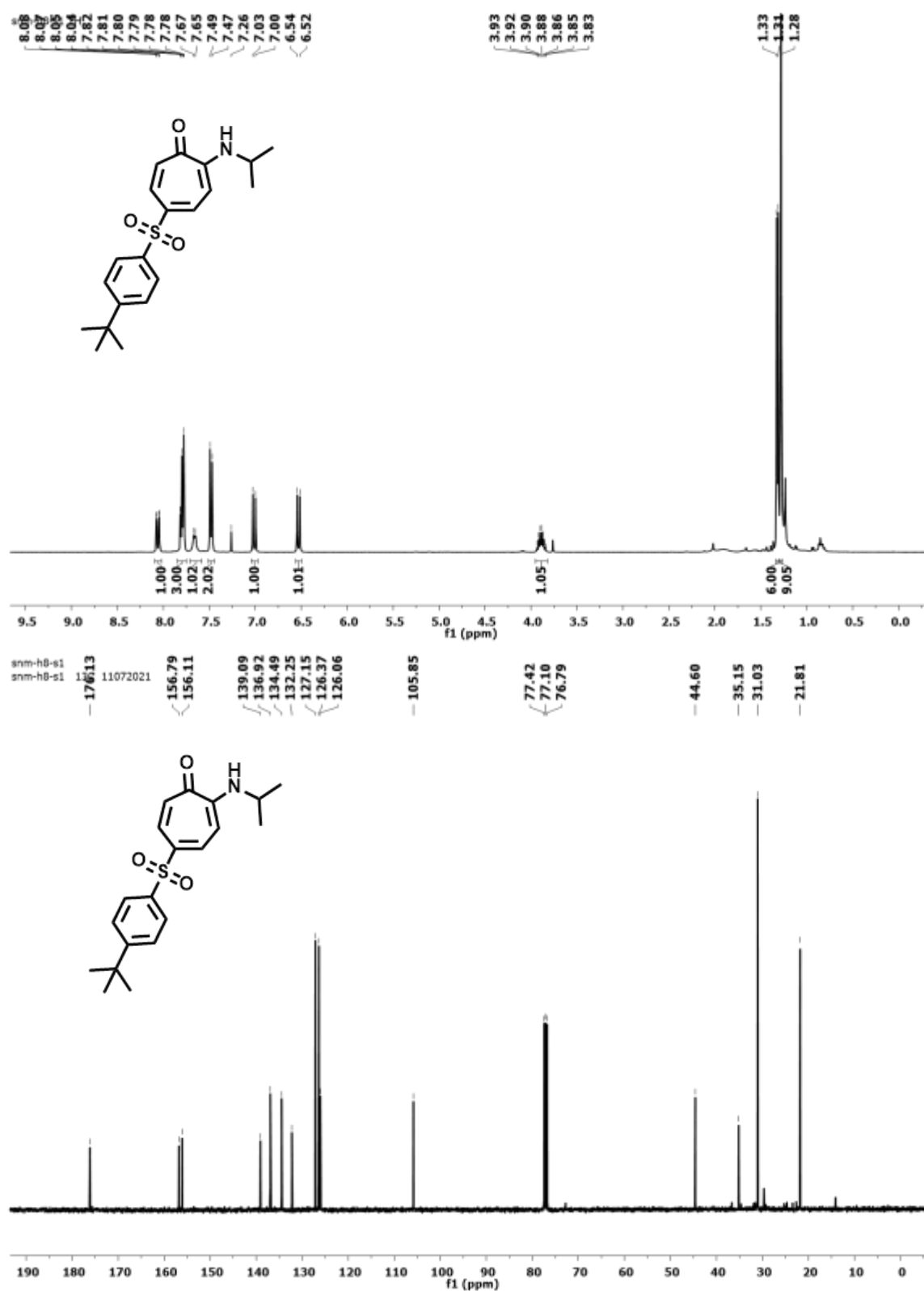
$^1\text{H}$ ,  $^{13}\text{C}$  NMR (400MHz,  $\text{CDCl}_3$ ) and HRMS of **10a**



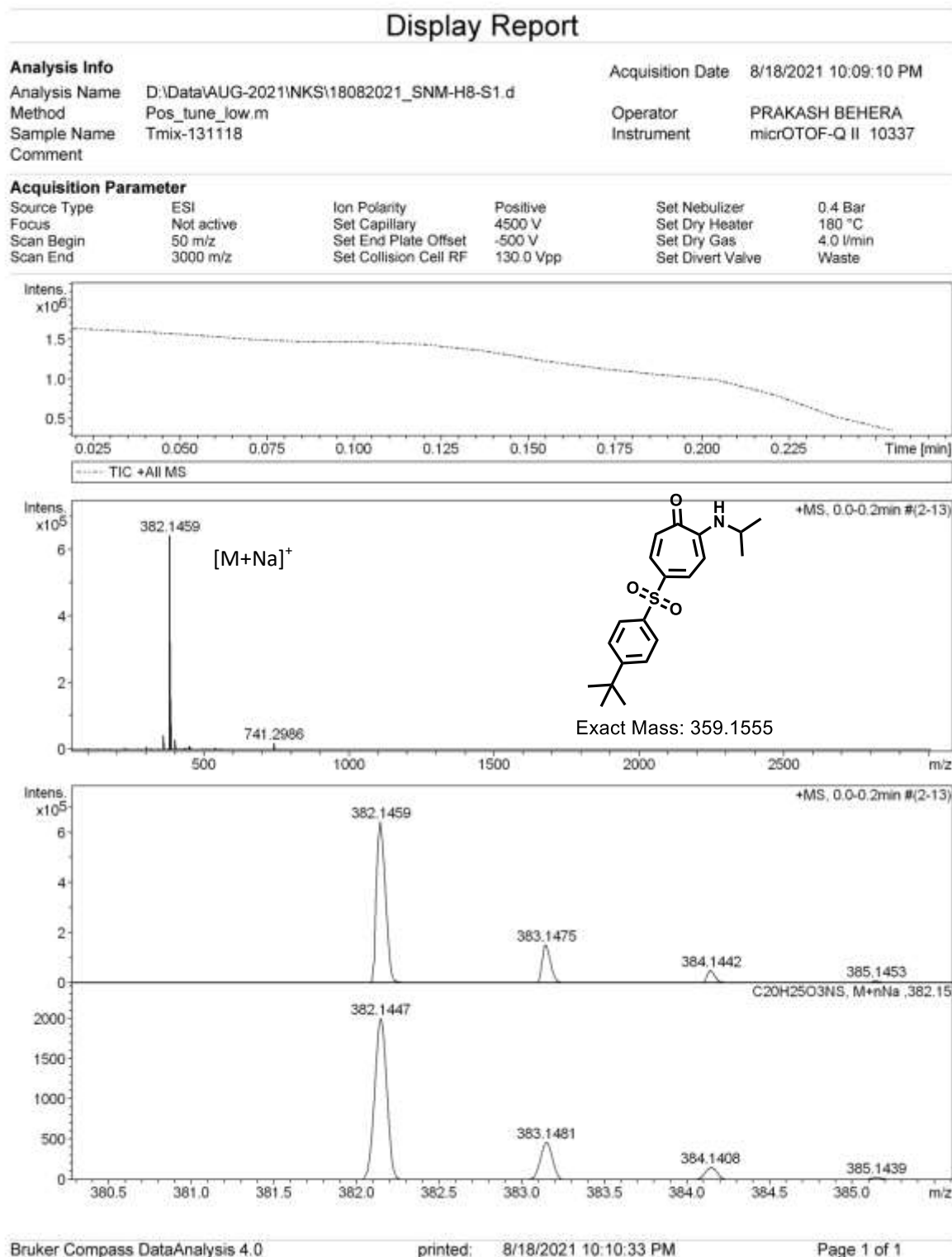
**Figure A47.**  $^1\text{H}/^{13}\text{C}$  NMR (400MHz,  $\text{CDCl}_3$ ) spectra of compound **10a** in  $\text{CDCl}_3$

**Figure A48.** ESI-MS/HRMS spectra of compound **10a**

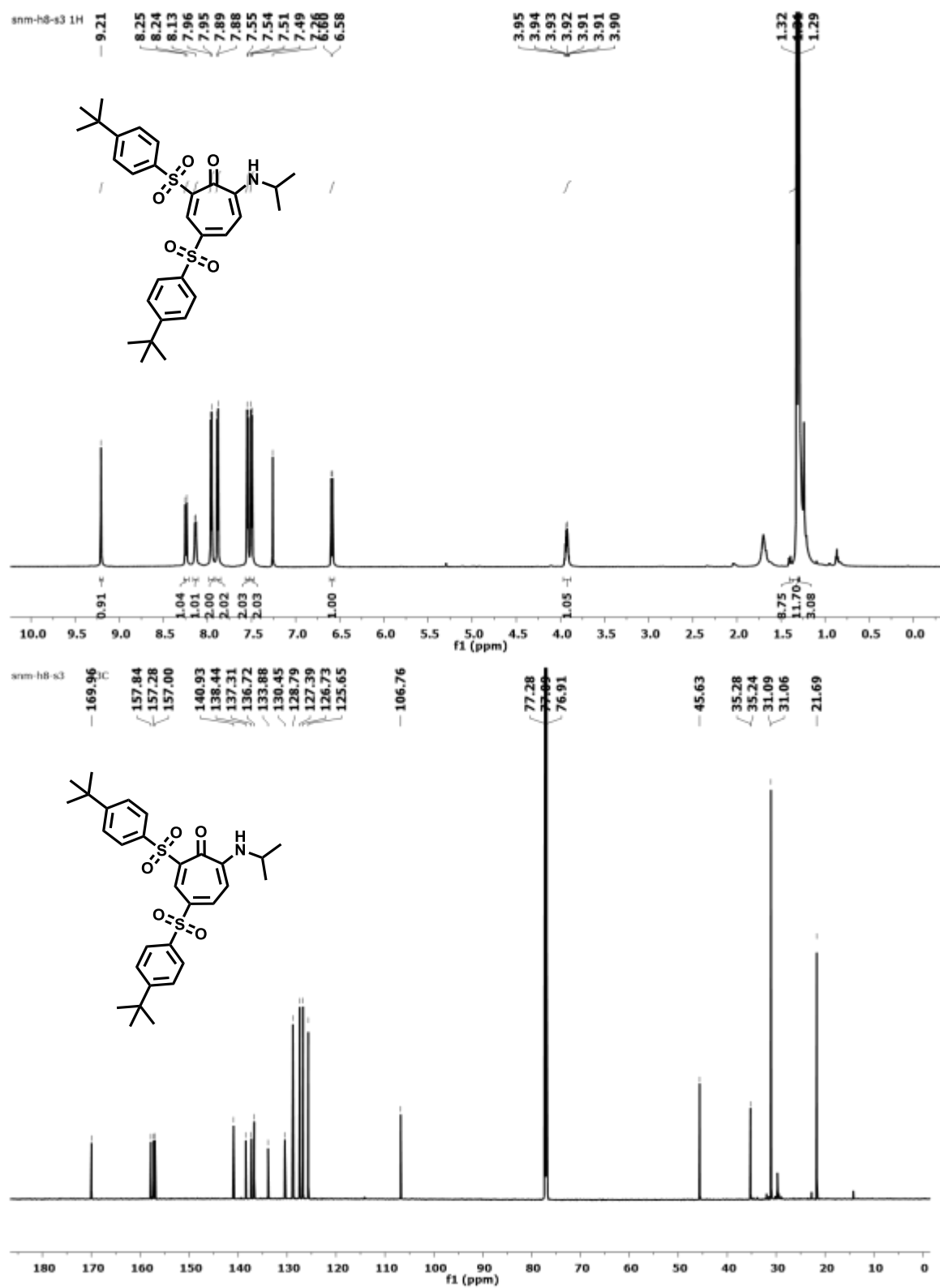
$^1\text{H}$ ,  $^{13}\text{C}$  NMR (400MHz,  $\text{CDCl}_3$ ) and HRMS of **10b**



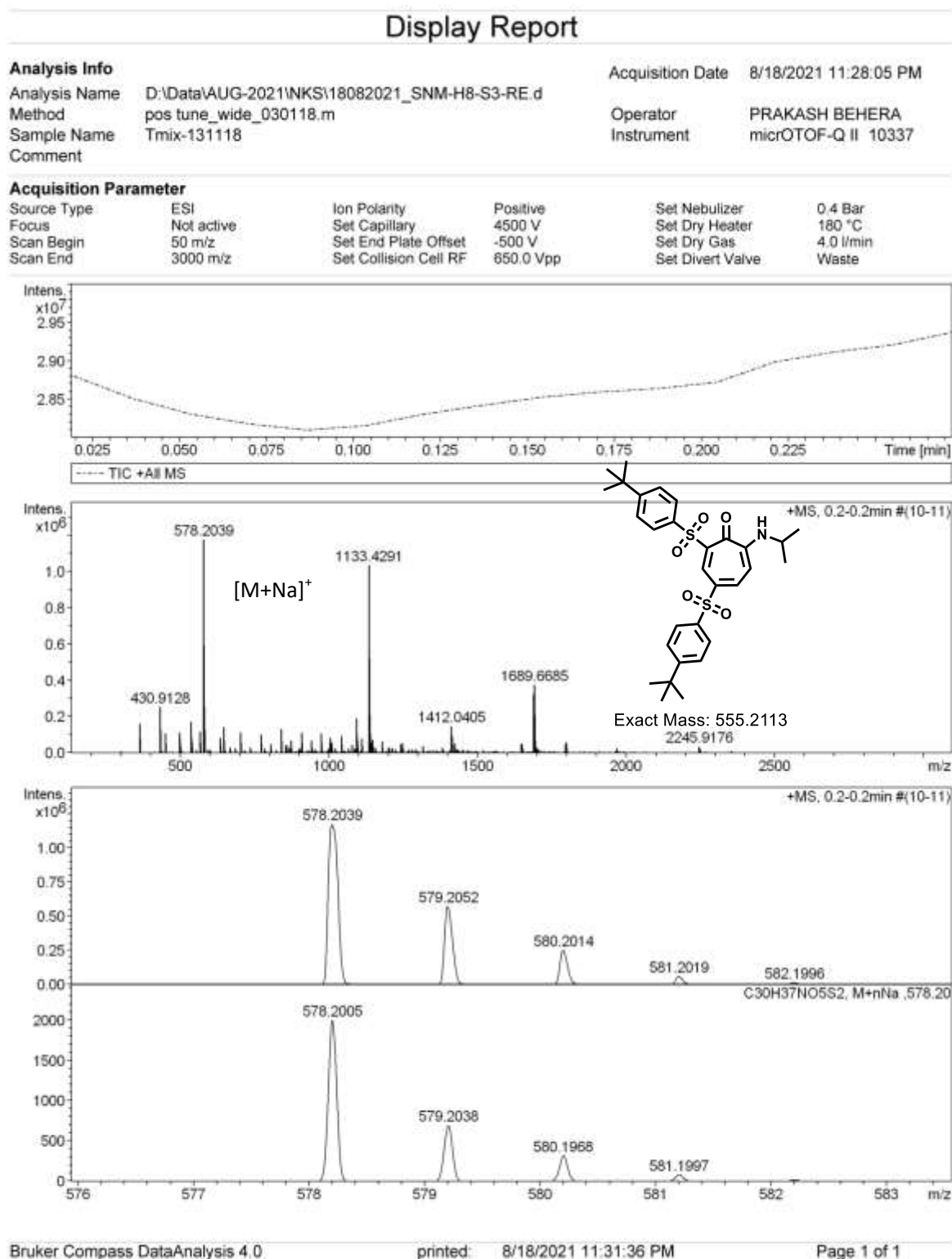
**Figure A49.**  $^1\text{H}/^{13}\text{C}$  NMR (400MHz,  $\text{CDCl}_3$ ) spectra of compound **10b** in  $\text{CDCl}_3$

**Figure A50.** ESI-MS/HRMS spectra of compound **10b**

$^1\text{H}$ ,  $^{13}\text{C}$  NMR (700MHz,  $\text{CDCl}_3$ ) and HRMS of **10c**



**Figure A51.**  $^1\text{H}/^{13}\text{C}$  NMR (700MHz,  $\text{CDCl}_3$ ) spectra of compound **10c** in  $\text{CDCl}_3$

Figure A52. ESI-MS/HRMS spectra of compound **10c**

$^1\text{H}$ ,  $^{13}\text{C}$  NMR (700MHz,  $\text{CDCl}_3$ ) and HRMS of **11a**

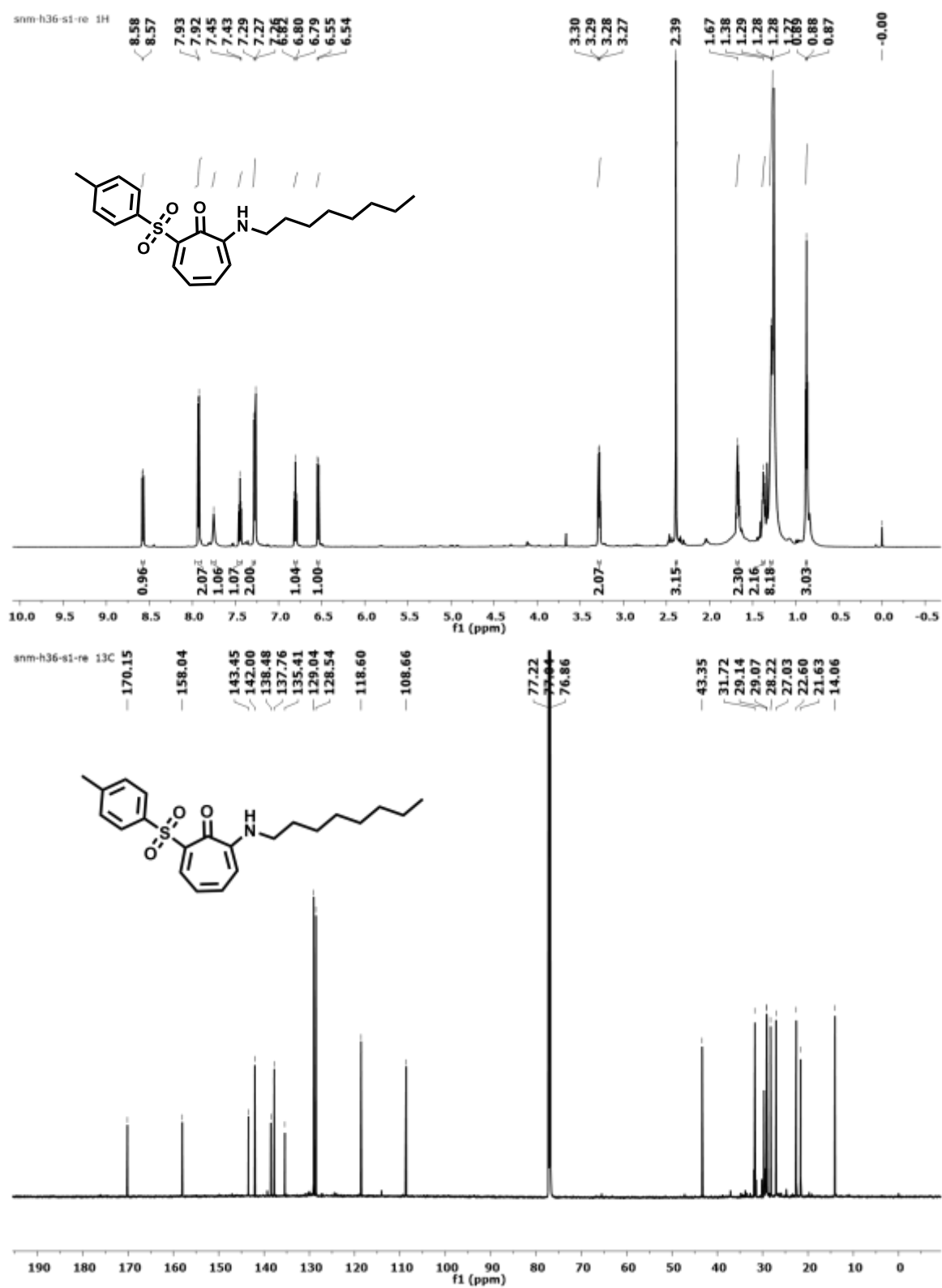


**Figure A53.**  $^1\text{H}/^{13}\text{C}$  NMR (700MHz,  $\text{CDCl}_3$ ) spectra of compound **11a** in  $\text{CDCl}_3$

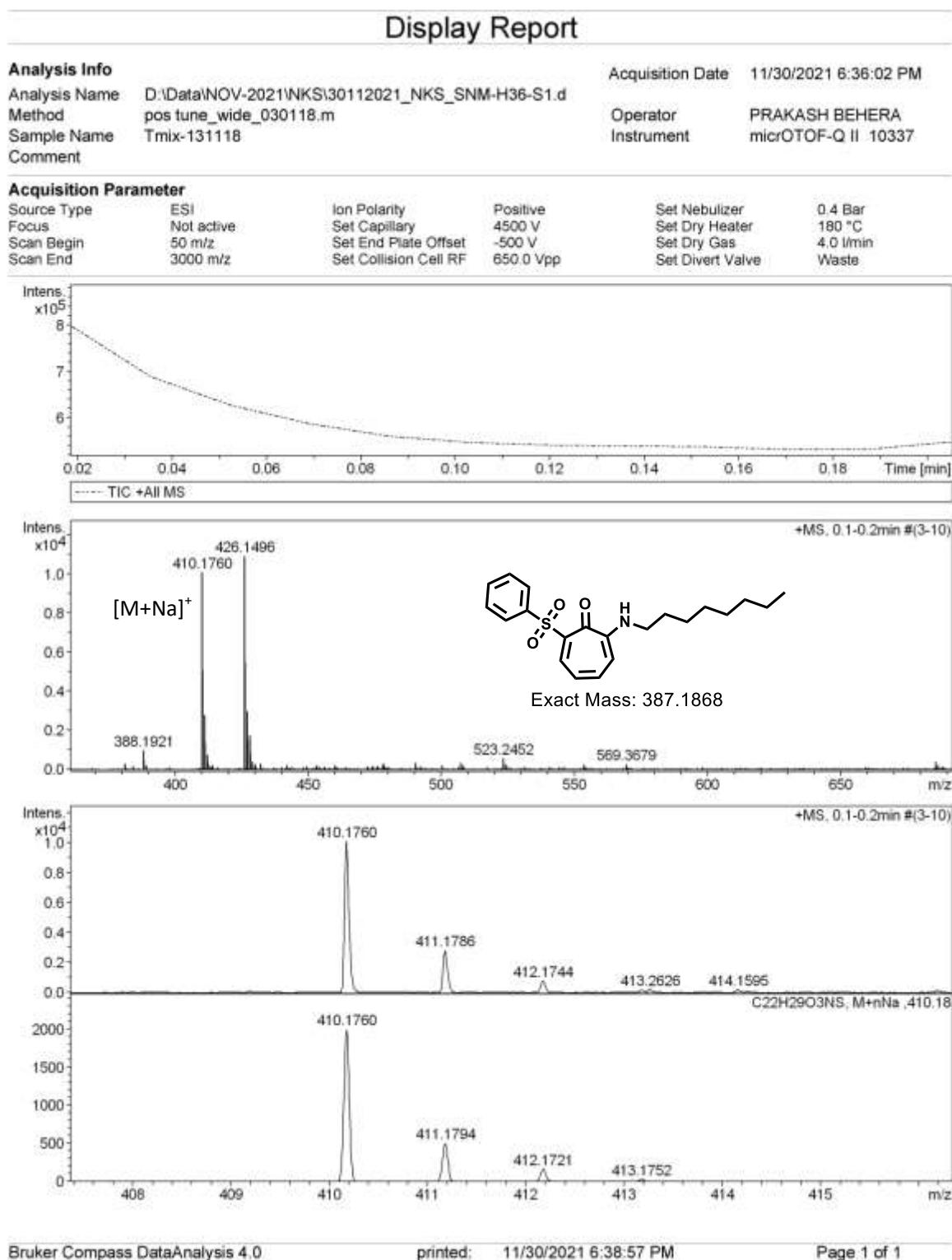
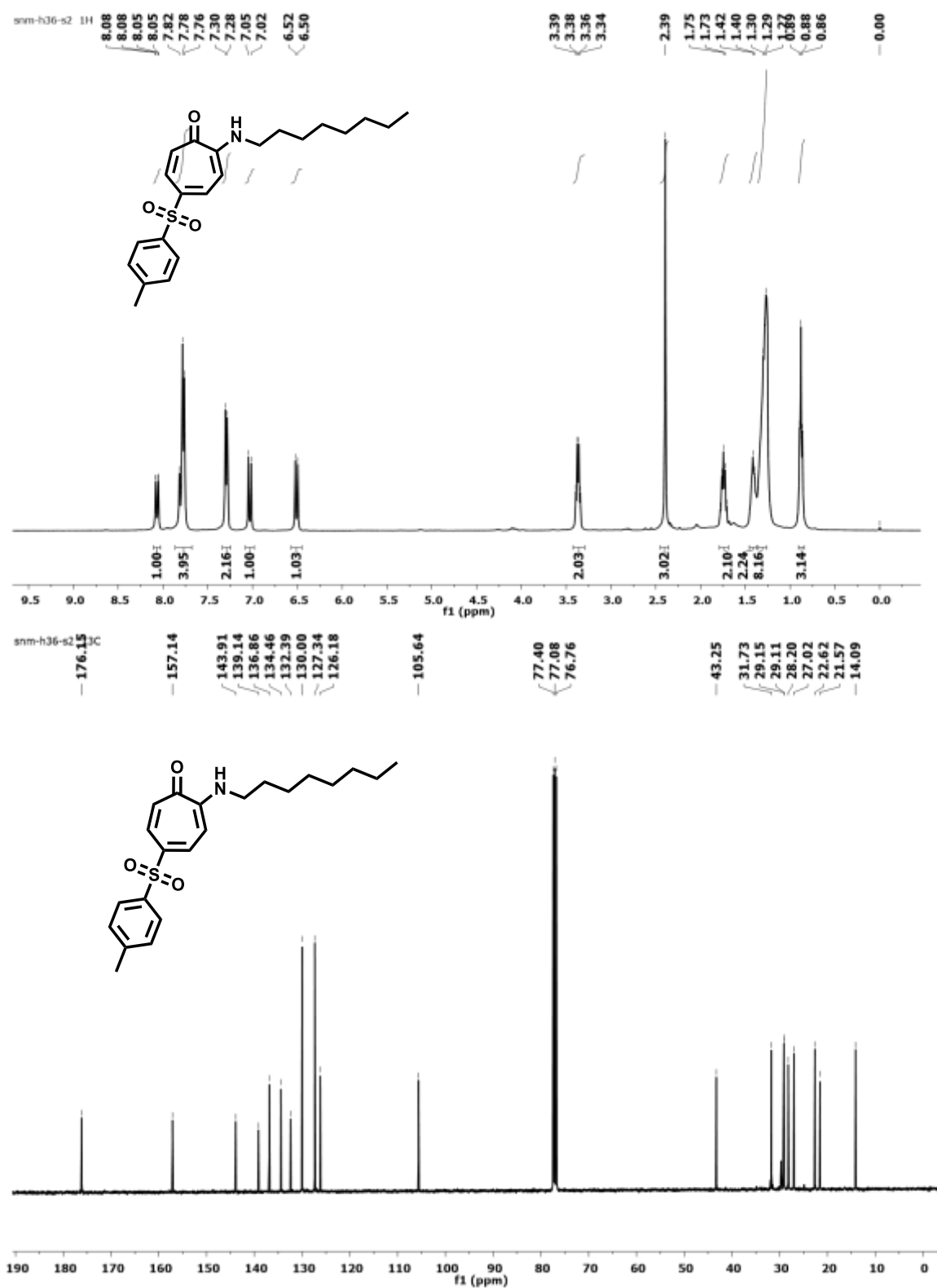


Figure A54. ESI-MS/HRMS spectra of compound 11a



$^1\text{H}$ ,  $^{13}\text{C}$  NMR (400MHz,  $\text{CDCl}_3$ ) and HRMS of **11b**



**Figure A55.**  $^1\text{H}/^{13}\text{C}$  NMR (400MHz,  $\text{CDCl}_3$ ) spectra of compound **11b** in  $\text{CDCl}_3$

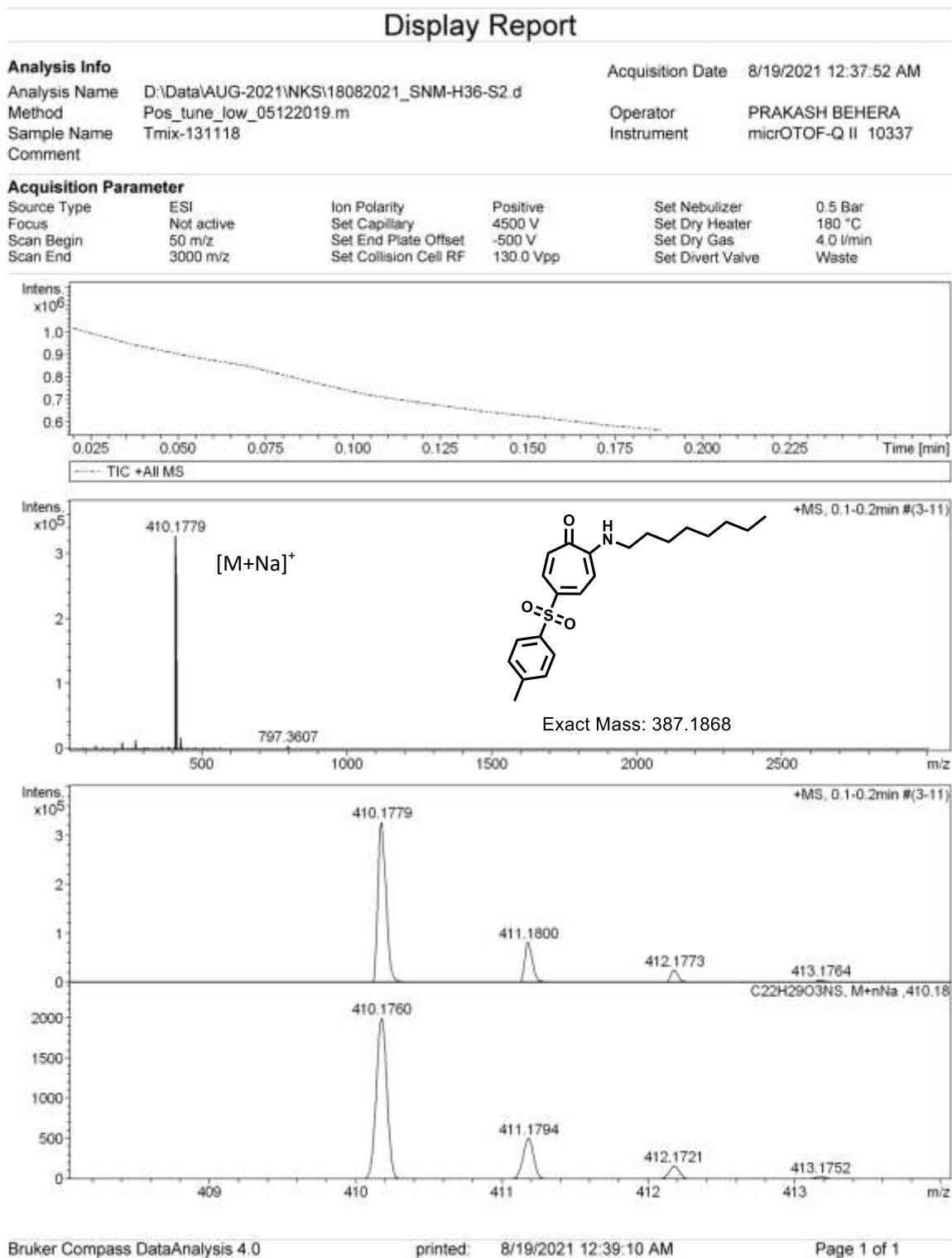
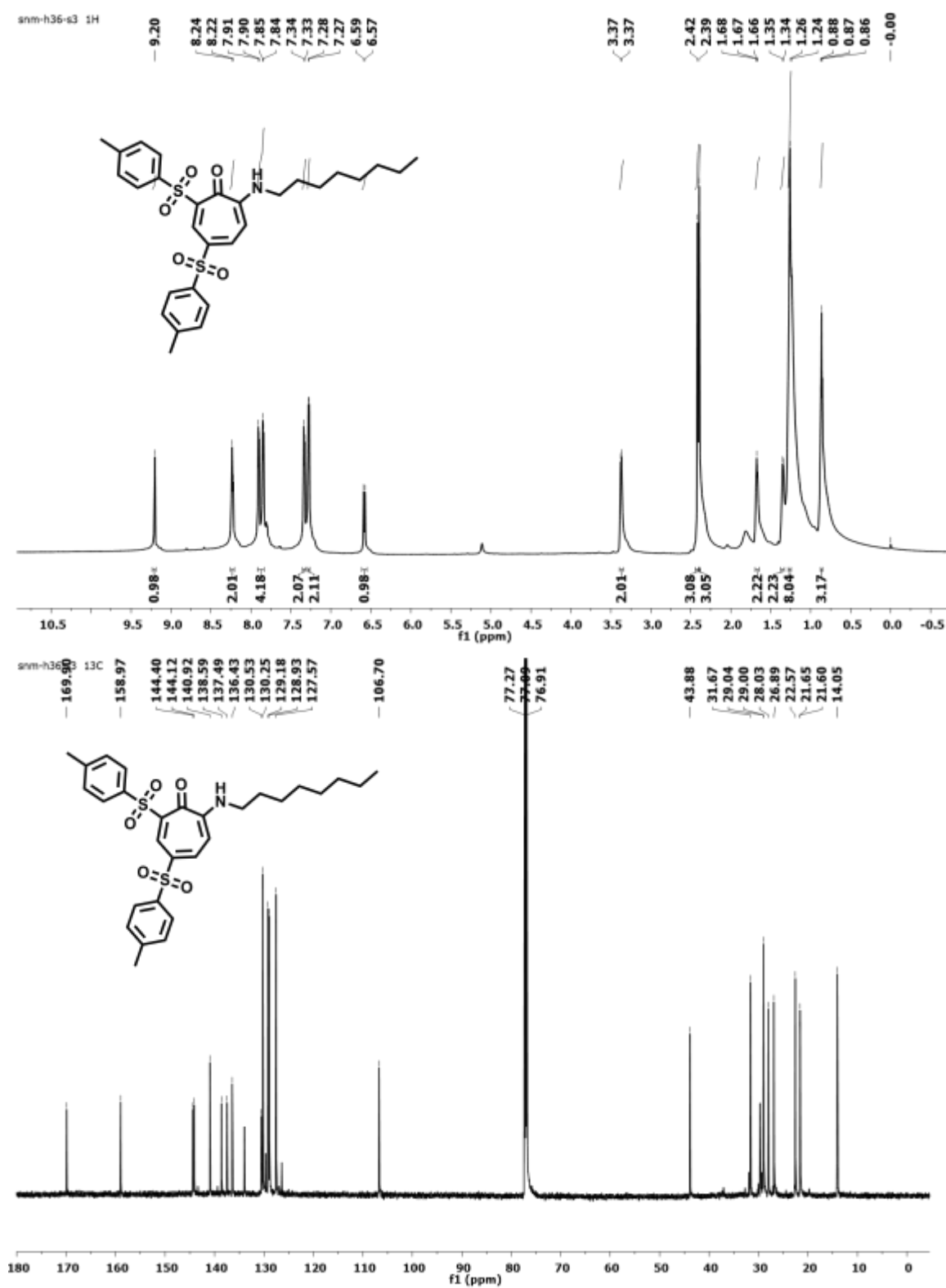


Figure A56. ESI-MS/HRMS spectra of compound 11b

$^1\text{H}$ ,  $^{13}\text{C}$  NMR (700MHz,  $\text{CDCl}_3$ ) and HRMS of **11c**



**Figure A57.**  $^1\text{H}/^{13}\text{C}$  NMR (700MHz,  $\text{CDCl}_3$ ) spectra of compound **11c** in  $\text{CDCl}_3$

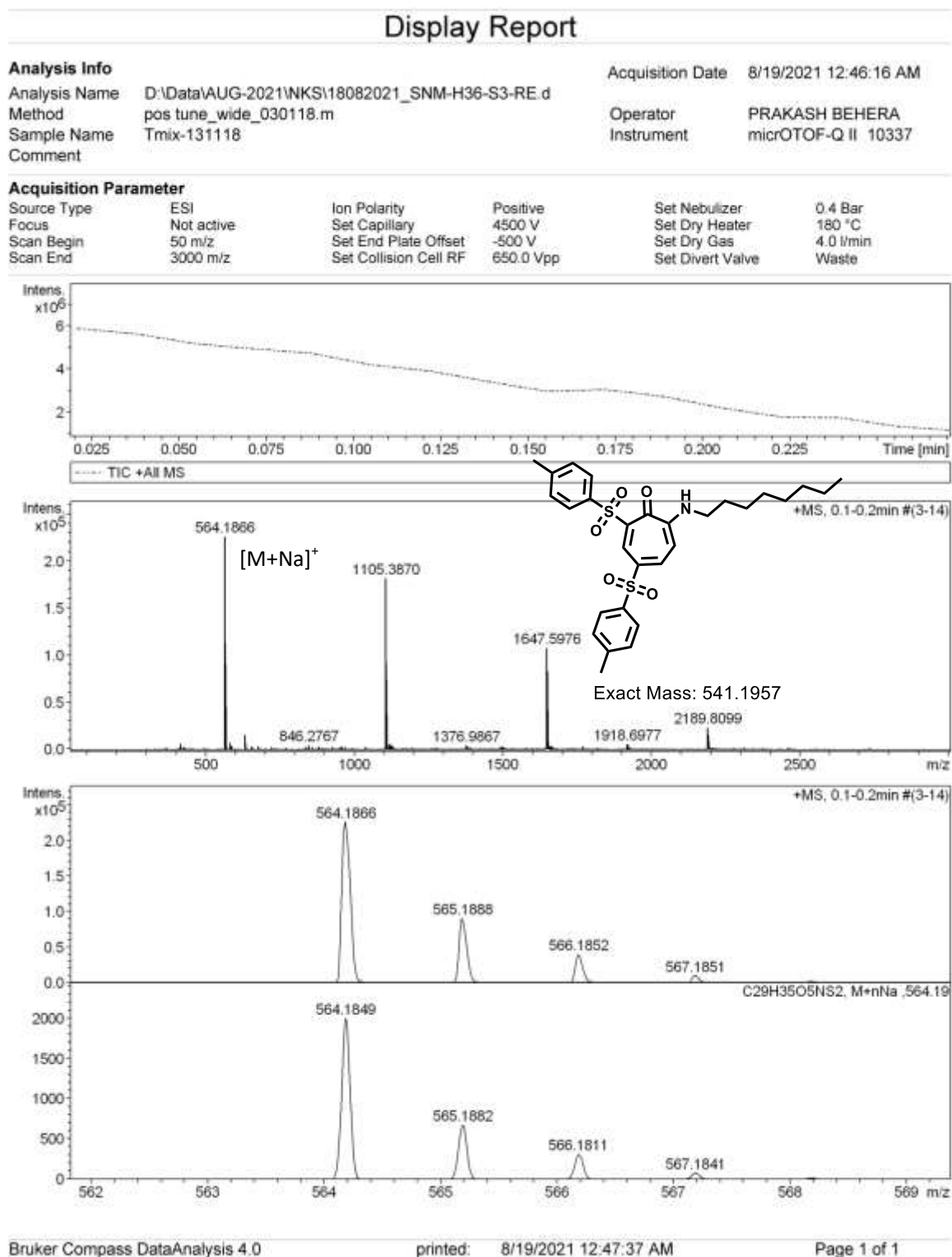


Figure A58. ESI-MS/HRMS spectra of compound 11c

## 2. Crystal data of compound 3b

**Table A1:** Crystal data and structure refinement for 3b

Identification code	<b>3b</b> (CCDC No. 2169438)
Empirical formula	C <sub>21</sub> H <sub>18</sub> NO <sub>3</sub> S
Formula weight	364.42
Temperature/K	302(1)
Crystal system	triclinic
Space group	P-1
a/Å	5.9955(3)
b/Å	7.9879(4)
c/Å	19.5137(10)
$\alpha$ /°	90.226(4)
$\beta$ /°	92.804(4)
$\gamma$ /°	98.340(4)
Volume/Å <sup>3</sup>	923.49(8)
Z	2
$\rho_{\text{calc}}$ /cm <sup>3</sup>	1.311
$\mu$ /mm <sup>-1</sup>	0.195
F(000)	382.0
Crystal size/mm <sup>3</sup>	0.01 × 0.01 × 0.001
Radiation	MoK $\alpha$ ( $\lambda$ = 0.71073)
2 $\theta$ range for data collection/°	6.602 to 61.584
Index ranges	-7 ≤ h ≤ 8, -11 ≤ k ≤ 10, -24 ≤ l ≤ 27
Reflections collected	17232
Independent reflections	4678 [R <sub>int</sub> = 0.0393, R <sub>sigma</sub> = 0.0359]
Data/restraints/parameters	4678/0/236
Goodness-of-fit on F <sup>2</sup>	1.029
Final R indexes [I ≥ 2 $\sigma$ (I)]	R <sub>1</sub> = 0.0544, wR <sub>2</sub> = 0.1426
Final R indexes [all data]	R <sub>1</sub> = 0.0828, wR <sub>2</sub> = 0.1574
Largest diff. peak/hole / e Å <sup>-3</sup>	0.35/-0.36

## **CHAPTER 3**

### **PART-B**

---

# **Troponylsulfone Conjugated Nucleosides: Synthesis, Photophysics and HeLa cell Imaging**

---

#### **3B.1 Introduction**

#### **3B.2 Objective**

#### **3B.3 Results and Discussion**

#### **3B.4 Conclusion**

#### **3B.5 Experimental Procedure**

#### **3B.6 References and Notes**

#### **3B.7 Appendix**

### 3B.1 Introduction

Nucleic acids (DNA/RNA) are the primary genetic component of cells that regulate various intricate biological processes.<sup>1,2</sup> The nucleic acid composition was extensively studied and analyzed, resulting in the discovery of modified nucleosides in addition to the primary constituent units (A/T/G/C/U).<sup>3</sup> This discovery brought up fresh perspectives on the interaction between genetic information and cellular biological processes, and the introduction of fluorescent nucleosides brought revolutionary changes in nucleic acid chemistry.<sup>4,5</sup> Emissive nucleosides have emerged as an instrumental category of chemical and biological tools for the molecular-level understanding of nucleic acid structures, activities, locations, and interactions.<sup>6,7</sup> Their luminescence permits the exploration of nucleic acid pathways, dynamics, or drug interactions and facilitates the fabrication of biophysical and diagnostic assays.<sup>8</sup> Non-emissive Natural nucleobases can be helpful as emissive tools by significant structural modifications. Fluorescent nucleosides bearing chemically modified nucleobases have been particularly widely studied because of their environment-sensitive fluorescence properties.<sup>9</sup> Environment-sensitive fluorophores (ESF) can sense changes in the microenvironment (polarity, viscosity), secondary structures, or intramolecular interactions. The response reflects useful photophysical properties such as the shift in absorption or emission wavelengths (solvatochromism) along with the change in fluorescence lifetime, quantum yield, color, etc.<sup>10–12</sup> Moreover, chemically modified nucleosides have received increasing attention because of their importance as antiviral, antifungal, antitumor, antimicrobial, and anticancer drugs.<sup>13</sup> Based on their molecular structure and relations to the natural nucleobases, fluorescent nucleoside analogs are popularly categorized as isomorphous nucleosides, pteridines, size-expanded nucleosides, and extended nucleosides.<sup>14,15</sup> It involves the replacement of the purine or pyrimidine heterocycle or through covalent modification of the natural heterocyclic base or their analogs. Functionalization of the canonical nucleoside

scaffolds and their close derivative delivers a general approach to synthesizing base-modified nucleosides.<sup>16</sup> Different methods like click chemistry, Sonogashira coupling, Stille coupling, Suzuki-Miyaura coupling, and Heck coupling have been widely used to synthesize modified nucleosides.<sup>17</sup> However, most modifications include the benzenoid and heterocyclic aromatic scaffolds. In the repertoire of functional DNA synthesis, the non-benzenoid moiety-based nucleoside analogs are not well explored. Tropolone is a seven-membered non-benzenoid aromatic scaffold whose derivatives constitute troponoid natural products.<sup>18</sup> Tropolone has unique hydrogen bonding, photophysical properties, and metal chelating abilities, and therapeutic-utility.<sup>19,20</sup> In the literature, sulfone derivatives are bioactive molecules that serve as popular antibiotics and potential drug candidates for treating AIDS/HIV infection and Alzheimer's disease.<sup>21–23</sup> Various research groups have explored modified nucleosides containing sulfone/ sulfonamide.<sup>24–26</sup> Previously, we have also reported Alkylaminotroponyl sulfone (ATS) derivatives which exhibited remarkable anti-Quorum Sensing activity against *Pseudomonas aeruginosa* (Figure 3B.1-A).<sup>27</sup> Recently, we have reported different Troponyl deoxyuridine nucleoside analogs exhibiting polarity sensitive and pH dependent fluorescence, synthesized mainly by using Sonogashira cross coupling reactions (Figure 3B.1-B).<sup>28–30</sup> These results encouraged us to tailor modified nucleosides using troponyl sulfones. Herein, we have described the synthesis of two novel troponyl sulfone conjugated nucleosides. This chapter also covers photophysical and biochemical evaluations of ATS derivatives and the two modified nucleosides.

### 3B.2 Objective

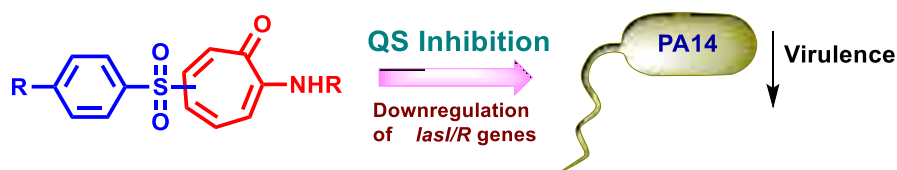
Fluorescent nucleoside analogs (FNAs) have emerged as powerful biochemical tools in investigating the structure and dynamics of nucleic acids and their interactions with various biomolecules. Recently, Tropolone comprising nucleosides and their DNA oligonucleotides, have been introduced by our group, which exhibit fluorescence



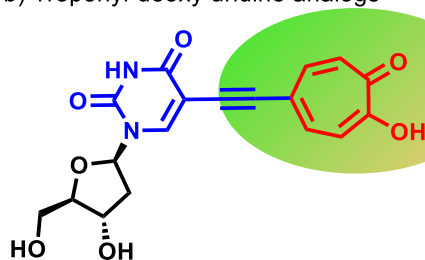
characteristics. Lately, we have reported various aminotroponyl sulfones (ATS), which show remarkable bioactivity as inhibitors of quorum sensing in pathogenic bacteria PA14 strain. In range of non benzenoid conjugated DNA analogs, the incorporation of aminotroponyl sulfonyl moiety into DNA was intended, to explore their photophysical properties and biological relevance.

### Previous Reports

a) Alkylaminotroponyl sulfone (ATS) derivatives as *Pseudomonas aeruginosa* QS inhibitor



b) Troponyl deoxy uridine analogs



c) This Report:

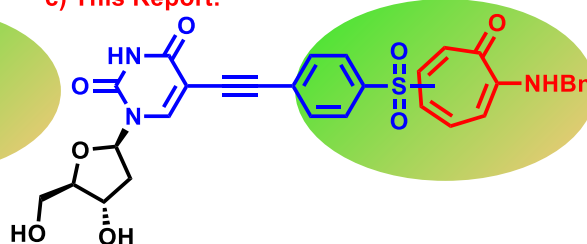
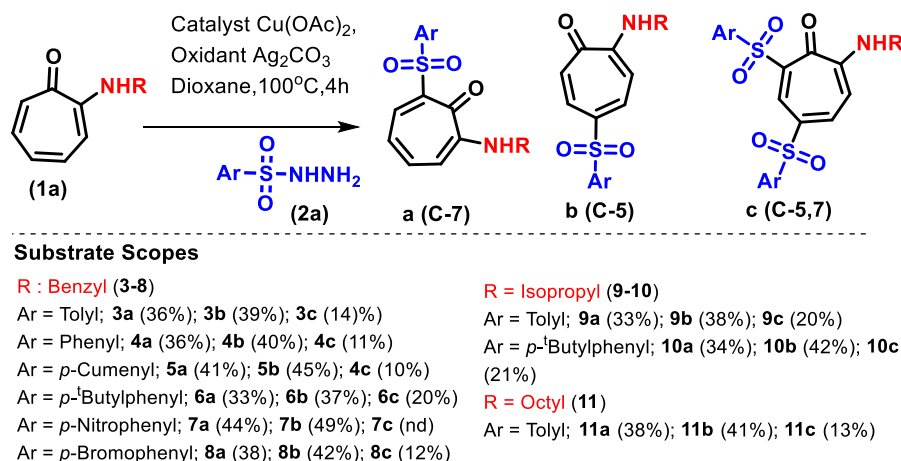


**Figure 3B.1.** (A) Alkylaminotroponyl sulfone (ATS) derivatives as *Pseudomonas aeruginosa* Quorum Sensing (QS) inhibitors, (B) Previously reported troponyl thymidine analogues, (C) This report- synthesis and biochemical evaluations of <sup>ATS</sup>dT analogs.

### 3B.3 Results and Discussion

The synthesis of alkylaminotroponyl sulfone (ATS) derivatives from the commercially available Tropolone molecule was previously reported by our group.<sup>27</sup> This was achieved by metal catalyzed C-H activation method using different aminotropones and sulfonyl hydrazides. Following the reported procedure, Tropolone was converted into N-alkylaminotropones derivatives (**1**).<sup>31</sup> In Scheme 3B.1, the aminotroponone (**1a**) was treated with *p*-tolylsulfonyl hydrazide (**2a**) in presence of the Cu-catalyst Cu(OAc)<sub>2</sub> (10 mol%) and an oxidant Ag<sub>2</sub>CO<sub>3</sub> at 100 °C in solvent dioxane. After completion of the reaction, we isolated

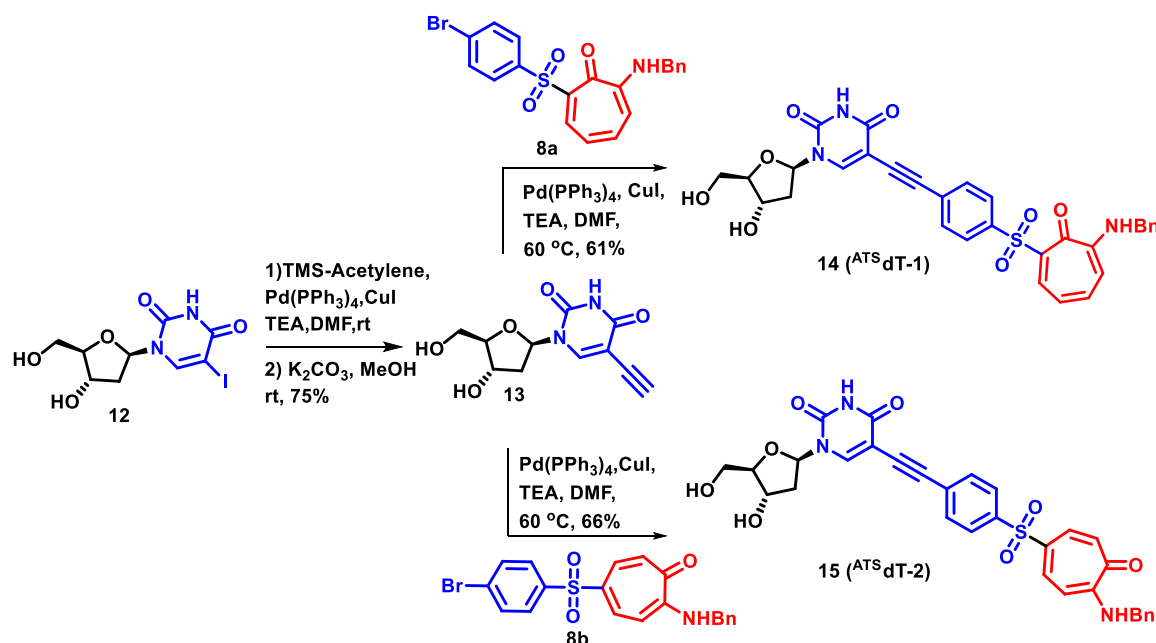
three types of ATS derivatives (**3a/3b/3c**) such as C-7 sulfonylated (**3a**), C-5 sulfonylated (**3b**) and C-5,7 disulfonylated (**3c**) with overall yield ca. 89%. We also synthesized other 23 ATS derivatives by performing a similar experiment with other alkylaminotropones (**1**) and arylsulfonyl hydrazides (**2**) that produced respective alkylaminotroponyl sulfones. All the experimental details are provided in Chapter 3A.<sup>27</sup>



**Scheme 3B.1.** Cu-catalyzed arylsulfonylation of *N*-benzylaminotroponone via C(sp<sup>2</sup>)-H activation.

Among the 26 ATS derivatives, two derivatives (**8a/8b**) contain a bromo group, allowing them to be used for further synthetic utility. Thus we envisioned the synthesis of modified nucleosides bearing troponyl sulfone unit by employing the Sonogashira cross-coupling reactions (Scheme 3B.2). We began the synthesis of the rationally designed ATS mediated nucleosides from commercially available 2'-deoxy-5-iodouridine (**12**). 2'-deoxy-5-iodouridine (**12**) was converted into 2'-deoxy-5-ethynyluridine (**13**) in two steps. The alkyne group of nucleoside **13** was individually coupled with Br-ATS (**8a** and **8b**) by the Sonogashira coupling using Pd(PPh<sub>3</sub>)<sub>4</sub> catalyst, and CuI as co-catalyst to get two different nucleosides <sup>ATS</sup>dT-1 (**14**) and <sup>ATS</sup>dT-2 (**15**) respectively. The products were obtained in good yield, 61% for compound **14** and 66% for compound **15**. The yield of **15** was slightly more

than that of **14**. All the compounds were characterized by  $^1\text{H}/^{13}\text{C}$  NMR, ESI-HRMS analyses (see Appendix).



**Scheme 3B.2.** Synthesis of troponyl sulfone conjugated nucleoside  $^{\text{ATS}}$ dT-1 (**14**) and  $^{\text{ATS}}$ dT-2 (**15**)

We conducted photophysical studies for the newly synthesized compounds  $^{\text{ATS}}$ dT-1(**14**) and  $^{\text{ATS}}$ dT-2(**15**) and obtained their quantum yields. Before investigating the properties of nucleosides, we studied the photophysical properties of ATS derivatives. We took compound **3a** as the model compound and studied its photophysical properties in various organic solvents, i.e., toluene, dichloromethane, dimethoxysulfoxide, acetonitrile, and methanol (Table 3B.1, Figure 3B.2). We observed that the solvent polarity had only a minor influence on the absorption properties. The analysis of absorption spectra of **3a** revealed absorptions at 348 nm and 433 nm in DMSO with very little solvatochromism (by 4-5 nm blue shift). Upon excitation we observed broad and solvent polarity dependent emissions. Emission intensity decreased when the polarity of the solvent increased to ACN/MeOH and experienced a 36 nm red shift in DMSO (503 nm) solvent from DCM (467 nm). It exhibited

lower quantum yields in relatively polar solvents (ACN, MeOH) than non-polar ones. In DMSO the quantum yield was highest (.013).

**Table 3B.1.** Summary table of photophysical properties of compound **3a** in different solvents.

solvent	$\lambda_{\text{abs}}(\text{nm})$	Abs	$\lambda_{\text{em}}(\text{nm})$	Stoke's shift (nm)	$\Phi$ (%)
Toluene	345, 429	0.18583	473	128	1.06
DCM	345, 428	0.18581	467	122	0.93
DMSO	348, 433	0.16255	503	155	1.34
ACN	344, 427	0.15707	478	134	0.54
MeOH	345, 428	0.17085	485	140	0.59

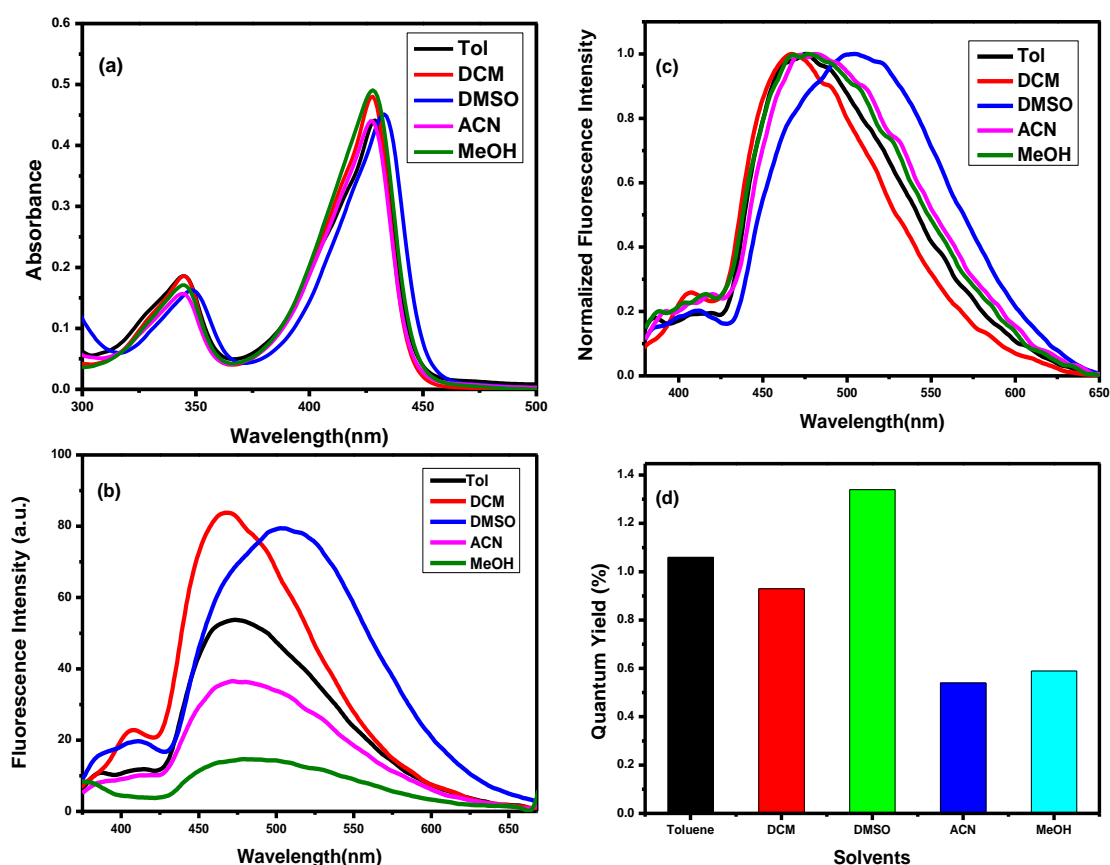


**Figure 3B.2.** (A) Absorption, (B) Emission, (C) Normalized emission spectra, (D) Quantum yield of compound **3a** in different solvents at  $10^{-5}$  M concentration.

We performed all photophysical studies in the DMSO solvent for all the rest of the ATS compounds. The details are provided in Table 3B.2. All C-5 sulfonylated, C-7 sulfonylated and C-5,7 disulfonylated derivatives possessed their own distinct absorption and emission spectra pattern. In Figure 3B.3-A, normalized UV-Vis and fluorescence spectra of compounds **3a**, **3b**, and **3c** are provided, which shows the differences. Compound **3a** has two absorption maxima, as discussed earlier, whereas compound **3b** has three ( $\lambda_{\text{abs}} = 360 \text{ nm}, 384 \text{ nm}, 407 \text{ nm}$ ) and **3c** has two ( $\lambda_{\text{abs}} = 361 \text{ nm}, 433 \text{ nm}$ ) with a shoulder peak near 433 nm. This spectral nature owes to multiple transitions, such as  $\pi-\pi^*$ ,  $n-\pi^*$ , and intramolecular charge transfer like their parent moiety topolone/aminotropone.<sup>32</sup> ATS derivatives were quite independent of various substituents present in *p*-position of benzene ring (except **7a-b**, due to the presence of the nitro group). UV-vis spectra of all C-7 derivatives (except **7a**) showed two absorption maxima ranging from 343 nm- 351 nm and 432 nm- 436 nm. Upon excitation at a lower wavelength absorption band, we observed broad emissions in the range of 485 nm- 510 nm. But in the case of C-5 derivatives (excluding **7b**), three peaks were present in absorption spectra around 360 nm, 385 nm and 407 nm. These compounds showed emission bands near around 460 nm upon excitation. All di-substituted sulfonyl compounds exhibited two absorption maxima around 361 nm and 433 nm along with a shoulder peak near 411 nm. For the nitro derivatives (**7a-b**) we couldn't get any emission band and quantum yield as nitro group is a common fluorescence quencher.<sup>33</sup> C-7 and C-5, 7 disulfonylated compounds had significantly higher quantum yield than that of C-5 derivatives, where the quantum yield values were either identical for C-7 and C-5, 7 sulfone derivatives or slightly higher for C-5,7 sulfones (Figure 3B.3-B). Among all compounds, **5c** was the most fluorescent one having 1.45 % quantum yield.

**Table 3B.2.** Summary table of photophysical properties of the compound **3<sub>a/b/c</sub>-11<sub>a/b/c</sub>** in DMSO.

Cpd S.N.	$\lambda_{\text{abs}}(\text{nm})$	Absorbance	$\lambda_{\text{em}}(\text{nm})$	Stoke's shift (nm)	$\Sigma_{\text{max}} (\text{M}^{-1}\text{cm}^{-1})$	$\Phi$ (%)
3a	348, 433	0.16255, 0.45123	503	155	45123	1.34
3b	360, 384, 407	0.46756, 0.44355, 0.39452	461	101	46756	0.61
3c	361, 433	0.2382, 0.38605	501	140	38605	1.39
4a	349, 433	0.17982, 0.54823	506	157	54823	0.86
4b	360, 386, 407	0.3987, 0.38466, 0.37004	461	101	39870	0.49
4c	361, 432	0.13169, 0.21733	502	141	21733	1.25
5a	348, 433	0.13585, 0.37647	492	144	37647	1.2
5b	360, 386, 407	0.48777, 0.4646, 0.41302	460	100	48777	0.52
5c	361, 433	0.16389, 0.24183	491	130	24183	1.45
6a	349, 433	0.08457, 0.27525	504	155	27525	0.99
6b	360, 384, 407	0.37198, 0.3434, 0.32057	464	104	37198	0.79
6c	361, 411, 433	0.24486, 0.21428, 0.21389	483	122	24486	1.06
7a	343, 436	0.13404, 0.40918	xxx	xxx	40918	xxx
7b	398, 408	0.60987, 0.59064	xxx	xxx	59064	xxx
8a	349, 434	0.1665, 0.51099	510	148	51099	1.19
8b	362, 387, 407	0.44835, 0.45631, 0.41229	458	96	45631	0.74
8c	361, 433	0.15007, 0.24759	478	117	24759	1.29
9a	350, 432	0.15544, 0.43389	512	162	43389	0.62
9b	361, 383, 407	0.4689, 0.45494, 0.35519	468	107	46890	0.53
9c	363, 431	0.24805, 0.37976	508	145	37976	1.03
10a	351, 432	0.10777, 0.23539	485	134	23539	1.15
10b	361, 383, 407	0.44984, 0.44287, 0.34504	467	106	44984	0.82
10c	363, 431	0.3234, 0.4909	508	145	49090	1.11
11a	351, 434	0.12573, 0.31185	504	153	31185	1.09
11b	362, 385, 408	0.55052, 0.54891, 0.43413	472	110	55052	0.79
11c	363, 432	0.24854, 0.37323	498	135	37323	1.06

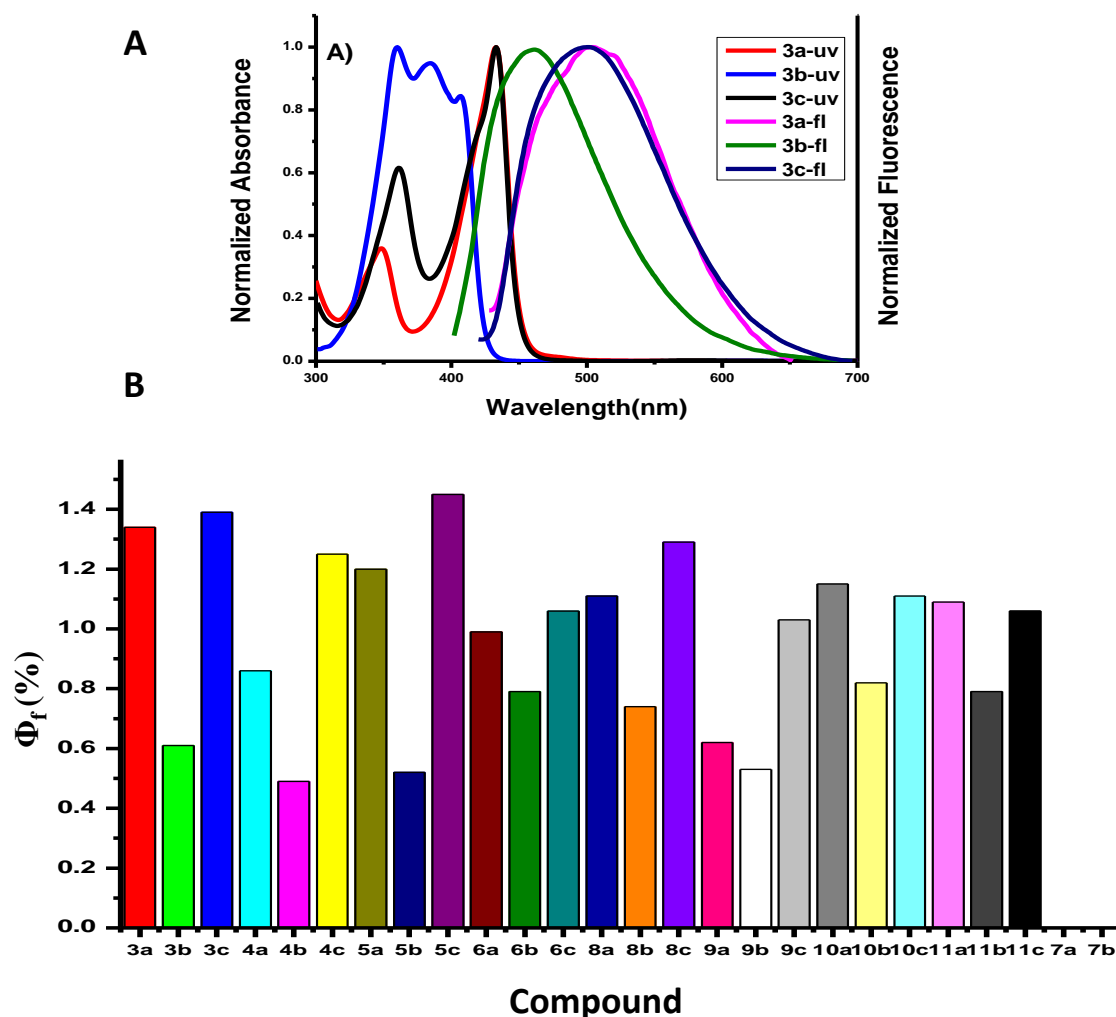


**Figure 3B.3.** (A) Normalized absorptions and emissions of compound **3a**, **3b** and **3c** in DMSO solvent, (B) Quantum yield of all ATS derivatives (**3a/b/c-11a/b/c**) in DMSO solvent

The spectroscopic and photophysical properties of both the modified nucleosides <sup>ATS</sup>dT-1 (**14**) and <sup>ATS</sup>dT-2 (**15**) were measured in different solvents of varying polarity. Both nucleosides exhibited different spectral properties (Table 3B.3, Figure 3B.4). <sup>ATS</sup>dT-1 (**14**) showed two absorption maxima around 330 nm and 430 nm in all solvents along with a 5 nm red shift in DMSO solvent and emitted in the range of 473–506 nm depending on solvent polarity. The normalized emission spectra of nucleoside (**14**) were generated, which shows the characteristic red shift by increasing the polarity of solvents (Figure 3B.4-C). The maximum difference in the emission wavelength ( $\Delta\lambda_{em}$ ) is ~33 nm ( $\lambda_{em}^{MeOH} - \lambda_{em}^{DCM}$ ).

For comparative studies, we plotted bar diagram of quantum yields vs solvents (Figure 3B.4-D). This indicates that the quantum yield of <sup>ATS</sup>dT-1 (**14**) is relatively high in non-polar solvents (1.56 % in DCM, 1.67% in DMSO) than in polar solvents (0.63% in methanol). In case of <sup>ATS</sup>dT-2 (**15**), we observed multiple absorption peaks, unlike <sup>ATS</sup>dT-1 (**14**) (Figure 3B.4-E). For instance, in DMSO solvent absorption maxima occur at 332 nm, 365 nm along with two shoulder peaks around 390 nm and 406 nm. The normalized emission spectra of nucleoside **15** depicted red-shift with increasing polarity of solvents (Figure 3B.4-G). The maximum difference in the emission wavelength ( $\Delta\lambda_{em}$ ) is ~20 nm ( $\lambda_{em}^{MeOH} - \lambda_{em}^{DCM}$ ). The bar diagram of quantum yields vs. solvents (Figure 3B.4-H) for <sup>ATS</sup>dT-2 (**15**) indicates that quantum yield of **15** is relatively high in non-polar solvents (0.71% in toluene, 0.65 % in DMSO) than polar solvents (0.36% in methanol). Therefore both the nucleosides are environmentally sensitive fluorescent (ESF) nucleosides where the Quantum yield of nucleoside <sup>ATS</sup>dT-1 (**14**) is nearly two fold higher than that of <sup>ATS</sup>dT-2 (**15**).

**Table 3B.3.** Summary table of photophysical properties of the compound <sup>ATS</sup>dT-1(**14**) and <sup>ATS</sup>dT-2 (**15**) in different solvents

Cpd	Solvent	$\lambda_{abs}(nm)$	Absorbance	$\lambda_{em}(nm)$	Stokes shift (nm)	$\Phi$ (%)
14	Toluene	330, 360	0.28888, 0.31963	442	82	0.71
	DCM	327, 358	0.31046, 0.35144	432	74	0.61
	DMSO	332, 365	0.30222, 0.33656	452	87	0.65
	ACN	325, 359	0.31763, 0.34633	440	81	0.57
	MeOH	325, 359	0.32881, 0.35044	452	93	0.36
15	Toluene	330, 430	0.02459, 0.17843	474	44	1.17
	DCM	325, 430	0.26807, 0.21381	473	43	1.56
	DMSO	330, 435	0.43842, 0.38264	506	71	1.67
	ACN	330, 430	0.41213, 0.33866	488	58	0.72
	MeOH	325, 430	0.34591, 0.26368	506	76	0.63



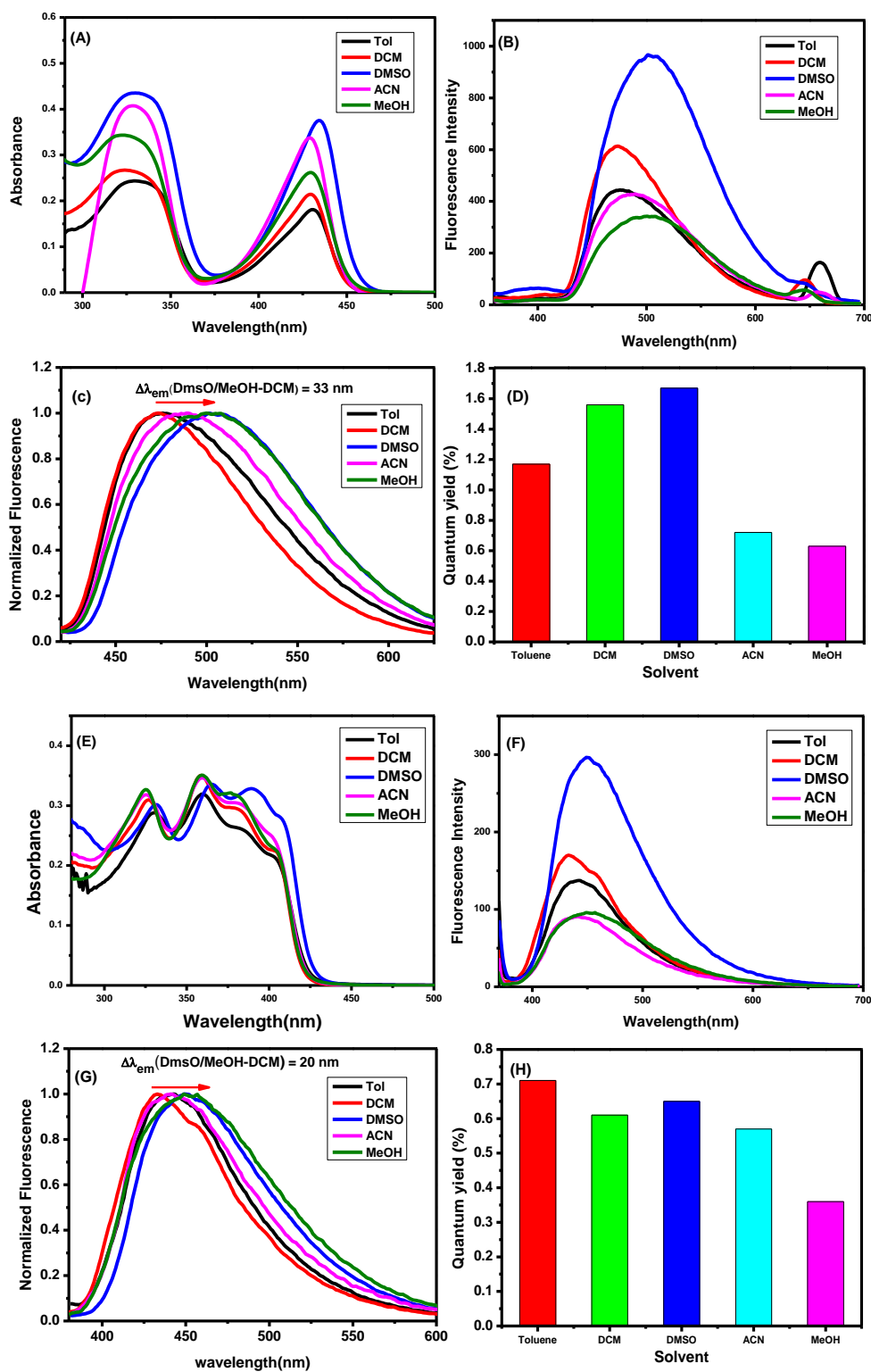


**Figure 3B.4.** Absorption (A), Emission spectra (B, C) and Quantum yield (D) of  $^{ATS}dT-1$  (14); Absorption (E), Emission spectra (F, G) and Quantum yield (H) of  $^{ATS}dT-2$  (15) in different solvents.

To examine fluorophoric behavior of <sup>ATS</sup>dT-1 (**14**) and <sup>ATS</sup>dT-2 (**15**), we performed their DFT calculation in gas phase and extracted their HOMO and LUMO diagrams (Figure 3B.5). (opt freq b3lyp/6-31g geom = connectivity). Geometrically optimized structure of <sup>ATS</sup>dT-1 (**14**) shows that sulfonyl-phenyl-thymine residues are almost in the same plane while benzyl-troponyl ring is nearly perpendicular to sulfonyl-phenyl-thymine ring system. The HOMO-LUMO of <sup>ATS</sup>dT-1 (**14**) shows that Troponyl residue has a major contribution in the HOMO while thymine-phenyl-sulfonyl-troponyl residues are involved in LUMO. The energy difference of their HOMO-LUMO is 3.3eV. The optimized structure of <sup>ATS</sup>dT-2 (**15**) shows that benzyl-troponyl is non-planar with sulfonyl-phenyl-thymine ring over troponyl ring which perpendicular almost to <sup>ATS</sup>dT-2 (**15**). However, the benzyl unit is nearly perpendicular to the troponyl ring in compound **15**. Thymine-phenyl-sulfonyl-troponyl residues are contributed in HOMO and LUMO in <sup>ATS</sup>dT-2 (**15**) with almost the same energy differences, contrastingly to <sup>ATS</sup>dT-1 (**14**). In both cases, troponyl molecular orbitals are involved HOMO-LUMO and made significant contributions to be fluorescent.

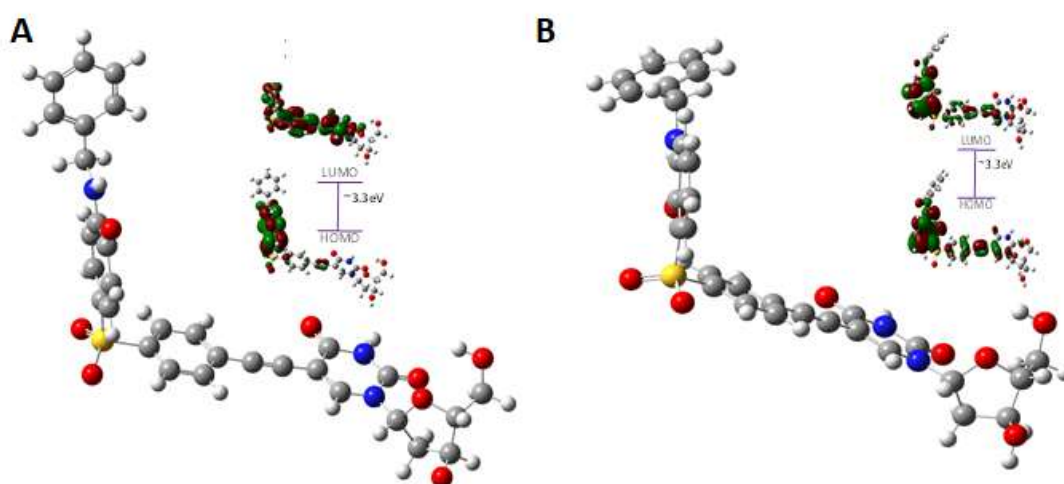


**Figure 3B.5.** Geometrically optimized structure HOMO-LUMO diagrams and their energy differences using DFT calculation: (A) <sup>ATS</sup>dT-1 (**14**) and (B) <sup>ATS</sup>dT-1 (**15**).

The cytotoxicity activities of nucleosides <sup>ATS</sup>dT-1 (**14**) and <sup>ATS</sup>dT-2 (**15**) were studied against HEK293T (Human embryonic kidney) and HeLa (human cervical carcinoma) cell lines using MTS assay. The cytotoxicity activity assay was required to assess the utility of the modified nucleosides (**14/ 15**) as probes in confocal microscopy imaging studies. The MTS assay results are provided in Figure 3B.6. We couldn't find any significant cytotoxicity with <sup>ATS</sup>dT-1 (**14**) and <sup>ATS</sup>dT-2 (**15**) in both cell lines. The cytotoxicity activity of troponyl sulfones was studied previously, where compound **5c** also didn't show any noticeable effect. Thus, it was concluded that **5c** and both nucleosides (**14/ 15**) are suitable for imaging studies.

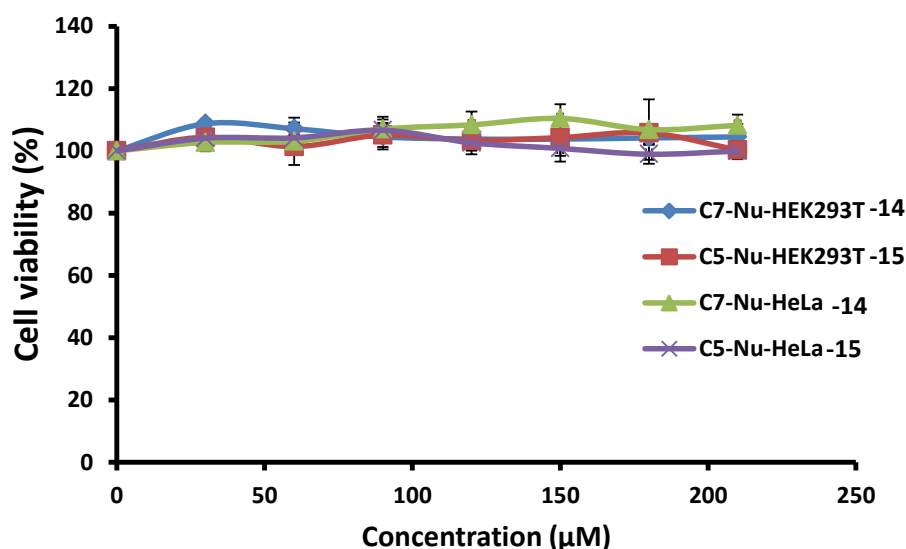


**Figure 3B.6.** Cell proliferation assays of <sup>ATS</sup>dT-1 (**14**) and <sup>ATS</sup>dT-1 (**15**).

Compound **5c** was examined as a luminescent probe for confocal microscopy imaging in HeLa cells. The cells were incubated in media containing 100 μM of a given compound for 12 and 24 h following the standard protocol and studied by confocal microscopy. HeLa cells were visualized under bright light and different channels such as FITC (green channel,  $\lambda_{\text{ex}}$  490 nm) and TRITC (red channel,  $\lambda_{\text{ex}}$  570 nm). The staining pattern demonstrates diffusion of the compound over all the cytoplasm and membrane. The membranous localization was verified by a co-staining experiment with a lipid staining dye (BODIPY 493/503) (Figure

3B.7-A-F). The colocalization of the given compound was quantified in HeLa cells using Pearson's coefficients ( $r$ ). Pearson's coefficient ( $r$ ) values were estimated by using JACoP plugin in Fiji: Image.<sup>34</sup> The calculated ' $r$ ' value for compound **5c** was found to be 0.98, which suggests the significant co-existence of BODIPY dye and the compound in the cytoplasm/membrane area. The cellular staining pattern was the same when the incubation time was 24 h.

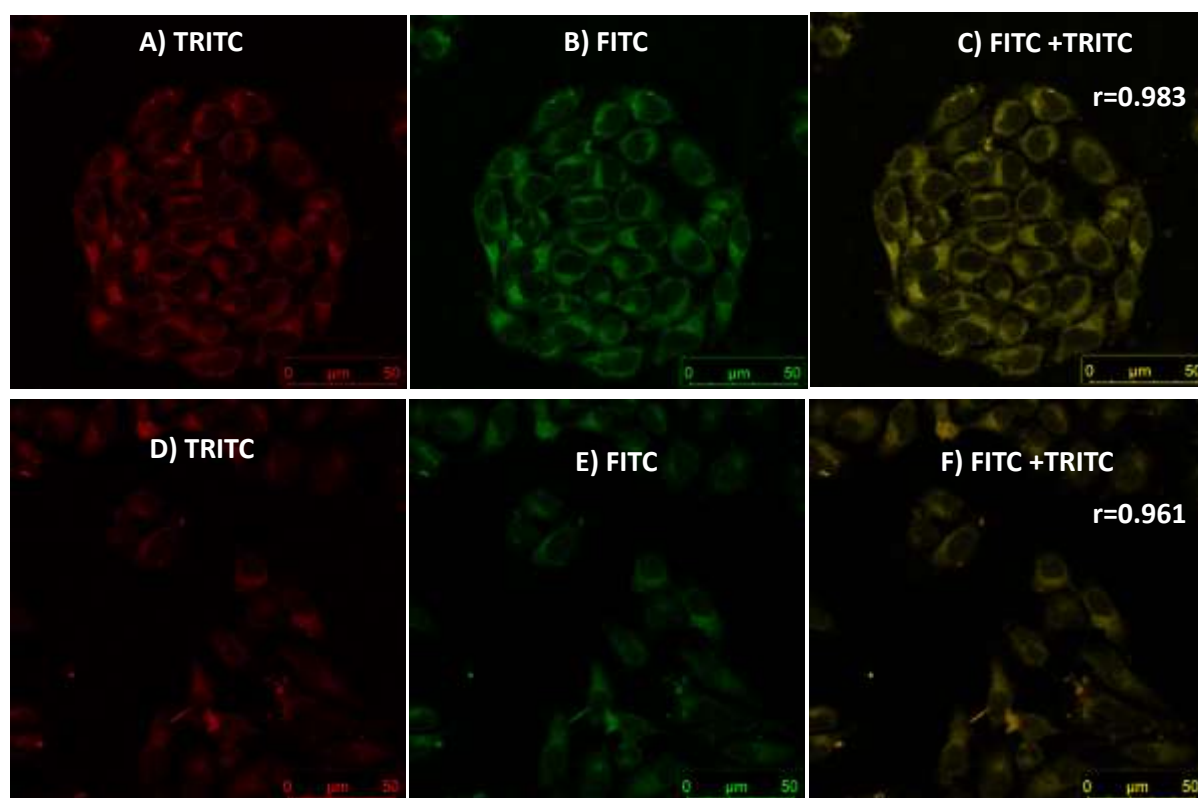


**Figure 3B.7.** Confocal microscopic images of HeLa cells incubated with compound **5c** (A-C, 12 h incubation time; D-F, 24 h incubation time) along with BODIPY dye staining.

As probes and sensors, fluorescent nucleoside analogs have been employed to monitor intracellular processes, including RNA and DNA replication and transcription.<sup>35–37</sup> Additionally, nucleoside probes have been created that can assess specific enzyme reactions and endogenous genetic circuits in live cells. Recently, a nucleoside-based, environment-sensitive fluorescence-lifetime sensor for DNA interactions was introduced.<sup>38–40</sup> Fluorescent

nucleoside analogs exhibit improved cell permeability and are applied for labeling biomolecules in vitro/Vivo conditions. Herein we examined the cell permeability of fluorescent nucleoside analogs <sup>ATS</sup>dT-1 (**14**) and <sup>ATS</sup>dT-2 (**15**) into HeLa cell lines. These were incubated with HeLa cells following the standard protocol as compound **5c** and studied by confocal microscopy. HeLa cells were visualized under bright light and different channels such as DAPI (blue channel,  $\lambda_{ex}$  358 nm), FITC and TRITC. The cells, treated with nucleosides and stained with DAPI, were visualized, where <sup>ATS</sup>dT-1 (**14**) (Figure 3B.8-A-F) and <sup>ATS</sup>dT-2 (**15**) (Figure 3B.8-G-L) are majorly found to be located in the nucleus. In Figure 3B.8-A/G, DAPI-stained and nucleoside-treated cells clearly show the localization of DAPI at the cellular nucleus. Under FITC (green) channel, confocal images of **14/ 15** treated cells show cell-internalization without transfecting reagents. Similar observations were noticed under TRITC (red) channel. The colocalization studies of both the nucleosides with DAPI were performed in both channels (green/red). For red and green channel, Pearson's coefficient values (r) are 0.96 and 0.97, respectively, for <sup>ATS</sup>dT-1 (**14**). In the case of <sup>ATS</sup>dT-2 (**15**), Pearson's coefficient values (r) are 0.95 and 0.91 for red and green channels, respectively. These results strongly support the localization of nucleosides (**14/ 15**) nucleoside in nucleus of HeLa cells. The results were same for both 12h (Figure 3B.8) and 24 h (Figure 3B.9) incubation time. To sum up, confocal microscopy imaging studies revealed that:

- (a) Staining patterns of ATS derivative (**5c**) and sulfone nucleosides (**14** and **15**) are different.
- (b) ATS derivative **5c** preferably localize in cytoplasm/ membrane, whereas nucleosides localize over cellular nucleus.
- (c) Compounds (**5c**, **14** and **15**) are not cytotoxic against HeLa cells.

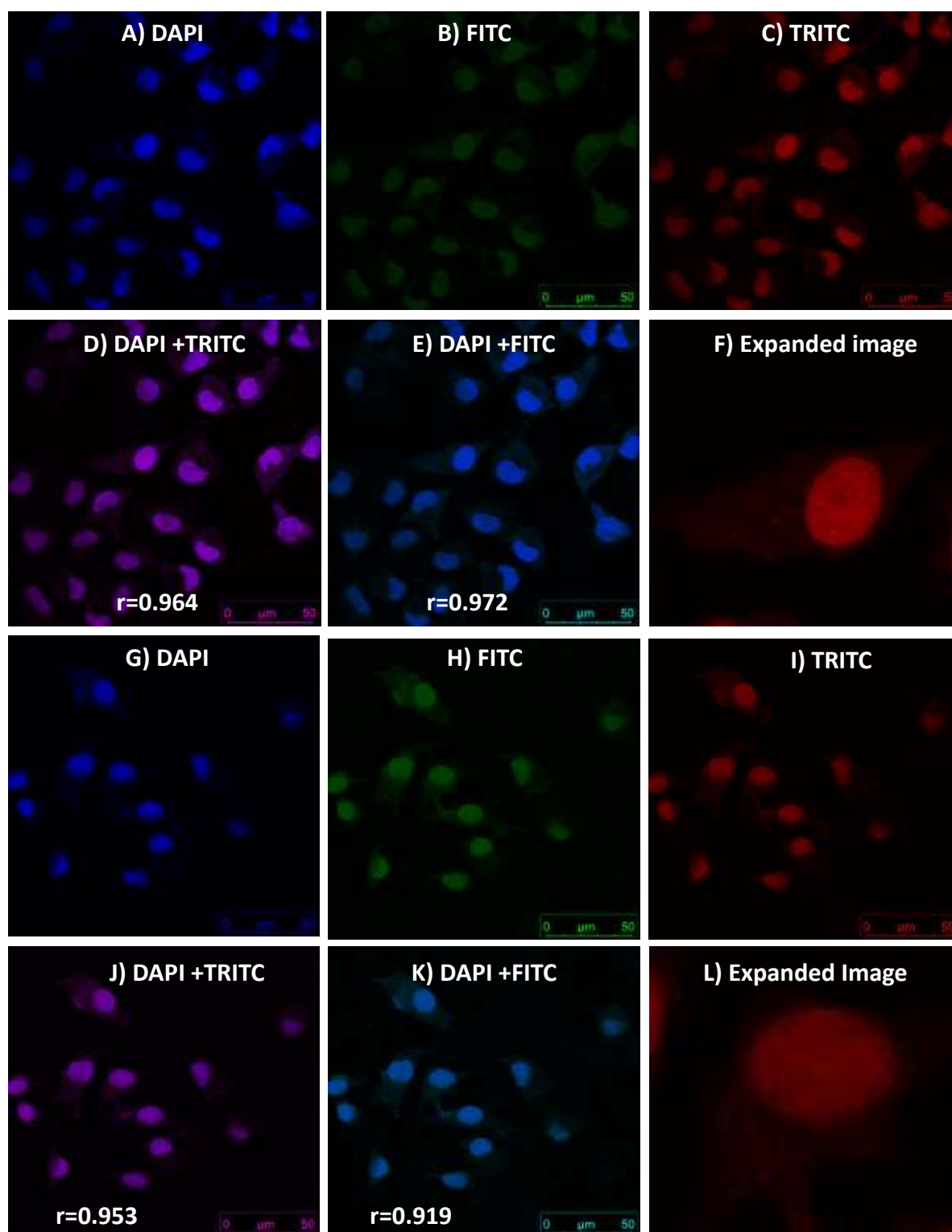


**Figure 3B.8.** Confocal microscopic images of HeLa cells incubated with <sup>ATS</sup>dT-1 (**14**) (A-F) and <sup>ATS</sup>dT-2 (**15**) (G-L) along with DAPI staining for colocalization (12 h incubation time).

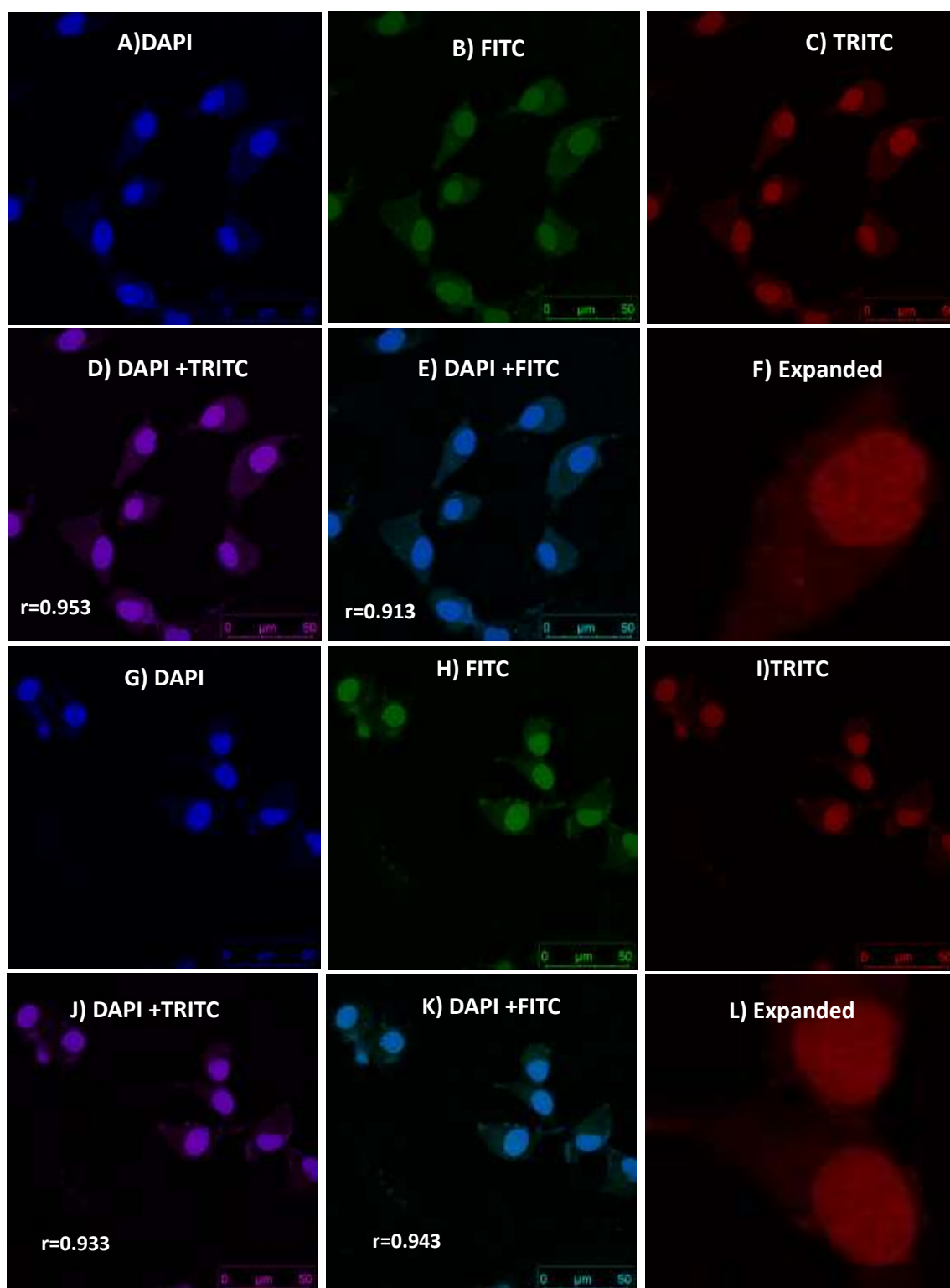


**Figure 3B.9.** Confocal microscopic images of HeLa cells incubated with <sup>ATS</sup>dT-1 (**14**) (A-F) and <sup>ATS</sup>dT-2 (**15**) (G-L) along with DAPI staining for colocalization (24 h incubation time).

### 3B.4 Conclusion

In summary, we have incorporated troponyl sulfone moiety in nucleosides and synthesized two modified thymidine analogs <sup>ATS</sup>dT-1 (**14**) and <sup>ATS</sup>dT-2 (**15**), where sulfone units were attached to C-7 and C-5 positions of troponone ring, respectively. Their photophysical studies were performed along with the previously reported ATS derivatives. Compound **5c** had the highest quantum yield of 1.45% among the twenty-six ATS derivatives. Both the nucleosides showed solvatochromism and the quantum yield of compound **14** was two-fold higher than compound **15**. Fluorescence behaviours of the nucleosides almost resemble with their parent moiety, i.e., sulfone units. These nucleosides showed no significant cytotoxicity toward HEK293T or HeLa cell lines. Therefore, we used them as fluorescent probes in the imaging of HeLa cells with confocal microscopy. Compound **5c** and troponyl sulfone conjugated nucleosides (**14/ 15**) exhibited different cellular staining patterns. The former was localized in the cytoplasm and membrane region, whereas the nucleosides were localized inside the cellular nucleus. These molecules possess Aminotroponone unit, which is an excellent metal chelating unit. So, it could be beneficial for designing metal-ion-based probes for finding target-specific biochemical activity and therapeutic applications. Hence, both nucleosides are promising fluorescent nucleoside analogs and can be explored further for their biochemical applications.

### 3B.5 Experimental section

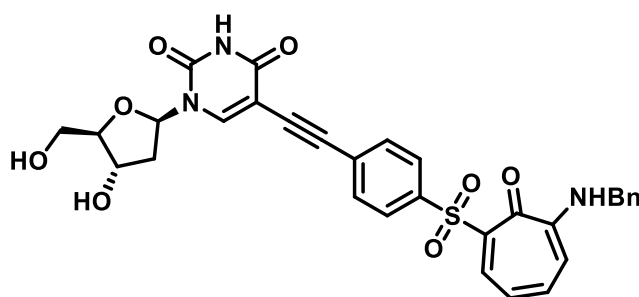
*General information:* All the materials were purchased from commercial suppliers and were used as received. DMF and DCM were distilled over CaH<sub>2</sub> and stored over 4Å molecular sieves. Reactions were monitored by thin layer chromatography, visualized by UV and Ninhydrin. Column chromatography was performed in 230-400 mesh silica. Mass spectra (HRMS) were obtained from Bruker microTOF-Q II Spectrometer and the samples were



prepared in methanol and injected in methanol and water mixture. NMR spectra were recorded on Bruker 400 MHz and Bruker 700 MHz NMR spectrometer at room temperature and processed using Mnova software from Mestrelab Research. Absorption spectra were obtained using Jasco V-730 spectrometer and Fluorescence spectra were obtained from Agilent spectrophotometer and Perkin-Elmer LS-55 using Xenon lamp. Confocal Images were taken in Leica Microscope.

#### *Characterization data of products*

5-((4-((6-(benzylamino)-7-oxocyclohepta-1,3,5-trien-1-yl)sulfonyl)phenyl)ethynyl)-1-((2R,4S,5R)-4-hydroxy-5-(hydroxymethyl)tetrahydrofuran-2-yl)pyrimidine-2,4(1H,3H)-dione (**14**): To 5-ethynyl-2'-deoxy Uridine (**13**) (0.05 g, 0.198 mmol) dissolved in dry DMF



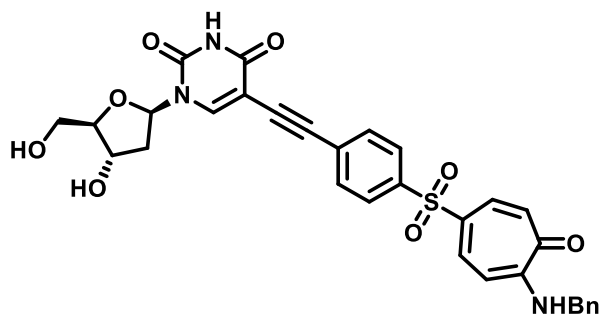
(5 ml), compound **8a** (0.102 g, 0.238 mmol), Tetrakis (triphenylphosphine) palladium (0.023 g, 0.019 mmol), copper (I) iodide (0.007 g, 0.04 mmol) and triethylamine (0.110 ml, 0.793 mmol)

were added and stirred under argon atmosphere over night at temp 60 °C. After reaction completion, the solvents were evaporated under reduced pressure and the reaction mixture passed through silica column using methanol and dichloromethane as eluent obtain x mg of yellow solid in 61 % yield. <sup>1</sup>H NMR (700 MHz, DMSO) δ 11.77 (s, 1H), 9.31 (t, J = 6.2 Hz, 1H), 8.47 (s, 1H), 8.36 (d, J = 10.1 Hz, 1H), 7.93 (d, J = 8.0 Hz, 2H), 7.63 (d, J = 8.0 Hz, 2H), 7.53 (t, J = 10.1 Hz, 1H), 7.35 – 7.23 (m, 5H), 6.85 (t, J = 9.8 Hz, 1H), 6.78 (d, J = 10.8 Hz, 1H), 6.13 (t, J = 6.2 Hz, 1H), 5.29 (s, 1H), 5.20 (s, 1H), 4.64 (d, J = 6.3 Hz, 2H), 4.26 (s, 1H), 3.82 (d, J = 2.5 Hz, 1H), 3.69 – 3.64 (m, 1H), 3.62 – 3.58 (m, 1H), 2.20 – 2.15 (m, 2H). <sup>13</sup>C NMR (176 MHz, DMSO) δ 170.00, 161.78, 158.66, 149.85, 145.30, 143.25, 141.39, 137.01, 134.32, 131.49, 129.12, 128.88, 127.84, 127.59, 127.18, 118.78, 110.28, 97.94, 91.18, 88.07,

86.39, 85.45, 70.24, 61.17, 46.20, 46.13, HRMS ESI-Tof Calcd for  $C_{13}H_{27}O_8N_3S$ :  $[M+Na]^+$  624.1411, Found 624.1391.

5-(((4-((4-(benzylamino)-5-oxocyclohepta-1,3,6-trien-1-yl)sulfonyl)phenyl)ethynyl)-1-((2R,4S,5R)-4-hydroxy-5-(hydroxymethyl)tetrahydrofuran-2-yl)pyrimidine-2,4(1H,3H)-

dione (**15**): To 5-ethynyl-2'-deoxy Uridine (**13**) (0.05 g, 0.198 mmol) dissolved in dry DMF



(5 ml), compound **8b** (0.102 g, 0.238 mmol), Tetrakis (triphenylphosphine) palladium (0.023 g, 0.019 mmol), copper (I) iodide (0.007 g, 0.04 mmol) and triethylamine (0.110 ml, 0.793 mmol) were

added and stirred under argon atmosphere over night at temp 60 °C. After reaction completion, the solvents were evaporated under reduced pressure and the reaction mixture passed through silica column using methanol and dichloromethane as eluent obtain x mg of pale yellow solid in 66 % yield.  $^1H$  NMR (700 MHz, DMSO)  $\delta$  11.76 (s, 1H), 9.36 (t,  $J$  = 6.6 Hz, 1H), 8.47 (s, 1H), 7.92 (dd,  $J$  = 11.2, 1.6 Hz, 1H), 7.88 (d,  $J$  = 8.4 Hz, 2H), 7.77 (dd,  $J$  = 12.2, 1.9 Hz, 1H), 7.64 (d,  $J$  = 8.3 Hz, 2H), 7.36 – 7.31 (m, 4H), 7.27 (t,  $J$  = 6.9 Hz, 1H), 6.95 (d,  $J$  = 12.3 Hz, 1H), 6.73 (d,  $J$  = 11.4 Hz, 1H), 6.11 (t,  $J$  = 6.4 Hz, 1H), 5.28 (s, 1H), 5.19 (s, 1H), 4.69 (d,  $J$  = 6.6 Hz, 2H), 4.26 (d,  $J$  = 3.2 Hz, 1H), 3.83 – 3.79 (m, 1H), 3.66 (d,  $J$  = 10.2 Hz, 1H), 3.59 (d,  $J$  = 9.7 Hz, 1H), 2.19 – 2.15 (m, 2H).  $^{13}C$  NMR (176 MHz, DMSO)  $\delta$  176.29, 161.73, 157.99, 149.83, 145.47, 141.59, 137.42, 136.99, 133.93, 132.53, 130.43, 129.15, 127.89, 127.81, 127.71, 127.64, 126.20, 106.60, 97.80, 90.92, 88.07, 86.96, 85.47, 70.21, 61.15, 46.20, 46.15. HRMS ESI-Tof Calcd for  $C_{13}H_{27}O_8N_3S$ :  $[M+Na]^+$  624.1411, Found 624.1453.

*Cell proliferation assay and imaging studies:* For the detailed procedure, follow Chapter 2 (A/B).

*Photophysical studies:* For the detailed procedure, follow Chapter 2B.

#### 4B.6 References and Notes

- (1) Liu, H.; Wang, Y.; Zhou, X. Labeling and Sequencing Nucleic Acid Modifications Using Bio-Orthogonal Tools. *RSC Chem. Biol.* **2022**, 3 (8), 994–1007.
- (2) Dahm, R. Discovering DNA: Friedrich Miescher and the Early Years of Nucleic Acid Research. *Hum. Genet.* **2008**, 122, 565–581.
- (3) Jaenisch, R.; Bird, A.; Epigenetic Regulation of Gene Expression: How the Genome Integrates Intrinsic and Environmental Signals,. *Nat. Genet.* **2003**, 33 (3), 245–254.
- (4) Chakraborty, A.; Ravi, S. P.; Shamiya, Y.; Cui, C.; Paul, A. Harnessing the Physicochemical Properties of DNA as a Multifunctional Biomaterial for Biomedical and Other Applications. *Chem. Soc. Rev.* **2021**, 50 (13), 7779–7819.
- (5) Benson, S.; De Moliner, F.; Tipping, W.; Vendrell, M. Miniaturized Chemical Tags for Optical Imaging. *Angew. Chemie Int. Ed.* **2022**, 61 (34), e202204788.
- (6) Xu, W.; Chan, K. M.; Kool, E. T. Fluorescent Nucleobases as Tools for Studying DNA and RNA. *Nat. Chem.* **2017**, 9 (11), 1043–1055.
- (7) Sinkeldam, R. W.; Greco, N. J.; Tor, Y. Fluorescent Analogs of Biomolecular Building Blocks: Design, Properties, and Applications. *Chem. Rev.* **2010**, 110 (5), 2579–2619.
- (8) Stendevad, J.; Hornum, M.; Wüstner, D.; Kongsted, J. Photophysical Investigation of Two Emissive Nucleosides Exhibiting Gigantic Stokes Shifts. *Photochem. Photobiol. Sci.* **2019**, 18, 1858–1865.
- (9) Seio, K.; Kanamori, T.; Masaki, Y. Solvent-and Environment-Dependent Fluorescence of Modified Nucleobases. *Tetrahedron Lett.* **2018**, 59 (21), 1977–1985.

- (10) Güixens-Gallardo, P.; Hocek, M. Acetophenyl-thienyl-aniline-linked Nucleotide for Construction of Solvatochromic Fluorescence Light-up DNA Probes Sensing Protein-DNA Interactions. *Chem. Eur. J.* **2021**, *27* (24), 7090–7093.
- (11) Karimi, A.; Börner, R.; Mata, G.; Luedtke, N. W. A Highly Fluorescent Nucleobase Molecular Rotor. *J. Am. Chem. Soc.* **2020**, *142* (34), 14422–14426.
- (12) Ghosh, P.; Kropp, H. M.; Betz, K.; Ludmann, S.; Diederichs, K.; Marx, A.; Srivatsan, S. G. Microenvironment-Sensitive Fluorescent Nucleotide Probes from Benzofuran, Benzothiophene, and Selenophene as Substrates for DNA Polymerases. *J. Am. Chem. Soc.* **2022**, *144* (23), 10556–10569.
- (13) Skiba, J.; Kowalczyk, A.; Fik, M. A.; Gapinska, M.; Trzybinski, D.; Woźniak, K.; Vrček, V.; Czerwieniec, R.; Kowalski, K. Luminescent Pyrenyl-GNA Nucleosides: Synthesis, Photophysics and Confocal Microscopy Studies in Cancer HeLa Cells. *Photochem. Photobiol. Sci.* **2019**, *18* (10), 2449–2460.
- (14) Saito, Y.; Hudson, R. H. E. Base-Modified Fluorescent Purine Nucleosides and Nucleotides for Use in Oligonucleotide Probes. *J. Photochem. Photobiol. C Photochem. Rev.* **2018**, *36*, 48–73.
- (15) Dziuba, D.; Didier, P.; Ciaco, S.; Barth, A.; Seidel, C. A. M.; Mély, Y. Fundamental Photophysics of Isomorphic and Expanded Fluorescent Nucleoside Analogues. *Chem. Soc. Rev.* **2021**, *50* (12), 7062–7107.
- (16) Shaughnessy, K. H. Palladium-Catalyzed Modification of Unprotected Nucleosides, Nucleotides, and Oligonucleotides. *Molecules* **2015**, *20* (5), 9419–9454.
- (17) Kapdi, A. R.; Maiti, D.; Sanghvi, Y. S. *Palladium-Catalyzed Modification of Nucleosides, Nucleotides and Oligonucleotides*; Elsevier, 2018.

- (18) Guo, H.; Roman, D.; Beemelmans, C. Tropolone Natural Products. *Nat. Prod. Rep.* **2019**, *36* (8), 1137–1155.
- (19) Muetterties, E. L.; Roesky, H.; Wright, C. M. Chelate Chemistry. V. Metal Chelates Based on Tropolone and Its Derivatives. *J. Am. Chem. Soc.* **1966**, *88* (21), 4856–4861.
- (20) Ononye, S. N.; VanHeyst, M. D.; Oblak, E. Z.; Zhou, W.; Ammar, M.; Anderson, A. C.; Wright, D. L. Tropolones as Lead-like Natural Products: The Development of Potent and Selective Histone Deacetylase Inhibitors. *ACS Med. Chem. Lett.* **2013**, *4* (8), 757–761.
- (21) Qiao, H.; Sun, S.; Yang, F.; Zhu, Y.; Zhu, W.; Dong, Y.; Wu, Y.; Kong, X.; Jiang, L.; Wu, Y. Copper (I)-Catalyzed Sulfonylation of 8-Aminoquinoline Amides with Sulfonyl Chlorides in Air. *Org. Lett.* **2015**, *17* (24), 6086–6089.
- (22) Liang, H.-W.; Jiang, K.; Ding, W.; Yuan, Y.; Shuai, L.; Chen, Y.-C.; Wei, Y. Selective Remote C–H Sulfonylation of Aminoquinolines with Arylsulfonyl Chlorides via Copper Catalysis. *Chem. Commun.* **2015**, *51* (95), 16928–16931.
- (23) Chen, G.; Zhang, X.; Zeng, Z.; Peng, W.; Liang, Q.; Liu, J. Copper-Catalyzed Remote C–H Sulfonylation of 8-Aminoquinoline Amides with Arylsulfonyl Hydrazides. *ChemistrySelect* **2017**, *2* (5), 1979–1982.
- (24) Chrominski, M.; Ziemkiewicz, K.; Kowalska, J.; Jemielity, J. Introducing SuFNucs: Sulfamoyl-Fluoride-Functionalized Nucleosides That Undergo Sulfur Fluoride Exchange Reaction. *Org. Lett.* **2022**, *24* (27), 4977–4981.
- (25) Dadová, J.; Orság, P.; Pohl, R.; Brázdová, M.; Fojta, M.; Hocek, M. Vinylsulfonamide and Acrylamide Modification of DNA for Cross-linking with Proteins. *Angew. Chemie* **2013**, *125* (40), 10709–10712.

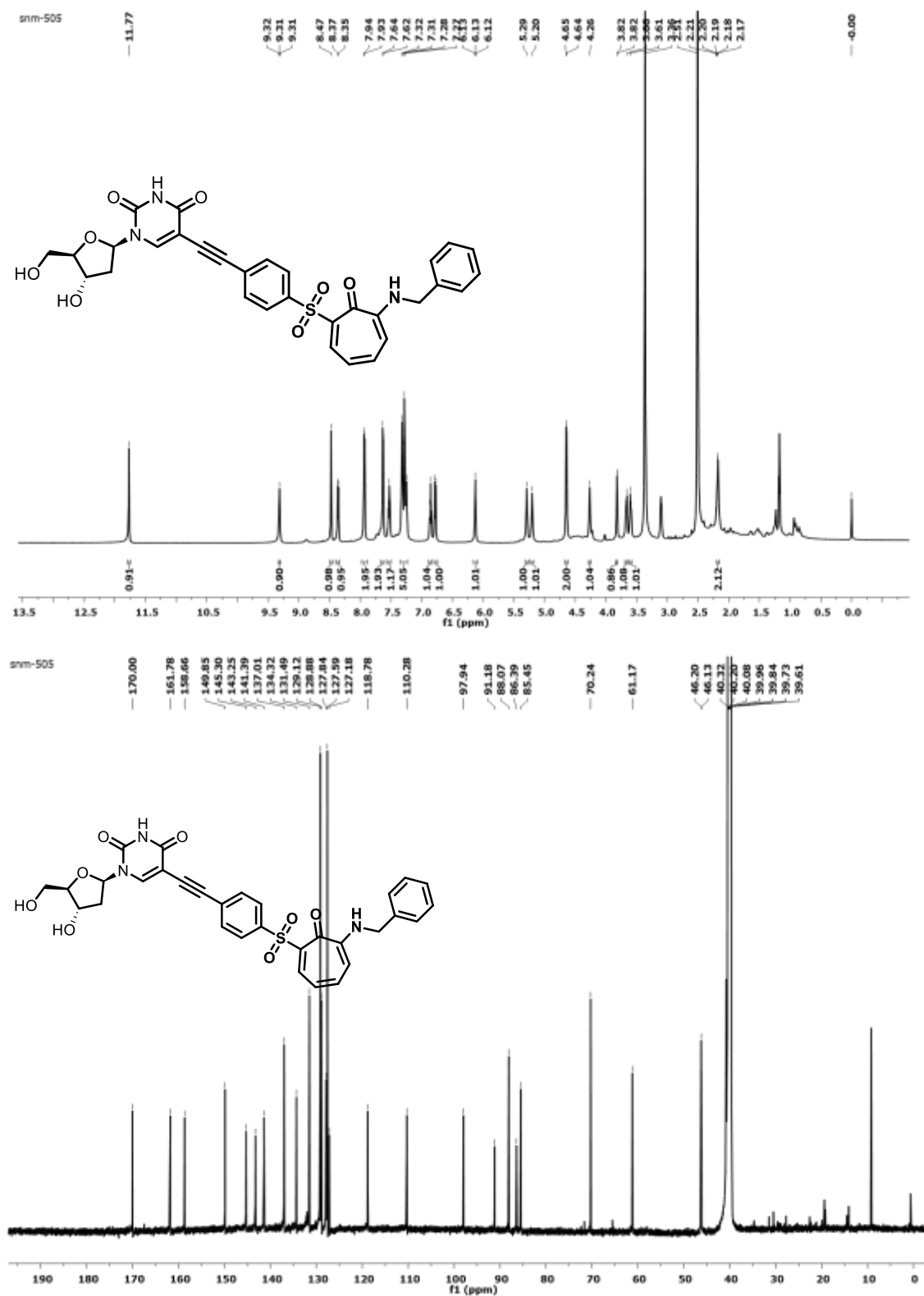
- (26) Suzol, S. H.; Howlader, A. H.; Wen, Z.; Ren, Y.; Laverde, E. E.; Garcia, C.; Liu, Y.; Wnuk, S. F. Pyrimidine Nucleosides with a Reactive ( $\beta$ -Chlorovinyl) Sulfone or ( $\beta$ -Keto) Sulfone Group at the C5 Position, Their Reactions with Nucleophiles and Electrophiles, and Their Polymerase-Catalyzed Incorporation into DNA. *ACS omega* **2018**, 3 (4), 4276–4288.
- (27) Meher, S.; Kumari, S.; Dixit, M.; Sharma, N. K. Cu-Catalyzed Synthesis of Alkylaminotroponyl Sulfones as Pseudomonas Aeruginosa Quorum Sensing Inhibitors Targeting LasI/R QS Circuitry. *Chem. Asian J.* **2022**, 17 (23), e202200866.
- (28) Meher, S.; Gade, C. R.; Sharma, N. K. Tropolone-Conjugated DNA: A Fluorescent Thymidine Analogue Exhibits Solvatochromism, Enzymatic Incorporation into DNA and HeLa Cell Internalization. *ChemBioChem* **2022**, e202200732.
- (29) Bollu, A.; Sharma, N. K. Tropolone-Conjugated DNA: Fluorescence Enhancement in the Duplex. *ChemBioChem* **2019**, 20 (11), 1467–1475.
- (30) Bollu, A.; Panda, S. S.; Sharma, N. K. Fluorescent DNA Analog: 2-Aminotroponyl-Pyrrolyl-2'-Deoxyuridiny DNA Oligo Enhance Fluorescence in DNA-Duplex as Compared to 2-Aminotroponyl-Ethynyl-2'-Deoxyuridiny DNA Oligo. *Nucleosides. Nucleotides Nucleic Acids* **2022**, 1–15.
- (31) Palai, B. B.; Soren, R.; Sharma, N. K., BODIPY Analogues: Synthesis and Photophysical Studies of Difluoro Boron Complexes from 2-Aminotropone Scaffolds through N, O-Chelation. *Org. Biomol. Chem.* **2019**, 17 (26), 6497–6505.
- (32) Breheret, E. F.; Martin, M. M. Electronic Relaxation of Troponoids: Tropolone Fluorescence. *J. Lumin.* **1978**, 17 (1), 49–60.
- (33) Zhao, C.-X.; Liu, T.; Xu, M.; Lin, H.; Zhang, C.-J. A Fundamental Study on the

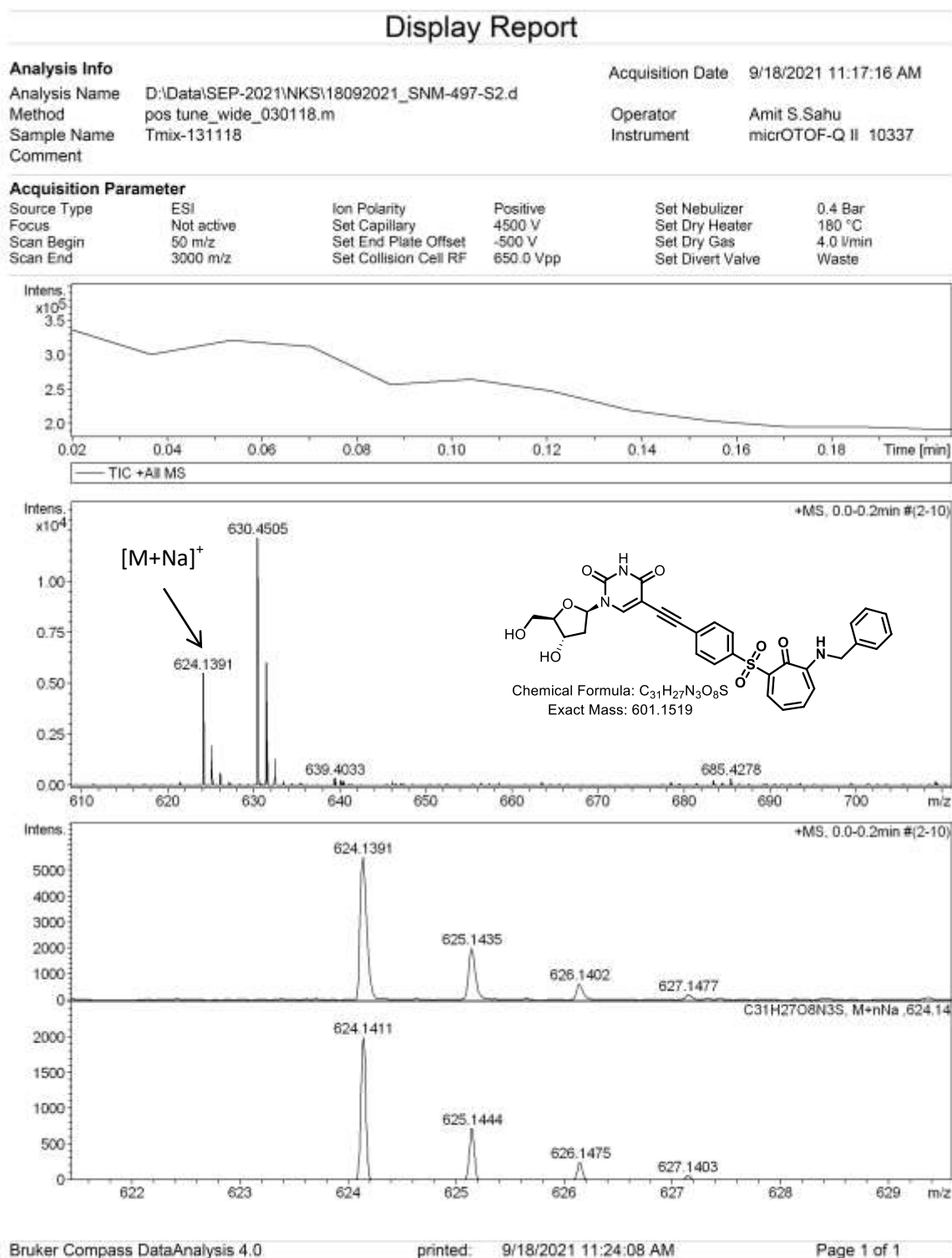
- Fluorescence-Quenching Effect of Nitro Groups in Tetraphenylethene AIE Dyes with Electron-Withdrawing Groups. *Chinese Chem. Lett.* **2021**, *32* (6), 1925–1928.
- (34) Dunn, K. W.; Kamocka, M. M.; McDonald, J. H. A Practical Guide to Evaluating Colocalization in Biological Microscopy. *Am. J. Physiol. Physiol.* **2011**, *300* (4), C723–C742.
- (35) Kuba, M.; Pohl, R.; Kraus, T.; Hocek, M. Nucleotides Bearing Red Viscosity-Sensitive Dimethoxy-Bodipy Fluorophore for Enzymatic Incorporation and DNA Labeling. *Bioconjug. Chem.* **2022**.
- (36) Loehr, M. O.; Luedtke, N. W. A Kinetic and Fluorogenic Enhancement Strategy for Labeling of Nucleic Acids. *Angew. Chemie* **2022**, *134* (22), e202112931.
- (37) Manna, S.; Sarkar, D.; Srivatsan, S. G. A Dual-App Nucleoside Probe Provides Structural Insights into the Human Telomeric Overhang in Live Cells. *J. Am. Chem. Soc.* **2018**, *140* (39), 12622–12633.
- (38) Bag, S. S.; Gogoi, H. Design of “Click” Fluorescent Labeled 2'-Deoxyuridines via C5-[4-(2-Propynyl (Methyl) Amino)] Phenyl Acetylene as a Universal Linker: Synthesis, Photophysical Properties, and Interaction with BSA. *J. Org. Chem.* **2018**, *83* (15), 7606–7621.
- (39) Zou, G.; Liu, C.; Cong, C.; Fang, Z.; Yang, W.; Luo, X.; Jia, S.; Wu, F.; Zhou, X. 5-Formyluracil as a Cornerstone for Aluminum Detection in Vitro and in Vivo: A More Natural and Sustainable Strategy. *Chem. Commun.* **2018**, *54* (93), 13107–13110.
- (40) Samaan, G. N.; Wyllie, M. K.; Cizmic, J. M.; Needham, L.-M.; Nobis, D.; Ngo, K.; Andersen, S.; Magennis, S. W.; Lee, S. F.; Purse, B. W. Single-Molecule Fluorescence Detection of a Tricyclic Nucleoside Analogue. *Chem. Sci.* **2021**, *12* (7), 2623–2628.

**4B.7 Appendix**

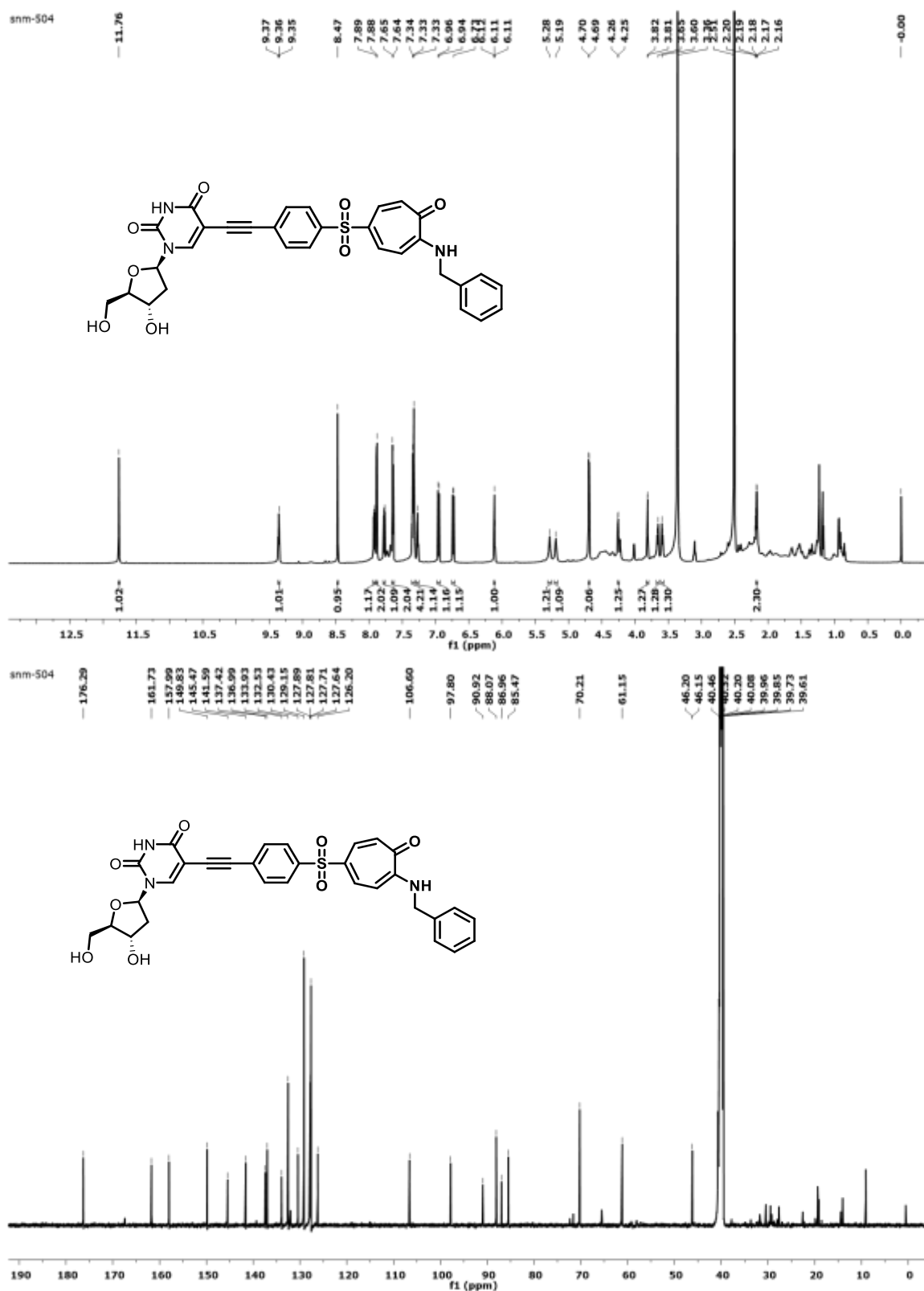
1.  $^1\text{H}$ ,  $^{13}\text{C}$  NMR (700MHz, DMSO) and HRMS of **14**.....232
2.  $^1\text{H}$ ,  $^{13}\text{C}$  NMR (700MHz, DMSO) and HRMS of **15**.....234



1.  $^1\text{H}$ ,  $^{13}\text{C}$  NMR (700MHz, DMSO) and HRMS of **14****Figure A1.**  $^1\text{H}/^{13}\text{C}$  NMR (700MHz, DMSO) spectra of compound **14** in DMSO- $d_6$



**Figure A2.** ESI-MS/HRMS spectra of compound **14**

2.  $^1\text{H}$ ,  $^{13}\text{C}$  NMR (700MHz, DMSO) and HRMS of **15**Figure A3.  $^1\text{H}/^{13}\text{C}$  NMR (700MHz, DMSO) spectra of compound **15** in DMSO- $d_6$

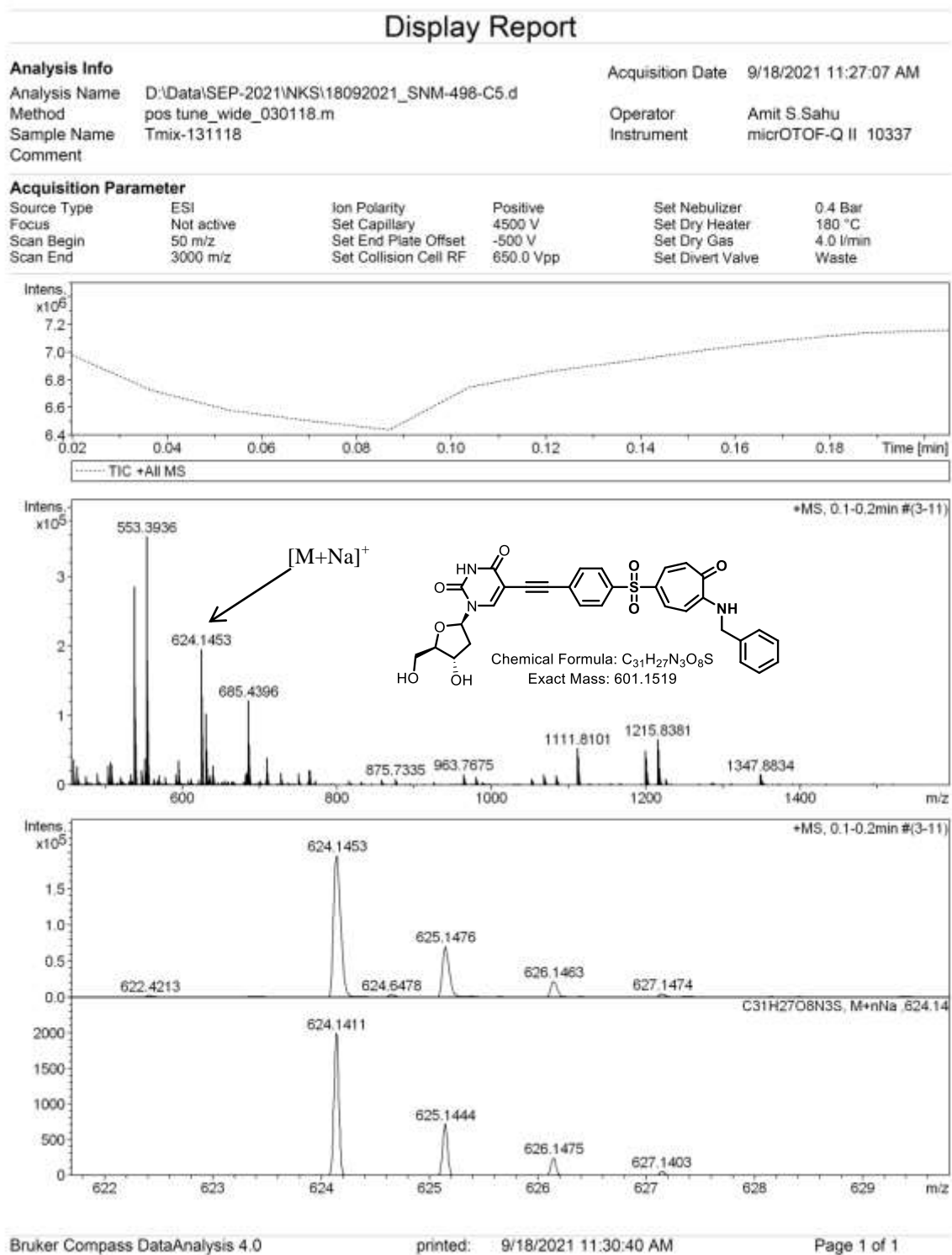


Figure A4. ESI-MS/HRMS spectra of compound 15

## CHAPTER 4

### PART-A

---

# Azulene tethered *N*-aryl Nucleobases: Synthesis, Morphology and Biochemical Evaluations

---

#### 4A.1 Introduction

#### 4A.2 Objective

#### 4A.3 Results and Discussion

#### 4A.4 Conclusion

#### 4A.5 Experimental Section

#### 4A.6 References and Notes

#### 4A.7 Appendix

### 4A.1 Introduction

*N*-substituted nucleoside derivatives have emerged as potential bioactive molecules in the quest for antimicrobial, antitumor, antineoplastic, antiviral and anticancer agents.<sup>1</sup> These derivatives also serve as agonists or antagonists for various receptors and enzymes.<sup>2</sup> The synthesis and characteristics of nucleic acid analogs with *N*-aryl-modified nucleobases has recently been the subject of research. These analogs possess a  $\pi$  electron-rich backbone with a bisaryl-like linkage to the nucleobase instead of ribose phosphate of native nucleic acid (DNA and RNA).<sup>3</sup> These aryl-nucleobases have ability to form supramolecular self-assembly structures through non-covalent interactions. Different non-covalent interactions like hydrogen bonding,  $\pi$  -  $\pi$  stacking, and metal chelating properties could be utilized in the self-organization and supramolecular assembly of nucleobases, which opens up the possibility for the synthesis of functional nanomaterials. Nucleobases have also the ability to chelate with metal ions and form metal-mediated supramolecular structure and it provides an opportunity for the synthesis of nanodevices and bioactive molecules .<sup>4</sup>

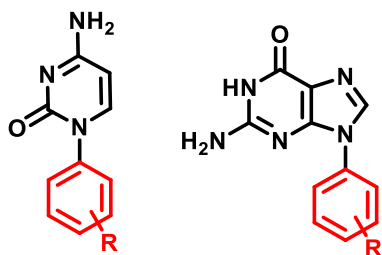
There are also ample reports on the synthetic routes toward *N*-aryl nucleobases that include nucleophilic aromatic substitution ( $S_NAr$ ), crosscoupling reactions, and multi-step reactions, where different phenyl derivatives and heterocycles were anchored to nucleobases.<sup>2,5</sup> Regioselective *N*-arylation of pyrimidine and purine nucleobases, i.e., *N*<sup>1</sup>-arylation of pyrimidines and *N*<sup>9</sup>- arylation of purines via ( $S_NAr$ ) was first reported by Khalifi et al. by using  $SiO_2$  and  $Cs_2CO_3$  at 150 °C temperature.<sup>1</sup> Similar reactions have also been executed in ionic liquids in the presence of ZnO or  $KF/Al_2O_3$ .<sup>2,5</sup> The Cu-mediated *N*-arylation of nucleobases is accomplished by employing various aryl boronic acids.<sup>6</sup> Ulven and co-workers have demonstrated the direct *N*<sup>9</sup>-arylation of purines with aryl halides using ligands like DPPhen/ BHPphen.<sup>5</sup> Still, the reported methods are associated with one or more drawbacks like low selectivity, usage of expensive reagents, long reaction time, high

temperature, unsatisfactory yield, tedious experimental procedures, narrow substrate scope/no generalization, and difficulties in the isolation of products.<sup>2,5</sup> The aryl components of *N*-aryl-nucleobases are mainly derived from the benzenoid aromatic scaffolds. However, non-benzenoid aromatic systems (tropolone and azulene) also occur in nature, which should be explored for the synthesis of *N*-aryl nucleobases. In the literature, azulene and its related derivatives are gaining interest due to its reversible stimuli-responsive nature, antibacterial properties, and potential medicinal and bioimaging applications. Azulene displays a characteristic deep blue color and a significant dipole moment due to an asymmetric  $\pi$ -polarization between the 5- and the 7-membered rings that contribute to the design of advanced functional materials.<sup>7</sup> Amination reaction has been established in the chemistry of azulene derivatives by several groups, such as Nozoe et al., Shoji et al., Mąkosza, Ostrowski, and their co-workers.<sup>8</sup> Azulene and its amino functionalized derivatives are viewed as crucial components and precursors of organic electronic materials and pharmaceuticals.<sup>8</sup> Thus, we planned to execute the synthesis and biochemical evaluation of new *N*-aryl nucleobases comprising non-benzenoid aryl scaffold, azulene derivatives.

#### 4A.2 Objective

In this chapter, we have described the synthesis and structural organization of new *N*-aryl nucleobases comprising non-benzenoid aryl scaffold, azulene derivative, by crystal X-ray diffractometer and transmission electron microscopy (TEM) and scanning electron microscopy (SEM) techniques. For practical utility, we have also performed the synthesis of azulenyl cytosine-silver complex and its bioactivity against *Pseudomonas aeruginosa* (PA14).

## Previous Reports



## This Report

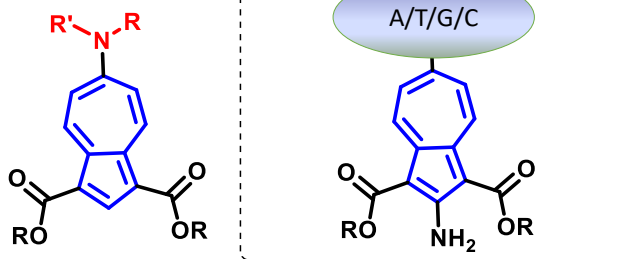
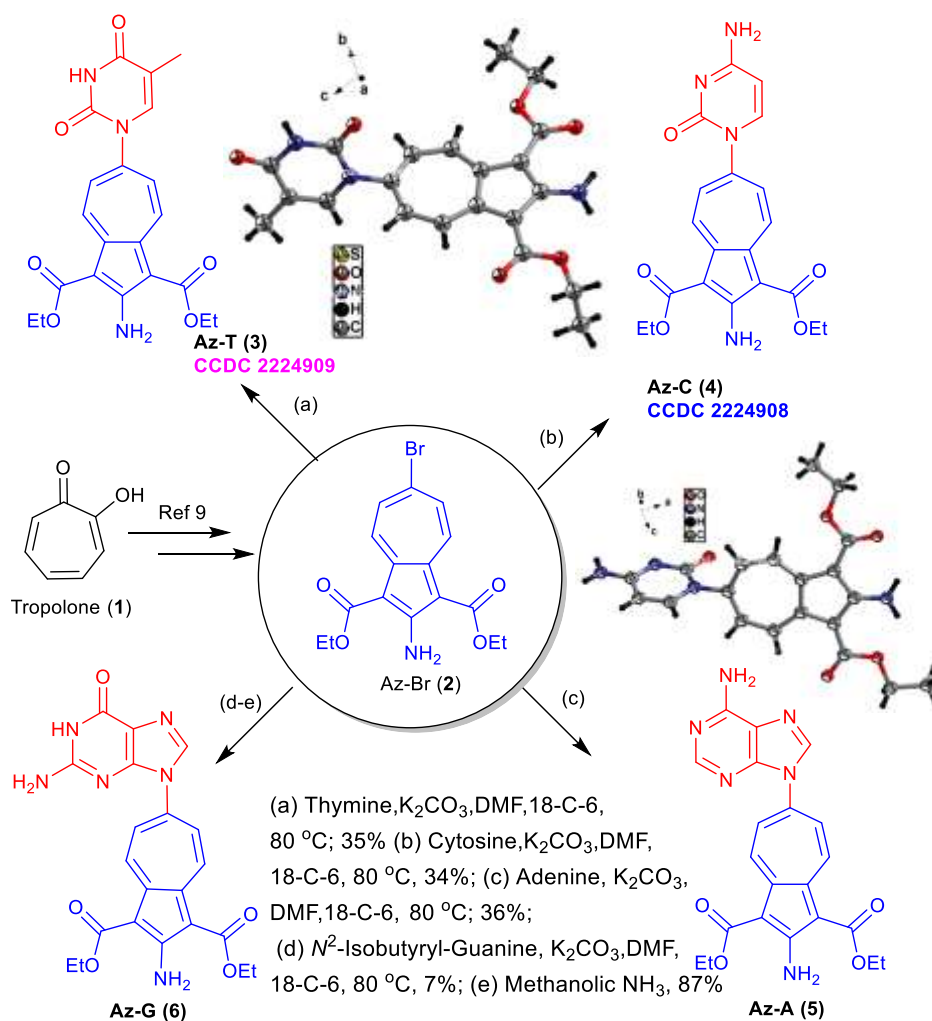


**Figure 4A.1.** Previously reported *N*-aryl nucleobases, amino-azulene derivatives and this report.

### 4A.3 Results and Discussion

We synthetically derivatized Tropolone (**1**) into 2-amino-6-bromoazulene-1,3-dicarboxylate, Az-Br (**2**) by following the reported procedure.<sup>9</sup> This bromo azulene derivative was subjected to regioselective *N*-arylation of native nucleobases under anhydrous basic conditions (18-Crown-6/K<sub>2</sub>CO<sub>3</sub>) with prolonged heating (72 hr at ~80 °C) in DMF as a solvent. As resultant, thymine (T) produced *N*<sup>1</sup>-azulenyl thymine derivative (Az-T, **3**) in a good yield. Similarly, we synthesized other *N*<sup>1</sup>-azulenyl derivative Az-C (**4**) and *N*<sup>9</sup>-Az-A (**5**) from respective nucleobases cytosine and adenine (Scheme 4B.1). However, its *N*<sup>9</sup>-Az-G (**6**) was synthesized from the *N*<sup>2</sup>-isobutyryl guanine derivative followed by deprotection under methanolic ammonia. All these derivatives were well characterized by NMR and HRMS spectral analyses (see Appendix). Pleasantly, we obtained the single crystal of Az-T (**3**) and Az-C (**4**) in solvent DMSO at 4 °C with slow evaporation method. Their crystals were studied by X-ray techniques, which confirmed their respective structure of Az-T (**3**) and Az-C (**4**). Their ORTEP diagrams are depicted in Scheme 4B.1, while other crystal structure parameters are provided in the Appendix. We also deposited their X-ray data to the cambridge crystallographic Data Centre (CCDC) with number 2224909 for Az-T (**3**) and 2224908 for Az-C (**4**).





**Scheme 4A.1.** Synthesis of *N*-azulenyl Nucleobases.

We analyzed the molecular packing of the solved crystals Az-C (4) and Az-T (3) using software (Diamond). The packing diagram of Az-C (4) shows the formation of a self-assembly supramolecular structure through H-bonding (Figure 4A.2-A). The crystal structure of Az-C shows the non-planar structural orientation of Azulene and cytosine aromatic ring residues with a twist angle of  $\sim 75^\circ$  (Figure 4A.2-B). Cytosine residue of Az-C (4) forms hydrogen bonding with neighbouring cytosine residues at bond length  $\sim 2.0\text{\AA}$  (Figure 4A.2-C). An antiparallel Cytosine-Cytosine planar structure is formed with two hydrogen bonds (N-H---N), while these pair are connected through another cytosine-cytosine pair through one

N-H...O hydrogen bond. Azulene residue also exhibits hydrogen bonding with opposite anti-parallel azulene residue at a distance  $\sim 2.0\text{\AA}$  (Figure 4A.2-D). Notably, both residues of Az-C (**4**) have hydrogen bond donor (N-H)/acceptor (O/N) atoms and form hydrogen bonds with acceptable bond length and bond angle between donor and acceptor atoms. Their packing diagram shows hydrogen bonds between cytosine-cytosine and azulene-azulene residues.

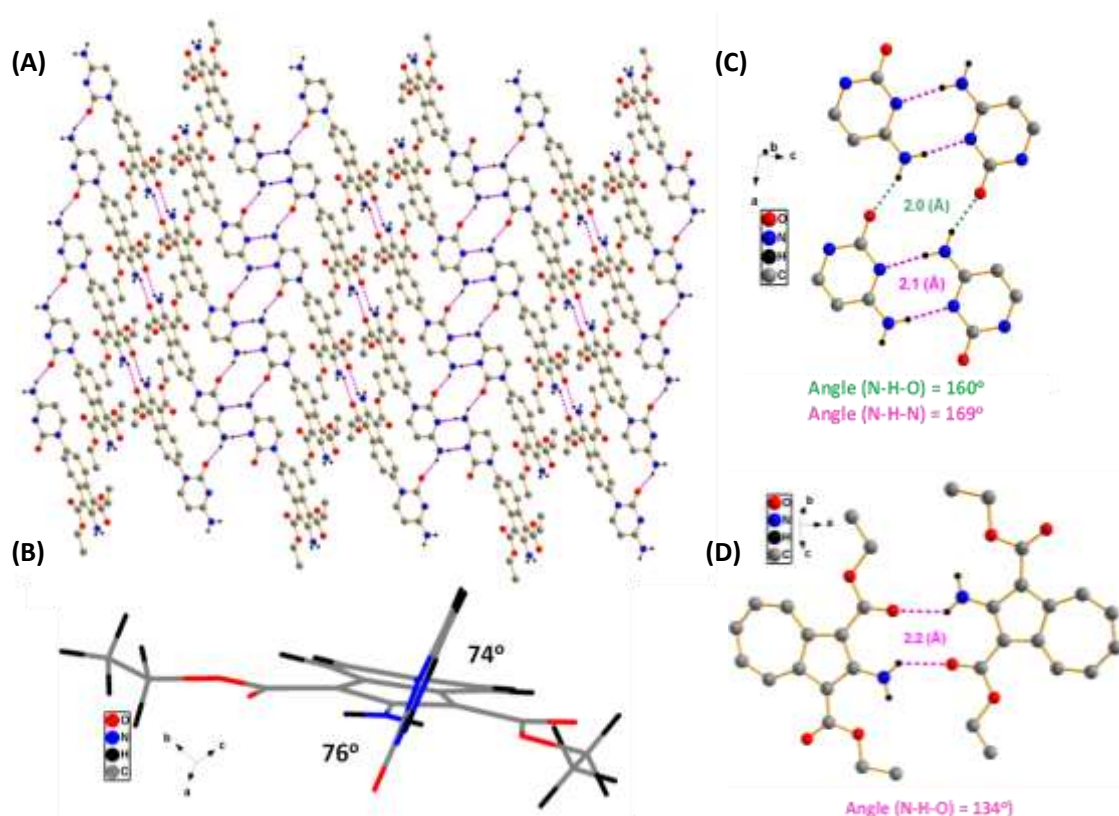


**Figure 4A.2.** Crystal structure and packing diagram of Az-C (**4**).

The packing diagram of Az-T (**3**) crystal shows the formation of a new supramolecular self-assembly structure owing to the  $\pi$ - $\pi$  interactions. Its azulenyl ring exhibit  $\pi$ - $\pi$  stacking with another antiparallel azulene ring at a distance  $3.7\text{ \AA}$ , while its thymine ring shows  $\pi$ - $\pi$  stacking with another thymine ring of Az-T (**3**) in the same fashion with distance  $3.7\text{ \AA}$  (Figure 4A.3-A/B). Thymine and azulene residues of Az-T (**3**) are non-planar with a twist angle  $\sim 72^\circ$ . This assembly forms unique step-type structures such as T-Az-T-Az.

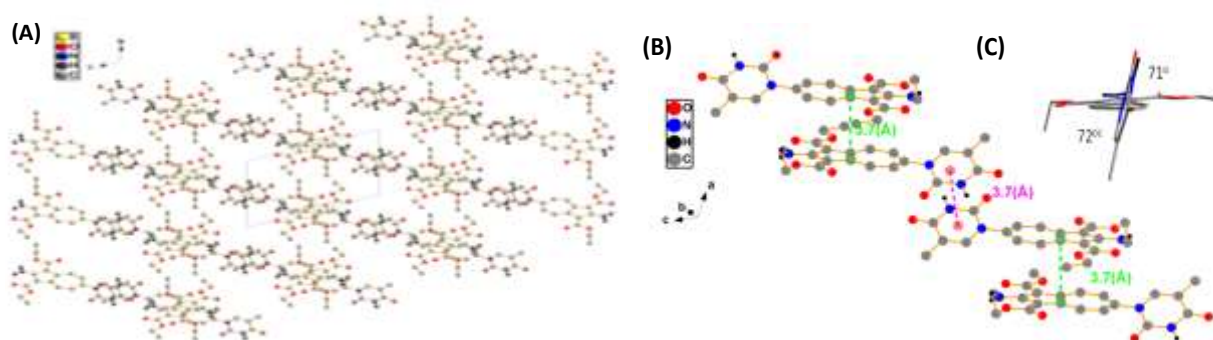


**Figure 4A.3.** Crystal structure and packing diagram of Az-T (**3**).

The UV-Vis spectra of four *N*-azulenyl nucleobases (**3-6**) in MeOH are shown in Appendix, Figure A15. The absorption maxima ( $\lambda_{\text{max}}$ ) and their molar extinction coefficients ( $\epsilon$ ) are summarized in Appendix (Table A3). The spectra for all the four compounds indicate the presence of several electronic transitions with apparent maxima at 270 and 331 nm with a shoulder positioned at around 320 nm. The strong absorption band at  $\lambda_{\text{max}} = 331$  nm is a result of  $S_0$ - $S_3$  transition, which is a known pattern for azulene derivatives.<sup>10</sup> There are two additional broader bands located at lower energy with apparent maxima at 412 and 465 nm, which can be assigned to weak  $S_0$ - $S_2$  and  $S_0$ - $S_1$  transitions, respectively, which is commonly seen in azulene derivatives.<sup>11</sup> However, these compounds don't show any fluorescence properties.

We also performed DFT calculation (B3lyp/631-G) of all four derivatives (**3-6**) and obtained the optimized structure in gas phase (See Appendix). We extracted their HOMO-LUMO diagrams and energy gap (Appendix, Figure A17). Their optimized structures (Figure 4A.4) reveal that both rings are non-planar to each other and contribute to the respective HOMO and LUMO through nucleobase (A/T/G/C) rings. The HOMO-LUMO energy gap is almost constant ( $\sim 3.5$  eV). Thus photophysical properties of azulenyl nucleobase (**3-6**) are nearly the same with all four derivatives.

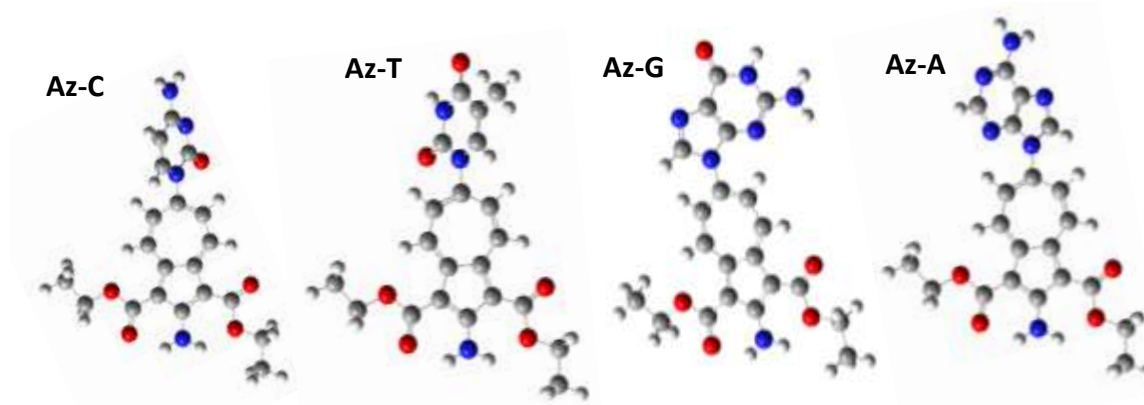


**Figure 4A.4.** Optimized structures of Az-A/T/G/C (**3-6**) nucleobases.

Further, we studied the surface morphology of the *N*-azulenyl nucleobases (**3-6**) by Transmission electron microscope (TEM) and scanning electron microscope (SEM) imaging techniques. Their TEM/SEM images at different scales are provided in Figure 4A.5 and the Appendix. In case of Az-C (**4**), the existence of well-dispersed nanofibers was noticed. The HRTEM images show a well-developed network structure composed of a three-dimensional entangled fibrous network (Figure 4A.5-A/B). According to the literature, the existence of nanofibers results in the trapping of more solvent with greater void volumes.<sup>12</sup> This kind of networking structure was further supported by SEM images (Figure 4A.5-C/D). Crystal packing diagram of Az-C (**4**) also shows the formation of supramolecular self-assembly owing to intermolecular hydrogen bonding between azulene and cytosine residues. We noticed similar types of networking patterns in SEM/TEM images of Az-A (**5**) and Az-G (**6**) (Appendix, Figure A18/19). In contrast, Az-T (**3**) doesn't show any networking and gives a clear view of unique supramolecular structure as plant-like morphology. Interestingly, it resembles boat lily plants closely, and the image creates an illusion of boat lily plants grown on soil in the SEM images (Figure 4A.5-F/G). The morphological information obtained from the Az-T (**3**) SEM images was further supported by TEM analysis (Figure 4A.5-E). The TEM study at different magnifications confirms that nanospheres aggregate to give a plant-like morphology. Its crystal packing diagram shows the formation of three-dimensional

supramolecular structures owing to the antiparallel  $\pi$ - $\pi$  interactions between azulene or thymine residues. The elemental mapping and the energy dispersive X-ray analysis (EDAX) of the four compounds are provided in Appendix. Thus *N*-azulenyl nucleobases are promising molecules for developing novel nanomaterials.

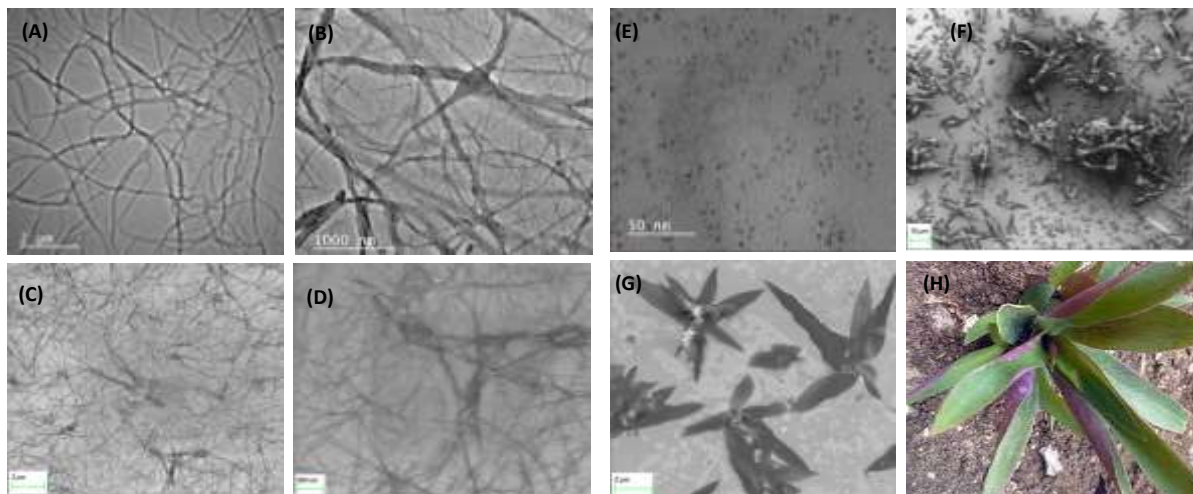


**Figure 4A.5.** (A, B) HRTEM and (C, D) FESEM images of Az-C (**4**); (E) HRTEM and (F, G) FESEM images of Az-T (**3**), (H) an image of boat lily plant.

In literature, silver complexes/nanoparticles (AgNPs) have shown direct antimicrobial and anti-inflammatory effects and are frequently used in the medical industry to prevent infection in burns and open wounds.<sup>13, 14</sup> Recently, antibacterial resistance has turned into a global issue, and there is always urgency in the development of new antibacterial drugs to treat lung, skin, eye, wound, blood-borne, and urinary tract infections occurring in both hospitals and the community caused by different pathogenic bacteria such as *Pseudomonas aeruginosa* (PA). Hence, we synthesized the silver complex of Az-C and evaluated its morphology and antibacterial activity. In the Az-C-Ag complex (**8**) ligand: metal ratio is 2:1 (Confirmed by HRMS (Appendix, Figure A13)). In Figure 4A.6-A, The absorption spectrum of Az-C-Ag complex (**8**) has a wavelength maximum at 310 nm with a shoulder peak at 330 nm and has a red tail extending to longer wavelengths compared to Az-C (**4**). Herein we



assumed the formation of Az-C-Ag complex by  $N^3$ -atom of two Az-C with Ag ion in antiparallel fashion (Figure 4A.6-B).

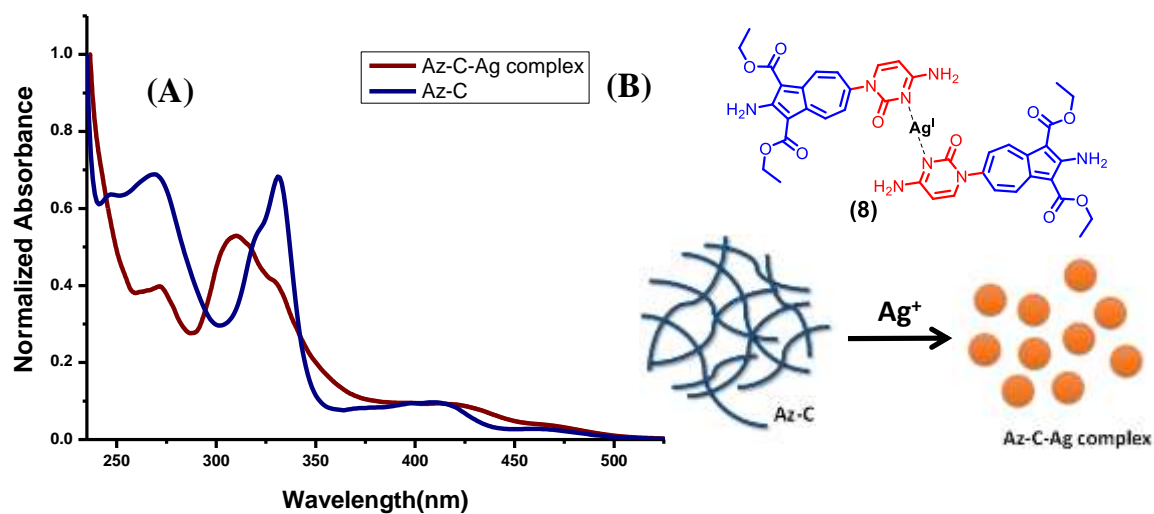


**Figure 4A.6.** (A) UV-Vis spectra of Az-C (**4**) and Az-C-Ag complex (**8**), (B) Graphical representation of the synthesis of compound **8**.

The SEM/TEM (Figure 4A.7-A-C) results of compound **8** give a clear indication regarding the shape and size of the nanoparticles. These silver nanoparticles were spherical and measured  $\sim 5$ – $30$  nm. The well-resolved lattice fringes obtained by HRTEM (Figure 4A.7-B) further confirm the formation of AgNP.<sup>14</sup> The elemental mapping and EDAX spectrum are provided in the Appendix.

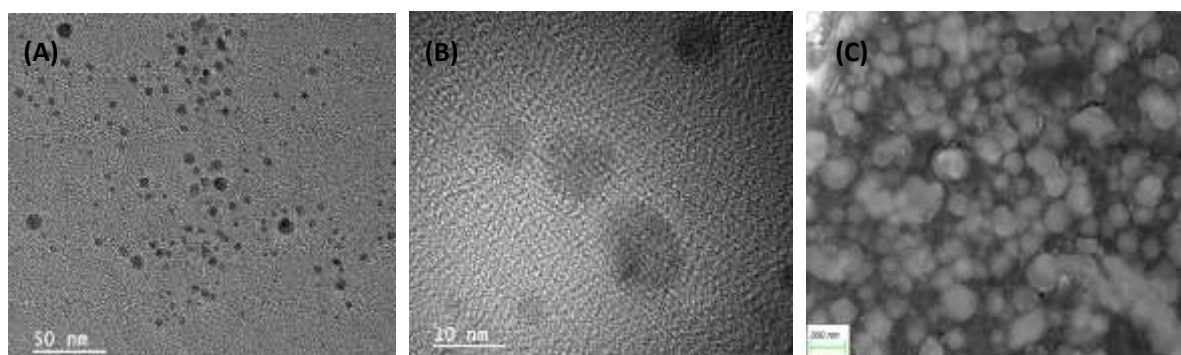


**Figure 4A.7.** (A, B) HRTEM and (C) FESEM images of Az-C-Ag complex (**8**).

For practical utility, we examined the antimicrobial activities of Az-C silver complex (8). The antimicrobial activity of Az-C-Ag nanoparticles was measured against the pathogenic microorganism *Pseudomonas aeruginosa* (PA14) on Luria-Bertani agar (LB) plates using the disc diffusion method. We measured the zones of clearance at different concentrations of Az-C-Ag complex (8), from 5-100  $\mu\text{M}$  (Figure 4A.8). The Minimum Inhibitory Concentration (MIC) was 20  $\mu\text{M}$  for exhibiting a zone of clearance with a diameter of  $\sim 15$  mm. Below this concentration, i.e., 5  $\mu\text{M}$  and 10  $\mu\text{M}$ , we couldn't notice any antibiotic activity (Figure 4A.8-C). The zone of inhibition diameter was 24 mm when the concentration was 100  $\mu\text{M}$  (Figure 4A.8-B).

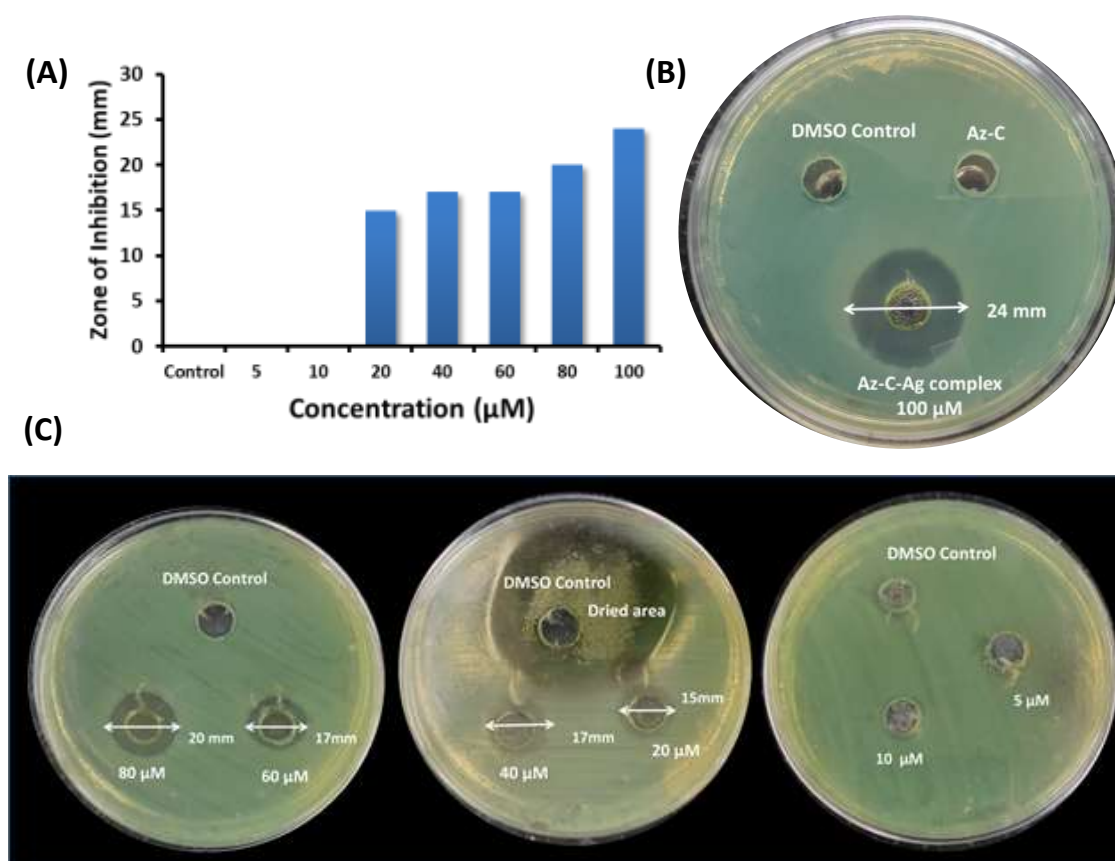


**Figure 4A.8.** (A) Plot for concentration-dependent antimicrobial activity of silver nanoparticles (Az-C-silver complex) (8) against PA14 by disc diffusion assay, (B) Image of LB plate showing zone of clearance for compound 8 at 100  $\mu\text{M}$  concentration.

Finally, when we evaluated the cytotoxicity of the Azulenyl nucleobases (**3-6**)/Az-C-Ag complex (**8**), with HEK293T cell line (Figure 4A.9-A/B), all four derivatives (**3-6**) showed no cytotoxic effects with HEK293T cell lines even with high concentrations (100  $\mu$ M) except for Az-C-Ag complex ( $IC_{50} \sim 71 \mu$ M). In literature, The cytotoxicity of silver nanoparticles is well documented.<sup>15</sup>

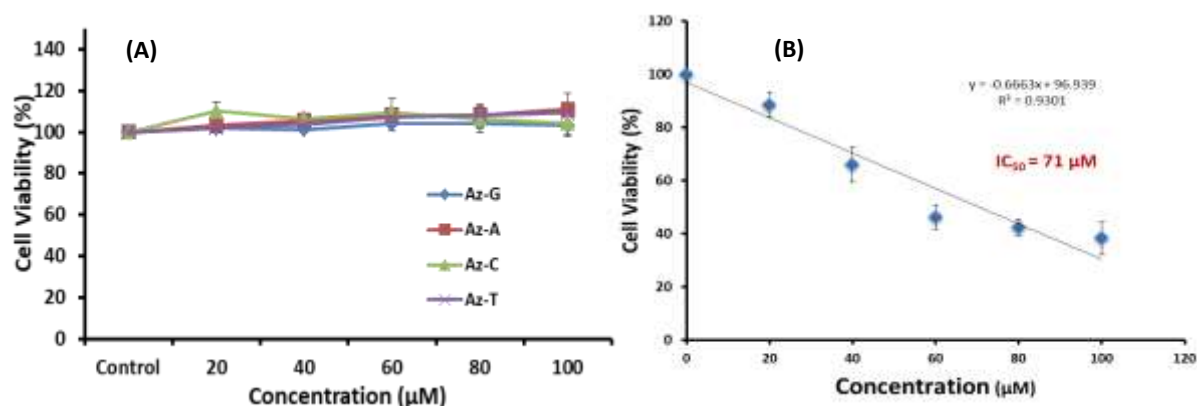


**Figure 4A.9.** (A) Plots for Cell viability assay of compounds Az-T (**3**), Az-C (**4**), Az-A (**5**), Az-G (**6**) and (B) Az-C-Ag complex (**8**) for HEK293T cell line.

#### 4A.4 Conclusion

In summary, we have synthesized four new *N*-azulenyl nucleobases showing unique morphology in SEM/TEM, such as the resemblance of Az-T SEM images with Boat lily plant structure. The introduction of  $Ag^+$  ions breaks the networking structure of Az-C and forms nanocomposites that exhibit antibacterial properties towards PA (MIC  $\sim 20 \mu$ M). Thus Az-C-Ag complex is a promising antibiotic drug candidate. It will be interesting to study the properties of *N*-azulenyl nucleobases by modifying the functional groups present in azulene moiety in the future.



#### 4A.5 Experimental Section

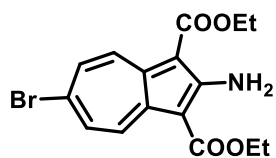
*General information:* Unless otherwise noted, materials were purchased from commercial suppliers and were used as received. DMF was distilled over  $\text{CaH}_2$  and stored over 4Å molecular sieves. Reactions were monitored by thin layer chromatography, visualized by UV and Ninhydrin. Column chromatography was performed in 100-200 mesh silica. Mass spectra (HRMS) were obtained from Bruker microTOF-Q II and Waters Spectrometer and the samples were prepared in methanol and injected in methanol and water mixture. NMR spectra were recorded on Bruker 400 MHz and Bruker 700 MHz NMR spectrometer at room temperature and processed using Mnova software from Mestrelab Research. The crystal data were collected on a Rigaku Oxford diffractometer. Absorption spectra were obtained using Jasco V-730 spectrometer. The surface morphologies of compounds were studied with field emission scanning electron microscopy (FESEM, Merlin Compact with a GEMINI-I/GEMINI-II electron column, Zeiss Pvt. Ltd., Germany) and high-resolution transmission electron microscopy (HRTEM, JEOL 2100F). FTIR analysis of the samples was carried out by the PerkinElmer FTIR spectrometer equipped with an attenuated total reflectance accessory.

*General procedure for the preparation of N-Azulenyl Nucleobases:* In a round bottom flask a mixture of Nucleobase (1 equiv.) (Thymine/ Cytosine/ Adenine/ N-isobutyryl-Guanine), Diethyl 2-amino-6-bromoazulene-1,3-dicarboxylate (1.2 equiv.),  $\text{K}_2\text{CO}_3$  (4 equiv.) and 18-C-6 (0.02 equiv.) in anh. DMF was stirred and heated in an oil bath at 80 °C for 72 h. After cooling it to room temperature the mixture was filtered through a pad of celite and the solution was evaporated in reduced pressure. The residue was subjected to column chromatography using 100-200 mesh silica gel and MeOH: DCM as solvent system to get the desired products. In case of guanine, we didn't get regioselectivity unlike in other cases. All

the compounds were completely soluble in DMSO but Az-A wasn't, when concentration was high.

### Characterization data of products

Diethyl 2-amino-6-bromoazulene-1,3-dicarboxylate(**2**): Following the reported procedure, the



title compound was synthesized and obtained as a deep purple

solid.<sup>9,16</sup> <sup>1</sup>H NMR (400 MHz, CDCl<sub>3</sub>) δ 8.82 (d, *J* = 11.5 Hz, 2H),

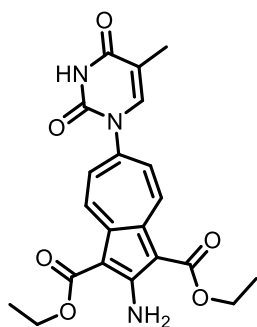
7.81 (s, 2H), 7.78 (d, 2H), 4.46 (q, *J* = 7.1 Hz, 2H), 1.47 (t, *J* = 7.1

Hz, 3H). <sup>13</sup>C NMR (101 MHz, CDCl<sub>3</sub>) δ 166.23, 162.34, 144.33,

135.31, 129.45, 128.37, 101.00, 60.07, 14.61. HRMS (ESI) calcd for C<sub>16</sub>H<sub>16</sub>BrNO<sub>4</sub>: [M+Na]<sup>+</sup>

388.0155, found 388.0135.

Diethyl 2-amino-6-(5-methyl-2,4-dioxo-3,4-dihydropyrimidin-1(2H)-yl)azulene-1,3-



dicarboxylate(**3**): Following the general procedure the title compound

was isolated by column chromatography (eluent: dichloromethane) as

a yellow solid in 35% yield (46 mg). <sup>1</sup>H NMR (400 MHz, DMSO) δ

11.53 (s, 1H), 9.05 (d, *J* = 11.5 Hz, 2H), 7.94 (s, 2H), 7.76 (s, 1H),

7.71 (d, *J* = 11.5 Hz, 2H), 4.41 (q, *J* = 7.1 Hz, 4H), 1.83 (s, 3H), 1.40

(t, *J* = 7.1 Hz, 6H). <sup>13</sup>C NMR (101 MHz, DMSO) δ 165.75, 164.83, 161.98, 151.07, 145.07,

141.81, 141.48, 132.91, 128.96, 110.00, 100.39, 60.28, 14.87, 12.33, HRMS (ESI) calcd for

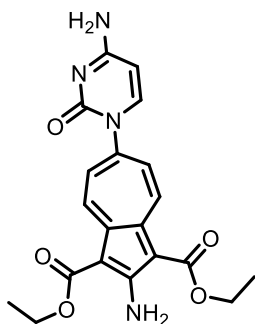
C<sub>21</sub>H<sub>21</sub>N<sub>3</sub>O<sub>6</sub>: [M+Na]<sup>+</sup> 434.1323, found 434.1309, FT-IR (cm<sup>-1</sup>) 3497, 3374, 3168, 3061,

2972, 2954, 2922, 2849, 2818, 2377, 2332, 2322, 1701, 1678, 1647, 1597, 1560, 1532, 1507,

1492, 1456, 1427, 1376, 1302, 1283, 1233, 1188, 1151, 1115, 1073, 1039, 986, 931, 854,

819, 790, 753, 686, 640, 613, 592, 560.

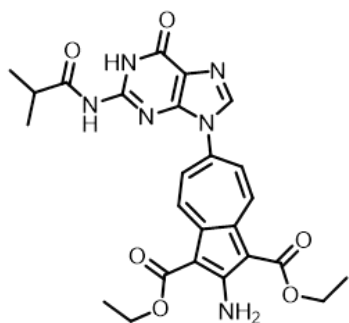
Diethyl 2-amino-6-(4-amino-2-oxopyrimidin-1(2H)-yl)azulene-1,3-dicarboxylate (**4**) :



Following the general procedure the title compound was isolated by column chromatography (eluent: dichloromethane) as a yellow solid in 34% yield (49 mg).  $^1\text{H}$  NMR (700 MHz, DMSO)  $\delta$  9.05 (d,  $J$  = 10.6 Hz, 2H), 7.90 (s, 2H), 7.80 (d,  $J$  = 7.2 Hz, 1H), 7.64 (d,  $J$  = 10.6 Hz, 2H), 7.51 (s, 1H), 7.40 (s, 1H), 5.86 (d,  $J$  = 7.1 Hz, 1H),

4.41 (q,  $J$  = 13.2, 6.1 Hz, 4H), 1.40 (t,  $J$  = 7.0 Hz, 6H).  $^{13}\text{C}$  NMR (176 MHz, DMSO)  $\delta$  166.38, 166.11, 165.79, 161.80, 155.10, 146.18, 144.88, 144.35, 132.83, 129.13, 100.14, 94.84, 60.19, 14.88. HRMS (ESI) calcd for  $\text{C}_{20}\text{H}_{20}\text{N}_4\text{O}_5$ :  $[\text{M}+\text{H}]^+$  397.1506, found 397.1501, FT-IR ( $\text{cm}^{-1}$ ), 3512, 3394, 3332, 3278, 3162, 3085, 3054, 2954, 2921, 2859, 2366, 2343, 1692, 1673, 1628, 1596, 1544, 1510, 1495, 1442, 1429, 1382, 1371, 1315, 1278, 1237, 1222, 1183, 1139, 1121, 1104, 1027, 988, 928, 865, 805, 780, 765, 650, 604.

Diethyl 2-amino-6-(2-isobutyramido-6-oxo-1,6-dihydro-9H-purin-9-yl)azulene-1,3-



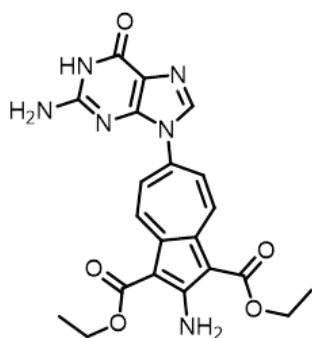
dicarboxylate (**7**): Following the general procedure the title compound was isolated by column chromatography (eluent: dichloromethane) as a yellow solid in 7% yield (7 mg).  $^1\text{H}$  NMR (700 MHz,  $\text{CDCl}_3$ )  $\delta$  12.25 (s, 1H), 9.60 (s, 1H), 8.87 (d,  $J$  = 11.0 Hz, 2H), 8.03 (s, 1H), 7.76 (s, 2H), 7.46 (d,  $J$  = 11.0

Hz, 2H), 4.44 (q,  $J$  = 7.1 Hz, 4H), 2.93 – 2.82 (m, 6.9 Hz, 1H), 1.46 (t,  $J$  = 7.1 Hz, 6H), 1.27 (d,  $J$  = 6.8 Hz, 6H),  $^{13}\text{C}$  NMR (176 MHz,  $\text{CDCl}_3$ )  $\delta$  179.19, 165.89, 162.47, 155.56, 148.37, 148.25, 144.27, 138.91, 135.81, 128.90, 127.85, 121.58, 101.37, 60.25, 36.41, 19.03, 14.63, HRMS (ESI) calcd for  $\text{C}_{21}\text{H}_{21}\text{N}_3\text{O}_6$ :  $[\text{M}+\text{H}]^+$  507.1951, found 507.1992.

Diethyl 2-amino-6-(2-amino-6-oxo-1,6-dihydro-9H-purin-9-yl)azulene-1,3-dicarboxylate (**6**):

Following the procedure for deprotection of isobutyryl group, the title compound was isolated as a yellow solid in 87% yield (15 mg).  $^1\text{H}$  NMR (700 MHz, DMSO)  $\delta$  9.12 (d,  $J$  =

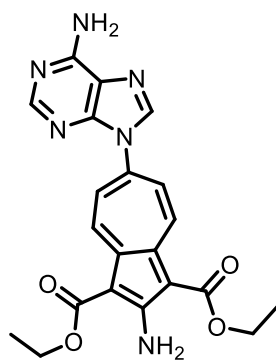
11.5 Hz, 2H), 8.40 (s, 1H), 8.12 (s, 1H), 7.98 (s, 1H), 7.94 (s, 1H), 7.93 (d,  $J = 3.7$  Hz, 2H),



6.65 (s, 2H), 4.44 – 4.40 (m,  $J = 11.4, 5.7$  Hz, 4H), 1.41 (t,  $J = 7.1$  Hz, 6H),  $^{13}\text{C}$  NMR (176 MHz, DMSO)  $\delta$  165.79, 161.84, 157.33, 154.58, 151.70, 144.52, 137.87, 137.46, 130.73, 130.32, 129.43, 117.50, 100.52, 60.29, 14.93, HRMS (ESI) calcd for  $\text{C}_{21}\text{H}_{20}\text{N}_6\text{O}_5$ :  $[\text{M}+\text{H}]^+$  437.1573, found 437.1571, FT-IR ( $\text{cm}^{-1}$ ), 3487, 3451,

3338, 3169, 3117, 2979, 2904, 2839, 2726, 2198, 2108, 1940, 1720, 1667, 1630, 1584, 1534, 1510, 1483, 1431, 1378, 1353, 1278, 1169, 1115, 1070, 1028, 963, 835, 776, 684, 624, 590, 553.

Diethyl 2-amino-6-(6-amino-9H-purin-9-yl)azulene-1,3-dicarboxylate (**5**) Following the



general procedure the title compound was isolated by column chromatography (eluent: dichloromethane) as a yellow solid in 36% yield (46 mg).  $^1\text{H}$  NMR (400 MHz, DMSO)  $\delta$  9.16 (d,  $J = 11.3$  Hz, 2H), 8.61 (s, 1H), 8.24 (s, 1H), 8.08 (d,  $J = 11.3$  Hz, 2H), 7.92 (s, 2H), 7.38 (s, 2H), 4.43 (q,  $J = 6.9$  Hz, 4H), 1.42 (t,  $J = 7.0$  Hz, 6H). HRMS (ESI) calcd for  $\text{C}_{21}\text{H}_{20}\text{N}_6\text{O}_4$ :  $[\text{M}+\text{H}]^+$  421.1619,

found 421.1605, FT-IR ( $\text{cm}^{-1}$ ) 3430, 3313, 3176, 3123, 2954, 2917, 2850, 2352, 2336, 2327, 2320, 2308, 1682, 1671, 1660, 1644, 1634, 1591, 1567, 1554, 1531, 1505, 1470, 1454, 1443, 1426, 1415, 1382, 1368, 1336, 1308, 1260, 1194, 1169, 1112, 1064, 1015, 967, 842, 796, 733, 691, 669, 646, 606.

*Disk diffusion test for concentration-dependent antibiotic activity:* The antimicrobial activity of silver nanoparticles (**8**) against pathogenic microorganism *Pseudomonas aeruginosa* (PA14) was measured on Luria-Bertani agar (LB) plates using the disk diffusion method. In this assay, the LB agar solution was poured into the disk while hot and is allowed to cool for gelation. Then PA14 was spread over the agar using a cotton swab. Small wells were made in

the agar gel plate with the head of 1 ml tip. 100  $\mu$ l of the sample (DMSO control, Az-C-Ag complex (**8**) in different concentrations) was poured onto the agar plates. The plates were incubated at 37°C for 12 h. After the incubation period, the zones of inhibition around silver were measured and compared with the zone of inhibition of each antibiotic disc.

*Cell proliferation assay:* For the detailed instructions, see Chapter 2.

#### 4A.6 References and Notes

- (1) Khalafi-Nezhad, A.; Zare, A.; Parhami, A.; Soltani Rad, M. N.; Nejabat, G. R. Regioselective N-Arylation of Some Pyrimidine and Purine Nucleobases. *Synth. Commun.* **2006**, *36* (23), 3549–3562.
- (2) Zare, A.; Hasaninejad, A.; Khalafi-Nezhad, A.; Moosavi-Zare, A. R.; Beyzavi, M. H.; Khedri, F.; Asadi, F.; Hayati, N.; Asifi, A. A Highly Efficient Protocol for the Synthesis of N-Aryl Nucleobases Using Zinc Oxide in Ionic Liquids. *J. Iran. Chem. Soc.* **2010**, *7* (2), 461–469.
- (3) Jacobsen, M. F.; Knudsen, M. M.; Gothelf, K. V. Efficient N-Arylation and N-Alkenylation of the Five DNA/RNA Nucleobases. *J. Org. Chem.* **2006**, *71* (24), 9183–9190.
- (4) Pu, F.; Ren, J.; Qu, X. Nucleobases, Nucleosides, and Nucleotides: Versatile Biomolecules for Generating Functional Nanomaterials. *Chem. Soc. Rev.* **2018**, *47* (4), 1285–1306.
- (5) Larsen, A. F.; Ulven, T. Direct N 9-Arylation of Purines with Aryl Halides. *Chem. Commun.* **2014**, *50* (39), 4997–4999.
- (6) Tao, L.; Yue, Y.; Zhang, J.; Chen, S.; Yu, X. A Mild and Efficient Method for N-

- Arylnucleobase Synthesis via the Cross-Coupling Reactions of Nucleobases with Arylboronic Acids Catalyzed by Simple Copper Salts. *Helv. Chim. Acta* **2008**, *91* (6), 1008–1014.
- (7) Clikeman, T. T.; Bukovsky, E. V.; Kuvychko, I. V.; San, L. K.; Deng, S. H. M.; Wang, X.-B.; Chen, Y.-S.; Strauss, S. H.; Boltalina, O. V. Poly (Trifluoromethyl) Azulenes: Structures and Acceptor Properties. *Chem. Commun.* **2014**, *50* (47), 6263–6266.
- (8) Shoji, T.; Sugiyama, S.; Takeuchi, M.; Ohta, A.; Sekiguchi, R.; Ito, S.; Yatsu, T.; Okujima, T.; Yasunami, M. Synthesis of 6-Amino- and 6-Arylazoazulenes via Nucleophilic Aromatic Substitution and Their Reactivity and Properties. *J. Org. Chem.* **2019**, *84* (3), 1257–1275.
- (9) Murfin, L. C.; Weber, M.; Park, S. J.; Kim, W. T.; Lopez-Alled, C. M.; McMullin, C. L.; Pradaux-Caggiano, F.; Lyall, C. L.; Kociok-Köhn, G.; Wenk, J. Azulene-Derived Fluorescent Probe for Bioimaging: Detection of Reactive Oxygen and Nitrogen Species by Two-Photon Microscopy. *J. Am. Chem. Soc.* **2019**, *141* (49), 19389–19396.
- (10) Matěnová, M.; Horhoiu, V. L.; Dang, F.-X.; Pospíšil, P.; Alster, J.; Burda, J. V.; Balaban, T. S.; Pšenčík, J. Energy Transfer in Aggregates of Bacteriochlorophyll *c* Self-Assembled with Azulene Derivatives. *Phys. Chem. Chem. Phys.* **2014**, *16* (31), 16755–16764.
- (11) Zhang, J.; Petoud, S. Azulene-moiety-based Ligand for the Efficient Sensitization of Four Near-infrared Luminescent Lanthanide Cations: Nd<sup>3+</sup>, Er<sup>3+</sup>, Tm<sup>3+</sup>, and Yb<sup>3+</sup>. *Chem. Eur. J.* **2008**, *14* (4), 1264–1272.
- (12) Lalitha, K.; Prasad, Y. S.; Maheswari, C. U.; Sridharan, V.; John, G.; Nagarajan, S. Stimuli Responsive Hydrogels Derived from a Renewable Resource: Synthesis, Self-

- Assembly in Water and Application in Drug Delivery. *J. Mater. Chem. B* **2015**, *3* (27), 5560–5568.
- (13) Mistry, L.; El-Zubir, O.; Dura, G.; Clegg, W.; Waddell, P. G.; Pope, T.; Hofer, W. A.; Wright, N. G.; Horrocks, B. R.; Houlton, A. Addressing the Properties of “Metallo-DNA” with a Ag (i)-Mediated Supramolecular Duplex. *Chem. Sci.* **2019**, *10* (11), 3186–3195.
- (14) Singh, P.; Kim, Y. J.; Wang, C.; Mathiyalagan, R.; Yang, D. C. The Development of a Green Approach for the Biosynthesis of Silver and Gold Nanoparticles by Using Panax Ginseng Root Extract, and Their Biological Applications. *Artif. cells, nanomedicine, Biotechnol.* **2016**, *44* (4), 1150–1157.
- (15) Feng, D.; Zhang, R.; Zhang, M.; Fang, A.; Shi, F. Synthesis of Eco-Friendly Silver Nanoparticles Using Glycyrrhizin and Evaluation of Their Antibacterial Ability. *Nanomaterials* **2022**, *12* (15), 2636.
- (16) Ito, A.; Ishii, A.; Amaki, T.; Fukuda, K.; Yamasaki, R.; Okamoto, I. Synthesis and Conformational Analysis of N-Aryl-N-(6-Azulenyl) Acetamides. *Tetrahedron Lett.* **2019**, *60* (29), 1929–1933.

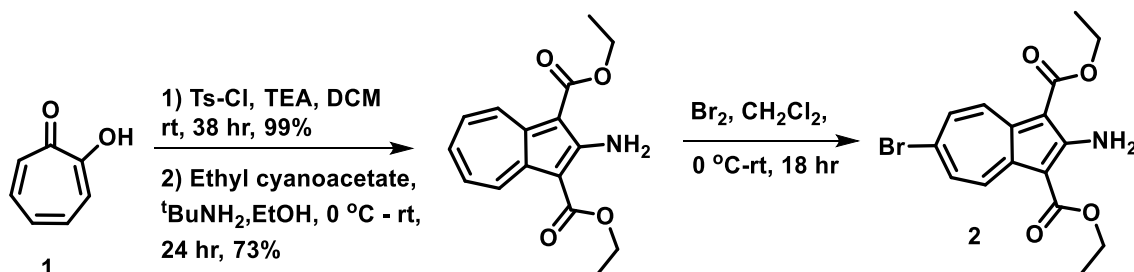
**4A.7 Appendix**

1. Synthesis of Diethyl 2-amino-6-bromoazulene-1,3-dicarboxylate ( <b>2</b> ).....	256
2. Procedure for the preparation of Silver complex Az-C-Ag ( <b>8</b> ).....	256
3. $^1\text{H}$ , $^{13}\text{C}$ NMR (400MHz, $\text{CDCl}_3$ ) and HRMS of compound <b>2</b> .....	257
4. $^1\text{H}$ , $^{13}\text{C}$ NMR (400MHz, DMSO) and HRMS of compound <b>3</b> .....	259
5. $^1\text{H}$ , $^{13}\text{C}$ NMR (700MHz, DMSO) and HRMS of compound <b>4</b> .....	261
6. $^1\text{H}$ , $^{13}\text{C}$ NMR (700MHz, $\text{CDCl}_3$ ) and HRMS of compound <b>7</b> .....	263
7. $^1\text{H}$ NMR (400MHz, $\text{CDCl}_3$ ) and HRMS of compound <b>5</b> .....	264
8. $^1\text{H}$ , $^{13}\text{C}$ NMR (700MHz, $\text{CDCl}_3$ ) and HRMS of compound <b>6</b> .....	266
9. FT-IR Spectra .....	269
10. Crystal structures and data .....	269
11. Photophysical studies.....	271
12. Optimized structure and HOMO- LUMO energy gap .....	272
13. Field Emission Scanning Electronic Microscopy (FESEM) and High-Resolution Transmission Electron Microscopy (HRTEM).....	273

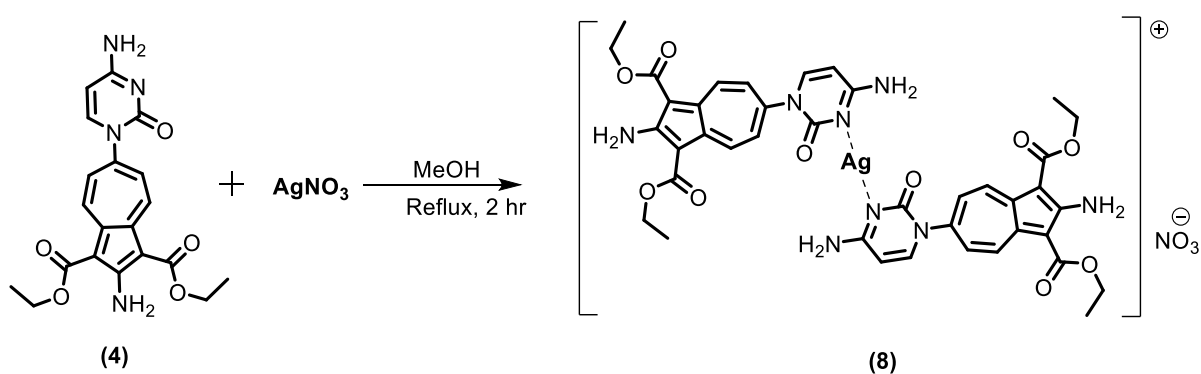


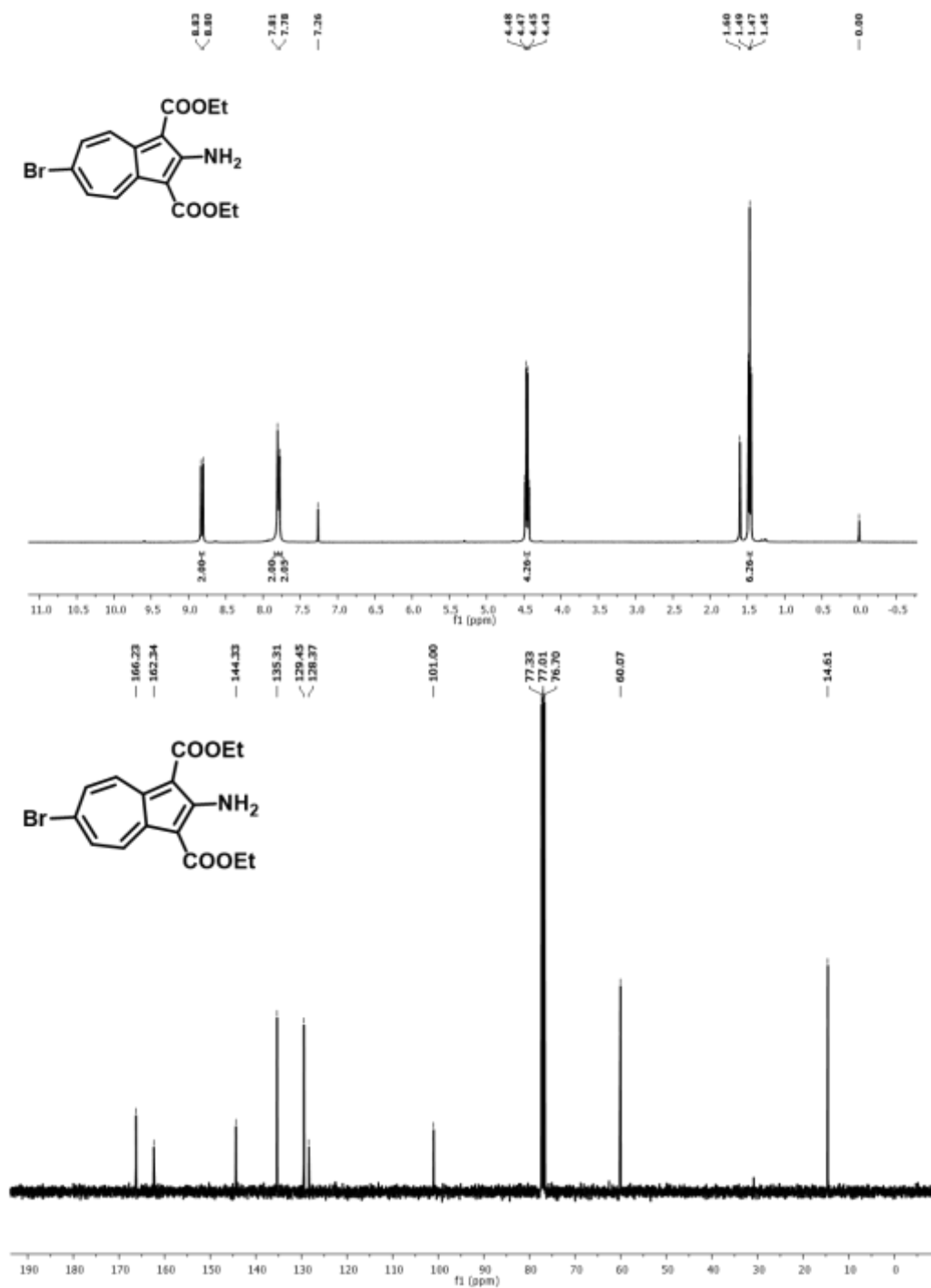
1. Synthesis of Diethyl 2-amino-6-bromoazulene-1,3-dicarboxylate (**2**)

Diethyl 2-amino-6-bromoazulene-1,3-dicarboxylate (**2**) was synthesized from commercially available Tropolone by following the reported procedure.<sup>9, 16</sup>

2. Procedure for the preparation of Silver complex Az-C-Ag (**8**)

Az-C (**4**) (.025 mmol, 2.0 equiv.) was dissolved in MeOH (2 ml). To this solution, another solution (0.5 ml) of AgNO<sub>3</sub> (0.12 mmol, 1.0 equiv.) was added slowly. The mixture was heated under reflux (77 °C) for 2 h in the dark. The solution was filtered while still warm. After cooling it to room temperature diethyl ether solution was added to precipitate the compound. The compound was dried under reduced pressure, washed with n-pentane and dried again, giving the product (**8**) in 62% yield.



3.  $^1\text{H}$ ,  $^{13}\text{C}$  NMR (400MHz,  $\text{CDCl}_3$ ) and HRMS of compound **2****Figure A1.**  $^1\text{H}/^{13}\text{C}$  NMR (400MHz,  $\text{CDCl}_3$ ) spectra of compound **2**.

## Display Report

## Analysis Info

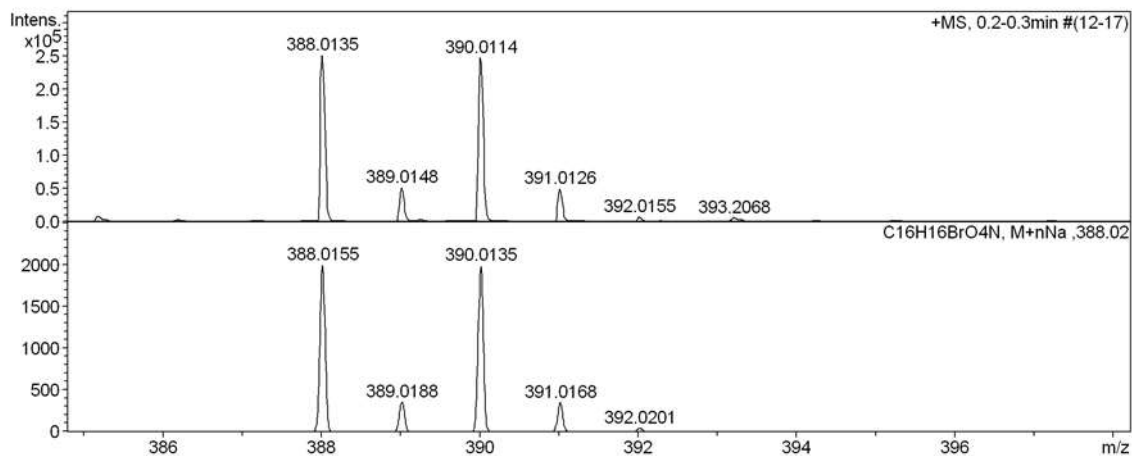
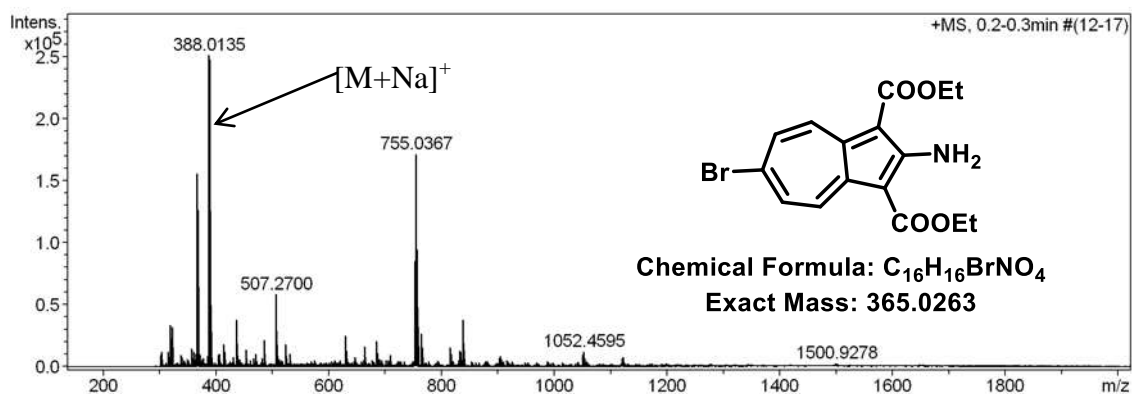
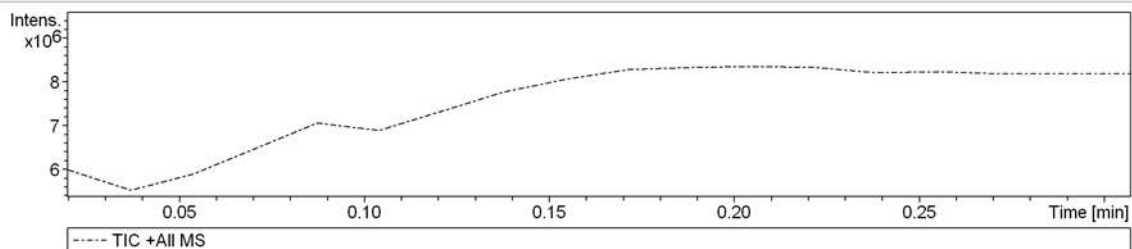
Analysis Name D:\Data\JULY-2020\NKS\26072020\_NKS\_SNM-braz.d  
 Method pos tune\_wide\_030118.m  
 Sample Name Tmix-131118  
 Comment

Acquisition Date 7/26/2020 8:30:50 PM

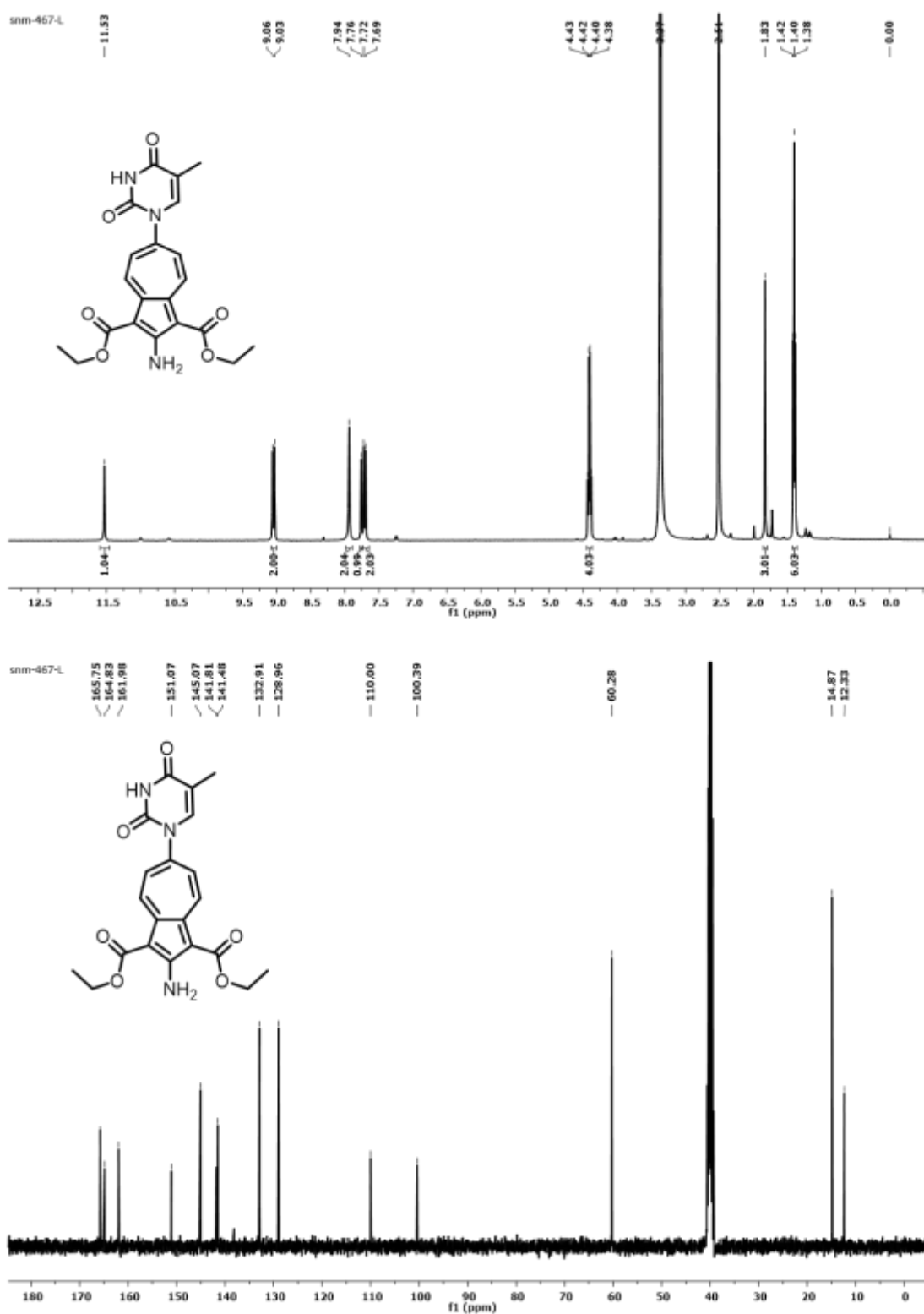
Operator PRAKASH BEHERA  
 Instrument micrOTOF-Q II 10337

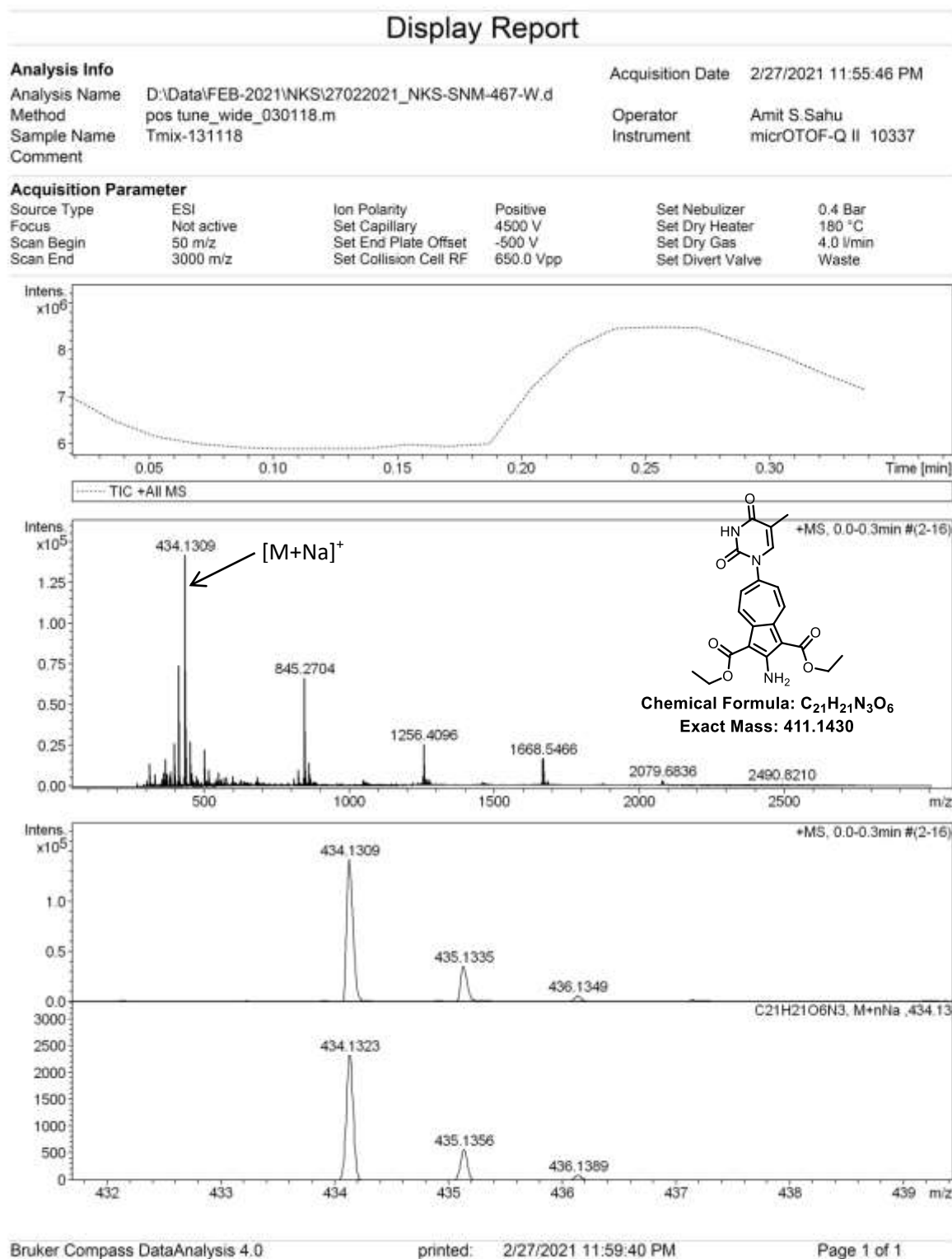
## Acquisition Parameter

Source Type	ESI	Ion Polarity	Positive	Set Nebulizer	0.4 Bar
Focus	Not active	Set Capillary	4500 V	Set Dry Heater	180 °C
Scan Begin	50 m/z	Set End Plate Offset	-500 V	Set Dry Gas	4.0 l/min
Scan End	3000 m/z	Set Collision Cell RF	650.0 Vpp	Set Divert Valve	Waste

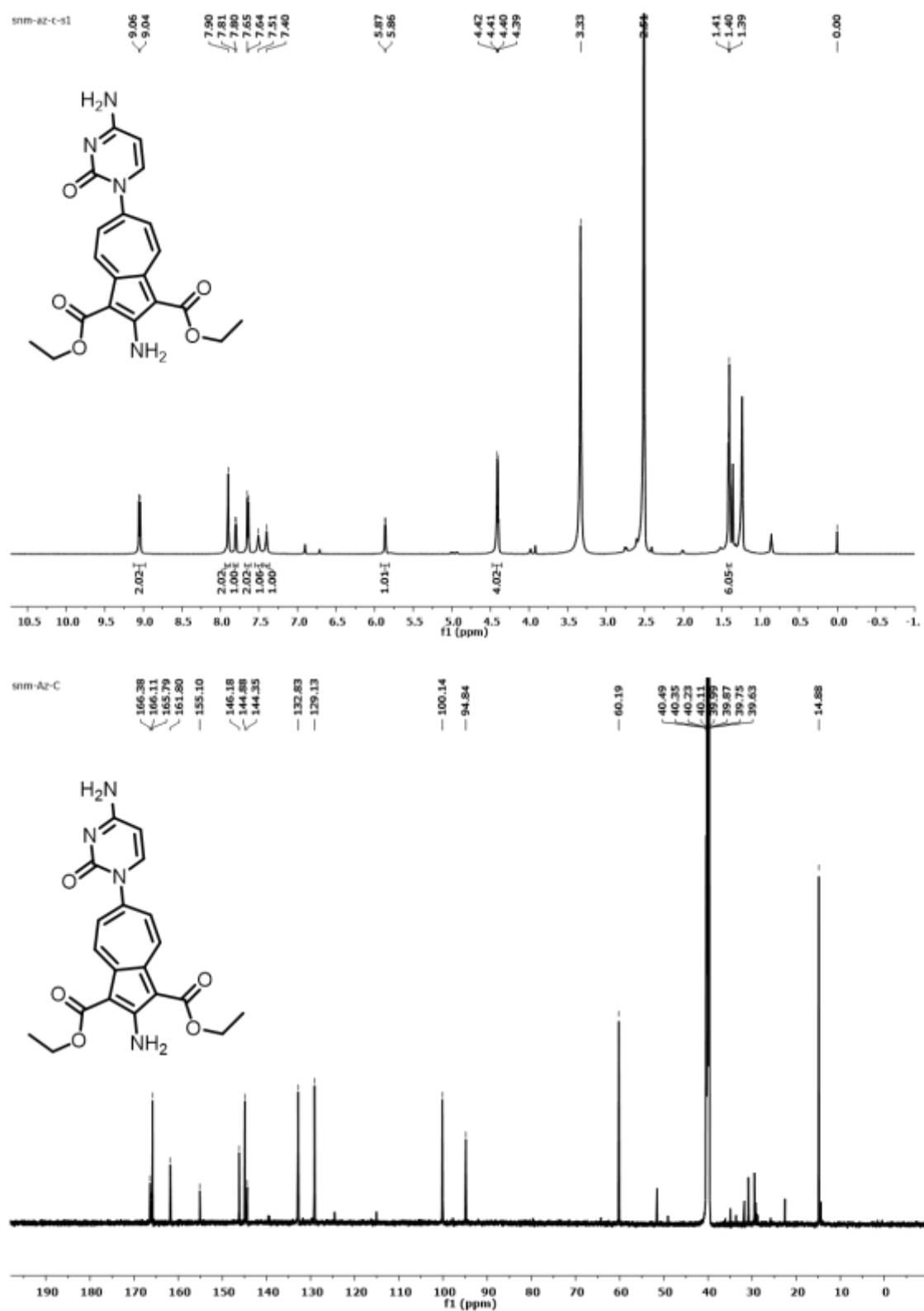


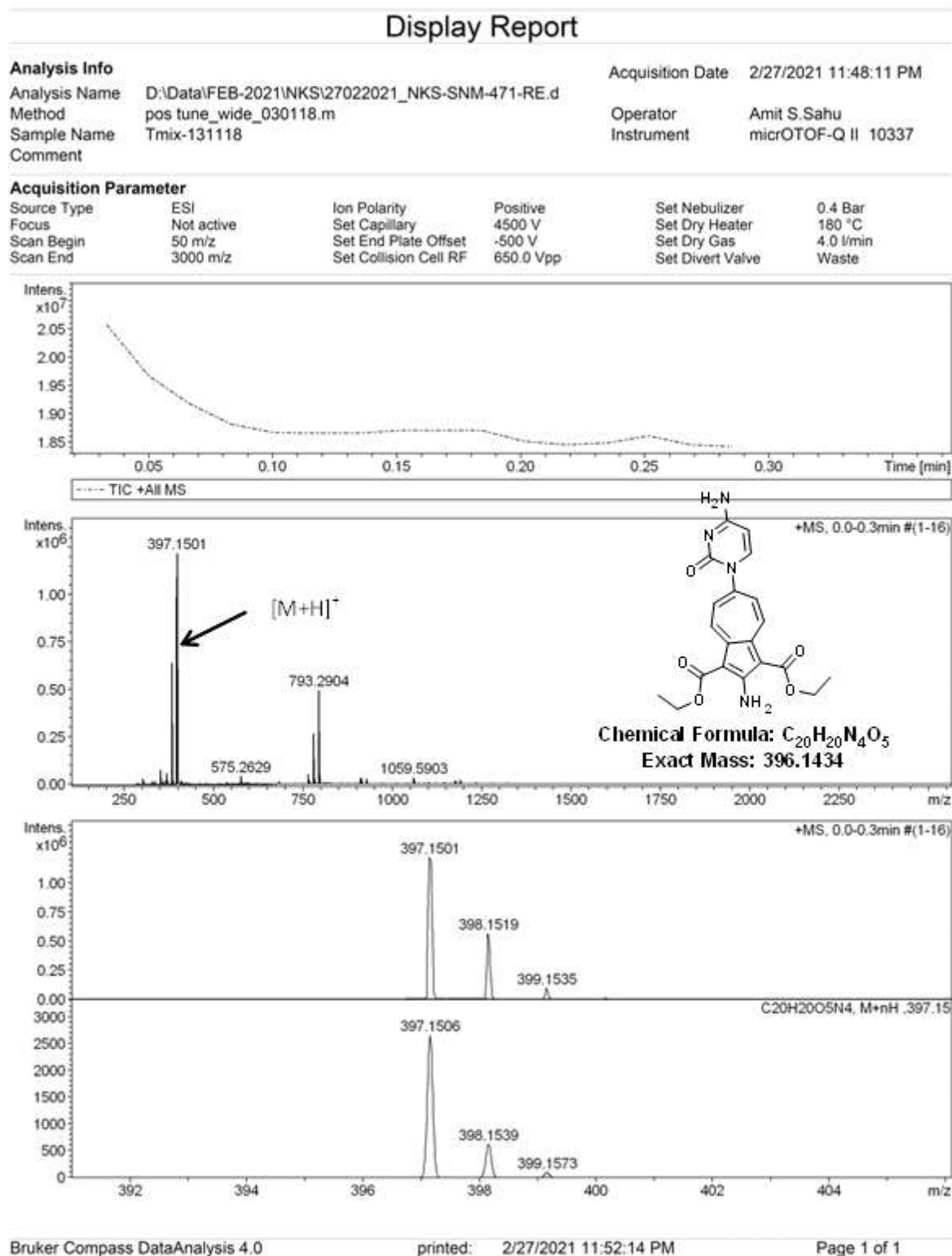
**Figure A2.** ESI-MS/HRMS spectra of compound **2**.

4.  $^1\text{H}$ ,  $^{13}\text{C}$  NMR (400MHz, DMSO) and HRMS of compound **3****Figure A3.**  $^1\text{H}/^{13}\text{C}$  NMR (400MHz, DMSO) spectra of compound **3** in DMSO-  $d_6$ .

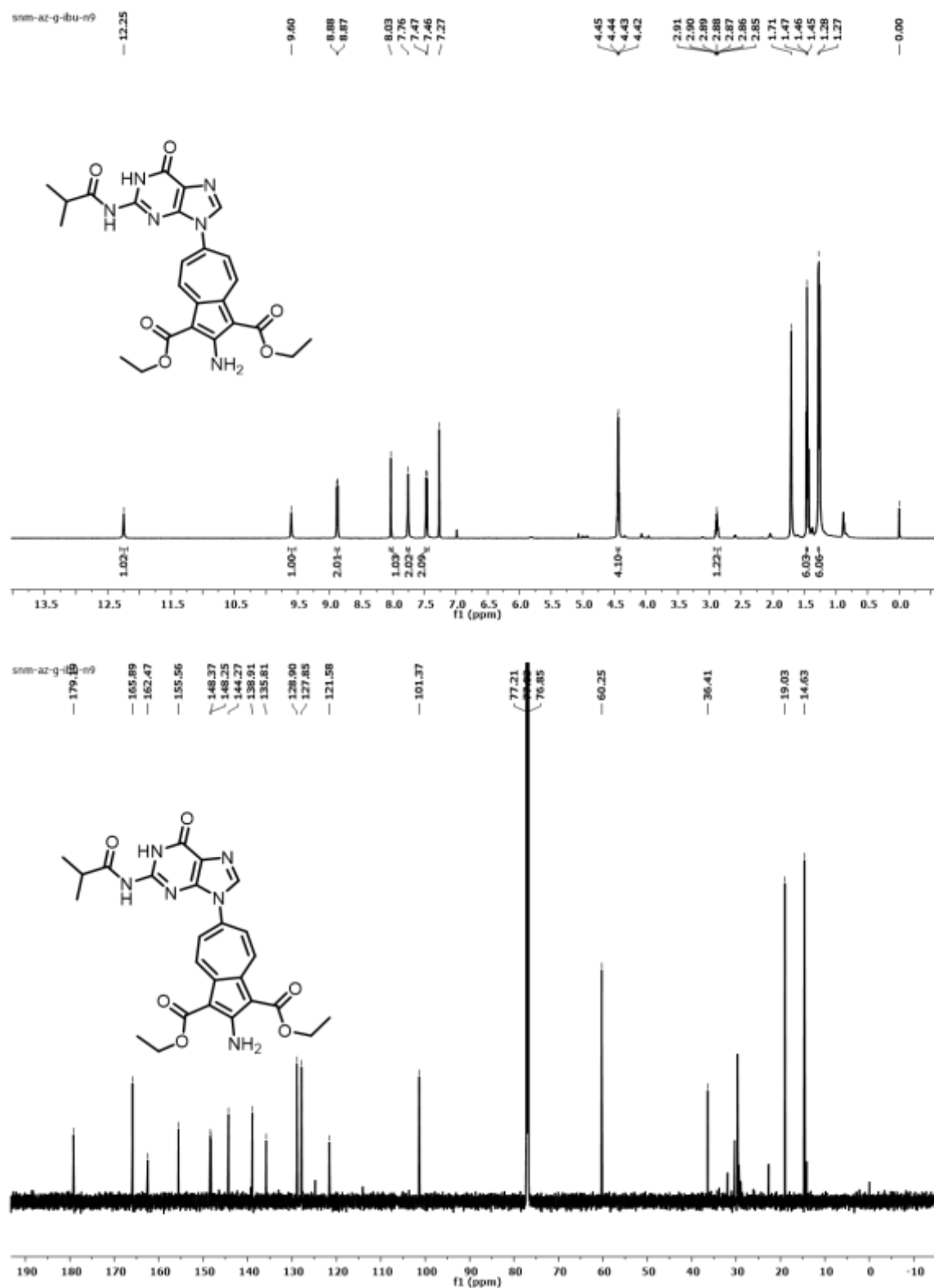


**Figure A4.** ESI-MS/HRMS spectra of compound **3**.

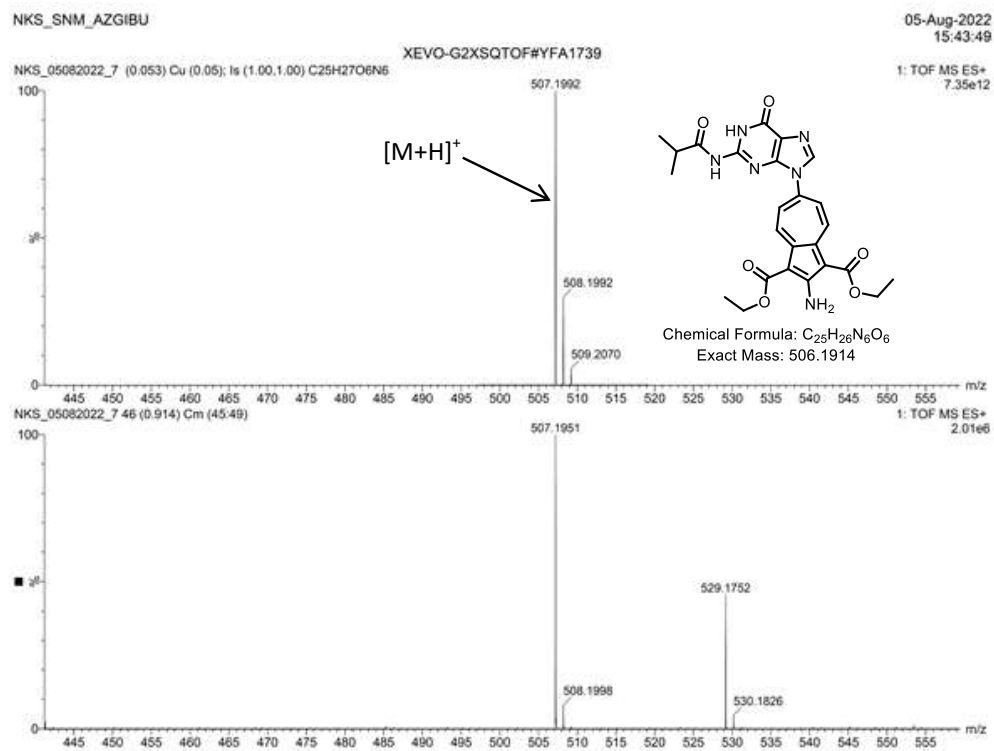
5.  $^1\text{H}$ ,  $^{13}\text{C}$  NMR (700MHz, DMSO) and HRMS of compound **4****Figure A5.**  $^1\text{H}/^{13}\text{C}$  NMR (700MHz, DMSO) spectra of compound **4** in DMSO- $d_6$ .



**Figure A6.** ESI-MS/HRMS spectra of compound **4**.

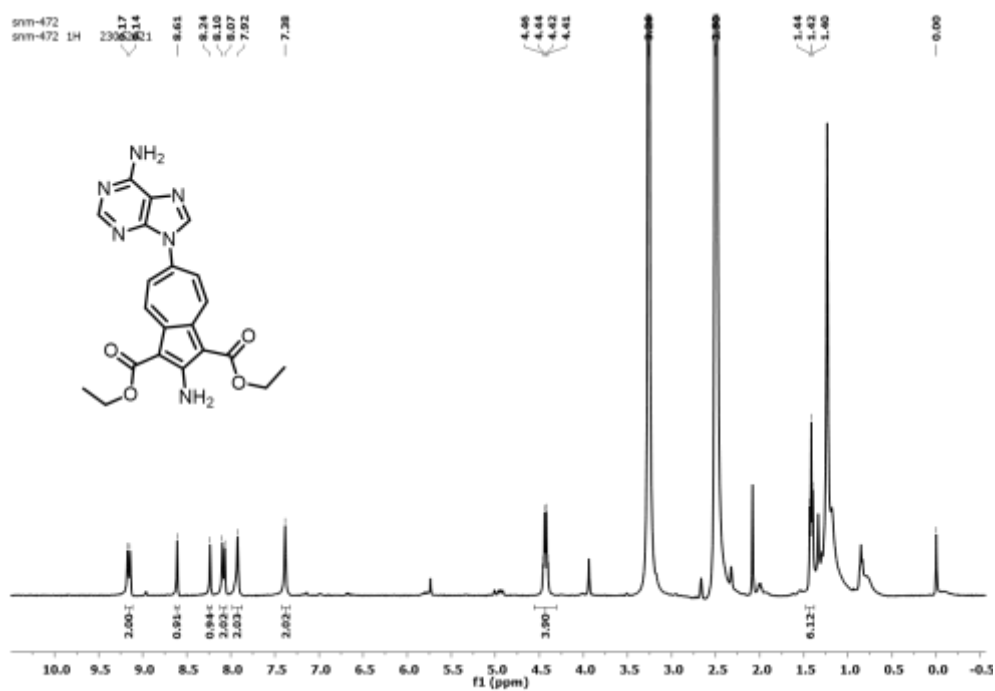
6.  $^1\text{H}$ ,  $^{13}\text{C}$  NMR (700MHz,  $\text{CDCl}_3$ ) and HRMS of compound **7**Figure A7.  $^1\text{H}/^{13}\text{C}$  NMR (700MHz,  $\text{CDCl}_3$ ) spectra of compound **7** in  $\text{CDCl}_3$ .



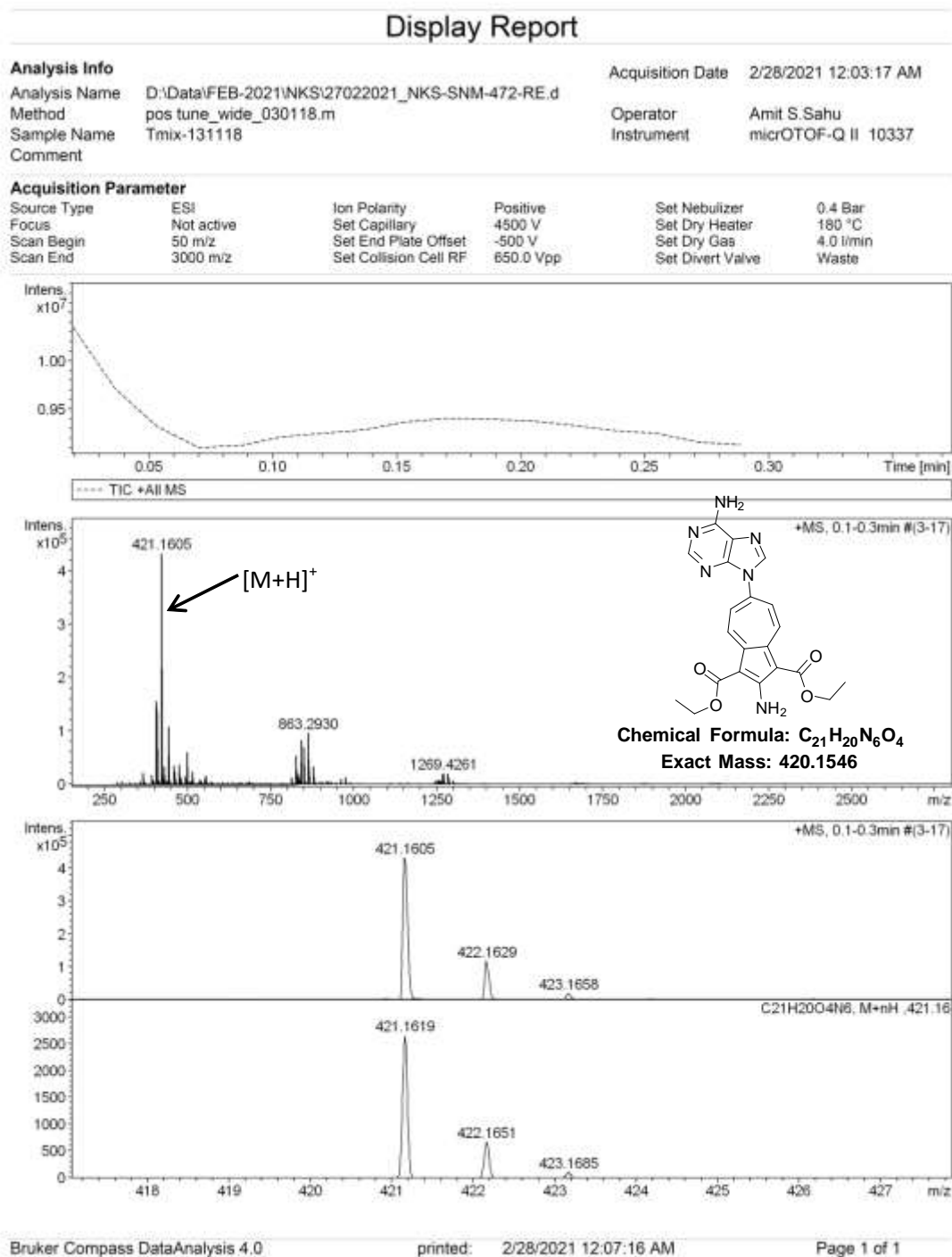


**Figure A8.** ESI-MS/HRMS spectra of compound **7**

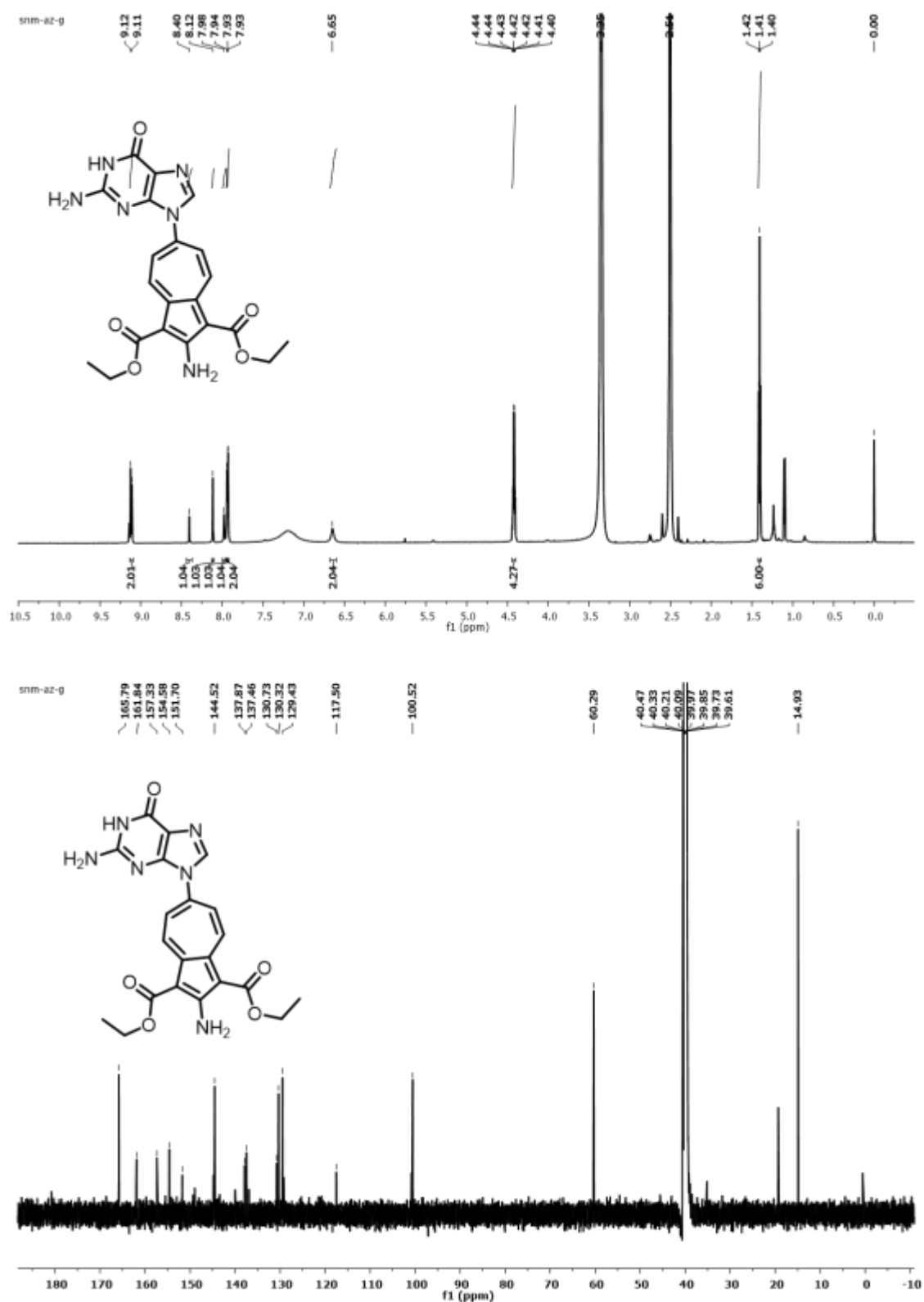
7. <sup>1</sup>H NMR (400MHz, CDCl<sub>3</sub>) and HRMS of compound **5**



**Figure A9.** <sup>1</sup>H NMR (400MHz, CDCl<sub>3</sub>) spectra of compound **5** in DMSO-d<sub>6</sub>.



**Figure A10.** ESI-MS/HRMS spectra of compound **5**.

8.  $^1\text{H}$ ,  $^{13}\text{C}$  NMR (700MHz,  $\text{CDCl}_3$ ) and HRMS of compound **6**Figure A11.  $^1\text{H}/^{13}\text{C}$  NMR (700MHz,  $\text{DMSO}$ ) spectra of compound **6** in  $\text{DMSO-d}_6$ .

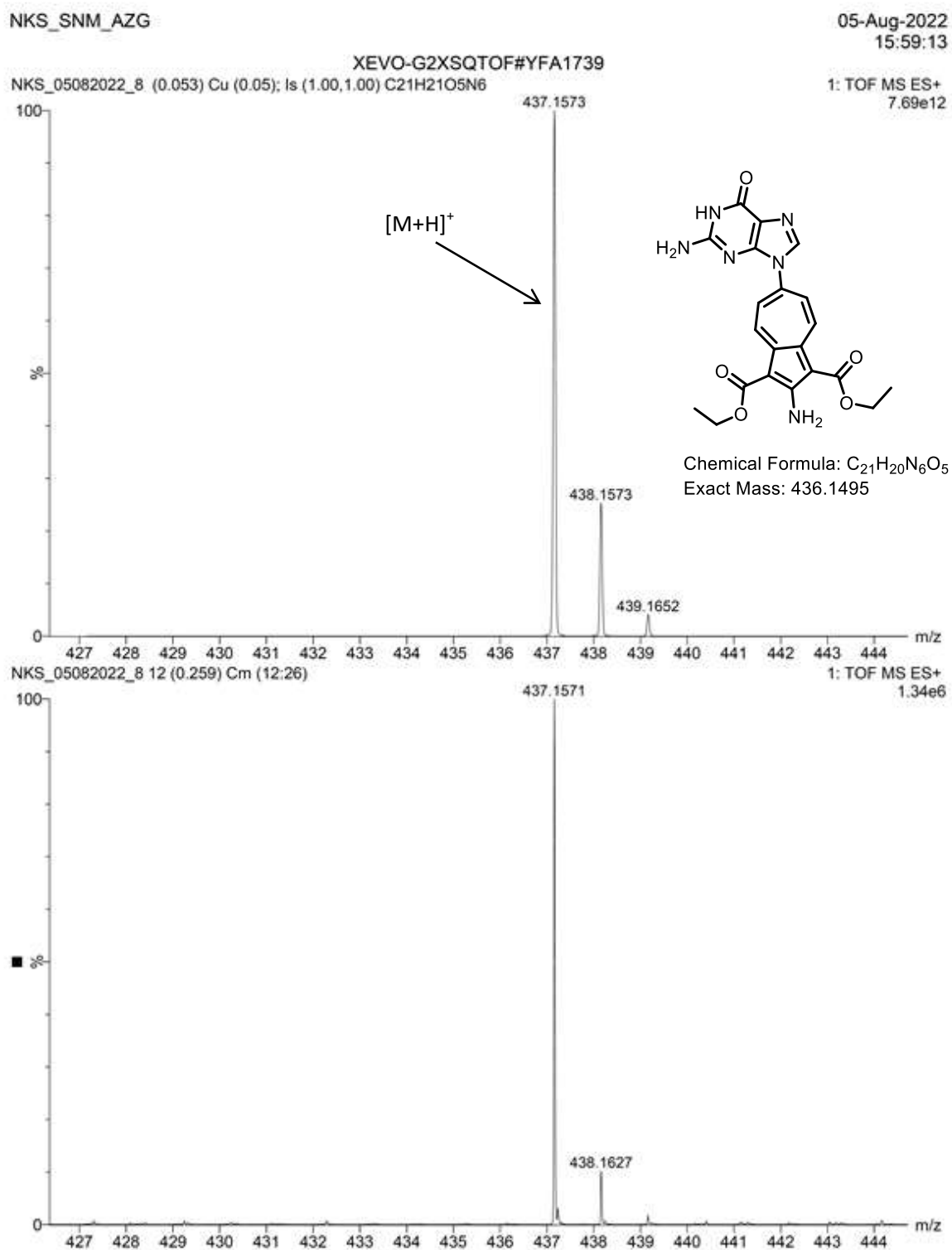


**Figure A12.** ESI-MS/HRMS spectra of compound **6**.

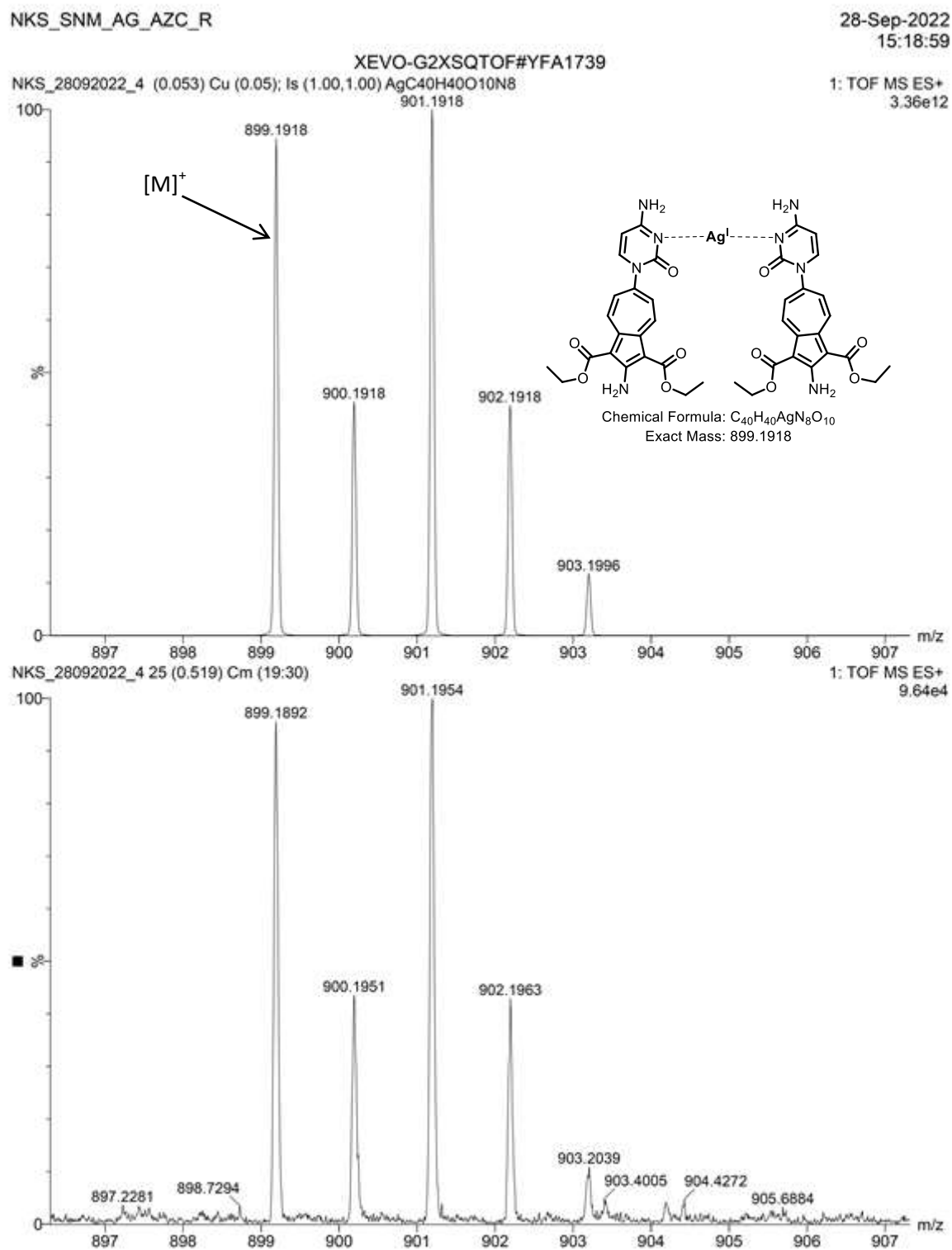
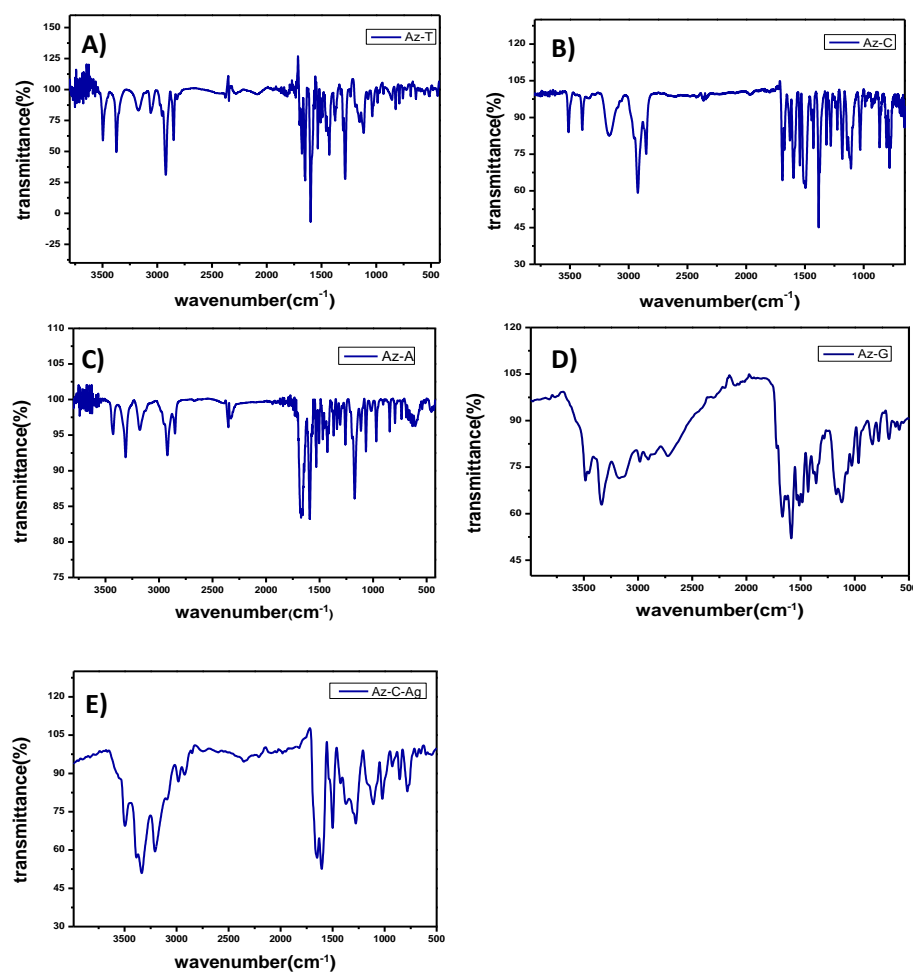


Figure A13. ESI-MS/HRMS spectra of compound **8**.

## 9. FT-IR Spectra



**Figure S14.** FT-IR spectra of compounds **3** (A), **4** (B), **5** (C), **6** (D) and **8** (E).

## 10. Crystal structures and data

Good quality crystals of compounds were obtained in solvent DMSO at 4 °C by slow evaporation method. The crystals data of compound **3** and **4** were collected on a Rigaku Oxford diffractometer at 293 K. Selected data collection parameters and other crystallographic results are summarized below. The program package SHELXTL1 and Olex2 was used for structure solution and packing diagram carried out by DIAMOND3.2 software.

CCDC **2224909** and **2224908** contains the supplementary crystallographic data for Az-T (**3**) and Az-C (**4**) respectively. These data can be obtained free of charge via <https://www.ccdc.cam.ac.uk/data>

**Table A1. Crystal data and structure refinement for Az-C (4)**

Identification code	NKS_SNM_AZ_C (1)
Empirical formula	C <sub>20</sub> H <sub>20</sub> N <sub>4</sub> O <sub>5</sub>
Formula weight	396.41
Temperature/K	303(2)
Crystal system	triclinic
Space group	P-1
a/Å	6.8930(1)
b/Å	12.3968(2)
c/Å	15.7410(2)
α/°	99.503(1)
β/°	93.061(1)
γ/°	100.462(1)
Volume/Å <sup>3</sup>	1299.74(3)
Z	2
ρ <sub>calc</sub> /g/cm <sup>3</sup>	1.0128
μ/mm <sup>-1</sup>	0.619
F(000)	417.5
Crystal size/mm <sup>3</sup>	0.01 × 0.001 × 0.001
Radiation	Cu Kα (λ = 1.54184)
2θ range for data collection/°	10.1 to 151.06
Index ranges	-8 ≤ h ≤ 6, -15 ≤ k ≤ 15, -19 ≤ l ≤ 19
Reflections collected	19861
Independent reflections	5195 [R <sub>int</sub> = 0.2111, R <sub>sigma</sub> = 0.2123]
Data/restraints/parameters	5195/0/264
Goodness-of-fit on F <sup>2</sup>	1.046
Final R indexes [I ≥ 2σ (I)]	R <sub>1</sub> = 0.0694, wR <sub>2</sub> = 0.2080
Final R indexes [all data]	R <sub>1</sub> = 0.1022, wR <sub>2</sub> = 0.2215
Largest diff. peak/hole / e Å <sup>-3</sup>	1.40/-1.20

**Table A2. Crystal data and structure refinement for Az-T (3)**

Identification code	SNM-T AZ
Empirical formula	C <sub>23</sub> H <sub>27</sub> N <sub>3</sub> O <sub>7</sub> S
Formula weight	489.55
Temperature/K	256(40)
Crystal system	triclinic

Space group	P-1
a/Å	8.7670(1)
b/Å	10.6359(2)
c/Å	14.1150(2)
$\alpha/^\circ$	108.665(1)
$\beta/^\circ$	99.074(1)
$\gamma/^\circ$	101.146(1)
Volume/Å <sup>3</sup>	1188.79(3)
Z	2
$\rho_{\text{calc}}/\text{g cm}^{-3}$	1.3675
$\mu/\text{mm}^{-1}$	1.632
F(000)	518.4
Crystal size/mm <sup>3</sup>	0.01 × 0.001 × 0.001
Radiation	Cu K $\alpha$ ( $\lambda$ = 1.54184)
2 $\Theta$ range for data collection/ $^\circ$	6.8 to 150.92
Index ranges	-10 ≤ h ≤ 8, -13 ≤ k ≤ 12, -17 ≤ l ≤ 17
Reflections collected	18490
Independent reflections	4820 [ $R_{\text{int}}$ = 0.0394, $R_{\text{sigma}}$ = 0.0277]
Data/restraints/parameters	4820/0/312
Goodness-of-fit on $F^2$	1.027
Final R indexes [ $I \geq 2\sigma(I)$ ]	$R_1$ = 0.0442, $wR_2$ = 0.1372
Final R indexes [all data]	$R_1$ = 0.0463, $wR_2$ = 0.1404
Largest diff. peak/hole / e Å <sup>-3</sup>	0.50/-0.37

## 11. Photophysical studies

All the UV –Visible spectra of the compounds **3**, **4**, **5**, **6** and **8** (10  $\mu\text{M}$ ) were measured in MeOH solvent using a UV-Visible spectrophotometer with a cell of 1 cm path length. All spectroscopy samples were prepared from concentrated DMSO stock solutions; hence, all samples contain 0.4 v% or 0.2 v% DMSO.

**Table A3.** Photophysical parameters of compounds **3**, **4**, **5**, **7** and **8**

S. N.	Compound	$\lambda_{\text{abs}}(\text{nm})$	Absorbance	$\epsilon_{331}(\text{M}^{-1} \text{cm}^{-1})$
1	Az-T ( <b>3</b> )	331	0.301	30100
2	Az-C ( <b>4</b> )	331	0.532	53200
3	Az-A ( <b>5</b> )	331	0.348	34800
4	Az-G ( <b>6</b> )	331	0.301	30100
5	Az-C-Ag ( <b>8</b> )	310	0.527	52700



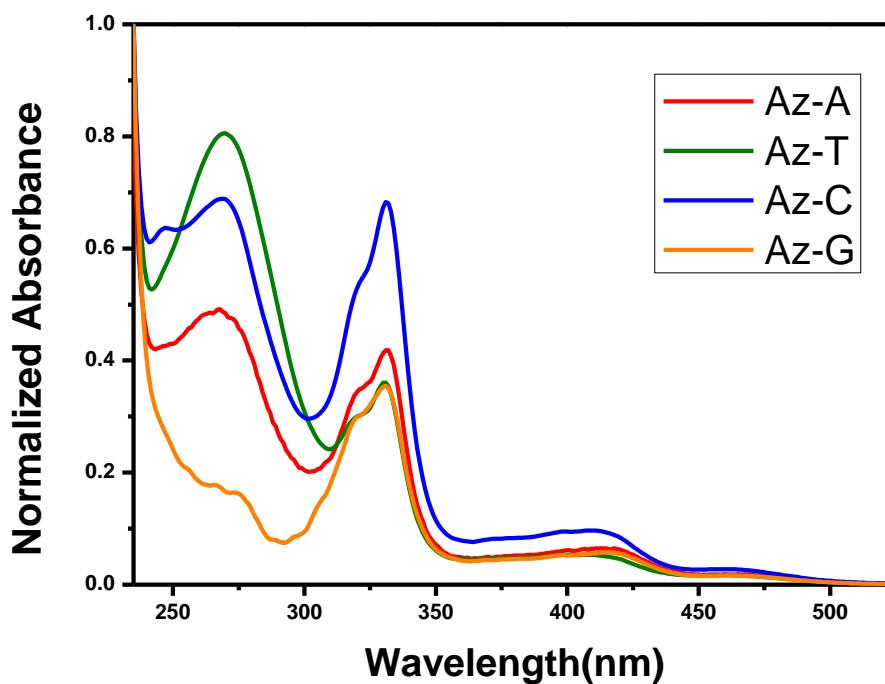


**Figure A15.** UV-Vis spectra of Az-T (**3**), Az-C (**4**), Az-A (**5**) and Az-G (**6**).

## 12. Optimized structure and HOMO- LUMO energy gap

The HOMO-LUMO energy gap for compounds Az-T (**3**), Az-C (**4**), Az-A (**5**) and Az-G (**6**) has been calculated using Gaussian 09 software and B3LYP/6-31+G\* level of theory in vacuum.

**Table A4.** Calculated HOMO and LUMO gap at B3LYP/6-31+G\* level of theory in vacuum

S.N.	Cpd	HOMO (eV)	LUMO (eV)	$\Delta$ (eV)
1	Az-C	-5.5488	-2.067	-3.482
2	Az-A	-5.6032	-2.122	-3.482
3	Az-T	-5.7664	-2.258	-3.509
4	Az-G	-6.0112	-2.502	-3.509

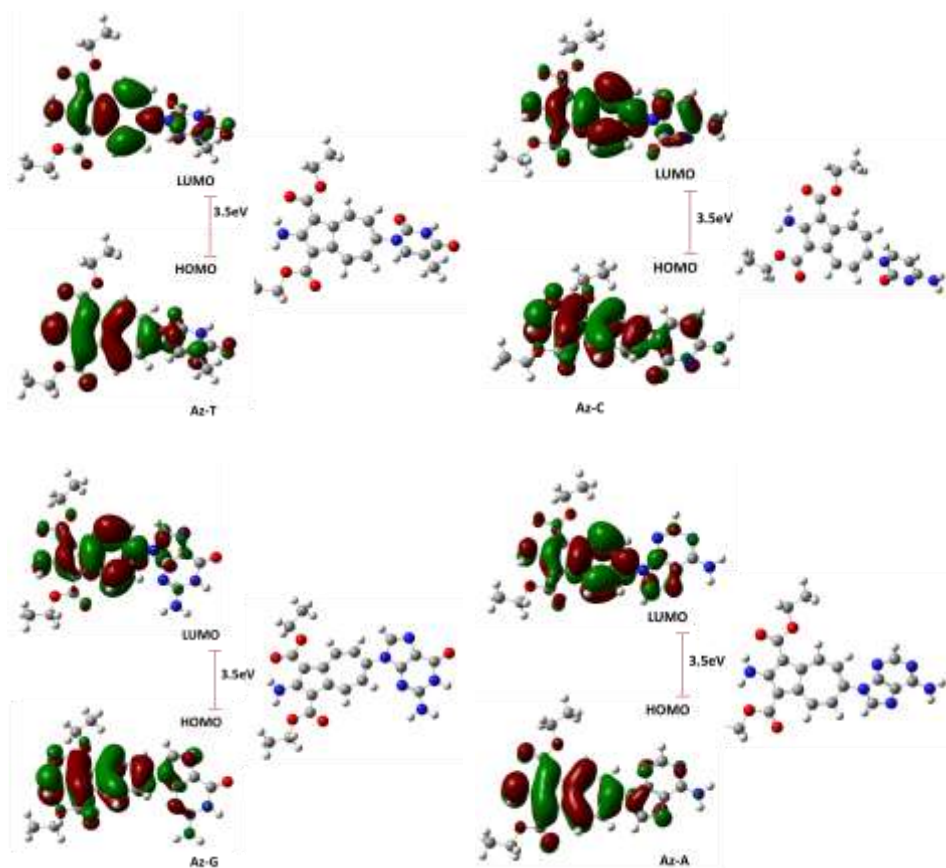


**Figure A16.** Optimized structure and HOMO- LUMO energy gap (atomic unit in eV) of compounds Az-T (**3**), Az-C (**4**), Az-A (**5**) and Az-G (**6**) at B3LYP/6-31+G\* level of theory in vacuum.

### 13. Field Emission Scanning Electronic Microscopy (FESEM) and High-Resolution Transmission Electron Microscopy (HRTEM)

Thin layer of samples of Az-T (**3**), Az-C (**4**), Az-A (**5**), Az-G (**6**) and Az-C-Ag complex (**8**) were prepared individually by drop casting EtOH solution of the samples on silicon wafer. These wafers were dried and kept under vacuum before recording their SEM-images. SEM images at nano-scales, at selectively resolution (~200 nm to ~2-10  $\mu\text{m}$ ) are illustrated along with Elemental mapping and EDAX spectrum in following Figures. For TEM images a dilute solution of the sample was prepared in ethanol solvent and drop casted onto a copper grid (200 mesh) and dried properly prior to the HRTEM analysis.

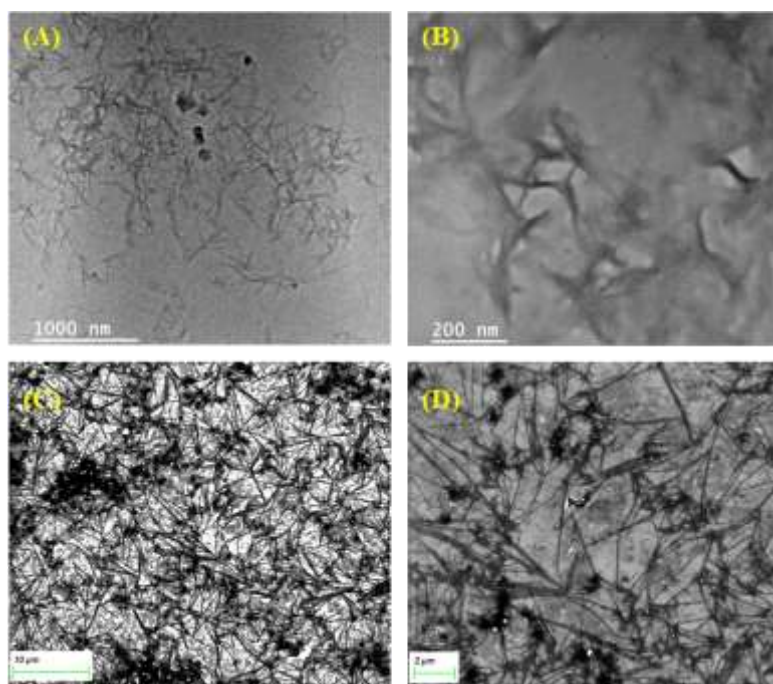


**Figure A18.** HRTEM images (A, B) and FESEM images (C, D) for compound **5** (Az-A) at different magnification.

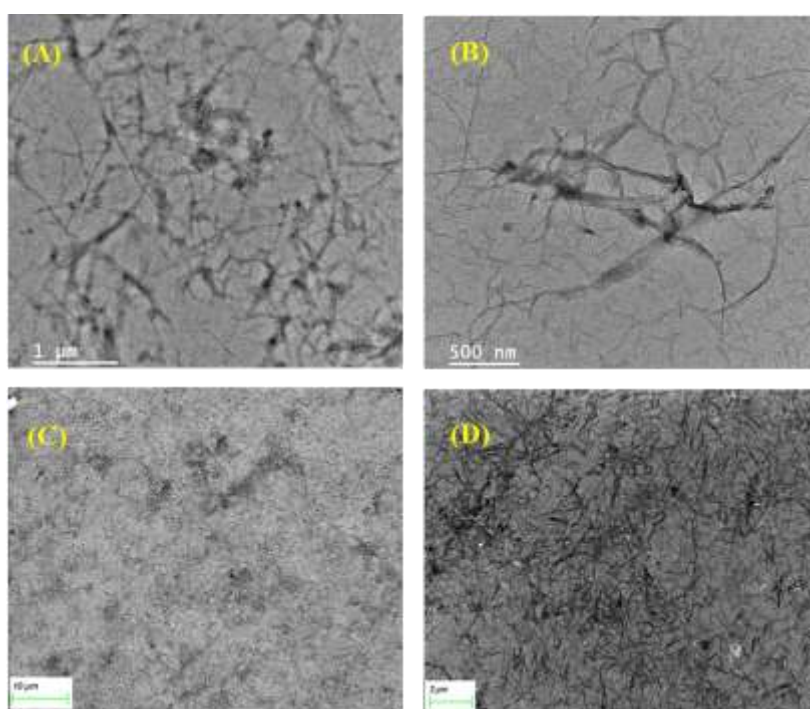


**Figure A19.** HRTEM images (A, B) and FESEM images (C, D) for compound **6** (Az-G) at different magnification.

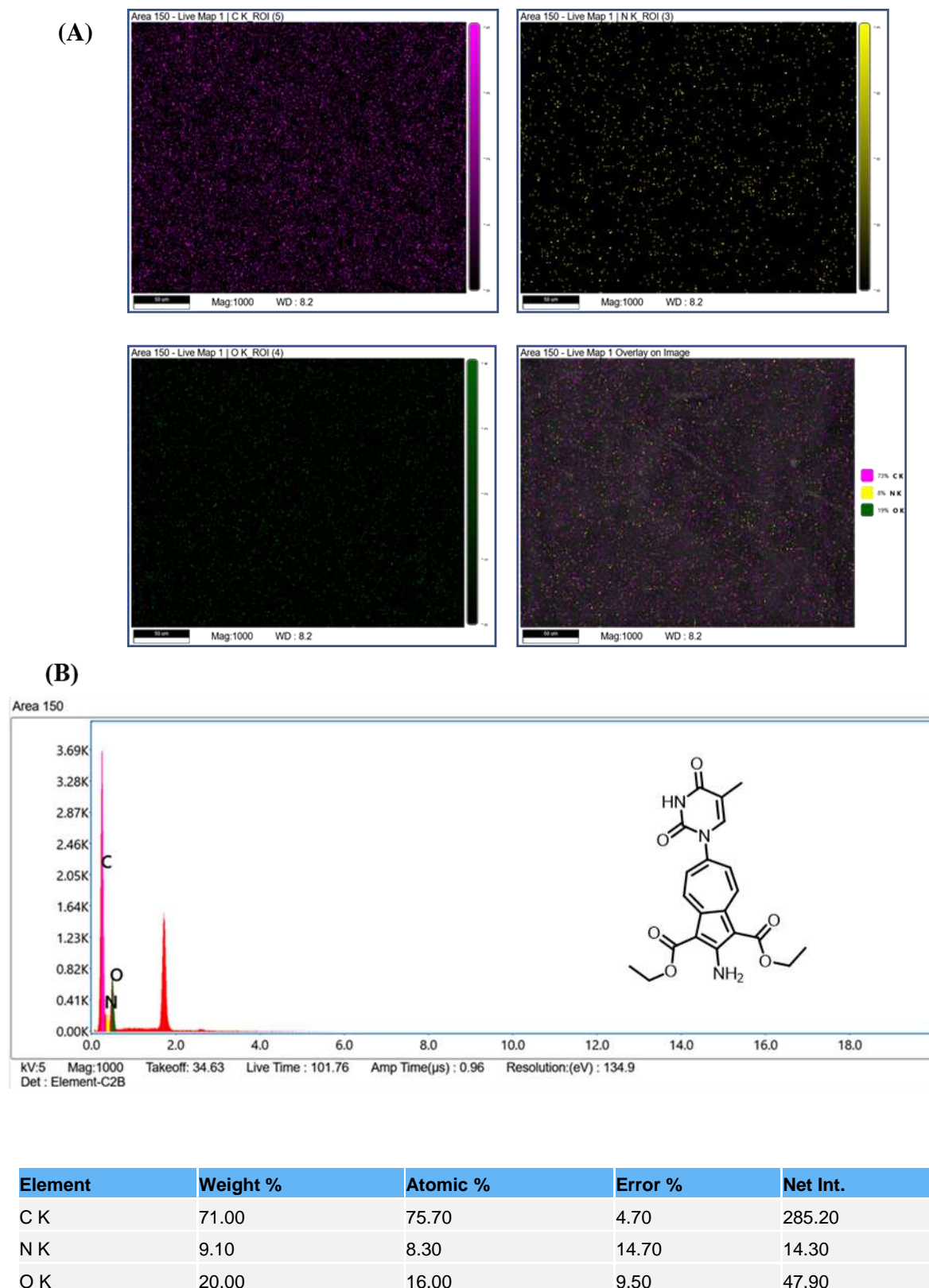


**Figure A20.** (A) Elemental mapping and (B) EDAX spectrum of compound **4** (Az-C) showing the presence of C, N and O.

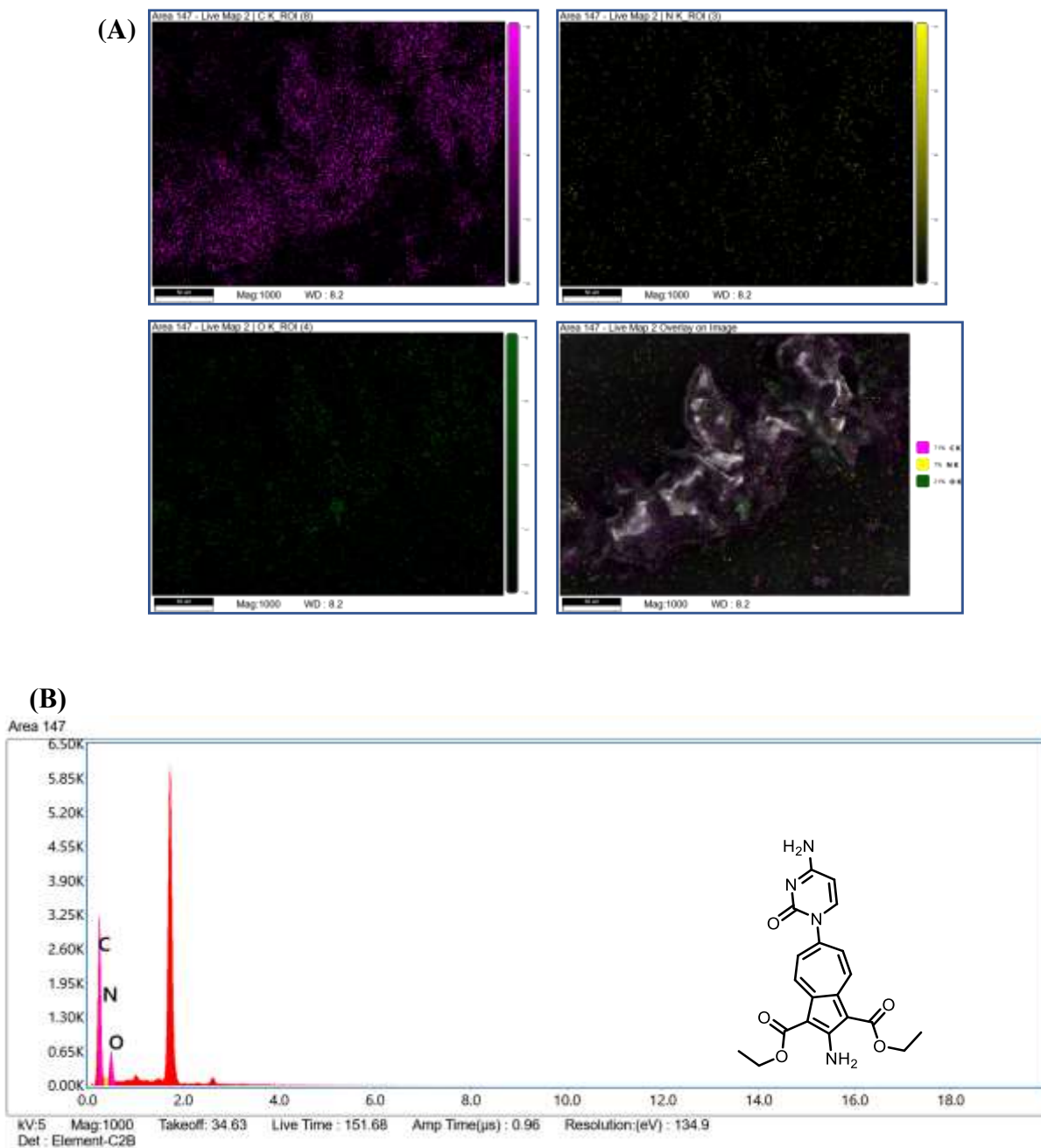
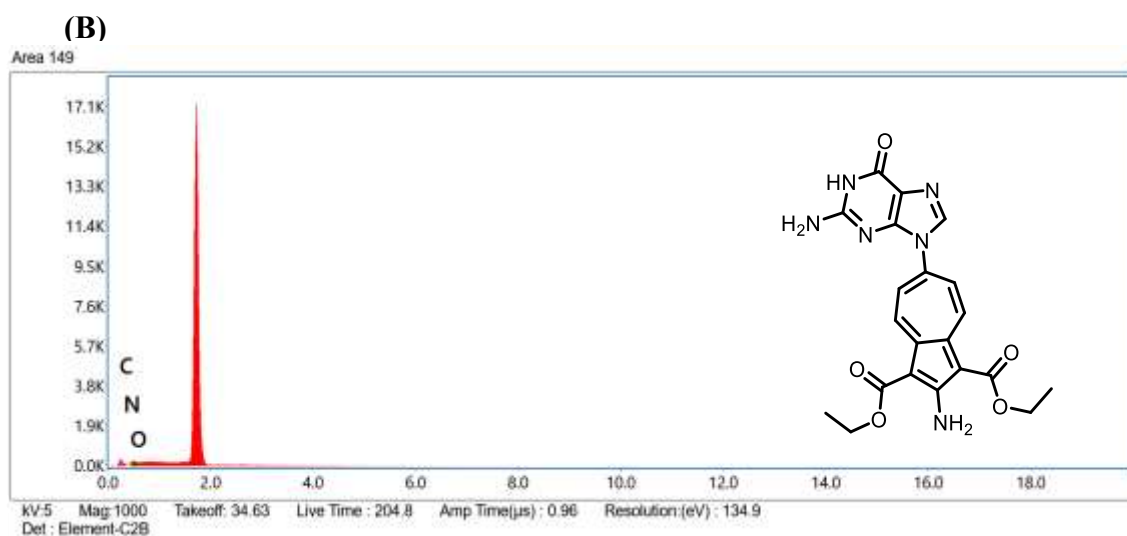
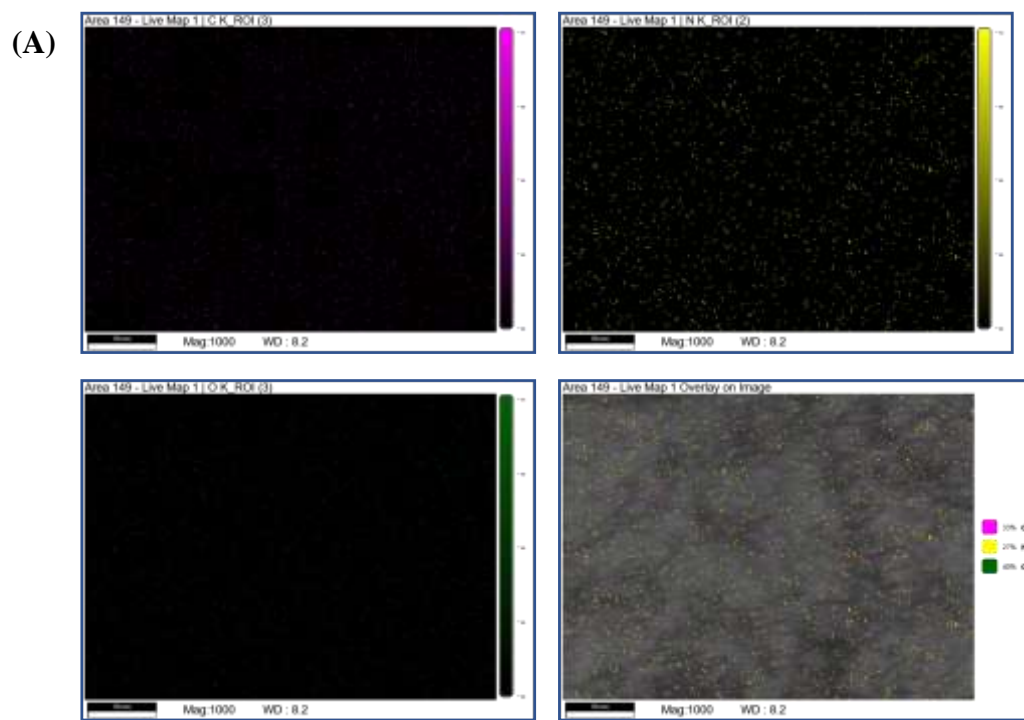


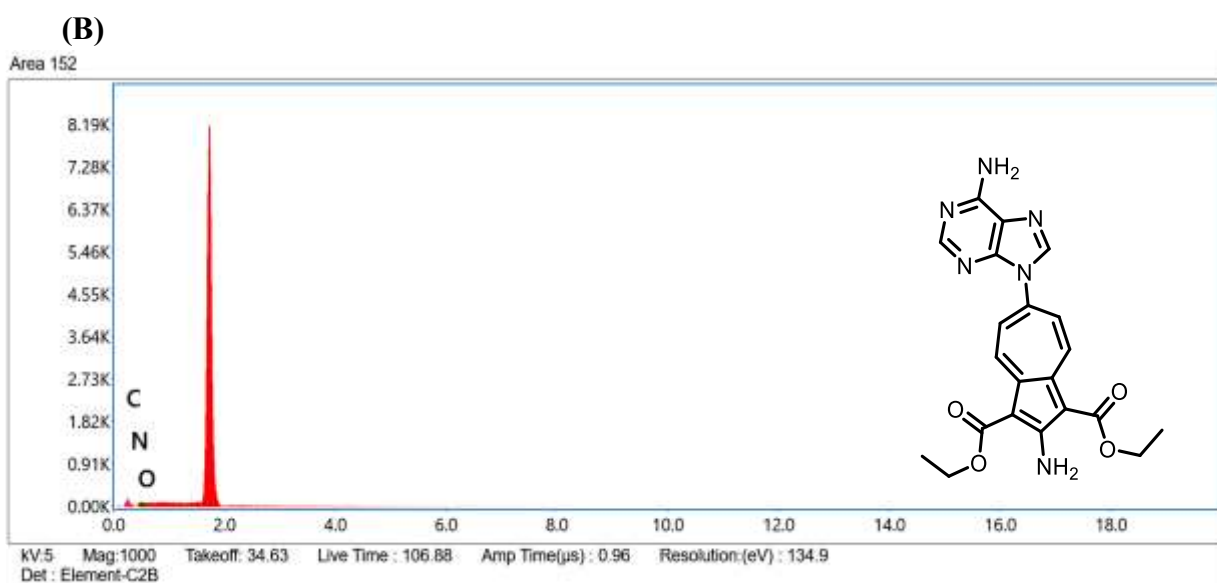
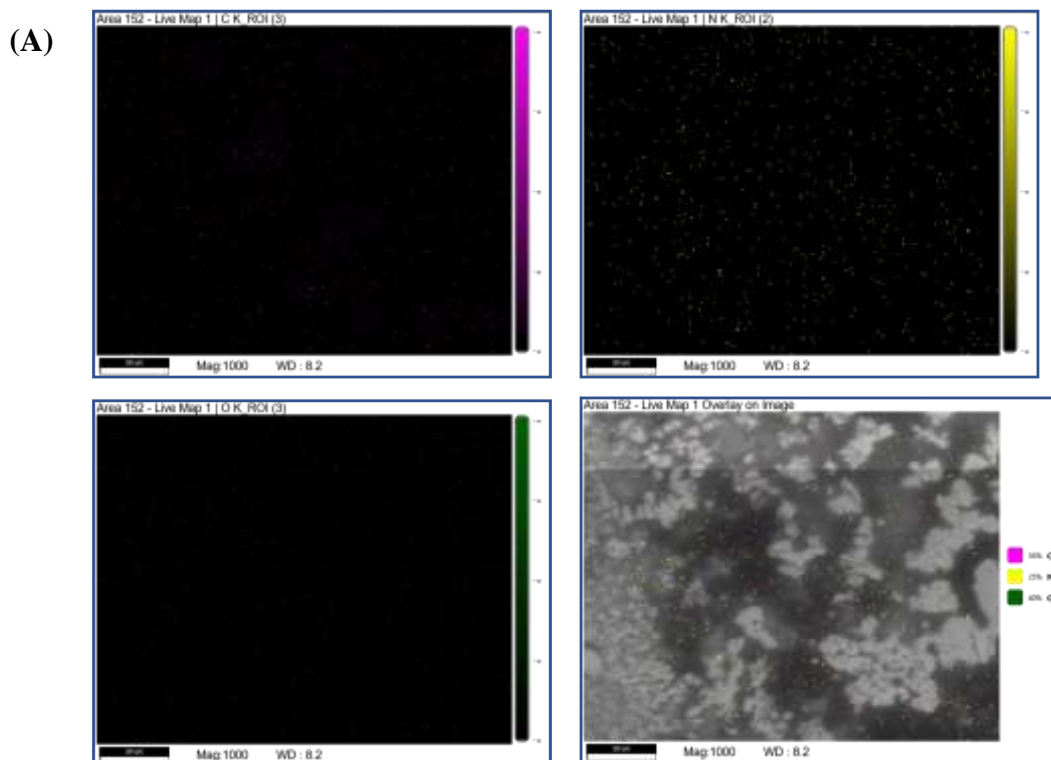
**Figure A21.** (A) Elemental mapping and (B) EDAX spectrum of compound **3** (Az-T) showing the presence of C, N and O.





Element	Weight %	Atomic %	Error %	Net Int.
C K	42.70	48.40	7.90	11.70
N K	23.30	22.70	17.40	3.40
O K	34.00	28.90	14.30	6.00

**Figure A22.** (A) Elemental mapping and (B) EDAX spectrum of compound **6** (Az-G) showing the presence of C, N and O.



Element	Weight %	Atomic %	Error %	Net Int.
C K	46.30	52.30	8.60	12.80
N K	19.10	18.50	25.60	2.70
O K	34.60	29.30	15.50	6.20

**Figure A23.** (A) Elemental mapping and (B) EDAX spectrum of compound **5** (Az-A) showing the presence of C, N and O.

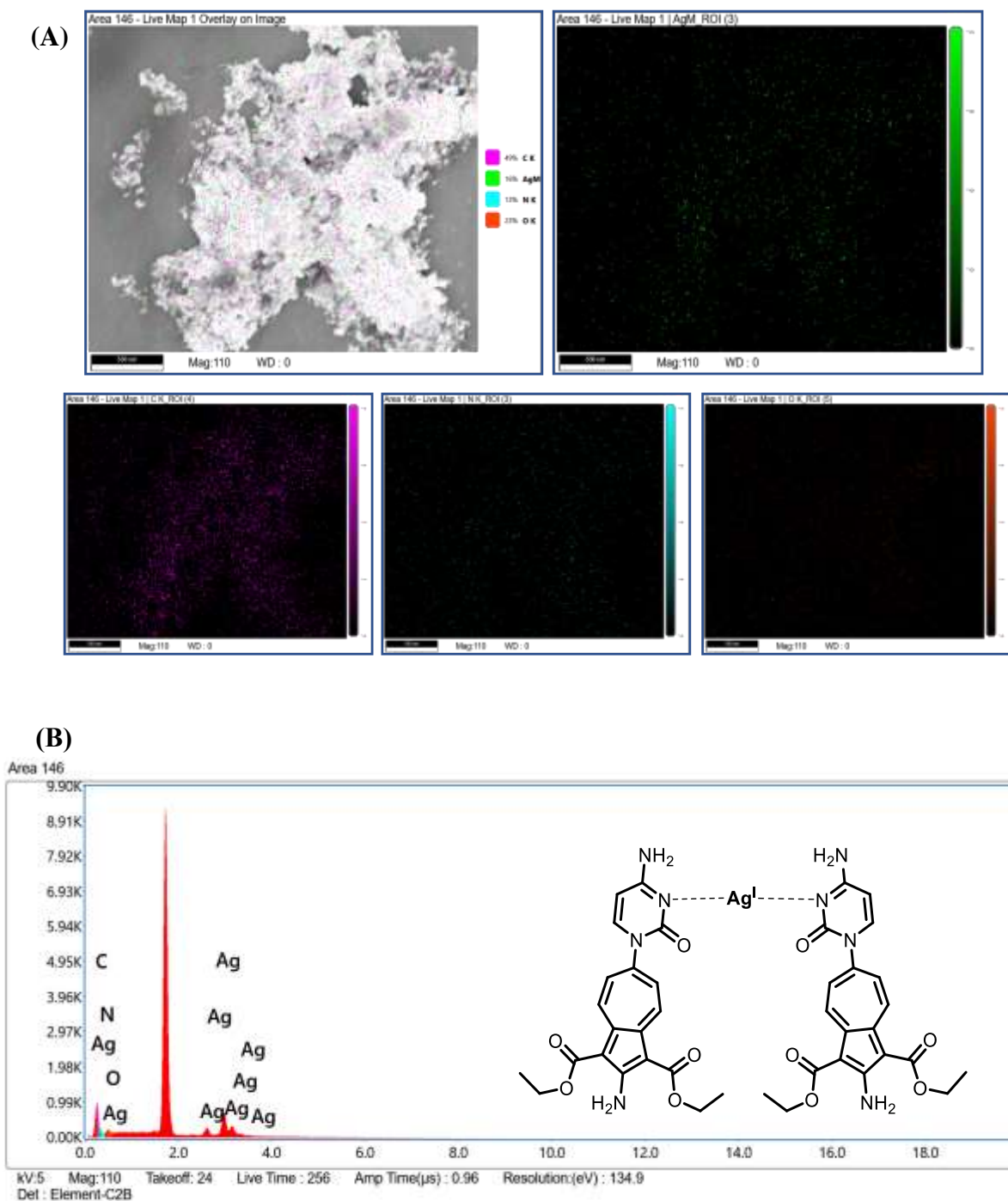


**Figure A24.** (A) Elemental mapping and (B) EDAX spectrum of compound **8** (Az-C-Ag complex) showing the presence of C, N, O and Ag.



## **CHAPTER 4**

### **PART-B**

---

#### **Azulene Tethered C-nucleoside: Synthesis and Morphological studies**

---

##### **4B.1 Introduction**

##### **4B.2 Objective**

##### **4B.3 Results and Discussion**

##### **4B.4 Conclusion**

##### **4B.5 Experimental Section**

##### **4B.6 References and Notes**

##### **4B.7 Appendix**

### 4B.1 Introduction

Nucleic acids (DNA/RNA) are undeniably one of the most fundamental biomolecules involved in the origins of chemical evolution, which stores, transfers, and replicates genetic information.<sup>1</sup> These molecules contain the natural *N*-glycosidic bond connecting the anomeric carbon of a sugar moiety to the nitrogen atom of a heterocyclic base.<sup>2</sup> One effective method for examining nucleic acid structure and function is to alter the base moiety linked to ribose unit, which resulted in the synthesis of many non-natural analogs of DNA nucleosides in recent years.<sup>3–6</sup> C-Nucleosides is an important class of modified nucleosides characterized by replacing a labile glycosidic C-N bond with a stable C-C bond. While natural and synthetic *N*-nucleosides are susceptible to enzymatic and acid-catalyzed hydrolysis of the nucleosidic bond, their C-analogues are much more stable.<sup>7–10</sup> Naturally occurring C-nucleosides possess exciting activities, including antibacterial, anticancer, antifungal, antiviral, and antitumor properties. The development of novel synthetic methodologies allowed the preparation of a large variety of synthetic analogs, which found numerous applications in medicinal chemistry and chemical biology.<sup>11</sup> In the literature, there are two critical approaches for synthesizing C-nucleosides.<sup>12,13</sup> One method involves coupling a premade aglycone to a sugar derivative. On the other, a functional group is introduced at the anomeric position of the sugar derivative and is followed by the construction of a heterocyclic base. There are several synthetic methods to prepare C-nucleosides: (a) additions of organometallics to ribono- or 2-deoxyribo lactones, (b) electrophilic substitutions of electron-rich aromatics with sugars under Lewis acid catalysis, (c) coupling of halogens with organometallics, (d) Heck-type coupling of aryl iodides with glycals or opening of glycal epoxides with aryl aluminum reagents.<sup>14–27</sup> Various synthetic aryl-C-nucleosides capable of  $\pi$ -stacking are studied as building blocks in chemical biology. Several Artificial Expanded Genetic Information Systems (AEGIS) have been successfully developed as prime examples

of synthetic biology in recent years. It is an emerging interdisciplinary field with the decisive goal of designing systems in which artificial chemical systems mimic high-level behaviors of living matter.<sup>28,29</sup> Several artificial base pairs have been developed based on hydrogen bonding, hydrophobic interactions and metal binding properties.<sup>30,31</sup> The aromatic glycones in C-nucleosides generally contain benzenoid and heterocyclic aromatic scaffolds (Figure 4B.1-a/b). Conversely, this field doesn't fully cover non-benzenoid aromatic systems (tropolone/azulene). Azulene is a bright-blue, bicyclic, 10  $\pi$ -electron isomer of naphthalene. It is stabilized by resonance contributions from cyclopentadienyl anion and tropylium cation that provides a dipole moment distinguishing azulene from common fused benzenoids. Azulene and its derivatives are getting attention due to their reversible stimuli-responsive nature, composite and self-assembled architectures, antibacterial properties, and potential medicinal and bioimaging applications.<sup>32–35</sup> However, there is only a single Japanese patent (JPH07027768A) available, reporting an azulenyl C-nucleoside where sugar ring is attached to the 5-membered ring of azulene (Figure 4B.1-c). In this repertoire, we have synthesized a C-nucleoside containing azulene derivative, where the sugar ring is attached to the seven-membered ring (C-6 position) of azulene moiety. We have also examined its structural organization by crystal X-ray diffractometer, transmission electron microscopy (TEM) and scanning electron microscopy (SEM) techniques along with cytotoxicity effect on HEK293T cell line.

## 4B.2 Objective

Azulenyl C-nucleosides are not well explored. Hence, in this chapter, we have rationally designed azulene tethered c-nucleoside, where the sugar ring is attached to the C-6 position of azulene moiety. This was achieved by performing multiple-step reactions from the starting materials (a) glycal derivative and (b) Bromo azulene derivative. Here we have also explored its morphology and cytotoxicity.

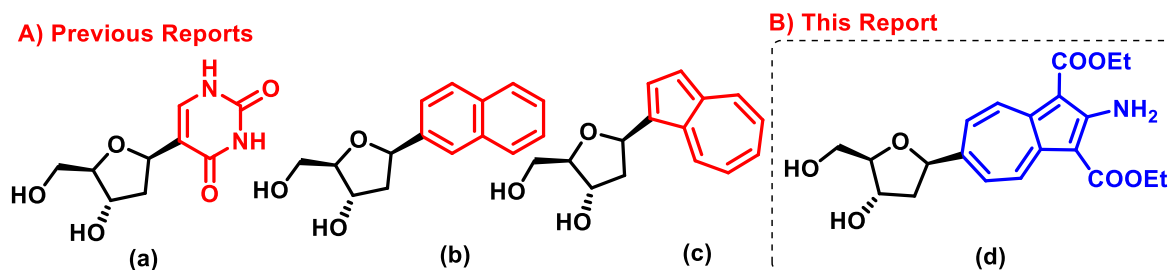
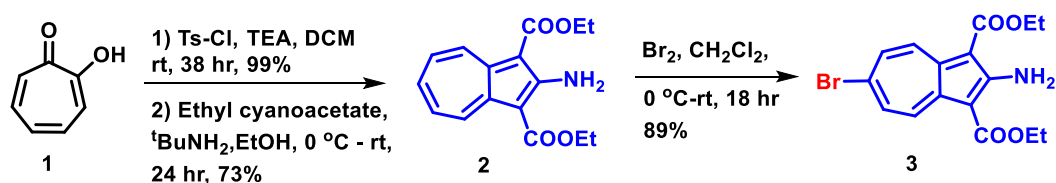


**Figure 4B.1.** (A) Previously reported C-nucleosides and (B) this report.

### 4B.3 Results and Discussion

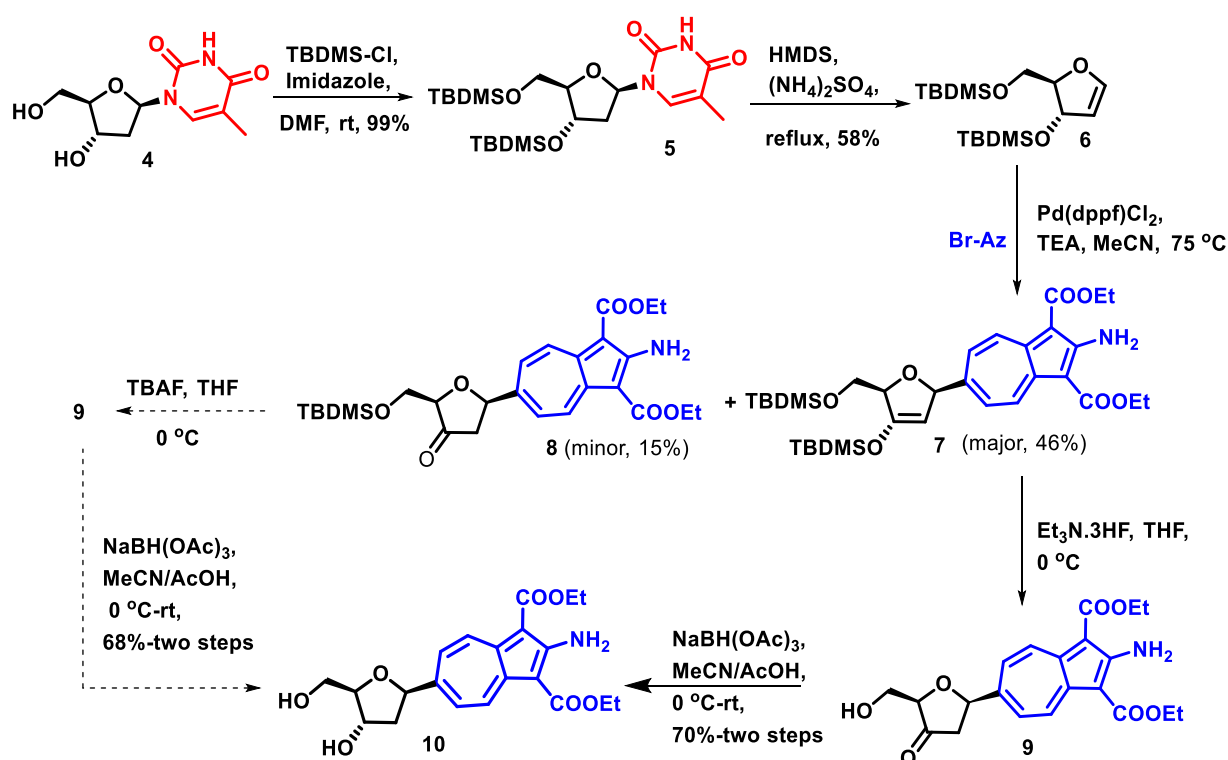
We derivatized Tropolone (**1**) into 2-amino-6-bromoazulene-1,3-dicarboxylate, Az-Br (**3**) by following the reported procedure (Scheme 4B.1).<sup>32</sup> First, tosylation of compound **1** with TsCl in TEA/DCM was carried out at rt to produce tosyloxypone (99% yield). The tosylate was transformed into the azulene derivative (**2**, 73% yield) using ethyl cyanoacetate and *t*-butylamine. Bromination of **2** using Br<sub>2</sub> in DCM gave diethyl 2-amino-6-bromoazulene-1, 3-dicarboxylate (**3**) in quantitative yield (89%).



**Scheme 4B.1.** Synthesis of diethyl 2-amino-6-bromoazulene-1, 3-dicarboxylate (**3**).

Next we planned to synthesize C-Nucleosides (**10**) containing azulene moiety in four steps using a Heck-type coupling reaction as the central step (Scheme 4B.2). First of all, glycal (**6**) was synthesized in a yield of 57% by *tert*-butyldimethylsilyl (TBDMS) protection of Thymidine (**4**) at the 3'- and 5'- positions and subsequent elimination of thymine.<sup>36,37</sup> For the Heck-type coupling between the bromo-azulene derivative (**3**) and the glycal (**6**), Pd(dppf)Cl<sub>2</sub> [dppf = 1,1'-bis(diphenylphosphino)ferrocene] was used as the catalyst of choice. Here we obtained the desired glycoside (**7**) in 46% yield as a major product along

with some minor product, i.e., mono-TBDMS protected glycoside (**8**) in 15% yield. Both were processed separately to get the final product (**10**). After deprotection of the glycoside **7** at their 3' and 5' positions and reduction of the intermediate 3'-keto derivatives (**9**) by treatment with  $\text{NaBH}(\text{OAc})_3$ , C-nucleoside (**10**) was obtained in 70% yield. Similarly, compound **8** was subjected to subsequent deprotection and reduction to get the desired azulenyl C-nucleoside (**10**). All these derivatives were well characterized by NMR and HRMS spectral analyses (see Appendix).

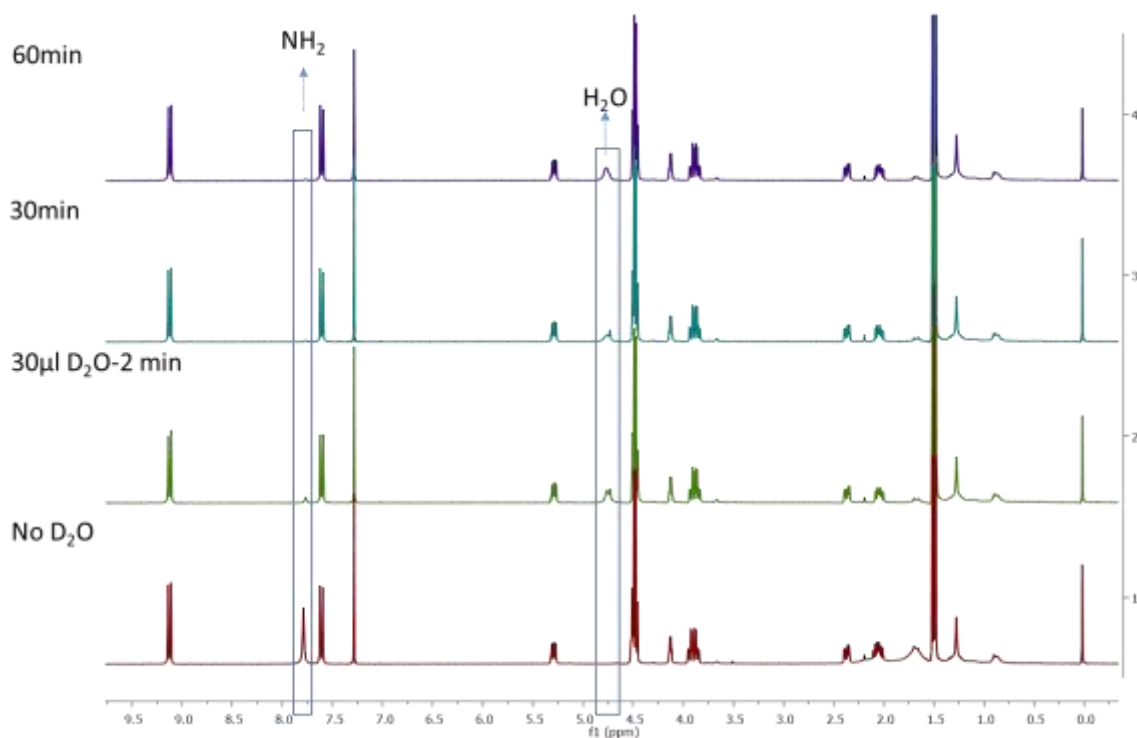


**Scheme 4B.2.** Synthesis of azulenyl C-nucleoside (**10**).

Here, it should be noted that (a) the palladium-catalyzed coupling reaction and (b) the final reduction are highly stereoselective. The stereoselectivity results are a consequence of substrate control because (a) the lower face of glycal (**6**) is effectively shielded by the sterically bulky TBDMS group in the 3'-position to give only the desired  $\beta$ -anomers<sup>23</sup> and (b) the free 5'-hydroxy group binds to the boron atom of  $\text{NaBH}(\text{OAc})_3$  thereby leading to a

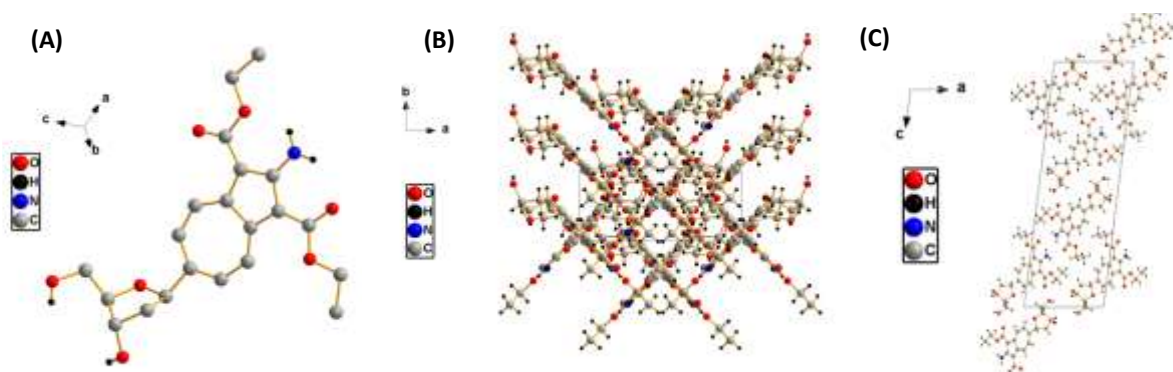
hydride attack of the C=O bond from the top to recover the 2'-deoxyribofuranoside configuration.<sup>38</sup> Another important instruction is to use Et<sub>3</sub>N.3HF instead of commonly used TBAF in THF for deprotection of di-TBDMS protected glycoside (desilylation step).<sup>39</sup> Otherwise, it can lead to an inseparable mixture of compounds causing less product yield. In case of mono-TBDMS deprotection the use of TBAF is fine.

We performed the D<sub>2</sub>O exchange NMR experiment to confirm the NH<sub>2</sub> group (Figure 4B.2). After recording <sup>1</sup>H NMR spectra, we added 30 µl of D<sub>2</sub>O to the same NMR tube and mixed it well. After that, we recorded <sup>1</sup>H NMR spectra after 2 min and observed a decrease in intensity of a singlet peak at 7.75 δ ppm value. After some time, it vanished completely where other peaks were intact. This depicts that the said peak corresponds to hydrogen atoms of NH<sub>2</sub> group present in the azulene ring of C-nucleoside.



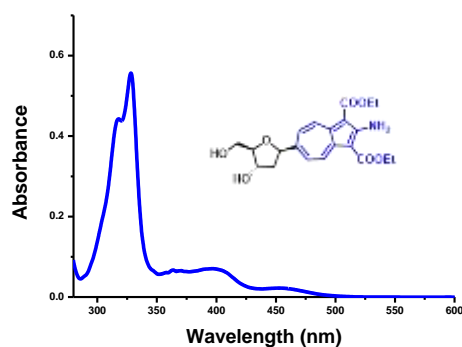
**Figure 4B.2.** D<sub>2</sub>O exchange NMR experiment of C-nucleoside (10).

Pleasantly, we obtained the single crystal of azulenyl C-nucleoside (**10**) in solvent  $\text{CDCl}_3$  at 4 °C with slow evaporation method. Their crystals were studied by X-ray techniques. Their ORTEP diagrams are depicted in Figure 4B.3-A, while other crystal structure parameters are provided in the Appendix. We analyzed the molecular packing of the solved crystals 10 using software (Diamond). The packing diagram of compound (**10**) crystal shows the formation of a new supramolecular self-assembly structure owing to the  $\pi$ - $\pi$  interactions (Figure 4B.3-B/C). Its azulenyl ring exhibit  $\pi$ - $\pi$  stacking with another azulene ring. It only exhibited intra-molecular hydrogen bonding between the hydrogen atom of  $\text{NH}_2$  and oxygen atom of two ester groups.



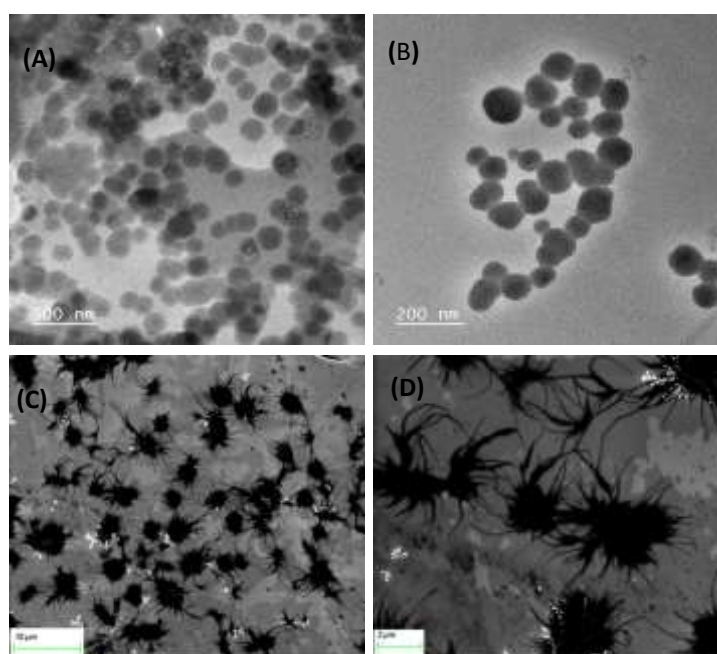
**Figure 4B.3.** Crystal structure and packing diagram of azulenyl C-nucleoside (**10**).

The UV-Vis spectrum of azulenyl C-nucleoside (**10**) in Acetonitrile is shown in Figure 4B.4. The spectrum indicates the presence of several electronic transitions with apparent maxima at 328 nm with a shoulder positioned at around 316 nm. The strong absorption band at  $\lambda_{\text{max}} = 328$  nm is a result of  $S_0$ - $S_3$  transition, which is a known pattern for azulene derivatives.<sup>40</sup> There are two additional broader bands located at lower energy with apparent maxima at 400 and 455 nm, which can be assigned to weak  $S_0$ - $S_2$  and  $S_0$ - $S_1$  transitions, respectively, which is commonly seen in azulene derivatives.<sup>34</sup> However, we didn't notice any fluorescence properties.



**Figure 4B.4.** UV-Vis spectrum of C-nucleoside (**10**) in acetonitrile at 10 μM concentration.

The morphology of the C-nucleoside (**10**) was characterized by Transmission electron microscope (TEM) and scanning electron microscope (SEM) imaging techniques. Their TEM/SEM images at different scales and EDAX data are provided in Figure 4B.5. From the HRTEM analysis, we observed nanoparticles of spherical shape. The images showed that the nanoparticles possessed weak connectivity with restrained dispersity. The spherical shapes were not the same in size and exhibited moderate agglomeration. This kind of structure was further supported by SEM images, where we observed a fragile networking pattern among the micro-aggregates. Its crystal packing diagram explains this, where we noticed  $\pi$ - $\pi$  stacking and no intermolecular H-bonding.





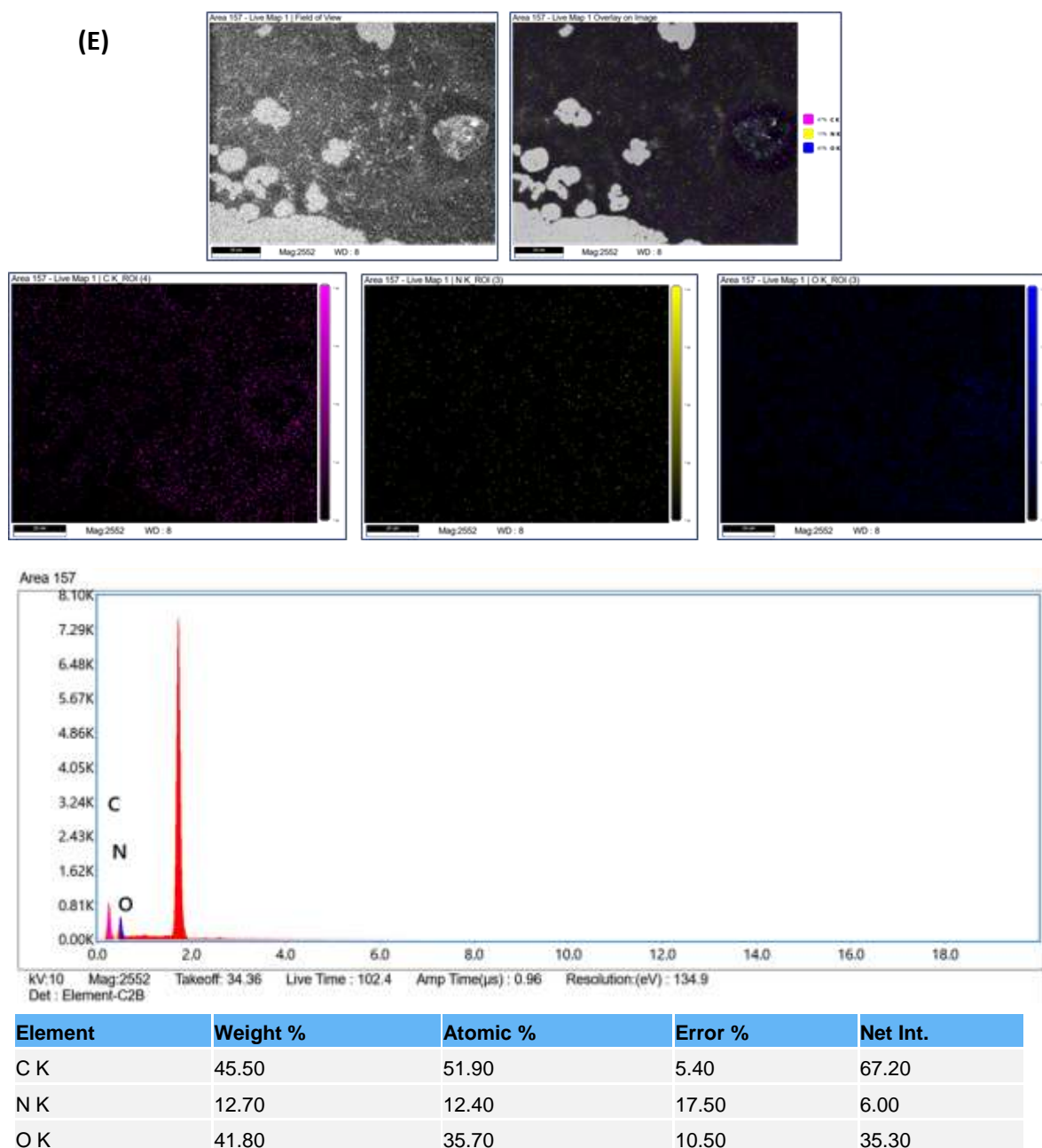


**Figure 4B.5.** (A, B) HRTEM, (C, D) FESEM images at different magnifications and (E) EDAX analysis of azulenyl C-nucleoside (**10**)

For practical utility, we evaluated the cytotoxicity of the Azulenyl nucleoside (**10**), with HEK293T and HeLa cell lines. It showed no cytotoxic effects in both the cases, even with high concentrations (100  $\mu$ M). So it can be used for further biological evaluations. The concentration-dependent cell viability is provided in Figure 4B.6.

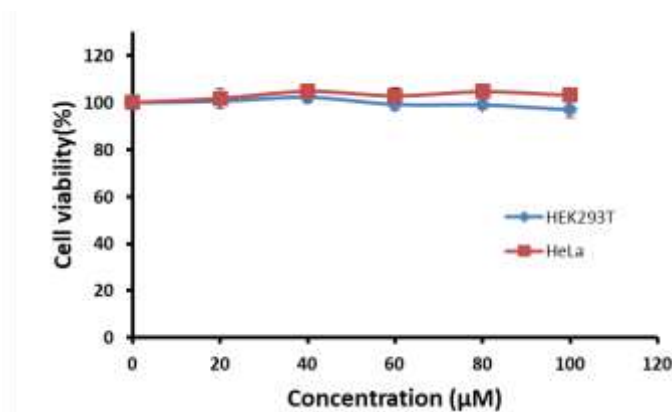


**Figure 4B.6.** Cell proliferation assay of compound **10** in HEK293 and HeLa cells.

#### 4B.4 Conclusion

In summary, we have synthesized azulene tethered C-nucleoside, where the sugar ring is attached to the C-6 position of azulene moiety. The synthesis involves multiple steps and Heck-type coupling reaction was the central step where we could attach the azulenyl unit to the sugar ring. The crystal packing diagrams explain the existence of  $\pi$ - $\pi$  stacking between azulene rings. This reflects in the morphology studies. In TEM analysis, we noticed non-uniform spherical-shaped nanoparticles, which are weakly linked with each other. We couldn't detect any significant cytotoxicity towards HEK293 and HeLa cell lines when treated with Azulenyl C-nucleoside. Hence this can be useful for different biochemical applications.

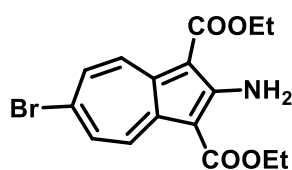
#### 4B.5 Experimental section

*General information:* All materials were purchased from commercial suppliers and used without any purifications. Acetonitrile and DMF were distilled over  $\text{CaH}_2$  and stored over 4Å molecular sieves. THF was distilled over sodium metal and stored over sodium metal. Reactions were monitored by thin layer chromatography, visualized by UV, Ninhydrin and phosphomolybdic acid. Column chromatography was performed in 100-200 mesh silica.

Mass spectra (HRMS) were obtained from Bruker microTOF-Q II and Waters Spectrometer and the samples were prepared in methanol and injected in methanol and water mixture. NMR spectra were recorded on Bruker 400 MHz NMR spectrometer at room temperature and processed using Mnova software from Mestrelab Research. The crystal data were collected on a Rigaku Oxford diffractometer. Absorption spectra were obtained using Jasco V-730 spectrometer. The surface morphologies of compounds were studied with field emission scanning electron microscopy (FESEM, Merlin Compact with a GEMINI-I/GEMINI-II electron column, Zeiss Pvt. Ltd., Germany) and high-resolution transmission electron microscopy (HRTEM, JEOL 2100F).

#### *Characterization data of products*

Diethyl 2-amino-6-bromoazulene-1,3-dicarboxylate (**3**): Following the reported procedure,



the title compound was synthesized and obtained as a deep purple

solid.<sup>32</sup> <sup>1</sup>H NMR (400 MHz, CDCl<sub>3</sub>) δ 8.82 (d, *J* = 11.5 Hz, 2H),

7.81 (s, 2H), 7.78 (d, 2H), 4.46 (q, *J* = 7.1 Hz, 2H), 1.47 (t, *J* = 7.1

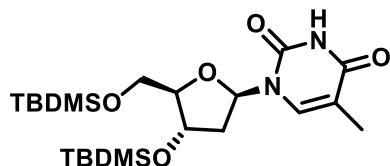
Hz, 3H). <sup>13</sup>C NMR (101 MHz, CDCl<sub>3</sub>) δ 166.23, 162.34, 144.33, 135.31, 129.45, 128.37,

101.00, 60.07, 14.61. HRMS (ESI) calcd for C<sub>16</sub>H<sub>16</sub>BrNO<sub>4</sub>: [M+Na]<sup>+</sup> 388.0155, found

388.0135.

1-((2R,4S,5R)-4-((tert-butyldimethylsilyl)oxy)-5-(((tert-

butyldimethylsilyl)oxy)methyl)tetrahydrofuran-2-yl)-5-methylpyrimidine-2,4(1H,3H)-dione



(**5**): A mixture of Thymidine (10.0 g, 41.3 mmol) and

imidazole (11.8 g, 173 mmol) in anhydrous DMF was stirred

at room temperature for 10 min. Then tert-butyldimethylsilyl

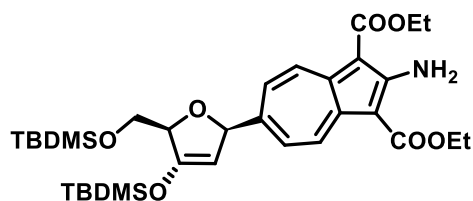
chloride (13.1 g, 86.7 mmol) was added slowly, and the mixture was continued stirring for another 18 h. After adding water (100 mL), the reaction mixture was extracted with hexane,

dried with Na<sub>2</sub>SO<sub>4</sub> purified by column chromatography (EtOAc:Hexane), and fractions obtained were concentrated under vacuum to give **4** (19.3 g, 99%) as a white solid; <sup>1</sup>H NMR (400 MHz, CDCl<sub>3</sub>) δ 8.55 (s, 1H), 7.49 (s, 1H), 6.41 – 6.31 (m, *J* = 7.7, 6.0 Hz, 1H), 4.46 – 4.35 (m, 1H), 3.95 (d, *J* = 2.3 Hz, 1H), 3.89 (dd, *J* = 11.4, 2.4 Hz, 1H), 3.78 (dd, *J* = 11.3, 2.2 Hz, 1H), 2.32 – 2.20 (m, *J* = 13.0, 5.7, 2.4 Hz, 1H), 2.07 – 1.98 (m, 1H), 1.93 (s, 3H), 0.93 (d, *J* = 14.0 Hz, 18H), 0.13 (s, 6H), 0.10 (d, *J* = 2.7 Hz, 6H), <sup>13</sup>C NMR (101 MHz, CDCl<sub>3</sub>) δ 163.63, 150.18, 135.50, 110.82, 87.85, 84.84, 72.28, 63.00, 41.39, 25.94, 25.75, 18.41, 12.53, -4.64, -4.83, -5.36, -5.45, C<sub>22</sub>H<sub>42</sub>N<sub>2</sub>O<sub>5</sub>Si<sub>2</sub>: [M+Na]<sup>+</sup> 493.2524, found 493.2498.

tert-butyl(((2R,3S)-3-((tert-butyldimethylsilyl)oxy)-2,3-dihydrofuran-2-yl)methoxy)dimethylsilane (**6**): A mixture of compound **5** (3.00 g, 6.40 mmol) and ammonium sulfate (337 mg, 2.55 mmol) was dissolved in hexamethyldisilazane (11.7 g, 72.5 mmol) in a dry flask, and the resulting mixture was heated at reflux condition for 4 h. After the solvents were removed under vacuum, the residue was dissolved in CH<sub>2</sub>Cl<sub>2</sub>. The solution was washed with saturated NaHCO<sub>3</sub> solution, water, and brine, dried with Na<sub>2</sub>SO<sub>4</sub>, and concentrated under vacuum. The crude was subjected to silica gel column chromatography (EtOAc:Hexane) to give **4** (1.27 g, 58%) as a yellowish oil, <sup>1</sup>H NMR (400 MHz, CDCl<sub>3</sub>) δ 6.47 (d, *J* = 2.4 Hz, 1H), 5.01 (t, *J* = 2.6 Hz, 1H), 4.86 (t, *J* = 2.1 Hz, 1H), 4.32 – 4.25 (m, *J* = 6.1, 2.7 Hz, 1H), 3.69 (dd, *J* = 10.7, 5.7 Hz, 1H), 3.51 (dd, *J* = 10.7, 6.3 Hz, 1H), 0.89 (d, *J* = 2.6 Hz, 18H), 0.09 (s, 6H), 0.07 (d, *J* = 3.7 Hz, 6H), <sup>13</sup>C NMR (101 MHz, CDCl<sub>3</sub>) δ 148.98, 103.41, 88.97, 75.99, 62.83, 25.91, 25.89, 18.40, 18.10, -4.25, -4.40, -5.33, -5.36, HRMS ESI-Tof Calcd for C<sub>22</sub>H<sub>42</sub>N<sub>2</sub>O<sub>5</sub>Si<sub>2</sub>: [M+Na]<sup>+</sup> 367.2095, Found 367.2087.

diethyl-2-amino-6-((2R,5R)-4-((tert-butyldimethylsilyl)oxy)-5-(((tert-butyldimethylsilyl)oxy)methyl)-2,5-dihydrofuran-2-yl)azulene-1,3-dicarboxylate (**7**): A mixture of **6** (0.272 g, 0.790 mmol), **3** (0.320 g, 0.870 mmol), and triethylamine (0.5 ml, 1.97

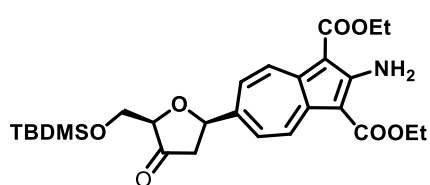
mmol) was dissolved in acetonitrile (10 mL) in a dry round bottom flask, and the resulting mixture was degassed by using a long needle and a balloon containing inert gas. [1,1'-Bis(diphenylphosphino)ferrocene] dichloropalladium(II) (0.161 g, 0.197 mmol) was added,



and the mixture was heated at 75 °C for 9 h. After this, the reaction mixture was concentrated under vacuum, and the crude product was purified by silica gel column chromatography (EtOAc:Hexane) to give **7**

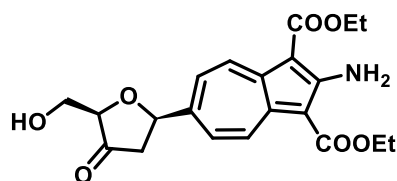
(0.228 g, 46%) as major product.  $^1\text{H}$  NMR (400 MHz,  $\text{CDCl}_3$ )  $\delta$  9.11 (d,  $J$  = 11.1 Hz, 2H), 7.80 (s, 2H), 7.76 (d,  $J$  = 11.2 Hz, 2H), 5.77 (d,  $J$  = 3.2 Hz, 1H), 4.81 (s, 1H), 4.64 (s, 1H), 4.46 (q,  $J$  = 7.1 Hz, 4H), 4.00 – 3.84 (m,  $J$  = 14.8, 11.4, 2.7 Hz, 2H), 1.47 (t,  $J$  = 7.1 Hz, 6H), 0.94 (d,  $J$  = 6.2 Hz, 18H), 0.21 (d,  $J$  = 9.6 Hz, 6H), 0.11 (d,  $J$  = 8.2 Hz, 6H),  $^{13}\text{C}$  NMR (101 MHz,  $\text{CDCl}_3$ )  $\delta$  166.73, 162.65, 151.62, 147.62, 145.42, 132.21, 131.05, 102.56, 99.69, 87.54, 84.38, 63.66, 59.74, 26.13, 25.59, 18.68, 18.10, 14.74, -4.87, -4.97, -5.13, -5.25, HRMS ESI-Tof Calcd for  $\text{C}_{33}\text{H}_{51}\text{NO}_7\text{Si}_2$ :  $[\text{M}+\text{Na}]^+$  652.3096, Found 652.3103

diethyl 2-amino-6-((2R,5R)-5-(((tert-butyldimethylsilyl)oxy)methyl)-4-oxotetrahydrofuran-2-yl)azulene-1,3-dicarboxylate (**8**): This was obtained as a minor (0.061 g, 15%) product in the



coupling step.  $^1\text{H}$  NMR (400 MHz,  $\text{CDCl}_3$ )  $\delta$  9.13 (d,  $J$  = 11.2 Hz, 2H), 7.84 (s, 2H), 7.78 (d,  $J$  = 11.3 Hz, 2H), 5.27 (dd,  $J$  = 11.0, 5.9 Hz, 1H), 4.46 (q,  $J$  = 7.1 Hz, 4H), 4.11 (t,  $J$  = 2.0 Hz, 1H), 4.03 (t,  $J$  = 2.4 Hz, 2H), 2.89 (dd,  $J$  = 17.7, 5.9 Hz, 1H), 2.45 (dd,  $J$  = 17.7, 11.1 Hz, 1H), 1.47 (t,  $J$  = 7.1 Hz, 6H), 0.93 (s, 9H), 0.16 (s, 3H), 0.10 (s, 3H),  $^{13}\text{C}$  NMR (101 MHz,  $\text{CDCl}_3$ )  $\delta$  213.28, 166.62, 162.79, 145.39, 145.15, 130.93, 130.62, 100.16, 82.80, 80.05, 62.73, 59.92, 47.24, 25.87, 14.64, -5.34, -5.68, HRMS ESI-Tof Calcd for  $\text{C}_{27}\text{H}_{37}\text{NO}_7\text{Si}$ :  $[\text{M}+\text{Na}]^+$  538. 2232, Found 538.2223.

diethyl 2-amino-6-((2R,5R)-5-(hydroxymethyl)-4-oxotetrahydrofuran-2-yl)azulene-1,3-



dicarboxylate (**9**): Et<sub>3</sub>N:3HF (233  $\mu$ L, 1.30 mmol) was

added to a solution of compound **7** (0.100 g, 0.162 mmol)

in THF (5 mL), and the mixture was kept for stirring at

room temperature for 14 h. After the reaction was completed, solvents were removed under

reduced pressure. Then the crude product was dissolved in MeOH (2 mL), and a 1 M aqueous

solution of sodium hydroxide (8 mL) was added to neutralize the mixture. Then the solvents

were evaporated under reduced pressure. The crude product was purified by column eluted

with gradient CH<sub>2</sub>Cl<sub>2</sub>:MeOH to get compound **9** for analysis purpose only. <sup>1</sup>H NMR (400

MHz, CDCl<sub>3</sub>)  $\delta$  9.11 (d,  $J$  = 11.1 Hz, 2H), 7.80 (s, 2H), 7.64 (d,  $J$  = 11.1 Hz, 2H), 5.29 (dd,  $J$

= 10.9, 5.9 Hz, 1H), 4.46 (q,  $J$  = 7.1 Hz, 4H), 4.12 (t,  $J$  = 3.3 Hz, 1H), 4.03 (d,  $J$  = 3.2 Hz,

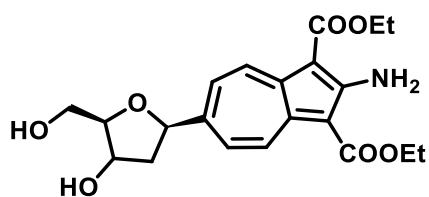
2H), 2.95 (dd,  $J$  = 18.1, 5.9 Hz, 1H), 2.53 (dd,  $J$  = 18.1, 10.9 Hz, 1H), 1.47 (t,  $J$  = 7.1 Hz,

6H), <sup>13</sup>C NMR (101 MHz, CDCl<sub>3</sub>)  $\delta$  212.85, 166.46, 162.72, 145.38, 143.69, 130.78, 130.27,

100.35, 82.69, 80.05, 61.61, 59.96, 46.30, 14.66, HRMS ESI-Tof Calcd for C<sub>21</sub>H<sub>23</sub>NO<sub>7</sub> :

[M+Na]<sup>+</sup> 424.1367, Found 424.1357.

diethyl 2-amino-6-((2R,4S,5R)-4-hydroxy-5-(hydroxymethyl)tetrahydrofuran-2-yl)azulene-



1,3-dicarboxylate (**10**): Compound **9** without any

purification was dissolved in AcOH/MeCN (1:1, 6 mL),

and the solution was cooled to 0 °C. NaBH(OAc)<sub>3</sub> (0.05

g, 0.240 mmol) was added, and the reaction mixture was

kept for stirring at room temperature for two hours and then neutralized with EtOH/water

(1:1, 5 mL). The resulting mixture was concentrated under vacuum, and the crude was

subjected to silica gel chromatography (CH<sub>2</sub>Cl<sub>2</sub>:MeOH) to give **10** (45.6 mg, 70%-two step)

as a yellow solid; <sup>1</sup>H NMR (400 MHz, CDCl<sub>3</sub>)  $\delta$  9.10 (d,  $J$  = 11.1 Hz, 2H), 7.75 (s, 2H), 7.58

(d,  $J$  = 11.2 Hz, 2H), 5.31 – 5.22 (m, 1H), 4.46 (q,  $J$  = 7.1 Hz, 4H), 4.10 (dd,  $J$  = 7.5, 4.4 Hz,

1H), 3.93 – 3.81 (m,  $J = 11.6, 4.6$  Hz, 2H), 2.38 – 2.31 (m,  $J = 13.3, 5.6, 1.4$  Hz, 1H), 2.06 – 1.98 (m,  $J = 13.3, 10.3, 6.4$  Hz, 2H), 1.47 (t,  $J = 7.1$  Hz, 6H),  $^{13}\text{C}$  NMR (101 MHz,  $\text{CDCl}_3$ )  $\delta$  166.57, 162.46, 145.89, 145.25, 130.95, 130.27, 100.00, 87.75, 82.46, 73.67, 63.43, 59.86, 45.20, 14.67, HRMS ESI-Tof Calcd for  $\text{C}_{21}\text{H}_{25}\text{NO}_7$  :  $[\text{M}+\text{Na}]^+$  426.1523, Found 426.1513.

#### 4B.6 reference and Notes

- (1) Takezawa, Y.; Shionoya, M. Metal-Mediated DNA Base Pairing: Alternatives to Hydrogen-Bonded Watson–Crick Base Pairs. *Acc. Chem. Res.* **2012**, *45* (12), 2066–2076.
- (2) Li, Q.; Groaz, E.; Persoons, L.; Daelemans, D.; Herdewijn, P. Synthesis and Antitumor Activity of C-7-Alkynylated and Arylated Pyrrolotriazine C-Ribonucleosides. *ACS Med. Chem. Lett.* **2020**, *11* (8), 1605–1610.
- (3) Ren, R. X.-F.; Chaudhuri, N. C.; Paris, P. L.; Rumney IV, S.; Kool, E. T. Naphthalene, Phenanthrene, and Pyrene as DNA Base Analogues: Synthesis, Structure, and Fluorescence in DNA. *J. Am. Chem. Soc.* **1996**, *118* (33), 7671–7678.
- (4) Xu, W.; Chan, K. M.; Kool, E. T. Fluorescent Nucleobases as Tools for Studying DNA and RNA. *Nat. Chem.* **2017**, *9* (11), 1043–1055.
- (5) Meher, S.; Gade, C. R.; Sharma, N. K. Tropolone-Conjugated DNA: A Fluorescent Thymidine Analogue Exhibits Solvatochromism, Enzymatic Incorporation into DNA and HeLa Cell Internalization. *ChemBioChem* **2023**, *24* (4), e202200732.
- (6) Karimi, A.; Börner, R.; Mata, G.; Luedtke, N. W. A Highly Fluorescent Nucleobase Molecular Rotor. *J. Am. Chem. Soc.* **2020**, *142* (34), 14422–14426.
- (7) Giofrè, S. V.; Romeo, R.; Carnovale, C.; Mancuso, R.; Cirimi, S.; Navarra, M.;

- Garozzo, A.; Chiacchio, M. A. Synthesis and Biological Properties of 5-(1 H-1, 2, 3-Triazol-4-Yl) Isoxazolidines: A New Class of c-Nucleosides. *Molecules* **2015**, *20* (4), 5260–5275.
- (8) Miller, P. S.; Hecht, S. M. Antisense/Antigene Oligonucleotides. *Bioorganic Chem. Acids* **1996**, 347–374.
- (9) Wellington, K. W.; Benner, S. A. A Review: Synthesis of Aryl C-Glycosides via the Heck Coupling Reaction. *Nucleosides, Nucleotides, and Nucleic Acids* **2006**, *25* (12), 1309–1333.
- (10) Zhang, M.; Kong, L.; Gong, R.; Iorio, M.; Donadio, S.; Deng, Z.; Sosio, M.; Chen, W. Biosynthesis of C-Nucleoside Antibiotics in Actinobacteria: Recent Advances and Future Developments. *Microb. Cell Fact.* **2022**, *21* (1), 2.
- (11) De Clercq, E. C-Nucleosides to Be Revisited: Miniperspective. *J. Med. Chem.* **2016**, *59* (6), 2301–2311.
- (12) Knutsen, L. J. S. The Chemistry of 2'-Deoxyribo-C-Nucleosides. *Nucleosides Nucleotides* **1992**, *11* (5), 961–983.
- (13) Watanabe, K. A. The Chemistry of C-Nucleosides. *Chem. Nucleosides Nucleotides Vol. 3* **1994**, 421–535.
- (14) Novák, P.; Pohl, R.; Katora, M.; Hocek, M. Synthesis of C-Aryldeoxyribosides by [2+ 2]-Cyclotrimerization Catalyzed by Rh, Ni, Co, and Ru Complexes. *Org. Lett.* **2006**, *8* (10), 2051–2054.
- (15) Brotschi, C.; Leumann, C. J. Transition Metal Ligands as Novel DNA-Base Substitutes. *Nucleosides, Nucleotides and Nucleic Acids* **2003**, *22* (5–8), 1195–1197.



- (16) Reese, C. B.; Wu, Q. Conversion of 2-Deoxy-d-Ribose into 2-Amino-5-(2-Deoxy- $\beta$ -d-Ribofuranosyl) Pyridine, 2'-Deoxypseudouridine, and Other C-(2'-Deoxyribonucleosides). *Org. Biomol. Chem.* **2003**, *1* (18), 3160–3172.
- (17) Aketani, S.; Tanaka, K.; Yamamoto, K.; Ishihama, A.; Cao, H.; Tengeiji, A.; Hiraoka, S.; Shiro, M.; Shionoya, M. Syntheses and Structure– Activity Relationships of Nonnatural  $\beta$ -C-Nucleoside 5'-Triphosphates Bearing an Aromatic Nucleobase with Phenolic Hydroxy Groups: Inhibitory Activities against DNA Polymerases. *J. Med. Chem.* **2002**, *45* (25), 5594–5603.
- (18) He, W.; Togo, H.; Yokoyama, M. Strategic Approach to C-Nucleosides via Sugar Anomeric Radical, Cation, and Anion with Sugar Tellurides. *Tetrahedron Lett.* **1997**, *38* (31), 5541–5544.
- (19) Singh, I.; Seitz, O. Diastereoselective Synthesis of  $\beta$ -Aryl-C-Nucleosides from 1, 2-Anhydrosugars. *Org. Lett.* **2006**, *8* (19), 4319–4322.
- (20) Farr, R. N.; Kwok, D. I.; Daves Jr, G. D. 8-Ethenyl-1-Hydroxy-4-. Beta.-D-Ribofuranosylbenzo [d] Naphtho [1, 2-b] Pyran-6-One and 8-Ethenyl-1-Hydroxy-4-(2'-Deoxy-. Beta.-D-Ribofuranosyl) Benzo [d] Naphtho [1, 2-b] Pyran-6-One. Synthetic C-Glycosides Related to the Gilvocarcin, Ravidomycin, and Ch. *J. Org. Chem.* **1992**, *57* (7), 2093–2100.
- (21) Hainke, S.; Arndt, S.; Seitz, O. Concise Synthesis of Aryl-C-Nucleosides by Friedel–Crafts Alkylation. *Org. Biomol. Chem.* **2005**, *3* (23), 4233–4238.
- (22) Beuck, C.; Singh, I.; Bhattacharya, A.; Hecker, W.; Parmar, V. S.; Seitz, O.; Weinhold, E. Polycyclic Aromatic DNA-Base Surrogates: High-Affinity Binding to an Adenine-Specific Base-Flipping DNA Methyltransferase. *Angew. Chemie Int. Ed.*

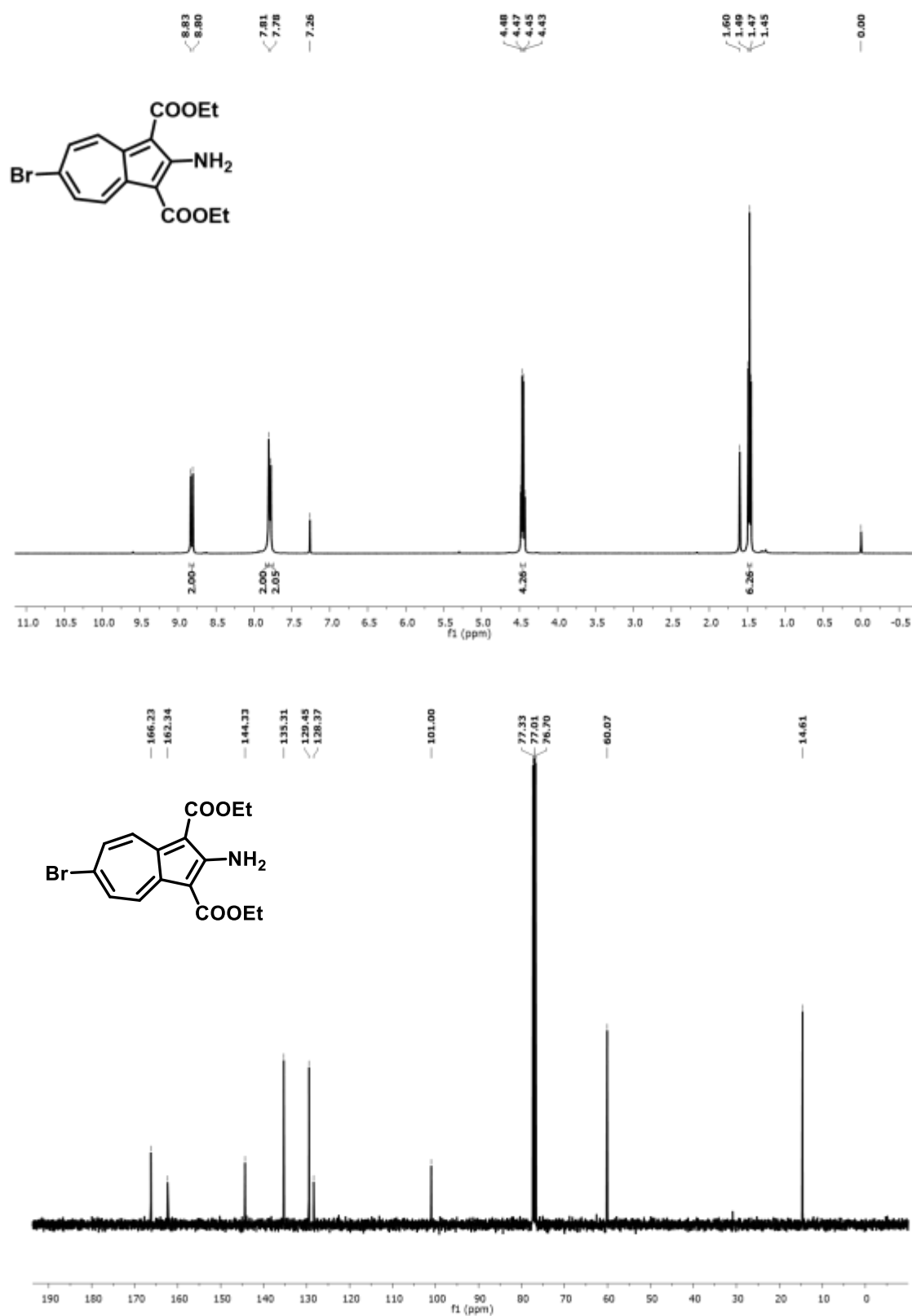
- 2003**, 42 (33), 3958–3960.
- (23) Daves Jr, G. D. C-Glycoside Synthesis by Palladium-Mediated Glycal-Aglycon Coupling Reactions. *Acc. Chem. Res.* **1990**, 23 (6), 201–206.
- (24) Urban, M.; Pohl, R.; Klepetářová, B.; Hocek, M. New Modular and Efficient Approach to 6-Substituted Pyridin-2-Yl C-Nucleosides. *J. Org. Chem.* **2006**, 71 (19), 7322–7328.
- (25) Son, S.; Fu, G. C. Copper-Catalyzed Asymmetric [4+ 1] Cycloadditions of Enones with Diazo Compounds to Form Dihydrofurans. *J. Am. Chem. Soc.* **2007**, 129 (5), 1046–1047.
- (26) Henry, A. A. *Efforts toward Expanding the Genetic Alphabet and the Substrate Repertoire of a DNA Polymerase*; The Scripps Research Institute, 2005.
- (27) Ren, R. X. F. Chaudhuri NC. Paris PL. Rumney IVS. Kool ET. *J. Am. Chem. Soc.* **1996**, 118, 7671.
- (28) Benner, S. A. Synthetic Biology: Act Natural. *Nature* **2003**, 421 (6919), 118.
- (29) Benner, S. A.; Sismour, A. M. Synthetic Biology. *Nat. Rev. Genet.* **2005**, 6 (7), 533–543.
- (30) Hocek, M. C-Nucleosides: Synthetic Strategies and Biological Applications. *Chem. Rev.* **2009**, 109 (12), 6729–6764.
- (31) Pu, F.; Ren, J.; Qu, X. Nucleobases, Nucleosides, and Nucleotides: Versatile Biomolecules for Generating Functional Nanomaterials. *Chem. Soc. Rev.* **2018**, 47 (4), 1285–1306.
- (32) Murfin, L. C.; Weber, M.; Park, S. J.; Kim, W. T.; Lopez-Alled, C. M.; McMullin, C.

- L.; Pradaux-Caggiano, F.; Lyall, C. L.; Kociok-Köhn, G.; Wenk, J. Azulene-Derived Fluorescent Probe for Bioimaging: Detection of Reactive Oxygen and Nitrogen Species by Two-Photon Microscopy. *J. Am. Chem. Soc.* **2019**, *141* (49), 19389–19396.
- (33) Puodziukynaite, E.; Wang, H.-W.; Lawrence, J.; Wise, A. J.; Russell, T. P.; Barnes, M. D.; Emrick, T. Azulene Methacrylate Polymers: Synthesis, Electronic Properties, and Solar Cell Fabrication. *J. Am. Chem. Soc.* **2014**, *136* (31), 11043–11049.
- (34) Zhang, J.; Petoud, S. Azulene-moiety-based Ligand for the Efficient Sensitization of Four Near-infrared Luminescent Lanthanide Cations: Nd<sup>3+</sup>, Er<sup>3+</sup>, Tm<sup>3+</sup>, and Yb<sup>3+</sup>. *Chem. Eur. J.* **2008**, *14* (4), 1264–1272.
- (35) Meher, S.; Sharma, N. K. Azulene Tethered N-Aryl Nucleobases: Synthesis, Morphology and Biochemical Evaluations. *New J. Chem.* **2023**.
- (36) Cameron, M. A.; Cush, S. B.; Hammer, R. P. Facile Preparation of Protected Furanoid Glycals from Thymidine. *J. Org. Chem.* **1997**, *62* (26), 9065–9069.
- (37) Krim, J.; Grünwald, C.; Taourirte, M.; Engels, J. W. Efficient Microwave-Assisted Synthesis, Antibacterial Activity and High Fluorescence of 5-Benzimidazolyl-2'-Deoxyuridines. *Bioorg. Med. Chem.* **2012**, *20* (1), 480–486.
- (38) Farr, R. N.; Daves Jr, G. D. Efficient Synthesis of 2'-Deoxy- $\beta$ -D-Furanosyl C-Glycosides. Palladium-Mediated Glycal-Aglycone Coupling and Stereocontrolled  $\beta$ - and  $\alpha$ -Face Reductions of 3-Keto-Furanosyl Moieties. **1990**.
- (39) Joubert, N.; Pohl, R.; Klepetářová, B.; Hocek, M. Modular and Practical Synthesis of 6-Substituted Pyridin-3-yl C-Nucleosides. *J. Org. Chem.* **2007**, *72* (18), 6797–6805.
- (40) Matěnová, M.; Horhoiu, V. L.; Dang, F.-X.; Pospíšil, P.; Alster, J.; Burda, J. V;

Balaban, T. S.; Pšenčík, J. Energy Transfer in Aggregates of Bacteriochlorophyll c Self-Assembled with Azulene Derivatives. *Phys. Chem. Chem. Phys.* **2014**, *16* (31), 16755–16764.

#### 4B.7 Appendix

1. $^1\text{H}$ , $^{13}\text{C}$ NMR (400MHz, $\text{CDCl}_3$ ) and HRMS of compound <b>3</b> .....	300
2. $^1\text{H}$ , $^{13}\text{C}$ NMR (400MHz, $\text{CDCl}_3$ ) and HRMS of compound <b>5</b> .....	302
3. $^1\text{H}$ , $^{13}\text{C}$ NMR (400MHz, $\text{CDCl}_3$ ) and HRMS of compound <b>6</b> .....	304
4. $^1\text{H}$ , $^{13}\text{C}$ NMR (400MHz, $\text{CDCl}_3$ ) and HRMS of compound <b>7</b> .....	306
5. $^1\text{H}$ , $^{13}\text{C}$ NMR (400MHz, $\text{CDCl}_3$ ) and HRMS of compound <b>8</b> .....	308
6. $^1\text{H}$ , $^{13}\text{C}$ NMR (400MHz, $\text{CDCl}_3$ ) and HRMS of compound <b>9</b> .....	310
7. $^1\text{H}$ , $^{13}\text{C}$ NMR (400MHz, $\text{CDCl}_3$ ) and HRMS of compound <b>10</b> .....	312

1.  $^1\text{H}$ ,  $^{13}\text{C}$  NMR (400MHz,  $\text{CDCl}_3$ ) and HRMS of compound **3****Figure A1.**  $^1\text{H}/^{13}\text{C}$  NMR (400MHz,  $\text{CDCl}_3$ ) spectra of compound **3** in  $\text{CDCl}_3$

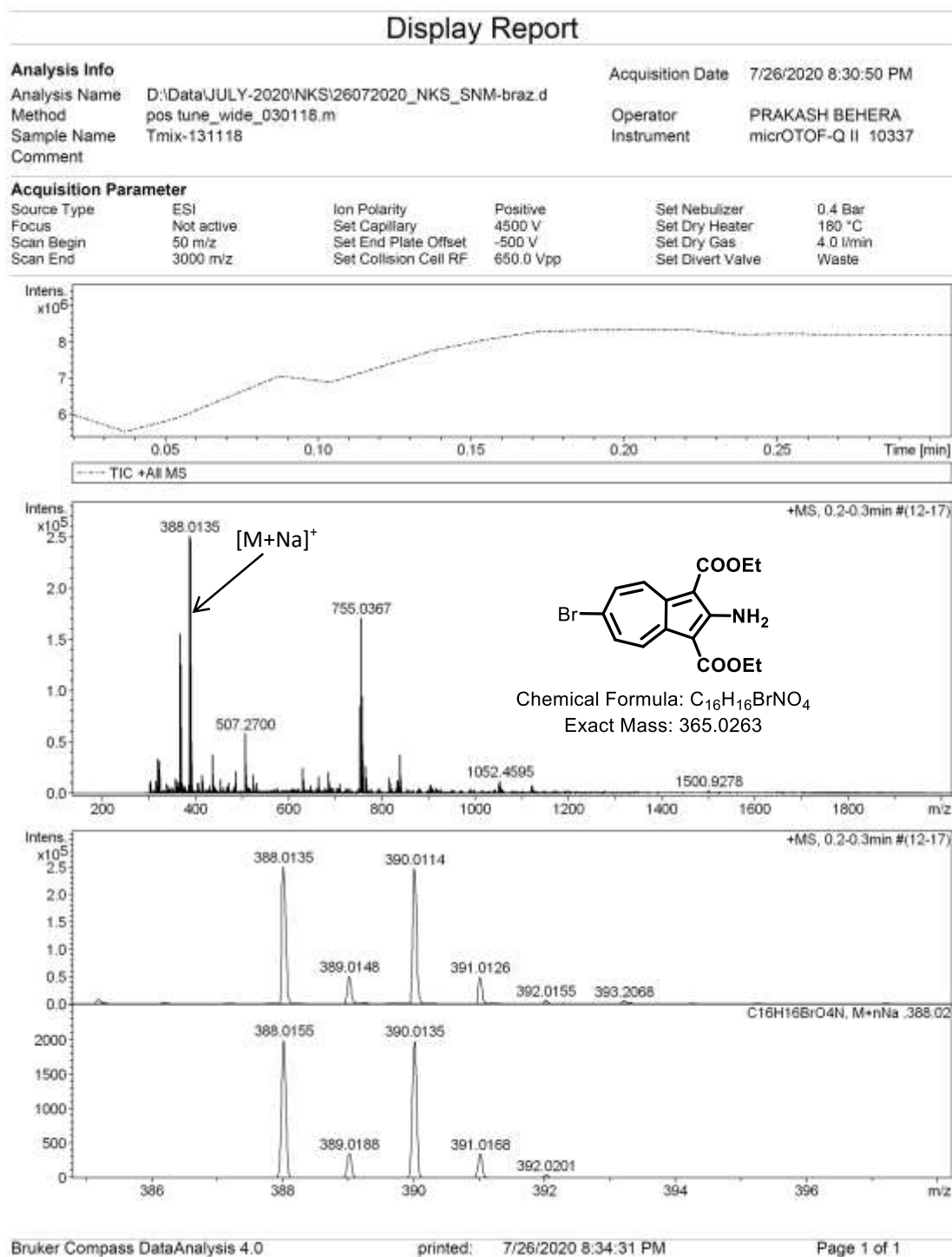
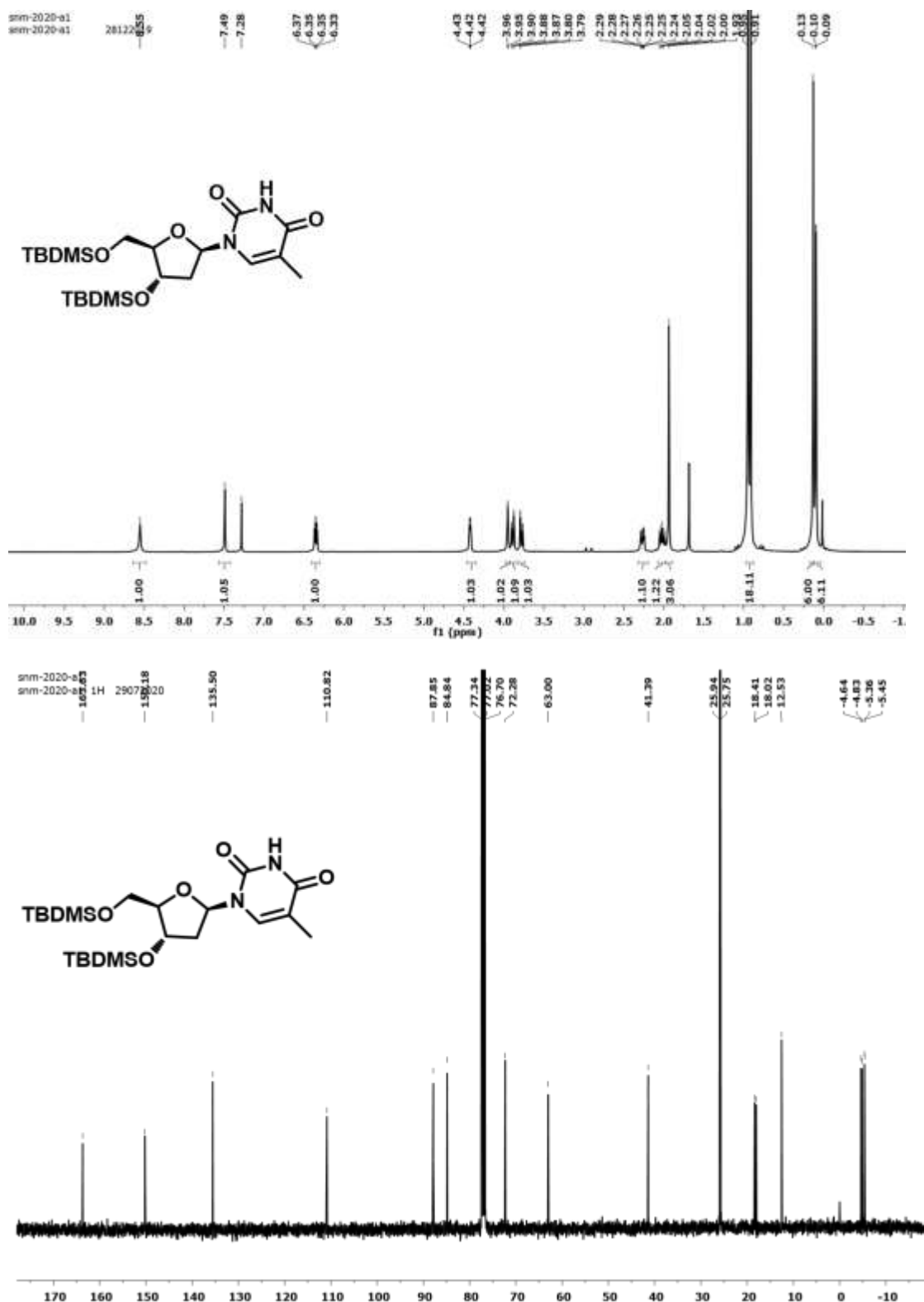


Figure A2. ESI-MS/HRMS spectra of compound 3

2.  $^1\text{H}$ ,  $^{13}\text{C}$  NMR (400MHz,  $\text{CDCl}_3$ ) and HRMS of compound **5**Figure A3.  $^1\text{H}/^{13}\text{C}$  NMR (400MHz,  $\text{CDCl}_3$ ) spectra of compound **5** in  $\text{CDCl}_3$

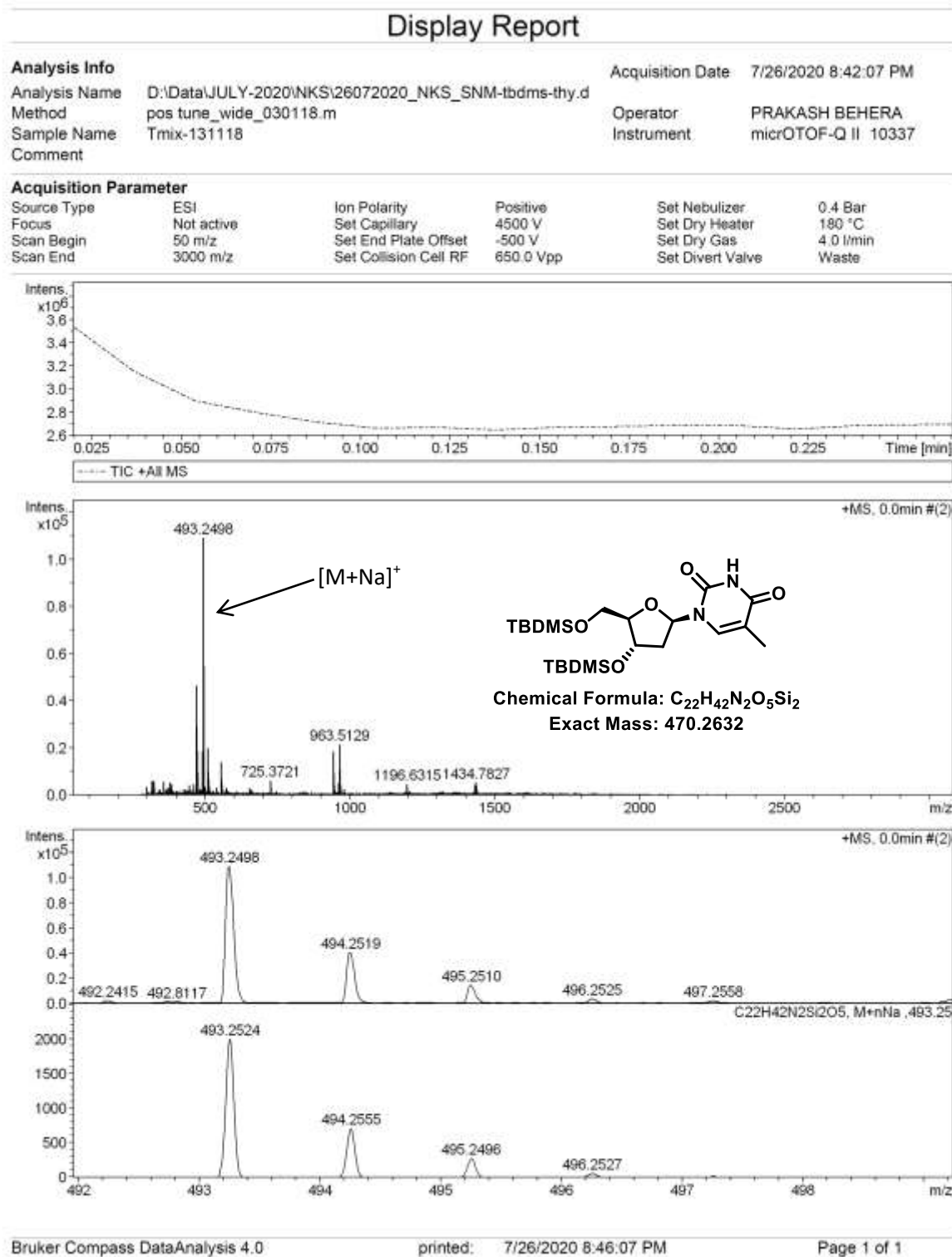
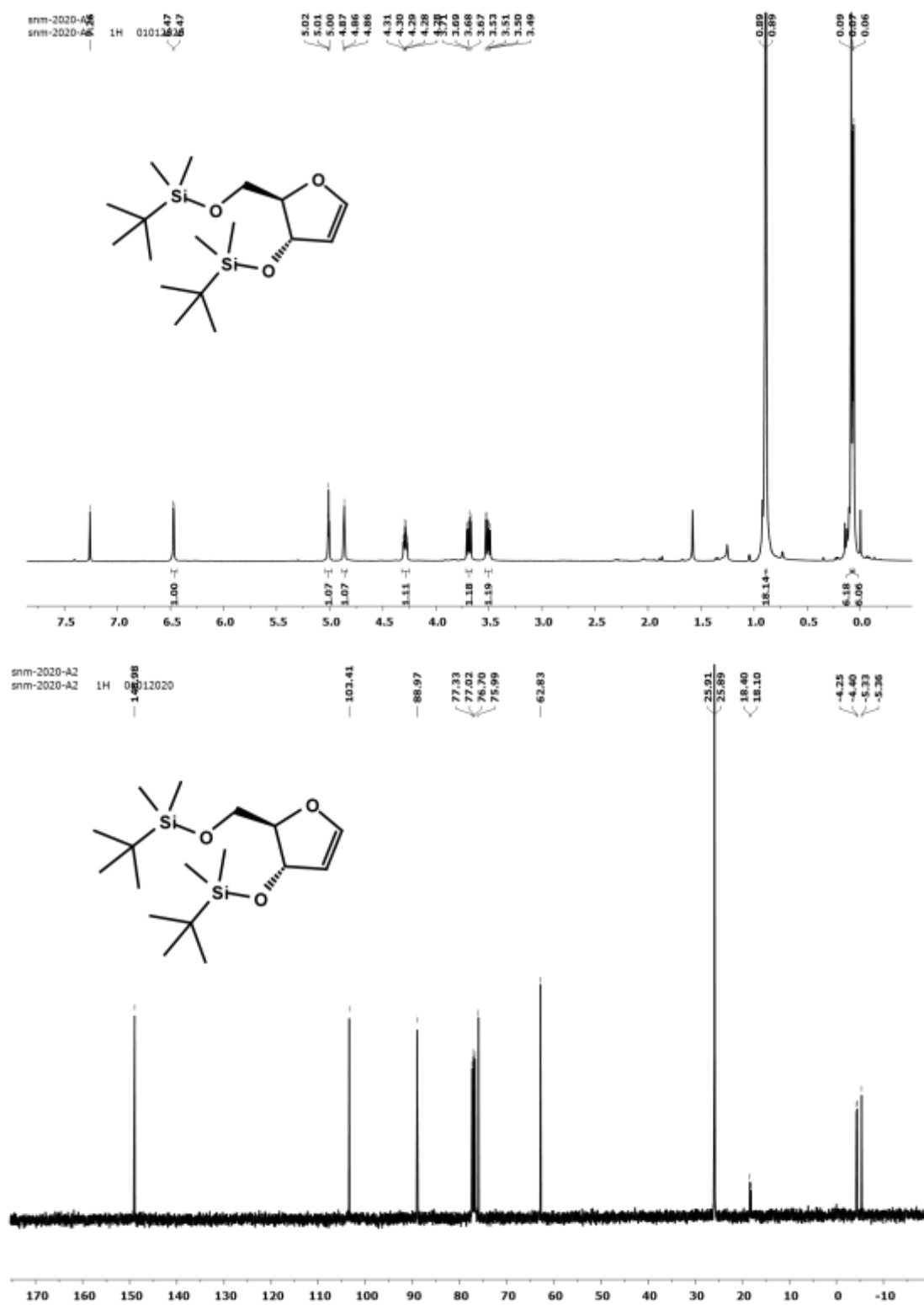


Figure A4. ESI-MS/HRMS spectra of compound 5



3.  $^1\text{H}$ ,  $^{13}\text{C}$  NMR (400MHz,  $\text{CDCl}_3$ ) and HRMS of compound **6**Figure A5.  $^1\text{H}/^{13}\text{C}$  NMR (400MHz,  $\text{CDCl}_3$ ) spectra of compound **6** in  $\text{CDCl}_3$

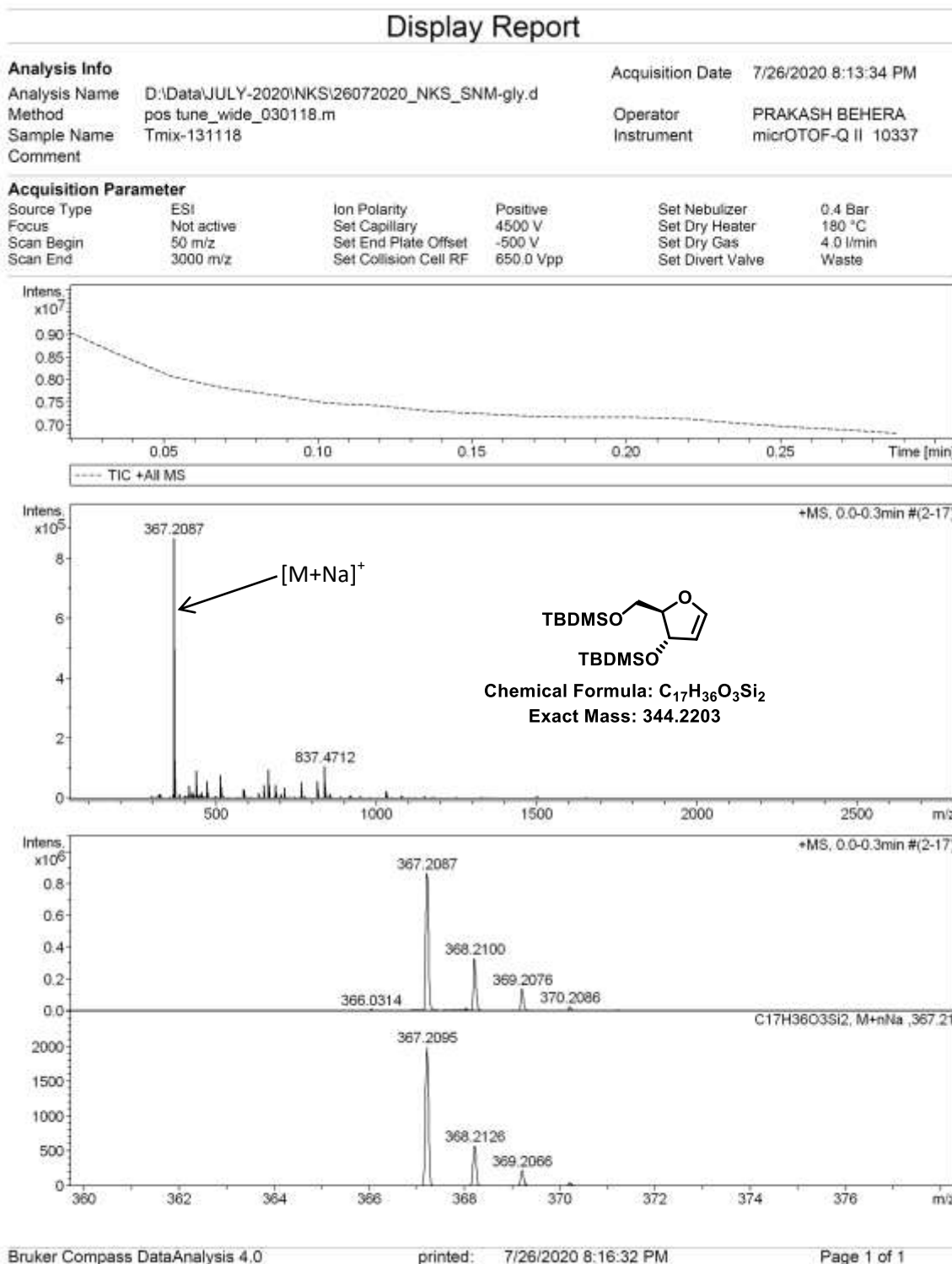
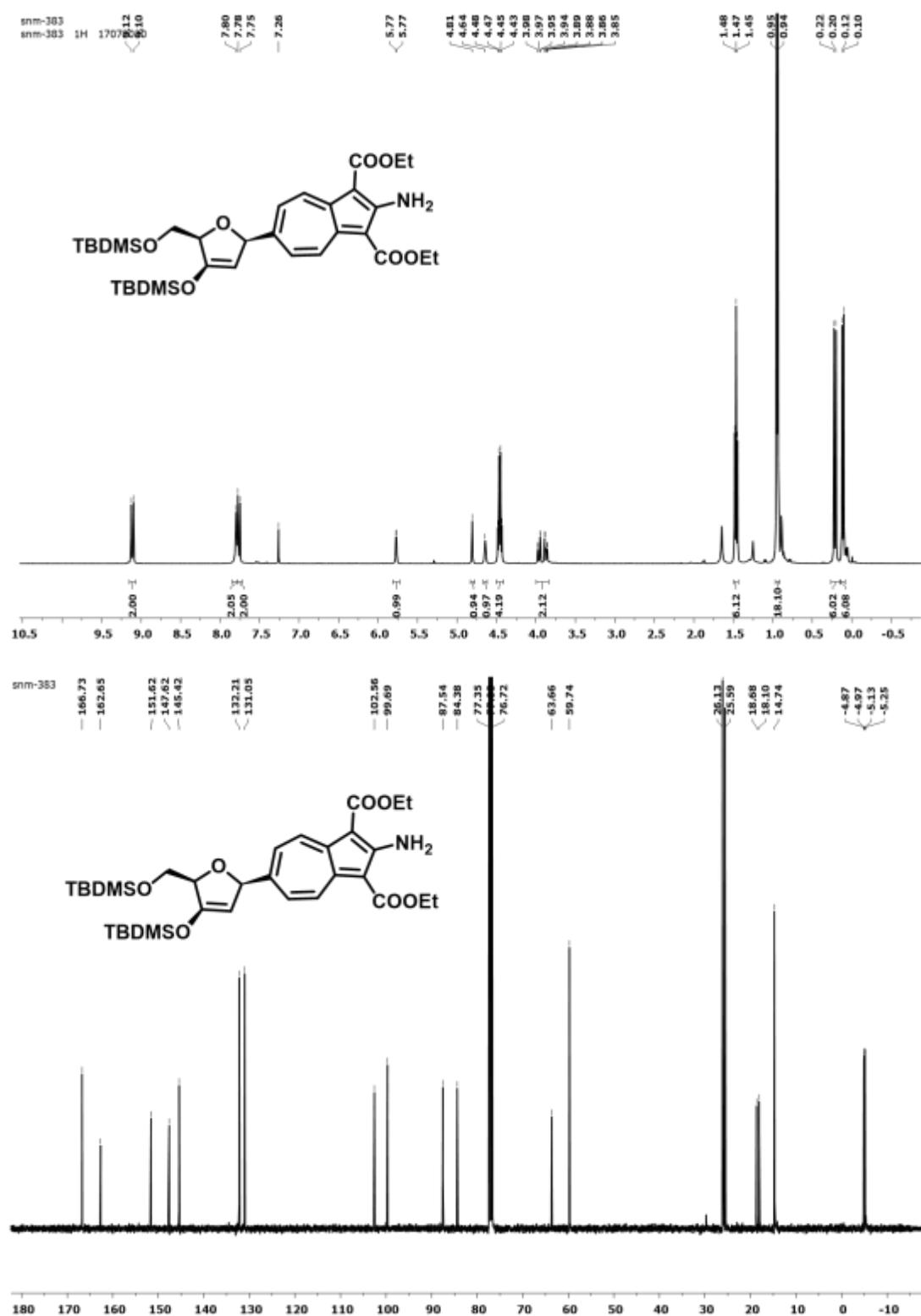


Figure A6. ESI-MS/HRMS spectra of compound 6

4.  $^1\text{H}$ ,  $^{13}\text{C}$  NMR (400MHz,  $\text{CDCl}_3$ ) and HRMS of compound **7**Figure A7.  $^1\text{H}/^{13}\text{C}$  NMR (400MHz,  $\text{CDCl}_3$ ) spectra of compound **7** in  $\text{CDCl}_3$

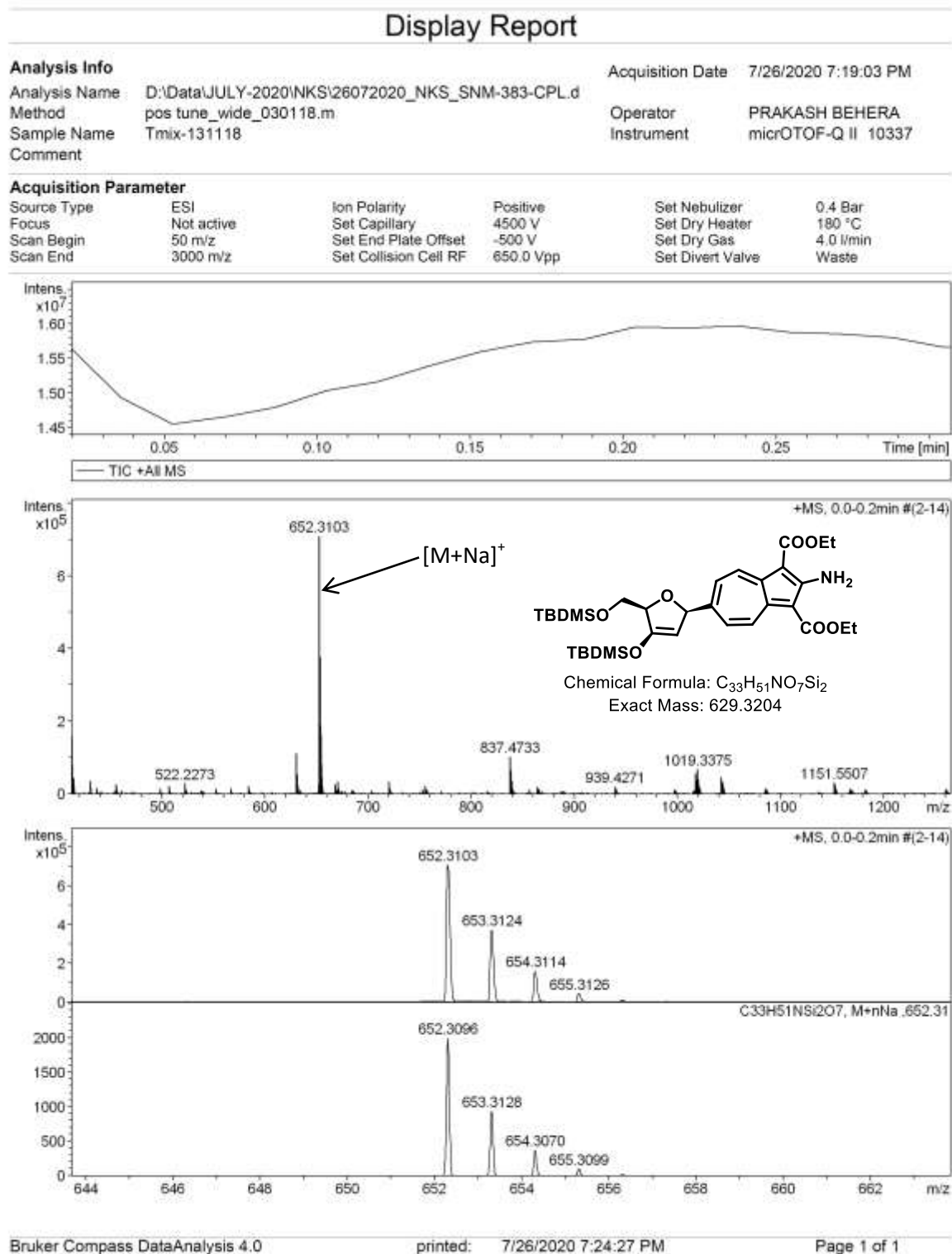
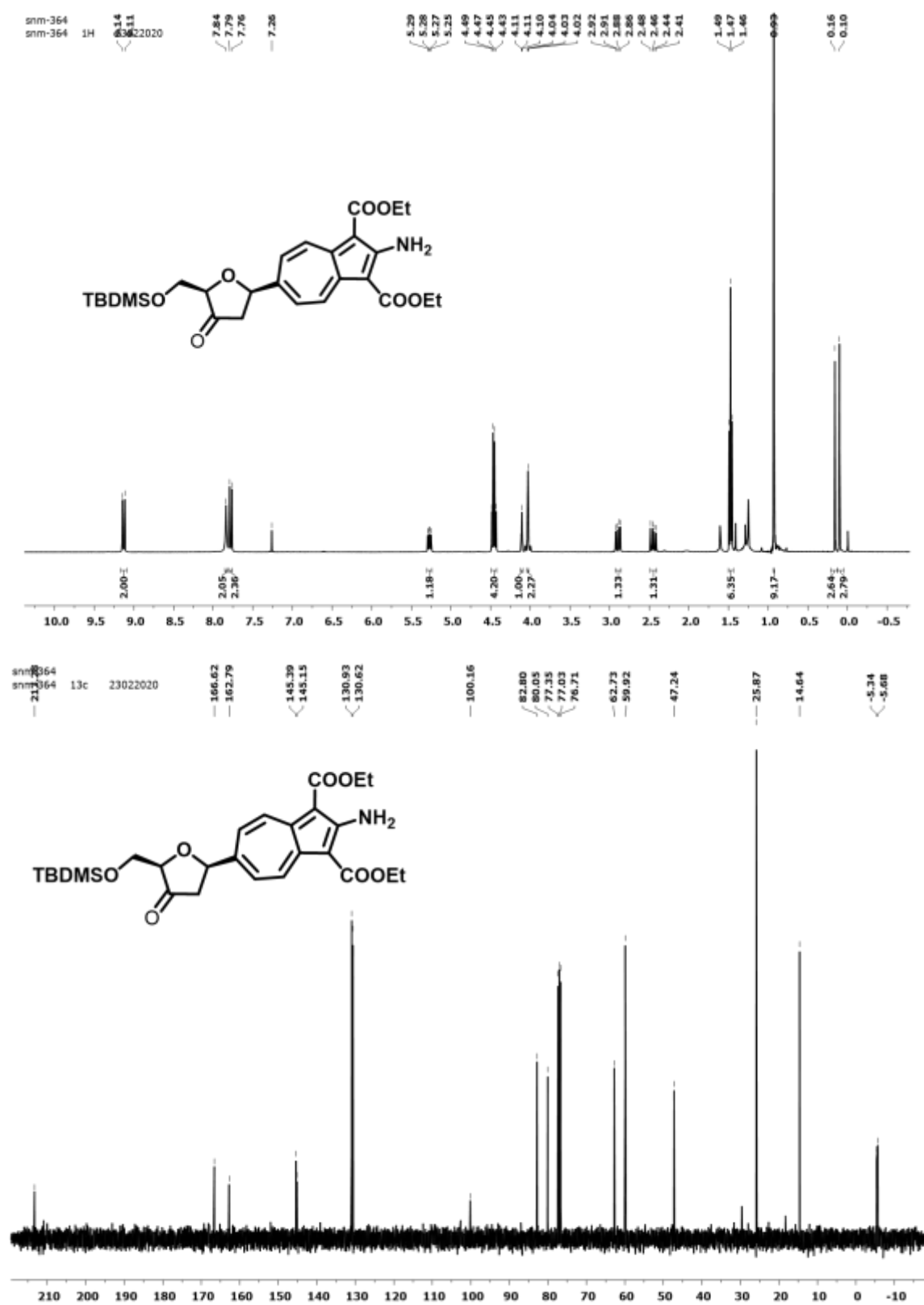
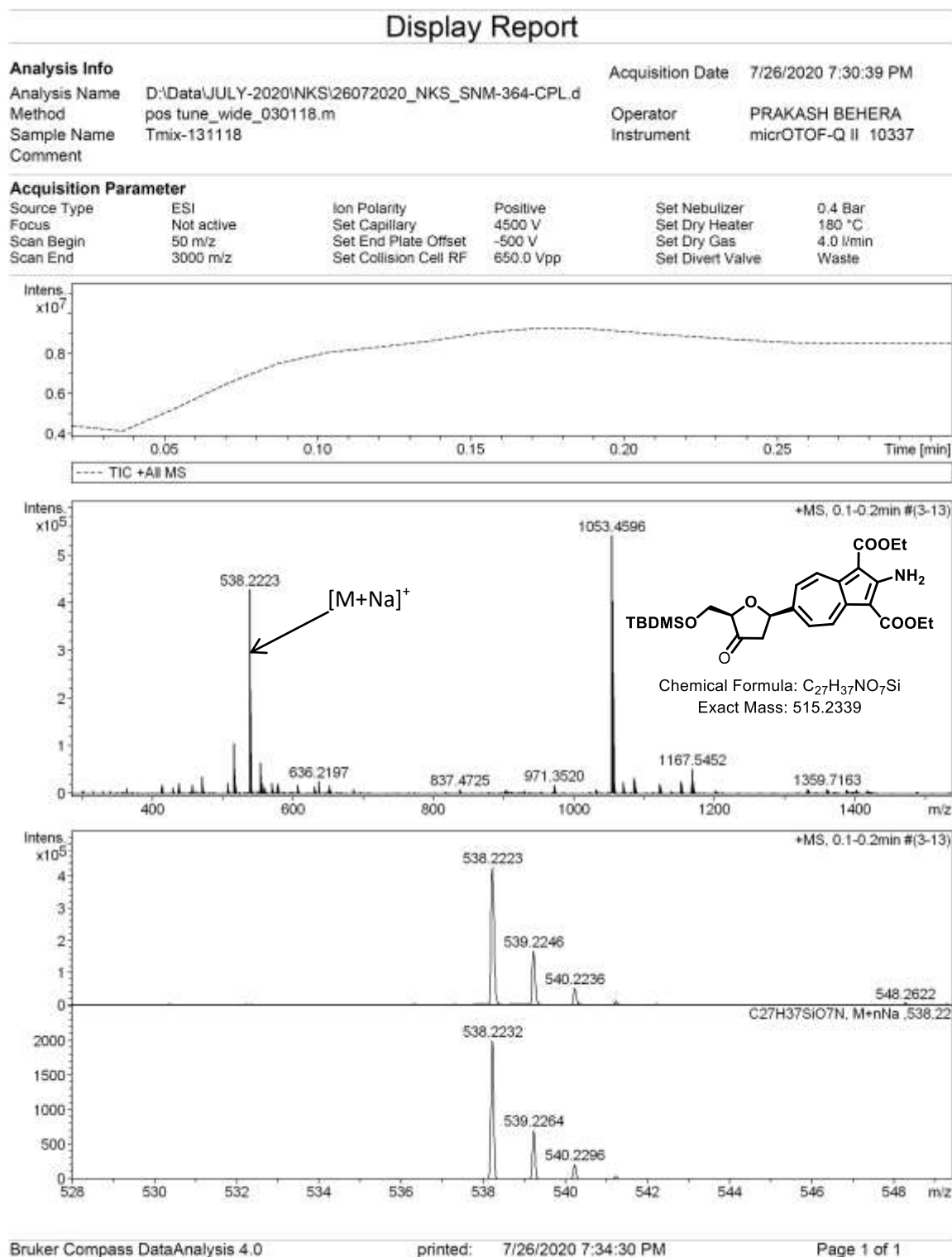
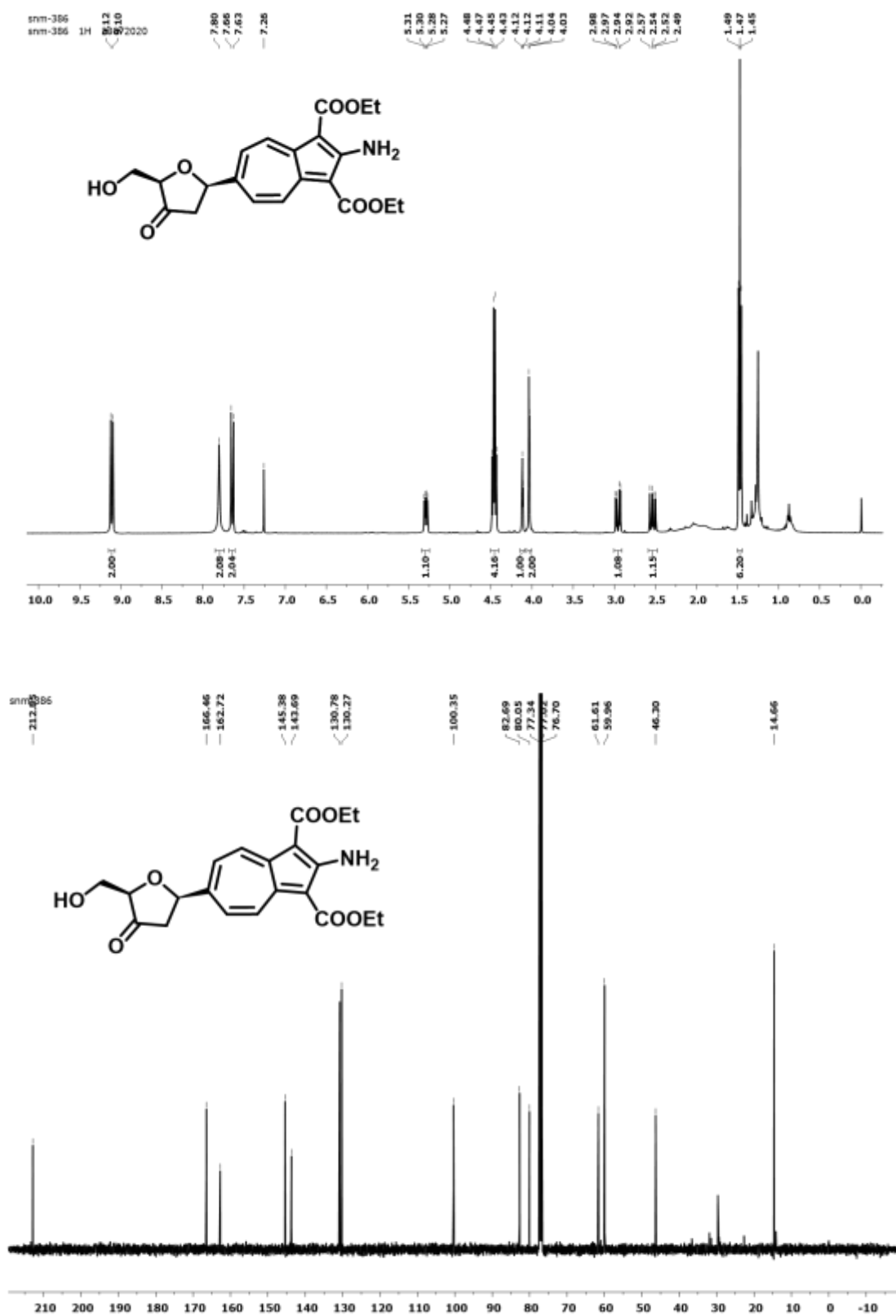
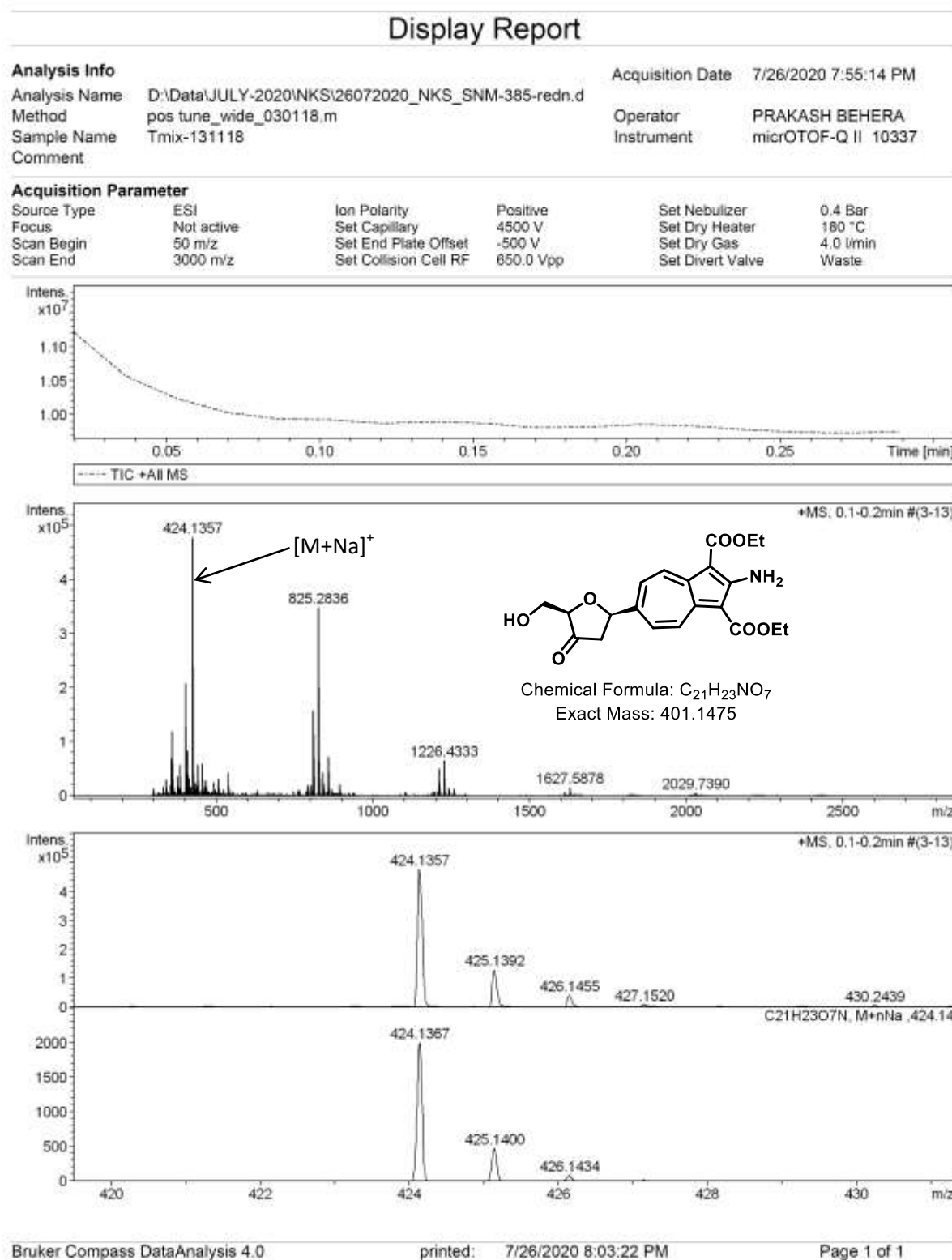


Figure A8. ESI-MS/HRMS spectra of compound 7

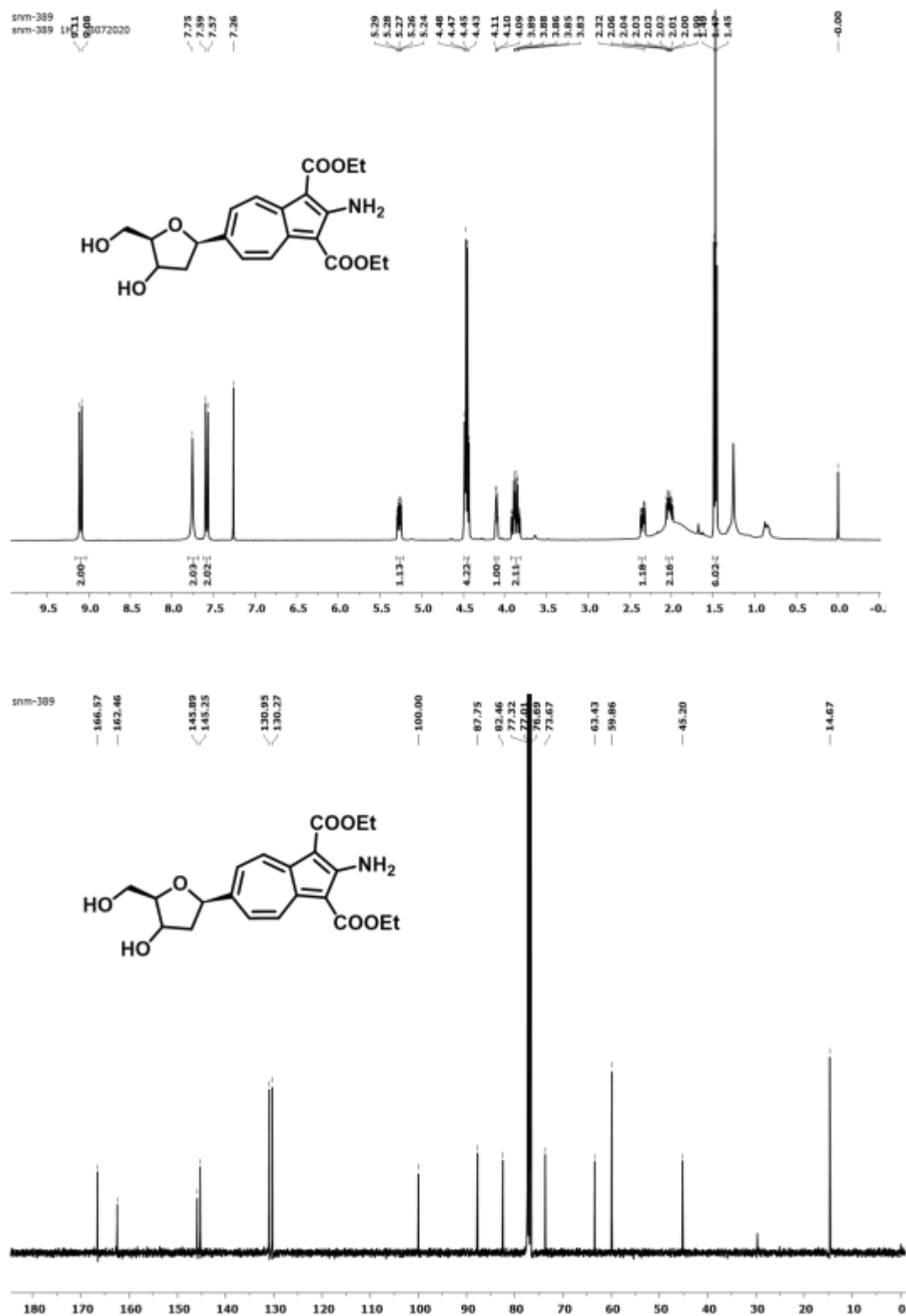
5.  $^1\text{H}$ ,  $^{13}\text{C}$  NMR (400MHz,  $\text{CDCl}_3$ ) and HRMS of compound **8**Figure A9.  $^1\text{H}/^{13}\text{C}$  NMR (400MHz,  $\text{CDCl}_3$ ) spectra of compound **8** in  $\text{CDCl}_3$

Figure A10. ESI-MS/HRMS spectra of compound **8**

6.  $^1\text{H}$ ,  $^{13}\text{C}$  NMR (400MHz,  $\text{CDCl}_3$ ) and HRMS of compound **9**Figure A11.  $^1\text{H}/^{13}\text{C}$  NMR (400MHz,  $\text{CDCl}_3$ ) spectra of compound **9** in  $\text{CDCl}_3$

**Figure A12.** ESI-MS/HRMS spectra of compound **9**



7.  $^1\text{H}$ ,  $^{13}\text{C}$  NMR (400MHz,  $\text{CDCl}_3$ ) and HRMS of compound **10**Figure A13.  $^1\text{H}/^{13}\text{C}$  NMR (400MHz,  $\text{CDCl}_3$ ) spectra of compound **10** in  $\text{CDCl}_3$

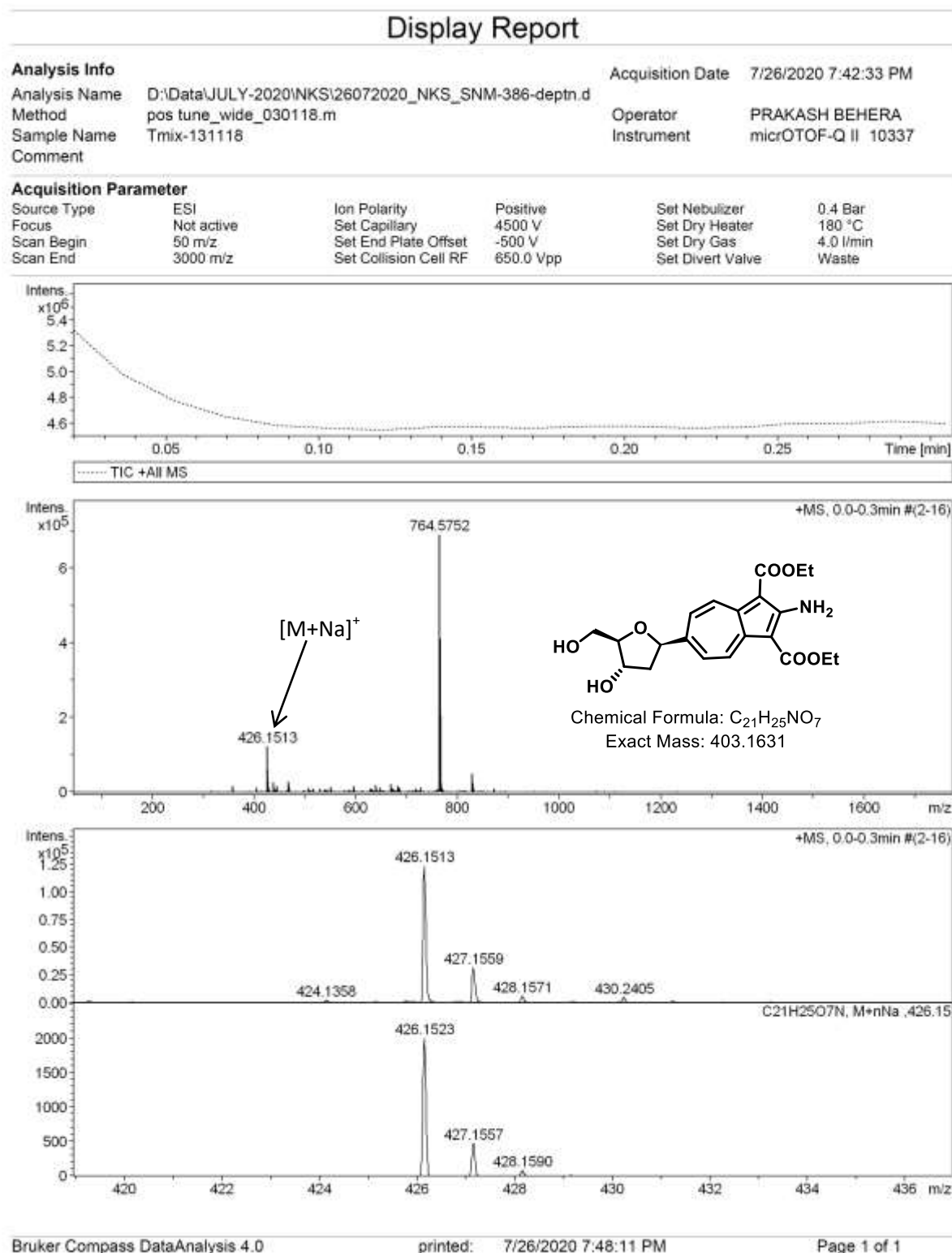


Figure A14. ESI-MS/HRMS spectra of compound 10

## **CHAPTER 5**

---

### **Troponylbodipy Cisplatin and C-nucleoside analogs: Synthesis and Biochemical evaluation**

---

#### **5.1 Introduction**

#### **5.2 Objective**

#### **5.3 Results and Discussion**

#### **5.4 Conclusion**

#### **5.5 Experimental Section**

#### **5.6 References and Notes**

#### **5.7 Appendix**

## 5.1 Introduction

Boron-dipyrromethene (BODIPY) dyes have been extensively used as trackers in cellular imaging studies. Their photophysical and photochemical properties make them suitable for bioimaging and therapeutic agents.<sup>1,2</sup> These dyes exhibit excellent photophysical properties, including a high molar absorption coefficient, strong fluorescence quantum yields, and photochemical and chemical stabilities.<sup>3,4</sup> As a result, they have been used in a wide range of applications, including biological imaging, sensors, photodynamic treatment, dye-sensitized solar cells, and light-emitting materials for electroluminescent devices.<sup>5–13</sup> Recent studies have revealed that BODIPY-appended transition metal complexes like Cisplatin-BODIPY can be used to detect drugs inside cells in real-time.<sup>14,15</sup> Since Rosenberg's accidental discovery of cisplatin's anticancer activity, a significant number of cisplatin variants have been synthesized and tested for their potential to kill cancer cells and limit tumor growth.<sup>16</sup> Cisplatin (Figure 5.1-a) and its analogs, carboplatin, and oxaliplatin, are well-known chemotherapy drugs. At the same time, nedaplatin, lobaplatin, and heptaplatin are being probed as prospective chemotherapeutic agents.<sup>17–19</sup> These drugs operate as transcription inhibitors by producing adducts with nuclear DNA, such as inter and/or intrastrand crosslinks via platinum(II) and the N<sup>7</sup> atoms of guanine residues, resulting in apoptotic cell death.<sup>20</sup> Platinum(II) drugs, cisplatin, and carboplatin treat 40–80% of cancer patients alone or in combination with other medications.<sup>21–23</sup> The method by which such substances do so consists of multiple steps, the first of which is cellular absorption. A platinum anticancer agent's efficacy is determined by its capacity to enter the cell and penetrate the nucleus, where the crucial target, DNA, is located.<sup>24</sup> Even with the clinical success of these bifunctional drugs, they suffer from dose-limiting and other side effects. These include poor tumor selectivity, intrinsic and acquired resistance, and reduced activity owing to the nuclear excision repair (NER) mechanism.<sup>25</sup> To compensate for the

shortcomings of such pharmacological molecules, monofunctional platinum(II) complexes were introduced.<sup>26–31</sup> When compared to traditional bifunctional platinum-based drugs, such complexes have significantly different anticancer efficacy due to altered cellular responses. For example, monofunctional Pt-BODIPY conjugates (Figure 5.1-c) sensitise anticancer action by increasing cellular accumulation after short photoirradiation duration when compared to cisplatin. More over tethering fluorophores to the complexes' Pt(II) centres could result in fluorescent molecules, allowing the complexes' cellular location to be studied using fluorescence imaging.<sup>32</sup>

The interactions between BODIPY compounds with biomolecules (DNA, RNA, and protein) have fascinated researchers in developing potential drug candidates.<sup>33</sup> The compounds bind to DNA in either covalent or noncovalent ways. Covalent binders have harmful side effects because the covalent binding mode is irreversible and has a high binding affinity. Noncovalent (electrostatic, major/minor groove, intercalation) binding modes are reversible and preferred over covalent ones.<sup>34–36</sup> So another approach was to link bodipy scaffold to the nucleosides by a linker to make fluorescent nucleic acids (FNA) because fluorescence has emerged as a helpful tool to study the structure and dynamics of nucleic acids. These modified nucleosides can act as Environment-sensitive fluorophores (ESF) and be used as probes for studying secondary structures, biomolecular interactions, imaging, microscopy, and metabolic studies.<sup>37–40</sup> It would be exciting to attach a bodipy analog to the sugar ring without using any linker, which is considered a C-nucleoside analog. C-nucleosides are a type of modified nucleoside that is distinguished by the replacement of a labile glycosidic C-N bond with a stable C-C bond. While natural and synthesized N-nucleosides are sensitive to enzymatic and acid-catalyzed nucleosidic bond hydrolysis, their C-analogues are far more stable.<sup>41,42</sup> There is a detailed description of tropolone and C-nucleosides in the previous chapters (Chapters 2 and 4A).

## 5.2 Objective

Tropolone is a seven-membered, nonbenzenoid aromatic compound possessing interesting properties. In this chapter, we have designed and synthesized a troponylbodipy appended cisplatin and a C-nucleoside derivative.

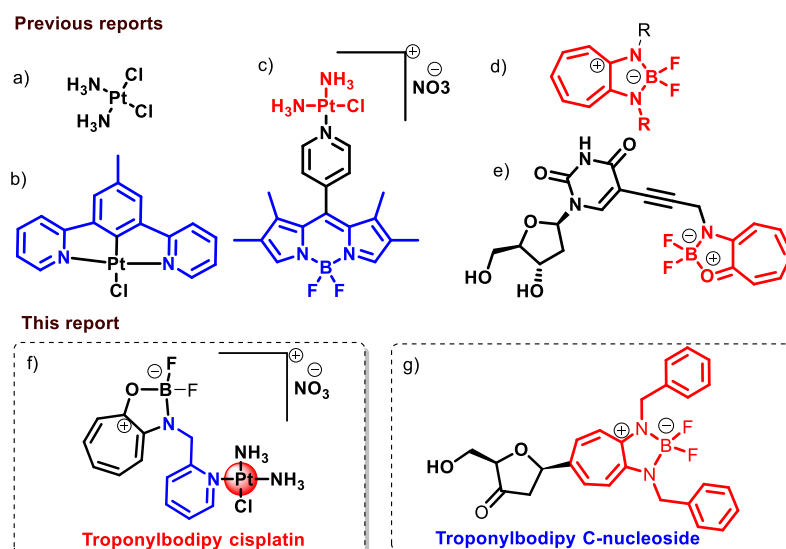
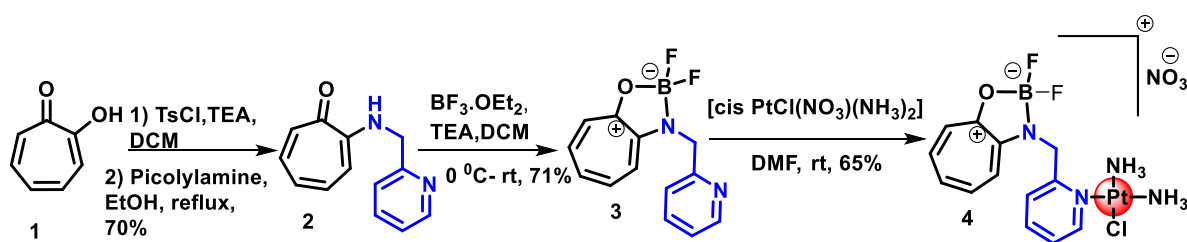


**Figure 5.1.** Previous and this reports on bodipy cisplatin and troponylbodipy nucleoside analogs.

## 5.3 Results and Discussion

We started the synthesis from commercially available tropolone (**1**). Following the reported procedure, Tropolone was derivatized into a difluoro boron complex of picolylaminotropone (**3**).<sup>43</sup> Here, picolylaminotropone (**2**) was treated with  $\text{BF}_3 \cdot \text{OEt}_2 / \text{TEA}$  in DCM to get the corresponding difluoro boron complex, i.e., picolylaminotropone boron complex (PTB) (**3**). Cisplatin was first treated with silver nitrate, followed by the addition of the ligand PTB (**3**) in DMF to get the platinum complex denoted as  $[\text{Pt}(\text{NH}_3)_2(\text{PTB})\text{Cl}](\text{NO}_3)$  (**4**) (Scheme 5.1).<sup>23,44</sup> The ligand and their platinum (II) complexes were characterized from the NMR and ESI-HRMS data (see Appendix). The ESI-HRMS mass spectra of complex **4**

revealed the  $[M-(NO_3)]^+$  peak in accordance with the calculated  $m/z$  values. The isotopic distribution pattern showed the presence of platinum and unipositive charge of the complexes (Figure A8, Appendix). Pt(II) complex (**4**) was diamagnetic, and its  $^1H$  NMR spectra also supported the formation of the product (Figure 5.2). It had characteristic two singlet peaks protons of two  $NH_3$  groups. The methylene protons ( $-CH_2-$ ) appeared as two doublets, which were a singlet in the case of the PTB ligand (**3**). There were also significant differences in  $^1H$  NMR spectra for the aromatic protons.



**Scheme 5.1.** Synthesis of the platinum complex  $[Pt(NH_3)_2(PTB)Cl](NO_3)$  (**4**).

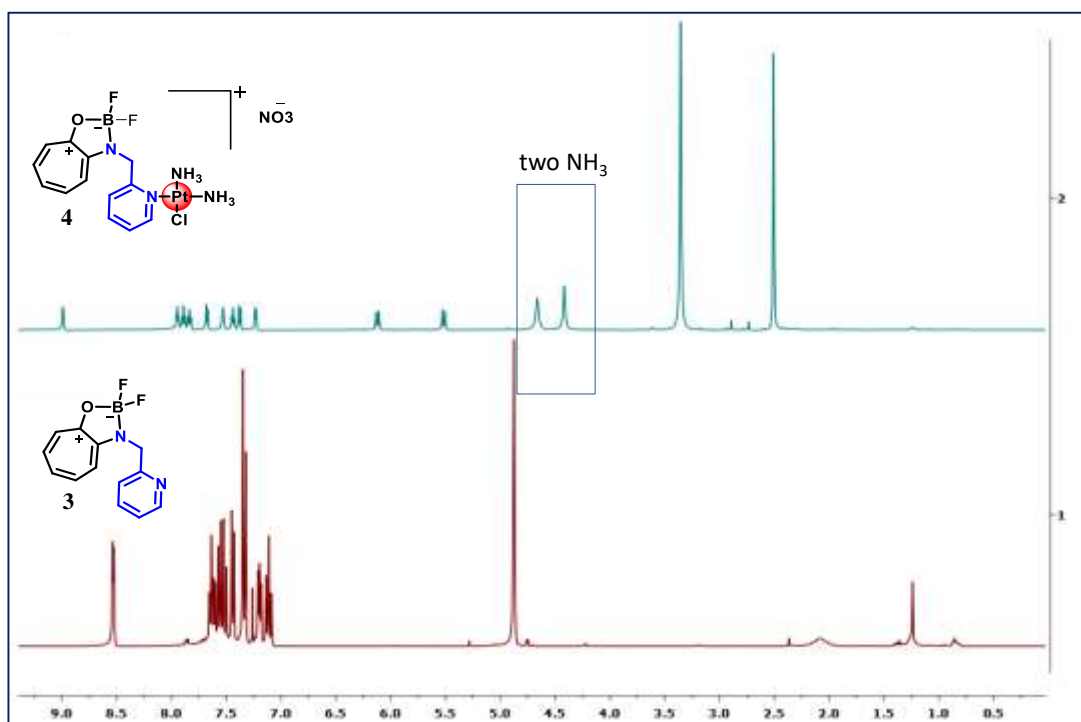


**Figure 5.2.**  $^1H$  NMR spectra comparison of compounds **3** and **4**.

The UV-Vis and fluorescence spectra of compounds **3** and **4** were recorded in PBS buffer (10 X) (Table 5.1, Figure 5.3). The spectral patterns were almost the same for both compounds. Compounds **3** and **4** displayed strong absorption bands near 333 and 375 nm, which are assignable to the electronic transition involving the picolylaminotroponyl-boron complex moiety. Both compounds showed an intense emission band at 433 nm ( $\lambda_{\text{ex}} = 333$  nm). The free ligand PTB (**3**) gave an emission spectrum with almost fivefold more quantum yield ( $\Phi_f = 10.3\%$ ) than the complex **4** ( $\Phi_f = 1.7\%$ ).

**Table 5.1.** Summary table of photophysical properties of compounds **3** and **4** in PBS buffer.

Cpd	$\lambda_{\text{abs}}$ (nm)	Abs	$\lambda_{\text{em}}$ (nm)	Stokes shift (nm)	OD (nm)	$\Phi(\%)$
4	333, 375	0.12173, 0.12978	433	100	326	1.7
3	333, 375	0.21588, 0.20661	433	100	340	10.3

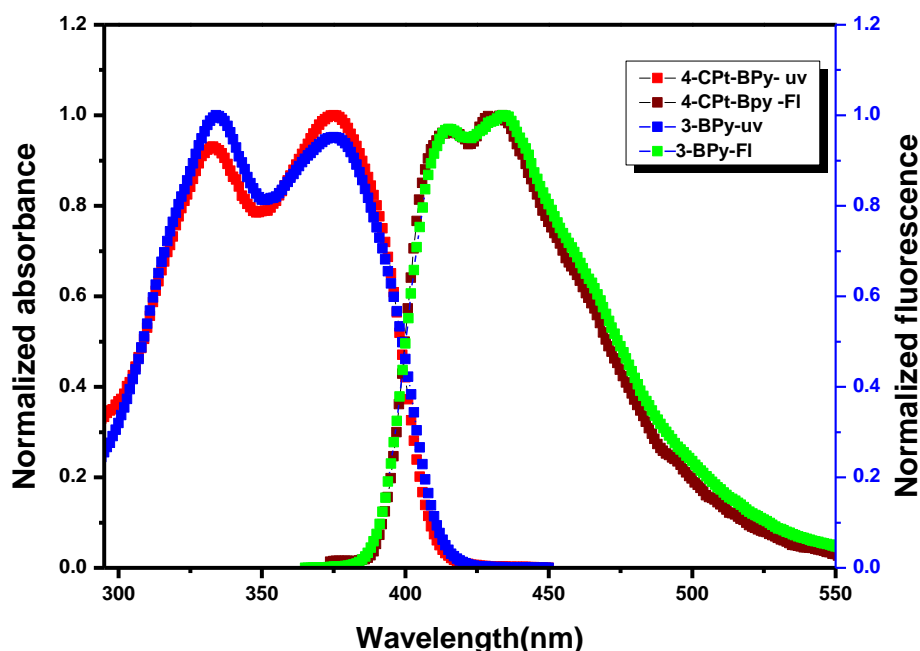


**Figure 5.3.** Normalized absorption and emission spectra of compounds **3** and **4** in PBS buffer at  $10^{-5}$  M concentration.



The biocompatibility of synthetic compounds is essential for their biomedical applications. Herein, the biocompatibility of compound **4** was evaluated by MTS assays towards HeLa and HEK293T cells. No significant cytotoxicity was observed, at a 100  $\mu\text{M}$  concentration for compound **4** after 24 h (Figure 5.4). Thus the biochemical applications of compound **4** can be further explored.

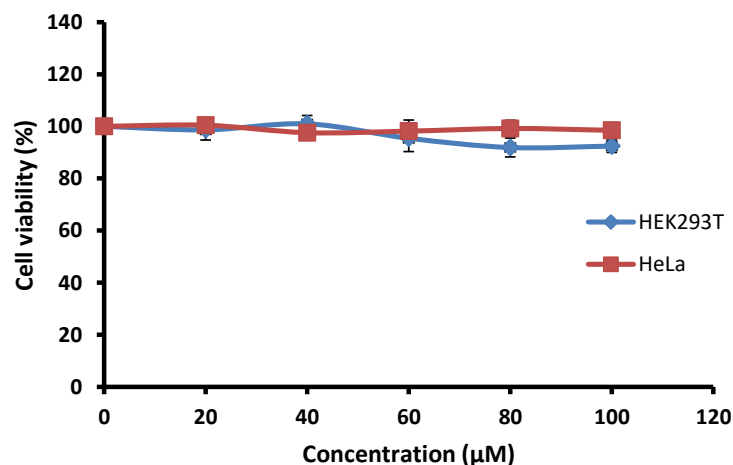


**Figure 5.4.** Cell proliferation assay of compound **4**.

The emissive complex **4** was used for cellular imaging in the HeLa cell line. Cells were treated with compound **4** (100  $\mu\text{M}$ ), co-stained with DAPI dye, and incubated for 24 h in the dark. Images were taken under bright light and different channels such as DAPI (blue channel,  $\lambda_{\text{ex}}$  358 nm), FITC (green channel,  $\lambda_{\text{ex}}$  490 nm) and TRITC (red channel,  $\lambda_{\text{ex}}$  570 nm). From the imaging studies, compound **4** was majorly found to be located in the cellular nucleus. In Figure 5.5, cells clearly show the localization of DAPI at the nucleus of cell. Under FITC (green) and TRITC (red) channels, the localization of compound **4** in the nucleus was observed. The merged images and colocalization studies further evidenced it. The extent of colocalization was estimated by Pearson's correlation coefficient (PCC) method using JACoP plugin in Fiji: ImageJ. Pearson's coefficient ( $r$ ) values for red and green channels were 0.96 and 0.95, respectively. However, the shapes of HeLa cells appeared slightly different

than their standard spindle shape, which needed more exploration. Compound **4** treated cells show cell internalization without transfecting reagents and can be used as a probe.

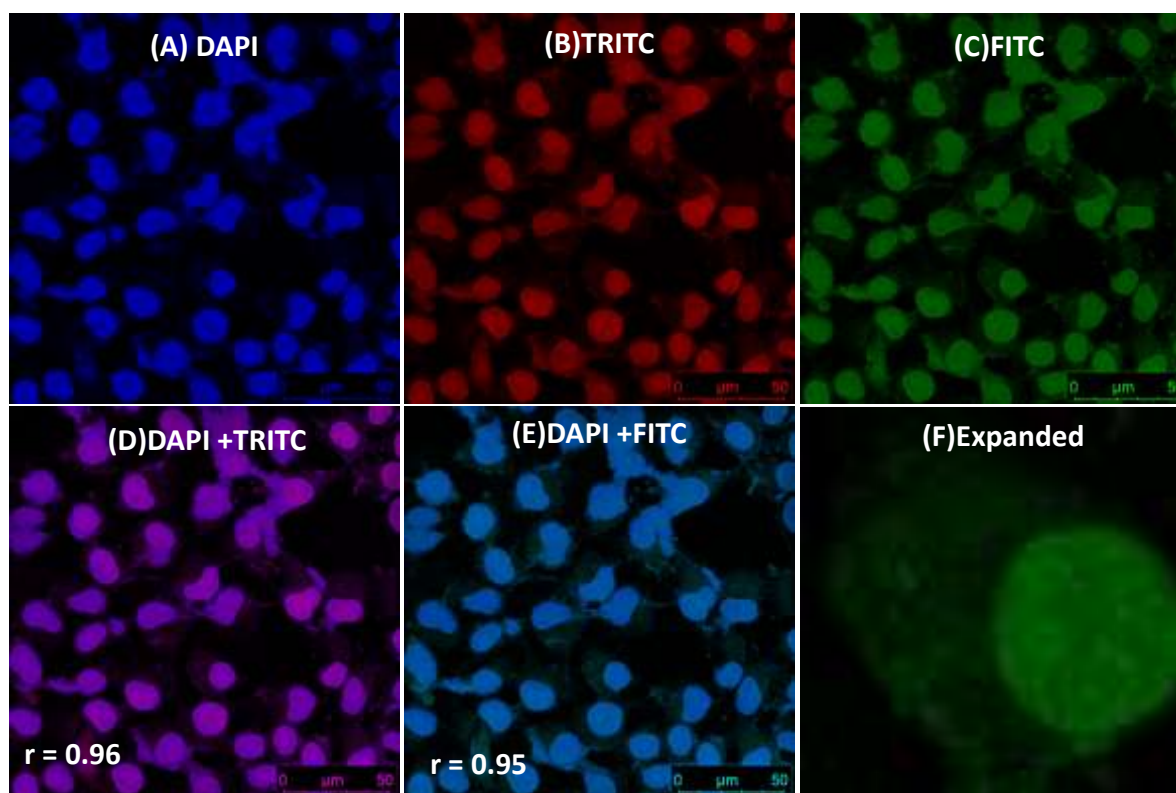
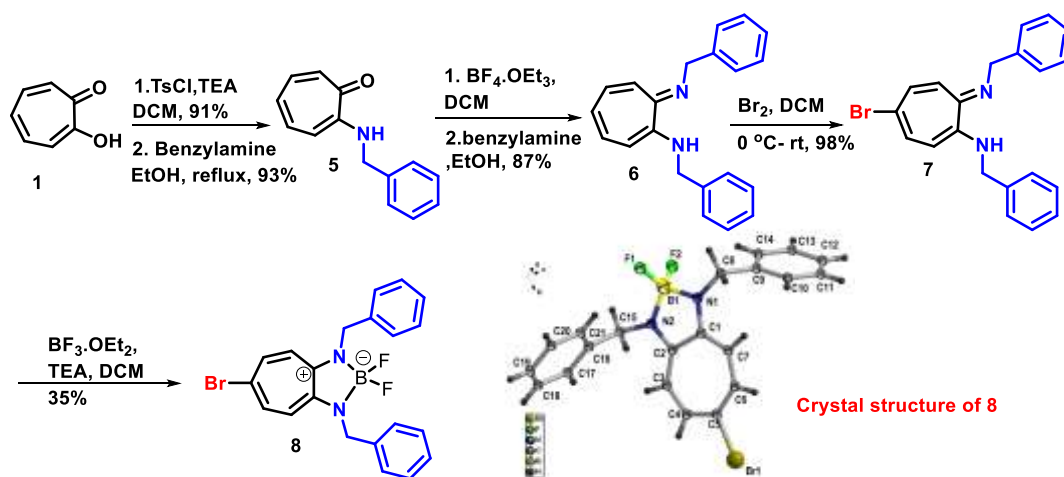


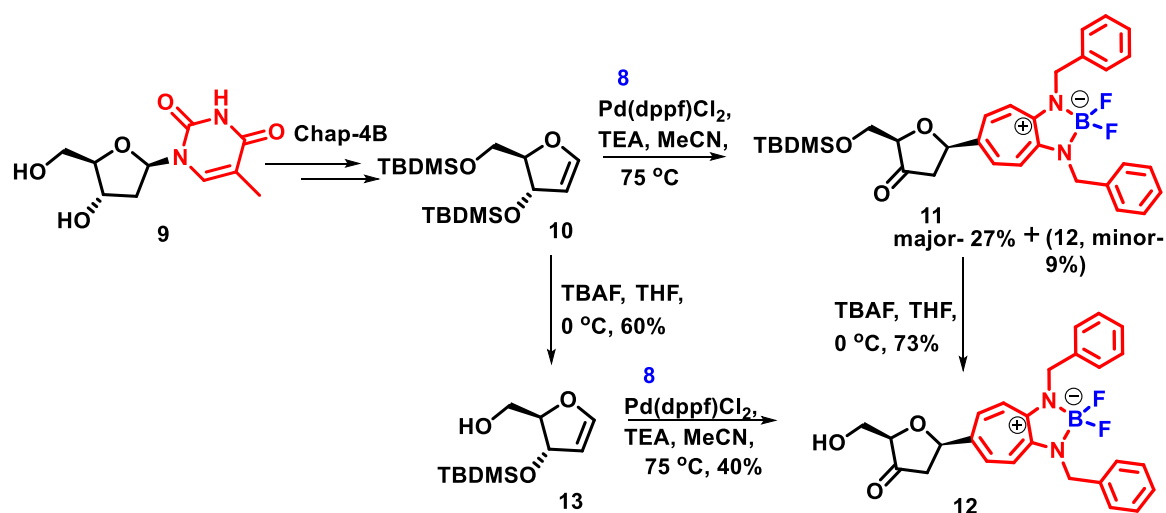
**Figure 5.5.** Confocal microscopic images of HeLa cells incubated with compound **4** (stained with DAPI) for 24 h at a concentration of 100  $\mu$ M.

We also designed troponyl bodipy containing C-nucleoside without any linker. In Scheme 5.2, tropolone was converted into 2-tosyloxypone and then treated with benzyl amine, which produced *N*-benzyl aminotropone (**5**) in good yield. *N*-benzyl aminotropone (**5**) was further converted into troponimine derivative (**6**) by treating sequentially with triethyloxonium tetrafluoroborate and benzyl amine. Up on treatment with Br<sub>2</sub> in DCM, bromination occurred selectively in the 5-position giving the bromo-troponimine derivative (**7**) in high yield. Synthetic steps up to compound **7** is well documented in literature.<sup>45,46</sup> From compound **7**, the corresponding difluoro boron complex, i.e., bromotroponylbodipy analog (**8**) was synthesized by using BF<sub>3</sub>.OEt<sub>2</sub>/TEA in DCM, which was isolated in 35% yield.



**Scheme 5.2.** Synthesis and crystal structure of bromotroponimine difluoro boron complex (8).

The synthesis of the target troponylbodipy C-nucleoside (**12**) was envisaged from the bromotroponimine difluoro boron complex (**8**) and glycal (**10**) steps by using a Heck-type coupling reaction as the major step (Scheme 5.3). Glycal (**10**) was synthesized as described in Chapter 4B. For the Heck-type coupling between the bromotroponylbodipy derivative (**8**) and the glycal (**10**), Pd(dppf)Cl<sub>2</sub> was used as the catalyst. Here we observed the coupling product with TBDMS deprotection giving two glycosides (**11**, 27% and **12**, 9%). Compound **11** was further deprotected using TBAF/THF to get the intermediate 3'-keto derivatives (**12**). The cause of TBDMS group deprotection may be the presence of boron moiety and temperature (75 °C). So to get only compound **12**, we followed a different route. Instead of glycal (**10**), we used mono-TBS protected glycal (**13**), and it can be synthesized by a single desilylation step from compound **10**.<sup>47</sup> Following this route, we got intermediate 3'-keto derivatives (**12**) in 40%. Further, we tried to reduce the 3'-keto group using NaBH(OAc)<sub>3</sub> but couldn't succeed, probably due to the steric hindrance. This work is still underway; we are trying to remove the 3'-keto group completely using tosylhydrazide derivatives.



**Scheme 5.3.** Synthesis of troponylbodipy 3'-keto C- nucleoside derivative (**12**).

## 5.4 Conclusion

In summary, we have synthesized a cisplatin derivative and a C-nucleoside having troponylbodipy moiety. The C-nucleoside can be incorporated into DNA in terminal position as a small fluorescent tag. The work on troponylbodipy C-nucleoside is in progress. The troponylbodipy cisplatin exhibited fivefold less fluorescence than the parent troponyl bodipy derivative. It was used for imaging to see the effect on HeLa cell lines. The compound was localized inside the cellular nucleus showing some structural perturbation. It showed no significant cytotoxicity toward HEK293T and HeLa cell lines. Currently, we exploring its bioactivities and works are still in progress.

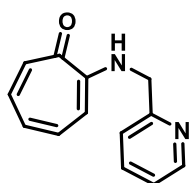
## 5.5 Experimental Section

*General informations:* Unless otherwise specified, all essential chemicals and solvents were acquired from commercial providers and used without additional purification. By distilling over Calcium hydride, anhydrous DCM, DMF, ACN solvents were freshly made and stored in 4 Å molecular sieves. Thin layer chromatography was used for monitoring the reactions, which were then visualised using UV and Ninhydrin. Column chromatography was carried

out on 100-200 mesh silica. The Bruker microTOF-Q II Spectrometer was used to obtain mass spectra, and the samples were prepared in methanol and injected in a methanol and water combination. At room temperature, NMR spectra were obtained on a Bruker AV- 400/ 700 ( $^1\text{H}$ : 400/ 700 MHz,  $^{13}\text{C}$ : 100.6 MHz,  $^{11}\text{B}$ : 128 MHz,  $^{19}\text{F}$ : 377 MHz). The crystal data were collected on a Rigaku Oxford diffractometer at 293 K. Absorption spectra were obtained using Jasco V- 730 spectrometer. Fluorescence spectra were obtained from Perkin-Elmer LS- 55 using Xenon lamp. Confocal images were taken in Leica Microscope.

#### *Characterization data of products*

2-((pyridin-2-ylmethyl)amino)cyclohepta-2,4,6-trien-1-one (**2**): Tropolone was converted in

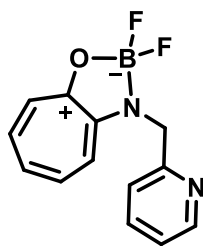


to 2- tosyloxytropone.<sup>43</sup> To a solution of 2- tosyloxytropone (3.6 mmol, 1 g) and picolylamines (7.2 mmol, 0.745 ml) dissolved in ethanol,  $\text{Et}_3\text{N}$  (10.8 mmol, 1.5 ml) was added. It was refluxed for 24 h and monitored by TLC.

After completion of the reaction all volatiles were evaporated under pressure. To the crude, 1.0 N HCl was added and extracted with dichloromethane (thrice). Then the organic layers were dried over  $\text{Na}_2\text{SO}_4$  and evaporated under reduced pressure. The resultant crude was subjected to column chromatography using EtOAc:Hexane mixture as mobile phase to get compound **2** (0.552 g, 70% yield),  $^1\text{H}$  NMR (400 MHz,  $\text{CDCl}_3$ )  $\delta$  8.62 (d,  $J$  = 4.7 Hz, 1H), 8.05 (s, 1H), 7.65 (td,  $J$  = 7.7, 1.6 Hz, 1H), 7.32 – 7.12 (m, 5H), 6.68 (t,  $J$  = 9.4 Hz, 1H), 6.53 (d,  $J$  = 10.3 Hz, 1H), 4.68 (d,  $J$  = 5.9 Hz, 2H),  $^{13}\text{C}$  NMR (101 MHz,  $\text{CDCl}_3$ )  $\delta$  177.12, 156.08, 155.26, 149.57, 137.36, 136.99, 136.22, 129.41, 122.80, 122.63, 121.18, 109.34, 48.23, HRMS ESI-Tof Calcd for  $\text{C}_{13}\text{H}_{12}\text{N}_2\text{O}$ :  $[\text{M}+\text{H}]^+$  213.1022, Found 213.1021.

2,2-difluoro-3-(pyridin-2-ylmethyl)-2,3-dihydrocyclohepta[d][1,3,2]oxazaborol-8a-ylum-2-uide (**3**): In anhydrous dichloromethane, compound **2** (0.3 g, 1.4 mmol) was dissolved, and  $\text{Et}_3\text{N}$  (3.8 ml, 27.5 mmol) was added. For the next step,  $\text{BF}_3\cdot\text{OEt}_2$  (3.4 ml, 27.5 mmol) was

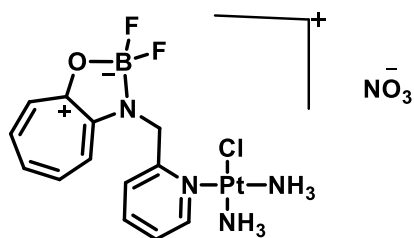
added to the reaction mixture and stirred at room temperature for about 24 h. The reaction



was monitor using TLC, and water was used to quench unreacted  $\text{BF}_3\cdot\text{OEt}_2$  before being extracted three times with dichloromethane. The collected organic layers were dried over  $\text{Na}_2\text{SO}_4$  and concentrated under reduced pressure. Using EtOAc:Hexane as the mobile phase, the crude

was subjected to column chromatography to get compound **3** (0.243 g, 71%).  $^1\text{H}$  NMR (700 MHz,  $\text{CDCl}_3$ )  $\delta$  8.53 (d,  $J = 4.6$  Hz, 1H), 7.63 (t,  $J = 7.7$  Hz, 1H), 7.57 (t, 1H), 7.52 (t,  $J = 10.2$  Hz, 1H), 7.44 (d,  $J = 7.8$  Hz, 1H), 7.34 (d,  $J = 10.7$  Hz, 2H), 7.20 (t, 1H), 7.11 (t,  $J = 9.8$  Hz, 1H), 4.88 (s, 2H),  $^{13}\text{C}$  NMR (176 MHz,  $\text{CDCl}_3$ )  $\delta$  167.82, 160.63, 155.87, 149.13, 141.91, 140.00, 137.39, 128.36, 122.93, 122.59, 120.06, 119.12, 49.38,  $^{19}\text{F}$  NMR (377 MHz,  $\text{CDCl}_3$ )  $\delta$  -137.33 – -137.94 (m),  $^{11}\text{B}$  NMR (128 MHz,  $\text{CDCl}_3$ )  $\delta$  6.07 (t,  $J = 18.3$  Hz), HRMS ESI-ToF Calcd for  $\text{C}_{13}\text{H}_{11}\text{BF}_2\text{N}_2\text{O}$ :  $[\text{M}+\text{K}]^+$  299.0566, Found 299.0520.

$[\text{Pt}(\text{NH}_3)_2(\text{PTB})\text{Cl}](\text{NO}_3)$  (**4**): To a solution of Cisplatin (0.15 g, 0.5 mmol) in 5 ml DMF,

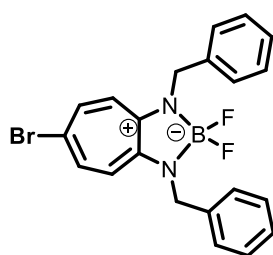


$\text{Ag}_2\text{NO}_3$  (0.076 g, 0.45 mmol) was added in the dark and stirred at rt for 24 h. The precipitate of  $\text{AgCl}$  was removed by filtration. Compound **3** (0.117 g, 0.45 mmol) was added to the solution and stirred for 24 h at rt. The

solvents were evaporated under in a rotavapor, and the residue was redissolved in 40 ml of MeOH. Unreacted Cisplatin was removed by filtration. Diethyl ether (60 ml) was added to the filtrate under vigorous stirring condition to obtain a solid precipitate. The precipitate was treated twice with diethyl ether before vacuum drying to get compound **4** (0.19 g, 65% yield) as an off-white solid. The compound was protected from light.  $^1\text{H}$  NMR (700 MHz, DMSO)  $\delta$  8.99 (d,  $J = 5.3$  Hz, 1H), 7.94 (t,  $J = 7.6$  Hz, 1H), 7.89 (t,  $J = 10.2$  Hz, 1H), 7.84 (t,  $J = 10.1$  Hz, 1H), 7.67 (d,  $J = 10.1$  Hz, 1H), 7.53 (t,  $J = 6.4$  Hz, 1H), 7.44 (t,  $J = 9.7$  Hz, 1H), 7.38 (d,  $J = 11.1$  Hz, 1H), 7.23 (d,  $J = 7.9$  Hz, 1H), 6.12 (d,  $J = 17.5$  Hz, 1H), 5.52 (d,  $J = 17.5$  Hz,

1H), 4.66 (s, 3H), 4.42 (s, 3H), <sup>13</sup>C NMR (176 MHz, DMSO) δ 167.42 (s), 160.49 (s), 158.16 (s), 154.74 (s), 143.90 (s), 142.15 (s), 140.32 (s), 130.89 (s), 125.22 (s), 123.38 (s), 121.87 (s), 120.01 (s), 48.41 (s), <sup>19</sup>F NMR (377 MHz, DMSO) δ -133.98 – -134.85 (m), <sup>11</sup>B NMR (128 MHz, DMSO) δ 6.01 (s), HRMS ESI-Tof Calcd for C<sub>13</sub>H<sub>17</sub>BClF<sub>2</sub>N<sub>4</sub>OPt<sup>+</sup>: [M]<sup>+</sup> 524.0801, Found 524.0781.

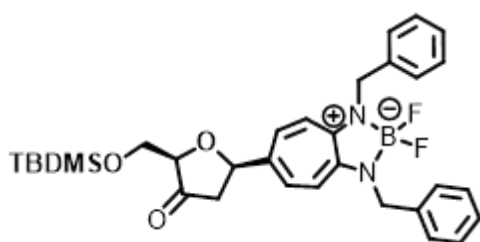
1,3-dibenzyl-6-bromo-2,2-difluoro-1,2-dihydro-2λ4,3λ4-cyclohepta[d][1,3,2]diazaborole (**8**):



Bromotroponimine derivative (**7**) (1 g, 2.6 mmol) was dissolved in dry DCM and to this Et<sub>3</sub>N (7.3 ml, 52.9 mmol) and BF<sub>3</sub>.OEt<sub>2</sub> (6.5 ml, 52.9 mmol) was added slowly with vigorous stirring at rt. The reaction mixture was evaporated in a rotavapor after completion.

Water was added to quench unreacted BF<sub>3</sub>.OEt<sub>2</sub> before being extracted three times with dichloromethane. The collected organic layers were dried over Na<sub>2</sub>SO<sub>4</sub> and concentrated. Using EtOAc:Hexane as the mobile phase, the crude was subjected to column chromatography to get compound **8** (0.39 g, 35%) as a yellow solid. <sup>1</sup>H NMR (400 MHz, CDCl<sub>3</sub>) δ 7.38 – 7.31 (m, 8H), 7.31 – 7.24 (m, 2H), 7.02 (d, *J* = 11.4 Hz, 2H), 6.16 (d, *J* = 11.3 Hz, 2H), 4.59 (s, 4H). <sup>19</sup>F NMR (377 MHz, CDCl<sub>3</sub>) δ -122.58 – -127.06 (m, 34.3 Hz). <sup>11</sup>B NMR (128 MHz, CDCl<sub>3</sub>) δ 5.82 (t, *J* = 34.4 Hz), HRMS ESI-Tof Calcd for C<sub>21</sub>H<sub>18</sub>BBrF<sub>2</sub>N<sub>2</sub>: [M+Na]<sup>+</sup> 449.0610, Found 449.0528.

1,3-dibenzyl-6-((2R,5R)-5-(((tert-butyl)dimethylsilyl)oxy)methyl)-4-oxotetrahydrofuran-2-yl)-2,2-difluoro-1,2,3,3a-tetrahydrocyclohepta[d][1,3,2]diazaborol-2-uide (**11**): A mixture of

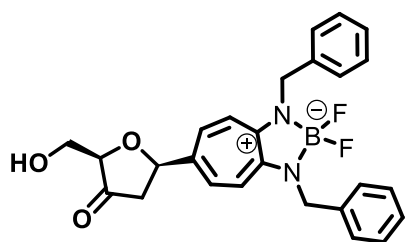


**10** (0.1 g, 0.29 mmol), **8** (0.14 g, 0.32 mmol), and triethylamine (0.12 ml, 0.87 mmol) was dissolved in acetonitrile (5 mL) in a dry round bottom flask, and the resulting mixture was degassed by using a long

needle and a balloon containing inert gas. [1,1'-Bis(diphenylphosphino)ferrocene]

dichloropalladium(II) (0.06 g, 0.072 mmol) was added, and the mixture was heated at 75 °C for 9 h. After this, the reaction mixture was concentrated under vacuum, and the crude product was purified by silica gel column chromatography (EtOAc:Hexane) to give **11** (0.045 g, 27%) as major product,  $^1\text{H}$  NMR (400 MHz,  $\text{CDCl}_3$ )  $\delta$  7.50 (d,  $J$  = 11.4 Hz, 2H), 7.40 (d,  $J$  = 7.3 Hz, 4H), 7.36 – 7.29 (m, 4.8 Hz, 4H), 7.29 – 7.22 (m, 3H), 6.74 (d,  $J$  = 11.2 Hz, 2H), 4.96 (dd,  $J$  = 10.8, 6.0 Hz, 1H), 4.85 (s, 4H), 3.97 (t,  $J$  = 2.1 Hz, 1H), 3.90 (d,  $J$  = 2.1 Hz, 2H), 2.74 – 2.66 (m, 6.0 Hz, 1H), 2.27 – 2.16 (m, 1H), 0.82 (s, 9H), 0.01 (d,  $J$  = 9.6 Hz, 6H),  $^{19}\text{F}$  NMR (377 MHz,  $\text{CDCl}_3$ )  $\delta$  -134.23 – -139.84 (m, 29.9 Hz),  $^{11}\text{B}$  NMR (128 MHz,  $\text{CDCl}_3$ )  $\delta$  5.44 (t,  $J$  = 29.6 Hz), HRMS ESI-Tof Calcd for  $\text{C}_{32}\text{H}_{39}\text{BF}_2\text{N}_2\text{O}_3\text{Si}$ :  $[\text{M}+\text{Na}]^+$  599.2689, Found 599.2612.

(2R,5R)-5-(1,3-dibenzyl-2,2-difluoro-1,2-dihydro-2H,3H-cyclohepta[d][1,3,2]diazaborol-6-



yl)-2-(hydroxymethyl)dihydrofuran-3(2H)-one (**12**): A mixture of **13** (0.05 g, 0.217 mmol), **8** (0.10 g, 0.24 mmol), and triethylamine (0.09 ml, 0.65 mmol) was dissolved in acetonitrile (5 mL) in a dry round bottom flask, and the

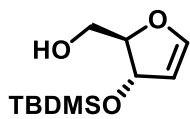
resulting mixture was degassed by using a long needle and a balloon containing inert gas.

[1,1'-Bis(diphenylphosphino)ferrocene] dichloropalladium(II) (0.044 g, 0.054 mmol) was added, and the mixture was heated at 75 °C for 9 h. After this, the reaction mixture was concentrated under vacuum, and the crude product was purified by silica gel column chromatography (EtOAc:Hexane) to give **12** (0.040 g, 40% yield). Compound **12** was also obtained as a minor product (0.015g, 9% yield) when coupling Heck reaction was performed using compound **10**. Compound **11** can be treated with TBAF/THF solution (desilylation) to get **12**. by  $^1\text{H}$  NMR (400 MHz,  $\text{CDCl}_3$ )  $\delta$  7.42 – 7.37 (m, 6H), 7.34 (t,  $J$  = 7.5 Hz, 4H), 7.29 – 7.22 (m, 1H), 6.77 (d,  $J$  = 11.3 Hz, 2H), 4.96 (dd,  $J$  = 10.9, 5.8 Hz, 1H), 4.86 (s, 4H), 3.97 (t,  $J$  = 3.2 Hz, 1H), 3.91 (s, 2H), 2.75 (dd,  $J$  = 18.1, 5.8 Hz, 1H), 2.32 (dd,  $J$  = 18.1, 10.9 Hz,



1H), <sup>19</sup>F NMR (377 MHz, CDCl<sub>3</sub>) δ -135.16 – -140.48 (m, Hz), <sup>11</sup>B NMR (128 MHz, CDCl<sub>3</sub>) δ 5.46 (t, *J* = 30.4 Hz). ESI-Tof mass for C<sub>26</sub>H<sub>25</sub>BF<sub>2</sub>N<sub>2</sub>O<sub>3</sub>: [M+Na]<sup>+</sup> 485.2088.

5'-TBS glycal (**13**): Following the reported procedure compound **10** was converted into compound **13**.<sup>47</sup> <sup>1</sup>H NMR (400 MHz, CDCl<sub>3</sub>) δ 6.52 (d, *J* = 2.2 Hz, 1H),



5.08 (t, *J* = 2.5 Hz, 1H), 4.83 (t, *J* = 2.1 Hz, 1H), 4.39 – 4.34 (m, 1H), 3.73 (dd, *J* = 11.9, 3.6 Hz, 1H), 3.62 (dd, *J* = 11.8, 6.7 Hz, 1H), 0.91 (s, 9H),

0.11 (s, 6H), <sup>13</sup>C NMR (101 MHz, CDCl<sub>3</sub>) δ 148.69, 104.33, 89.29, 75.77, 63.16, 29.70, 25.84, -4.29, -4.45, HRMS ESI-Tof Calcd for C<sub>11</sub>H<sub>22</sub>O<sub>3</sub>Si: [M+Na]<sup>+</sup> 253.1230, Found 253.1240.

## 5.6 References and Notes

- (1) Loudet, A.; Burgess, K. BODIPY Dyes and Their Derivatives: Syntheses and Spectroscopic Properties. *Chem. Rev.* **2007**, *107* (11), 4891–4932.
- (2) Ulrich, G.; Ziessel, R.; Harriman, A. ,The Chemistry of Fluorescent Bodipy Dyes: Versatility Unsurpassed. *Angew. Chemie Int. Ed.* **2008**, *47* (7), 1184–1201.
- (3) Piatkevich, K. D.; Subach, F. V; Verkhusha, V. V. Engineering of Bacterial Phytochromes for Near-Infrared Imaging, Sensing, and Light-Control in Mammals. *Chem. Soc. Rev.* **2013**, *42* (8), 3441–3452.
- (4) Boens, N.; Leen, V.; Dehaen, W. Fluorescent Indicators Based on BODIPY. *Chem. Soc. Rev.* **2012**, *41* (3), 1130–1172.
- (5) Zhang, X.; Xiao, Y.; Qian, X. .Highly Efficient Energy Transfer in the Light Harvesting System Composed of Three Kinds of Boron– Dipyrromethene Derivatives. *Org. Lett.* **2008**, *10* (1), 29–32.

- (6) Bozdemir, O. A.; Cakmak, Y.; Sozmen, F.; Ozdemir, T.; Siemiarczuk, A.; Akkaya, E. U. Synthesis of Symmetrical Multichromophoric BODIPY Dyes and Their Facile Transformation into Energy Transfer Cassettes. *Chem. Eur. J.* **2010**, *16* (21), 6346–6351.
- (7) Rousseau, T.; Cravino, A.; Bura, T.; Ulrich, G.; Ziessel, R.; Roncali, J. BODIPY Derivatives as Donor Materials for Bulk Heterojunction Solar Cells. *Chem. Commun.* **2009**, No. 13, 1673–1675.
- (8) Peters, C.; Billich, A.; Ghobrial, M.; Hoegenauer, K.; Ullrich, T.; Nussbaumer, P. Synthesis of Borondipyrromethene (BODIPY)-Labeled Sphingosine Derivatives by Cross-Metathesis Reaction. *J. Org. Chem.* **2007**, *72* (5), 1842–1845.
- (9) Domaille, D. W.; Zeng, L.; Chang, C. J. Visualizing Ascorbate-Triggered Release of Labile Copper within Living Cells Using a Ratiometric Fluorescent Sensor. *J. Am. Chem. Soc.* **2010**, *132* (4), 1194–1195.
- (10) Hudnall, T. W.; Gabbai, F. P. A BODIPY Boronium Cation for the Sensing of Fluoride Ions. *Chem. Commun.* **2008**, No. 38, 4596–4597.
- (11) Atilgan, S.; Ozdemir, T.; Akkaya, E. U. Selective Hg (II) Sensing with Improved Stokes Shift by Coupling the Internal Charge Transfer Process to Excitation Energy Transfer. *Org. Lett.* **2010**, *12* (21), 4792–4795.
- (12) Kolemen, S.; Cakmak, Y.; Erten-Ela, S.; Altay, Y.; Brendel, J.; Thelakkat, M.; Akkaya, E. U. Solid-State Dye-Sensitized Solar Cells Using Red and near-IR Absorbing Bodipy Sensitizers. **2010**.
- (13) Gorman, A.; Killoran, J.; O'Shea, C.; Kenna, T.; Gallagher, W. M.; O'Shea, D. F. In Vitro Demonstration of the Heavy-Atom Effect for Photodynamic Therapy. *J. Am.*

- Chem. Soc.* **2004**, *126* (34), 10619–10631.
- (14) Qiu, K.; Chen, Y.; Rees, T. W.; Ji, L.; Chao, H. Organelle-Targeting Metal Complexes: From Molecular Design to Bio-Applications. *Coord. Chem. Rev.* **2019**, *378*, 66–86.
- (15) Zhu, Z.; Wang, X.; Li, T.; Aime, S.; Sadler, P. J.; Guo, Z. Platinum (II)–Gadolinium (III) Complexes as Potential Single-Molecular Theranostic Agents for Cancer Treatment. *Angew. Chemie* **2014**, *126* (48), 13441–13444.
- (16) Johnstone, T. C.; Wilson, J. J.; Lippard, S. J. Monofunctional and Higher-Valent Platinum Anticancer Agents. *Inorg. Chem.* **2013**, *52* (21), 12234–12249.
- (17) Johnstone, T. C.; Suntharalingam, K.; Lippard, S. J. The next Generation of Platinum Drugs: Targeted Pt (II) Agents, Nanoparticle Delivery, and Pt (IV) Prodrugs. *Chem. Rev.* **2016**, *116* (5), 3436–3486.
- (18) Mügge, C.; Marzo, T.; Massai, L.; Hildebrandt, J.; Ferraro, G.; Rivera-Fuentes, P.; Metzler-Nolte, N.; Merlino, A.; Messori, L.; Weigand, W. Platinum (II) Complexes with O, S Bidentate Ligands: Biophysical Characterization, Antiproliferative Activity, and Crystallographic Evidence of Protein Binding. *Inorg. Chem.* **2015**, *54* (17), 8560–8570.
- (19) Dhar, S.; Gu, F. X.; Langer, R.; Farokhzad, O. C.; Lippard, S. J. Targeted Delivery of Cisplatin to Prostate Cancer Cells by Aptamer Functionalized Pt (IV) Prodrug-PLGA–PEG Nanoparticles. *Proc. Natl. Acad. Sci.* **2008**, *105* (45), 17356–17361.
- (20) Zhu, G.; Song, L.; Lippard, S. J. Visualizing Inhibition of Nucleosome Mobility and Transcription by Cisplatin–DNA Interstrand Crosslinks in Live Mammalian Cells. *Cancer Res.* **2013**, *73* (14), 4451–4460.

- (21) Thayer, A. M. Platinum Drugs Take Their Toll. *Chem. Eng. NEWS* **2010**, 88 (26), 24–28.
- (22) Lease, N.; Vasilevski, V.; Carreira, M.; De Almeida, A.; Sanau, M.; Hirva, P.; Casini, A.; Contel, M. Potential Anticancer Heterometallic Fe–Au and Fe–Pd Agents: Initial Mechanistic Insights. *J. Med. Chem.* **2013**, 56 (14), 5806–5818.
- (23) Sun, T.; Guan, X.; Zheng, M.; Jing, X.; Xie, Z. Mitochondria-Localized Fluorescent BODIPY-Platinum Conjugate. *ACS Med. Chem. Lett.* **2015**, 6 (4), 430–433.
- (24) Farrell, N. P. Multi-Platinum Anti-Cancer Agents. Substitution-Inert Compounds for Tumor Selectivity and New Targets. *Chem. Soc. Rev.* **2015**, 44 (24), 8773–8785.
- (25) Raza, M. K.; Gautam, S.; Howlader, P.; Bhattacharyya, A.; Kondaiah, P.; Chakravarty, A. R. Pyriplatin-Boron-Dipyrromethene Conjugates for Imaging and Mitochondria-Targeted Photodynamic Therapy. *Inorg. Chem.* **2018**, 57 (22), 14374–14385.
- (26) Park, G. Y.; Wilson, J. J.; Song, Y.; Lippard, S. J. Phenanthriplatin, a Monofunctional DNA-Binding Platinum Anticancer Drug Candidate with Unusual Potency and Cellular Activity Profile. *Proc. Natl. Acad. Sci.* **2012**, 109 (30), 11987–11992.
- (27) Mitra, K.; Patil, S.; Kondaiah, P.; Chakravarty, A. R. 2-(Phenylazo) Pyridineplatinum (II) Catecholates Showing Photocytotoxicity, Nuclear Uptake, and Glutathione-Triggered Ligand Release. *Inorg. Chem.* **2015**, 54 (1), 253–264.
- (28) Xue, X.; Zhu, C.; Chen, H.; Bai, Y.; Shi, X.; Jiao, Y.; Chen, Z.; Miao, Y.; He, W.; Guo, Z. A New Approach to Sensitize Antitumor Monofunctional Platinum (II) Complexes via Short Time Photo-Irradiation. *Inorg. Chem.* **2017**, 56 (7), 3754–3762.
- (29) Suryadi, J.; Bierbach, U. DNA Metalating–Intercalating Hybrid Agents for the

- Treatment of Chemoresistant Cancers. *Chem. Eur. J.* **2012**, *18* (41), 12926–12934.
- (30) Malina, J.; Farrell, N. P.; Brabec, V. DNA Condensing Effects and Sequence Selectivity of DNA Binding of Antitumor Noncovalent Polynuclear Platinum Complexes. *Inorg. Chem.* **2014**, *53* (3), 1662–1671.
- (31) Riddell, I. A.; Johnstone, T. C.; Park, G. Y.; Lippard, S. J. Nucleotide Binding Preference of the Monofunctional Platinum Anticancer-Agent Phenanthriplatin. *Chem. Eur. J.* **2016**, *22* (22), 7574–7581.
- (32) Jin, S.; Guo, Y.; Guo, Z.; Wang, X. Monofunctional Platinum (II) Anticancer Agents. *Pharmaceuticals* **2021**, *14* (2), 133.
- (33) Kalaierasi, G.; Umadevi, C.; Shanmugapriya, A.; Kalaivani, P.; Dallemer, F.; Prabhakaran, R. DNA (CT), Protein (BSA) Binding Studies, Anti-Oxidant and Cytotoxicity Studies of New Binuclear Ni (II) Complexes Containing 4 (N)-Substituted Thiosemicarbazones. *Inorganica Chim. Acta* **2016**, *453*, 547–558.
- (34) Arshad, N.; Ahmad, M.; Ashraf, M. Z.; Nadeem, H. Spectroscopic, Electrochemical DNA Binding and in Vivo Anti-Inflammatory Studies on Newly Synthesized Schiff Bases of 4-Aminophenazone. *J. Photochem. Photobiol. B Biol.* **2014**, *138*, 331–346.
- (35) Ragheb, M. A.; Eldesouki, M. A.; Mohamed, M. S. DNA Binding, Photo-Induced DNA Cleavage and Cytotoxicity Studies of Lomefloxacin and Its Transition Metal Complexes. *Spectrochim. Acta Part A Mol. Biomol. Spectrosc.* **2015**, *138*, 585–595.
- (36) Biyiklioglu, Z.; Barut, B.; Özel, A. Synthesis, DNA/BSA Binding and DNA Photocleavage Properties of Water Soluble BODIPY Dyes. *Dye. Pigment.* **2018**, *148*, 417–428.

- (37) Dziuba, D.; Pohl, R.; Hocek, M. Bodipy-Labeled Nucleoside Triphosphates for Polymerase Synthesis of Fluorescent DNA. *Bioconjug. Chem.* **2014**, *25* (11), 1984–1995.
- (38) Dziuba, D.; Jurkiewicz, P.; Cebecauer, M.; Hof, M.; Hocek, M. A Rotational BODIPY Nucleotide: An Environment-Sensitive Fluorescence-Lifetime Probe for DNA Interactions and Applications in Live-Cell Microscopy. *Angew. Chemie* **2016**, *128* (1), 182–186.
- (39) Güixens-Gallardo, P.; Humpolickova, J.; Miclea, S. P.; Pohl, R.; Kraus, T.; Jurkiewicz, P.; Hof, M.; Hocek, M. Thiophene-Linked Tetramethylbodipy-Labeled Nucleotide for Viscosity-Sensitive Oligonucleotide Probes of Hybridization and Protein–DNA Interactions. *Org. Biomol. Chem.* **2020**, *18* (5), 912–919.
- (40) Kuba, M.; Pohl, R.; Kraus, T.; Hocek, M. Nucleotides Bearing Red Viscosity-Sensitive Dimethoxy-Bodipy Fluorophore for Enzymatic Incorporation and DNA Labeling. *Bioconjug. Chem.* **2022**.
- (41) Hocek, M. C-Nucleosides: Synthetic Strategies and Biological Applications. *Chem. Rev.* **2009**, *109* (12), 6729–6764.
- (42) De Clercq, E. C-Nucleosides to Be Revisited: Miniperspective. *J. Med. Chem.* **2016**, *59* (6), 2301–2311.
- (43) Palai, B. B.; Soren, R.; Sharma, N. K. .BODIPY Analogues: Synthesis and Photophysical Studies of Difluoro Boron Complexes from 2-Aminotropone Scaffolds through N, O-Chelation. *Org. Biomol. Chem.* **2019**, *17* (26), 6497–6505.
- (44) Raza, M. K.; Gautam, S.; Garai, A.; Mitra, K.; Kondaiah, P.; Chakravarty, A. R. Monofunctional BODIPY-Appended Imidazoplatin for Cellular Imaging and

- Mitochondria-Targeted Photocytotoxicity. *Inorg. Chem.* **2017**, 56 (18), 11019–11029.
- (45) Dochnahl, M.; Löhnwitz, K.; Lühl, A.; Pissarek, J.-W.; Biyikal, M.; Roesky, P. W.; Blechert, S. Functionalized Aminotroponimate Zinc Complexes as Catalysts for the Intramolecular Hydroamination of Alkenes. *Organometallics* **2010**, 29 (12), 2637–2645.
- (46) Dochnahl, M.; Löhnwitz, K.; Pissarek, J.-W.; Roesky, P. W.; Blechert, S. Electronic Modification of an Aminotroponimate Zinc Complex Leading to an Increased Reactivity in the Hydroamination of Alkenes. *Dalt. Trans.* **2008**, No. 21, 2844–2848.
- (47) Coleman, R. S.; Madaras, M. L. Synthesis of a Novel Coumarin C-Riboside as a Photophysical Probe of Oligonucleotide Dynamics. *J. Org. Chem.* **1998**, 63 (16), 5700–5703.

## 5.7 Appendix

1. $^1\text{H}$ , $^{13}\text{C}$ NMR (400MHz, $\text{CDCl}_3$ ) and HRMS of compound <b>2</b> .....	335
2. $^1\text{H}$ , $^{13}\text{C}$ , $^{19}\text{F}$ , $^{11}\text{B}$ NMR (700/400MHz, $\text{CDCl}_3$ ) and HRMS of compound <b>3</b> .....	337
3. $^1\text{H}$ , $^{13}\text{C}$ , $^{19}\text{F}$ , $^{11}\text{B}$ NMR (700/400MHz, DMSO- $d_6$ ) and HRMS of compound <b>4</b> .....	340
4. $^1\text{H}$ , $^{19}\text{F}$ , $^{11}\text{B}$ NMR (400MHz, $\text{CDCl}_3$ ) and HRMS of compound <b>8</b> .....	343
5. $^1\text{H}$ , $^{19}\text{F}$ , $^{11}\text{B}$ NMR (400MHz, $\text{CDCl}_3$ ) and HRMS of compound <b>11</b> .....	345
6. $^1\text{H}$ , $^{19}\text{F}$ , $^{11}\text{B}$ NMR (400MHz, $\text{CDCl}_3$ ) and HRMS of compound <b>12</b> .....	347
7. $^1\text{H}$ , $^{13}\text{C}$ NMR (400MHz, $\text{CDCl}_3$ ) and HRMS of compound <b>13</b> .....	349
8. Crystaldata .....	351

1.  $^1\text{H}$ ,  $^{13}\text{C}$  NMR (400MHz,  $\text{CDCl}_3$ ) and HRMS of compound **2**

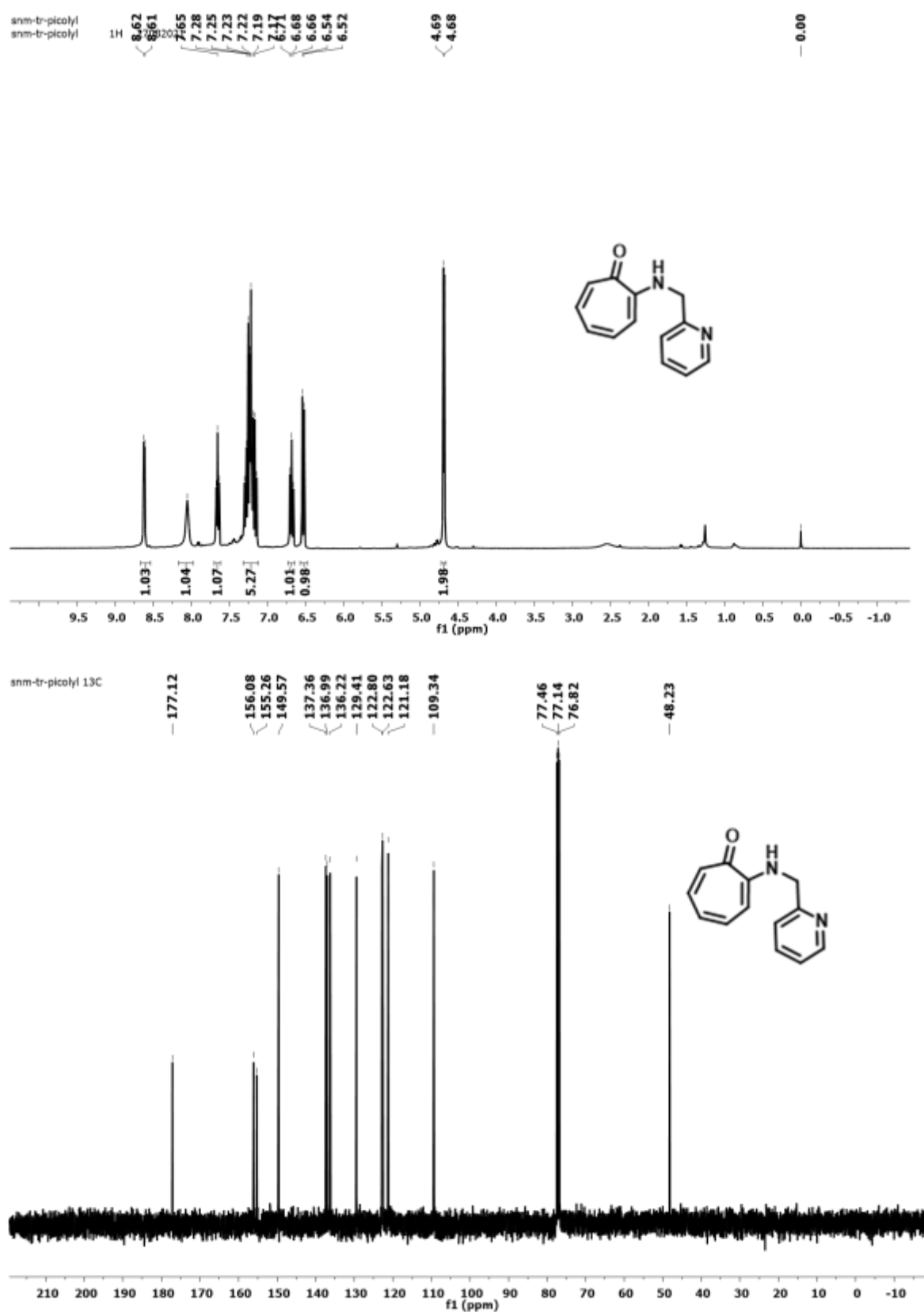


**Figure A1.**  $^1\text{H}/^{13}\text{C}$  NMR (400MHz,  $\text{CDCl}_3$ ) of Compound **2** in  $\text{CDCl}_3$



## Display Report

### Analysis Info

Analysis Name D:\Data\JAN-2019\NKS\29012019\_NKS-RCS-TR-PICO R.d  
 Method pos tune\_low\_16102018.m  
 Sample Name Tmix-131118  
 Comment

Acquisition Date 1/29/2019 7:36:22 PM

Operator PRAKASH BEHERA  
 Instrument micrOTOF-Q II 10337

### Acquisition Parameter

Source Type	ESI	Ion Polarity	Positive	Set Nebulizer	0.4 Bar
Focus	Active	Set Capillary	4500 V	Set Dry Heater	180 °C
Scan Begin	50 m/z	Set End Plate Offset	-500 V	Set Dry Gas	4.0 l/min
Scan End	3000 m/z	Set Collision Cell RF	300.0 Vpp	Set Divert Valve	Source

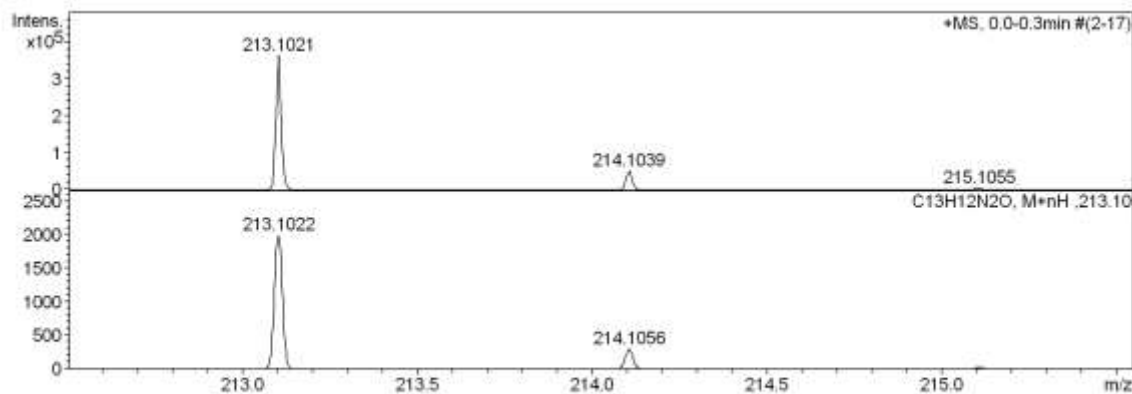
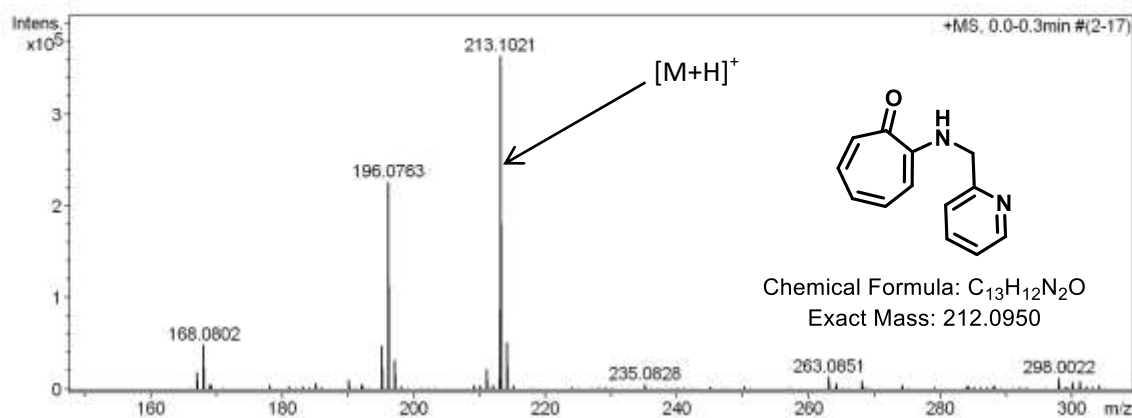
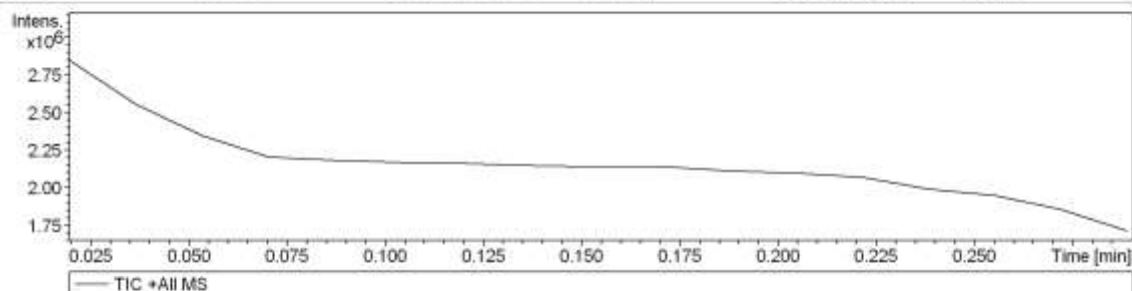


**Figure A2.** ESI-MS/HRMS spectra of compound 2

2.  $^1\text{H}$ ,  $^{13}\text{C}$ ,  $^{19}\text{F}$ ,  $^{11}\text{B}$  NMR (700/400MHz,  $\text{CDCl}_3$ ) and HRMS of compound **3**

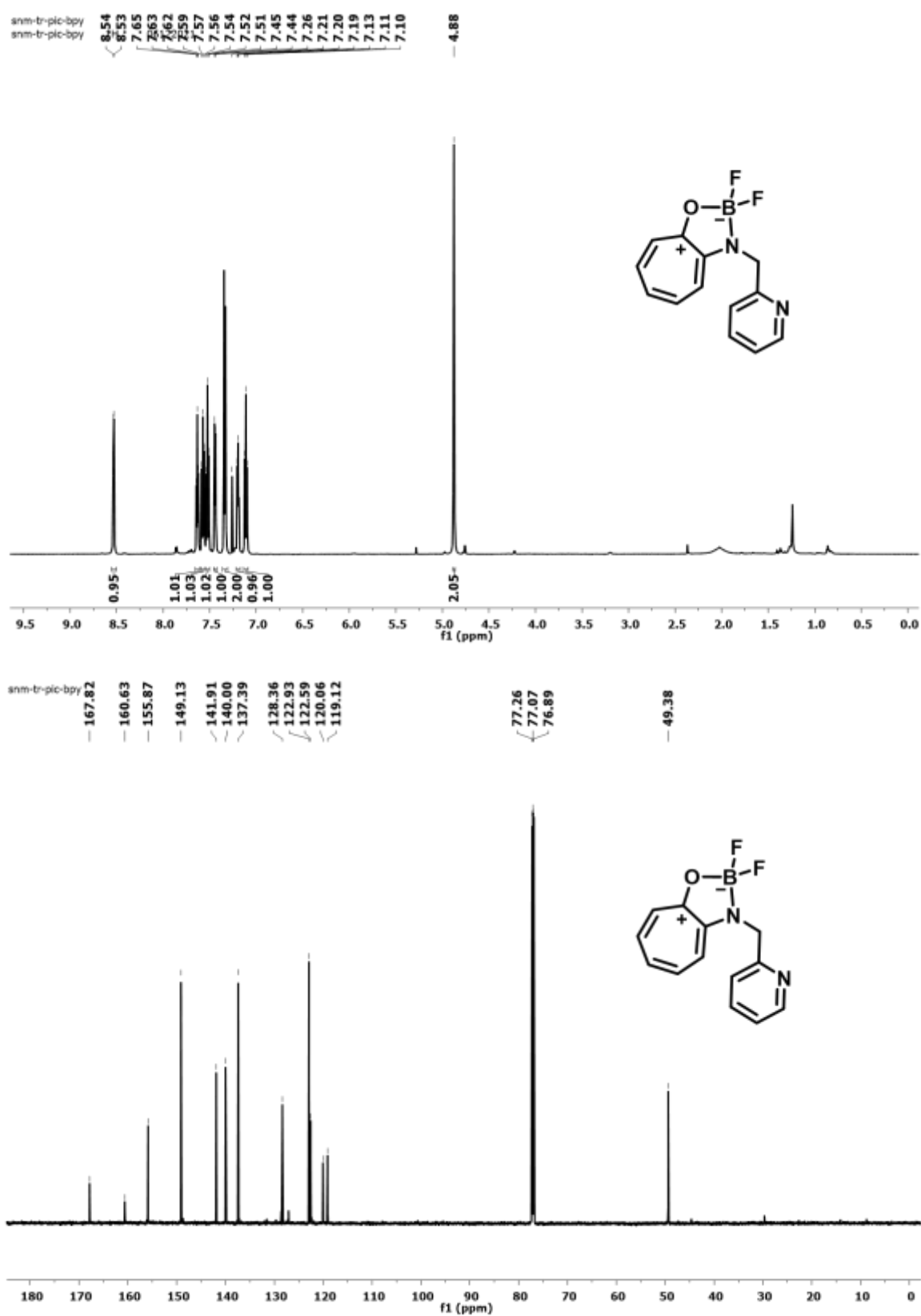


**Figure A3.**  $^1\text{H}/^{13}\text{C}$  NMR (700 MHz,  $\text{CDCl}_3$ ) of Compound **3** in  $\text{CDCl}_3$

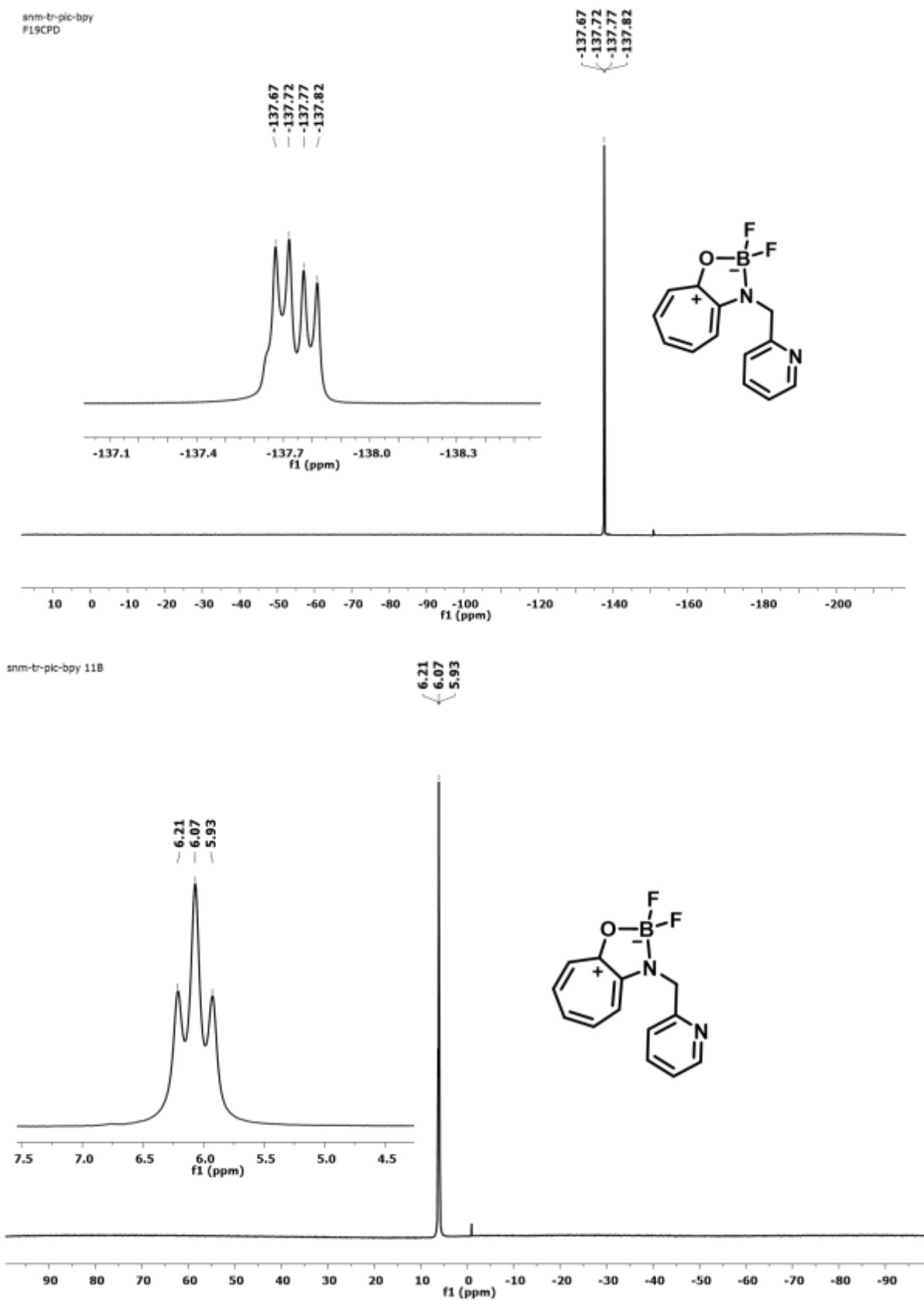


**Figure A4.**  $^{19}\text{F}/^{11}\text{B}$  NMR (400MHz,  $\text{CDCl}_3$ ) of Compound **3** in  $\text{CDCl}_3$

## Display Report

### Analysis Info

Analysis Name D:\Data\DEC-2021\NKS\07122021\_NKS-SNM-TR-PIC-BPY.d  
 Method pos tune\_wide\_030118.m  
 Sample Name Tmix-131118  
 Comment

Acquisition Date 12/7/2021 11:16:32 PM

Operator PRAKASH BEHERA  
 Instrument micrOTOF-Q II 10337

### Acquisition Parameter

Source Type	ESI	Ion Polarity	Positive	Set Nebulizer	0.4 Bar
Focus	Not active	Set Capillary	4500 V	Set Dry Heater	180 °C
Scan Begin	50 m/z	Set End Plate Offset	-500 V	Set Dry Gas	4.0 l/min
Scan End	3000 m/z	Set Collision Cell RF	650.0 Vpp	Set Divert Valve	Waste

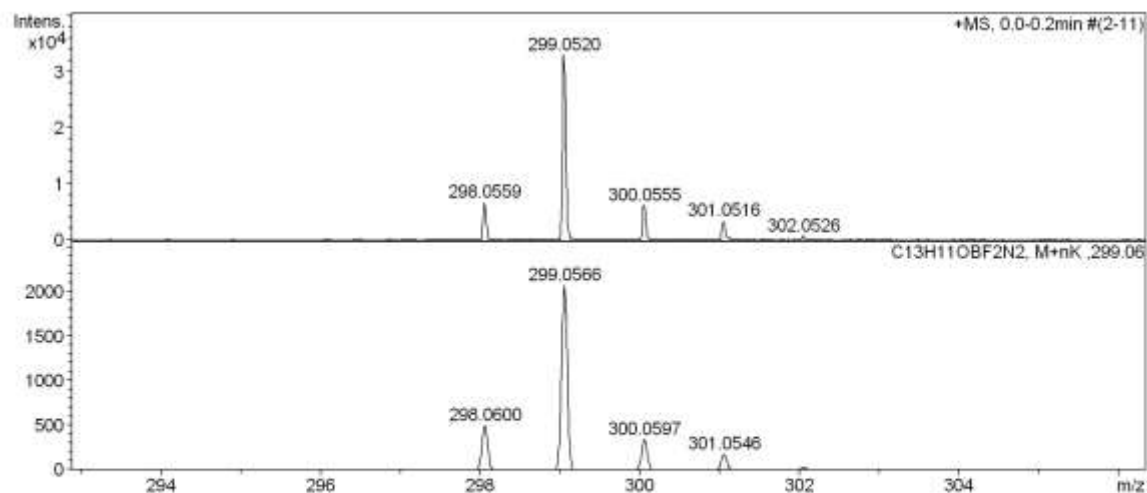
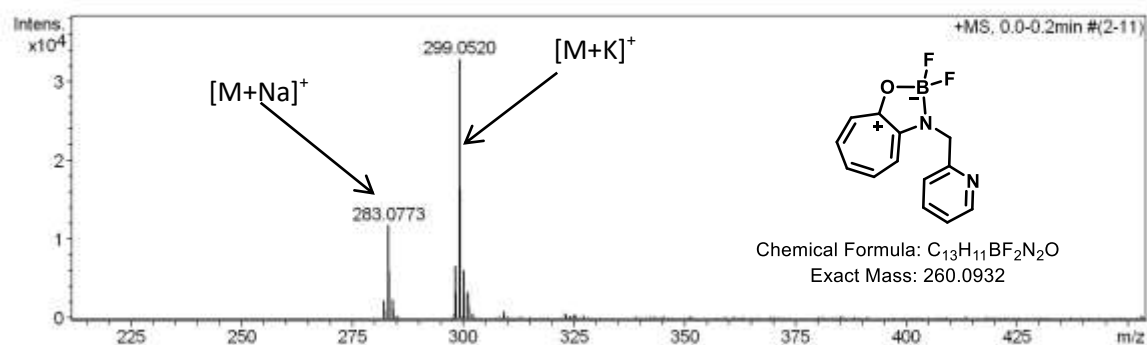
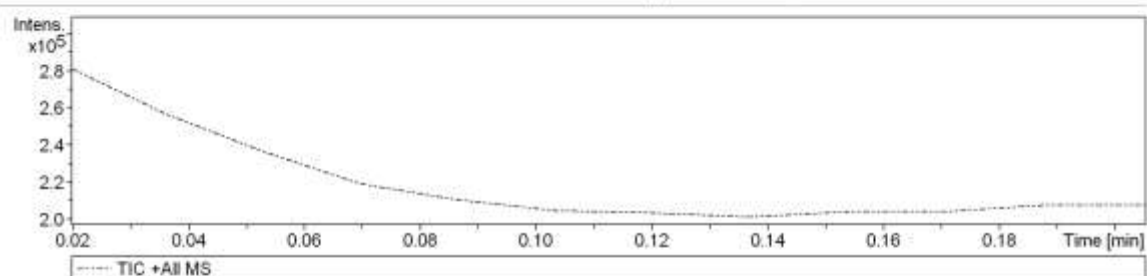


**Figure A5.** ESI-MS/HRMS spectra of compound **3**

3.  $^1\text{H}$ ,  $^{13}\text{C}$ ,  $^{19}\text{F}$ ,  $^{11}\text{B}$  NMR (700/400MHz, DMSO- $d_6$ ) and HRMS of compound **4**

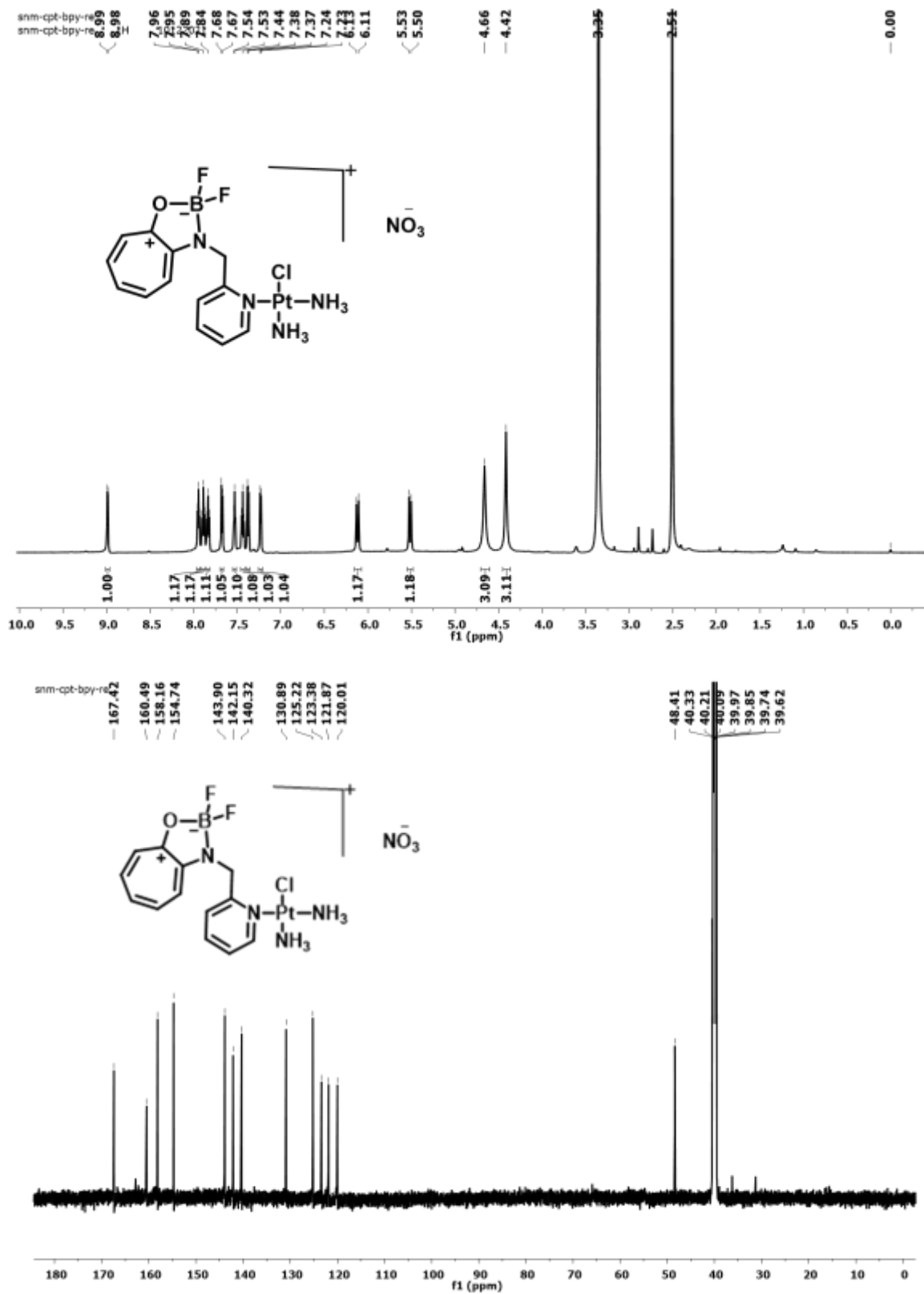


**Figure A6.**  $^1\text{H}/^{13}\text{C}$  NMR (700 MHz, DMSO) of Compound **4** in DMSO- $d_6$



## Display Report

### Analysis Info

Analysis Name D:\Data\NOV-2021\NKS\30112021\_NKS\_SNM-CISPLATIN.d  
 Method pos tune\_wide\_030118.m  
 Sample Name Tmix-131118  
 Comment

Acquisition Date 11/30/2021 6:44:26 PM

Operator PRAKASH BEHERA  
 Instrument micrOTOF-Q II 10337

### Acquisition Parameter

Source Type	ESI	Ion Polarity	Positive	Set Nebulizer	0.4 Bar
Focus	Not active	Set Capillary	4500 V	Set Dry Heater	180 °C
Scan Begin	50 m/z	Set End Plate Offset	-500 V	Set Dry Gas	4.0 l/min
Scan End	3000 m/z	Set Collision Cell RF	650.0 Vpp	Set Divert Valve	Waste

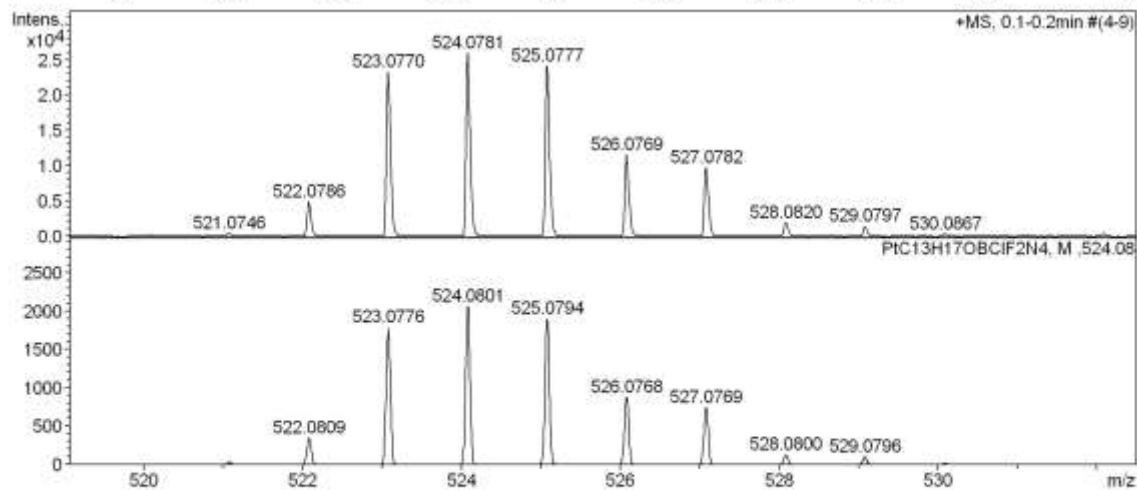
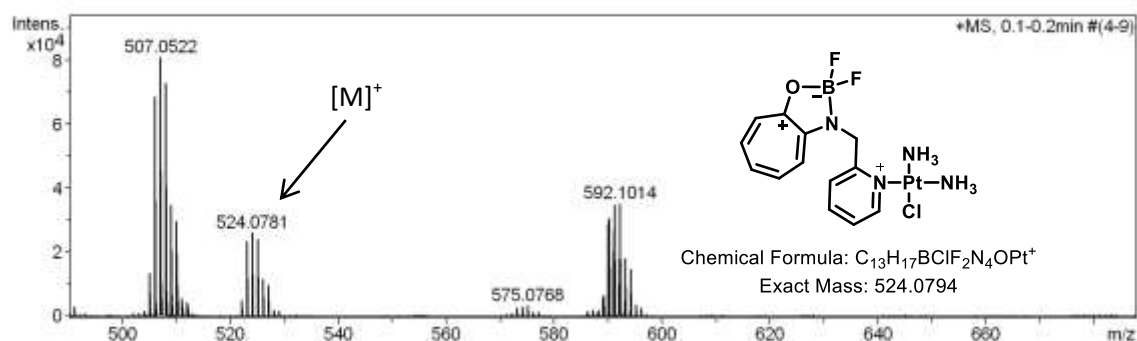
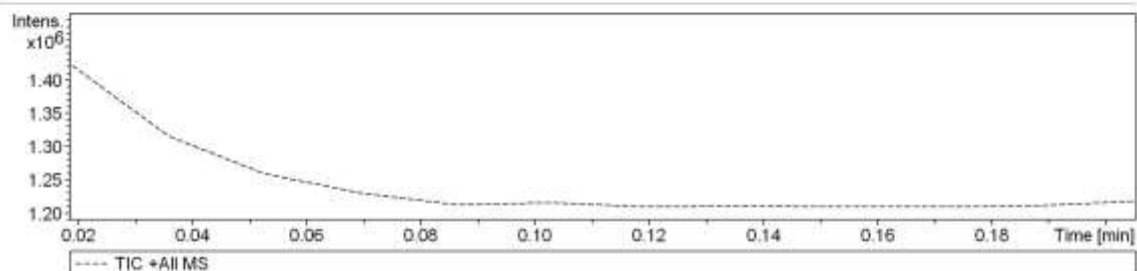


**Figure A8.** ESI-MS/HRMS spectra of compound **4**

4.  $^1\text{H}$ ,  $^{19}\text{F}$ ,  $^{11}\text{B}$  NMR (400MHz,  $\text{CDCl}_3$ ) and HRMS of compound **8**

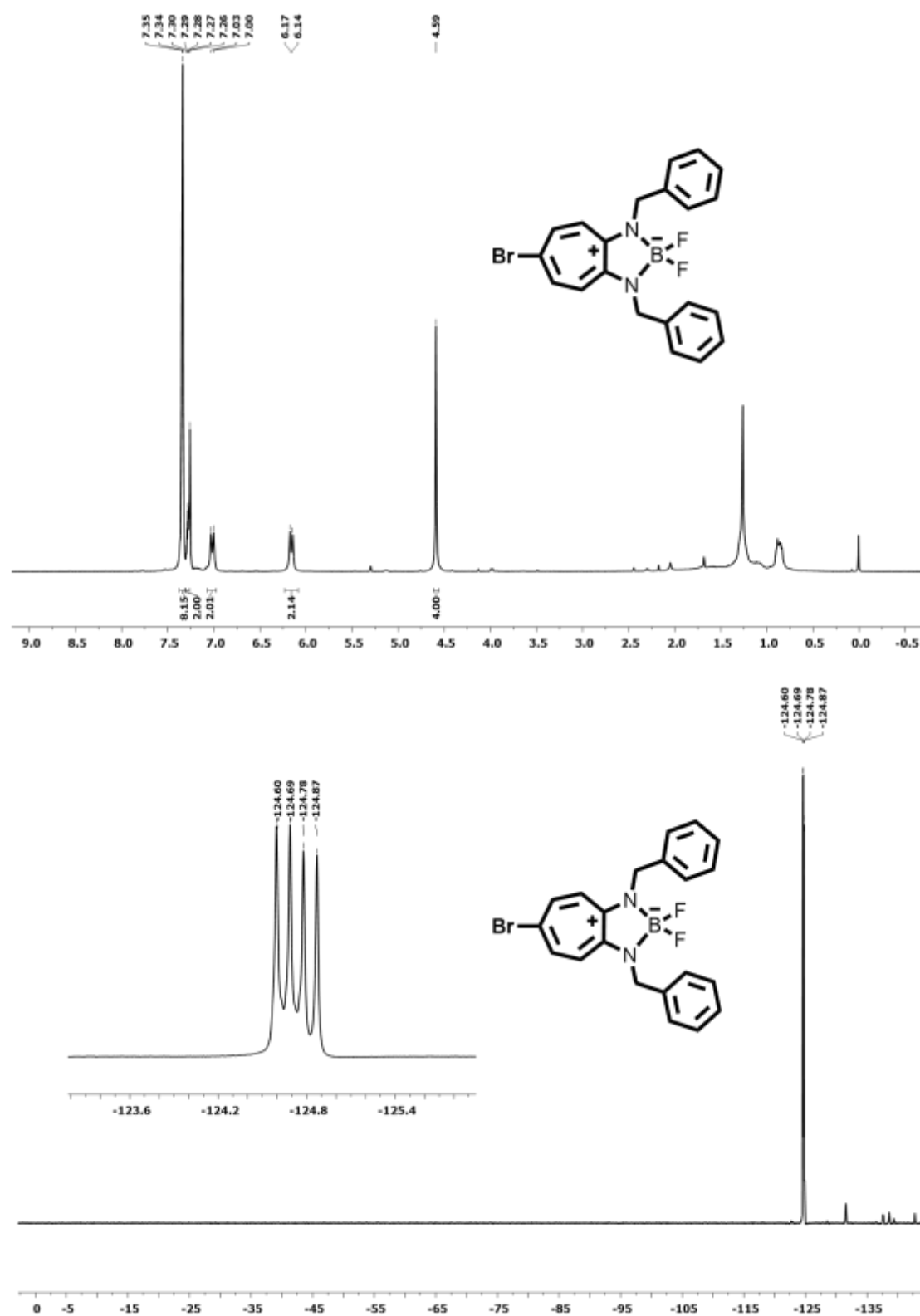
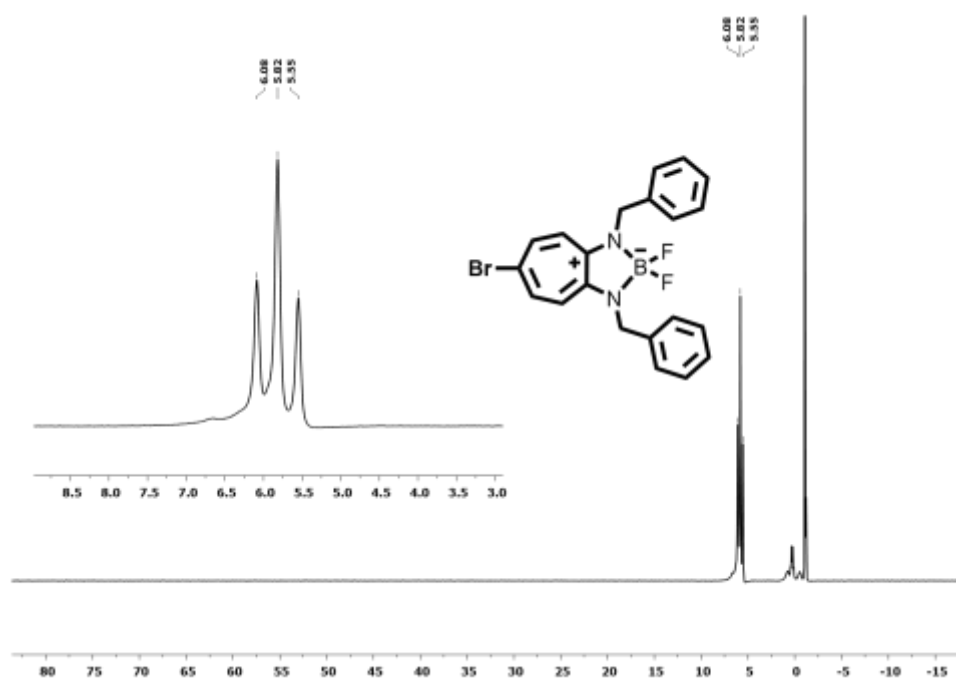
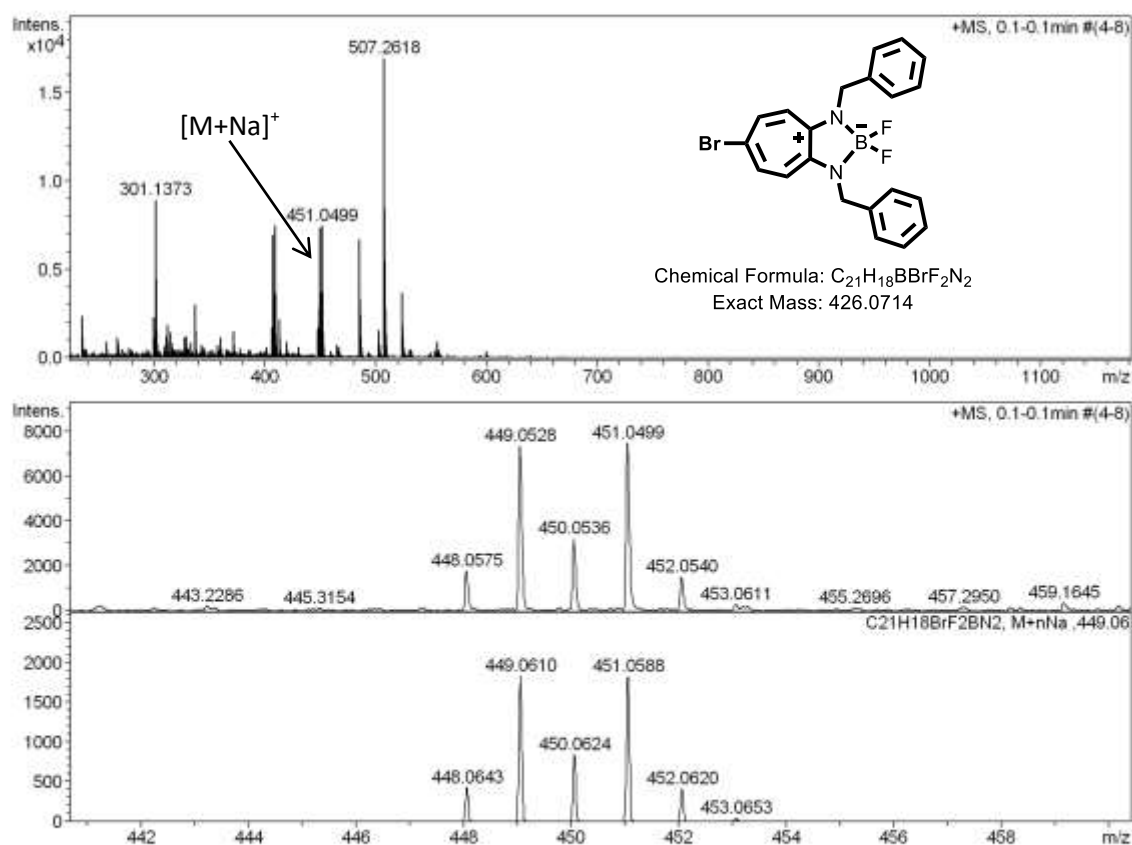


Figure A9.  $^1\text{H}/^{11}\text{B}$  FNMR (400 MHz,  $\text{CDCl}_3$ ) of Compound **8** in  $\text{CDCl}_3$





**Figure A10.**  $^{11}\text{B}$  NMR (400 MHz,  $\text{CDCl}_3$ ) of Compound **5** in  $\text{CDCl}_3$



**Figure A11.** ESI-MS/HRMS spectra of compound **8**

[illegible]

345

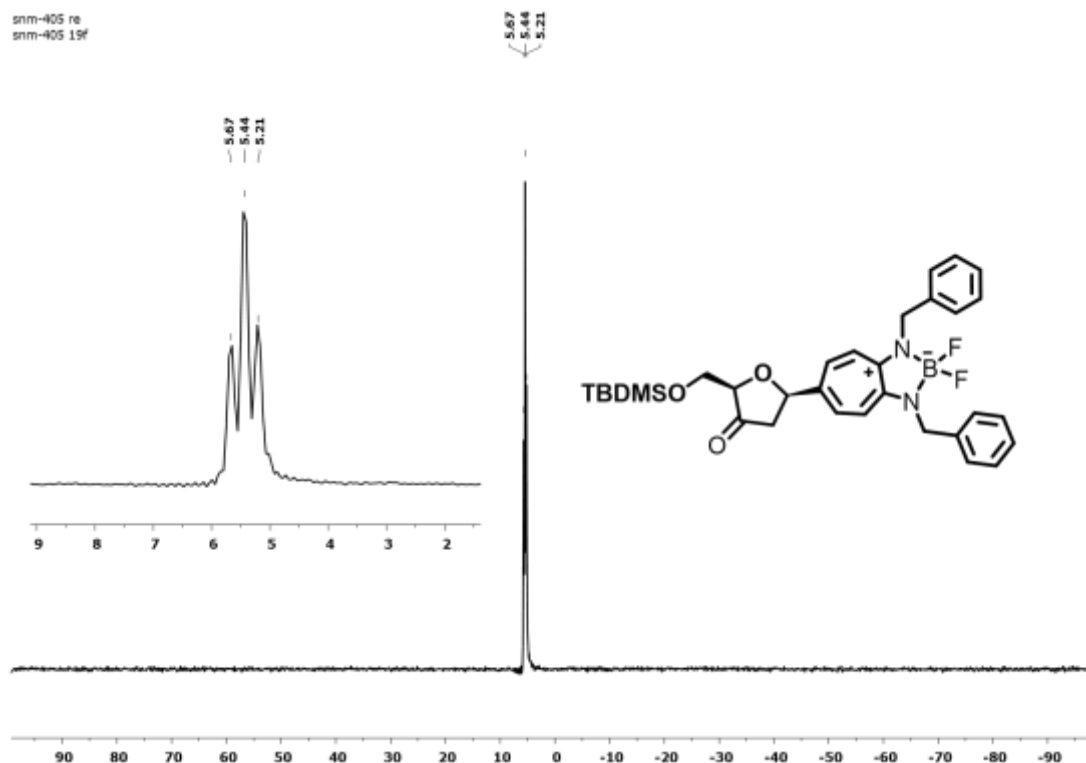


**Figure A13.**  $^{11}\text{B}$  NMR (400 MHz,  $\text{CDCl}_3$ ) of Compound **11** in  $\text{CDCl}_3$

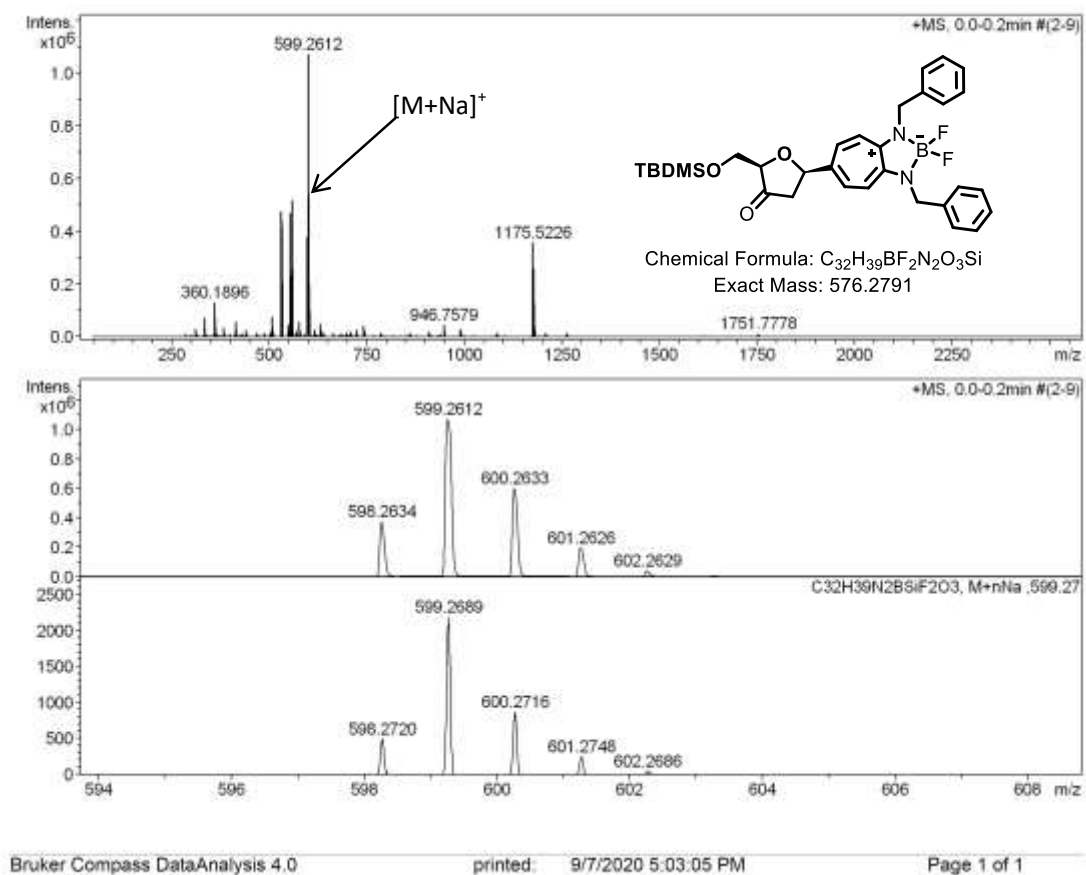


**Figure A14.** ESI-MS/HRMS spectra of compound **11**

6.  $^1\text{H}$ ,  $^{19}\text{F}$ ,  $^{11}\text{B}$  NMR (400MHz,  $\text{CDCl}_3$ ) and HRMS of compound **12**

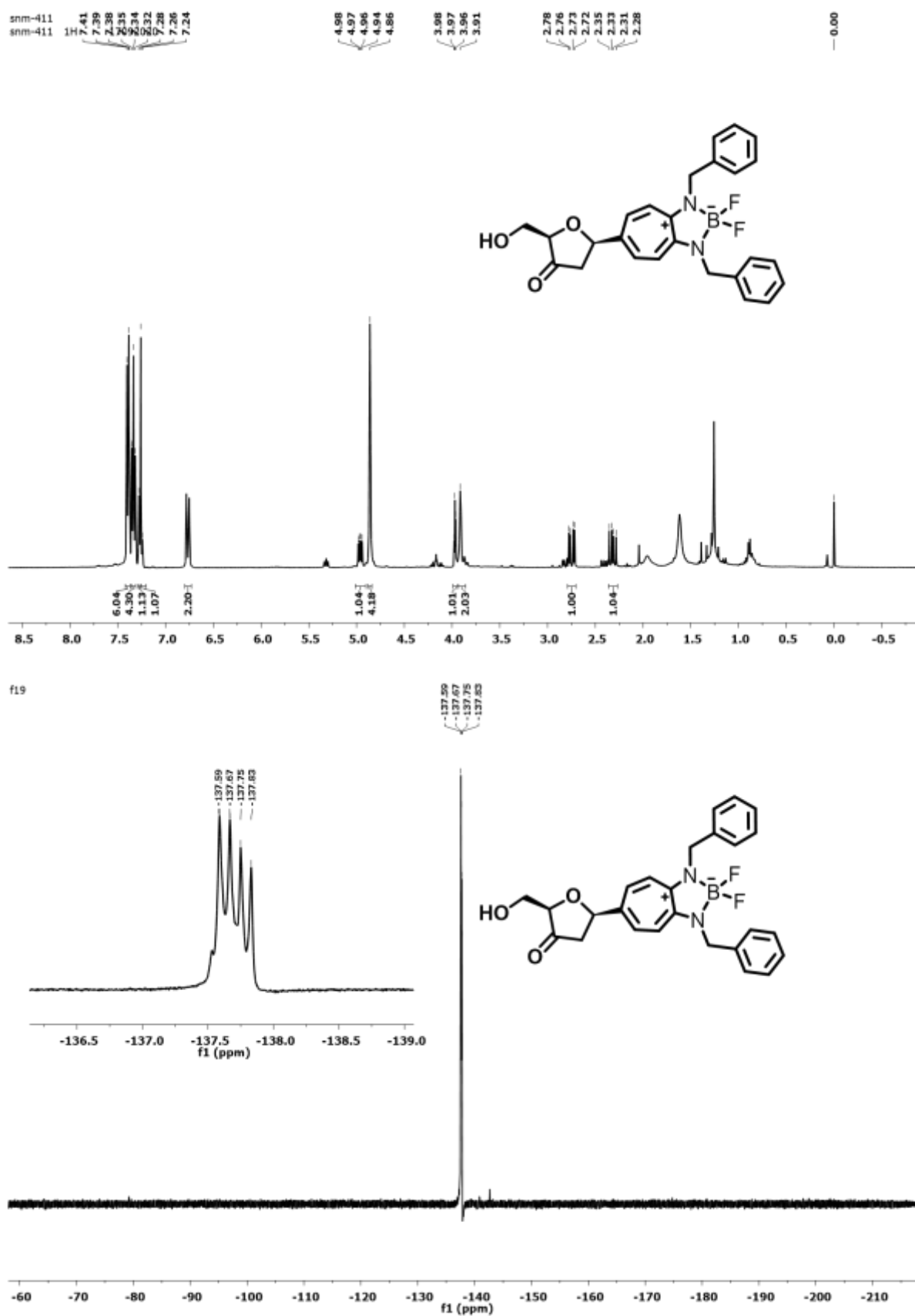
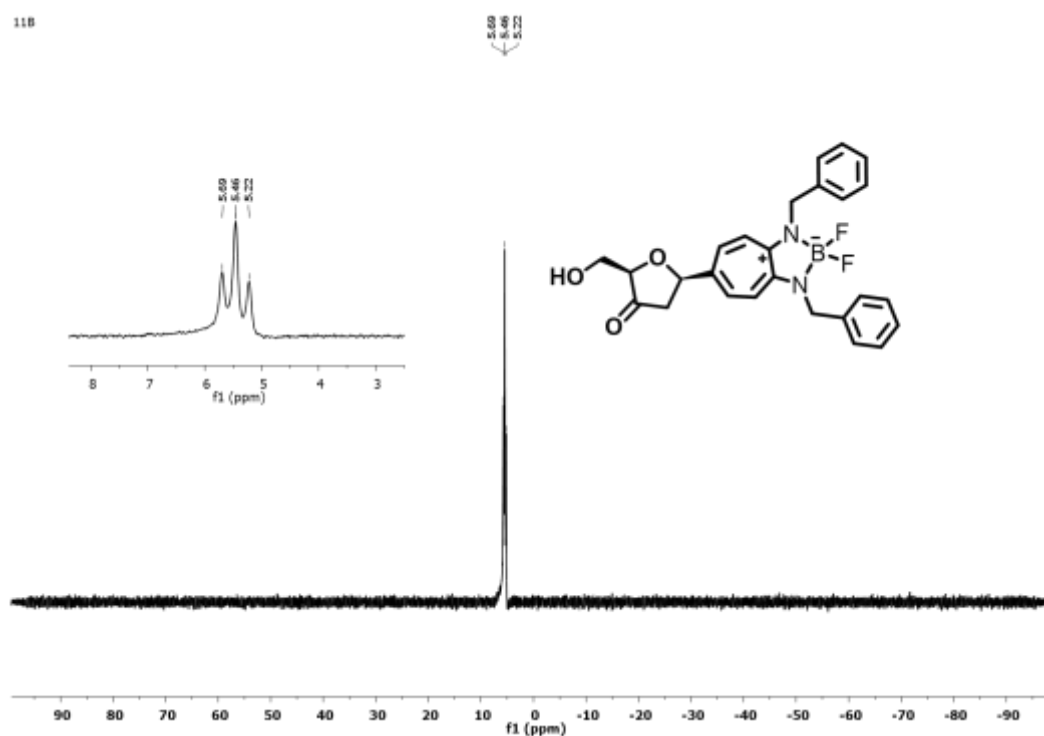
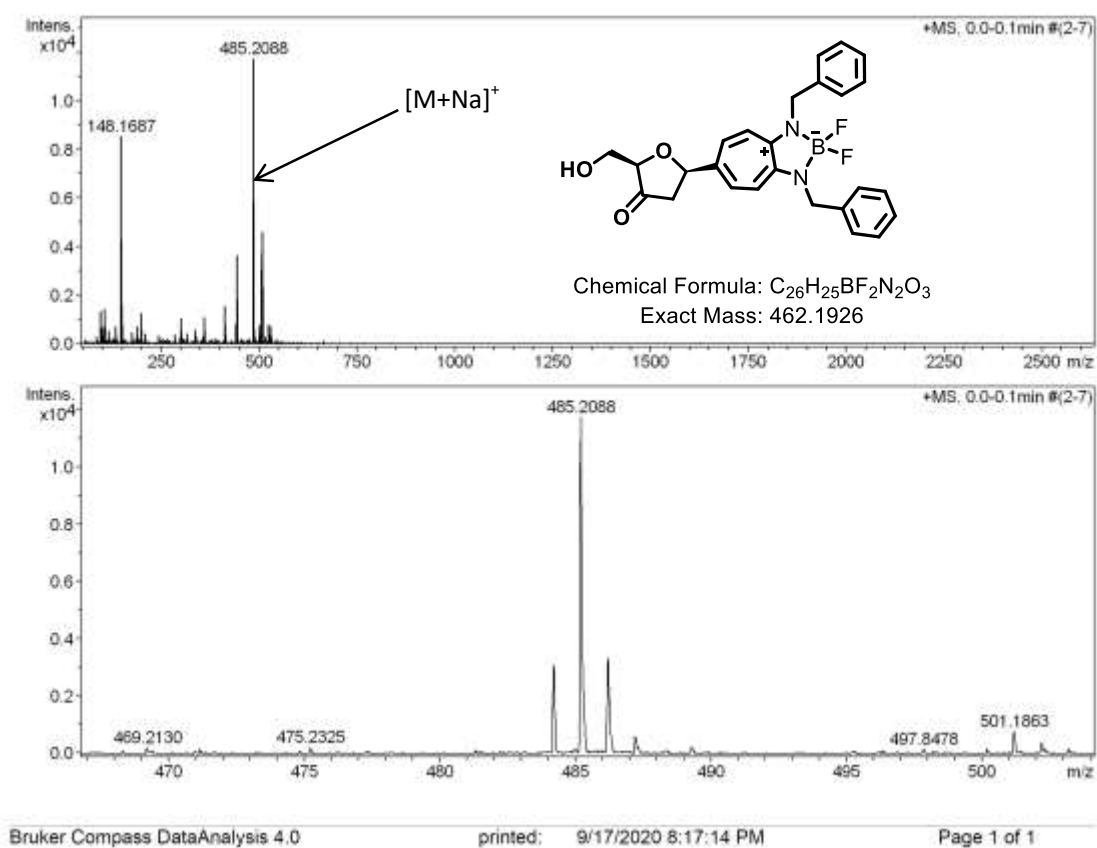


Figure A15.  $^1\text{H}/^{11}\text{F}$  NMR (400 MHz,  $\text{CDCl}_3$ ) of Compound **12** in  $\text{CDCl}_3$



**Figure A16.**  $^{11}\text{B}$  NMR (400 MHz,  $\text{CDCl}_3$ ) of Compound **12** in  $\text{CDCl}_3$



**Figure A17.** ESI-MS/HRMS spectra of compound **12**

7.  $^1\text{H}$ ,  $^{13}\text{C}$  NMR (400MHz,  $\text{CDCl}_3$ ) and HRMS of compound **13**

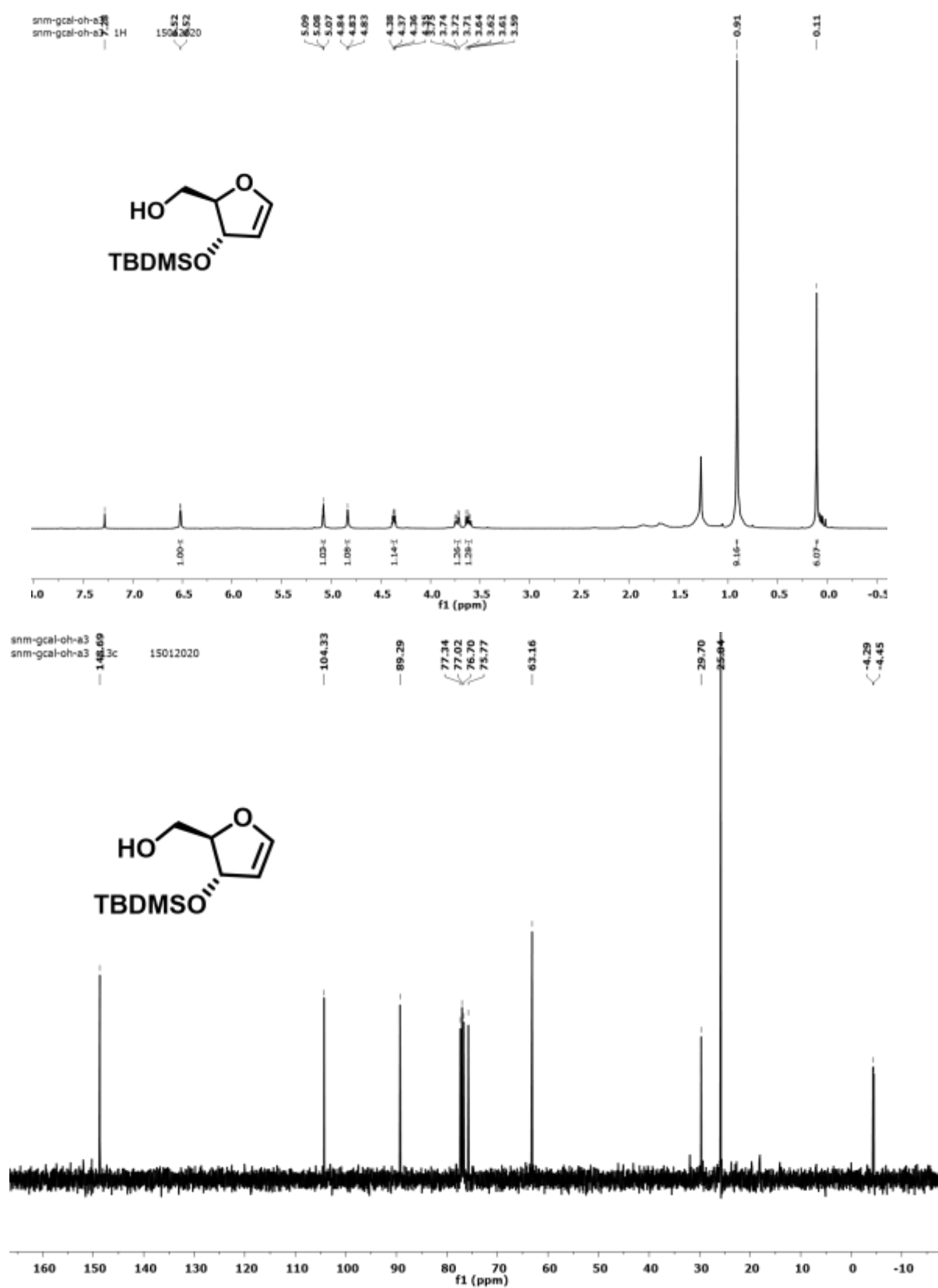


Figure A18.  $^1\text{H}/^{13}\text{C}$  NMR (400MHz,  $\text{CDCl}_3$ ) of Compound **13** in  $\text{CDCl}_3$

## Display Report

### Analysis Info

Analysis Name: D:\Data\JAN-2020\NKS\16012020\_NKS\_SNM-GCAL-OH.d  
 Method: Pos\_tune\_low\_05122019.m  
 Sample Name: Tmix-131118  
 Comment:

Acquisition Date: 1/16/2020 2:06:03 AM

Operator: Amit S.Sahu  
 Instrument: micrOTOF-Q II 10337

### Acquisition Parameter

Source Type	ESI	Ion Polarity	Positive	Set Nebulizer	0.5 Bar
Focus	Not active	Set Capillary	4500 V	Set Dry Heater	180 °C
Scan Begin	50 m/z	Set End Plate Offset	-500 V	Set Dry Gas	4.0 l/min
Scan End	3000 m/z	Set Collision Cell RF	130.0 Vpp	Set Divert Valve	Waste

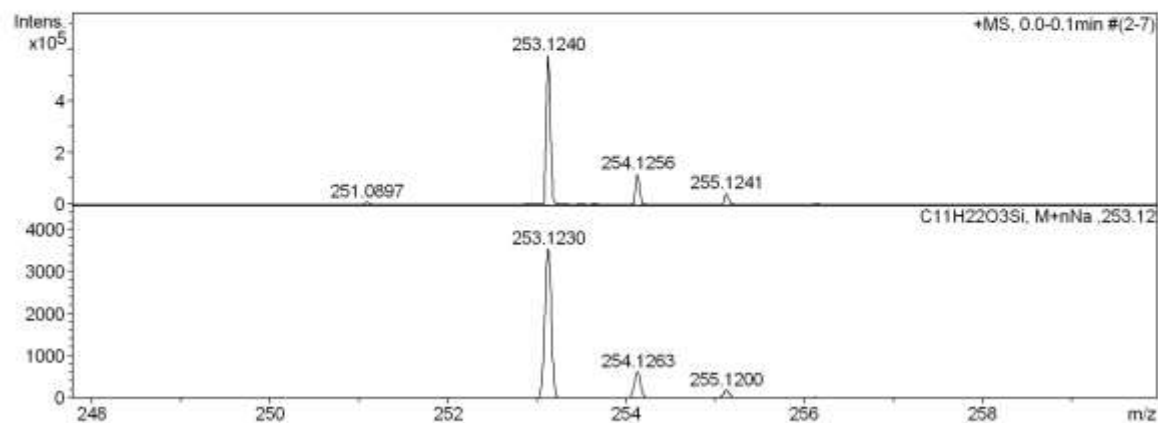
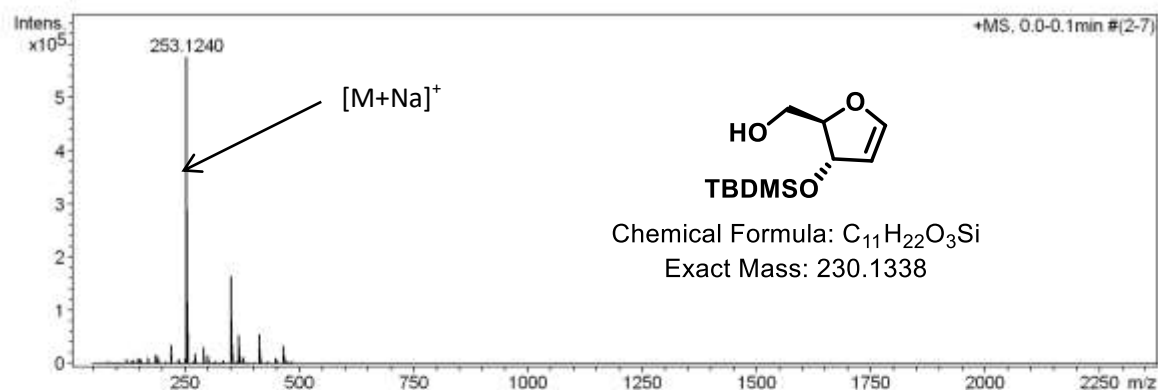
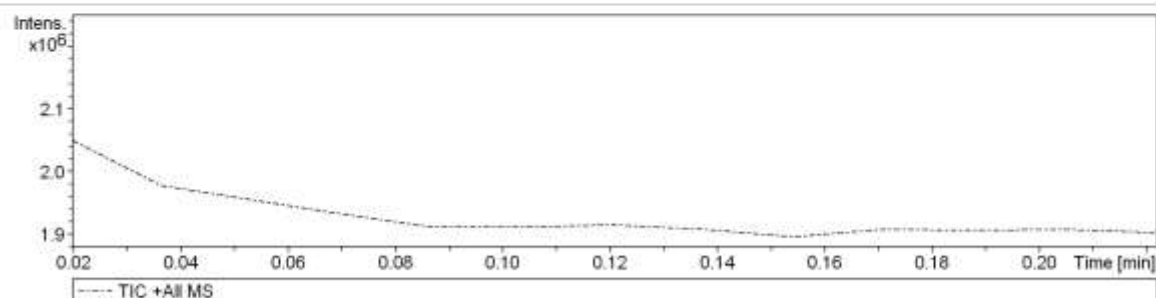


**Figure A19.** ESI-MS/HRMS spectra of compound **13**

## 8. Crystal data

**Table S1.** Crystal data and structure refinement for Compound **8**

Identification code	NKS_SNM_BPY_1
Empirical formula	C <sub>42</sub> H <sub>36</sub> B <sub>2</sub> Br <sub>2</sub> F <sub>4</sub> N <sub>4</sub>
Formula weight	854.23
Temperature/K	100.00(10)
Crystal system	monoclinic
Space group	P2 <sub>1</sub> /c
a/Å	18.5126(3)
b/Å	13.5365(2)
c/Å	15.0157(2)
α/°	90
β/°	92.693(2)
γ/°	90
Volume/Å <sup>3</sup>	3758.72(10)
Z	4
ρ <sub>calc</sub> /g/cm <sup>3</sup>	1.5094
μ/mm <sup>-1</sup>	3.210
F(000)	1727.4
Crystal size/mm <sup>3</sup>	0.002 × 0.001 × 0.001
Radiation	Cu Kα (λ = 1.54184)
2Θ range for data collection/°	8.1 to 149
Index ranges	-18 ≤ h ≤ 23, -17 ≤ k ≤ 17, -19 ≤ l ≤ 17
Reflections collected	31047
Independent reflections	7661 [R <sub>int</sub> = 0.0479, R <sub>sigma</sub> = 0.0320]
Data/restraints/parameters	7661/0/487
Goodness-of-fit on F <sup>2</sup>	1.022
Final R indexes [I ≥ 2σ (I)]	R <sub>1</sub> = 0.0366, wR <sub>2</sub> = 0.1022
Final R indexes [all data]	R <sub>1</sub> = 0.0388, wR <sub>2</sub> = 0.1041
Largest diff. peak/hole / e Å <sup>-3</sup>	0.53/-0.69



## CHAPTER 6

---

### **Synthesis and Mechanistic Insights of Cleavable Amide Bond Comprising $\beta$ -Troponylhydrazino Acid**

---

#### **6.1 Introduction**

#### **6.2 Objective**

#### **6.3 Results and Discussion**

#### **6.4 Conclusion**

#### **6.5 Experimental Section**

#### **6.6 References and Notes**

#### **6.7 Appendix**

## 6.1 Introduction

Natural amide bonds are pretty stable, with an estimated half-life of around ~350- 600 years for spontaneous hydrolysis at neutral pH and room temperature.<sup>1,2</sup> The natural amide bonds are resonance stabilized. The carbonyl group of the natural amide is inert toward the nucleophilic addition reaction.<sup>3,4</sup> The cleavage/hydrolysis of amide bonds could be achieved under extreme conditions, such as heating under strongly acidic or basic conditions. Though, the cyclic amides (*Lactams*) are more cleavable as compared to the linear amides because of ring-strained amides.<sup>5-7</sup> A large number of ring-strained lactams are synthesized and their poor stability is reported even under mild conditions because of the resonance decoupling through N-C=O torsion, which induces the strong electrophilicity at C=O group as ketonic carbonyl.<sup>8</sup> The cleavage of an amide bond without metal ions becomes a center point of discussions. Brown and co-workers have shown that the resonance decoupling enhances the hydrolysis rate in the strained amide bond because of the direct nucleophilic attack.<sup>3, 9</sup> For instance, the twisted amide of 1-aza-2-admantanone derivatives is highly strained lactam ring and readily cleavable under mild conditions.<sup>10</sup> This twisted amide also shows the dual reactivities such as (i) nucleophilic character of amine, and (ii) electrophilic of the carbonyl. The hydrolysis of linear amide bonds is also possible by decoupling the N-C=O resonance stability within the structurally modified amide bonds. However, the sequence-specific amide is cleaved/hydrolyzed with enzymes such as proteases. The zinc metal-dependent peptidase cleaves the specific amide bond through Zinc ions mediation. These results encourage synthetic chemists for the development of artificial peptidases.<sup>11</sup> Mashima and co-workers have explored the role of Zinc ion in the cleavage of amides bearing  $\beta$ -hydroxyethyl using Lewis acid  $\text{Zn}(\text{OTf})_2$ .<sup>12</sup> Recently, the activation of specific amide bonds are explored using a metal catalyst. For example, Garg, Houk and co-workers have shown the conversion of amide functional group into ester group by cleaving C-N bond of amide with Ni-catalyst.<sup>13</sup> The

cleavage of amide bond near-physiological conditions is still challenging. Booker-Milburn and Co-workers have reported the solvolysis of acyclic synthetic amide bonds at room temperature under neutral conditions via the formation of ketene intermediates.<sup>14</sup> They have shown that an electron-withdrawing group, at  $\alpha$ -position, of amide carbonyl enhances the protonation of sterically hindered amide amine and facilitates the formation of ketene by cleaving the C-N bond of amide. In a recent report, the cleavage of the terminal amide bond occurs with ammonium salt/aqueous hydrazine under heating conditions via hydrazinolysis.<sup>15</sup> The cleavage of modified *N*-terminal amide bonds, such as aminopyrazolonyloxy containing acetamides, is cleavable under mildly acidic conditions.<sup>16</sup> Another reactivity of amide bond as transamidation is also reported, such as the transamidation reaction of the amide bond using Zr/Hf-catalyst.<sup>17</sup> For the development of peptide-based materials, the various aromatic amino acids/peptides are synthesized and explored for novel peptidomimetics.<sup>18</sup> In addition to benzenoid aromatic peptides, recently, non-benzenoid aromatic amino acids/peptides are also synthesized from tropolone molecule and unnatural amino acid backbone for evaluating the role of tropolonyl carbonyl the structural and functional changes of peptides (Figure 6.1-a).<sup>19-</sup>

<sup>21</sup> The  $\alpha$ -troponylalkyl amino acid and their peptides exhibit rare characteristic chemical properties as the cleavage of amide bond under mild acidic conditions (5% TFA) alongwith the reversible amidation and transamidation activities under basic condions. However, their  $\beta$ -analogues as  $\beta$ -troponylalkyl amino acid derivatives are stable as like other natural amide bonds, even with neat TFA (~100%) (Figure 6.1-b). In repetreoire of unnatural peptidomimics,  $\alpha$ -hydrazino acids and their peptides as *N*-amino peptide (NAP) derivatives are explored, and found that those peptides exhibit improved biostability and bioactivity as compare to control (Figure 6.1-c).<sup>18, 22</sup> Thus, we designed a  $\beta$ -troponylhydrazino acid analogue to explore the role of troponyl group for novel peptidomimetics (Figure 6.1-d). This chapter describes the synthesis of  $\beta$ -troponylhydrazino acid and its hybrid peptides with amino group of natural  $\alpha$ -

amino acid/peptide ester derivative (Figure 6.1-b). For conformational studies, the DMSO- $d_6$  titration experiment and X-ray studies are performed with representative peptides. For practical utilities, the stability of such peptides are also investigated near physiological pH conditions (mild acidic/alkaline conditions) by NMR and ESI-Mass techniques, which reveal the cleavage of their amide bonds with dilute TFA (20%).

## 6.2 Objective

To examine the impact of troponyl-modified amino acids and peptides, we synthesized  $\beta$ -hydrazino acids analog as  $\beta$ -troponylhydrazino acids. We also studied the structural and conformational studies of their hybrid *di-/tri*-peptides with the natural amino acid and amide bond cleavage.

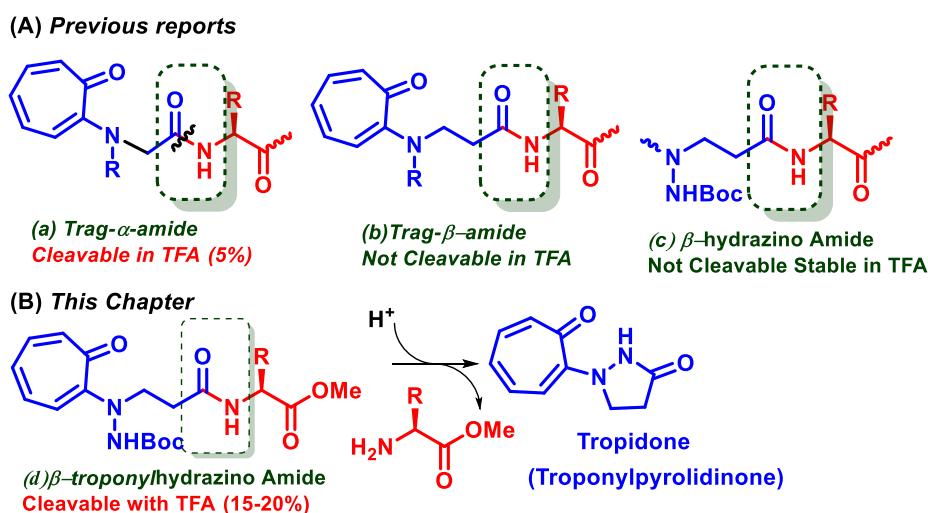
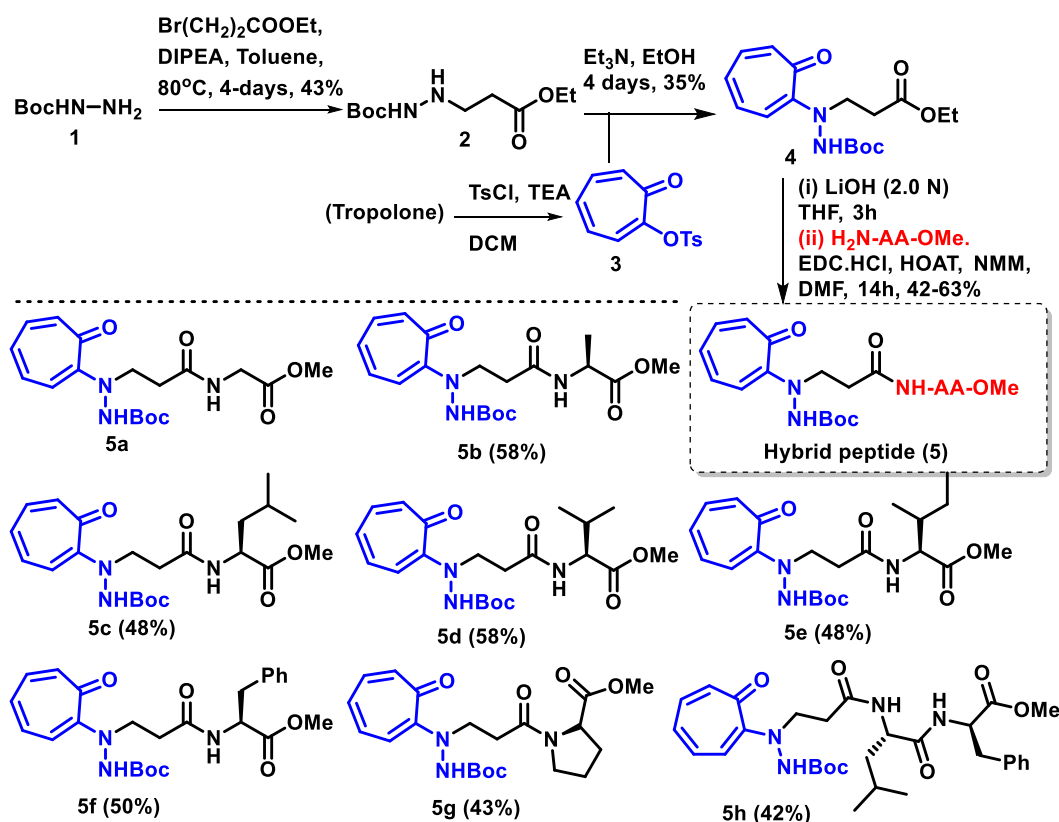


**Figure 6.1.** (A) Previously reported troponyl/hydrazine containing amides; (B) Rationally designed  $\beta$ -troponylhydrazinyl peptides & their instability under acidic conditions.

## 6.3 Results and Discussion

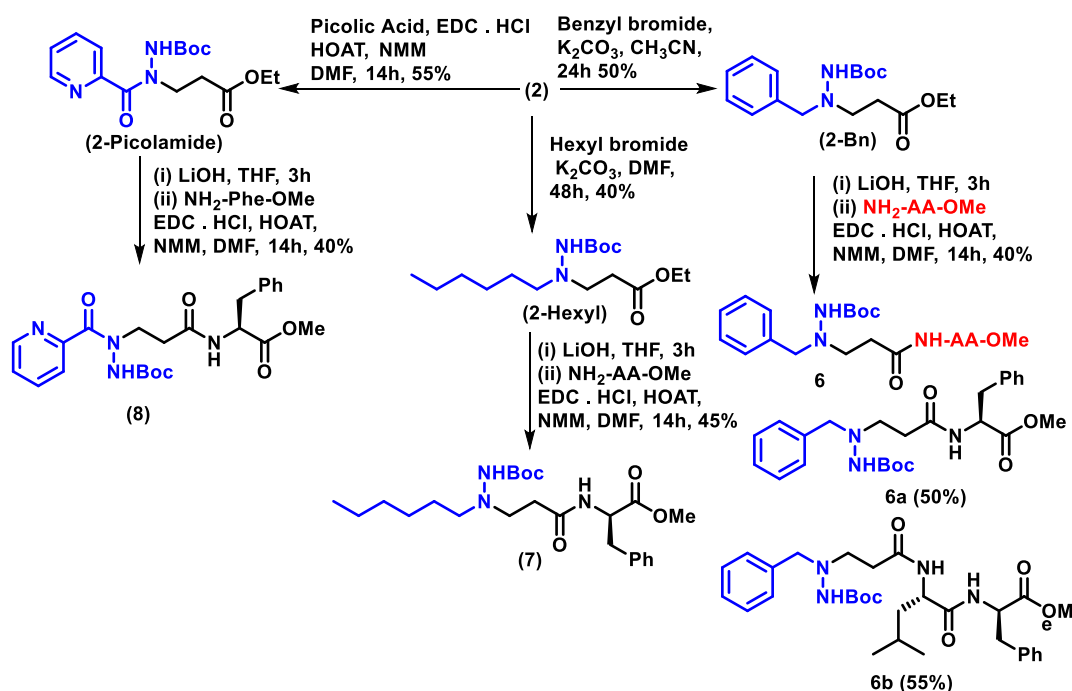
We used commercially available *N*-Boc-hydrazine (**1**) for *N*-alkylation with 3-bromopropionate ester under basic conditions that produced alkylated hydrazine derivative (**2**). This derivative was treated with *O*-tosylate tropolone (**3**) under reflux conditions for four

days for *N*-troponylation of amine that is converted into a new unnatural amino acid as 2-aminotroponyl hydrazine derivative (**4**). However, the *O*-tosylate tropolone (**3**) was derived from commercially available tropolone molecule. For the synthesis of amide bond, the ester group of derivative (**4**) was hydrolyzed into carboxylate derivative under alkaline conditions followed by coupling with various natural  $\alpha$ -L-amino acid esters (Gly, Ala, Leu, Val, Ile, Phe, Pro) /peptide ester (Leu-Phe) derivative using peptide coupling reagents. Subsequently, the hybrid *di*-/*tri*-peptide derivatives (**5a-5g/5h**) were isolated (Scheme 6.1). These peptides were characterized by NMR and ESI-HRMS (See Appendix). Pleasantly, we obtained the single crystal of one dipeptide (**5a**) from solvent mixture (EtOAc: Hexane) and analyzed by X-diffractometer, which confirmed the structures of peptide **5a** as Boc- $\beta$ -troponylhydrazino-glycine ester (Appendix, Table A4, Figure A69). Its crystal data was deposited to Cambridge Crystallographic Data Centre (CCDC) with the number CCDC 2003629 (**5a**).



**Scheme 6.1.** Synthesis of *N*-troponylated- $\beta$ -hydrazino acid/peptides.

For comparative studies, we synthesized three types of control  $\beta$ -hydrazino acid derivatives without containing troponyl scaffold from the same  $\beta$ -hydrazino acid ester (**2**) and their hybrid peptides with natural  $\alpha$ -amino acids (Scheme 6.2). The  $\beta$ -hydrazino acid ester (**2**) was treated with benzyl bromide under the basic condition, which produced *N*-benzyl- $\beta$ -hydrazino ester (**2-Bn**). Similarly, *N*-hexyl- $\beta$ -hydrazino ester (**2-hexyl**) was prepared ester (**2**) and hexyl bromide under basic condition. However, *N*-amide derivative of  $\beta$ -hydrazino acid ester (**2**) was developed with picolic acid under peptide coupling reaction conditions, which produced  $\beta$ -picolinyldhydrazino ester (**2-picolamide**). These non-troponyl  $\beta$ -hydrazino ester derivatives (**2-Bn/2-hexyl/2-picolamide**) were hydrolyzed into respective carboxylate with LiOH, and then directly coupled with amine group of  $\alpha$ -amino acid ester under peptide coupling conditions. As resultants, the control *di-/tri*-peptide  $\beta$ -benzylhydrazino peptides (**6a/6b**),  $\beta$ -picolinyldhydrazino peptide (**7**), and  $\beta$ -hexylhydrazino peptide (**8**) were synthesized for further studies. All the NMR and Mass spectra are provided in the Appendix. We attempted synthesis of *N*-phenyl- $\beta$ -hydrazino ester for control studies but couldn't achieve it.



**Scheme 6.2.** Synthesis of control *N*-alkylated- $\beta$ -hydrazino acid/peptides.

Herein, we also attempted the involvement of amine protons (BocNH/Amide NH) in intramolecular hydrogen bonding with carbonyl oxygen (troponyl/Boc/Amide) in solution state by DMSO- $d_6$ -titration  $^1\text{H}$ -NMR experiments. In this experiment, the chemical shift of intramolecular hydrogen bonded proton remains constant or exhibits small downfield shift (N-H), while the chemical shift of intermolecular hydrogen bonded proton shows significant downfield shift with increasing the concentration of DMSO- $d_6$  (strong hydrogen bond acceptor solvent).<sup>19</sup> The intramolecular hydrogen bond strength is inversely proportional to the downfield shift of N-H by DMSO addition. We assigned proton resonance signals of BocNH (NH1) and amide N-H (NH2) in troponylated dipeptides (**5a-5e**) and a control peptide (**7**). We performed DMSO titration experiment by recording the consecutive  $^1\text{H}$ -NMR spectra of respective peptides (**5a-5e/7**) in  $\text{CDCl}_3$  with successive addition of DMSO- $d_6$  in a small amount. Their  $^1\text{H}$ -NMR titration spectra are provided in the Appendix (Figure A35-40). We extracted the chemical shift value of BocNH and amide N-H with respect to the volume of DMSO- $d_6$  addition and then generated a plot as chemical shift (ppm) vs. DMSO- $d_6$  volume ( $\mu\text{L}$ ). These plots are depicted in Figure 6.2 (A & B), which exhibit a marginal downfield shift in the chemical shift of BocN-H/amide N-H in troponylated peptides (**5a-5e**) as compared to the BocN-H of control peptide (**7**). Importantly, we noticed that the extent of the downfield shift in BocNH and amide N-H are almost equal in of troponyl peptide (**5a/5c**). However, the extent of downfield shift in BocNH of troponyl peptide (**5b/5d/5e**) is lower than their respective amide N-H, which is almost equal to the control peptide (**7**). Hence intramolecular hydrogen bond in troponyl peptides (**5a-5e**) due to BocNH is equal to or stronger than the respective amide N-H. Our  $^1\text{H}$ -NMR titration results reveal the presence of two intramolecular hydrogen bonding in  $\beta$ -troponylhydrazino peptides, while one in control peptides. Herein, we propose the preferable intramolecular hydrogen bonding in  $\beta$ -troponylhydrazino peptides (**5a-5e**)/control peptide, as Figure 6.2-C. In troponyl peptides

(**5a-5e**), the intramolecular hydrogen bond between BocN-H---O=C (troponyl carbonyl), six-membered ring, could be slightly stronger than another intramolecular hydrogen bond between amide N-H---O=C (Boc carbonyl), nine membered ring in solution state. In literature, 9-membered ring  $\alpha$ -N-O turn is reported in peptides containing  $\alpha$ -aminoxy acid.<sup>23</sup>

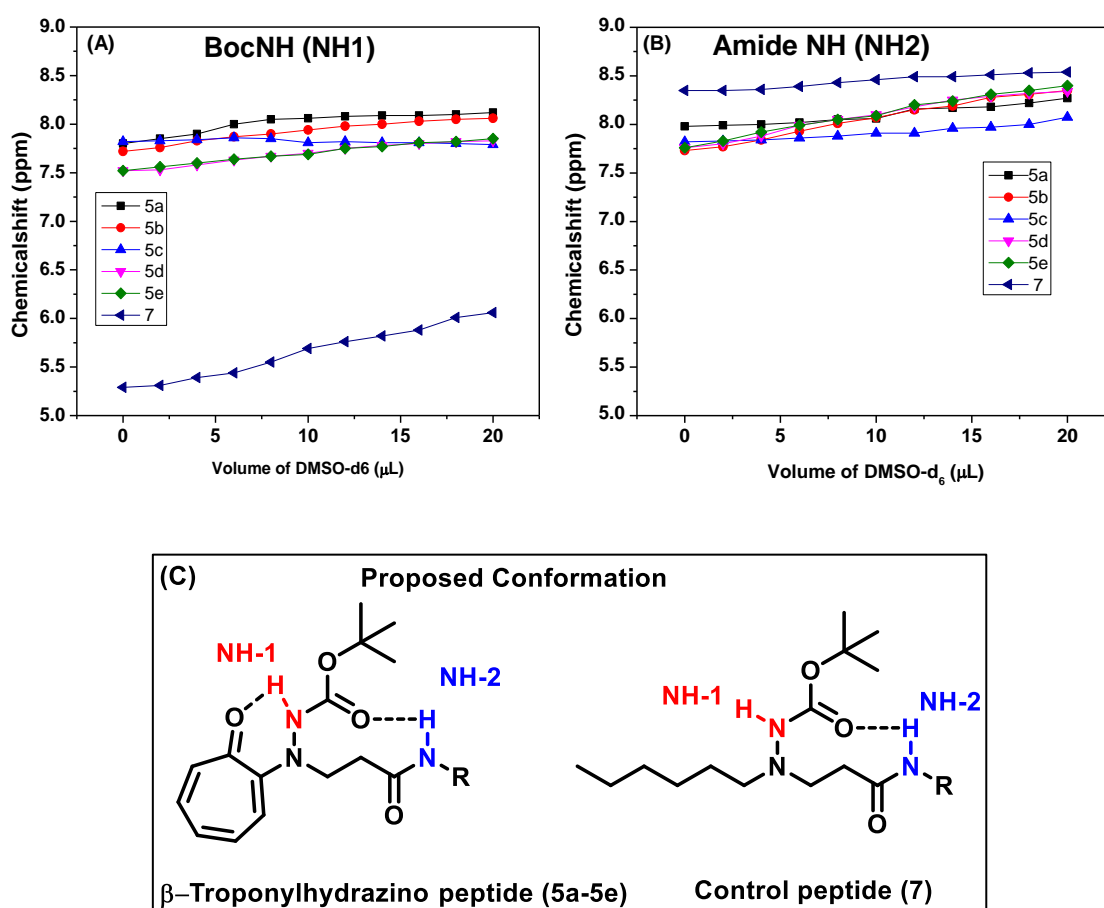
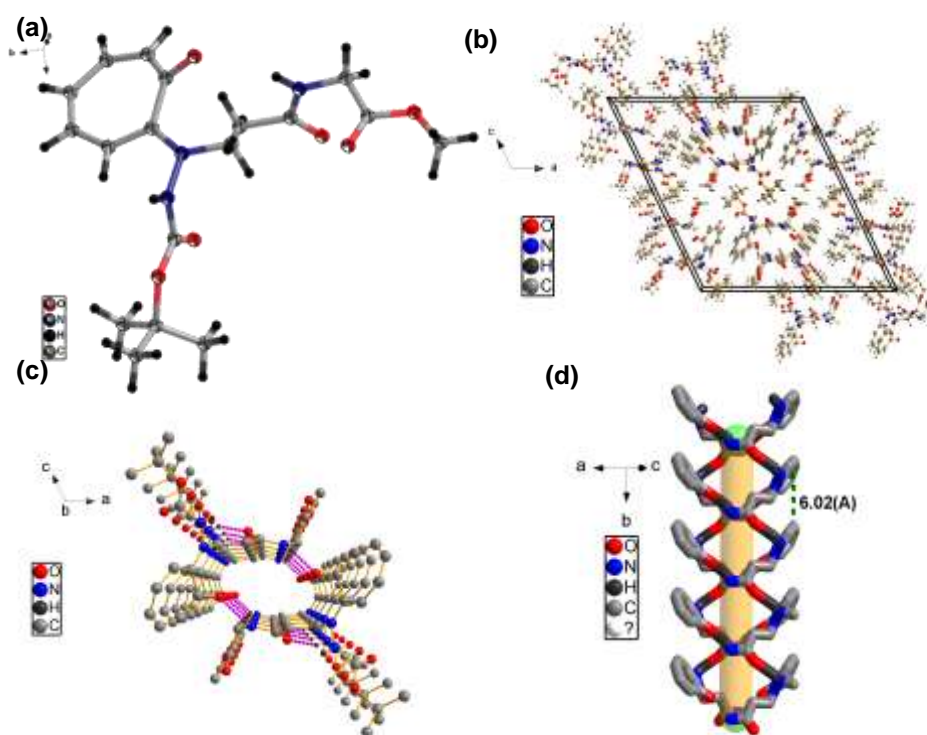


**Figure 6.2.** <sup>1</sup>H-NMR DMSO-d<sub>6</sub> titration plot for BocNH (A) and Amide NH (B), Proposed conformation of  $\beta$ -troponylhydrazino peptides/control peptide (C).

To investigate the role of troponyl carbonyl group in  $\beta$ -troponylhydrazino acid containing hybrid peptides, we attempted to crystallize the hybrid peptides under various solvent systems. Pleasantly, we obtained the single crystal of one dipeptide (**5a**) and one tripeptide (**5h**). Their crystal data are submitted to CCDC with number CCDC 2003629 for peptide **5a** and CCDC 2003628 for peptide **5h**. We extracted their packing diagram in unit cell and supramolecular self-assembly structure using software Diamod 3.2. The structural



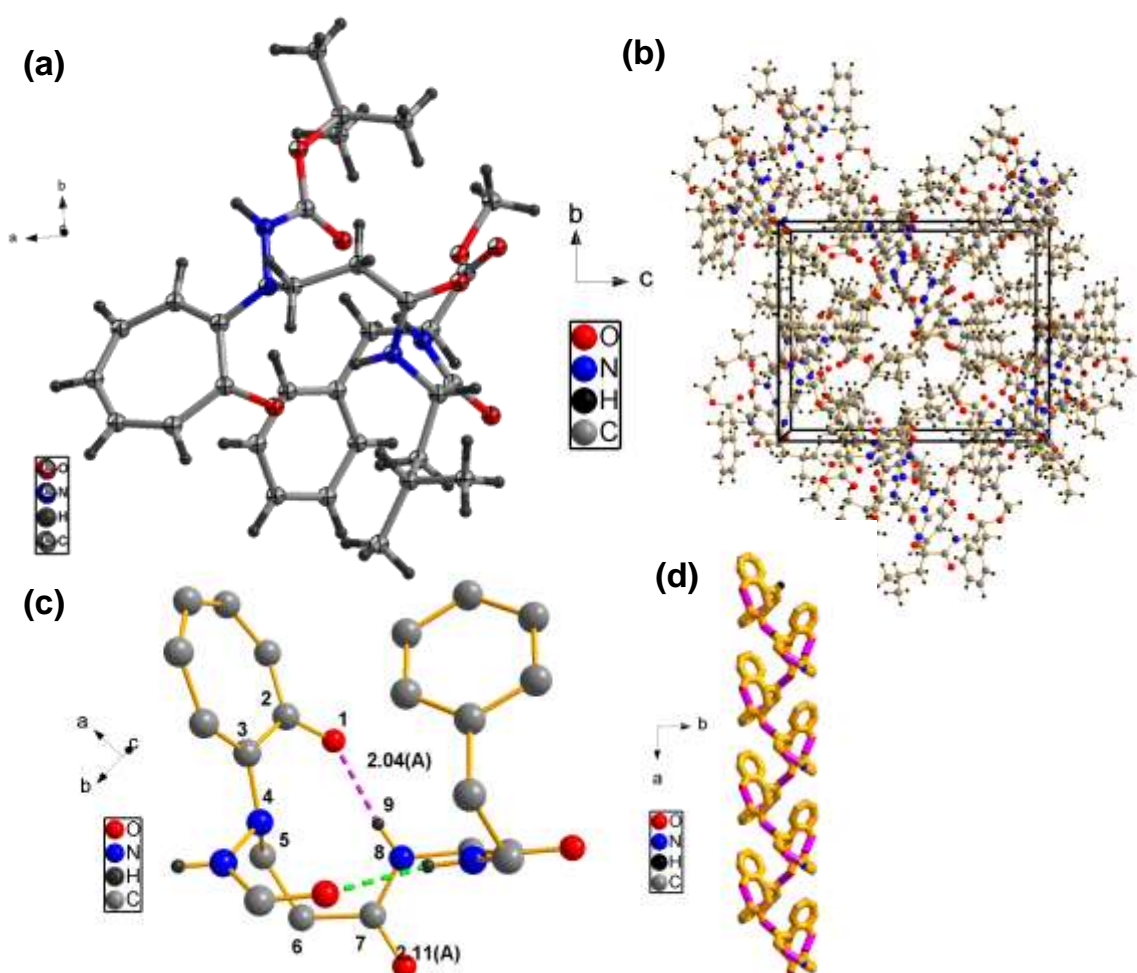
analyses of dipeptide (**5a**) in solid state are depicted in Figure 6.3, which includes ORTEP diagram (Figure 6.3-A), unit cell (Figure 6.3-B), packing arrangement (Figure 6.3-C), and supramolecular helical structure (Figure 6.3-D). Other crystal data are provided in the Appendix. Importantly, peptide **5a** forms an intermolecular hydrogen bonding between troponyl carbonyl with amide N-H ( $C=O \cdots H-N$ ) and hydrazine NH with amide carbonyl ( $N-H \cdots C=O$ ), which leads to a novel supramolecular helical structure with pitch 6.02 (Å) (Figure 6.3-D). Thus, troponyl carbonyl has a significant role in conformational changes of peptides for interesting supramolecular self-assembly structure in the solid state.



**Figure 6.3.** Conformational analyses of crystal peptide **5a\*** in solid state: analysis of crystal **5a\***: (A) ORTEP diagram; (B) Unit Cell packing; (C) Packing arrangement; (D) Helical supramolecular self-assembly structure. (\*Tertiary Butyl ester of **5a**).

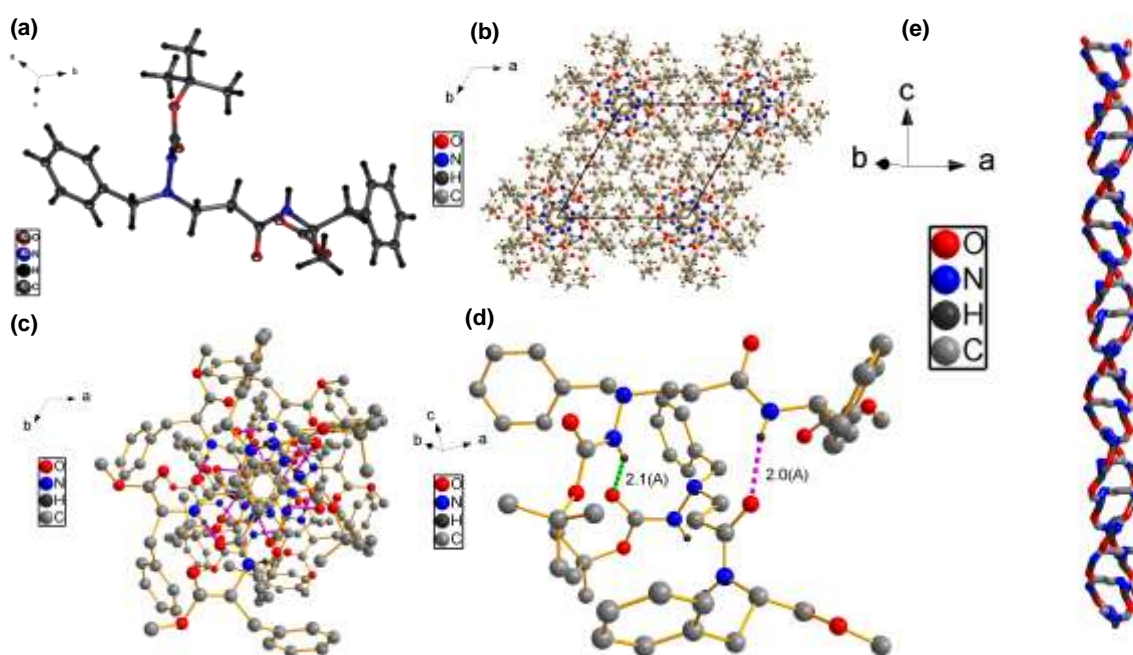
Similarly, The structural analyses data of tripeptide (**5h**) are depicted in Figure 6.4, which describes the ORTEP diagram (Figure 6.4-A), unit cell (Figure 6.4-B) and packing

diagram (Figure 6.4-C), and unique supramolecular helical structure (Figure 6.4-D). Other crystal data are provided in the Appendix. This peptide forms inter and intramolecular hydrogen bonding and generates a new supramolecular self-assembly helical structure. Most importantly, we noticed two intramolecular hydrogen bonding-(a) troponyl carbonyl with adjacent amide NH (Leu) ( $\text{C}=\text{O} \cdots \text{H}-\text{N}$ ,  $2.04\text{\AA}$ ) as  $i+9$  helical structure, and (b) Hydrazine Boc carbonyl with N-H of third residue (Phe) ( $\text{C}=\text{O} \cdots \text{H}-\text{N}$ ,  $2.1\text{\AA}$ ). Other carbonyl and NH of amide form intermolecular hydrogen bonding and assemble into the supramolecular helical structure.



**Figure 6.4.** Conformational analyses of crystal **5h** in solid state: (A) ORTEP diagram; (B) Unit Cell; (C) Hydrogen bonding pattern; (D) Helical supramolecular assembly.

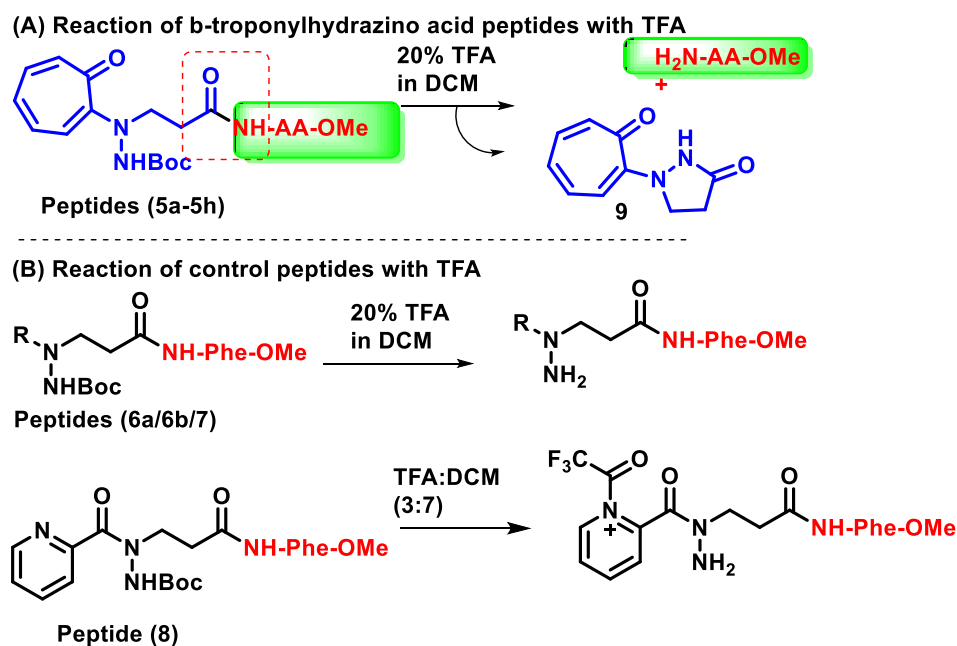
We also obtained the single crystal of control non-troponyl hybrid peptide (**6a**),  $\beta$ -benzylhydrazino acid containing peptide, and analyzed its structural conformation by X-ray studies (Figure 6.5). Other crystal data are provided in the Appendix. Their crystal data are submitted to CCDC with number CCDC 2003626 for peptide **6a**. The ORTEP /unit cell packing diagrams of **6a** are given in Figure 6.5-A/B. It has circular packing rearrangement by self-assembly through hydrogen bonding, as shown in Figure 6.5-C. There are two types of intermolecular hydrogen bonding existing as BocN-H---O=CBoc (2.1 Å) and Amide N-H-----O=C amide (2.0 Å) (Figure 6.5-D). These intermolecular hydrogen bonds of peptide **6a** form a unique ladder type of supramolecular helical structure (Figure 6.5-E). Thus non-troponyl  $\beta$ -hydrazino acid-containing peptide is also a building block of new peptidomimetics.



**Figure 6.5.** Conformational analyses of control peptide crystal (**6a**) in solid state: (A) ORTEP diagram; (B) Unit cell; (C) Packing arrangement; (D) Intermolecular hydrogenbondinnng; (E) Supramolecular self-assembly helical structure.

For peptide coupling at *N*-terminal of hybrid peptides, we attempted to remove the Boc group of *di*-/*tri*-peptides (**5a-5h**) with versatile reagent 20-30% TFA in DCM (Scheme

6.3). Unexpectedly, we isolated a new pyrazolidinone derivative as troponyl pyrazolidinone or *Troponylpyrazolidinone* (**9**) from all respective hybrid peptides (**5a-5h**) under similar conditions by unusual cleavage of the amide bond. The structure of Troponylpyrazolidinone (**9**) is confirmed by NMR and HRMS. Their spectra are provided in the Appendix. We also obtained the single crystal of Troponylpyrazolidinone (**9**) and analyzed it by X-ray diffractometer. Crystal details and unit cells are provided in the Appendix (Figure A72). The X-ray analysis result confirms the structure of Troponylpyrazolidinone (**9**). The X-ray data is also submitted to CCDC with number 2003627. The ORTEP diagram of one dipeptide (**5a**) and its cleaved product Troponylpyrazolidinone (**9**) are depicted in Figure 6.6. We noticed two types of intramolecular hydrogen bonds: (i) N-H of pyrrolidinone with tropolone carbonyl (1.8Å) and (ii) N-H of pyrazolidinone with its carbonyl (2.5Å). We also examined the instability of such amide bonds under different acids as HCl (4.0 N), HClO<sub>4</sub> (4.0 N), PTSA (10 equiv.), and AcOH (4.0 N) by ESI-Mass technique (See Appendix, Figure A68). For peptide **5a**, our mass analysis results reveal cleavage of the amide bond of **5a** with acids (HCl, HClO<sub>4</sub>, and PTSA) and the formation of the same cyclic derivative Troponylpyrazolidinone (**9**). We could not notice the cleavage of Boc group and amide bond cleavage with AcOH, which is a relatively weak organic acid. To examine the role of tropolone residue for the cleavage of such amide bonds, we performed control studies with similar types of non-troponyl- $\beta$ -alkylhydrazino acid containing hybrid peptides (**6a**, **6b**, **7** and **8**) and TFA (~20%) and analyzed by ESI-Mass and NMR techniques (Figure A49-52). Except for Boc group deprotection, we could not find the amide bond cleavage in control peptides. However, control peptide **8** also forms a trifluoroacylated salt derivative by acylation at the pyridine ring of picolamide residue. Hence troponyl residue has a critical role in cleavage of amide bonds containing  $\beta$ -troponylhydrazino acid (peptides **5a-5h**).



**Scheme 6.3.** Reaction of  $\beta$ -troponylhydrazino peptides/non-troponyl- $\beta$ -hydrazino peptides with TFA.

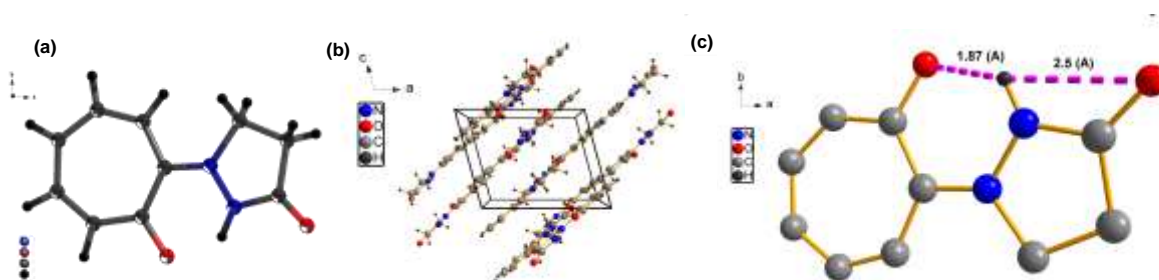


**Figure 6.6.** Conformational analyses of Troponylpyrazolidinone crystal (**9**): (A) ORTEP diagram; (B) unit cell packing; and (C) Intramolecular hydrogen bonding.

The cleavage of the amide bond in peptides (**5a-5h**), under acidic pH, was dependent only upon the concentration of peptides, and so considered as a first-order kinetic reaction. Thus we performed kinetic studies of dipeptides (**5a/5b**) cleavage with the time-dependent  $^1\text{H-NMR}$  experiment under acidic conditions (20% TFA in  $\text{CDCl}_3$ ). Their NMR spectra are provided in the Appendix (Figure A41-48). After the addition of TFA,  $^1\text{H-NMR}$  spectra arrays of dipeptide **5a** exhibit the significant downfield shift of  $\alpha$ -/ $\beta$ -hydrogen

resonance signals such as the resonance signal  $\delta 2.7$  ( $\alpha$ -H) shifted to  $\delta 3.0$ , and  $\delta 3.8$  ( $\beta$ -H) shifted to  $\delta 4.2$ . Simultaneously, the new signals appeared at  $\delta 3.2$  and  $\delta 4.4$ , which presumably belong to new cyclic derivative Troponylpyrazolidinone (**9**). The NMR spectral arrays also show an exponential decrease in the intensity  $\alpha$ -H signal ( $\delta 3.0$ ), while an exponential increase in the intensity of new signals ( $\delta 3.2$ ) happened with respect to time. After completing NMR experiments, we recorded their mass spectra, which are provided in the Appendix (Figure A49-52). Their mass spectra confirm the removal of the Boc group followed by the formation of cyclic compound **9**. Thus, the amide bond of a dipeptide (**5a**) was cleaved with TFA (20%). We repeated similar NMR kinetic experiments with another representative peptide (**5b**) and obtained almost similar results. To determine kinetic parameters (equilibrium constant and half-life of amide bond cleavage), we extracted mole fractions of reactant (**5a**) and its product (**9**) at different intervals of time from their respective NMR (See Appendix, Table A1 and A2). Then we generated a kinetic plot (Mole fraction vs. Time) for the cleavage amide bond (**5a**) and formation of a new cyclic product (**9**) (Figure 6.7A). We also obtained similar results with peptide (**5b**), and its kinetic plot is provided in the Appendix (Figure A56-A). Our kinetic results indicate that the cleavage of the amide bond (**5a/5b**) and the formation of the cyclic derivative are first-order kinetic reactions. Following our previous report,<sup>16</sup> we extracted equilibrium constant ( $k_a$ ) as  $0.016 \text{ min}^{-1}$  and  $0.009 \text{ min}^{-1}$  for peptides **5a** and **5b**, respectively (Figure 6.7B and Figure A56-B). We also compared our experimental kinetic results with the simulated kinetic model (COPASI) using reported software (See Appendix, Figure A57-S58).<sup>16, 24</sup> Then we calculated half-life of amide bond cleavage (**5a/5b**) from their respective logarithmic plots (mole fraction vs. time plot by following the previous reports (See Appendix). We obtained the half-life of 41.0 minutes and 71.0 minutes for cleavage of respective amide bonds in **5a** and **5b**. We performed a similar experiment with control peptide (**6a**), but we noticed only *N*-Boc group was deported. Thus only  $\beta$ -



troponylhydrazino acid-containing peptides are cleavable under acidic conditions, and the rate of cleavage in **5a/5b** also depends upon the substituent of  $\alpha$ -amino acid.

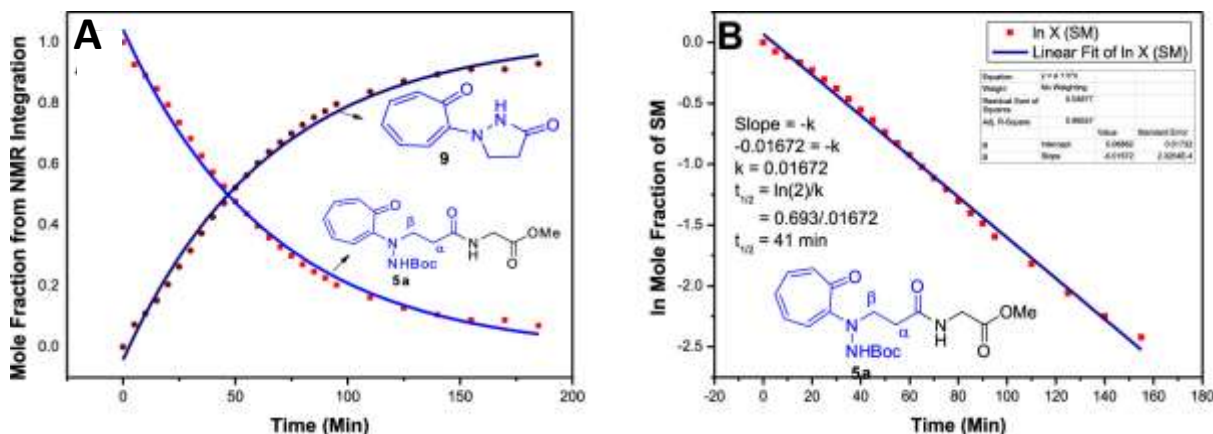


**Figure 6.7.** Time-dependent  $^1\text{H}$ -NMR kinetic plot-Mole Fraction vs. Time (min) with hybrid peptide **5a** (A) and its exponential plot for half-life calculation (B).

Troponyl derivative is a natural chromophore with characteristic absorption peaks.<sup>25</sup> Thus, we planned to monitor the amide bond cleavage reaction of troponylated peptides (**5a/5b**) by UV-Vis studies. We recorded the time-dependent UV-Vis spectra of hybrid peptide **5a** in acetonitrile (ACN) after the addition of 20% TFA (Figure 6.8). We noticed significant changes in the UV spectra of peptide **5a** after the addition of TFA (Figure 6.8), such as hypochromic ( $\sim\lambda_{330} \text{ nm}$ )/hyperchromic shifts ( $\sim\lambda_{400} \text{ nm}$ ) with isosbestic point ( $\sim\lambda_{355} \text{ nm}$ ). Notably, the electronic transition peak at  $\sim\lambda_{330} \text{ nm}$  collapsed into one peak at  $\sim\lambda_{400} \text{ nm}$  after 100 minutes under acidic conditions that matched the spectra of pure isolated Troponylpyrazolidinone (**9**) and their isosbestic point at  $\lambda_{350} \text{ nm}$  (Appendix, Figure A64). We noticed similar results with dipeptide **5b** from the time-dependent UV-Vis studies and mass analyses under the same acidic conditions (Appendix, Figure A65/66). Hence troponylhydrazino hybrid peptides produced the same cyclic intermediate Troponylpyrazolidinone (**9**) after removal *N*-Boc followed by the cleavage of amide bond under acidic conditions.

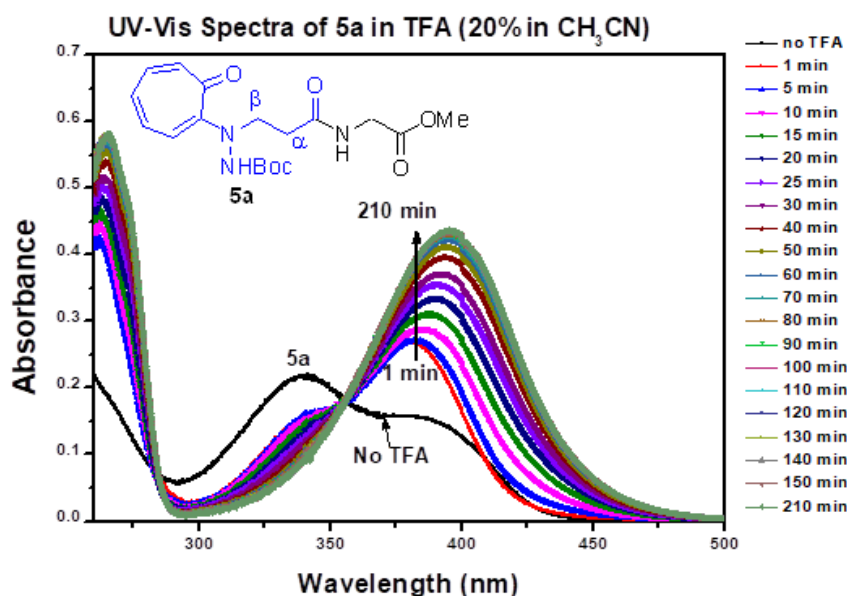


**Figure 6.8.** Time dependent UV-Spectra of dipeptide **6a** under acidic conditions (20% TFA in ACN).

Finally, we propose the plausible mechanism for the cleavage of  $\beta$ -troponylhydrazino containing amide bond (Figure 6.9). In first, TFA (20%) removed the *N*-Boc group of the peptide (**5**) and produced the protonated hydrazinyl derivative (**5-Boc**)\* under the acidic condition that facilitated the cleavage of an adjacent amide bond by the formation of new cyclic molecule troponylpyrazolidinone (**9**). We assumed that, the protonated hydrazinyl derivative (**5-Boc**)\* activated its amide bond when troponyl residue was present at *N*-atom. Herein, the delocalization of cationic hydrazinyl proton possibly occurs through troponyl ring as tautomeric intermediate (**T1** & **T2**), possessing hydrazine amine ( $\text{-NH}_2$ ) nucleophile. This nucleophile attacked at protonated amide carbonyl group *via* nucleophilic addition reaction and then generated a reactive *cyclic*-1,1-aminol intermediate (**T3**). Next, the protonation of aminol amine group followed by elimination led to the stable molecule *N*-troponylpyrazolidinone (**9**) and amine residue. In the case of control peptides, the delocalization of cationic hydrazinyl proton is not possible, and we could not notice the cleavage of amide bond or formation of troponylpyrazolidinone (**9**) under similar acidic



conditions. Thus tropolone played a crucial role in the cleavage of the amide bond in troponylated- $\beta$ -hydrazinopeptide (**5**) under acidic conditions, possibly through the proposed mechanism.

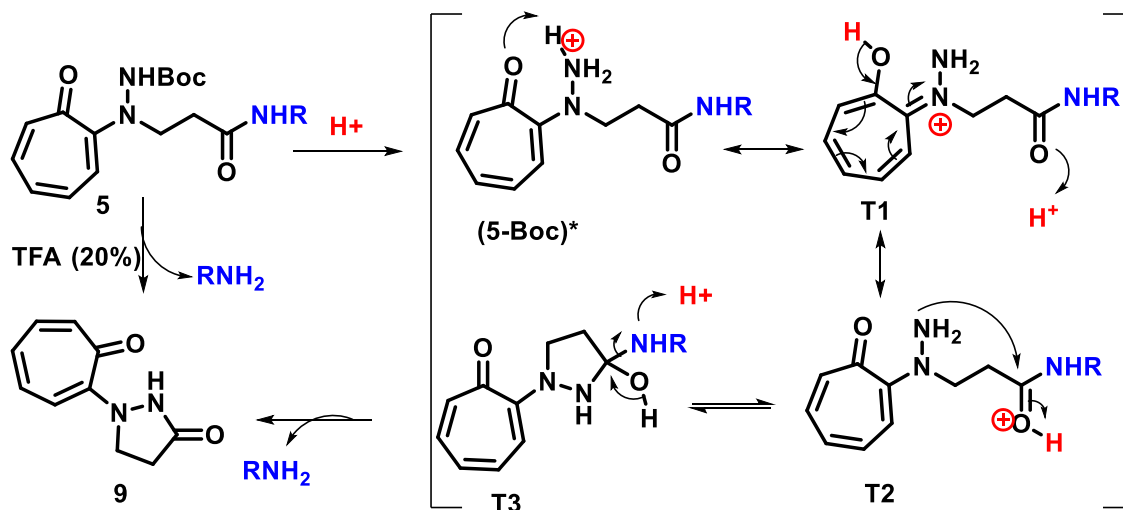


**Figure 6.9.** The proposed mechanism of  $\beta$ -troponylhydrazinyl peptides propenamide cleavage under mild acidic conditions.

## 6.4 Conclusion

$\beta$ -Troponylhydrazino acid analogs and their hybrid peptides are synthesized from natural amino acid derivatives. Conformational analyses of  $\beta$ -hydrazino acid-containing peptides are demonstrated by extracting hydrogen bonding in representative peptides in solid and state. The intramolecular hydrogen bonding of amide N-H has been shown in  $\beta$ -troponylhydrazino peptide by DMSO-titration methods in the solution state. X-ray studies reveal the role of troponyl group in the self-assembly of supramolecular structures in solid-state. Most importantly, the troponyl- $\beta$ -hydrazino acid-containing hybrid peptides show a unique feature as the cleavage of the amide bond through the formation of a new cyclic molecule Troponylpyrazolidinone under mild acidic conditions. Time-dependent NMR studies determine the equilibrium constant and half-life of amide cleavage. The cleavage of that amide bond and formation of Troponylpyrazolidinone are explained with the plausible

mechanism. Hence,  $\beta$ -troponylhydrazino acid could be a promising chromophoric acid-sensitive protecting group of free amines. It could also be helpful to estimate the free amine group by UV-Vis spectrophotometer.

## 6.5 Experimental Section

*General information:* All required materials were obtained from commercial suppliers and used without further purification. Dimethylformamide (DMF) was distilled over calcium hydride. Reactions were monitored by thin-layer chromatography (TLC), visualized by UV and Ninhydrin. Column chromatography was performed in 230-400 mesh silica. Mass spectra and HRMS were obtained from Bruker micrOTOF-Q II Spectrometer.  $^1\text{H}$  NMR,  $^{13}\text{C}$  NMR, were recorded on Bruker AV-400 or 700 MHz at 298 K.  $^1\text{H}$  and  $^{13}\text{C}$  NMR chemical shifts were recorded in ppm downfield from Tetramethylsilane or residual solvent peak. Splitting patterns are abbreviated as: s, Singlet; d, doublet; dd, doublet of doublet; t, triplet; q, quartet; dq, doublet of quartet; m, multiplet.

*General procedure for Hydrolysis of Ester into Acid:* Compounds having ester group (**4**), (**2-Bn**), (**2-Hexyl**) and (**2-Picolamide**) were dissolved in THF containing 2 equivalents of LiOH at 0 °C and then bring to room temperature with stirring. TLC monitored the completion of those ester hydrolysis reactions. The hydrolyses of *N*-allylated- $\beta$ -hydrazino esters were completed within 3 h. The solvents are evaporated under vacuum to half of its volume and adjusted the pH to 6-7 with 1M HCl, and then extracted thrice with EtOAc. The organic layers were combined, dried over  $\text{Na}_2\text{SO}_4$ , and concentrated under low pressure to afford the acid derivative products. Without any further characterization, we proceed for the next step (for amide coupling). These *N*-alkylated- $\beta$ -hydrazino acids were coupled with natural  $\alpha$ -amino acids in the presence of amide coupling reagents as HOAT (1.3 equivalent), *N*-methyl

morpholine (3 equivalent) was EDC.HCl (1.3 equivalent), and was dissolved in Dry DMF (1.5 M). After stirring for 10 min, cooled it to 0 °C and added

*General procedure for peptide synthesis:* After hydrolysis ester group into acid group it is directly used for peptide coupling reaction without any further purifications where the corresponding amines (1.2 equivalent), HOAT (1.3equivalent) were dissolved in Dry DMF (1.5 M). After stirring for 10 min, *N*-methyl morpholine (3 equivalent) was added drop wise and cooled it to 0 °C and added EDC.HCl (1.3 equivalent). After 20 min, it was allowed to warm to rt followed by heating at 55 °C for 14 h. The crude reaction mixture was evaporated under reduced pressure. The resultant crude was purified by column chromatography with MeOH in CH<sub>2</sub>Cl<sub>2</sub> (1-3%). The obtained product was characterized using <sup>1</sup>H/<sup>13</sup>C by NMR and HRMS by ESI-MS techniques. The characterization data of all synthesized hybrid peptides are provided below.

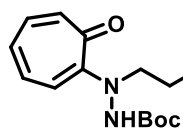
*General procedure for Boc deprotection:* 30% TFA in CH<sub>2</sub>Cl<sub>2</sub> (5 mL) was added to compound (**6a**) at room temperature and stirred for 3 h. The solvents were removed under vacuum and resulting in the red color residue (only in case of troponyl derivative). The residual viscous oil was purified via chromatography with 3% MeOH in CH<sub>2</sub>Cl<sub>2</sub>. The obtained product was characterized using <sup>1</sup>H/<sup>13</sup>C by NMR and HRMS by ESI-MS techniques.

#### *Characterization data of products*

tert-butyl-2-(3-ethoxy-3-oxopropyl)hydrazine-1-carboxylate (**2**): Experimental procedure and their characterization data for compounds (**2**) are previously reported.<sup>26</sup> A solution of 3-bromo-propionic acid ethyl ester (2 mL, 15.7mmol), DIPEA (2.6mL, 15.7mmol) and Boc-hydrazine (**1**) (3.1g, 23.55mmol) in toluene was heated at 80 °C for 4 days. After removal of the solvent under reduced pressure, the crude product was purified by column

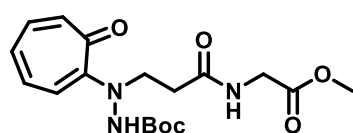
chromatography (Hexane:EtOAc) to give compound (**2**) which is a slightly yellow oil (1.58g, 43%).

tert-butyl-2-(3-ethoxy-3-oxopropyl)-2-(7-oxocyclohepta-1,3,5-trien-1-yl)hydrazine-1-



carboxylate (**4**): The Boc protected  $\beta$ -hydrazino acid derivative **2** (4.0g, 17.24mmol) was dissolved in ethanol containing TEA (7.20mL, 51.72mmol) and stirred at room temperature followed by addition of 2-tosyloxy tropolone derivative **3** (9.5g, 34.48mmol). This reaction mixture was allowed to reflux for 4 days till the disappearance of starting material (**2**). The reaction was monitored by TLC with 40% ethyl acetate in hexane. After completion of the reaction, the reaction mixture was concentrated under low pressure. The concentrated crude product was purified by silica gel column chromatography (230-400 mesh) in 20% Ethyl Acetate in Hexane as mobile phase. The purified product was obtained as solid yellow color 2.0g (35% yield) and then characterized by NMR ( $^1\text{H}/^{13}\text{C}$ ) and ESI-Mass techniques.  $^1\text{H}$  NMR (400 MHz, deuterated solvent  $\text{CDCl}_3$ )  $\delta$  7.58 (s, 1H), 7.20 – 6.95 (m, 4H), 6.84 – 6.74 (m, 1H), 4.15 (q,  $J$  = 7.1 Hz, 2H), 3.89 (t,  $J$  = 6.7 Hz, 2H), 2.76 (t,  $J$  = 6.8 Hz, 2H), 1.41 (s, 9H), 1.26 (t,  $J$  = 7.1 Hz, 3H),  $^{13}\text{C}$  NMR (176 MHz,  $\text{CDCl}_3$ )  $\delta$  181.63, 172.14, 157.26, 155.27, 136.36, 135.78, 133.60, 127.81, 81.35, 60.66, 49.62, 32.76, 29.65, 28.15, 14.13. HRMS (ESI-TOF)  $m/z$ :  $[\text{M}+\text{Na}]^+$  Calcd. for  $\text{C}_{17}\text{H}_{24}\text{N}_2\text{O}_5$  359.1572, found 359.1577.

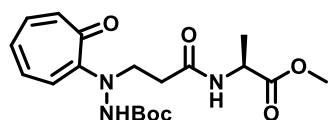
tert-butyl-2-(3-((2-methoxy-2-oxoethyl)amino)-3-oxopropyl)-2-(7-oxocyclohepta-1,3,5-trien-



1-yl)hydrazine-1-carboxylate (**5a**): The dipeptide was synthesized by following general procedure. 155mg (63% yield) of pure product was obtained as yellow color solid.  $^1\text{H}$  NMR (400 MHz, deuterated solvent  $\text{CDCl}_3$ )  $\delta$  7.97 (s, 1H), 7.81 (s, 1H), 7.28 (s, 1H), 7.23 – 7.03 (m, 3H), 6.86 (t, 1H), 4.04 (d,  $J$  = 5.0 Hz, 2H), 3.83 (t,  $J$  = 5.1 Hz, 2H), 3.73 (s, 3H), 2.65 (t,  $J$  = 5.9 Hz, 2H), 2.09 (s, 1H), 1.44 (s, 9H),  $^{13}\text{C}$  NMR (101 MHz,  $\text{CDCl}_3$ )  $\delta$  182.44, 172.17, 170.74, 157.26, 155.58,

137.24, 136.27, 134.00, 129.44, 81.47, 52.23, 50.78, 41.22, 34.62, 28.23. HRMS (ESI-TOF)  $m/z$ :  $[M+H]^+$  calcd. for  $C_{18}H_{25}N_3O_6$  380.1816, found 380.1817.

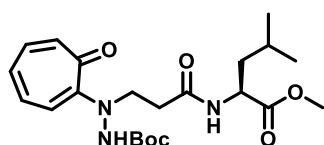
tert-butyl-(S)-2-(3-((1-methoxy-1-oxopropan-2-yl)amino)-3-oxopropyl)-2-(7-oxocyclohepta-



1,3,5-trien-1-yl)hydrazine-1-carboxylate (**5b**): The dipeptide was synthesized by following general procedure. 110mg (58%

yield) of pure product was obtained as yellow color solid.  $^1H$  NMR (700 MHz, deuterated solvent  $CDCl_3$ )  $\delta$  7.77 (s, 2H), 7.26 (s, 1H), 7.21 – 7.16 (m, 1H), 7.13 – 7.05 (m, 2H), 6.86 (t,  $J = 9.3$  Hz, 1H), 4.58 – 4.50 (m, 1H), 3.97 – 3.89 (m, 1H), 3.76 (s, 1H), 3.73 (s, 3H), 2.71 – 2.53 (m, 2H), 1.44 (s, 9H), 1.40 (d,  $J = 7.3$  Hz, 3H),  $^{13}C$  NMR (176 MHz,  $CDCl_3$ )  $\delta$  182.34, 173.82, 171.42, 157.26, 155.56, 137.09, 136.21, 133.95, 129.26, 81.49, 58.38, 52.35, 48.24, 34.63, 28.22, 17.53. HRMS (ESI-TOF)  $m/z$ :  $[M+Na]^+$  calcd. for  $C_{19}H_{27}N_3O_6$  416.1792, found 416.1828.

tert-butyl-(S)-2-(3-((1-methoxy-4-methyl-1-oxopentan-2-yl)amino)-3-oxopropyl)-2-(7-



oxocyclohepta-1,3,5-trien-1-yl)hydrazine-1-carboxylate (**5c**):

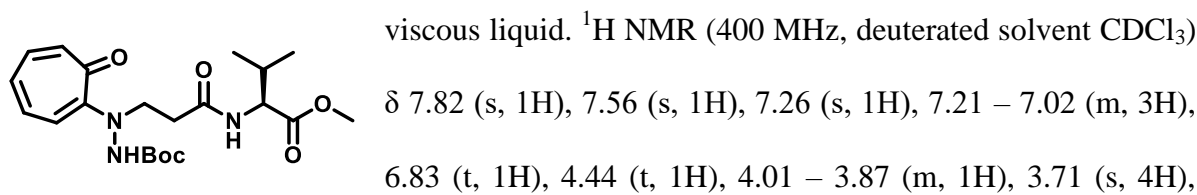
The dipeptide was synthesized by following general procedure.

135mg (48% yield) of pure product was obtained as yellow viscous liquid.  $^1H$  NMR (400 MHz, deuterated solvent  $CDCl_3$ )  $\delta$  7.80 (s, 2H), 7.34 (s, 1H), 7.24 – 7.00 (m, 3H), 6.86 (t, 1H), 4.54 (q,  $J = 7.7$  Hz, 1H), 3.97 – 3.83 (m, 1H), 3.71 (s, 4H), 2.75 – 2.48 (m, 2H), 1.76 – 1.64 (m, 1H), 1.63 – 1.57 (m, 2H), 1.44 (s, 9H), 0.91 (dd,  $J = 6.4$ , 4.2 Hz, 6H),  $^{13}C$  NMR (101 MHz,  $CDCl_3$ )  $\delta$  182.52, 173.92, 171.82, 157.24, 155.68, 137.38, 136.22, 134.04, 129.59, 81.38, 52.17, 51.14, 40.61, 36.66, 34.70, 28.21, 24.83, 22.88, 21.63. HRMS (ESI-TOF)  $m/z$ :  $[M+H]^+$  calcd. for  $C_{22}H_{33}N_3O_6$  436.2442, found 436.2451.

tert-butyl-(S)-2-(3-((1-methoxy-3-methyl-1-oxobutan-2-yl)amino)-3-oxopropyl)-2-(7-

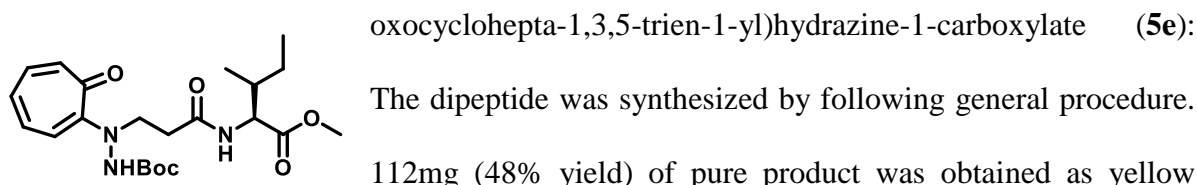
oxocyclohepta-1,3,5-trien-1-yl)hydrazine-1-carboxylate (**5d**): The dipeptide was synthesized

by following general procedure. 112mg (54% yield) of pure product was obtained as yellow



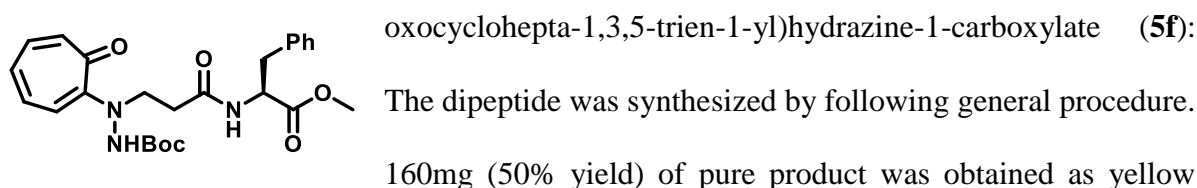
2.75 – 2.51 (m, 2H), 2.23 – 2.08 (m, 1H), 1.43 (s, 9H), 0.92 (dd,  $J = 6.6, 3.2$  Hz, 6H),  $^{13}\text{C}$  NMR (101 MHz,  $\text{CDCl}_3$ )  $\delta$  182.27, 172.79, 171.94, 157.31, 155.67, 137.06, 136.10, 133.95, 129.10, 81.39, 57.91, 52.01, 51.50, 34.91, 30.56, 28.21, 18.98, 18.00. HRMS (ESI-TOF)  $m/z$ :  $[\text{M}+\text{Na}]^+$  calcd. for  $\text{C}_{21}\text{H}_{31}\text{N}_3\text{O}_6$  444.2105, found 444.2147.

tert-butyl-2-(3-(((2S,3R)-1-methoxy-3-methyl-1-oxopentan-2-yl)amino)-3-oxopropyl)-2-(7-



viscous liquid.  $^1\text{H}$  NMR (400 MHz, deuterated solvent  $\text{CDCl}_3$ )  $\delta$  7.83 (s, 1H), 7.57 (s, 1H), 7.24 (s, 1H), 7.20 – 6.99 (m, 3H), 6.83 (t,  $J = 9.1$  Hz, 1H), 4.47 (t,  $J = 6.4$  Hz, 1H), 4.00 – 3.86 (m, 1H), 3.70 (s, 4H), 2.77 – 2.47 (m, 2H), 1.86 (s, 1H), 1.43 (s, 9H), 1.30 – 1.13 (m, 2H), 0.87 (t,  $J = 7.8$  Hz, 6H),  $^{13}\text{C}$  NMR (101 MHz,  $\text{CDCl}_3$ )  $\delta$  182.21, 172.80, 171.81, 157.29, 155.67, 137.00, 136.08, 133.95, 129.02, 81.39, 57.11, 51.95, 51.47, 37.22, 34.90, 28.20, 25.29, 15.48, 11.54. HRMS (ESI-TOF)  $m/z$ :  $[\text{M}+\text{Na}]^+$  calcd. for  $\text{C}_{22}\text{H}_{33}\text{N}_3\text{O}_6$  458.2262, found 458.2295.

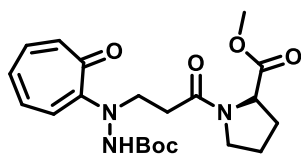
tert-butyl-(S)-2-(3-((1-methoxy-1-oxo-3-phenylpropan-2-yl)amino)-3-oxopropyl)-2-(7-



viscous liquid.  $^1\text{H}$  NMR (400 MHz, deuterated solvent  $\text{CDCl}_3$ )  $\delta$  7.73 (s, 1H), 7.60 (s, 1H), 7.27 – 7.13 (m, 7H), 7.11 – 7.03 (m, 2H), 6.86 (t, 1H), 4.84 (q,  $J = 7.8$  Hz, 1H), 3.78 (s, 2H),

3.71 (s, 3H), 3.16 (dd,  $J = 14.0, 5.5$  Hz, 1H), 3.04 (dd,  $J = 14.0, 8.1$  Hz, 1H), 2.66 – 2.47 (m, 2H), 1.44 (s, 9H),  $^{13}\text{C}$  NMR (101 MHz,  $\text{CDCl}_3$ )  $\delta$  182.24, 172.48, 171.55, 157.15, 155.41, 137.14, 136.52, 136.18, 133.95, 129.16, 128.44, 126.87, 81.41, 53.69, 52.27, 50.42, 37.48, 34.53, 28.23. HRMS (ESI-TOF)  $m/z$ :  $[\text{M}+\text{H}]^+$  calcd. for  $\text{C}_{25}\text{H}_{31}\text{N}_3\text{O}_6$  470.2286, found 470.2291.

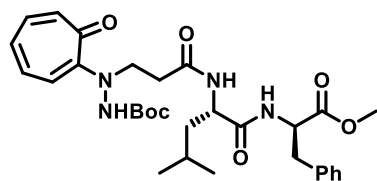
methyl-(3-(2-(tert-butoxycarbonyl)-1-(7-oxocyclohepta-1,3,5-trien-1-



yl)hydrazineyl)propanoyl)-L-prolinate (**5g**): The dipeptide was synthesized by following general procedure. 96mg (43% yield) of pure product was obtained as yellow viscous liquid.  $^1\text{H}$  NMR

(400 MHz, deuterated solvent  $\text{CDCl}_3$ )  $\delta$  7.92 (s, 1H), 7.18 – 6.99 (m, 4H), 6.75 (t,  $J = 9.0$  Hz, 1H), 4.53 – 4.45 (m, 1H), 4.03 (s, 2H), 3.75 (s, 3H), 3.69 – 3.63 (m, 1H), 3.59 – 3.51 (m, 1H), 2.98 – 2.84 (m, 1H), 2.77 – 2.65 (m, 1H), 2.25 – 2.13 (m, 1H), 2.07 – 1.95 (m, 3H), 1.45 (s, 9H),  $^{13}\text{C}$  NMR (101 MHz,  $\text{CDCl}_3$ )  $\delta$  181.09, 173.02, 170.67, 157.40, 155.09, 135.70, 133.96, 126.86, 117.90, 81.24, 58.64, 52.32, 50.68, 47.30, 33.27, 29.24, 28.23, 24.72. HRMS (ESI-TOF)  $m/z$ :  $[\text{M}+\text{Na}]^+$  calcd. for  $\text{C}_{21}\text{H}_{29}\text{N}_3\text{O}_6$  442.1949, found 442.1984.

*tert*-butyl-2-(3-(((*S*)-1-(((*R*)-1-methoxy-1-oxo-3-phenylpropan-2-yl)amino)-4-methyl-1-

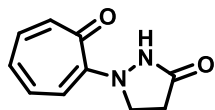


oxopentan-2-yl)amino)-3-oxopropyl)-2-(7-oxocyclohepta-1,3,5-trien-1-yl)hydrazine-1-carboxylate (**5h**). The tripeptide was synthesized by following general procedure.

320mg (42% yield) of pure product was obtained as yellow colour solid.  $^1\text{H}$  NMR (400 MHz, deuterated solvent  $\text{CDCl}_3$ )  $\delta$  8.41 (s, 1H), 7.93 (s, 1H), 7.26 – 7.05 (m, 8H), 7.02 (d,  $J = 6.7$  Hz, 2H), 6.94 – 6.82 (m, 1H), 4.78 (q,  $J = 7.4$  Hz, 1H), 4.49 – 4.38 (m, 1H), 3.98 (s, 1H), 3.67 (s, 3H), 3.58 (d,  $J = 12.3$  Hz, 1H), 3.09 (dd,  $J = 13.8, 5.6$  Hz, 1H), 2.91 (dd,  $J = 13.8, 7.4$  Hz, 1H), 2.69 – 2.54 (m, 2H), 1.78 – 1.65 (m, 1H), 1.64 – 1.52 (m, 2H), 1.46 (s, 9H), 0.89 (dd,  $J = 16.4, 6.4$  Hz, 6H),  $^{13}\text{C}$  NMR (101 MHz,  $\text{CDCl}_3$ )  $\delta$  181.86, 172.49, 172.17, 171.37, 157.55,

155.16, 137.20, 136.31, 136.23, 133.96, 129.18, 128.21, 126.74, 81.42, 53.17, 52.22, 48.73, 40.30, 37.57, 34.29, 28.22, 24.77, 23.02, 21.63. HRMS (ESI-TOF)  $m/z$ :  $[M+Na]^+$  calcd. for  $C_{31}H_{42}N_4O_7$  605.2918, found 605.2946.

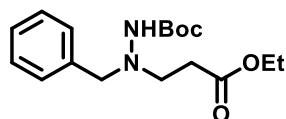
1-(7-oxocyclohepta-1,3,5-trien-1-yl)pyrazolidin-3-one (**9**): The Troponylpyrazolidinone was synthesized by following general procedure. The product was purified



by column chromatography with MeOH in  $CH_2Cl_2$  (2%). 18mg (94%) of pure product was obtained as red color solid and characterized by

NMR ( $^1H/^{13}C$ ) and mass spectroscopy.  $^1H$  NMR (400 MHz, deuterated solvent  $CDCl_3$ )  $\delta$  12.74 (s, 1H), 7.21 – 7.06 (m, 2H), 6.94 (d,  $J$  = 11.6 Hz, 1H), 6.64 (t,  $J$  = 9.3 Hz, 1H), 6.36 (d,  $J$  = 10.8 Hz, 1H), 3.99 (t,  $J$  = 8.6 Hz, 2H), 2.80 (t,  $J$  = 8.6 Hz, 2H),  $^{13}C$  NMR (101 MHz,  $CDCl_3$ )  $\delta$  178.12, 169.05, 150.01, 137.76, 135.62, 132.02, 124.59, 113.50, 47.68, 29.16. HRMS (ESI-TOF)  $m/z$ :  $[M+H]^+$  calcd. for  $C_{10}H_{10}N_2O_2$  191.0815, found 191.0815.

tert-butyl-2-benzyl-2-(3-ethoxy-3-oxopropyl)hydrazine-1-carboxylate (**2-Bn**): The Boc



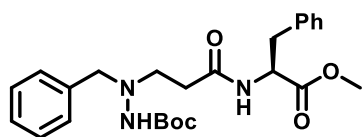
protected  $\beta$ -hydrazino acid derivative **2** (4.0g, 17.24mmol) was dissolved in acetonitrile and  $K_2CO_3$  (4.75g, 34.48mmol) was added

to it and stirred at RT followed by addition of benzyl bromide (3.07mL, 25.86 mmol). This reaction mixture was allowed to stirring at RT for 24 hrs. till the disappearance of starting material (**2**). The reaction was monitored by TLC with 40% ethyl acetate in hexane. After completion of the reaction, reaction mixture was filtrated and concentrated under reduced pressure to obtain crude product. The concentrated crude product was purified by silica gel column chromatography (230-400 mesh) in 10-20% Ethyl Acetate in Hexane as mobile phase. The desired product 2.8g (50%) was obtained as white colour solid and characterized by NMR ( $^1H/^{13}C$ ) and mass spectrometric methods.  $^1H$  NMR (400 MHz, deuterated solvent  $CDCl_3$ )  $\delta$  7.31 (d,  $J$  = 4.3 Hz, 4H), 7.27 (d,  $J$  = 3.8 Hz, 1H), 5.57 (s, 1H), 4.13 (q,  $J$  = 7.1 Hz, 2H), 4.01 (s, 2H), 3.13 (s, 2H), 2.54 (t,  $J$  = 6.9 Hz, 2H), 1.39 (s, 9H), 1.24 (t,  $J$  = 7.1 Hz, 3H),



$^{13}\text{C}$  NMR (101 MHz,  $\text{CDCl}_3$ )  $\delta$  172.40, 154.97, 136.81, 129.35, 128.23, 127.41, 79.95, 60.36, 51.56, 33.14, 28.27, 14.17. HRMS (ESI-TOF)  $m/z$ :  $[\text{M}+\text{Na}]^+$  calcd. for  $\text{C}_{17}\text{H}_{26}\text{N}_2\text{O}_4$  345.1785, found 345.1779.

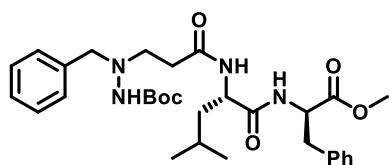
tert-butyl-(S)-2-benzyl-2-(3-((1-methoxy-1-oxo-3-phenylpropan-2-yl)amino)-3-



oxopropyl)hydrazine-1-carboxylate (**6a**): The dipeptide was synthesized by following general procedure. 150mg (50% yield) of pure product was obtained as white color solid.  $^1\text{H}$

NMR (400 MHz, deuterated solvent  $\text{CDCl}_3$ )  $\delta$  8.33 (s, 1H), 7.35 – 7.18 (m, 10H), 5.43 (s, 1H), 4.86 (q,  $J$  = 7.4 Hz, 1H), 3.98 (d,  $J$  = 12.5 Hz, 1H), 3.85 (d,  $J$  = 12.8 Hz, 1H), 3.72 (s, 3H), 3.24 (dd,  $J$  = 13.8, 5.6 Hz, 1H), 3.13 (dd,  $J$  = 13.9, 7.9 Hz, 1H), 3.09 – 2.99 (m, 1H), 2.99 – 2.90 (m, 1H), 2.45 – 2.28 (m, 2H), 1.38 (s, 9H),  $^{13}\text{C}$  NMR (101 MHz,  $\text{CDCl}_3$ )  $\delta$  172.43, 172.17, 155.60, 136.98, 135.53, 129.67, 129.34, 128.36, 127.71, 126.85, 80.37, 61.73, 53.73, 53.23, 52.16, 37.66, 33.77, 28.22. HRMS (ESI-TOF)  $m/z$ :  $[\text{M}+\text{H}]^+$  calcd. for  $\text{C}_{25}\text{H}_{33}\text{N}_3\text{O}_5$  456.2493, found 456.2501.

tert-butyl-2-benzyl-2-(3-(((S)-1-(((R)-1-methoxy-1-oxo-3-phenylpropan-2-yl)amino)-4-

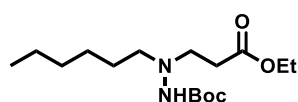


methyl-1-oxopentan-2-yl)amino)-3-oxopropyl)hydrazine-1-carboxylate (**6b**). The tripeptide was synthesized by following general procedure. 400 mg (55% yield) of pure

product was obtained as white color solid crystalline.  $^1\text{H}$  NMR (400 MHz, deuterated solvent  $\text{CDCl}_3$ )  $\delta$  8.45 (s, 1H), 7.33 (q,  $J$  = 9.2, 7.9 Hz, 3H), 7.28 – 7.18 (m, 5H), 7.15 (d,  $J$  = 6.7 Hz, 3H), 5.40 (d,  $J$  = 10.0 Hz, 1H), 4.84 (q,  $J$  = 7.5 Hz, 1H), 4.48 – 4.38 (m, 1H), 3.91 – 3.75 (m, 2H), 3.66 (s, 3H), 3.15 (dd,  $J$  = 13.8, 5.6 Hz, 1H), 3.01 (dd,  $J$  = 13.8, 7.5 Hz, 1H), 2.96 – 2.82 (m, 2H), 2.36 (t,  $J$  = 5.5 Hz, 2H), 2.00 – 1.81 (m, 1H), 1.71 – 1.59 (m, 2H), 1.36 (s, 9H), 0.91 (dd,  $J$  = 9.9, 6.1 Hz, 6H),  $^{13}\text{C}$  NMR (101 MHz,  $\text{CDCl}_3$ )  $\delta$  172.48, 172.30, 172.03, 156.22, 136.50, 134.54, 129.61, 129.44, 128.54, 128.37, 127.96, 126.80, 80.81, 62.66, 54.08, 53.19,

52.35, 52.17, 40.53, 38.02, 33.88, 28.15, 24.84, 23.10, 21.57. HRMS (ESI-TOF)  $m/z$ :  $[M+H]^+$  calcd. for  $C_{31}H_{44}N_4O_6$  569.3322, found 569.3334.

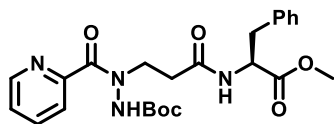
tert-butyl 2-(3-ethoxypropyl)-2-hexylhydrazine-1-carboxylate (**2-Hexyl**): The Boc protected



$\beta$ -hydrazino acid derivative **2** (4.0g, 17.24mmol) was dissolved in

acetonitrile and  $K_2CO_3$  (4.75g, 34.48mmol) was added to it and stirred at RT followed by addition of 1-Bromohexane (3.6mL, 25.86mmol). This reaction mixture was allowed to stir at 55°C for 48 hrs. till the disappearance of starting material (**2**). The reaction was monitored by TLC with 40% ethyl acetate in hexane. After completion of the reaction, reaction mixture was filtrated and concentrated under reduced pressure to obtain crude product. The concentrated crude product was purified by silica gel column chromatography (230-400 mesh) in 10-20% Ethyl Acetate in Hexane as mobile phase. The desired product 2.1g (40%) was obtained as slightly yellow colour liquid and characterized by NMR ( $^1H/^{13}C$ ) and mass spectrometric methods.  $^1H$  NMR (400 MHz, deuterated solvent  $CDCl_3$ )  $\delta$  5.41 (s, 1H), 4.10 (q,  $J = 7.1$  Hz, 2H), 2.98 (s, 2H), 2.67 (s, 2H), 2.50 (t,  $J = 6.5$  Hz, 2H), 1.41 (s, 11H), 1.32 – 1.18 (m, 9H), 0.85 (t,  $J = 6.5$  Hz, 3H),  $^{13}C$  NMR (101 MHz,  $CDCl_3$ )  $\delta$  172.56, 155.06, 79.68, 60.37, 58.20, 32.74, 31.69, 28.28, 26.73, 22.54, 14.15, 14.00. HRMS (ESI-TOF)  $m/z$ :  $[M+Na]^+$  calcd. for  $C_{16}H_{32}N_2O_4$  339.2254, found 339.2245.

tert-butyl-(R)-2-hexyl-2-(3-((1-methoxy-1-oxo-3-phenylpropan-2-yl)amino)-3-

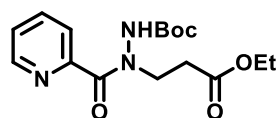


oxopropyl)hydrazine-1-carboxylate (**7**): The dipeptide was

synthesized by following general procedure. 150mg (45% yield) of pure product was obtained as white viscous liquid.  $^1H$  NMR (400 MHz, deuterated solvent  $CDCl_3$ )  $\delta$  8.45 – 8.30 (m, 1H), 7.34 – 7.16 (m, 5H), 5.35 (s, 1H), 4.81 (q,  $J = 7.8$  Hz, 1H), 3.70 (s, 3H), 3.15 (dd, 2H), 2.98 – 2.76 (m, 2H), 2.74 – 2.53 (m, 2H), 2.40 – 2.24 (m, 2H), 1.47 (s, 9H), 1.34 – 1.23 (m, 8H), 0.90 (t,  $J = 6.7$  Hz, 3H),  $^{13}C$  NMR (101 MHz,  $CDCl_3$ )  $\delta$  172.35, 172.26, 155.83, 137.14, 129.30, 128.58, 128.29, 126.70,

80.28, 58.33, 54.41, 53.74, 52.04, 37.56, 33.73, 31.79, 29.69, 28.30, 26.82, 26.67, 22.58, 14.06. HRMS (ESI-TOF)  $m/z$ :  $[M+Na]^+$  calcd. for  $C_{24}H_{39}N_3O_5$  472.2782, found 472.2783.

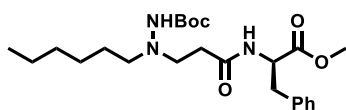
tert-butyl 2-(3-ethoxy-3-oxopropyl)-2-picolinoylhydrazine-1-carboxylate (**2-Picolamide**):



The Picolinoyl derivative peptide ester was synthesized by following general procedure. 1.6g (55% yield) of pure product was

obtained as yellow viscous liquid.  $^1H$  NMR (400 MHz, deuterated solvent  $CDCl_3$ )  $\delta$  8.54 (s, 1H), 7.90 – 7.69 (m, 3H), 7.41 – 7.28 (m, 1H), 4.16 (q,  $J$  = 7.0 Hz, 2H), 4.02 (t,  $J$  = 6.4 Hz, 2H), 2.77 (t,  $J$  = 6.7 Hz, 2H), 1.31 – 1.17 (m, 12H),  $^{13}C$  NMR (101 MHz,  $CDCl_3$ )  $\delta$  171.87, 169.76, 153.00, 147.74, 136.91, 124.81, 124.02, 81.43, 60.65, 45.30, 32.14, 27.84, 14.14. HRMS (ESI-TOF)  $m/z$ :  $[M+H]^+$  calcd. for  $C_{16}H_{23}N_3O_5$  338.1706, found 338.1710.

tert-butyl-(S)-2-(3-((1-methoxy-1-oxo-3-phenylpropan-2-yl)amino)-3-oxopropyl)-2-



picolinoylhydrazine-1-carboxylate (**8**): The tripeptide was synthesized by following general procedure. 120mg (40%

yield) of pure product was obtained as white viscous liquid.  $^1H$  NMR (400 MHz, deuterated solvent  $CDCl_3$ )  $\delta$  8.54 (d,  $J$  = 3.7 Hz, 1H), 7.82 – 7.75 (m, 1H), 7.70 (d,  $J$  = 7.6 Hz, 1H), 7.42 – 7.33 (m, 1H), 7.30 (d,  $J$  = 7.0 Hz, 1H), 7.28 – 7.21 (m, 2H), 7.17 (d,  $J$  = 7.0 Hz, 2H), 6.66 (s, 1H), 4.88 (q,  $J$  = 6.6 Hz, 1H), 4.07 (s, 1H), 3.91 (d,  $J$  = 12.9 Hz, 1H), 3.72 (s, 3H), 3.18 – 3.08 (m, 2H), 2.69 – 2.58 (m, 2H), 1.25 (s, 9H),  $^{13}C$  NMR (101 MHz,  $CDCl_3$ )  $\delta$  172.24, 170.83, 169.97, 147.93, 136.88, 136.04, 129.21, 128.61, 127.09, 124.76, 123.65, 81.54, 53.44, 52.31, 46.50, 37.80, 34.23, 27.90. HRMS (ESI-TOF)  $m/z$ :  $[M+H]^+$  calcd. for  $C_{24}H_{30}N_4O_6$  471.2220, found 471.2238.

General procedure for synthesis of *N*-Troponylpyrazolidinone (**9**): The Boc-protected troponyl peptides (~100mmol), containing  $\beta$ -troponyl hydrazino acid, was added to 20-30% TFA in DCM (~5.0mL) and stirred for 2-3 h at room temperature. The reaction was

monitored by TLC before characterization by ESI-Mass. The reaction mixture was purified through silica column chromatography technique. The yield of isolated cyclic product was ~94%.

## 6.6 References and Notes

1. Barrett, A. J. R., N. D.; J. F. Woessner, J. F., Enzymes can of course efficiently orchestrate amide cleavage under physiological conditions. Handbook of Proteolytic Enzymes, 2nd ed., Academic Press, San Diego, 2004; pp 1-30.
2. Radzicka, A.; Wolfenden, R., Rates of uncatalyzed peptide bond hydrolysis in neutral solution and the transition state affinities of proteases. *J. Am. Chem. Soc.* 1996, **118**, 6105-6109.
3. Bennet, A.; Somayaji, V.; Brown, R.; Santarsiero, B., The influence of altered amidic resonance on the infrared and carbon-13 and nitrogen-15 NMR spectroscopic characteristics and barriers to rotation about the NC (O) bond in some anilides and toluamides. *J. Am. Chem. Soc.* 1991, **113**, 7563-7571.
4. Lide, D. R., CRC Handbook of Chemistry and Physics, 3rd electronic ed. CRC, Boca Raton, Florida, 2000; pp 3-84
5. Clayden, J., Organic chemistry: Stabilizers cause instability. *Nature* 2012, **481**, 274-5.
6. Clayden, J.; Moran, W. J., The Twisted Amide 2-Quinuclidone: 60 Years in the Making. *Angew. Chem. Int. Ed. Engl.* 2006, **45**, 7118-7120.
7. Szostak, M.; Aubé, J., Medium-bridged lactams: a new class of non-planar amides. *Org. Biomol. Chem.* 2011, **9**, 27-35.

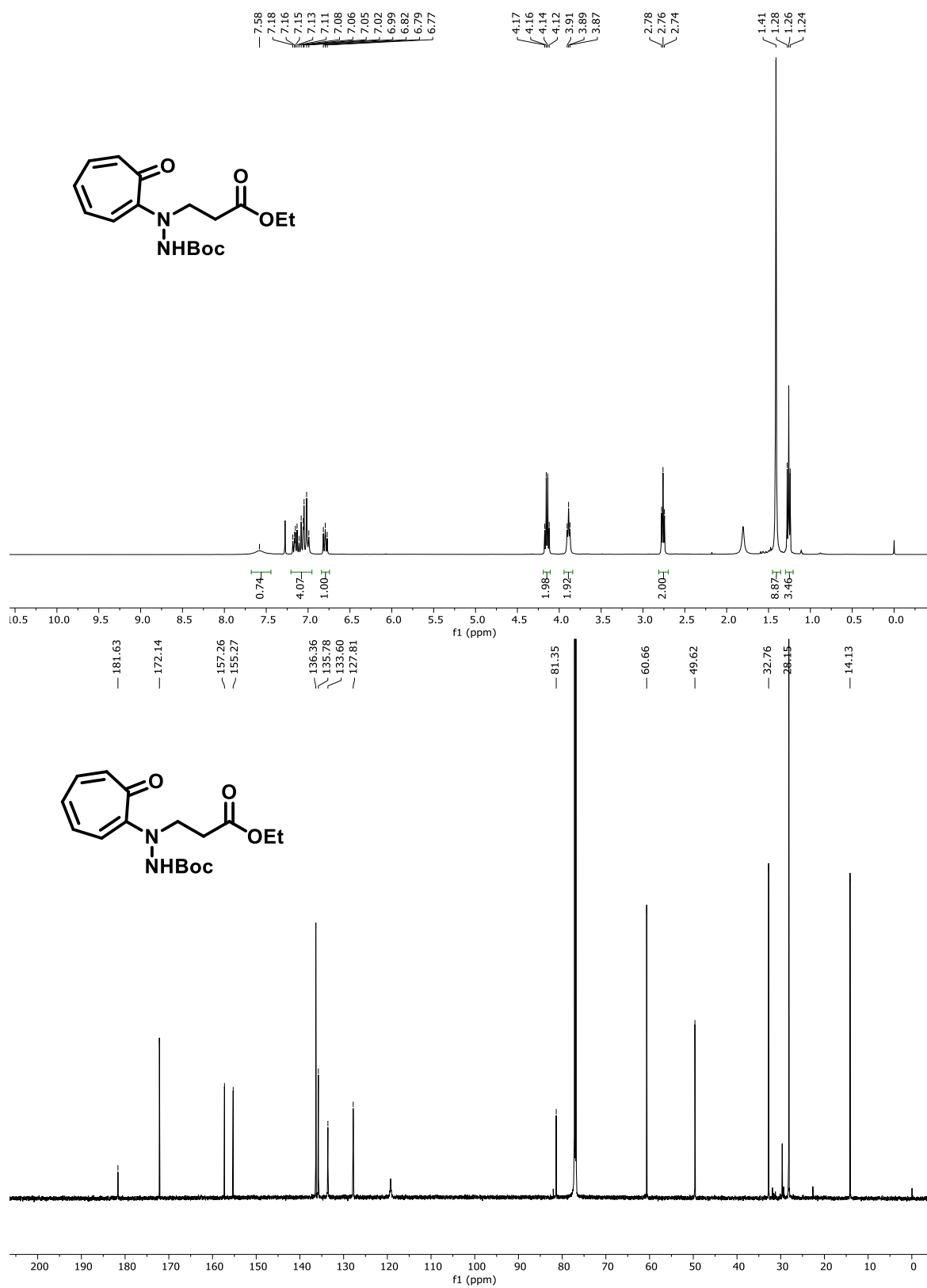
8. Tani, K.; Stoltz, B. M., Synthesis and structural analysis of 2-quinuclidonium tetrafluoroborate. *Nature* 2006, **441**, 731-4.
9. Somayaji, V.; Brown, R., Distorted amides as models for activated peptide NC: O units produced during enzyme-catalyzed acyl transfer reactions. 1. The mechanism of hydrolysis of 3, 4-dihydro-2-oxo-1, 4-ethanoquinoline and 2, 3, 4, 5-tetrahydro-2-oxo-1, 5-ethanobenzazepine. *J. Org. Chem.* 1986, **51**, 2676-2686.
10. Komarov, I. V.; Yanik, S.; Ishchenko, A. Y.; Davies, J. E.; Goodman, J. M.; Kirby, A. J., The most reactive amide as a transition-state mimic For cis-trans interconversion. *J. Am. Chem. Soc.* 2015, **137**, 926-930.
11. Balachandra, C.; Sharma, N. K., Novel fluorophores: Syntheses and photophysical studies of boron-aminotroponimines. *Dyes Pigm.* 2017, **137**, 532-538.
12. Kita, Y.; Nishii, Y.; Onoue, A.; Mashima, K., Combined catalytic system of scandium triflate and boronic ester for amide bond cleavage. *Adv. Synth. Catal.* 2013, **355**, 3391-3395.
13. Hie, L.; Nathel, N. F. F.; Shah, T. K.; Baker, E. L.; Hong, X.; Yang, Y.-F.; Liu, P.; Houk, K.; Garg, N. K., Conversion of amides to esters by the nickel-catalysed activation of amide C–N bonds. *Nature* 2015, **524**, 79.
14. Hutchby, M.; Houlden, C. E.; Haddow, M. F.; Tyler, S. N.; Lloyd-Jones, G. C.; Booker-Milburn, K. I., Switching pathways: room-temperature neutral solvolysis and substitution of amides. *Angew. Chem. Int. Ed. Engl.* 2012, **51**, 548-51.
15. Shimizu, Y.; Noshita, M.; Mukai, Y.; Morimoto, H.; Ohshima, T., Cleavage of unactivated amide bonds by ammonium salt-accelerated hydrazinolysis. *Chem. Commun.* 2014, **50**, 12623-12625.

16. Bollu, A.; Sharma, N. K., Cleavable Amide Bond: Mechanistic Insight into Cleavable 4-Aminopyrazolyloxy Acetamide at Low pH. *J. Org. Chem.* 2019, **84**, 5596-5602.
17. Stephenson, N. A.; Zhu, J.; Gellman, S. H.; Stahl, S. S., Catalytic transamidation reactions compatible with tertiary amide metathesis under ambient conditions. *J. Am. Chem. Soc.* 2009, **131**, 10003-10008.
18. Avan, I.; Hall, C. D.; Katritzky, A. R., Peptidomimetics via modifications of amino acids and peptide bonds. *Chem. Soc. Rev.* 2014, **43**, 3575-3594.
19. Balachandra, C.; Sharma, N. K., Synthesis and conformational analysis of new troponyl aromatic amino acid. *Tetrahedron* 2014, **70**, 7464-7469.
20. Balachandra, C.; Sharma, N. K., Instability of Amide Bond Comprising the 2-Aminotropone Moiety: Cleavable under Mild Acidic Conditions. *Org. Lett.* 2015, **17**, 3948-3951.
21. Balachandra, C.; Sharma, N. K., Direct/Reversible Amidation of Troponyl Alkylglycinates via Cationic Troponyl Lactones and Mechanistic Insights. *ACS Omega* 2018, **3**, 997-1013.
22. Kang, C. W.; Sarnowski, M. P.; Elbatrawi, Y. M.; Del Valle, J. R., Access to enantiopure  $\alpha$ -hydrazino acids for N-amino peptide synthesis. *J. Org. Chem.* 2017, **82**, 1833-1841.
23. Li, X.; Yang, D., Peptides of aminoxy acids as foldamers. *Chem. Commun.* 2006, 3367-3379.
24. Kent, E.; Hoops, S.; Mendes, P., Condor-COPASI: high-throughput computing for biochemical networks. *BMC Syst. Biol.* 2012, **6**, 91.

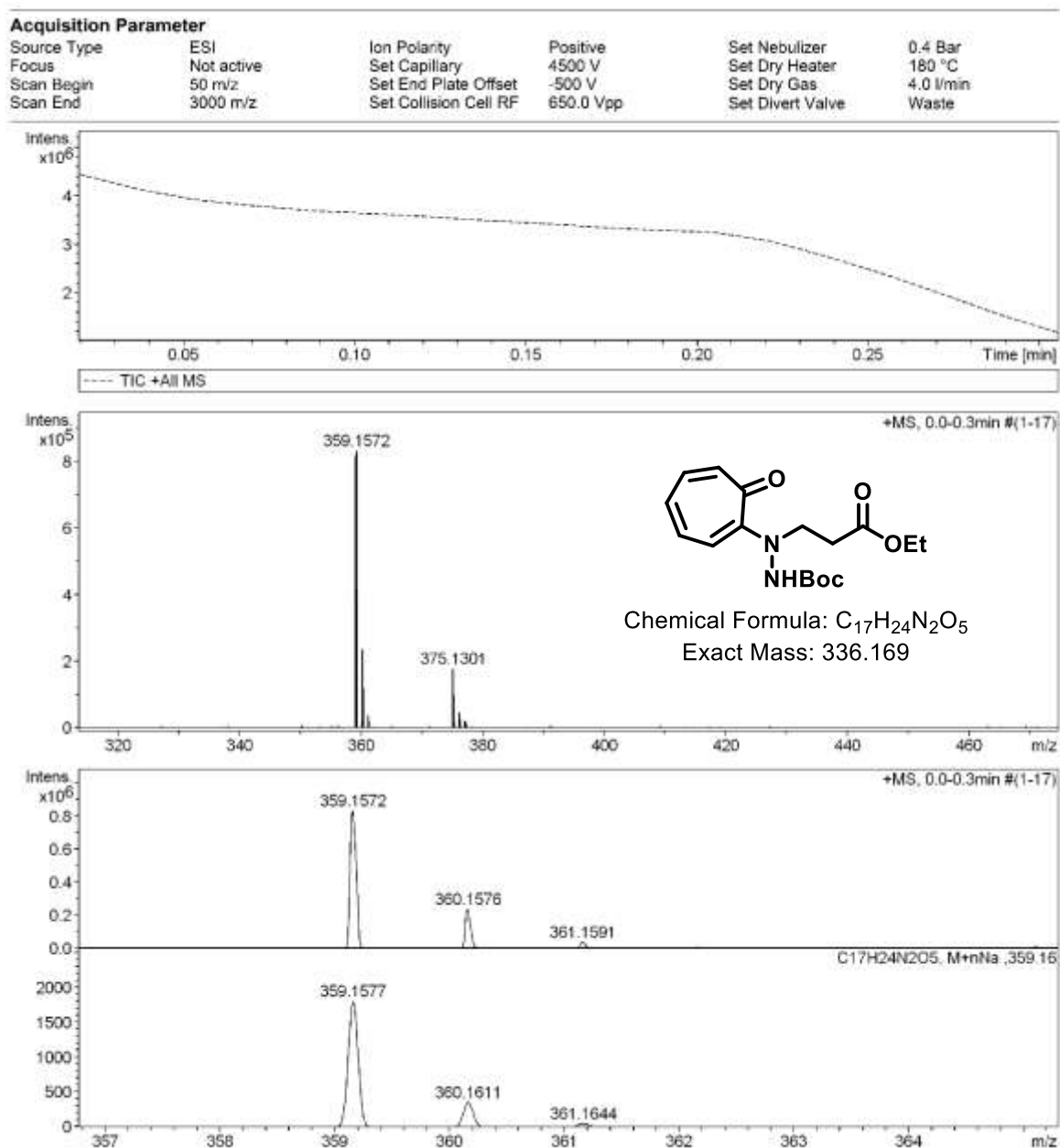
25. Breheret, E.; Martin, M., Electronic relaxation of troponoids: tropolone fluorescence. *J. Lumin.* 1978, **17**, 49-60.
26. Bordessa, A.; Keita, M.; Maréchal, X.; Formicola, L.; Lagarde, N.; Rodrigo, J.; Bernadat, G.; Bauvais, C.; Soulier, J.-L.; Dufau, L.,  $\alpha$ - and  $\beta$ -hydrazino acid-based pseudopeptides inhibit the chymotrypsin-like activity of the eukaryotic 20S proteasome. *Eur. J. Med. Chem.* 2013, **70**, 505-524.

## 6.7 Appendix

1. NMR ( $^1\text{H}/^{13}\text{C}$ ) and ESI-MS spectra of all synthesised Compounds .....	383
2. DMSO- $d_6$ titration experiments by $^1\text{H}$ -NMR of peptides ( <b>5a-5e</b> ) in $\text{CDCl}_3$ .....	417
3. Mass study of amide bond hydrolysis in compounds ( <b>5a-5h</b> ) in (20-30%) TFA .....	423
4. Mass study of Boc deprotection in compounds ( <b>6a/6b/7/8</b> ) in (20-30%) TFA.....	431
5. Time dependent $^1\text{H}$ -NMR spectra of amide bond hydrolysis in compounds ( <b>5a/5b</b> )....	435
6. Determination of rate constants ( $k_1$ ) and half-life ( $t_{1/2}$ ) of peptide derivatives ( <b>5a/5b</b> )..	437
7. COPASI Modelling Procedure and Results.....	442
8. ESI-MS spectra of compound ( <b>5a/5b</b> ) after time dependent NMR.....	443
9. Time dependent $^1\text{H}$ -NMR spectra of Boc deprotection in compounds ( <b>6a/8</b> ) .....	445
10. UV-Vis Spectroscopic studies for Tropolone ( <b>9</b> ) formation in hybrid dipeptide ( <b>5a/5b</b> )	447
11. UV-spectra of Tropolone ( <b>9</b> ) .....	449
12. Mass study of amide bond hydrolysis in compounds ( <b>5a</b> ) in different acid conditions.	449
13. X-Ray crystallographic Studies of new compounds <b>5a/ 9/ 5h/6a</b> .....	451

1. NMR ( $^1\text{H}/^{13}\text{C}$ ) and ESI-MS spectra of all synthesised Compounds



**Figure A1.**  $^1\text{H}$  and  $^{13}\text{C}$  NMR spectra of troponyl- $\beta$ -hydrazino ester (**4**) in  $\text{CDCl}_3$ **Figure A2.** ESI-MS/HRMS spectra of troponyl- $\beta$ -hydrazino ester (**4**)

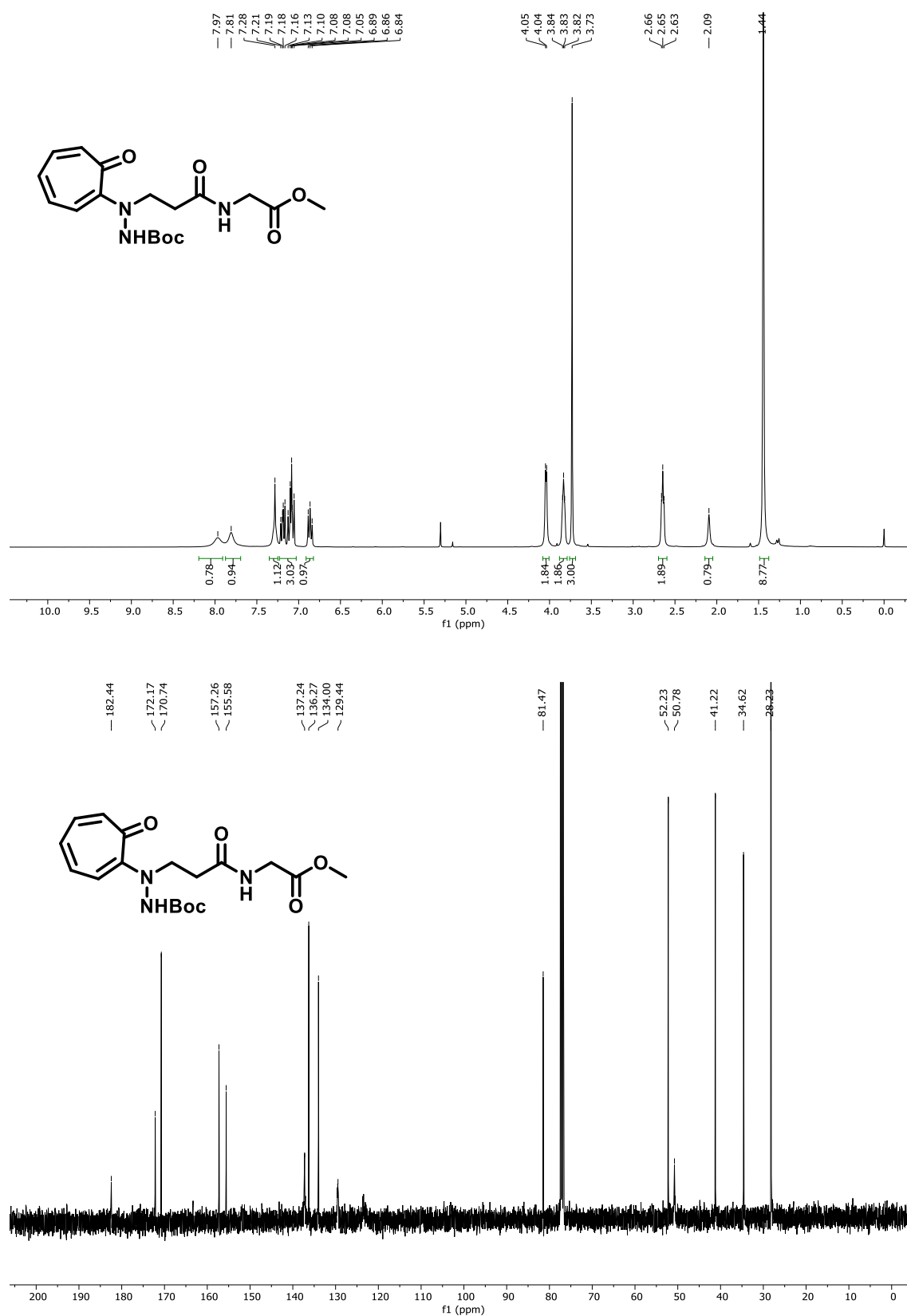
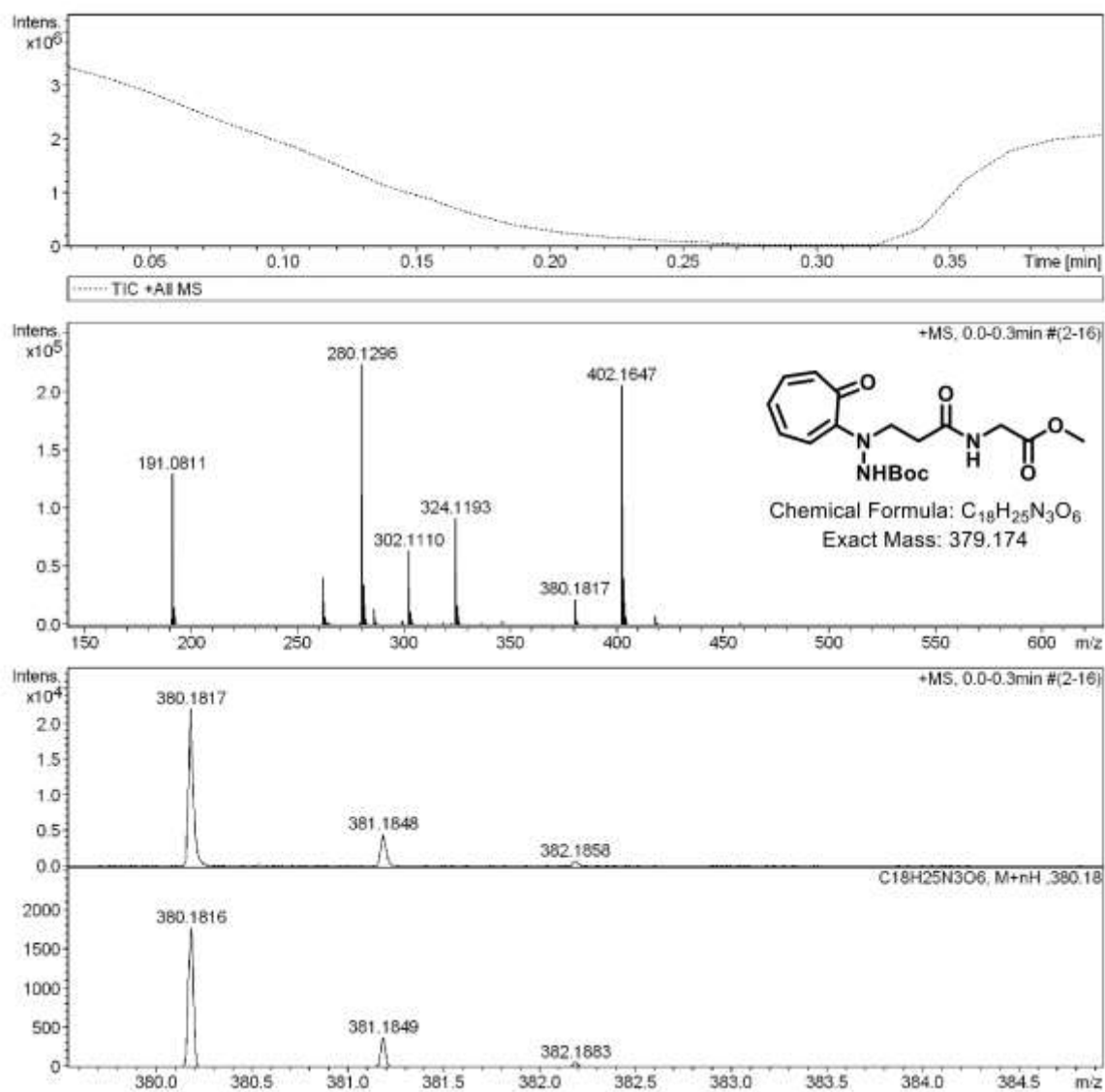


Figure A3.  $^1\text{H}$  and  $^{13}\text{C}$  NMR spectra of hybrid dipeptide (5a) in  $\text{CDCl}_3$

**Acquisition Parameter**

Source Type	ESI	Ion Polarity	Positive	Set Nebulizer	0.4 Bar
Focus	Active	Set Capillary	4500 V	Set Dry Heater	180 °C
Scan Begin	50 m/z	Set End Plate Offset	-500 V	Set Dry Gas	4.0 l/min
Scan End	3000 m/z	Set Collision Cell RF	300.0 Vpp	Set Divert Valve	Source

**Figure A4.** ESI-MS/HRMS spectra of hybrid dipeptide (**5a**)

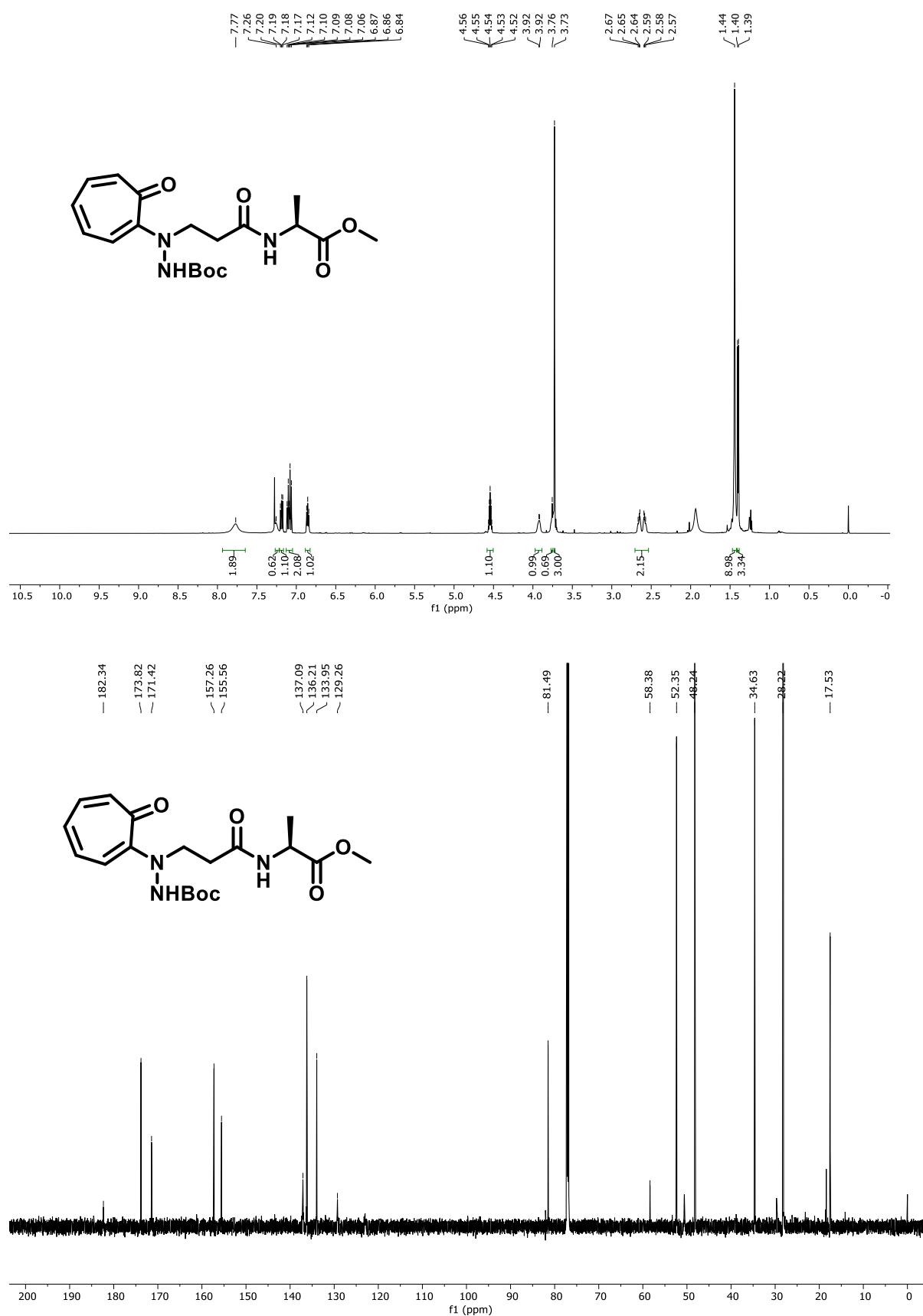
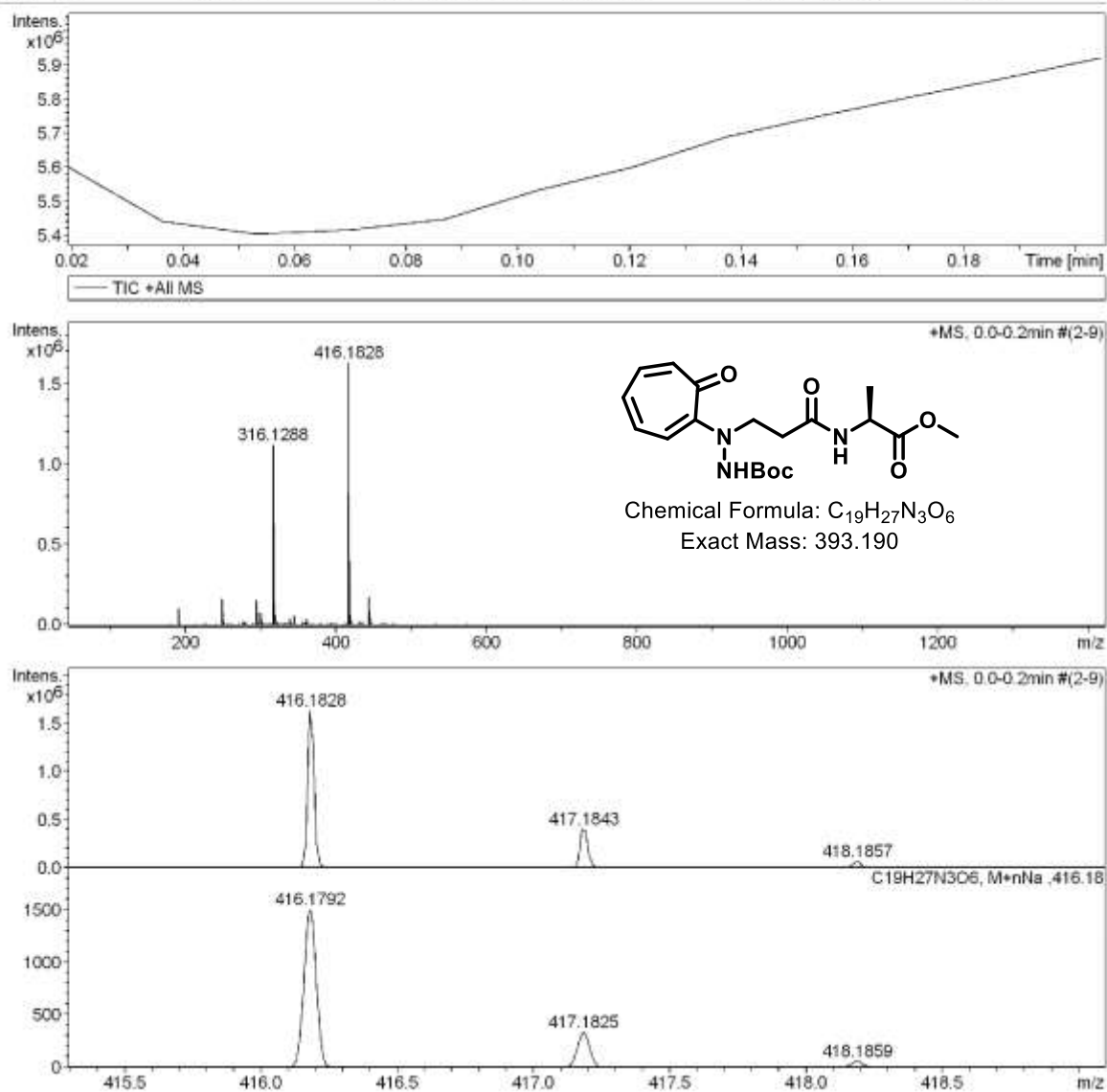
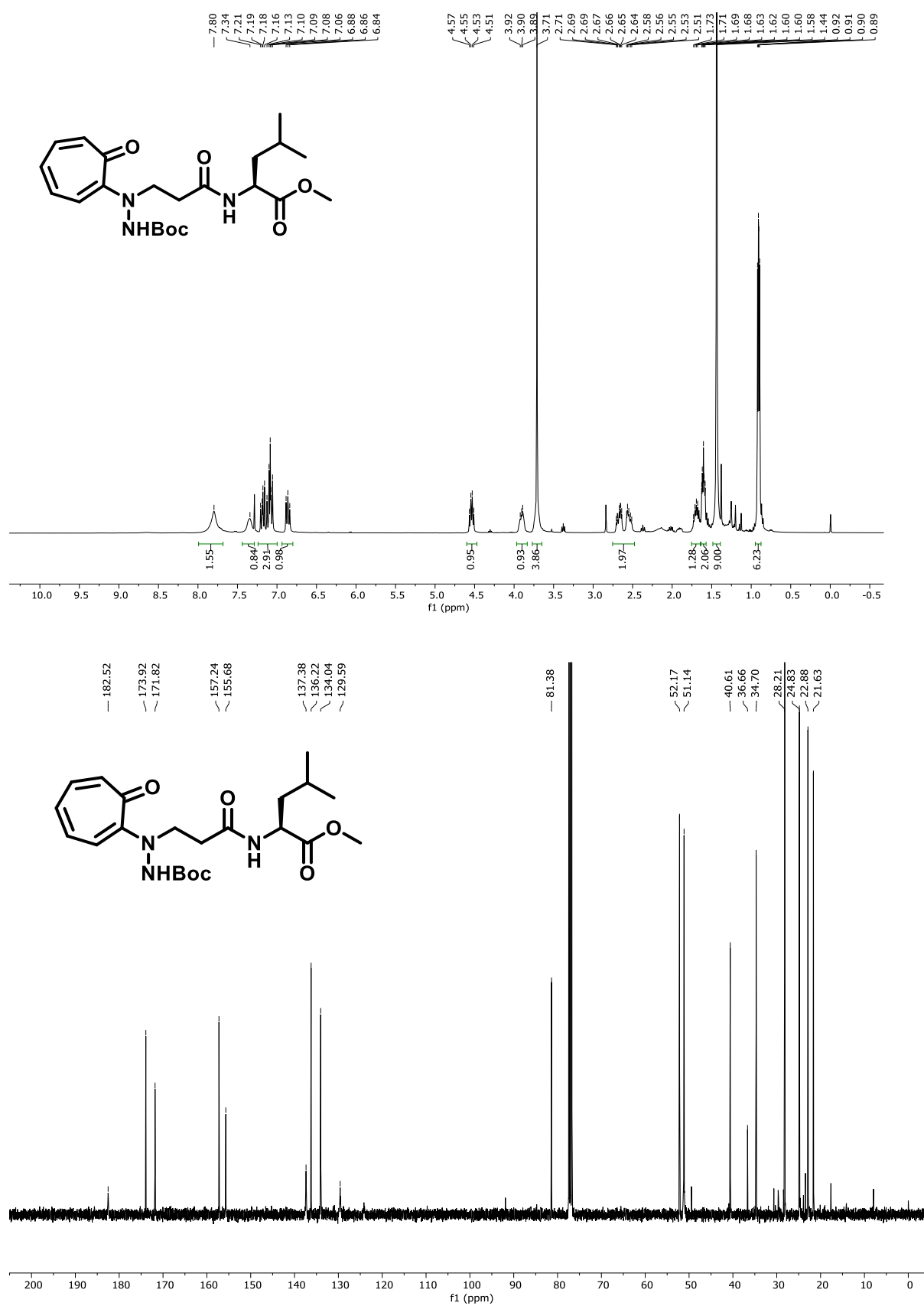


Figure A5.  $^1\text{H}$  and  $^{13}\text{C}$  NMR spectra of hybrid dipeptide (5b) in  $\text{CDCl}_3$

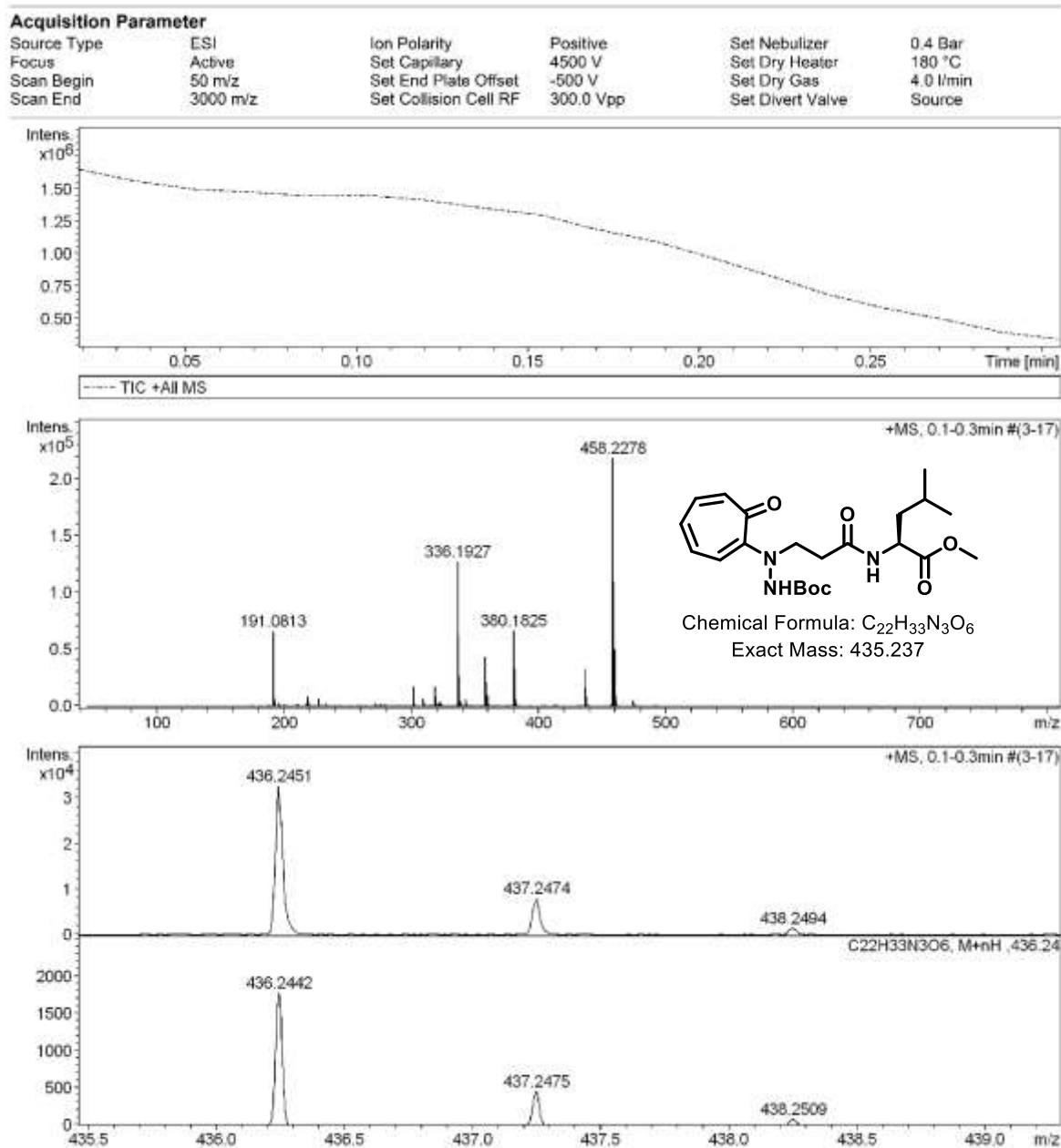
## Acquisition Parameter

Source Type	ESI	Ion Polarity	Positive	Set Nebulizer	0.4 Bar
Focus	Active	Set Capillary	4500 V	Set Dry Heater	180 °C
Scan Begin	50 m/z	Set End Plate Offset	-500 V	Set Dry Gas	4.0 l/min
Scan End	3000 m/z	Set Collision Cell RF	300.0 Vpp	Set Divert Valve	Source

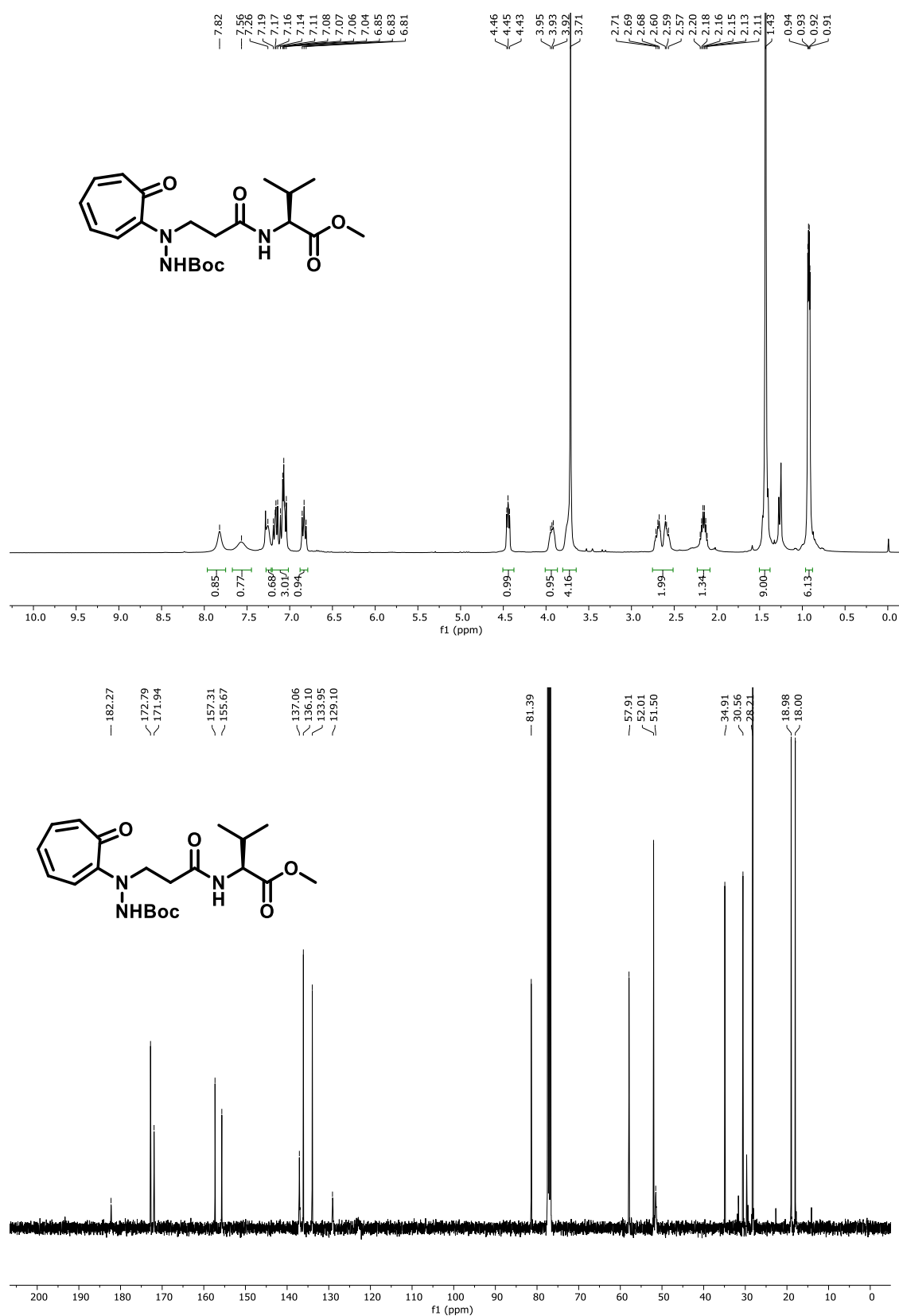
Figure A6. ESI-MS/HRMS spectra of hybrid dipeptide (**5b**)



**Figure A7.** <sup>1</sup>H and <sup>13</sup>C NMR spectra of hybrid dipeptide (5c) in CDCl<sub>3</sub>



**Figure A8.** ESI-MS/HRMS spectra of hybrid dipeptide (**5c**)

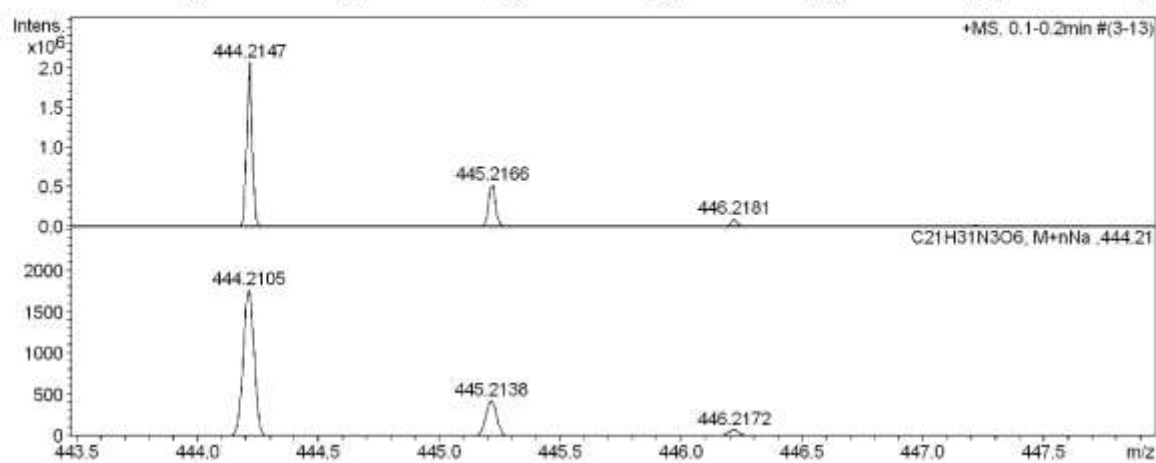
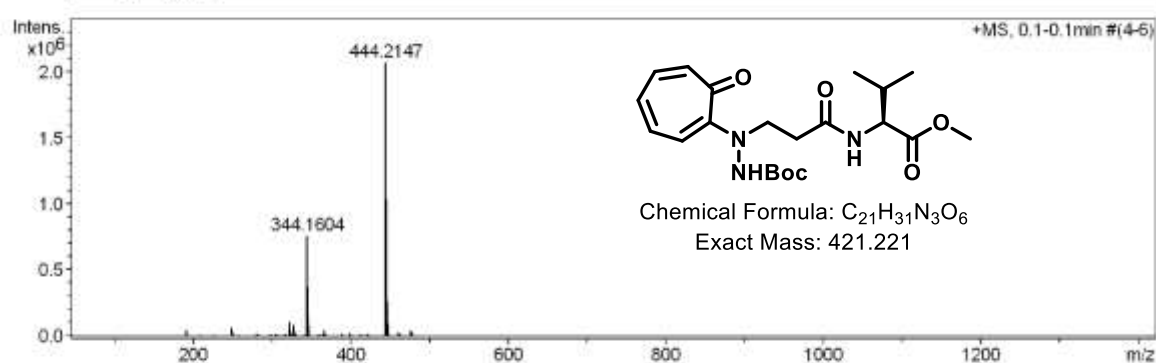
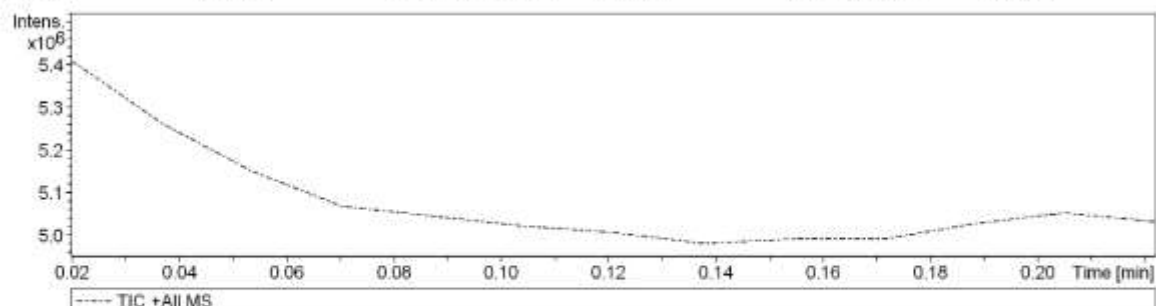


**Figure A9.** <sup>1</sup>H and <sup>13</sup>C NMR spectra of hybrid dipeptide (**5d**) in CDCl<sub>3</sub>



## Acquisition Parameter

Source Type	ESI	Ion Polarity	Positive	Set Nebulizer	0.4 Bar
Focus	Active	Set Capillary	4500 V	Set Dry Heater	180 °C
Scan Begin	50 m/z	Set End Plate Offset	-500 V	Set Dry Gas	4.0 l/min
Scan End	3000 m/z	Set Collision Cell RF	300.0 Vpp	Set Divert Valve	Source

Figure A10. ESI-MS/HRMS spectra of hybrid peptide (**5d**)

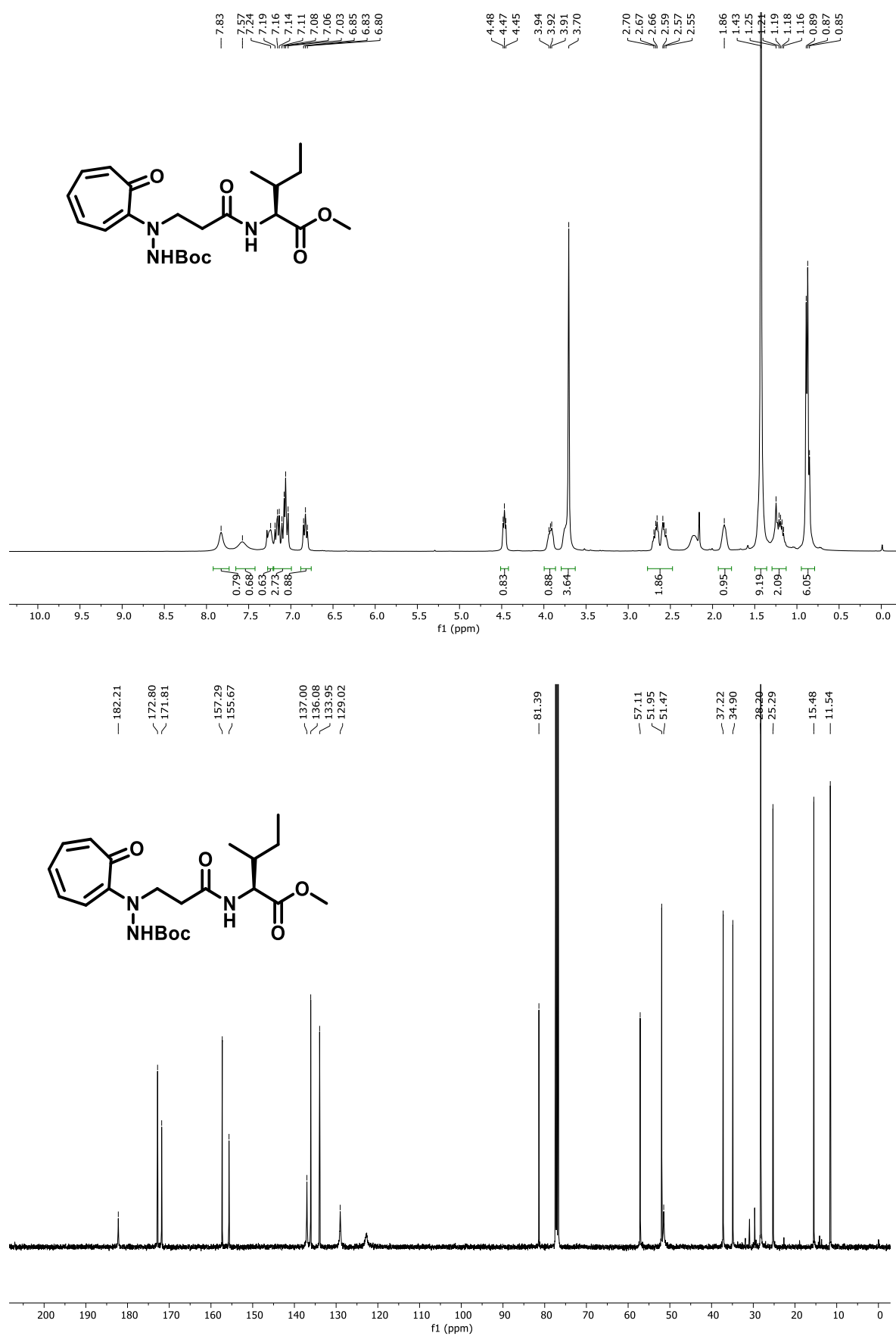


**Figure A11.** <sup>1</sup>H and <sup>13</sup>C NMR spectra of hybrid dipeptide (5e) in CDCl<sub>3</sub>

## Acquisition Parameter

Source Type	ESI	Ion Polarity	Positive	Set Nebulizer	0.4 Bar
Focus	Not active	Set Capillary	4500 V	Set Dry Heater	180 °C
Scan Begin	50 m/z	Set End Plate Offset	-500 V	Set Dry Gas	4.0 l/min
Scan End	3000 m/z	Set Collision Cell RF	400.0 Vpp	Set Divert Valve	Source

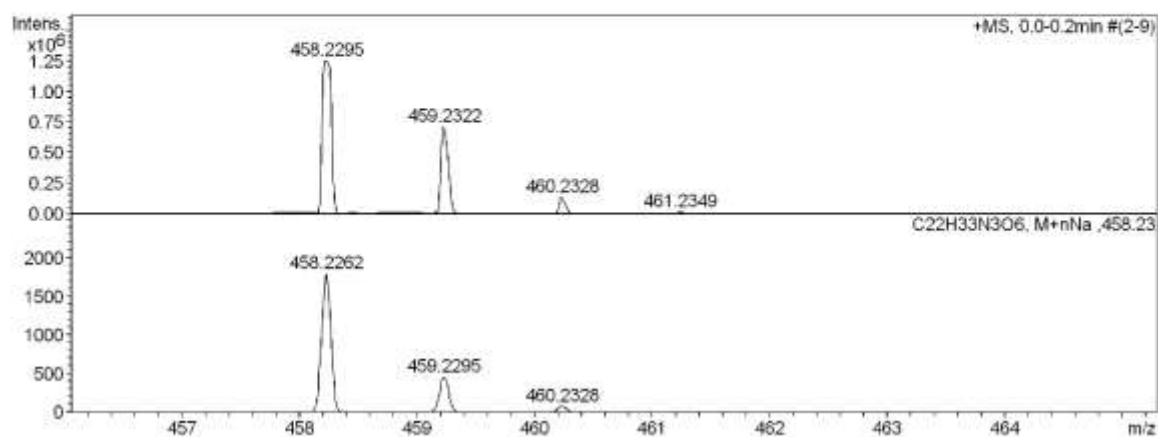
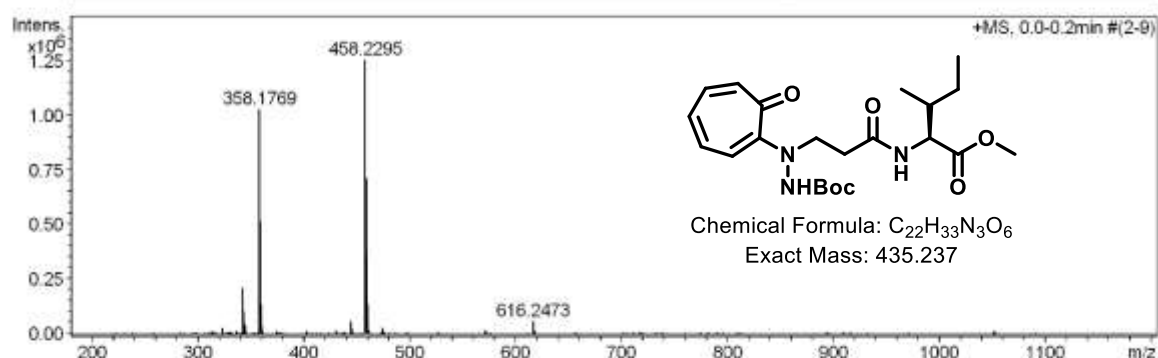
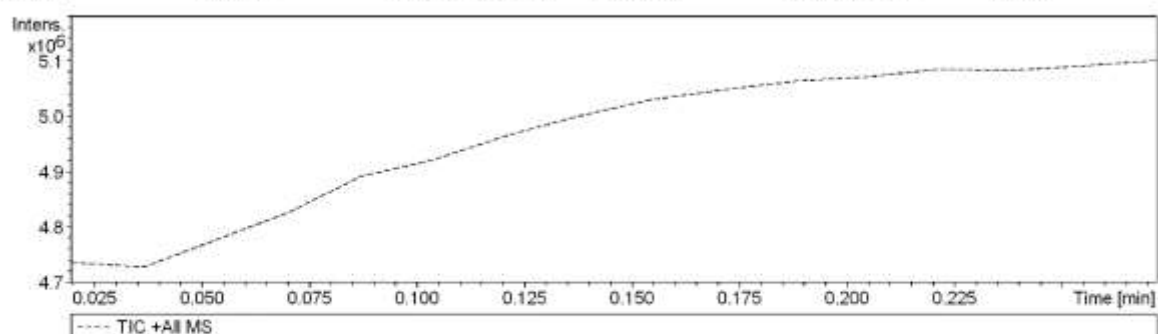


Figure A12. ESI-MS/HRMS spectra of hybrid peptide (5e)

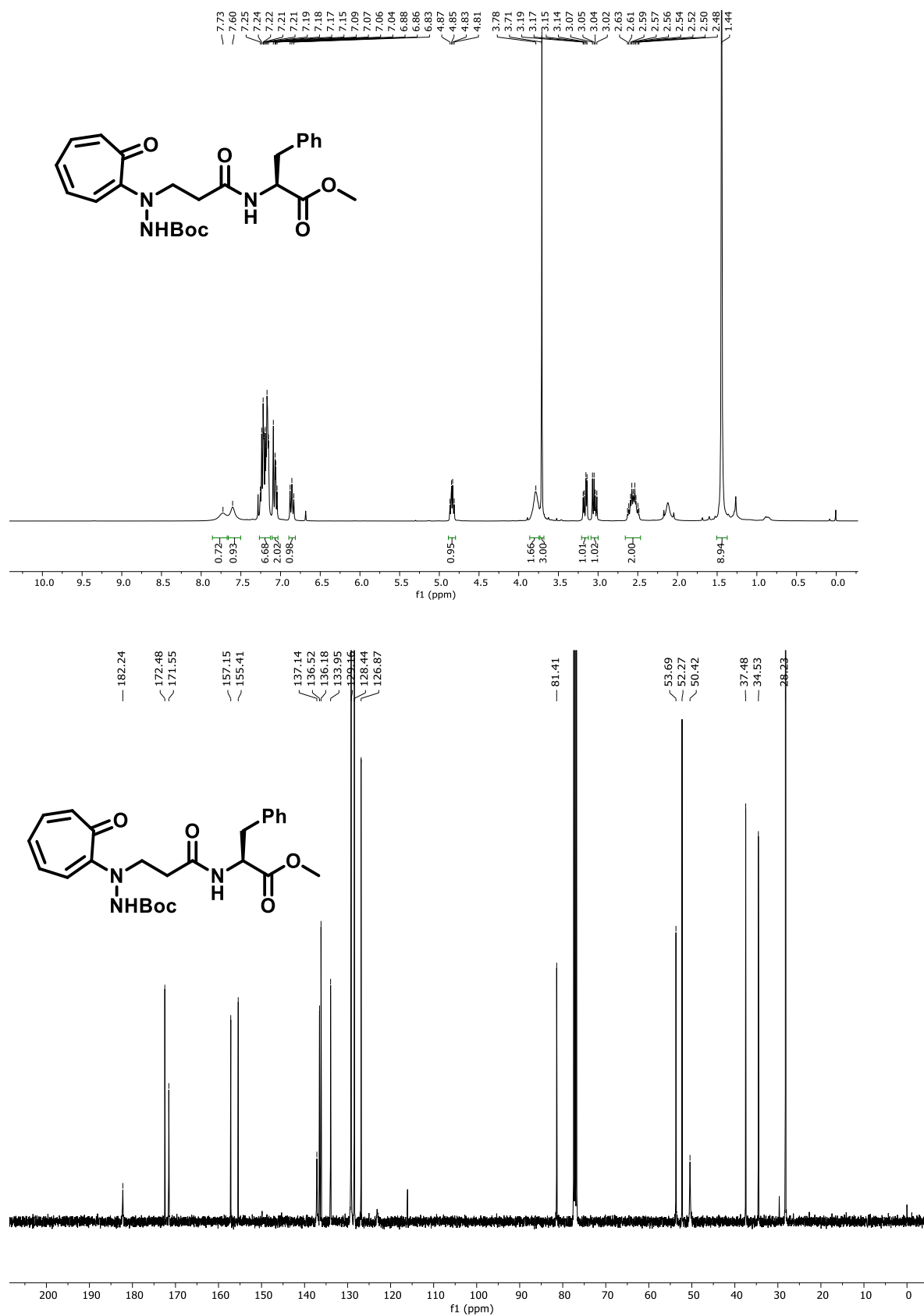
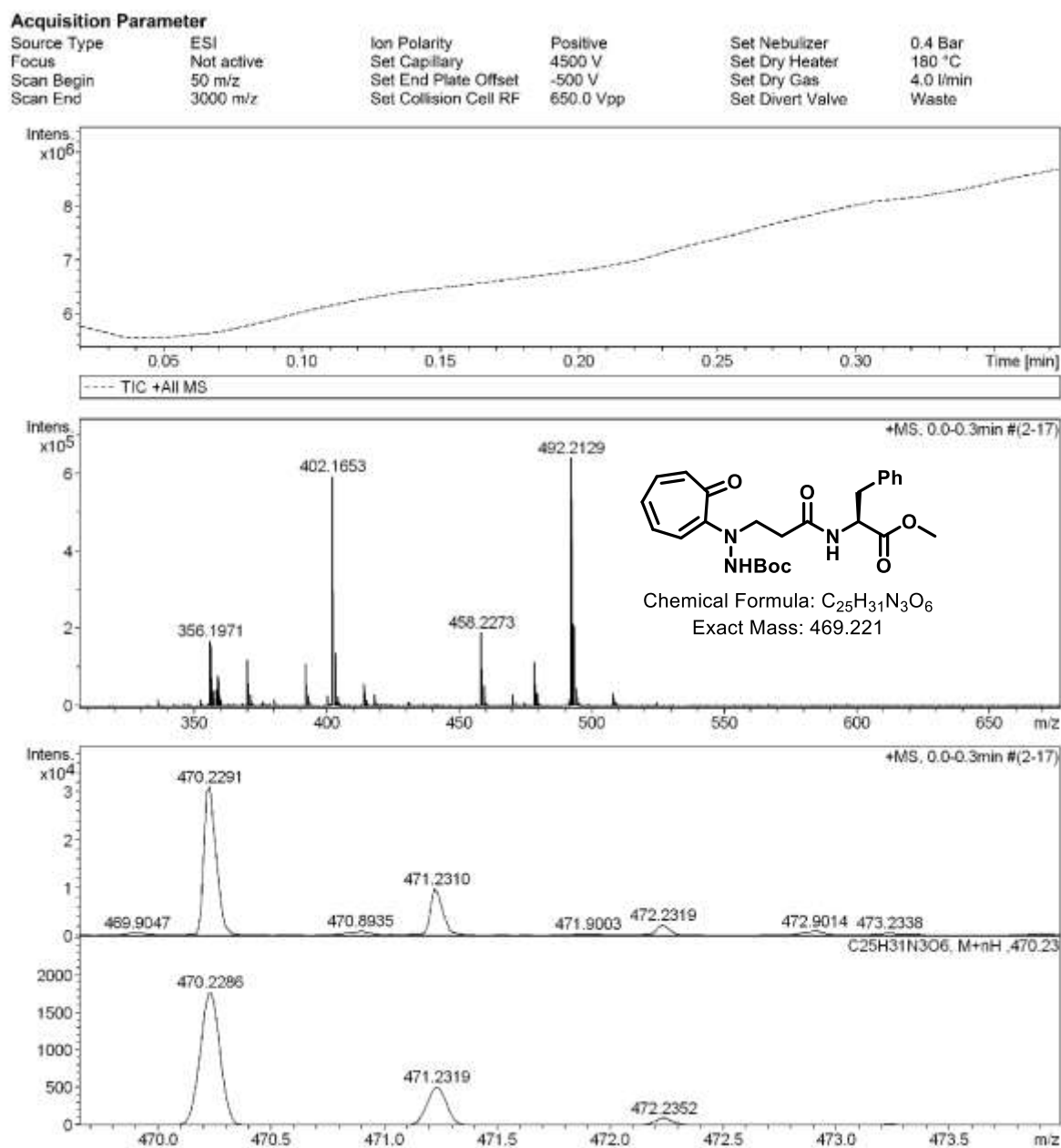
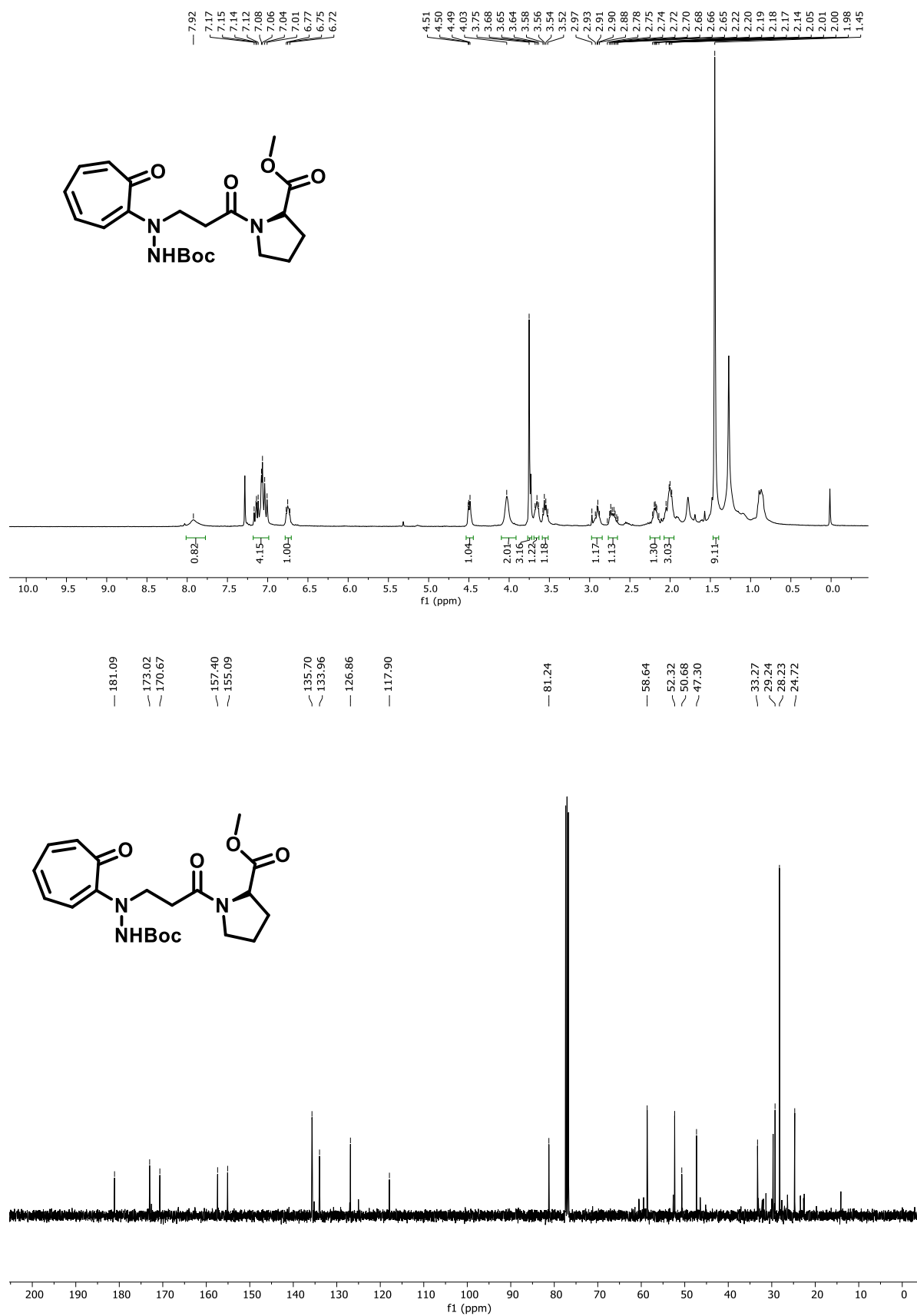


Figure A13. <sup>1</sup>H and <sup>13</sup>C NMR spectra of hybrid dipeptide (5f) in CDCl<sub>3</sub>



**Figure A14.** ESI-MS/HRMS spectra of hybrid dipeptide (**5f**)



**Figure A15.** <sup>1</sup>H and <sup>13</sup>C NMR spectra of hybrid dipeptide (**5g**) in CDCl<sub>3</sub>

## Acquisition Parameter

Source Type	ESI	Ion Polarity	Positive	Set Nebulizer	0.4 Bar
Focus	Not active	Set Capillary	4500 V	Set Dry Heater	180 °C
Scan Begin	50 m/z	Set End Plate Offset	-500 V	Set Dry Gas	4.0 l/min
Scan End	3000 m/z	Set Collision Cell RF	400.0 Vpp	Set Divert Valve	Source

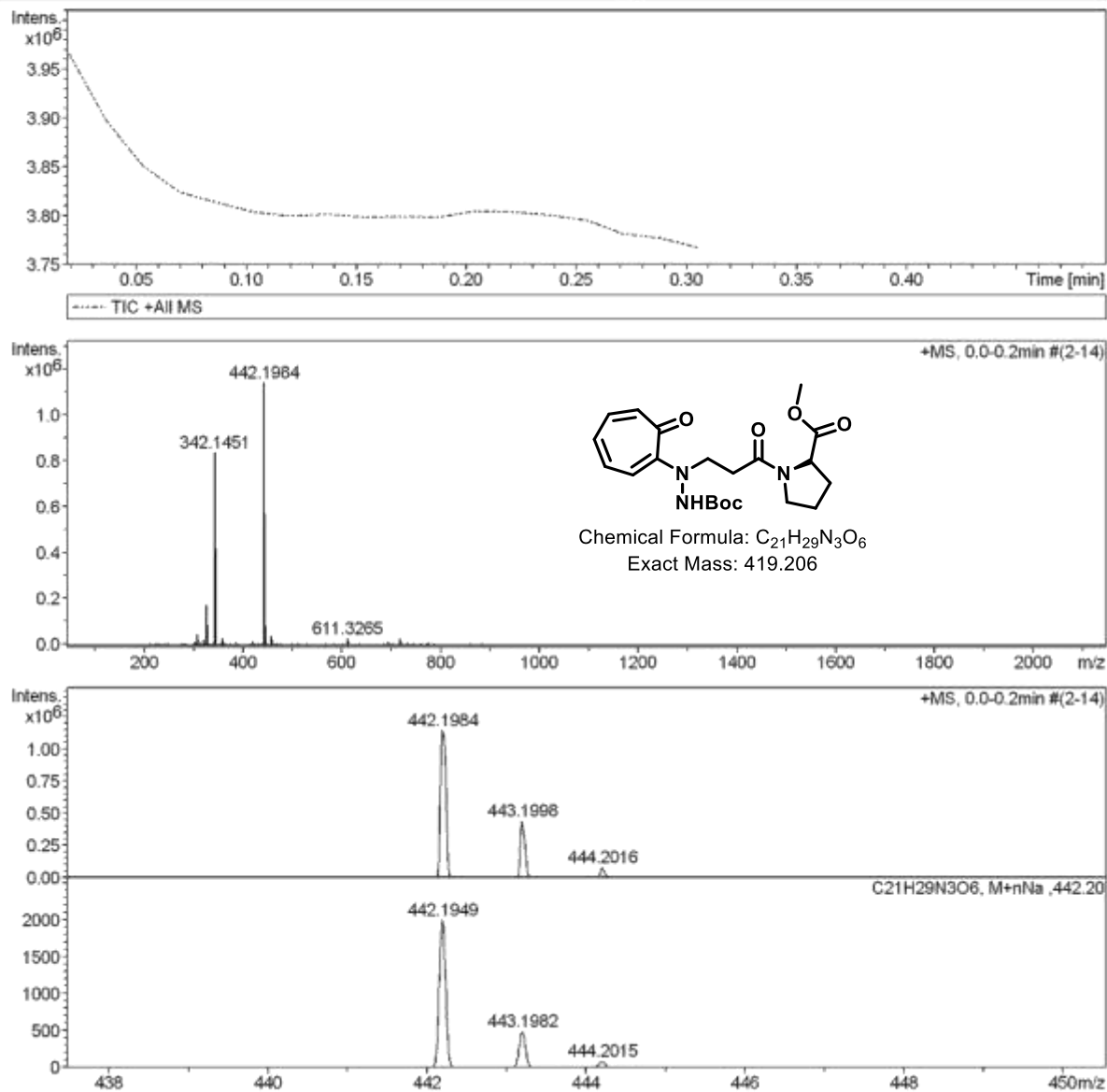


Figure A16. ESI-MS/HRMS spectra of hybrid dipeptide (5g)

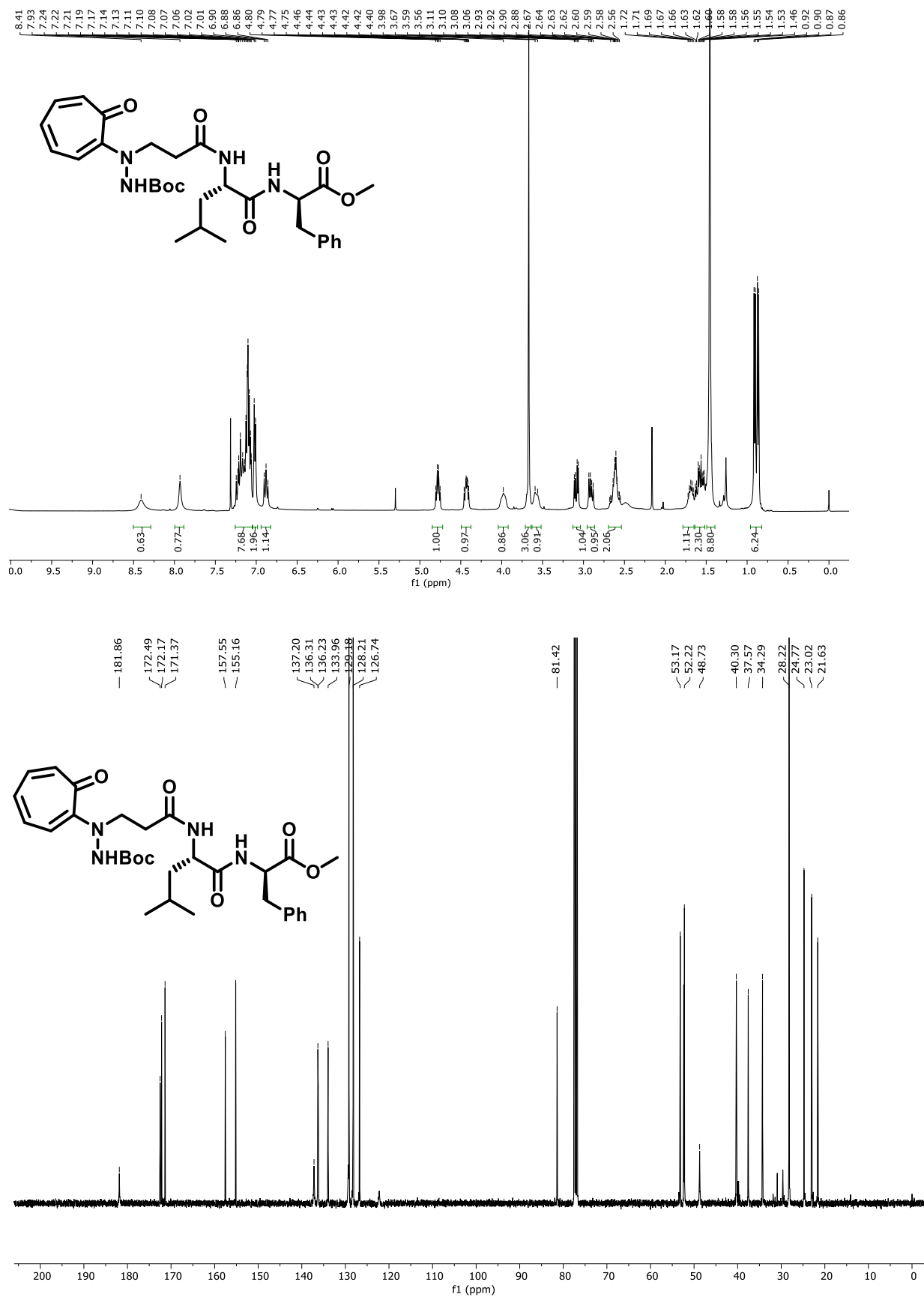
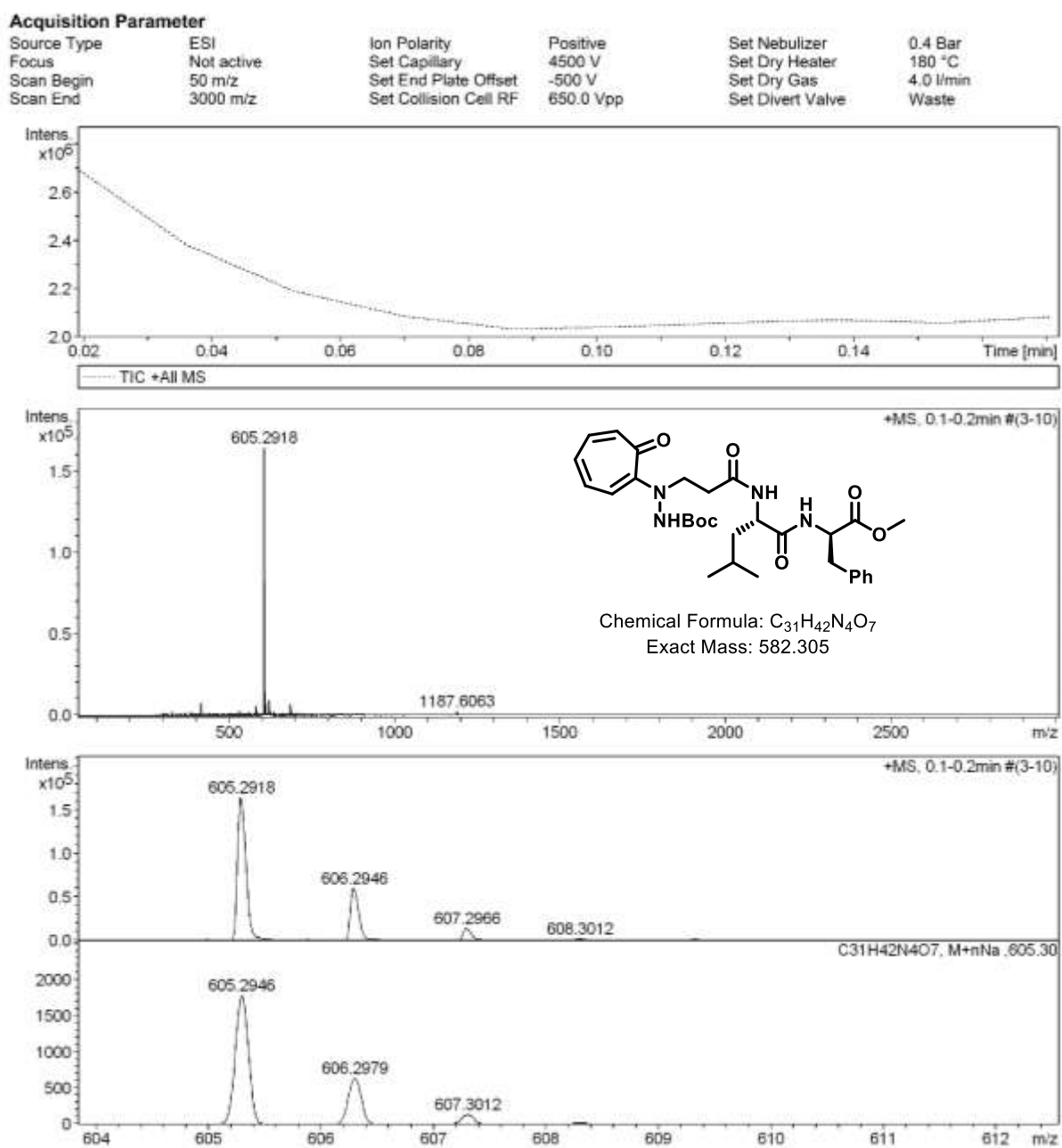


Figure A17. <sup>1</sup>H and <sup>13</sup>C NMR spectra of hybrid tripeptide (5h) in CDCl<sub>3</sub>





**Figure A18.** ESI-MS/HRMS spectra of hybrid tripeptide (5h)

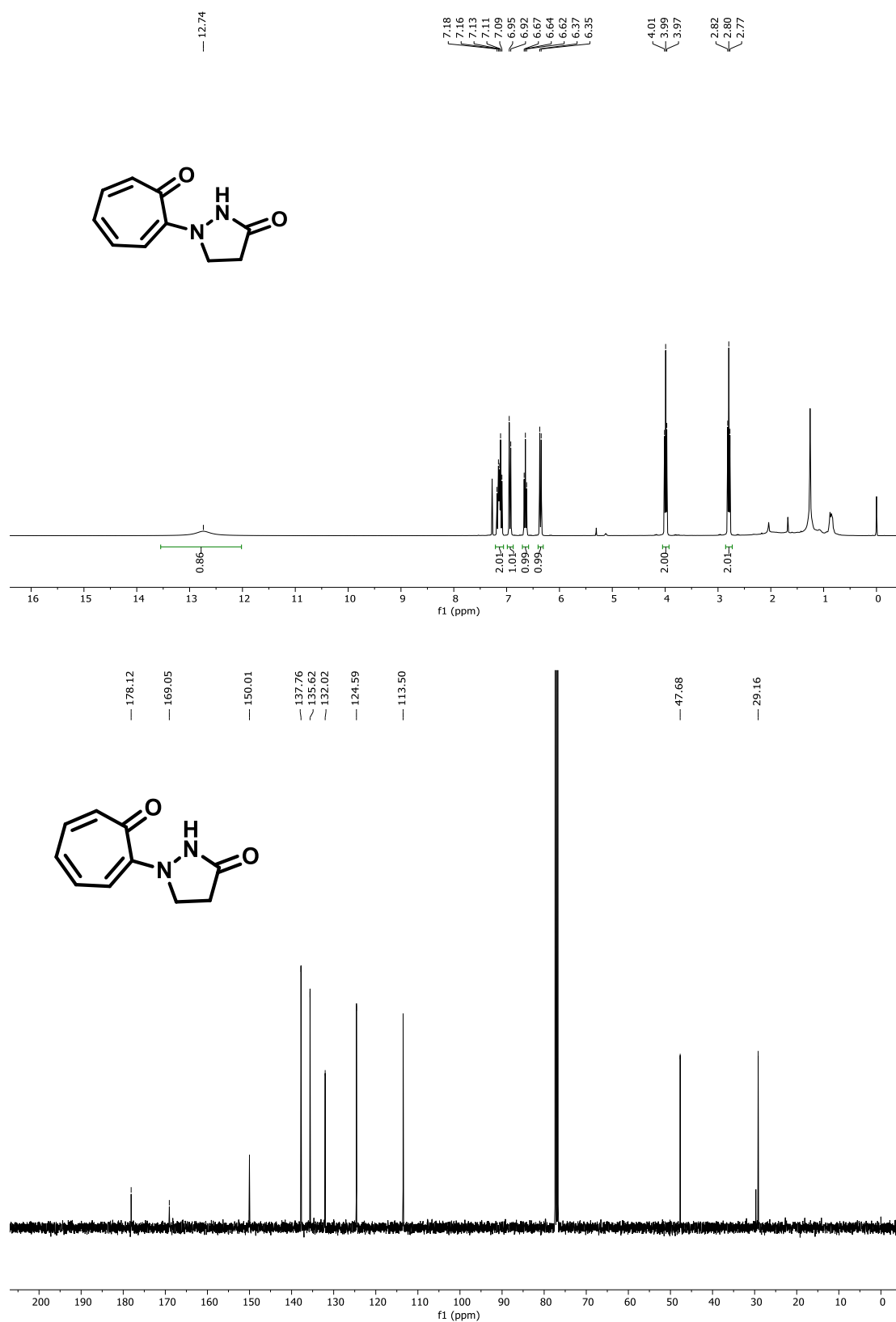
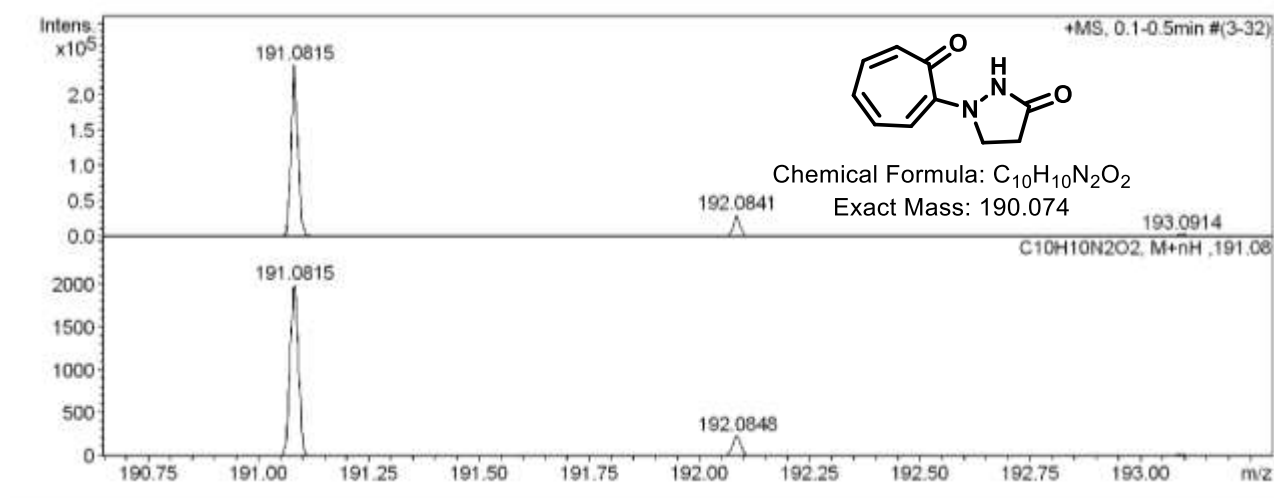
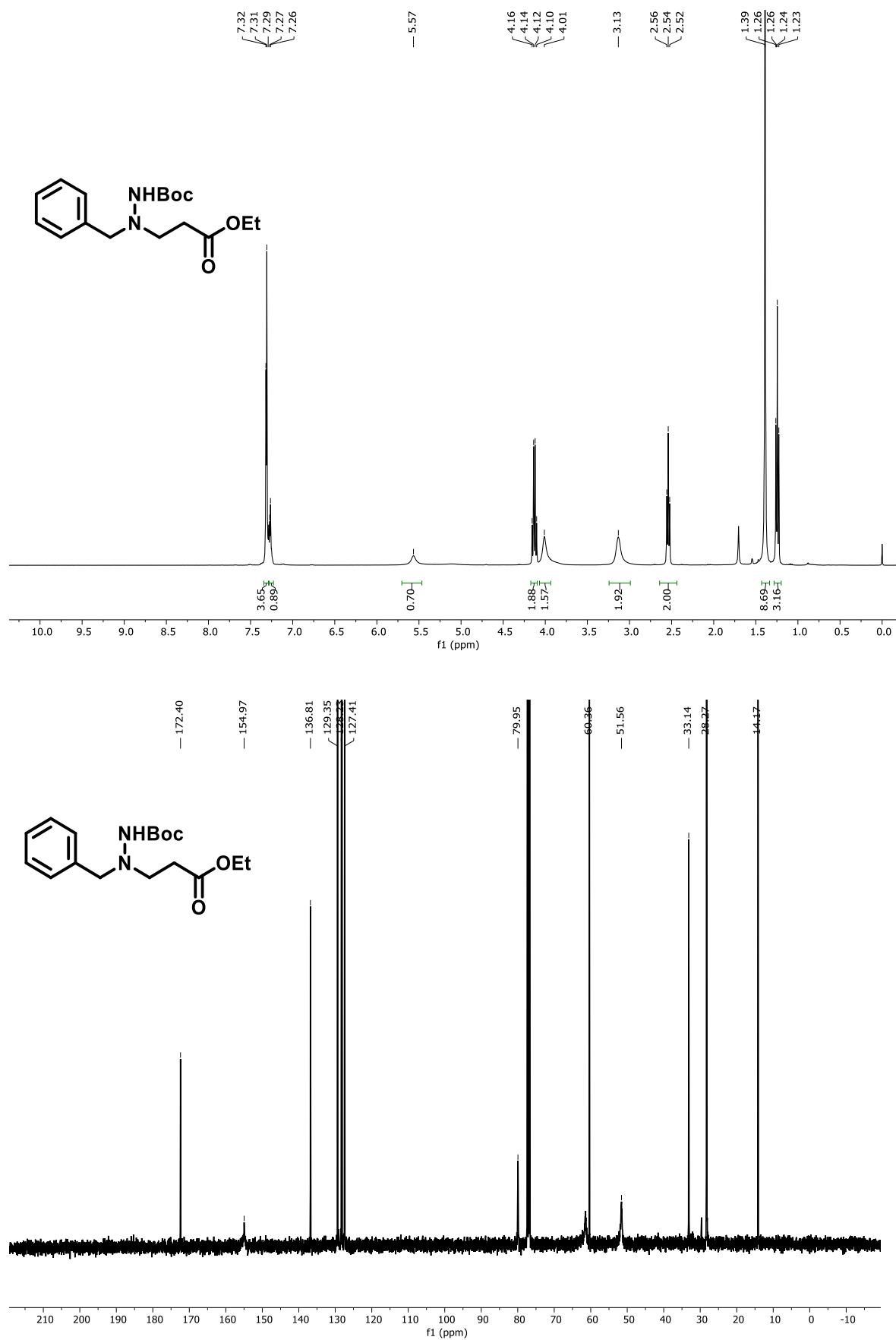


Figure A19. <sup>1</sup>H and <sup>13</sup>C NMR spectra of Tropicone (9) in CDCl<sub>3</sub>



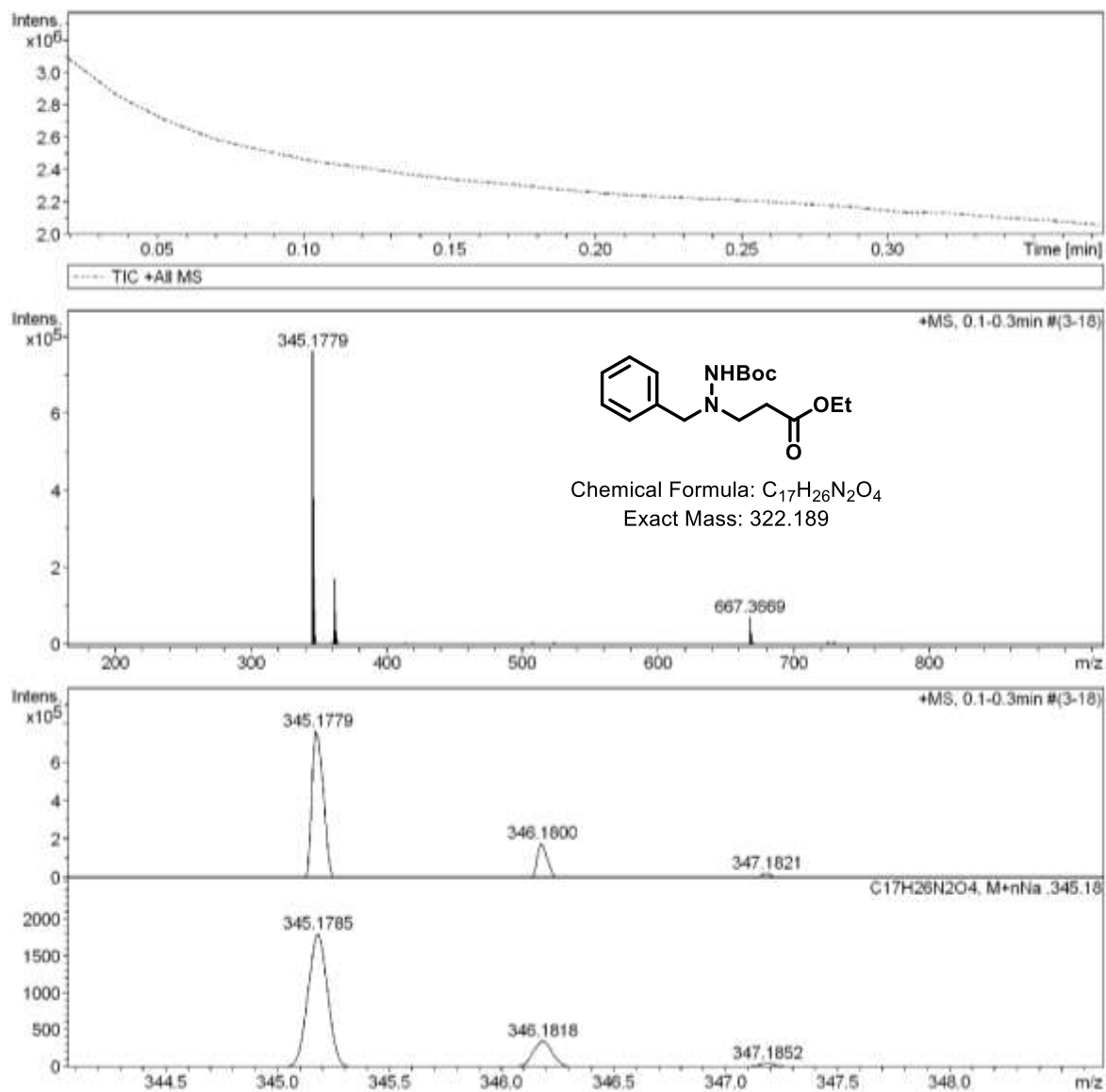
**Figure A20.** ESI-MS/HRMS spectra of Tropidone (9)



**Figure A21.** <sup>1</sup>H and <sup>13</sup>C NMR spectra of benzyl-β-hydrazino ester (**2-Bn**) in CDCl<sub>3</sub>

**Acquisition Parameter**

Source Type	ESI	Ion Polarity	Positive	Set Nebulizer	0.4 Bar
Focus	Not active	Set Capillary	4500 V	Set Dry Heater	180 °C
Scan Begin	50 m/z	Set End Plate Offset	-500 V	Set Dry Gas	4.0 l/min
Scan End	3000 m/z	Set Collision Cell RF	650.0 Vpp	Set Divert Valve	Waste

**Figure A22.** ESI-MS/HRMS spectra of benzyl-β-hydrazino ester (**2-Bn**)

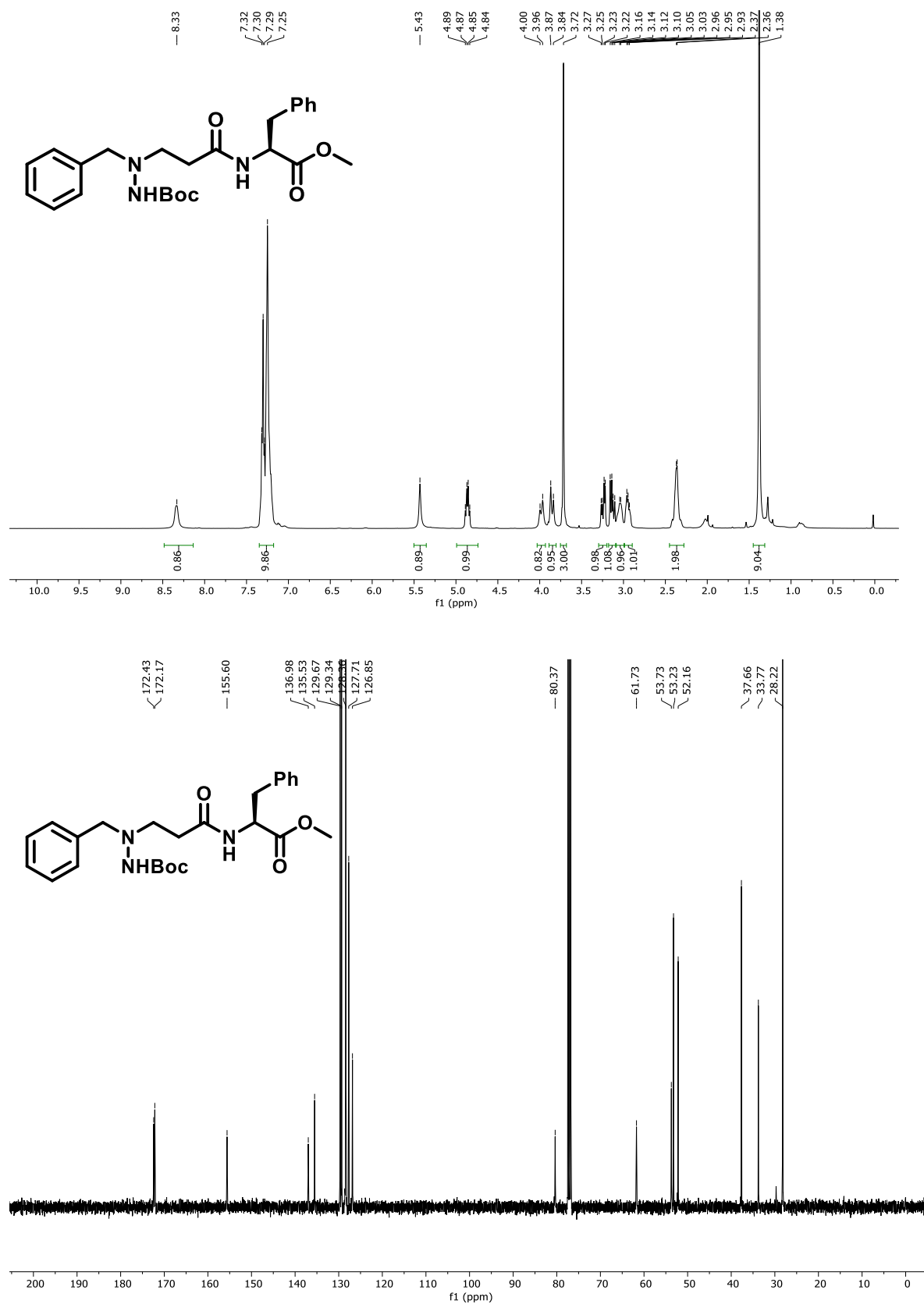
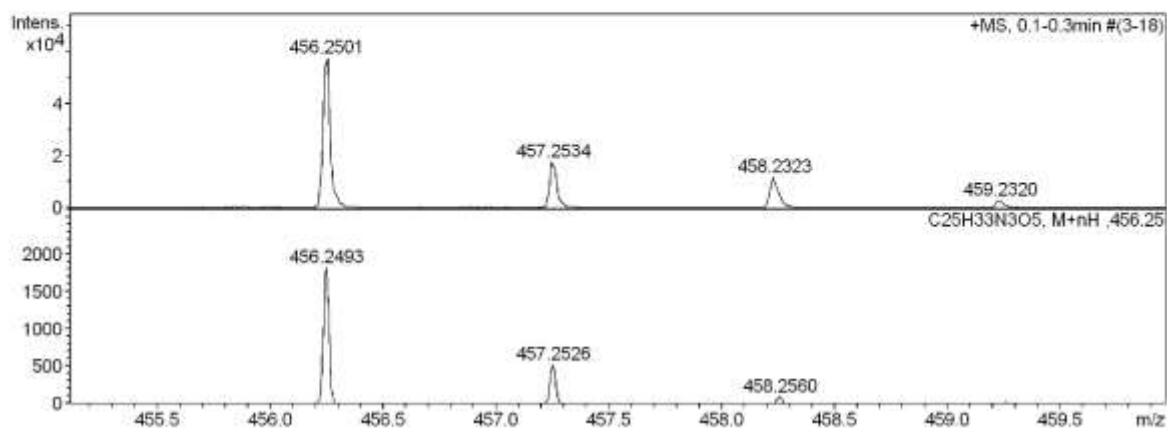
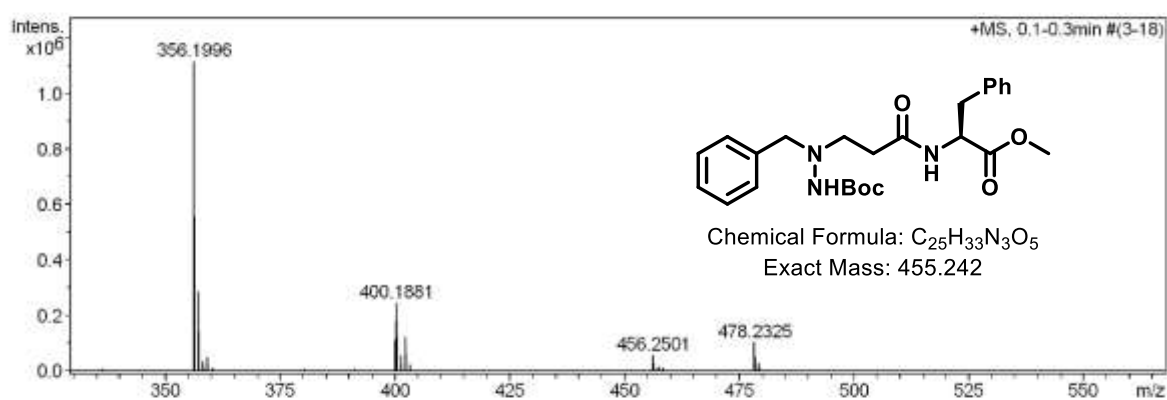
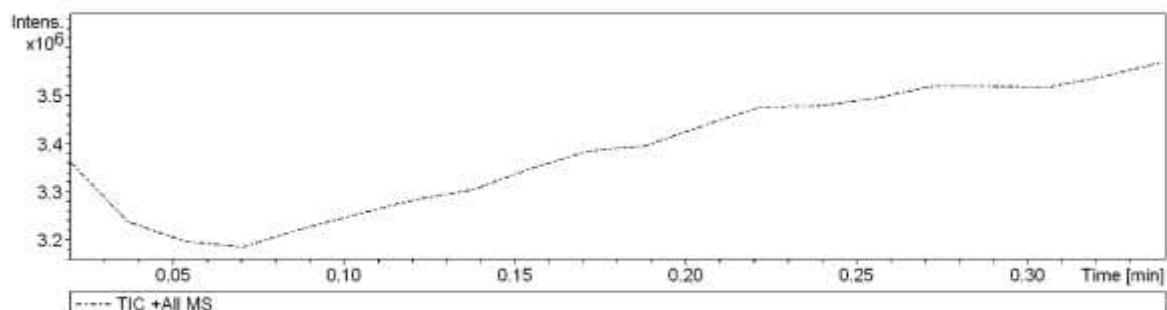
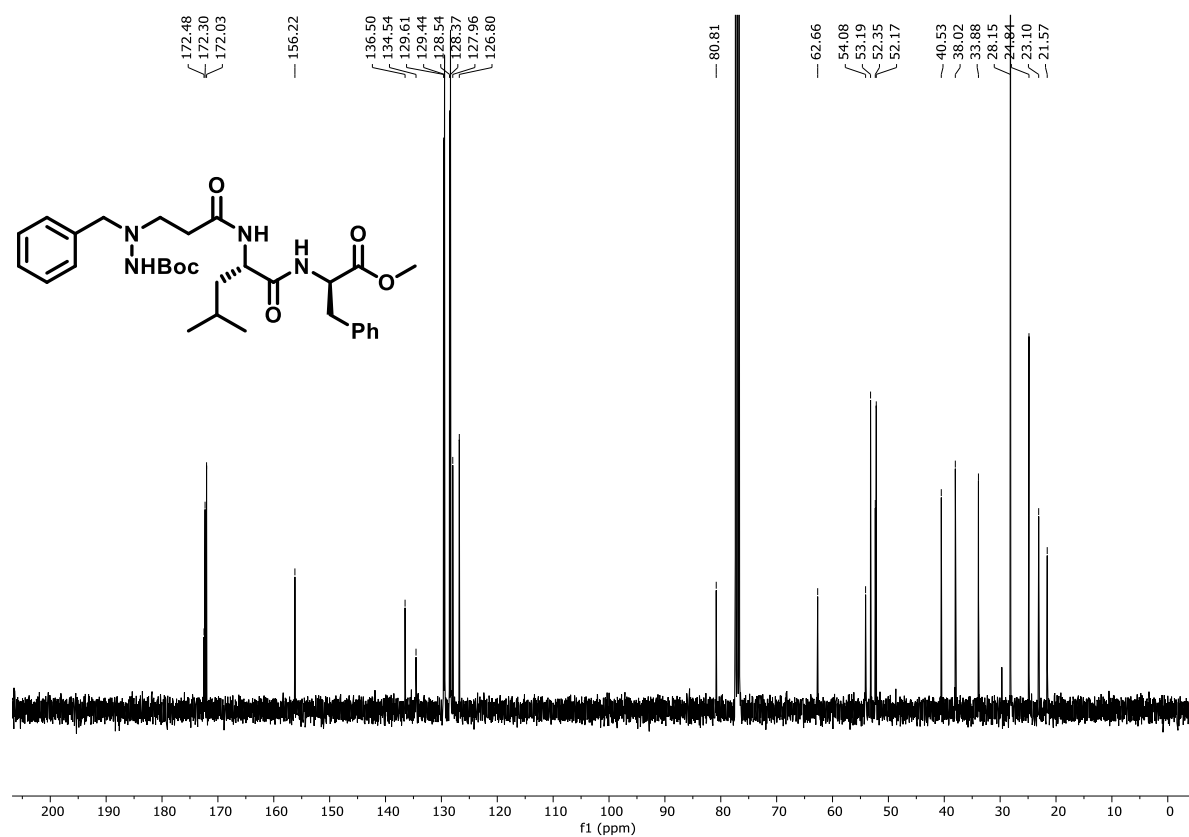
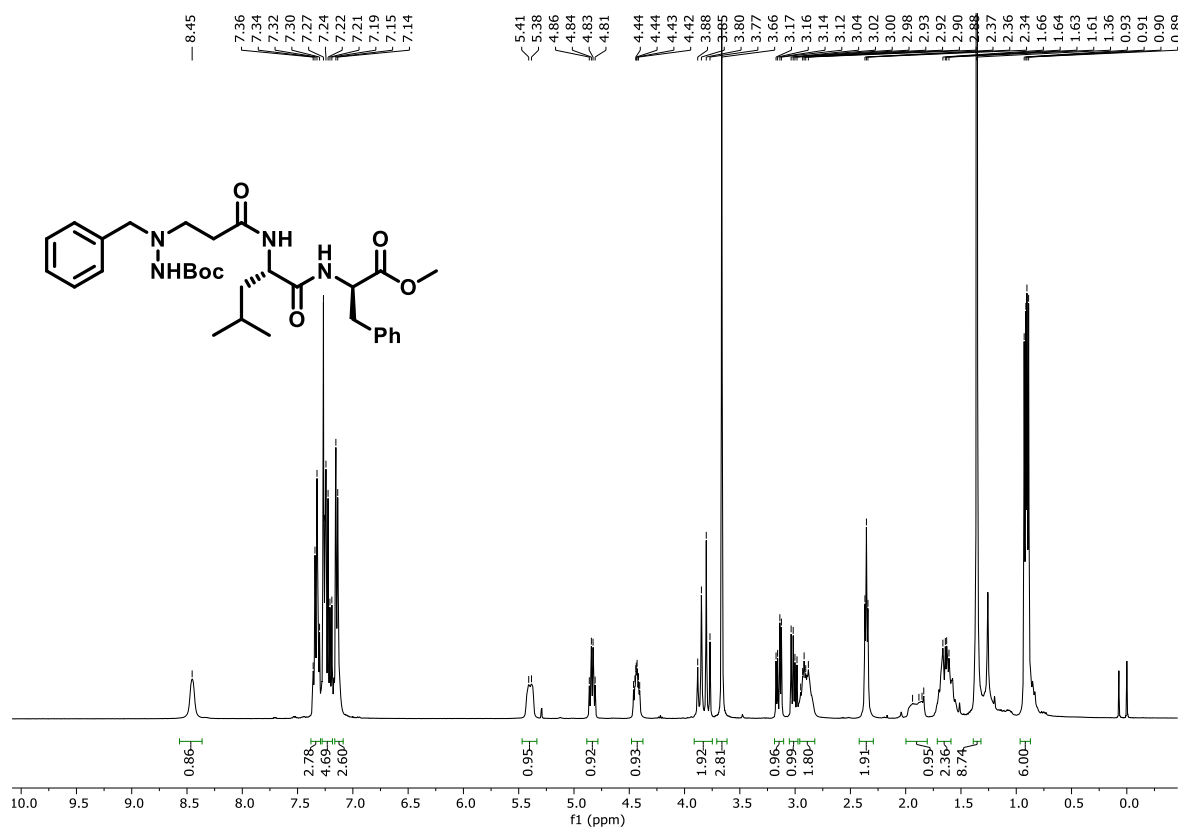


Figure A23.  $^1\text{H}$  and  $^{13}\text{C}$  NMR spectra of hybrid dipeptide (6a) in  $\text{CDCl}_3$

**Acquisition Parameter**

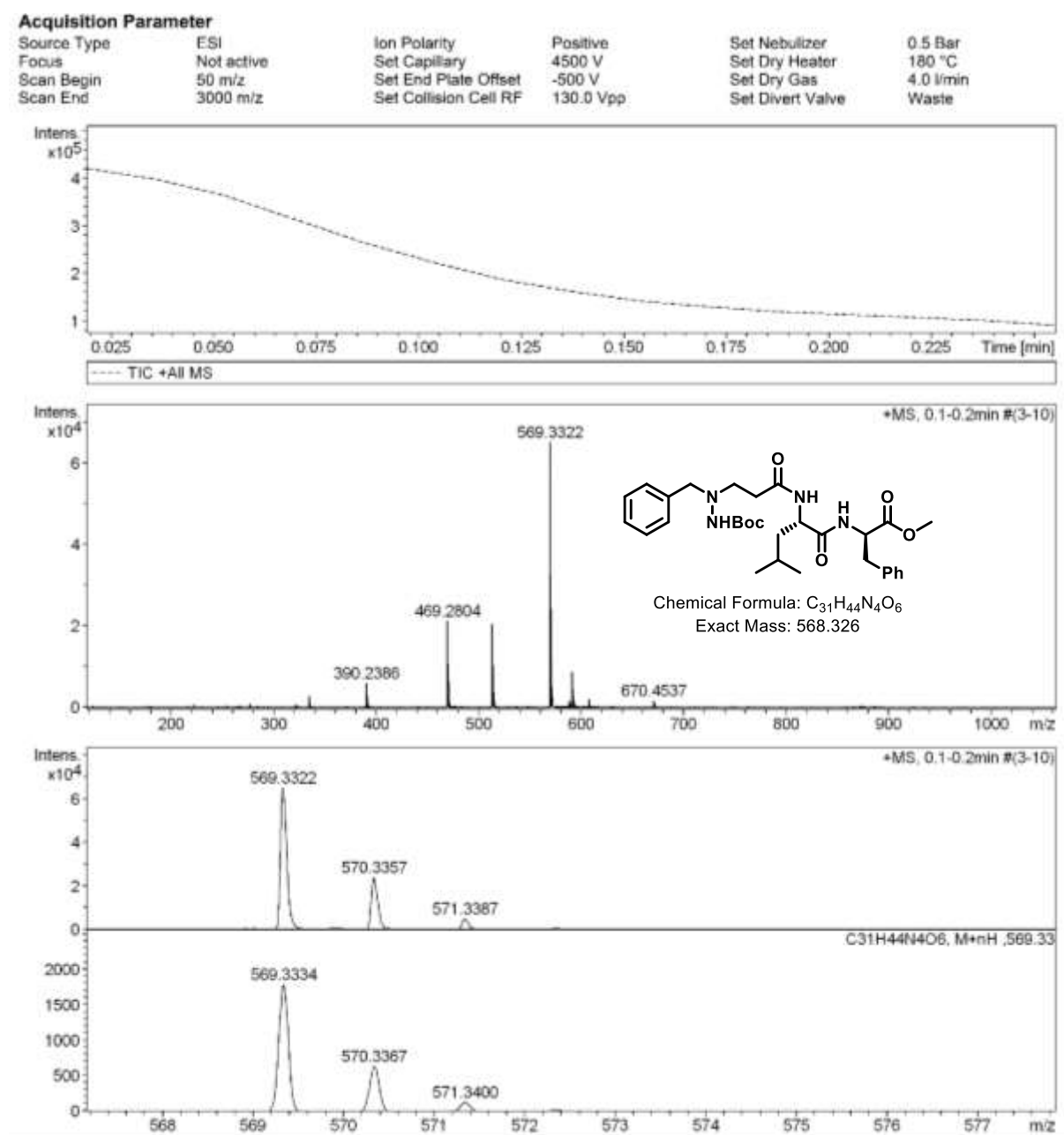
Source Type	ESI	Ion Polarity	Positive	Set Nebulizer	0.4 Bar
Focus	Active	Set Capillary	4500 V	Set Dry Heater	180 °C
Scan Begin	50 m/z	Set End Plate Offset	-500 V	Set Dry Gas	4.0 l/min
Scan End	3000 m/z	Set Collision Cell RF	300.0 Vpp	Set Divert Valve	Source

**Figure A24.** ESI-MS/HRMS spectra of hybrid dipeptide (**6a**)

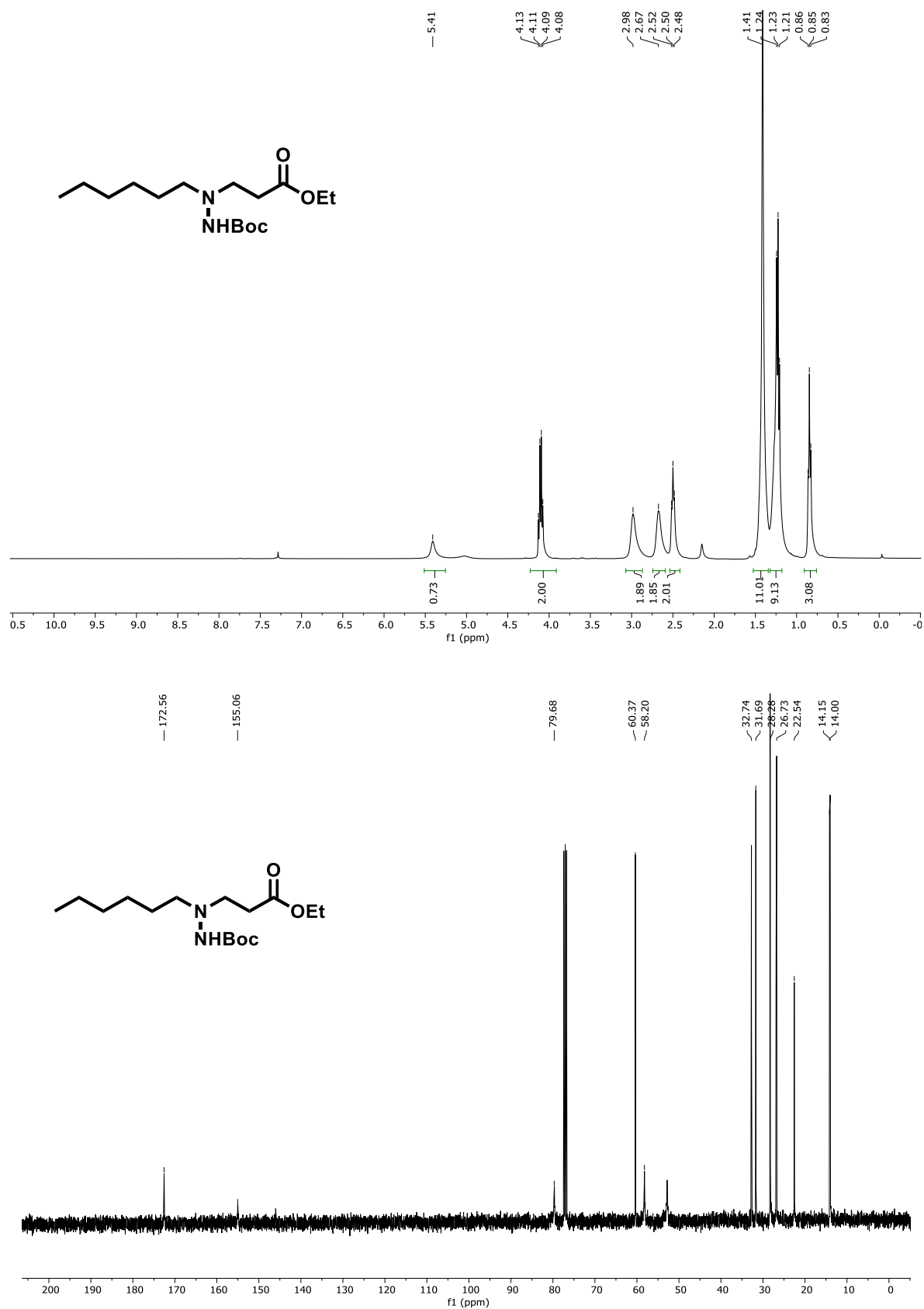


**Figure A25.** <sup>1</sup>H and <sup>13</sup>C NMR spectra of hybrid tripeptide (6b) in CDCl<sub>3</sub>





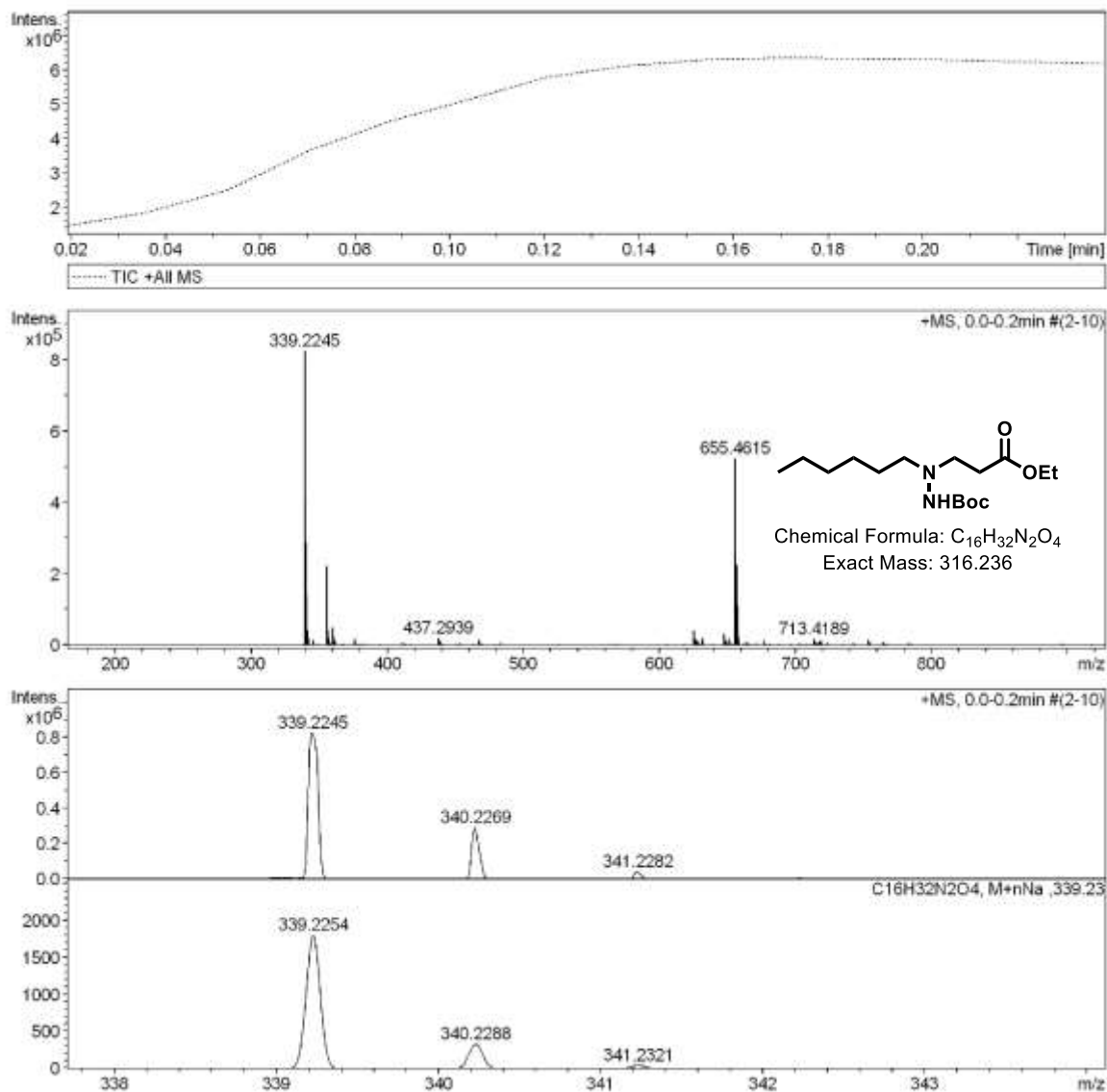
**Figure A26.** ESI-MS/HRMS spectra of hybrid tripeptide (6b)

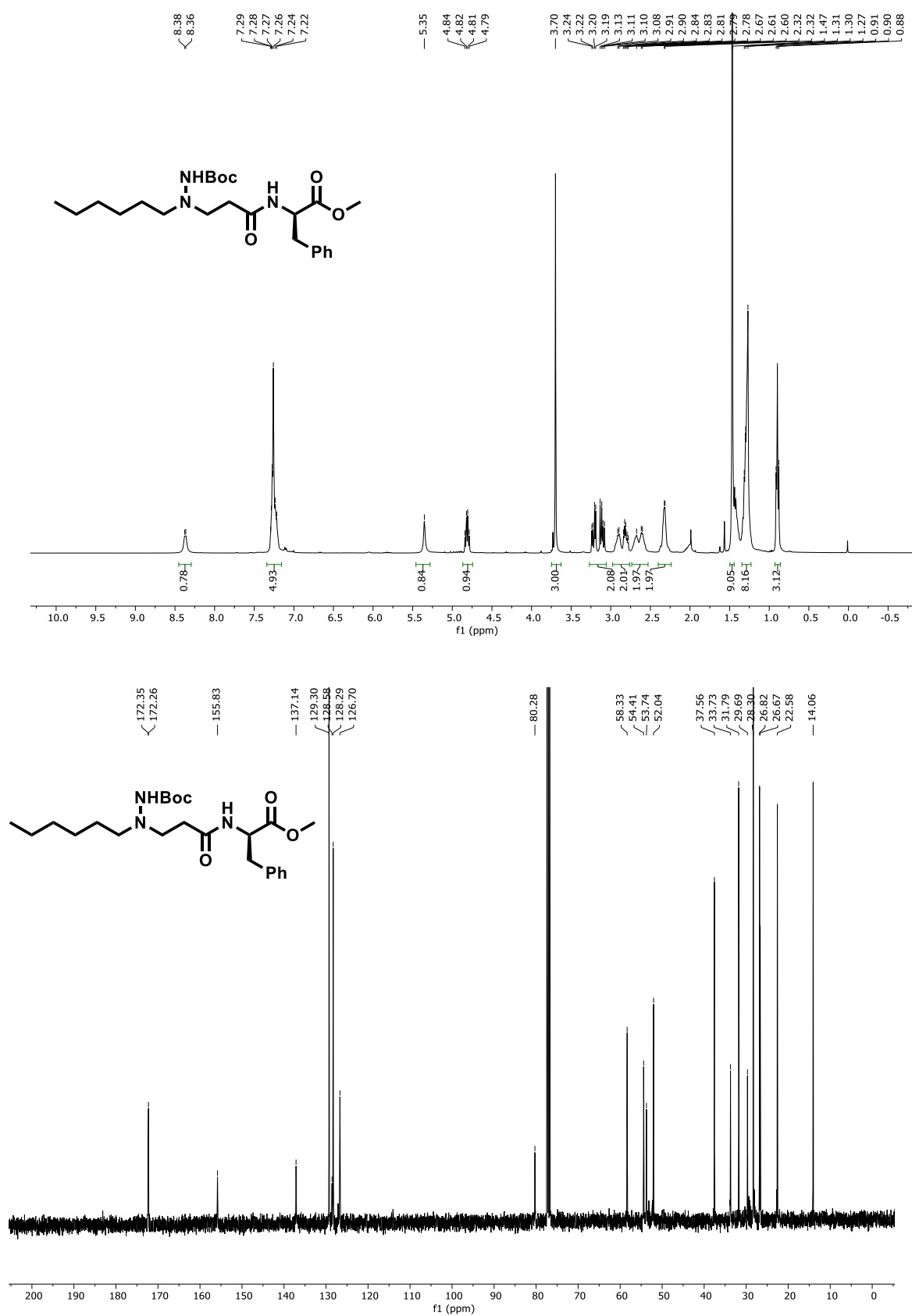


**Figure A27.** <sup>1</sup>H and <sup>13</sup>C NMR spectra of hexanyl-β-hydrazino ester (**2-Hexyl**) in CDCl<sub>3</sub>

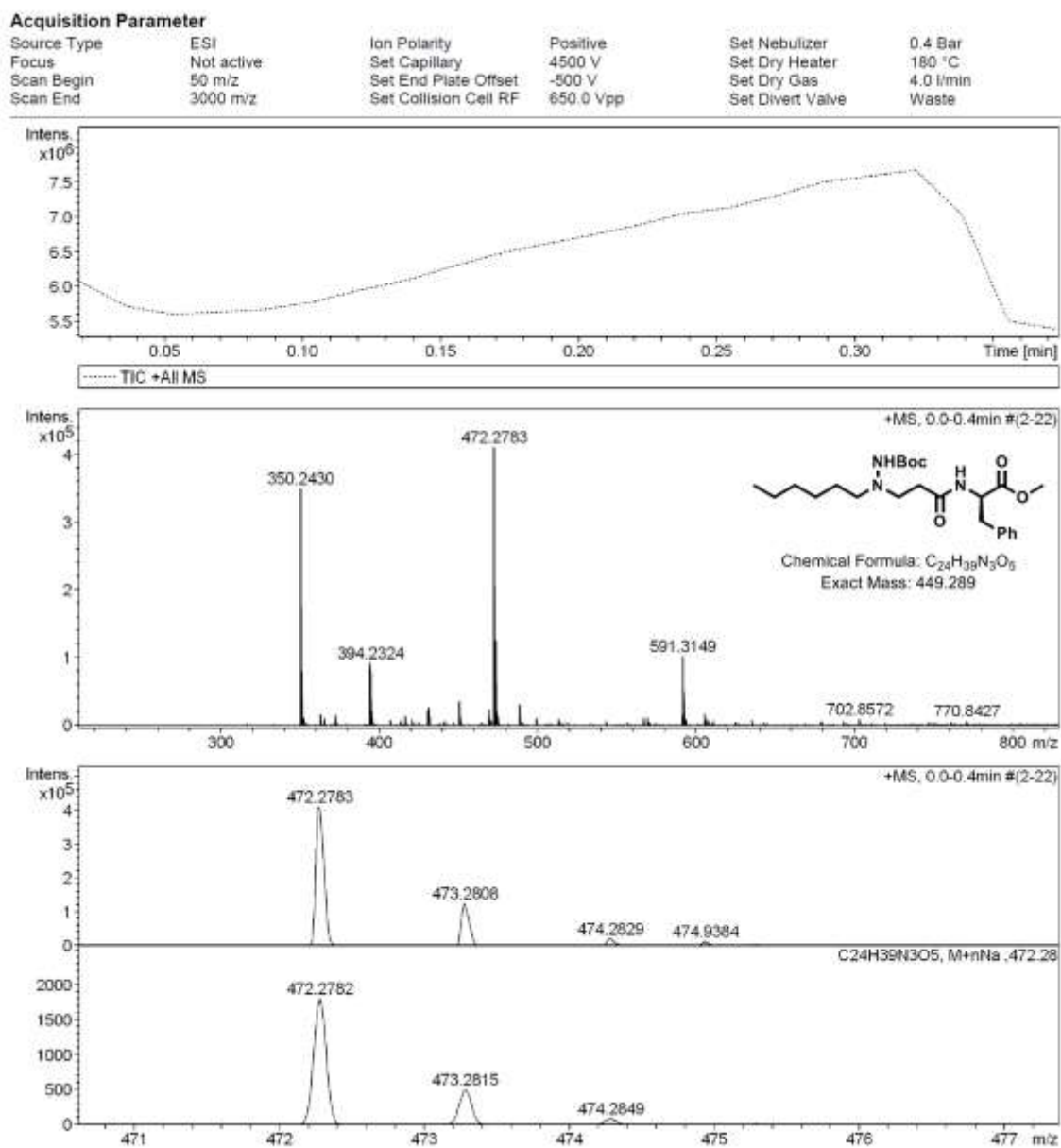
## Acquisition Parameter

Source Type	ESI	Ion Polarity	Positive	Set Nebulizer	0.4 Bar
Focus	Not active	Set Capillary	4500 V	Set Dry Heater	180 °C
Scan Begin	50 m/z	Set End Plate Offset	-500 V	Set Dry Gas	4.0 l/min
Scan End	3000 m/z	Set Collision Cell RF	650.0 Vpp	Set Divert Valve	Waste

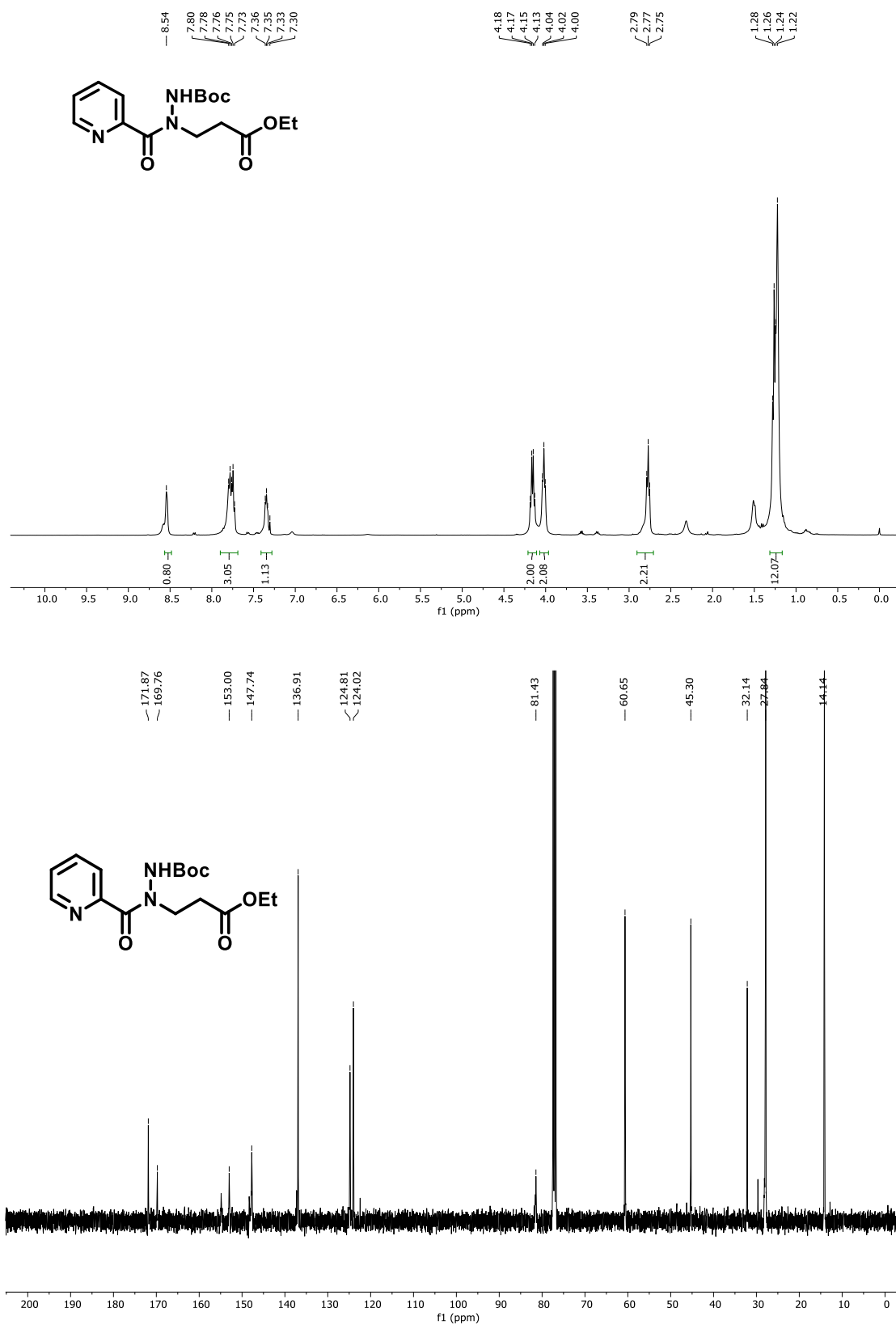
Figure A28. ESI-MS/HRMS spectra of hexanyl- $\beta$ -hydrazino ester (**2-Hexyl**)



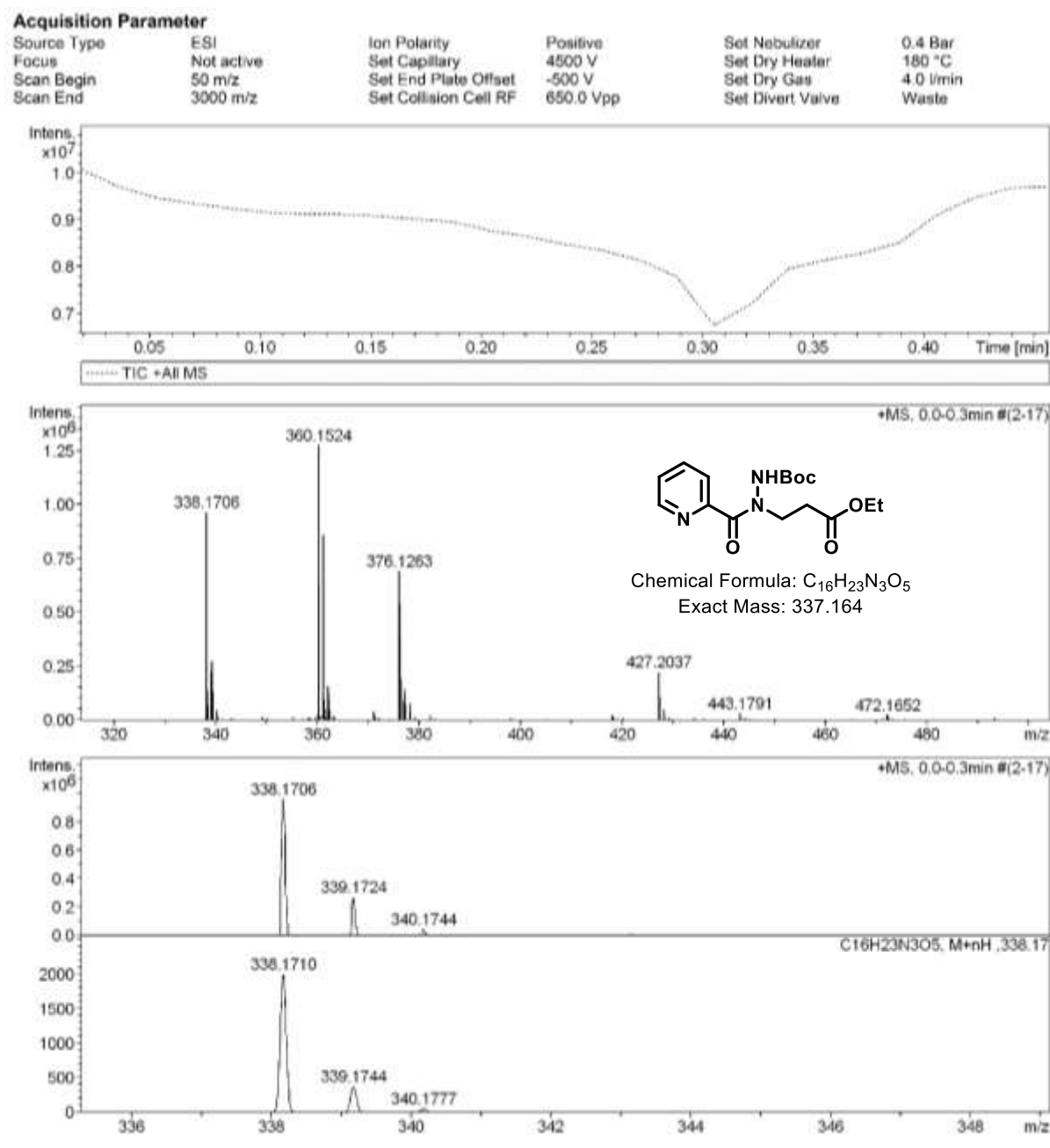
**Figure A29.** <sup>1</sup>H and <sup>13</sup>C NMR spectra of hybrid dipeptide (7) in CDCl<sub>3</sub>



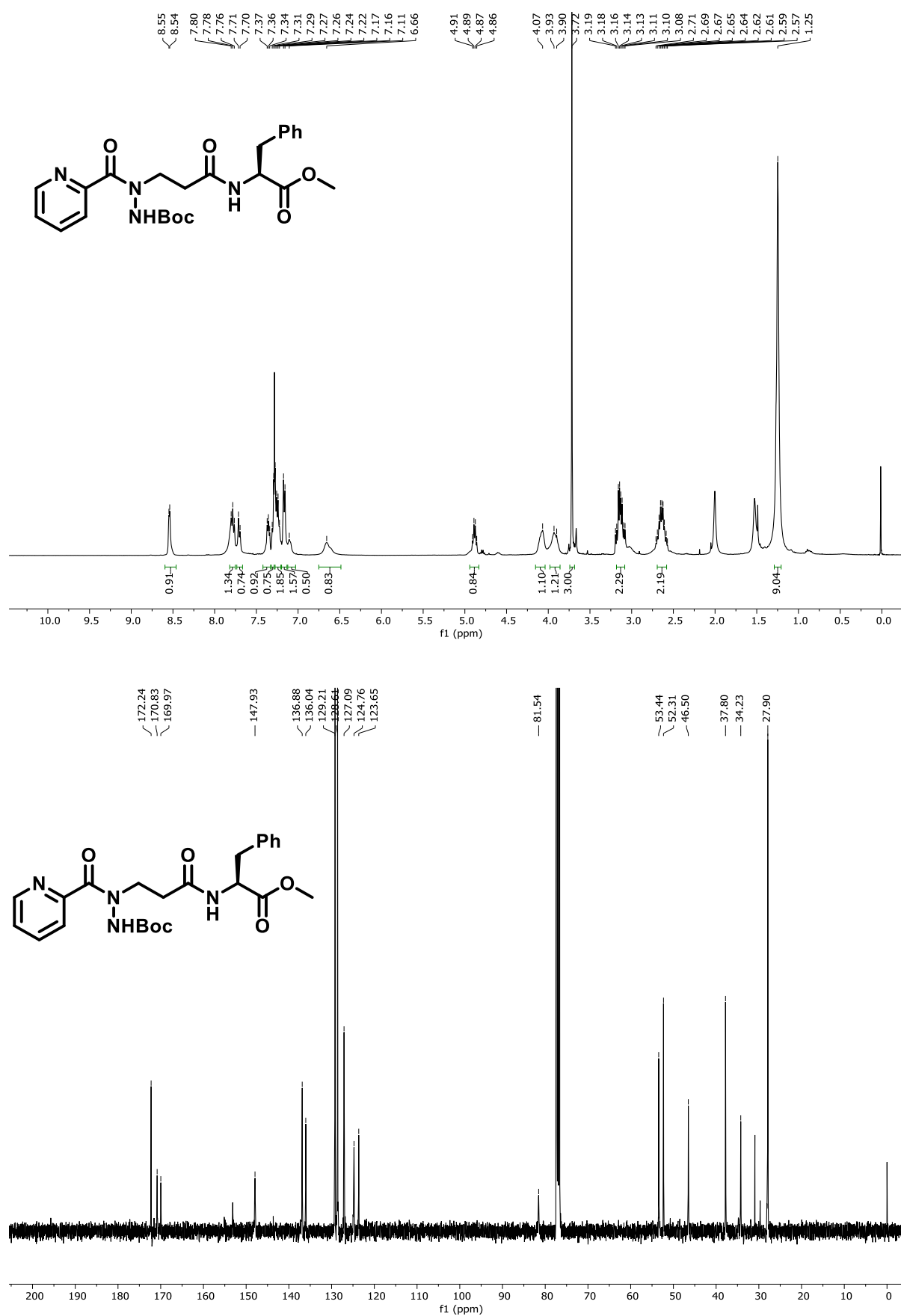
**Figure A30.** ESI-MS/HRMS spectra of hybrid dipeptide (7)



**Figure A31.**  $^1\text{H}$  and  $^{13}\text{C}$  NMR spectra of picolinyol- $\beta$ -hydrazino ester (2-Picolamide) in  $\text{CDCl}_3$

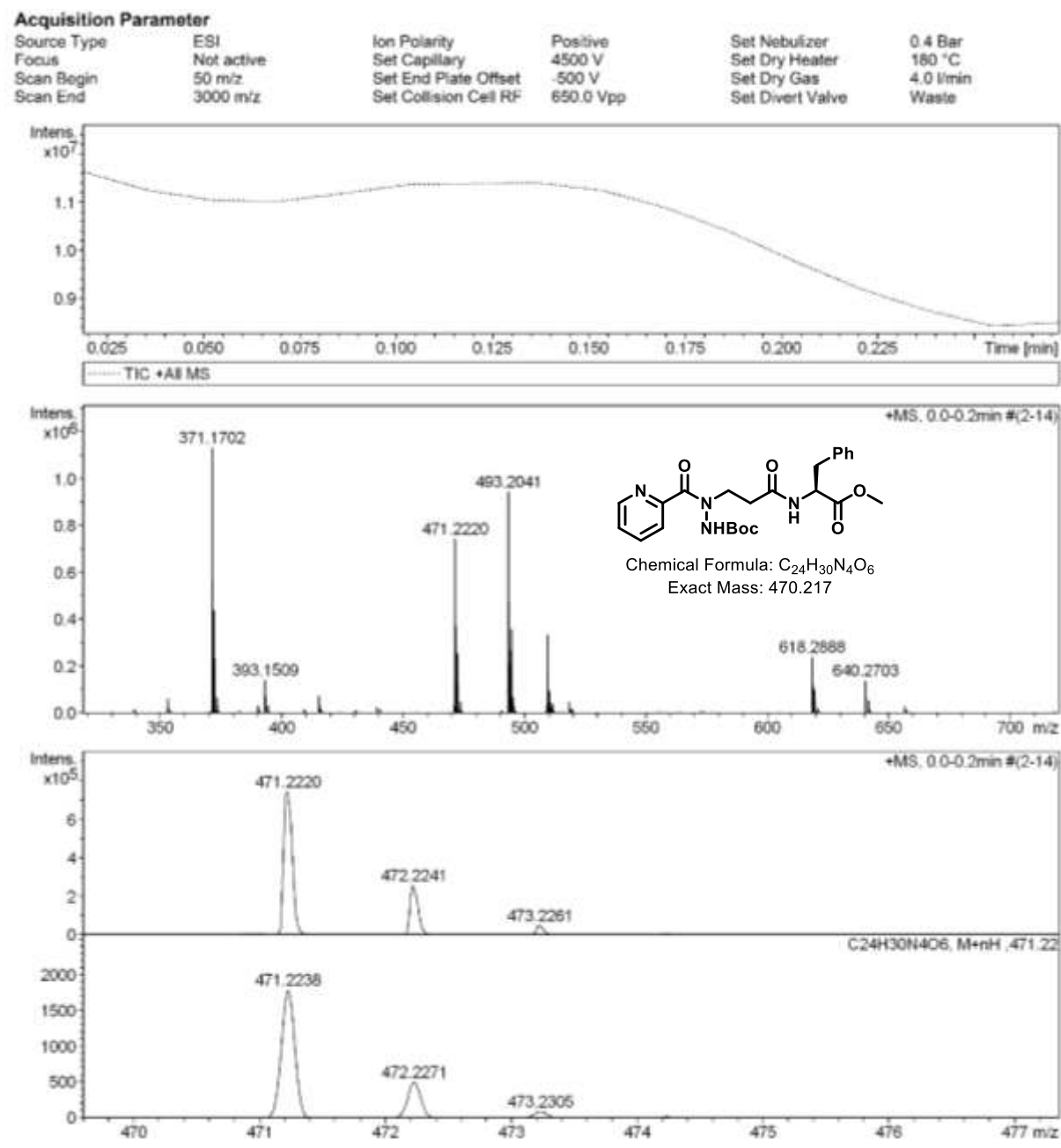


**Figure A32.** ESI-MS/HRMS spectra of picolinyol- $\beta$ -hydrazino ester (**2-Picolamide**)

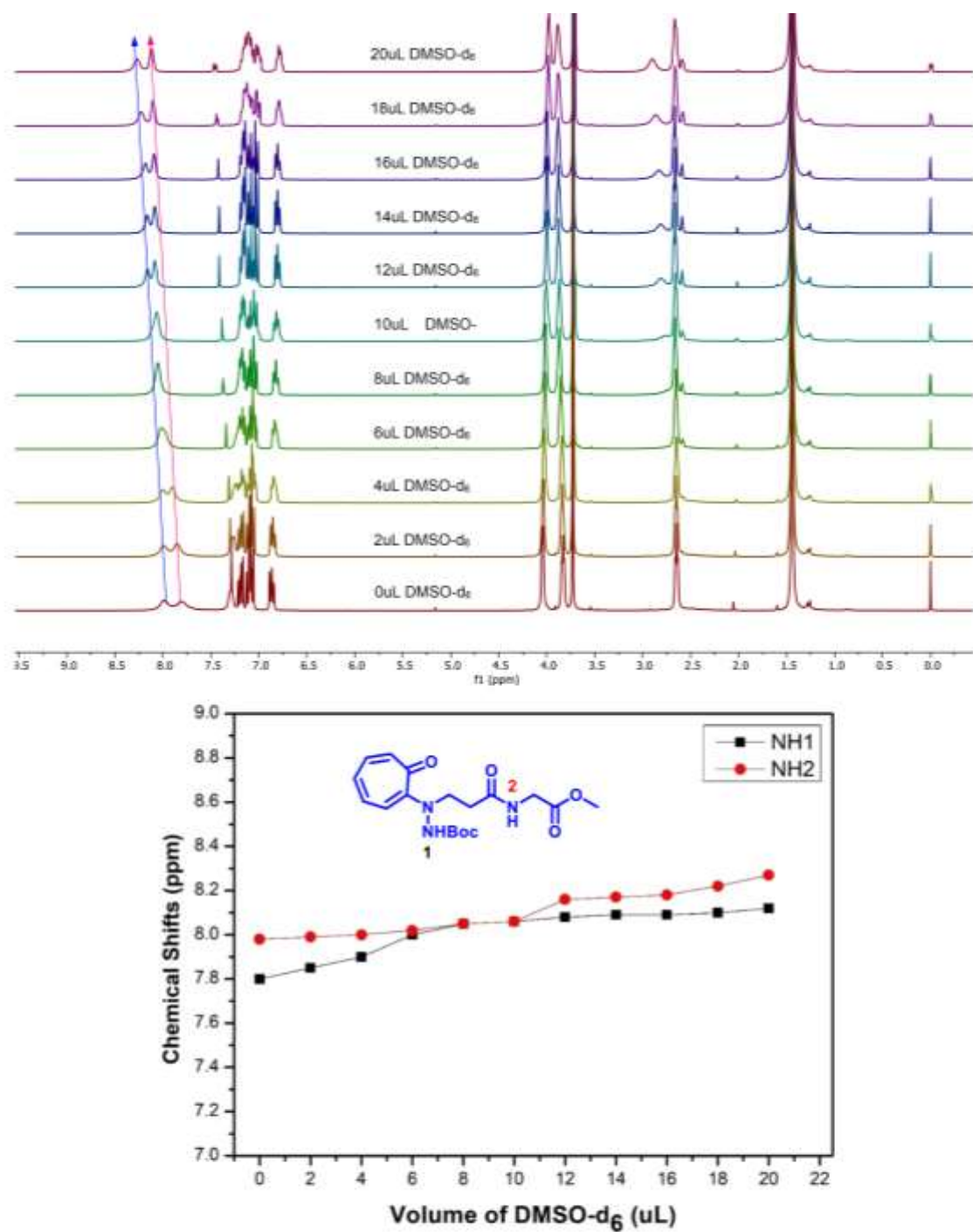


**Figure A33.**  $^1\text{H}$  and  $^{13}\text{C}$  NMR spectra of hybrid peptide (8) in  $\text{CDCl}_3$





**Figure A34.** ESI-MS/HRMS spectra of hybrid peptide (8)

2. DMSO-d<sub>6</sub> titration experiments by <sup>1</sup>H-NMR of peptides (**5a-5e**) in CDCl<sub>3</sub>

uL	0	2	4	6	8	10	12	14	16	18	20
NH <sub>1</sub>	7.8	7.85	7.9	8	8.05	8.06	8.08	8.09	8.09	8.1	8.12
NH <sub>2</sub>	7.98	7.99	8	8.02	8.05	8.06	8.16	8.17	8.18	8.22	8.27

Figure A35: <sup>1</sup>H-NMR of DMSO-d<sub>6</sub> titration of (**5a**) in CDCl<sub>3</sub>

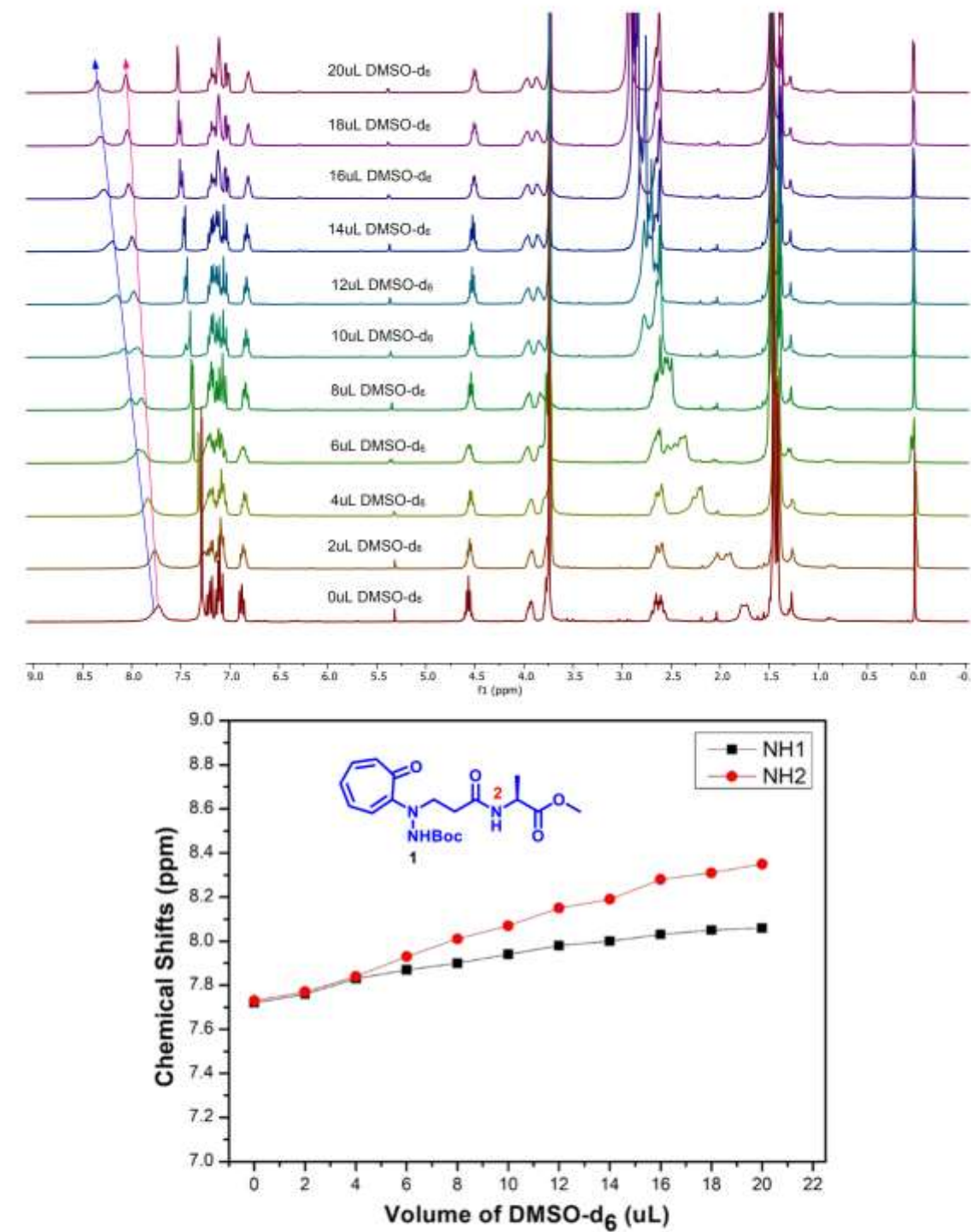
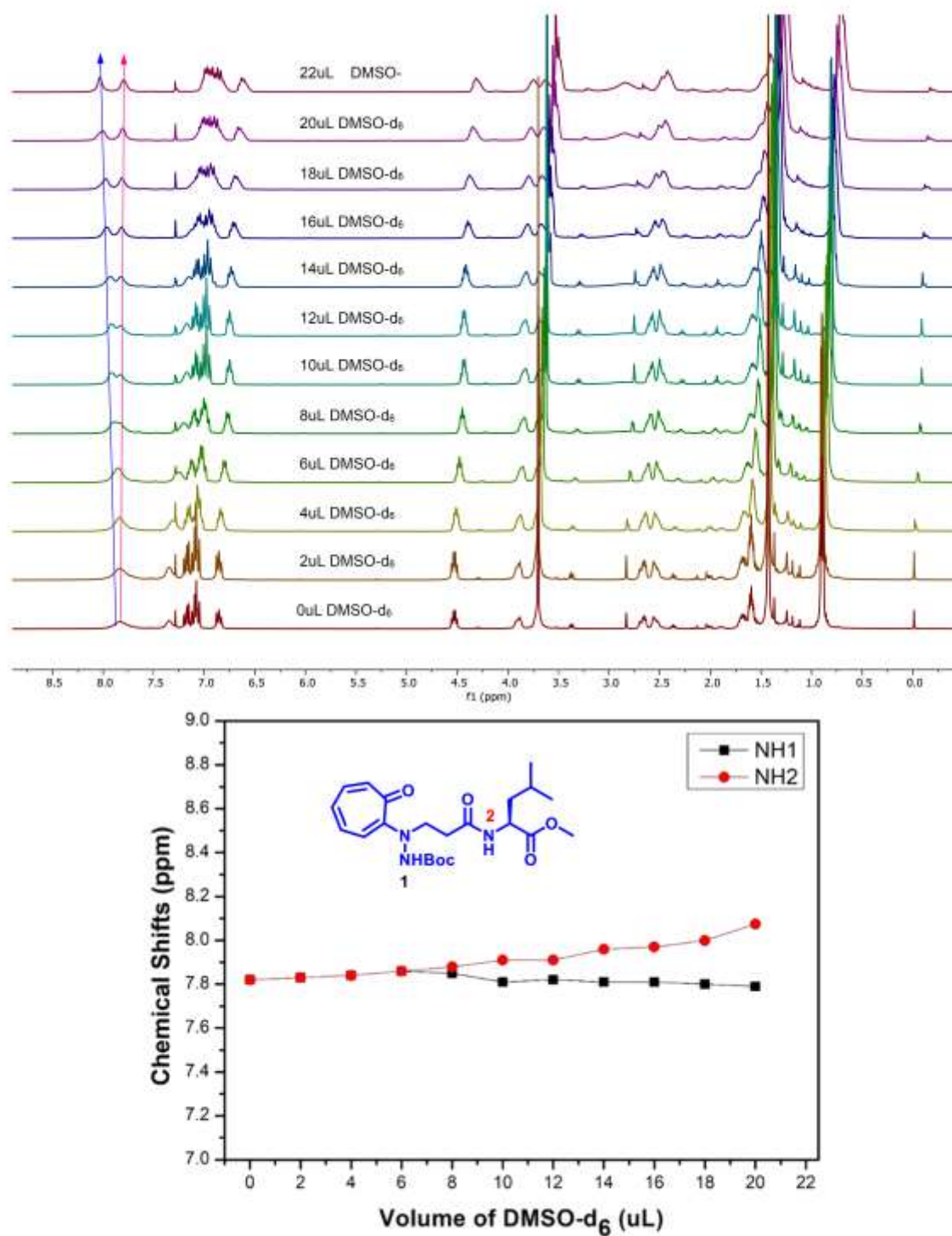
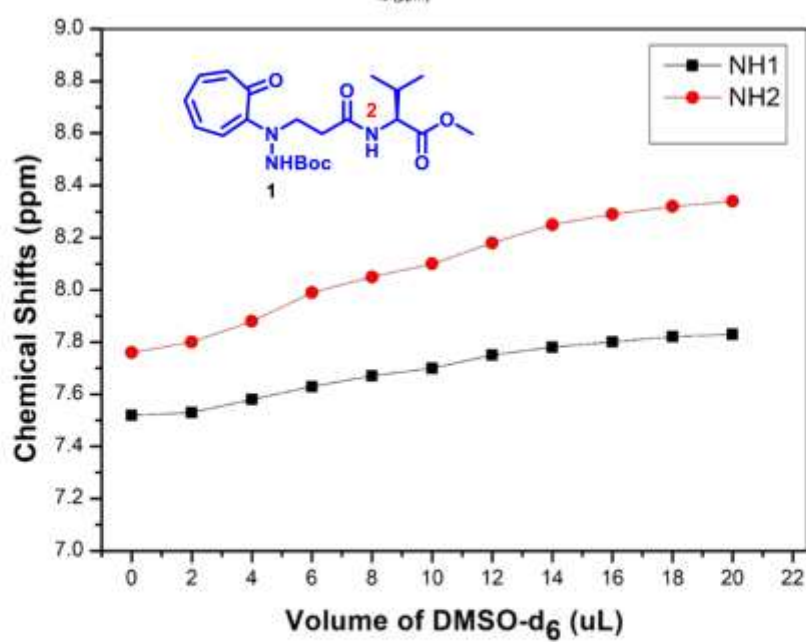
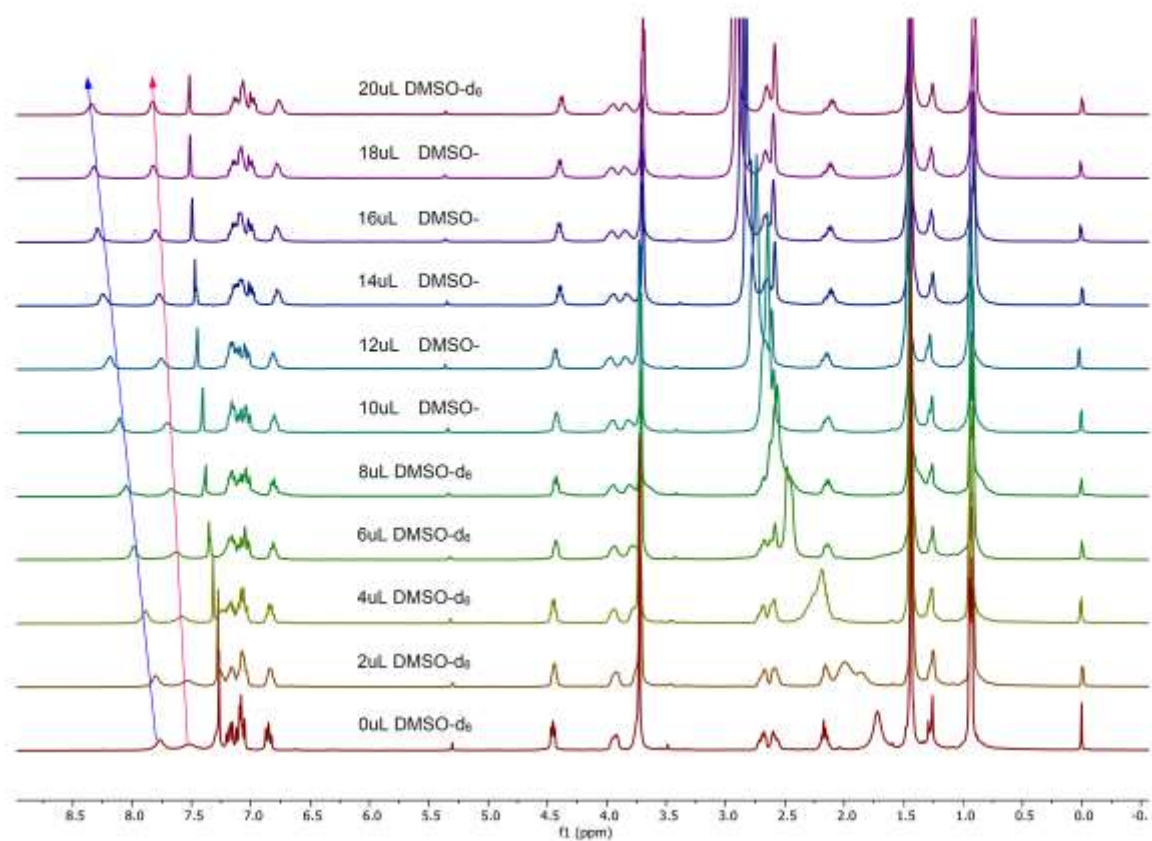


Figure A36.  $^1\text{H}$ -NMR of  $\text{DMSO-d}_6$  titration of (**5b**) in  $\text{CDCl}_3$



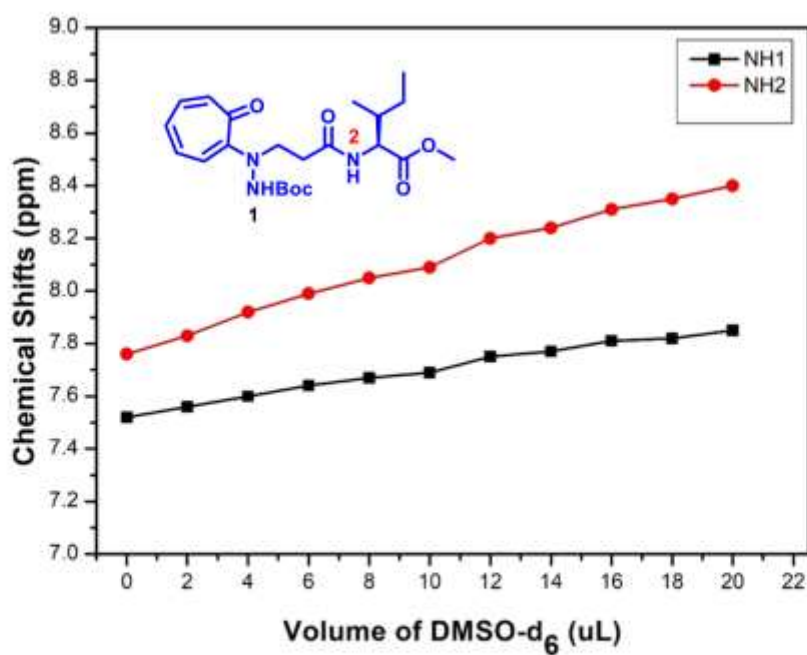
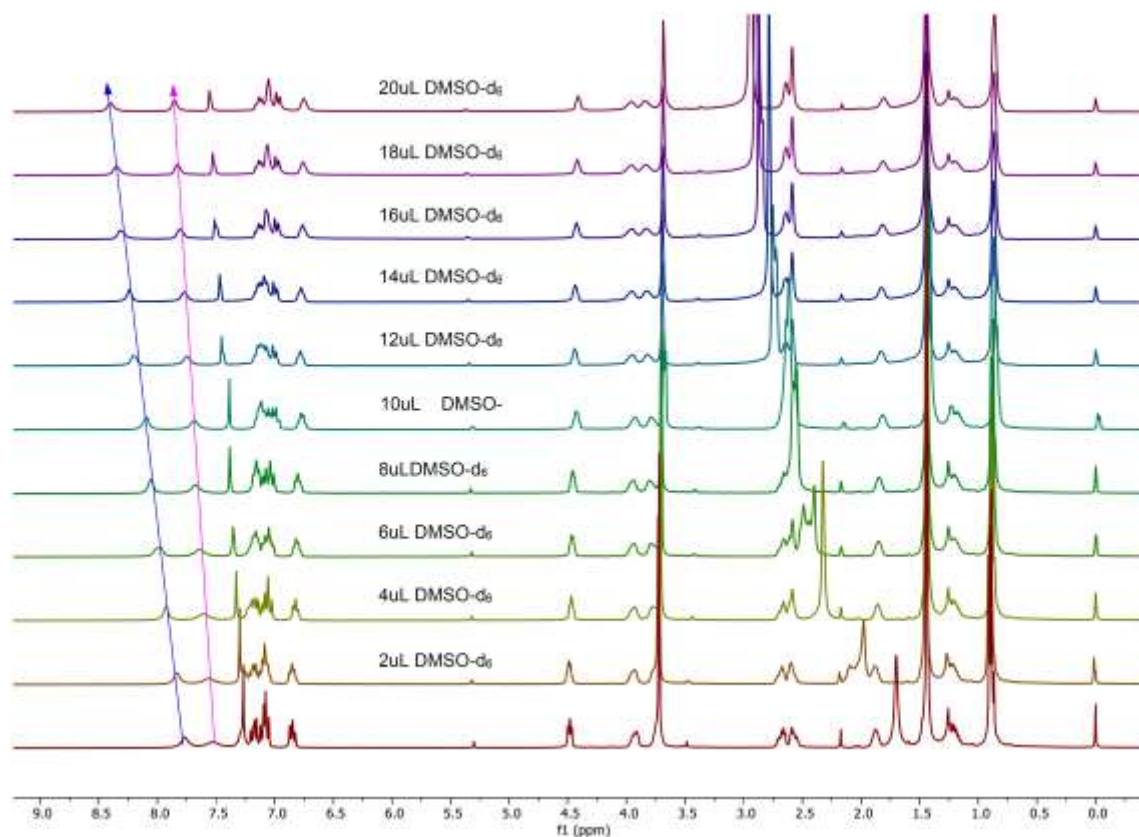
**Figure A37.**  $^1\text{H}$ -NMR of DMSO- $d_6$  titration of (**5c**) in  $\text{CDCl}_3$



uL	0	2	4	6	8	10	12	14	16	18	20
NH <sub>1</sub>	7.52	7.53	7.58	7.63	7.67	7.7	7.75	7.78	7.8	7.82	7.83
NH <sub>2</sub>	7.76	7.8	7.88	7.99	8.05	8.1	8.18	8.25	8.29	8.32	8.34

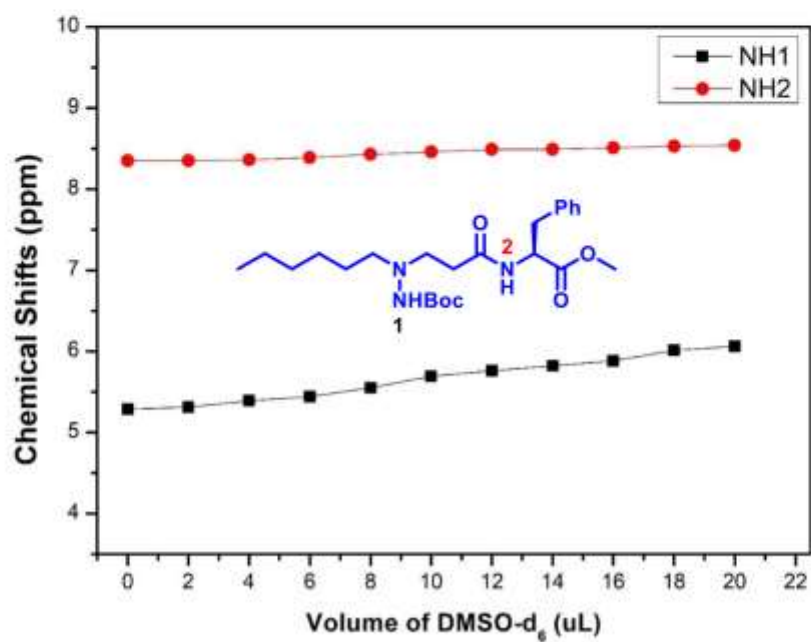
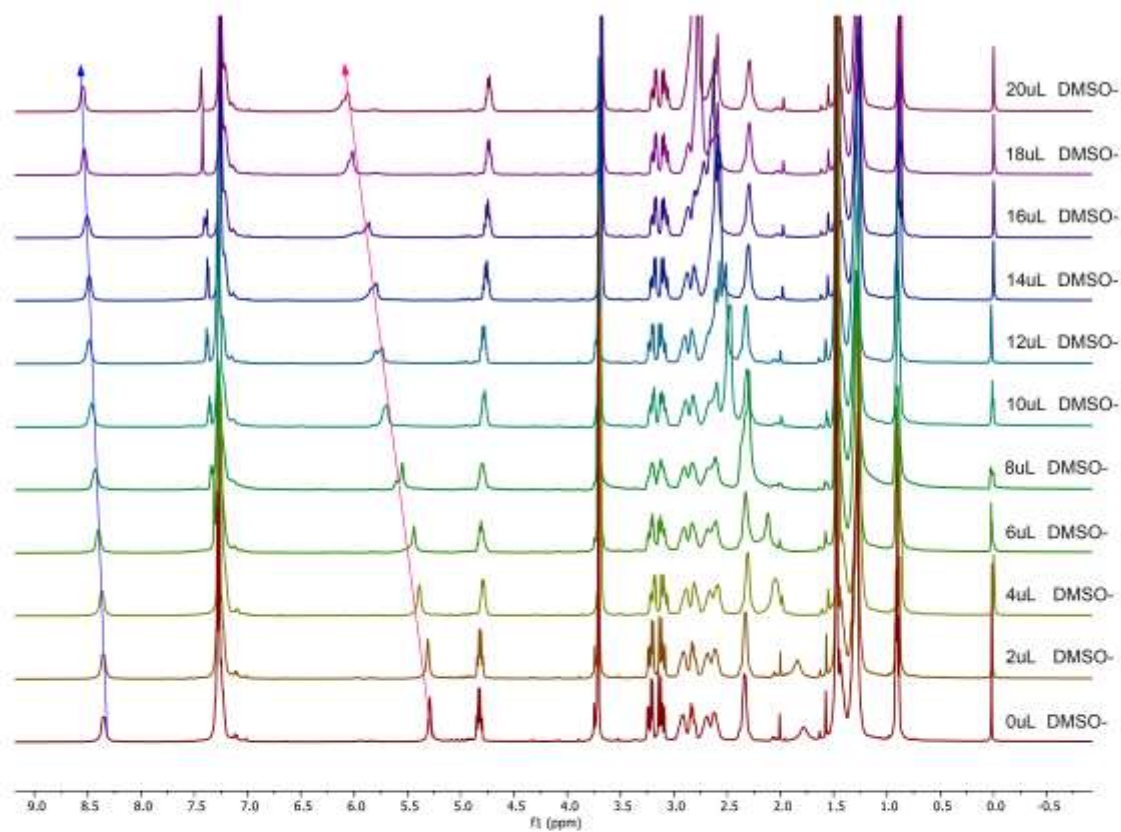
Figure A38. <sup>1</sup>H-NMR of DMSO-d<sub>6</sub> titration of (**5d**) in CDCl<sub>3</sub>





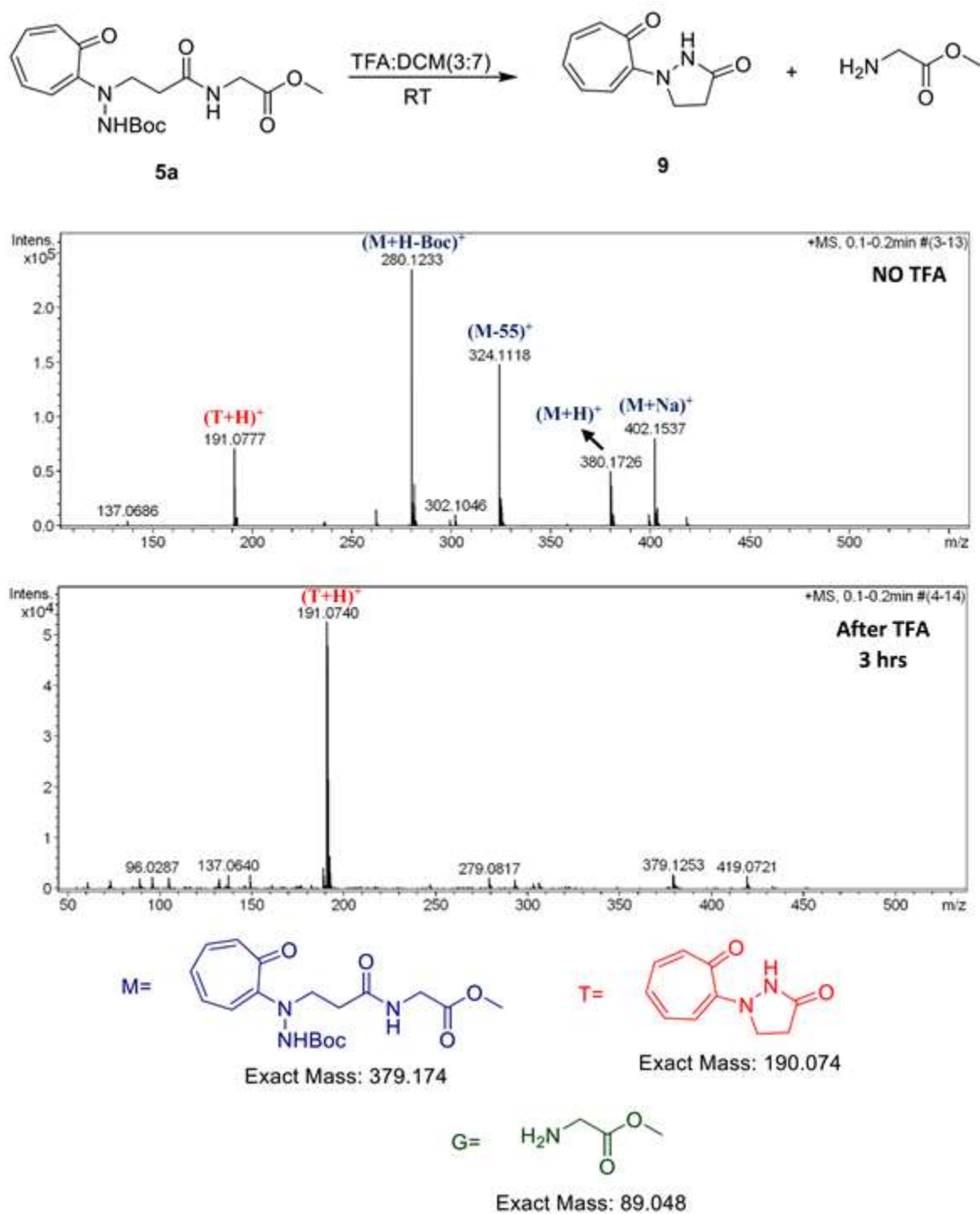
uL	0	2	4	6	8	10	12	14	16	18	20
NH <sub>1</sub>	7.52	7.56	7.6	7.64	7.67	7.69	7.75	7.77	7.81	7.82	7.85
NH <sub>2</sub>	7.76	7.83	7.92	7.99	8.05	8.09	8.2	8.24	8.31	8.35	8.4

Figure A39. <sup>1</sup>H-NMR of DMSO-d<sub>6</sub> titration of (5e) in CDCl<sub>3</sub>



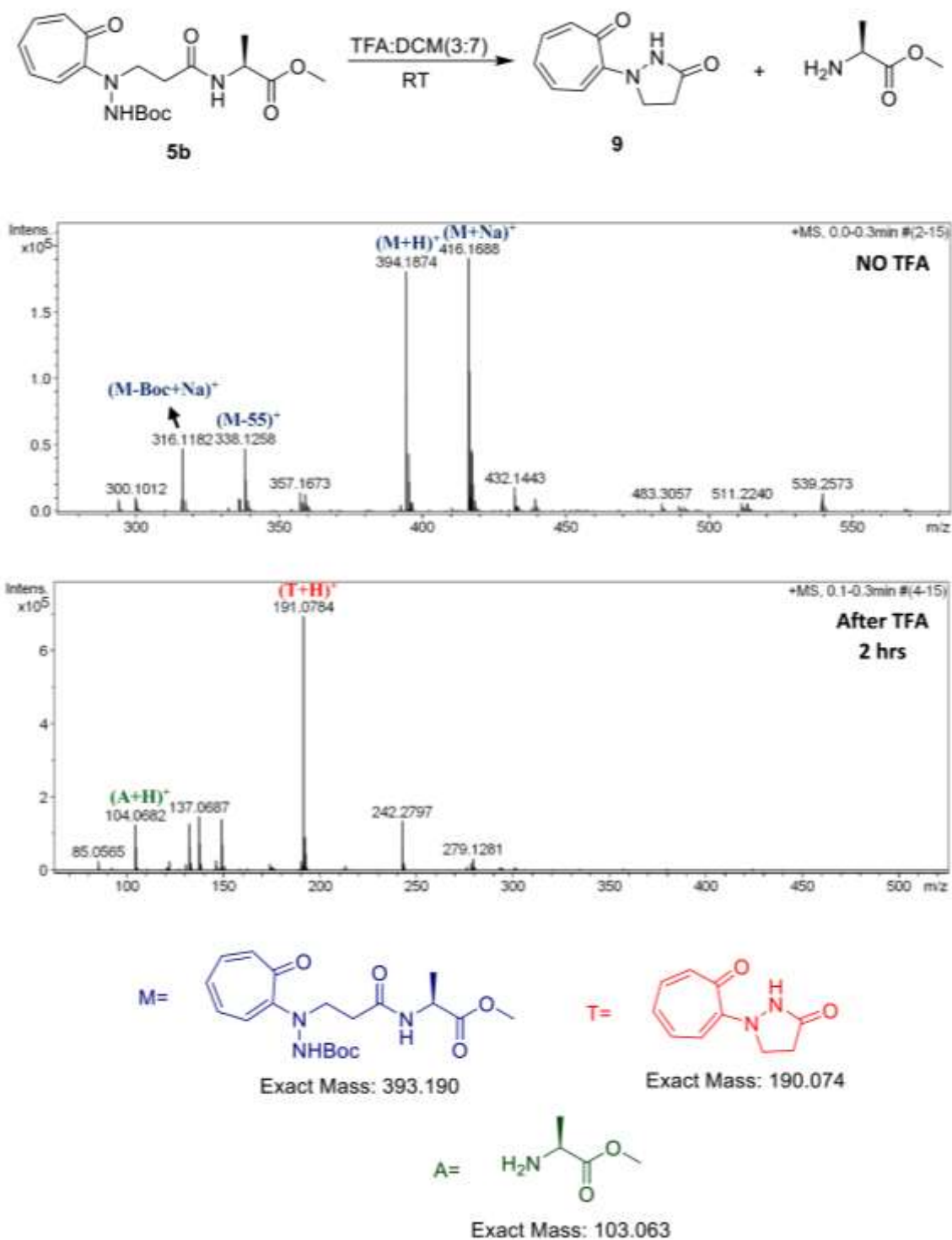
$\mu\text{L}$	0	2	4	6	8	10	12	14	16	18	20
$\text{NH}_1$	5.29	5.31	5.39	5.44	5.55	5.69	5.76	5.82	5.88	6.01	6.06
$\text{NH}_2$	8.35	8.35	8.36	8.39	8.43	8.46	8.49	8.49	8.51	8.53	8.54

**Figure A40.**  $\text{DMSO-d}_6$  titration of (**9**) in  $\text{CDCl}_3$

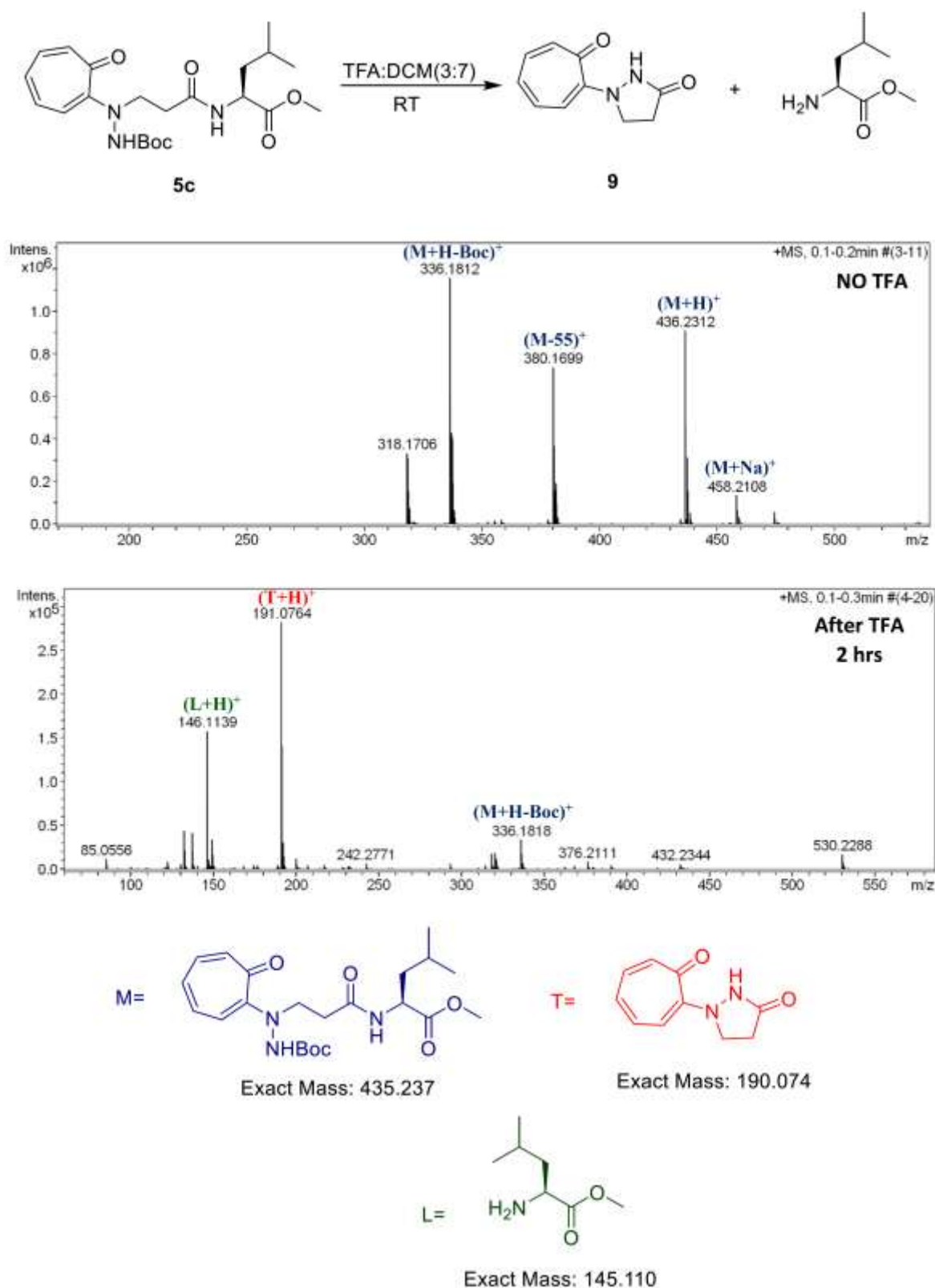
3. Mass study of amide bond hydrolysis in compounds (**5a-5h**) in (20-30%) TFA

**Figure A41.** ESI-MS spectra of compound **5a** at different time intervals in 30% TFA in CH<sub>2</sub>Cl<sub>2</sub>

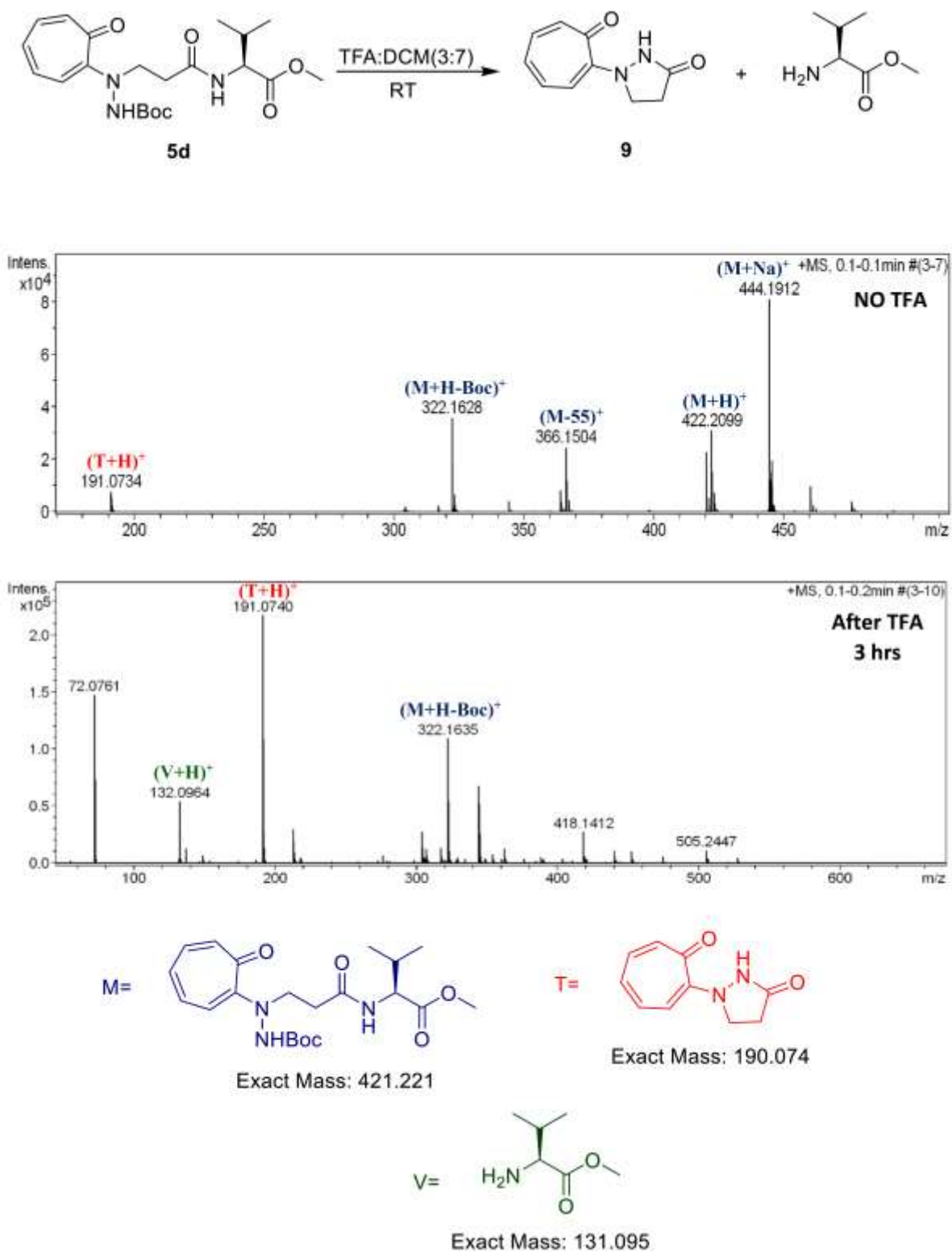




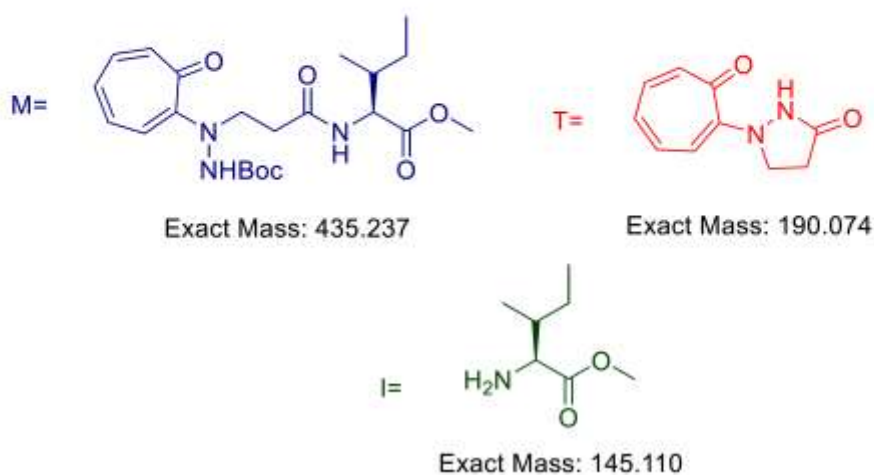
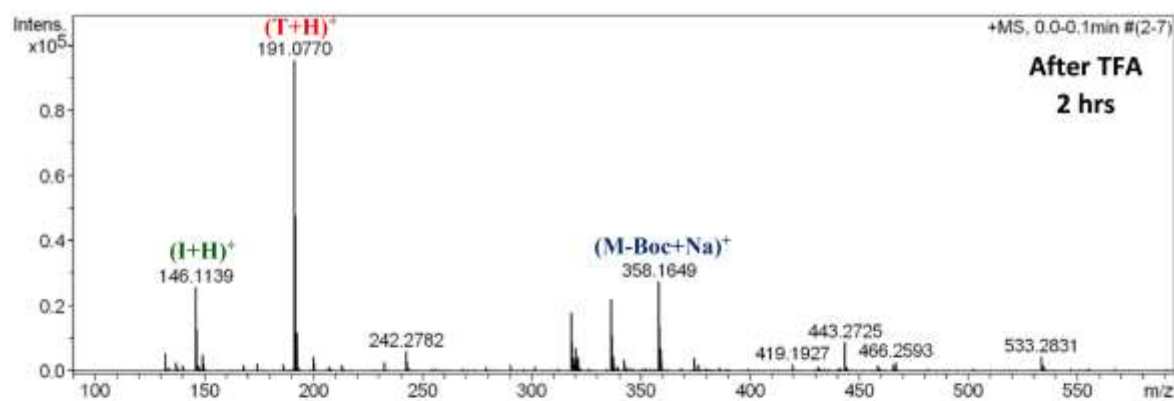
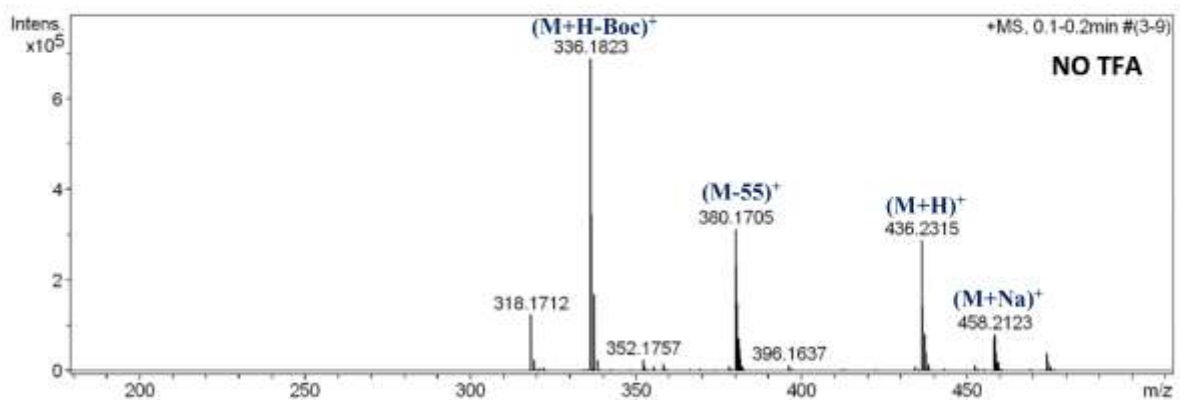
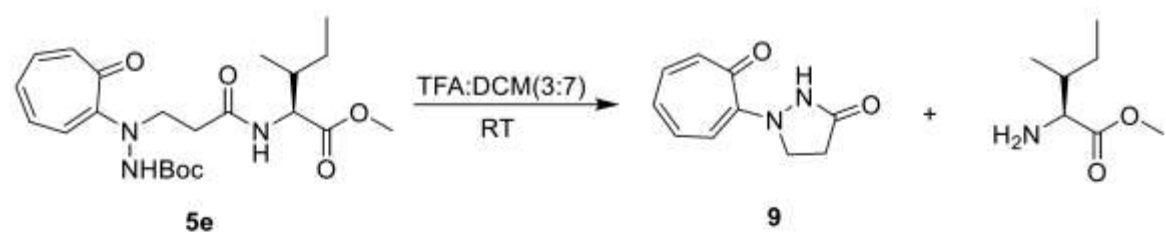
**Figure A42.** ESI-MS spectra of compound **5b** at different time intervals in 30% TFA in CH<sub>2</sub>Cl<sub>2</sub>



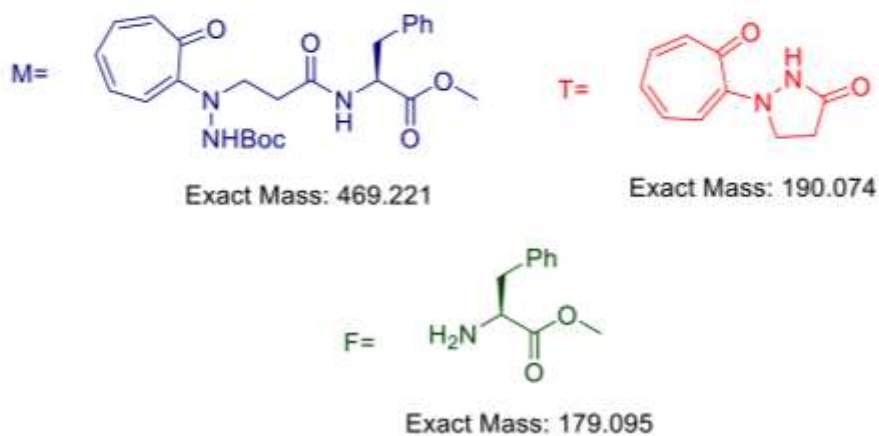
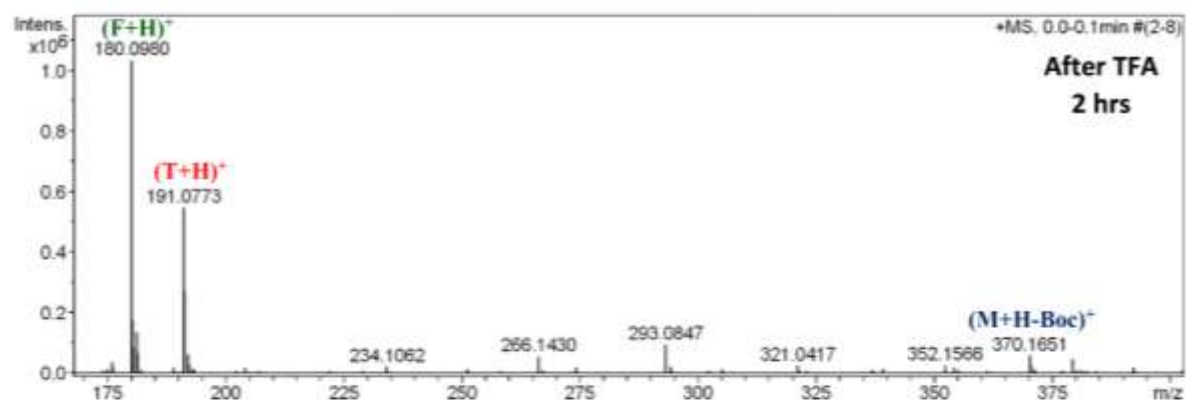
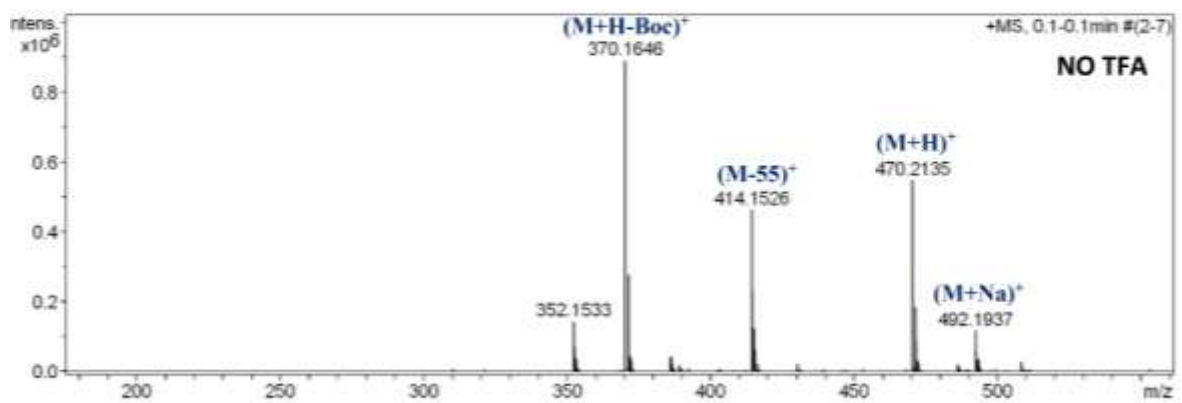
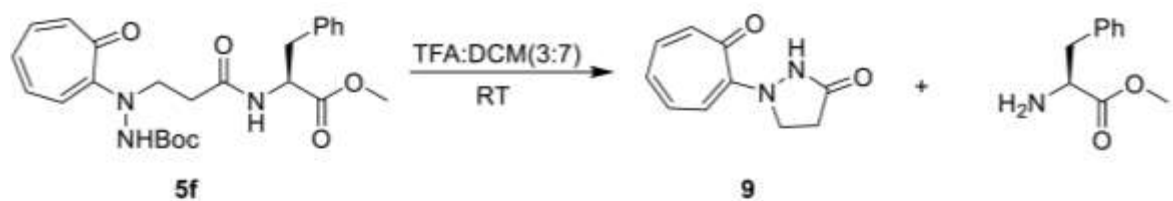
**Figure A43.** ESI-MS spectra of compound **5c** at different time intervals in 30% TFA in CH<sub>2</sub>Cl<sub>2</sub>



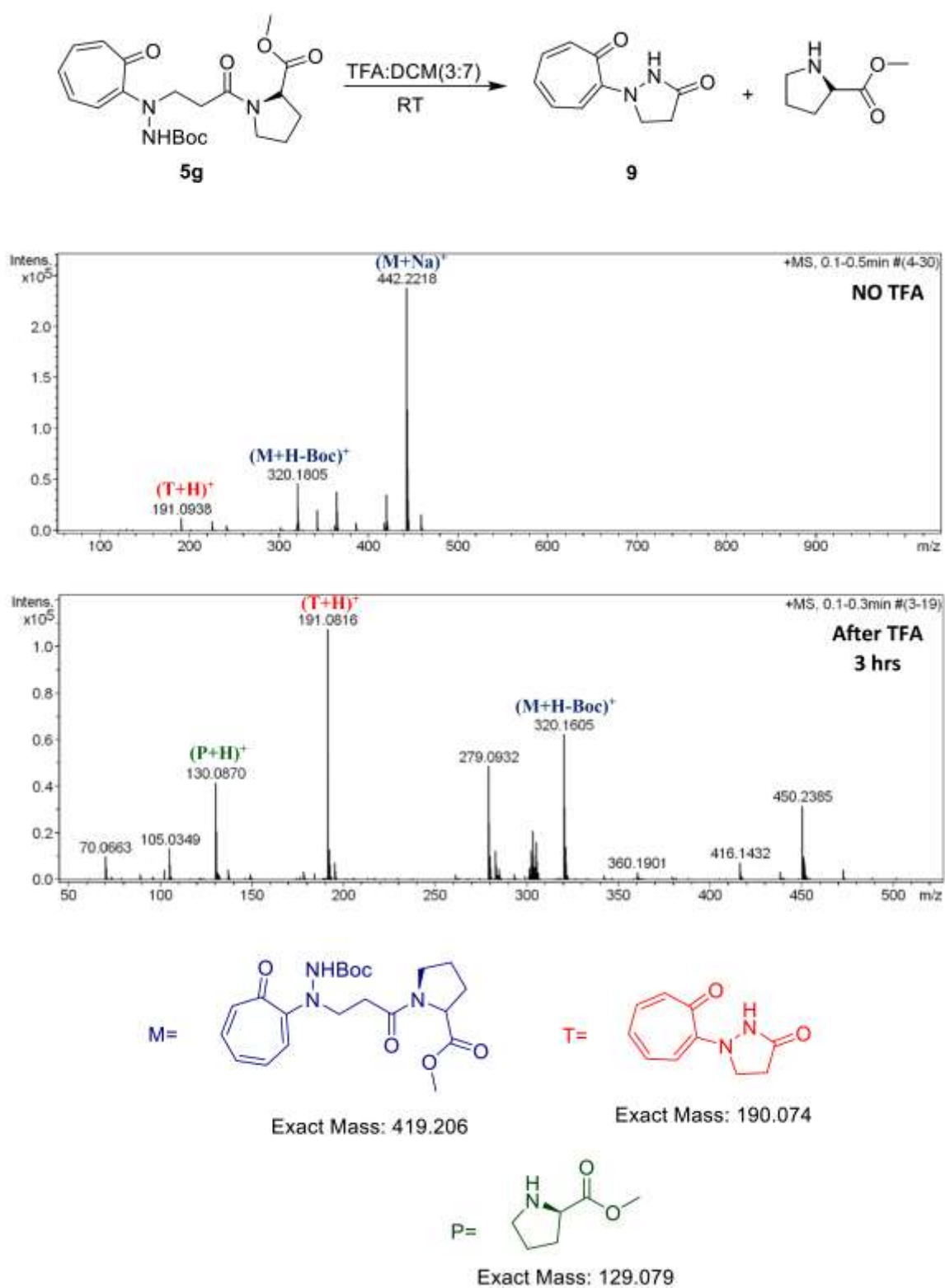
**Figure A44.** ESI-MS spectra of compound **5d** at different time intervals in 30% TFA in CH<sub>2</sub>Cl<sub>2</sub>



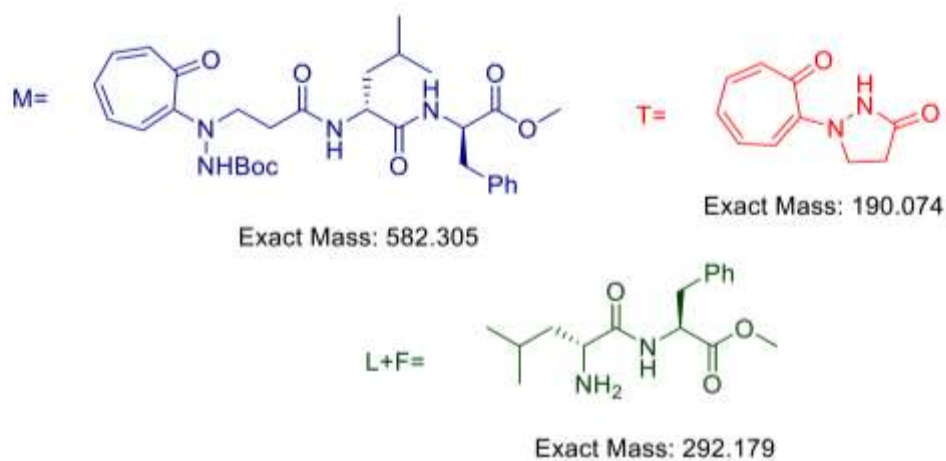
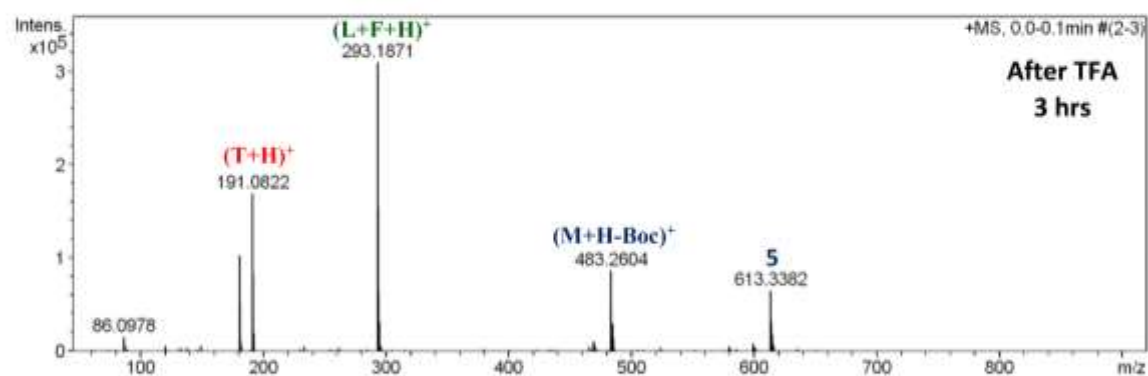
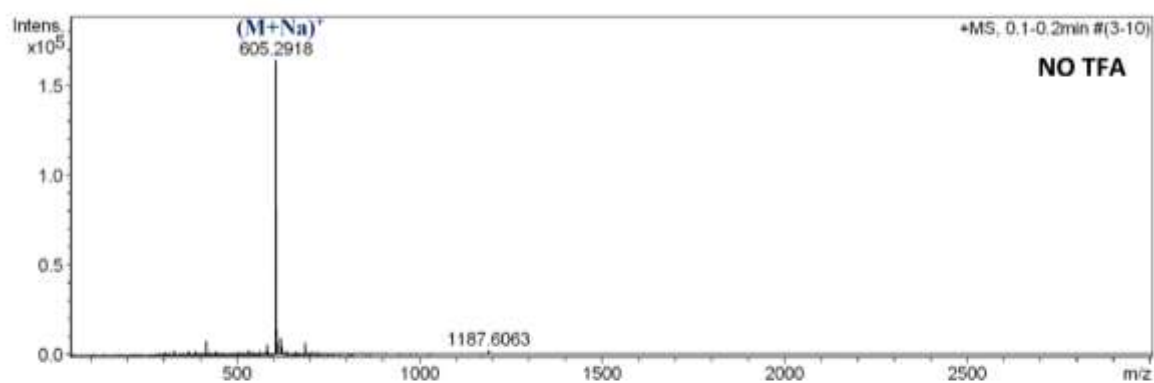
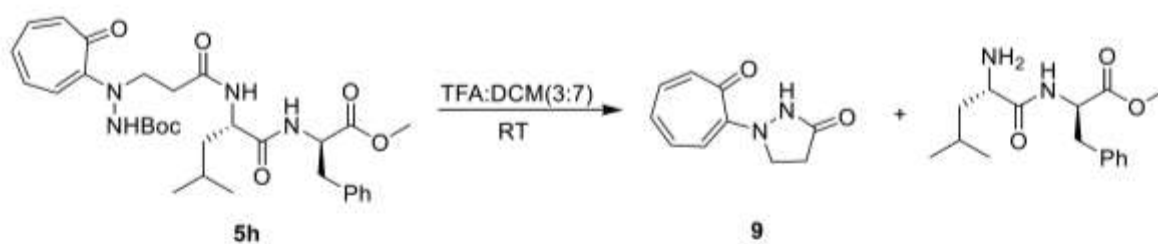
**Figure A45.** ESI-MS spectra of compound **5e** at different time intervals in 30% TFA in  $\text{CH}_2\text{Cl}_2$



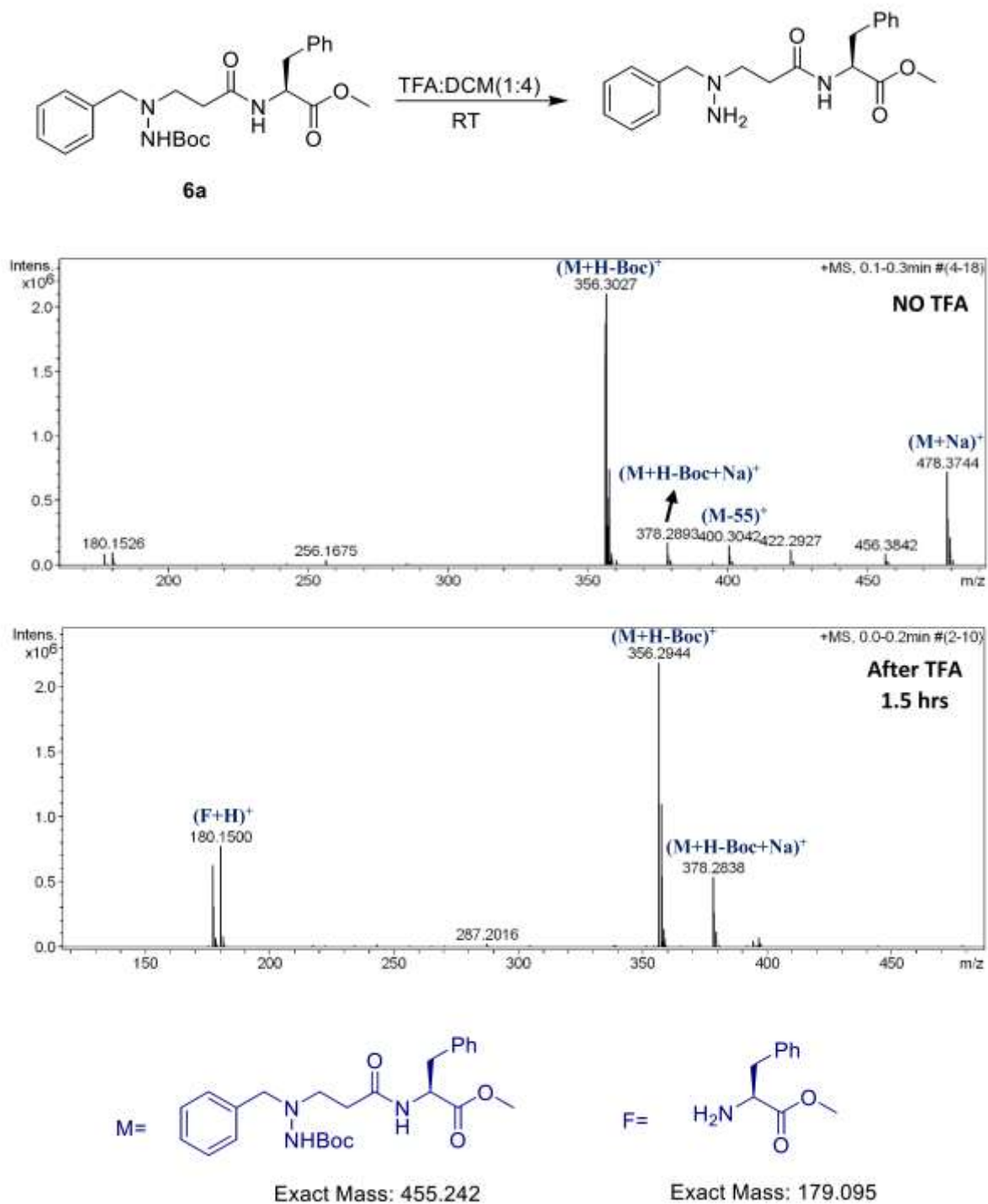
**Figure A46.** ESI-MS spectra of compound **5f** at different time intervals in 30% TFA in  $\text{CH}_2\text{Cl}_2$



**Figure A47.** ESI-MS spectra of compound **5g** at different time intervals in 30% TFA in CH<sub>2</sub>Cl<sub>2</sub>

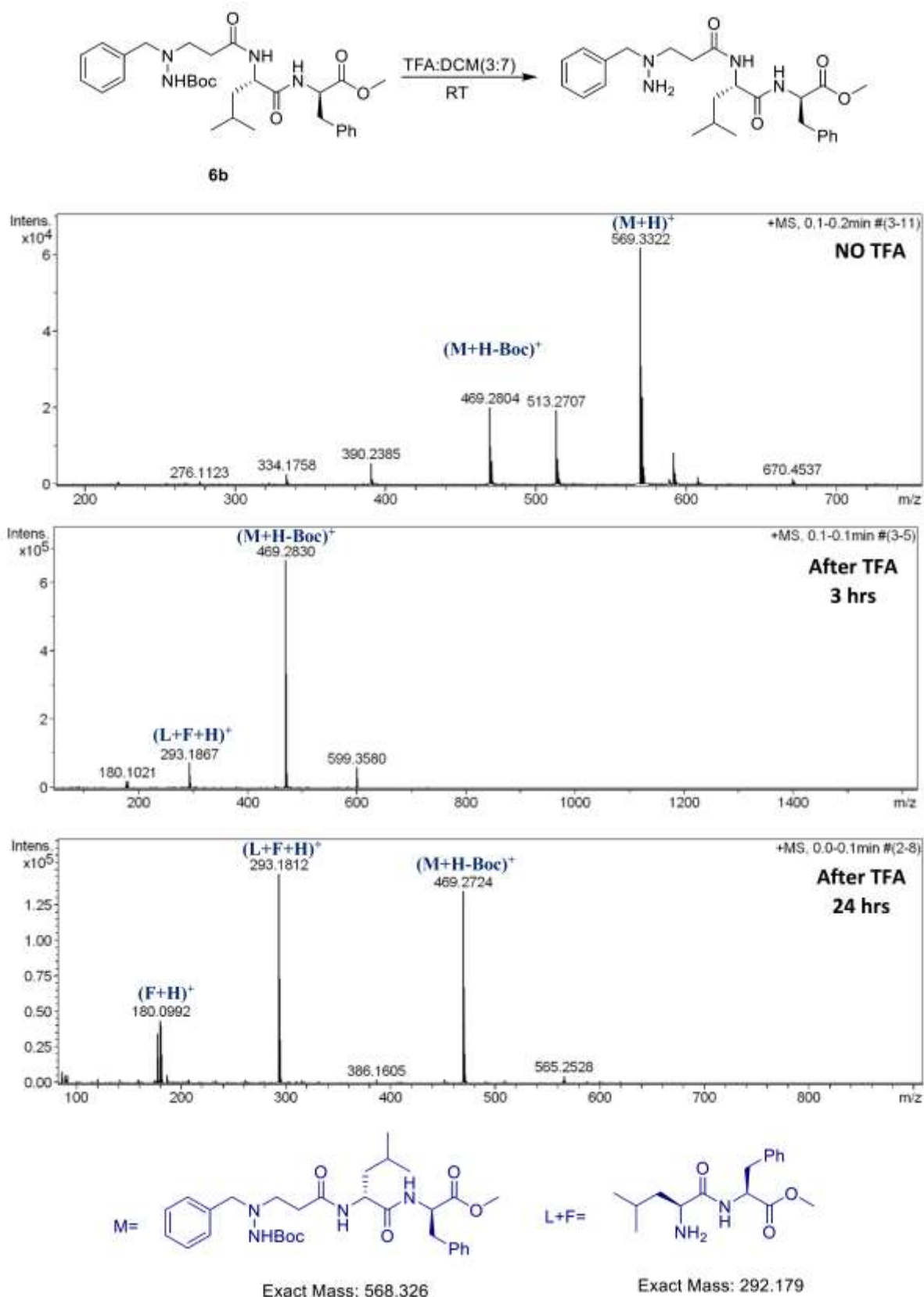


**Figure A48.** ESI-MS spectra of compound **5h** at different time intervals in 30% TFA in CH<sub>2</sub>Cl<sub>2</sub>

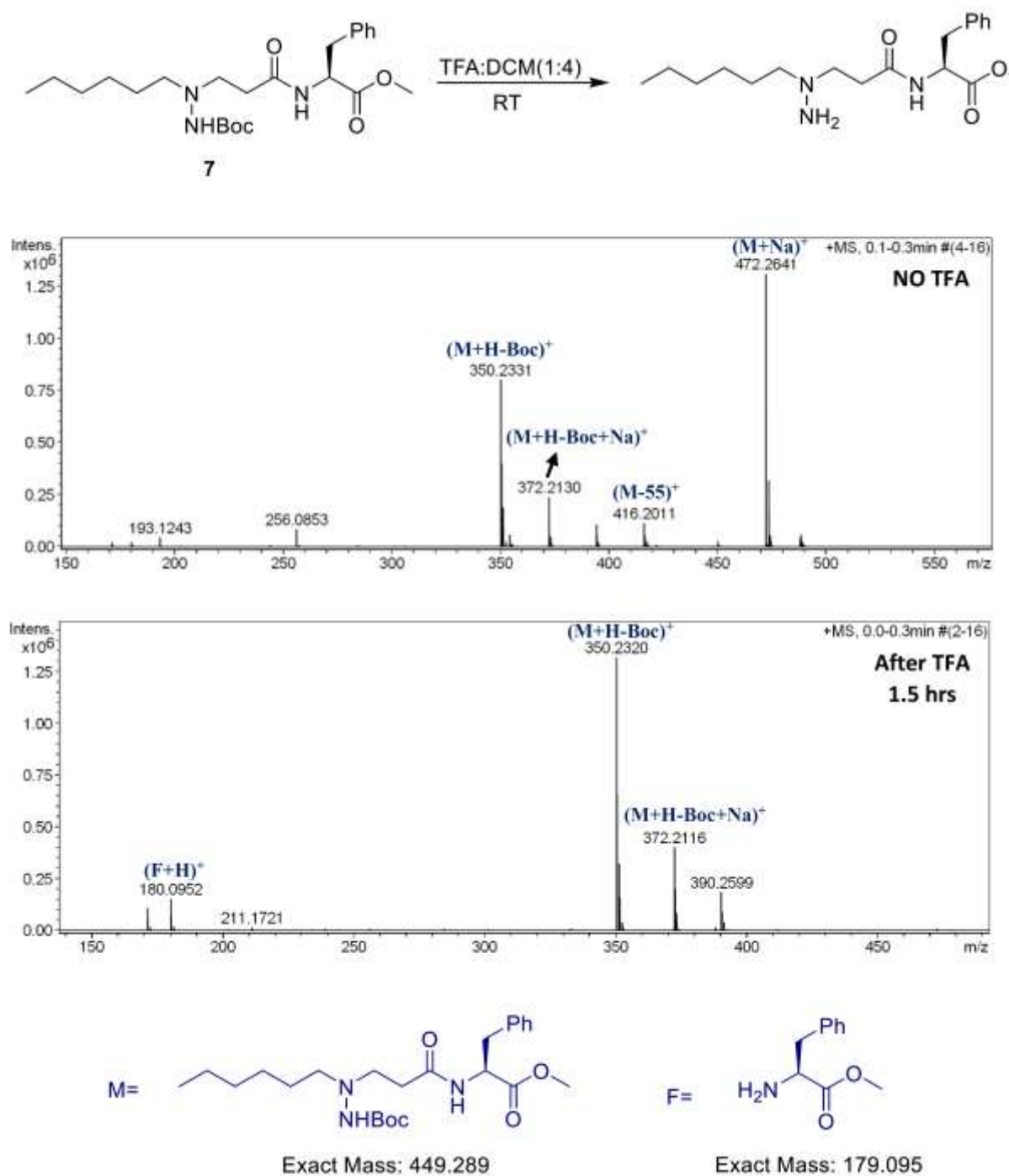
4. Mass study of Boc deprotection in compounds (**6a/6b/7/8**) in (20-30%) TFA

**Figure A49:** ESI-MS spectra of compound **6a** at different time intervals in 20% TFA in  $\text{CH}_2\text{Cl}_2$

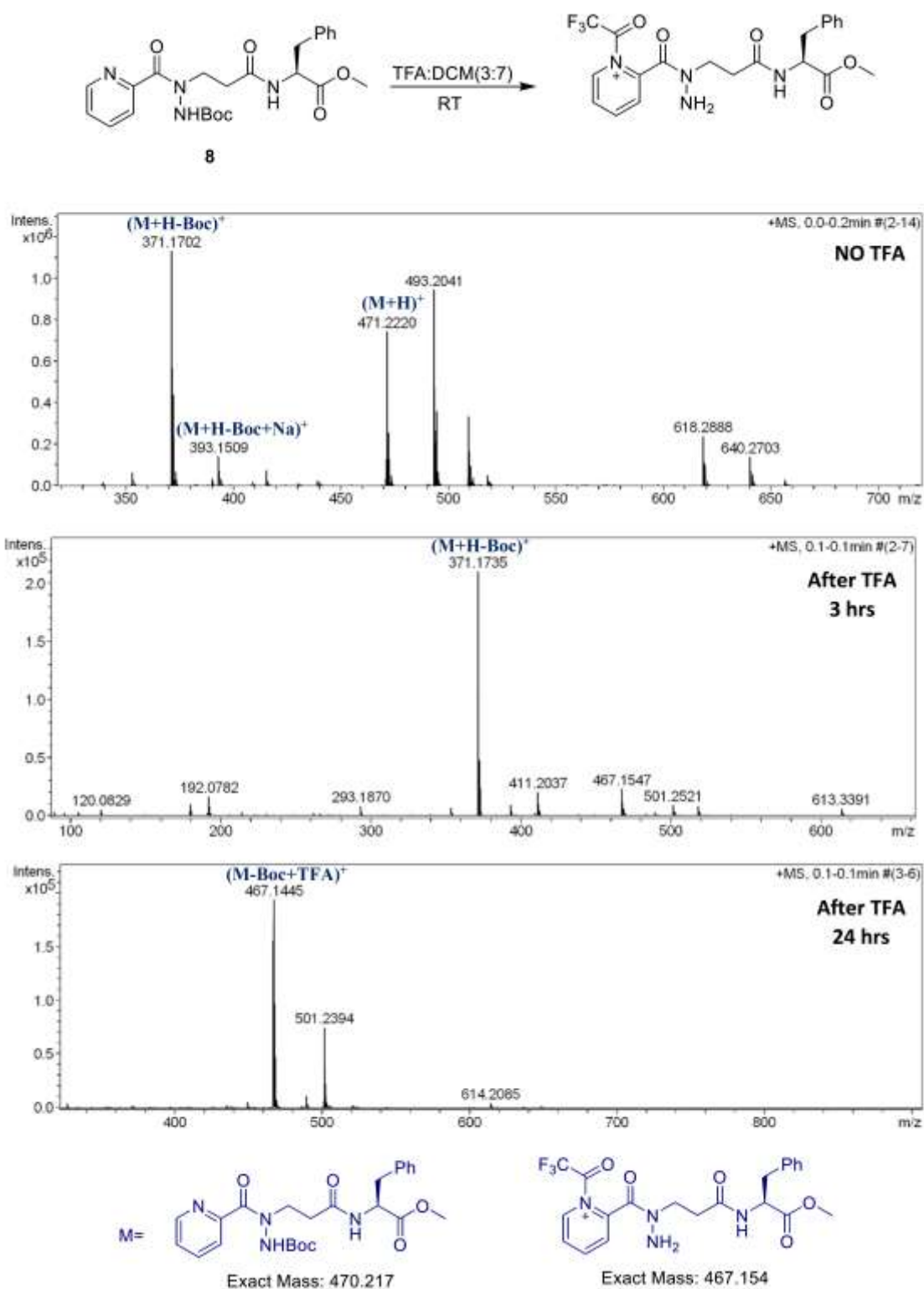




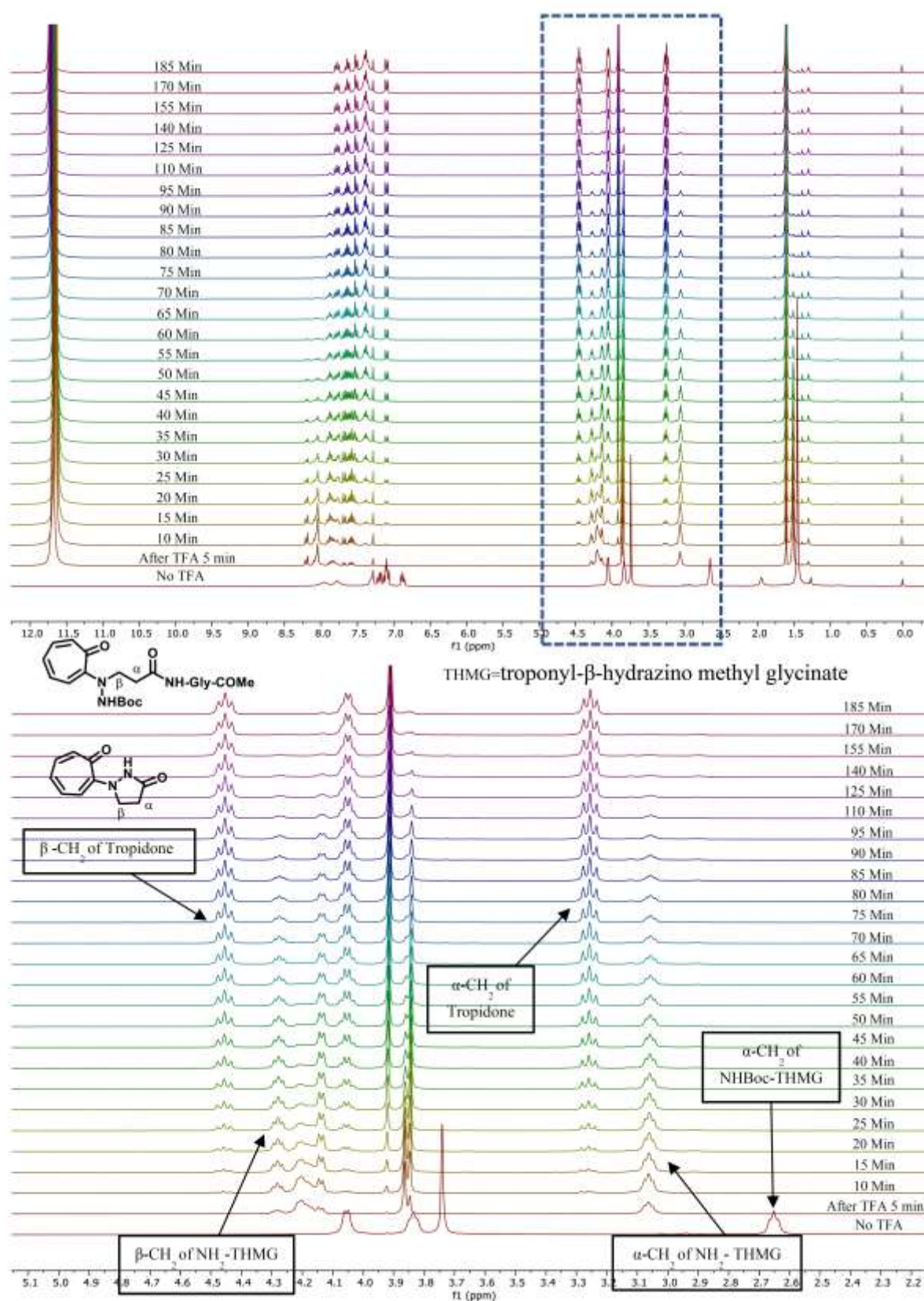
**Figure A50.** ESI-MS spectra of compound **6b** at different time intervals in 30% TFA in  $\text{CH}_2\text{Cl}_2$



**Figure A51.** ESI-MS spectra of compound **8** at different time intervals in 20% TFA in CH<sub>2</sub>Cl<sub>2</sub>



**Figure A52.** ESI-MS spectra of compound **7** at different time intervals in 30% TFA in CH<sub>2</sub>Cl<sub>2</sub>

5. Time dependent  $^1\text{H}$ -NMR spectra of amide bond hydrolysis in compounds (**5a/5b**)**Figure A53.** Time dependent  $^1\text{H}$ -NMR spectra of amide bond hydrolysis in compound (**5a**)



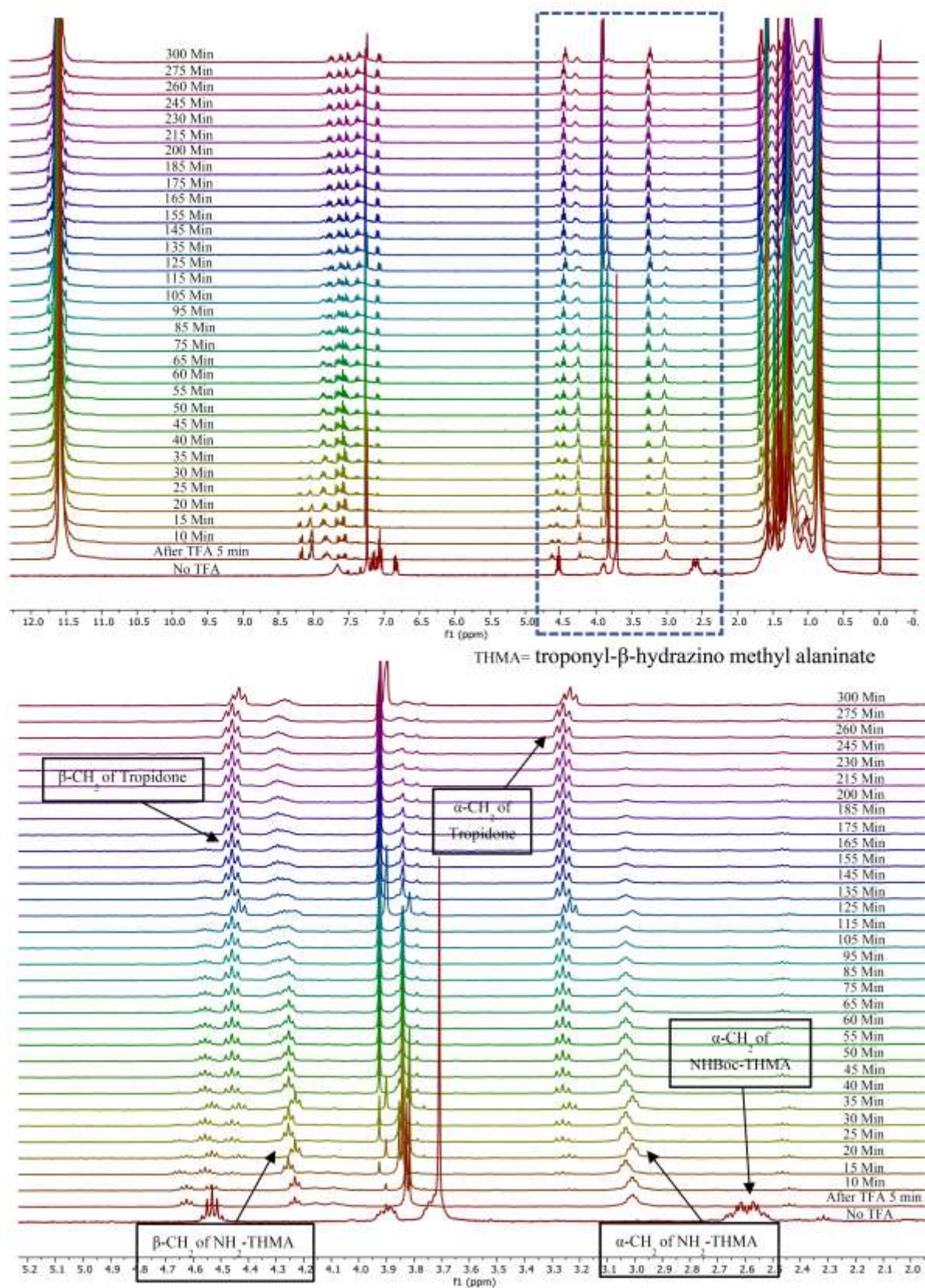
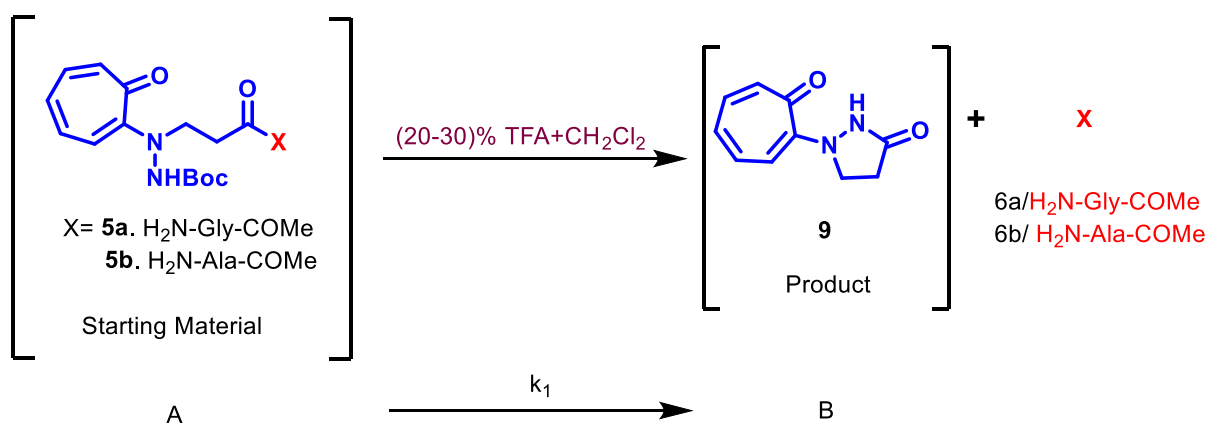


**Figure A54.** Time dependent  $^1\text{H}$ -NMR spectra of amide bond hydrolysis in compound (5b)

6. Determination of rate constants ( $k_1$ ) and half-life ( $t_{1/2}$ ) of peptide derivatives (**5a/5b**)

Procedure for rate constant determination for compounds troponyl- $\beta$ -hydrazino methyl glycinate (**5a**) and troponyl- $\beta$ -hydrazino methyl alaninate (**5b**): ~10 mg of troponyl- $\beta$ -hydrazino peptides was taken in 560  $\mu$ L of  $\text{CDCl}_3$  solution and its  $^1\text{H}$ NMR has been studied (Figure A52 and A53) before the addition of TFA then 140  $\mu$ L of TFA added to the  $\text{CDCl}_3$  solution, then every 5-15 min interval the spectra of troponyl- $\beta$ -hydrazino peptides were acquired. All the spectra baselines were corrected and solvent residual peak (TMS) were adjusted to zero. All the spectra were overlapped for precise integration and integrated using MestReNova NMR software. The mole fractions (x) were calculated from their desired peaks from area under the anticipated peak. From integrated NMR spectra, the Mole fraction (x) of  $\alpha\text{-CH}_2$  of troponyl- $\beta$ -hydrazino (Starting Material) peptide and Tropidone (Product) vs. time is plotted. The integral plots of Mole fraction (x) vs. Time were used to calculate the rate constants. After plotting the graph, we find out that the compounds compounds troponyl- $\beta$ -hydrazino methyl glycinate (**5a**) and troponyl- $\beta$ -hydrazino methyl alaninate (**5b**) are following consecutive first order kinetic pathway. Their rate laws are shown as



$$[B] = [A]_0 e^{-k_1 t} \dots\dots\dots (1)$$

$A_0$  = Initial of concentration of starting material (A) at time zero, (initial integral value)

T = Time;  $k_1$  = rate constants of the reaction;

Half-life of reaction ( $t_{1/2}$ ) =  $\ln(2)/k$

Rate constant and half-life of hybrid peptide (**5a**) and (**5b**): Herein we calculated the rate constant for hydrolysis of troponyl- $\beta$ -hydrazino peptides (**5a**) and (**5b**) with 20% TFA in  $\text{CDCl}_3$  by time dependent  $^1\text{H-NMR}$  studies. We have extracted integration of  $\beta\text{-CH}_2$  of troponyl- $\beta$ -hydrazino peptide and Tropidone at different interval of time by considering the  $\text{CH}_2$  residue troponyl- $\beta$ -hydrazino peptides (**5a**) and (**5b**) as reference with integration of 2.0.

**Table A1.** Integration of the  $\alpha\text{-CH}_2$  of troponyl- $\beta$ -hydrazino methyl glycinate (**5a**) and  $\alpha\text{-CH}_2$  of Tropidone at different time interval from their  $^1\text{H-NMR}$  spectra

S.No	Time	SM	Pdt	Total Integration	X of SM	X of Pdt	ln of X of SM	ln of X of Pdt
1	0	2	0	2	1	0	0	
2	5	1.9	0.15	2.05	0.9268293	0.073170732	-0.075985907	-2.614959778
3	10	1.87	0.23	2.1	0.8904762	0.10952381	-0.115998914	-2.211613315
4	15	1.72	0.31	2.03	0.8472906	0.15270936	-0.165711502	-1.879218775
5	20	1.67	0.43	2.1	0.7952381	0.204761905	-0.229113718	-1.585907415
6	25	1.54	0.55	2.09	0.7368421	0.263157895	-0.30538165	-1.335001067
7	30	1.43	0.66	2.09	0.6842105	0.315789474	-0.379489622	-1.15267951
8	35	1.33	0.79	2.12	0.6273585	0.372641509	-0.466237146	-0.987138422
9	40	1.17	0.87	2.04	0.5735294	0.426470588	-0.555946059	-0.852211875
10	45	1.06	0.95	2.01	0.5273632	0.472636816	-0.639865814	-0.749428016
11	50	0.97	1.06	2.03	0.4778325	0.522167488	-0.738495001	-0.649766885
12	55	0.86	1.11	1.97	0.4365482	0.563451777	-0.828856432	-0.573673527
13	60	0.79	1.2	1.99	0.3969849	0.603015075	-0.923856972	-0.505813082
14	65	0.73	1.3	2.03	0.3596059	0.640394089	-1.022746538	-0.445671529
15	70	0.65	1.33	1.98	0.3282828	0.671717172	-1.113879761	-0.397917902
16	75	0.58	1.36	1.94	0.2989691	0.701030928	-1.207415149	-0.355203273
17	80	0.54	1.45	1.99	0.2713568	0.728643216	-1.304320778	-0.316571082
18	85	0.49	1.5	1.99	0.2462312	0.753768844	-1.401484527	-0.282669531
19	90	0.45	1.54	1.99	0.2261307	0.773869347	-1.486642335	-0.256352222
20	95	0.43	1.69	2.12	0.2028302	0.797169811	-1.595386159	-0.22668756
21	110	0.32	1.65	1.97	0.1624365	0.837563452	-1.817467826	-0.177258255
22	125	0.25	1.71	1.96	0.127551	0.87244898	-2.059238834	-0.136451103
23	140	0.21	1.78	1.99	0.1055276	0.894472362	-2.248782387	-0.111521274
24	155	0.18	1.85	2.03	0.08867	0.911330049	-2.422834221	-0.092850154
25	170	0.18	1.86	2.04	0.0882353	0.911764706	-2.427748236	-0.09237332
26	185	0.14	1.86	2	0.07	0.93	-2.659260037	-0.072570693

SM = Starting Material, Pdt = Product, X = Mole Fraction

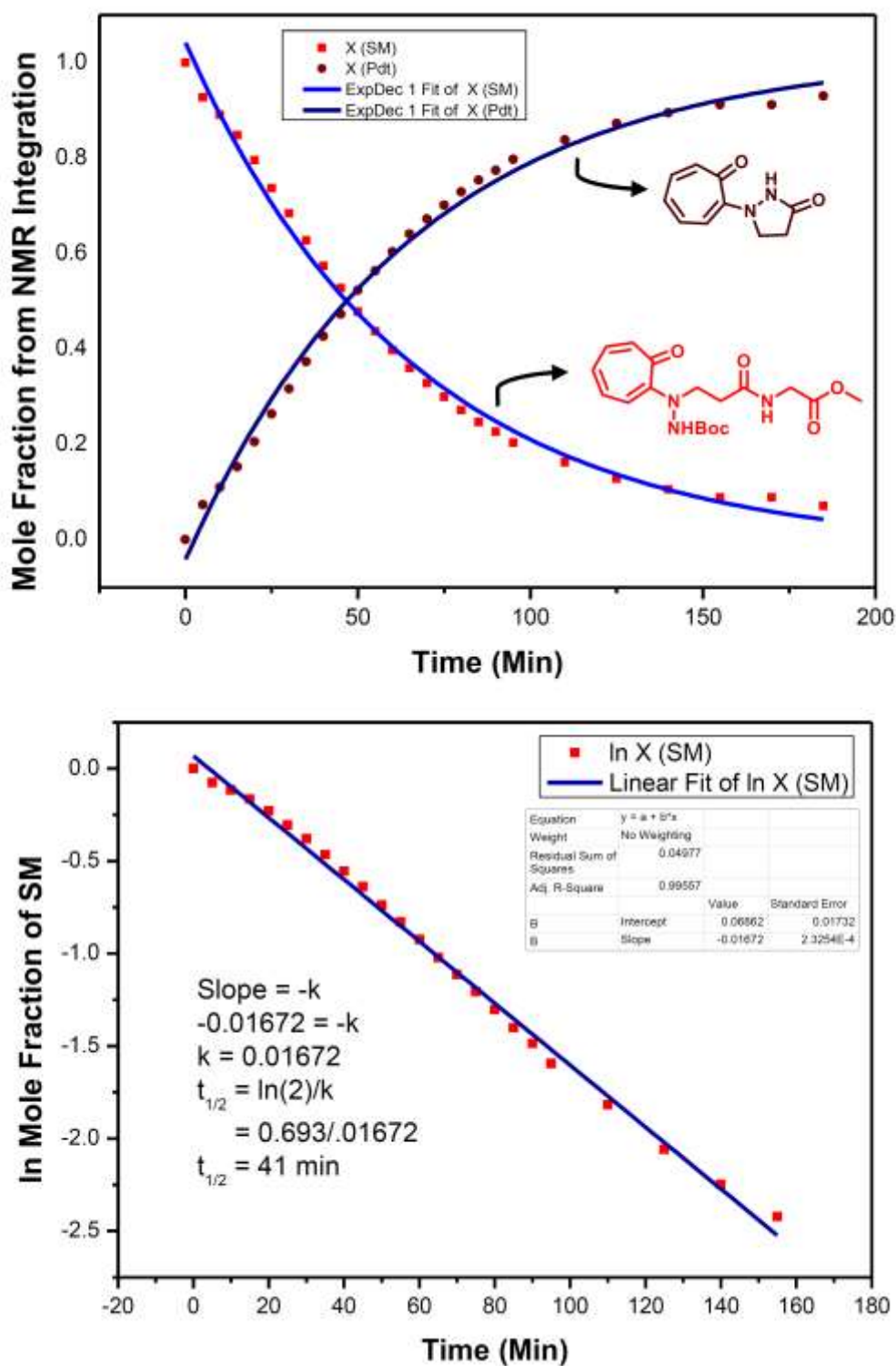


**Figure A55.** Time-dependent  $^1\text{H}$ -NMR kinetic plot-Mole Fraction vs. Time (min) with hybrid peptide **5a** (A) and its exponential plot for half-life calculation (B).



**Table A2.** Integration of the  $\alpha$ -CH<sub>2</sub> of troponyl- $\beta$ -hydrazino methyl alaninate (**5b**) and  $\alpha$ -CH<sub>2</sub> of Tropidone at different time interval from their <sup>1</sup>H-NMR spectra

S.No	Time	SM	Pdt	Total Integration	X of SM	X of Pdt	ln of X of SM	ln of X of Pdt
1	0	2	0	2	1	0	0	
2	5	1.97	0	1.97	1	0	0	
3	10	1.98	0.06	2.04	0.970588235	0.02941176	-0.02985296	-3.52636052
4	15	1.86	0.14	2.00	0.93	0.07	-0.07257069	-2.65926004
5	20	1.7	0.23	1.93	0.880829016	0.11917098	-0.12689175	-2.12719597
6	25	1.81	0.34	2.15	0.841860465	0.15813953	-0.172141	-1.8442775
7	30	1.75	0.44	2.19	0.799086758	0.20091324	-0.22428576	-1.6048821
8	35	1.58	0.53	2.11	0.748815166	0.25118483	-0.2892631	-1.38156622
9	40	1.6	0.62	2.22	0.720720721	0.27927928	-0.32750357	-1.275543
10	45	1.52	0.71	2.23	0.68161435	0.31838565	-0.38329125	-1.14449189
11	50	1.46	0.81	2.27	0.643171806	0.35682819	-0.4413434	-1.03050086
12	55	1.37	0.9	2.27	0.603524229	0.39647577	-0.50496909	-0.92514035
13	60	1.34	0.96	2.3	0.582608696	0.4173913	-0.54023951	-0.87373112
14	65	1.24	0.99	2.23	0.556053812	0.44394619	-0.58689021	-0.81205192
15	75	1.09	1.19	2.28	0.478070175	0.52192982	-0.73799775	-0.65022214
16	85	0.97	1.37	2.34	0.414529915	0.58547009	-0.88061014	-0.53534019
17	95	0.9	1.44	2.34	0.384615385	0.61538462	-0.95551145	-0.48550782
18	105	0.83	1.54	2.37	0.35021097	0.64978903	-1.04921953	-0.43110754
19	115	0.7	1.58	2.28	0.307017544	0.69298246	-1.18085039	-0.3667506
20	125	0.66	1.73	2.39	0.276150628	0.72384937	-1.28680881	-0.32317196
21	135	0.58	1.79	2.37	0.244725738	0.75527426	-1.40761713	-0.28067434
22	145	0.54	1.81	2.35	0.229787234	0.77021277	-1.47060147	-0.26108848
23	155	0.49	1.91	2.4	0.204166667	0.795833333	-1.58881863	-0.2283655
24	165	0.43	1.91	2.34	0.183760684	0.81623932	-1.694121	-0.20304769
25	175	0.4	1.92	2.32	0.172413793	0.82758621	-1.75785792	-0.189242
26	185	0.39	1.95	2.34	0.166666667	0.833333333	-1.79175947	-0.18232156
27	200	0.35	1.99	2.34	0.14957265	0.85042735	-1.89997305	-0.16201629
28	215	0.3	2.04	2.34	0.128205128	0.87179487	-2.05412373	-0.13720112
29	230	0.26	2.14	2.4	0.108333333	0.89166667	-2.22254239	-0.11466291
30	245	0.26	2.07	2.33	0.111587983	0.88841202	-2.19294192	-0.11831966
31	260	0.2	2.16	2.36	0.084745763	0.91525424	-2.46809953	-0.0885534
32	275	0.16	2.14	2.3	0.069565217	0.93043478	-2.66549059	-0.07210329
33	300	0.13	2.21	2.34	0.055555556	0.944444444	-2.89037176	-0.05715841

SM = Starting Material, Pdt = Product, X = Mole Fraction

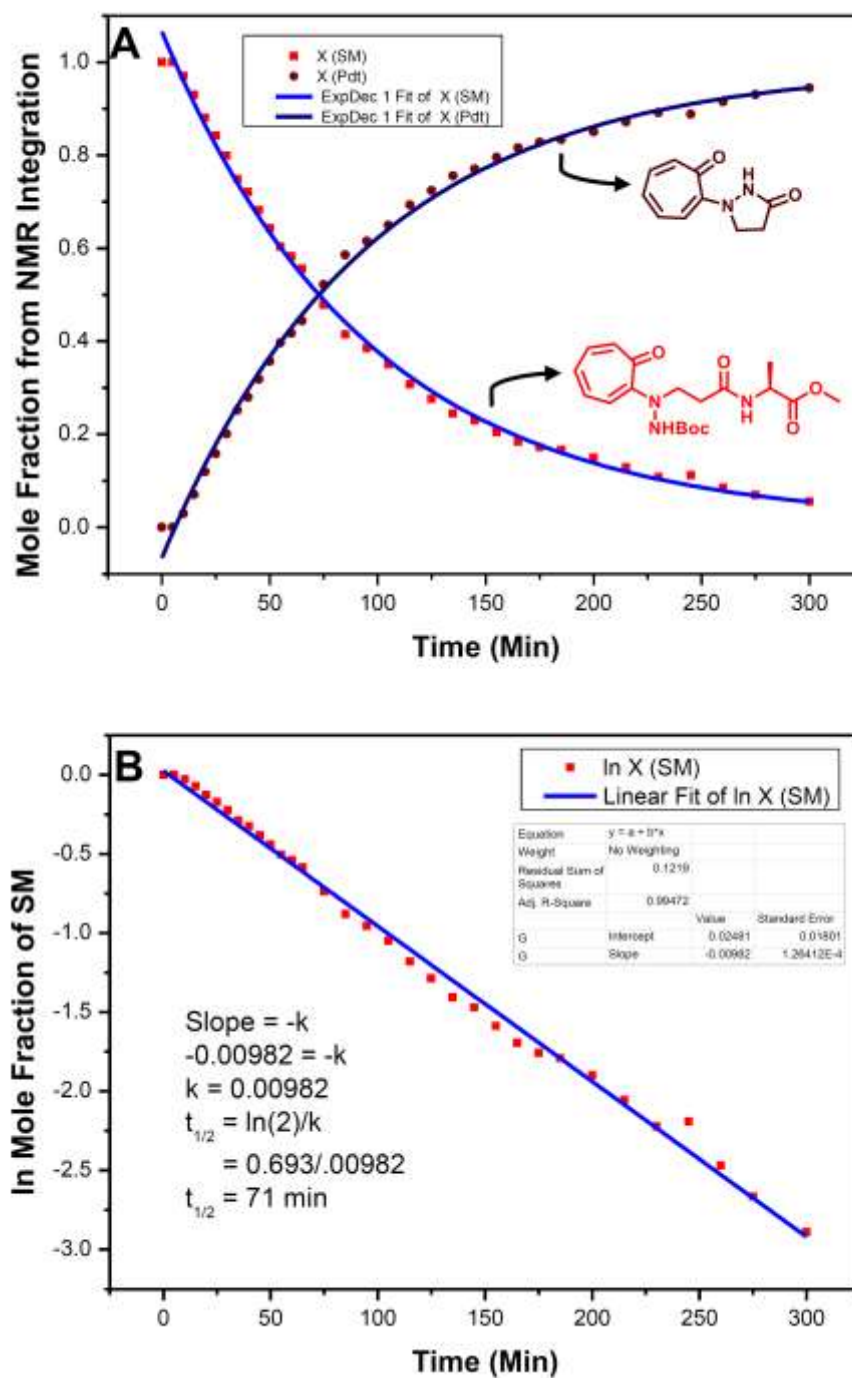
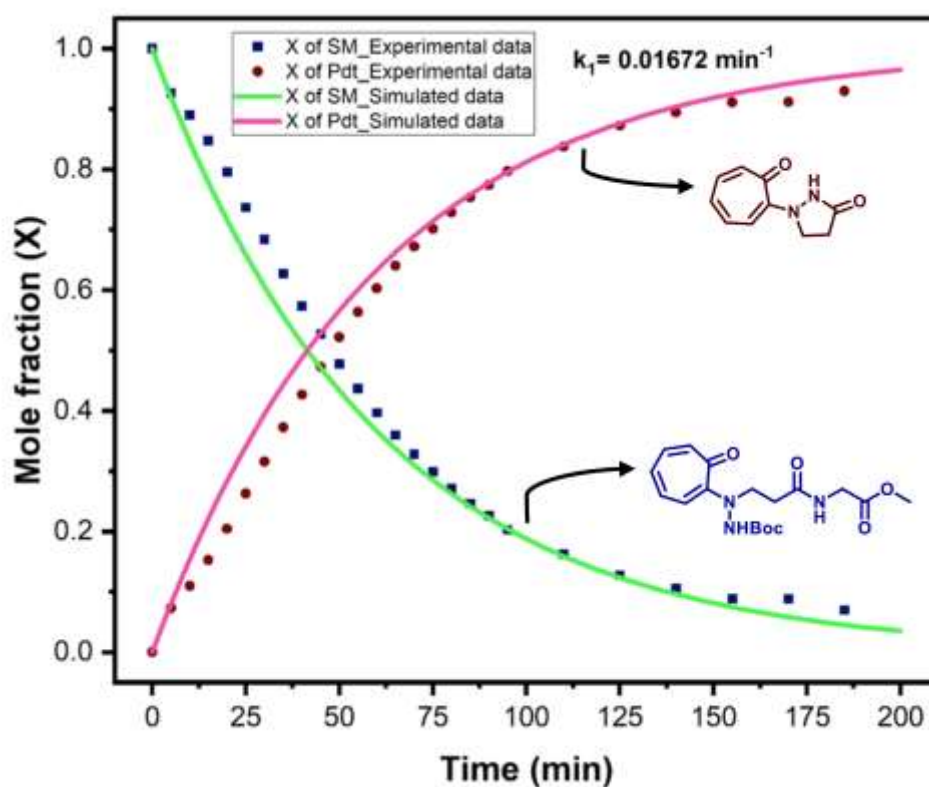


**Figure A56.** Time-dependent  $^1\text{H}$ -NMR kinetic plot-Mole Fraction vs. Time (min) with hybrid peptide **5b** (A); and its exponential plot for half-life calculation (B).

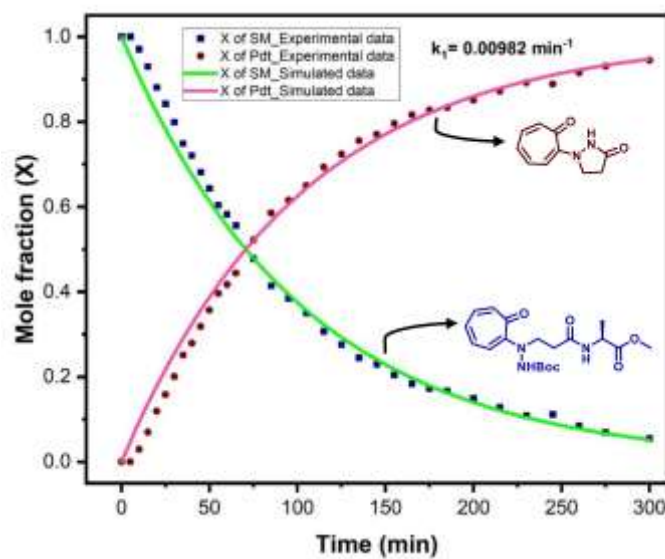
## 7. COPASI Modelling Procedure and Results

COPASI is software application for simulation and analyses of biochemical networks and their dynamics. Herein we use COPASI software for kinetic modelling and compared our experimental result with stimulated outputs. The observed rate constants were used to generate the concentration versus time fitting curves in the model, with initial volume of 0.5 ml and initial time, in minutes, as zero ( $t = 0$ ) and used with following reaction model:  $a \rightarrow b$

Plots were generated using Deterministic (LSODA) method in Time Course.

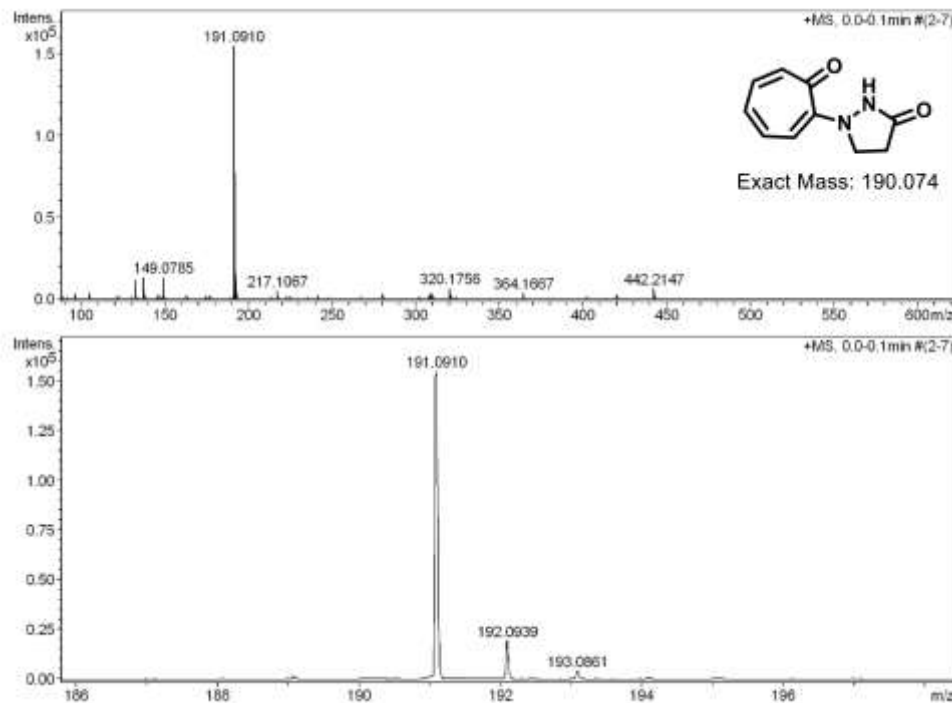


**Figure A57.** Experimental data and kinetic modelled data fitting (in COPASI) for hybrid dipeptide (**5a**).



**Figure A58.** Experimental data and kinetic modelled data fitting (in COPASI) for hybrid dipeptide (**5b**).

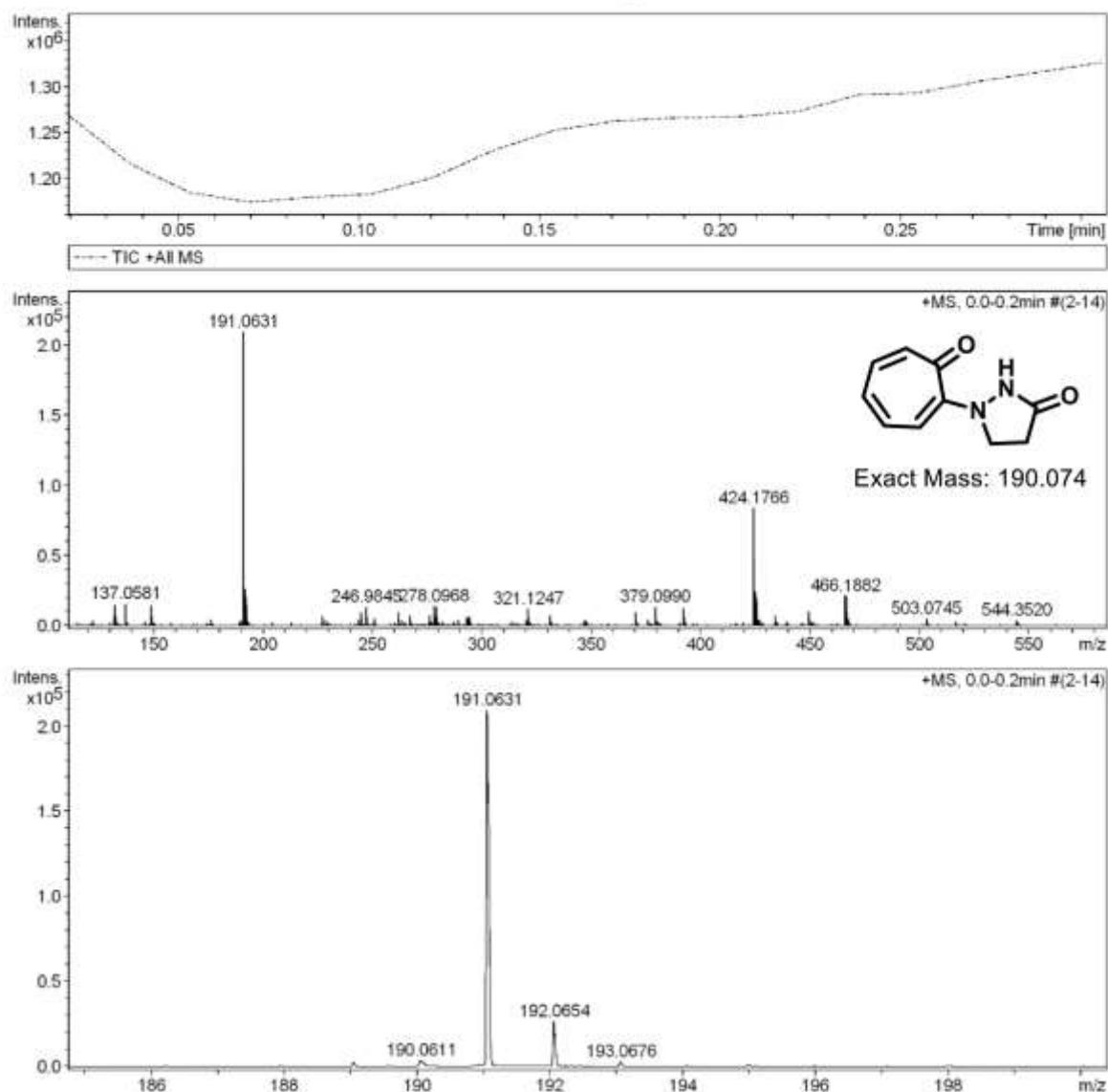
#### 8. ESI-MS spectra of compound (**5a/5b**) after time dependent NMR



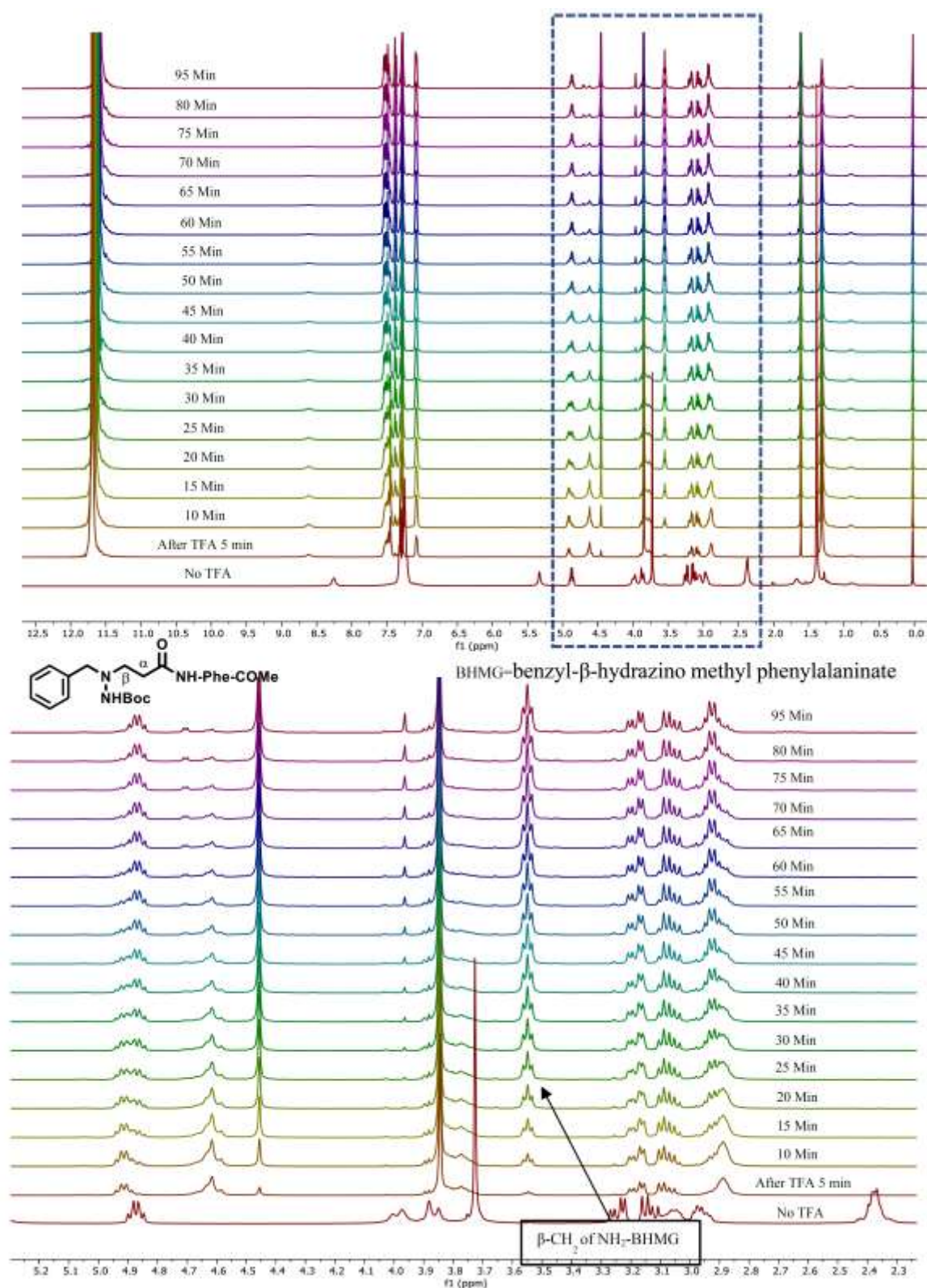
**Figure A59.** ESI-MS spectrum of amide bond hydrolysis (formation of Tropidone **9**) in hybrid dipeptide (**5a**) after time-dependent NMR

## Acquisition Parameter

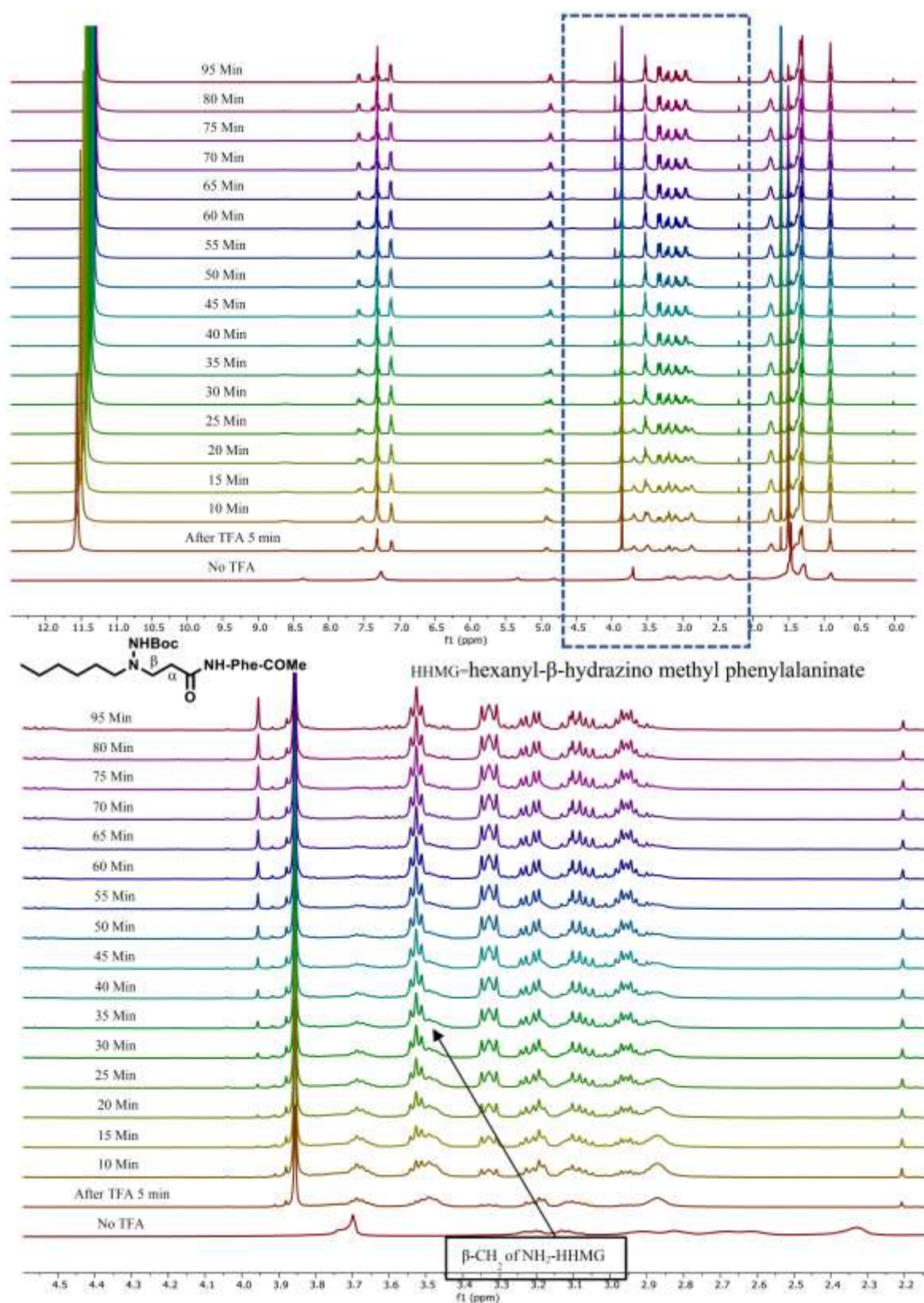
Source Type	ESI	Ion Polarity	Positive	Set Nebulizer	0.5 Bar
Focus	Not active	Set Capillary	4500 V	Set Dry Heater	180 °C
Scan Begin	50 m/z	Set End Plate Offset	-500 V	Set Dry Gas	4.0 l/min
Scan End	3000 m/z	Set Collision Cell RF	130.0 Vpp	Set Divert Valve	Waste



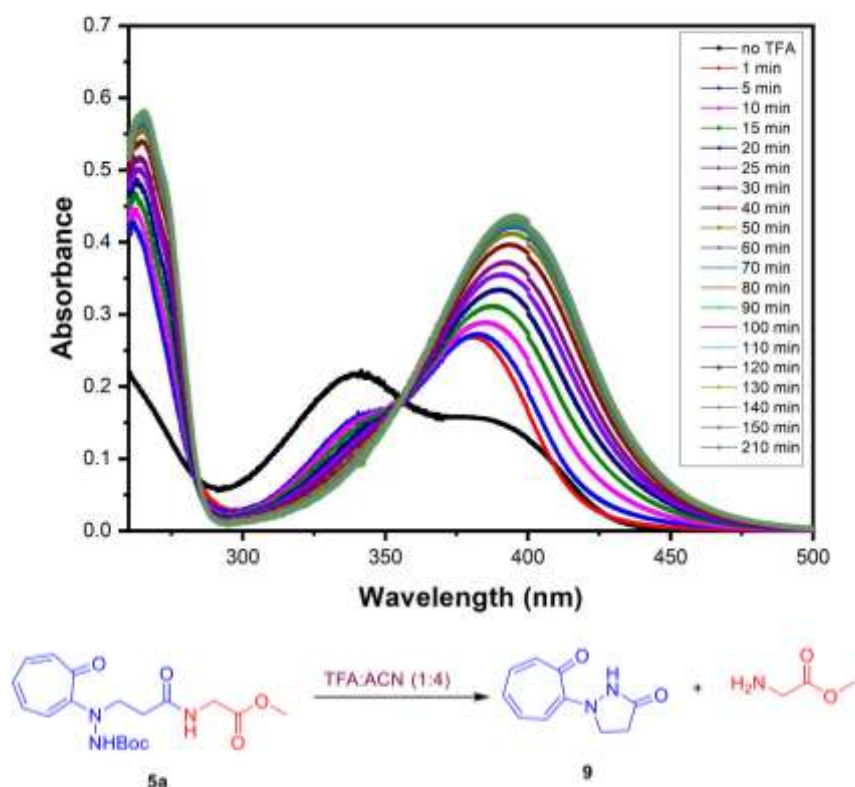
**Figure A60.** ESI-MS spectrum of amide bond hydrolysis (formation of Tropicidone **9**) in hybrid dipeptide (**5b**) after time-dependent NMR

9. Time dependent  $^1\text{H}$ -NMR spectra of Boc deprotection in compounds (**6a/8**)**Figure A61.** Time dependent  $^1\text{H}$ -NMR spectra of Boc Deprotection in compound (**6a**)

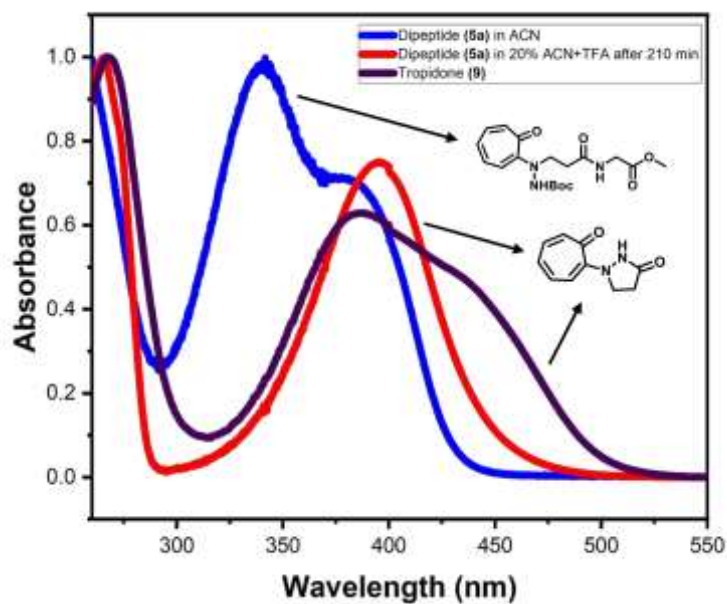




**Figure A62.** Time dependent  $^1\text{H}$ -NMR spectra of Boc Deprotection in compound (8)

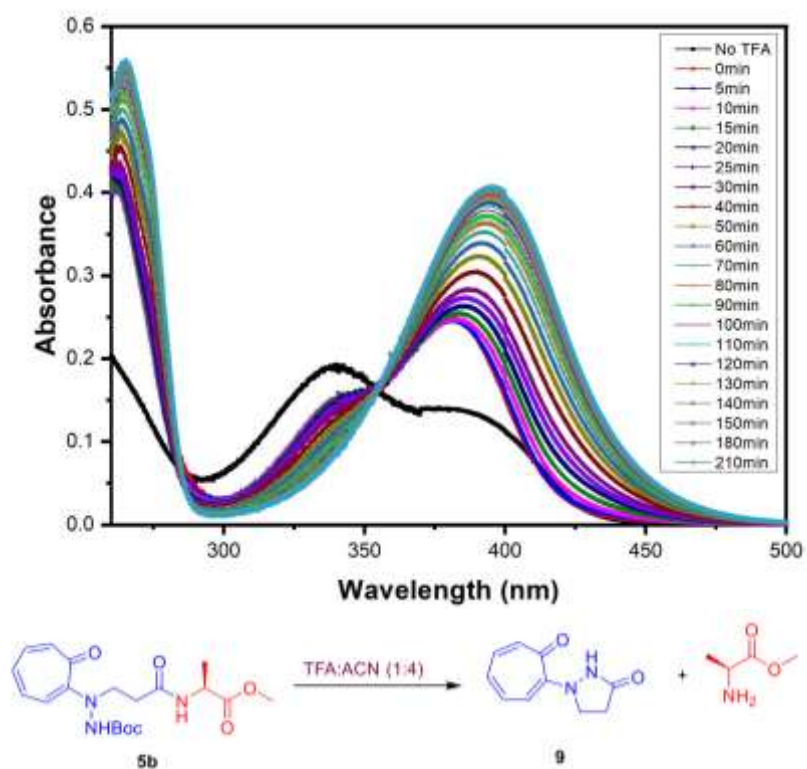
10. UV-Vis Spectroscopic studies for Tropolone (**9**) formation in hybrid dipeptide (**5a/5b**)

**Figure A63.** Amide cleavage monitoring of hybrid dipeptide **5a** by UV-Vis spectroscopy

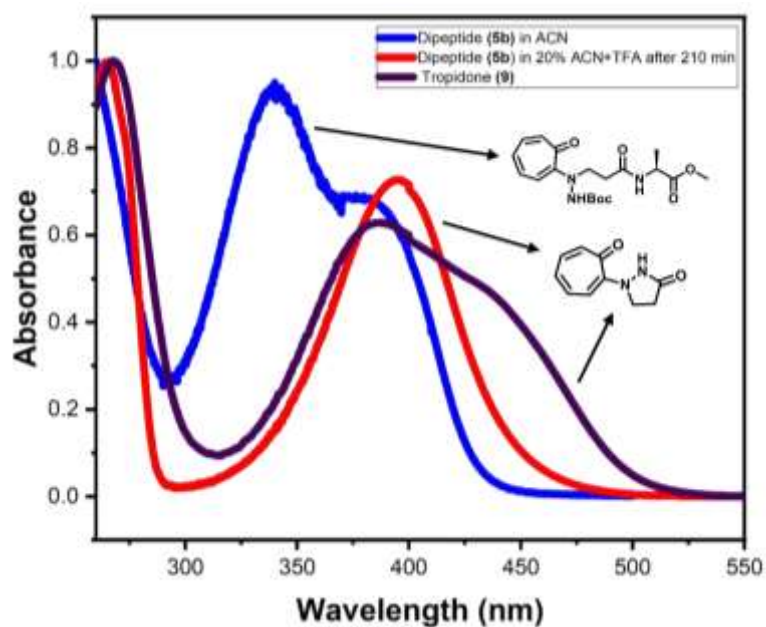


**Figure A64.** Comparison of hybrid dipeptide (**5a**) before and after TFA addition with Tropolone (**9**) by UV-Vis spectroscopy

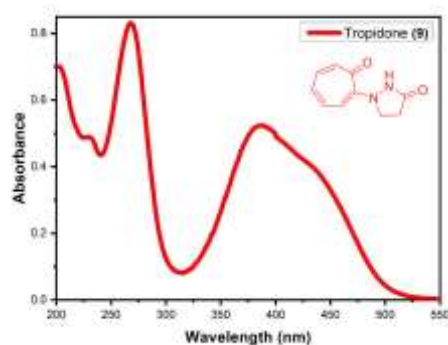




**Figure A65.** Time dependent UV-Vis spectra of peptide **5b** in 20% TFA (CH<sub>3</sub>CN)



**Figure A66.** Comparison of hybrid dipeptide (**5b**) before and after TFA addition with Tropidone (**9**) by UV-Vis spectroscopy.

11. UV-spectra of Tropidone (**9**)**Figure A67.** UV-spectra of Tropidone (**9**) in Acetonitrile12. Mass study of amide bond hydrolysis in compounds (**5a**) in different acid conditions**Table S3.** Amide bond hydrolysis in different acid condition

Reaction Condition	Compound (Starting Material)	Major Product formed after 2hrs	
30% TFA in CH <sub>2</sub> Cl <sub>2</sub>	THMG ( <b>5a</b> ) 	Amide Bond Hydrolysis	
4N HCl	THMG ( <b>5a</b> ) 	Amide Bond Hydrolysis	
4N HClO <sub>4</sub>	THMG ( <b>5a</b> ) 	Amide Bond Hydrolysis	
10eq PTSA	THMG ( <b>5a</b> ) 	Amide Bond Hydrolysis	
4N AcOH	THMG ( <b>5a</b> ) 	No Change	

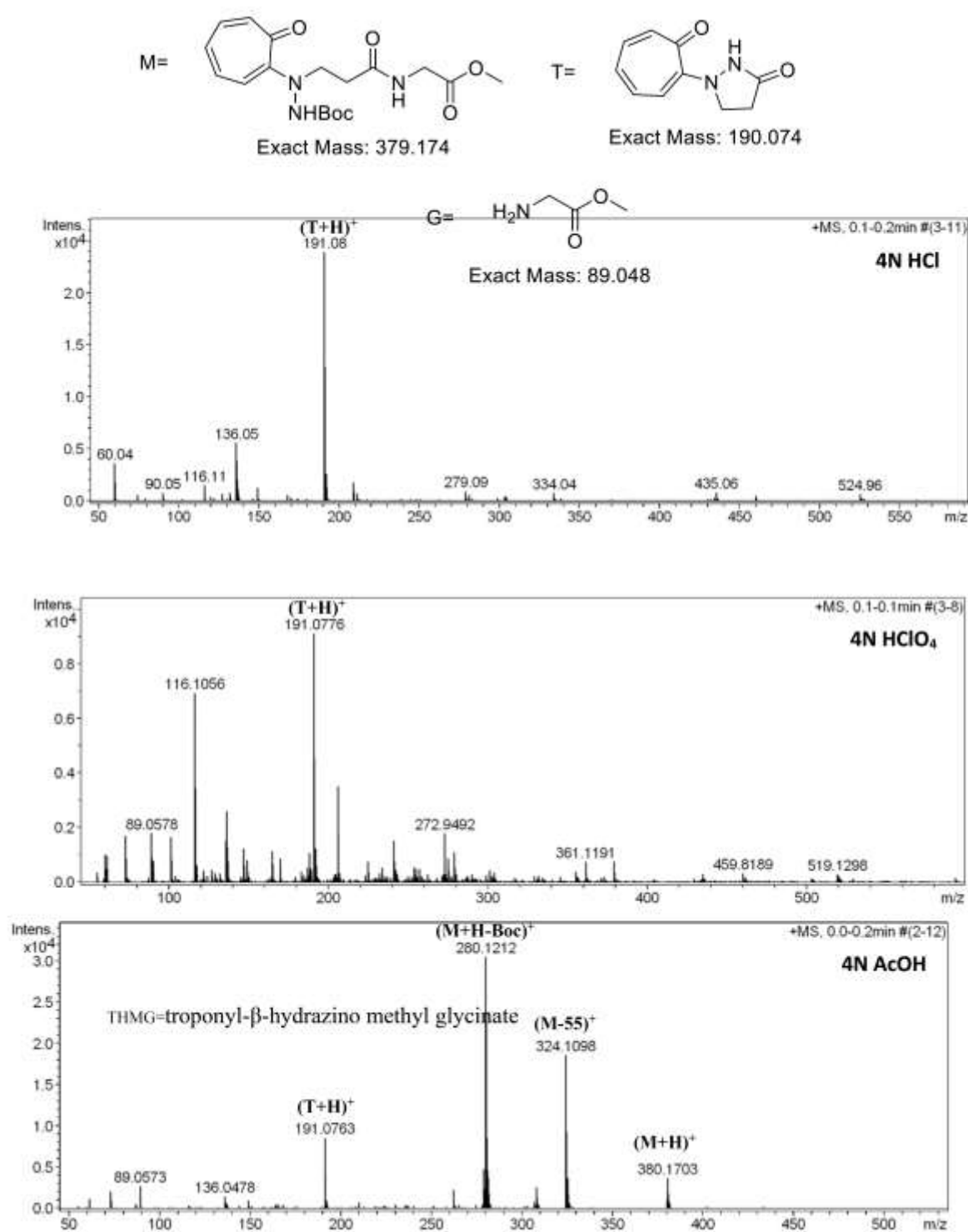


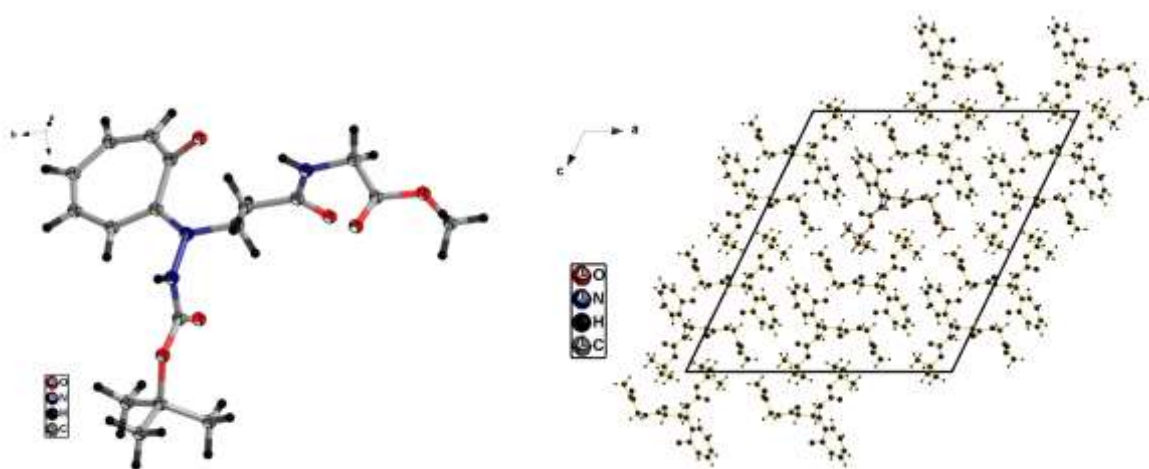
**Figure A68.** ESI-MS of hybrid dipeptide (**5a**) after 2 h in different acid (4N HCl, 4N HClO<sub>4</sub>, and 4N AcOH).

13. X-Ray crystallographic Studies of new compounds **5a/ 9/ 5h/6a**

A suitable single crystal of each complex was carefully selected under a polarizing microscope. Single crystal structure determination by X-ray diffraction was performed on a Siemens SMART-CCD diffractometer equipped with a normal focus, 2.4 kW sealed-tube X-ray source (*Mo*–*K* $\alpha$  radiation,  $\lambda = 0.71073\text{\AA}$ ) operating at 50 kV and 30 mA. Structures were solved by the direct method using SHELXT 2014 and refined on *F*<sup>2</sup> by a full-matrix least-squares technique using the SHELXL 2014 programs package. An empirical absorption correction based on symmetry equivalent reflections was applied using SADABS. The graphic programs DIAMOND 3.2 was used to draw the structures. Non-hydrogen atoms were refined anisotropically. In the refinement, hydrogens were treated as riding atoms using the SHELXL default parameters. The crystal structure of (**9**), (**5a**) and (**5h**) are deposited to the Cambridge crystallographic Data centre (CCDC) with CCDC with numbers CCDC 2003627, CCDC 2003629 and CCDC 2003628 respectively. The CCDC number of control peptide is 2003627.

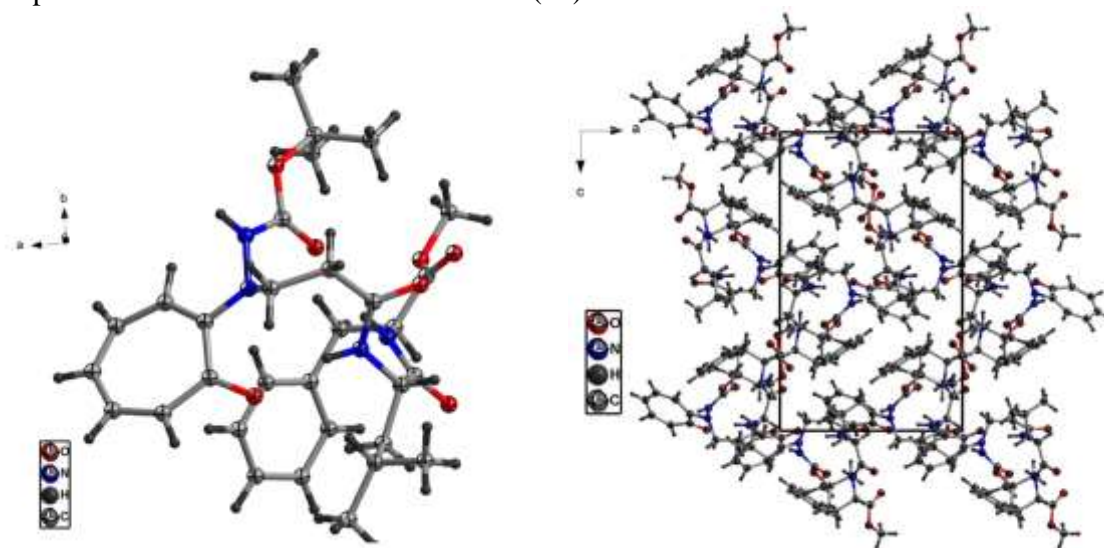
**Table A4.** Crystal data and structure refinement for Compound **5a**

CCDC Number	2003627
Identification code	data_nks_nrd_144(5a)
Empirical formula	C <sub>18</sub> H <sub>24</sub> N <sub>3</sub> O <sub>6</sub>
Formula weight	378.40
Temperature/K	293(2)
Crystal system	monoclinic
Space group	C2/c
a/Å	26.555(10)
b/Å	6.0271(13)
c/Å	28.976(13)
$\alpha/^\circ$	90
$\beta/^\circ$	115.99(5)
$\gamma/^\circ$	90
Volume/Å <sup>3</sup>	4168(3)
Z	8
$\rho_{\text{calc}}/\text{cm}^3$	1.206
$\mu/\text{mm}^{-1}$	0.091
F(000)	1608.0
Crystal size/mm <sup>3</sup>	0.215 × 0.125 × 0.012
Radiation	MoK $\alpha$ ( $\lambda$ = 0.71073)
2 $\theta$ range for data collection/ $^\circ$	6.828 to 52.744
Index ranges	-29 ≤ h ≤ 32, -6 ≤ k ≤ 7, -36 ≤ l ≤ 36
Reflections collected	20924
Independent reflections	4250 [ $R_{\text{int}}$ = 0.0802, $R_{\text{sigma}}$ = 0.0638]
Data/restraints/parameters	4250/0/252
Goodness-of-fit on F <sup>2</sup>	1.001
Final R indexes [ $I \geq 2\sigma(I)$ ]	$R_1$ = 0.0617, $wR_2$ = 0.1543
Final R indexes [all data]	$R_1$ = 0.1017, $wR_2$ = 0.1731
Largest diff. peak/hole / e Å <sup>-3</sup>	0.21/-0.19

**Figure A69.** ORTEP diagram and packing diagram in unit shell of hybrid dipeptide (**5a**)

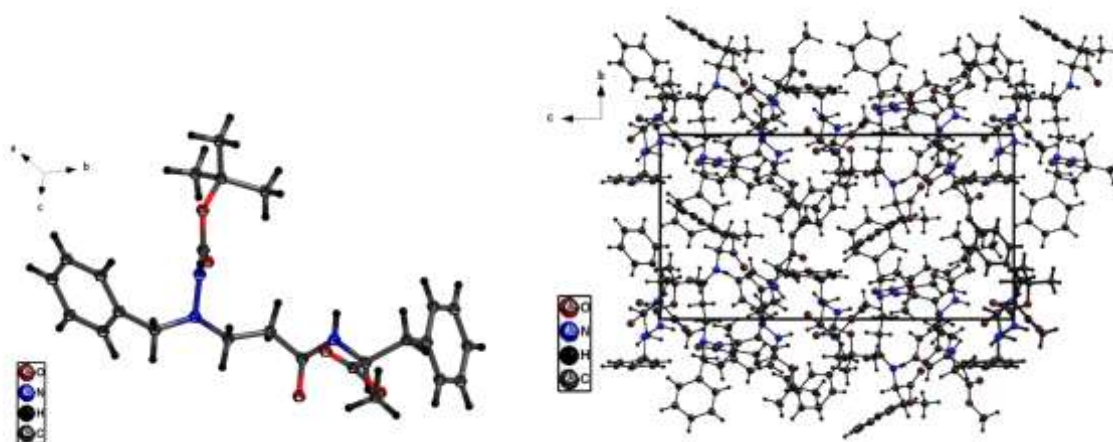
**Table A5.** Crystal data and structure refinement for Compound **5h**

CCDC	CCDC 2003628
Identification code	data_nks_nrd-tr-tptd ( <b>5h</b> )
Empirical formula	C <sub>1.97</sub> H <sub>2.67</sub> N <sub>0.25</sub> O <sub>0.44</sub>
Formula weight	37.00
Temperature/K	296.54(18)
Crystal system	orthorhombic
Space group	P212121
a/Å	11.5951(2)
b/Å	15.3645(3)
c/Å	18.9752(5)
$\alpha/^\circ$	90
$\beta/^\circ$	90
$\gamma/^\circ$	90
Volume/Å <sup>3</sup>	3380.49(13)
Z	63
$\rho_{\text{calc}}/\text{cm}^3$	1.145
$\mu/\text{mm}^{-1}$	0.667
F(000)	1248.0
Crystal size/mm <sup>3</sup>	0.01 × 0.002 × 0.001
Radiation	CuK $\alpha$ ( $\lambda = 1.54184$ )
2 $\theta$ range for data collection/ $^\circ$	7.404 to 148.948
Index ranges	-14 ≤ h ≤ 10, -19 ≤ k ≤ 18, -23 ≤ l ≤ 23
Reflections collected	25955
Independent reflections	6767 [R <sub>int</sub> = 0.0852, R <sub>sigma</sub> = 0.0553]
Data/restraints/parameters	6767/0/389
Goodness-of-fit on F <sup>2</sup>	1.057
Final R indexes [I ≥ 2 $\sigma$ (I)]	R <sub>1</sub> = 0.0683, wR <sub>2</sub> = 0.2023
Final R indexes [all data]	R <sub>1</sub> = 0.0811, wR <sub>2</sub> = 0.2176
Largest diff. peak/hole / e Å <sup>-3</sup>	0.17/-0.28
Flack parameter	0.04(16)

**Figure A70.** ORTEP diagram and packing diagram in unit shell of hybrid tripeptide (**5h**)

**Table A6.** Crystal data and structure refinement for Compound **6a**

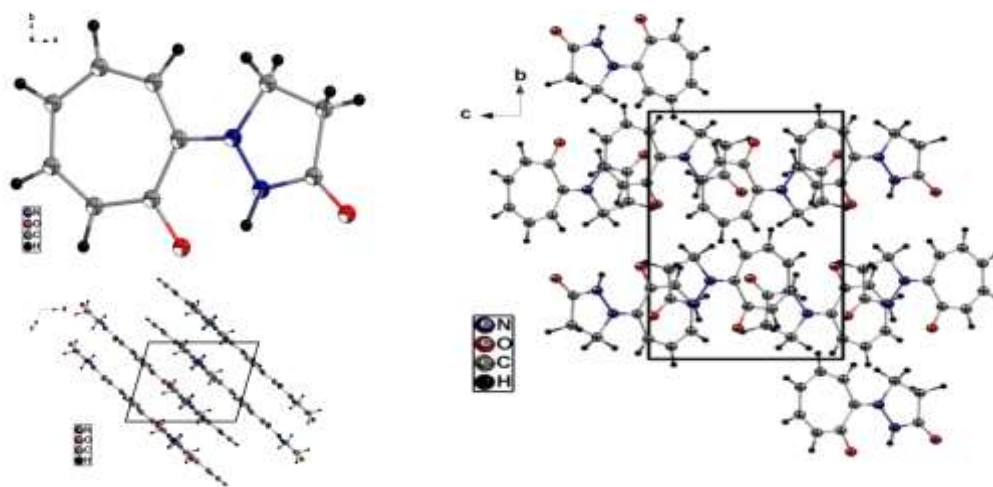
CCDC	CCDC 2003626
Identification code	data_nks_nrd_117( <b>6a</b> )
Empirical formula	C <sub>25</sub> H <sub>33</sub> N <sub>3</sub> O <sub>5</sub>
Formula weight	455.54
Temperature/K	112.1(4)
Crystal system	hexagonal
Space group	P6 <sub>1</sub>
a/Å	13.8479(6)
b/Å	13.8479(6)
c/Å	22.9802(10)
$\alpha/^\circ$	90.00
$\beta/^\circ$	90.00
$\gamma/^\circ$	120.00
Volume/Å <sup>3</sup>	3816.4(3)
Z	6
$\rho_{\text{calc}}/\text{cm}^3$	1.189
$\mu/\text{mm}^{-1}$	0.677
F(000)	1464.0
Crystal size/mm <sup>3</sup>	0.0012 $\times$ 0.0012 $\times$ 0.001
Radiation	CuK $\alpha$ ( $\lambda$ = 1.54184)
2 $\theta$ range for data collection/ $^\circ$	7.38 to 148.7
Index ranges	-14 $\leq h \leq$ 16, -17 $\leq k \leq$ 16, -27 $\leq l \leq$ 28
Reflections collected	20076
Independent reflections	4951 [ $R_{\text{int}}$ = 0.1942, $R_{\text{sigma}}$ = 0.1480]
Data/restraints/parameters	4951/1/303
Goodness-of-fit on F <sup>2</sup>	1.128
Final R indexes [ $I \geq 2\sigma(I)$ ]	$R_1$ = 0.1121, $wR_2$ = 0.2865
Final R indexes [all data]	$R_1$ = 0.1417, $wR_2$ = 0.3197
Largest diff. peak/hole / e Å <sup>-3</sup>	0.43/-0.57
Flack parameter	0.3(5)

**Figure A71.** ORTEP diagram and packing diagram in unit shell of hybrid tripeptide (**6a**)



**Table A7:** Crystal data and structure refinement for Tropicone (**9**)

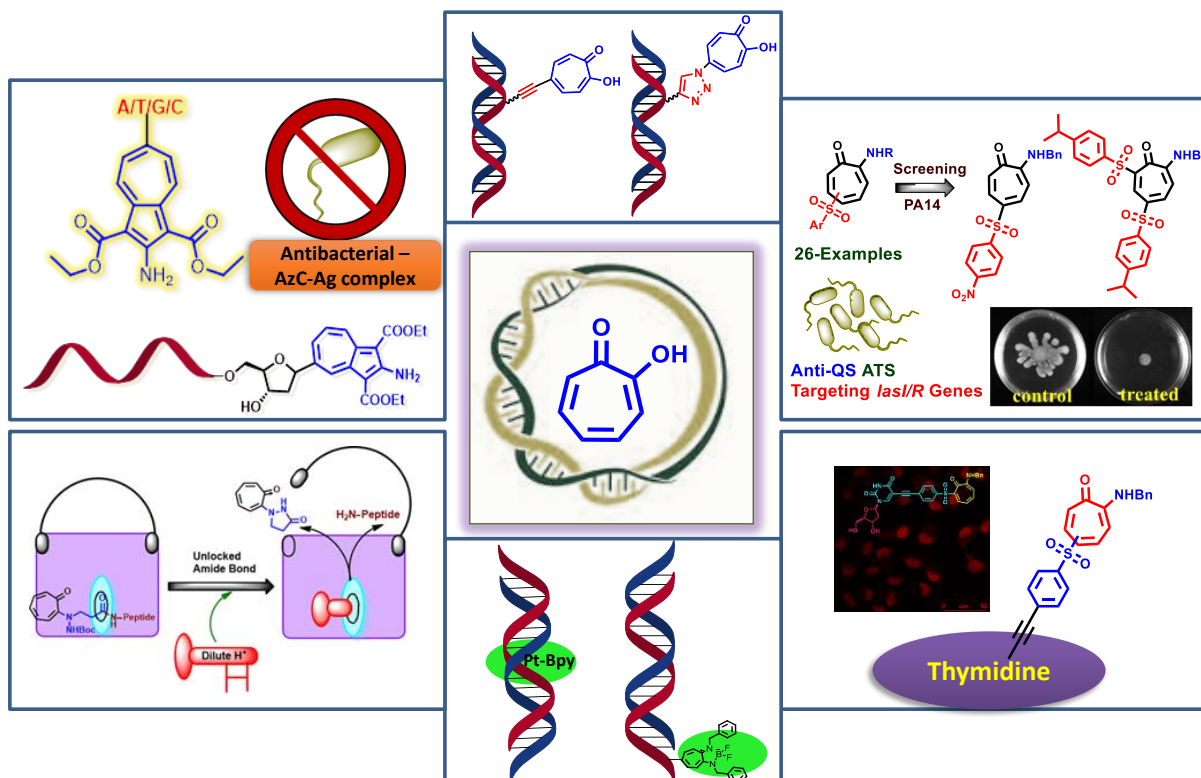
CCDC	2003627
Identification code	data_NKS_NRD_50 ( <b>9</b> )
Empirical formula	C <sub>10</sub> H <sub>10</sub> N <sub>2</sub> O <sub>2</sub>
Formula weight	190.20
Temperature/K	298.0
Crystal system	monoclinic
Space group	P2 <sub>1</sub> /c
a/Å	9.7164(4)
b/Å	12.3920(4)
c/Å	7.6809(3)
$\alpha/^\circ$	90
$\beta/^\circ$	105.389(4)
$\gamma/^\circ$	90
Volume/Å <sup>3</sup>	891.67(6)
Z	4
$\rho_{\text{calc}}/\text{cm}^3$	1.4167
$\mu/\text{mm}^{-1}$	0.834
F(000)	401.4
Crystal size/mm <sup>3</sup>	0.001 × 0.0001 × 0.0001
Radiation	Cu K $\alpha$ ( $\lambda$ = 1.54184)
2 $\Theta$ range for data collection/ $^\circ$	9.44 to 153.88
Index ranges	-11 ≤ h ≤ 12, -15 ≤ k ≤ 12, -9 ≤ l ≤ 9
Reflections collected	6532
Independent reflections	1838 [R <sub>int</sub> = 0.1030, R <sub>sigma</sub> = 0.0431]
Data/restraints/parameters	1838/0/127
Goodness-of-fit on F <sup>2</sup>	1.034
Final R indexes [I ≥ 2 $\sigma$ (I)]	R <sub>1</sub> = 0.0805, wR <sub>2</sub> = 0.2538
Final R indexes [all data]	R <sub>1</sub> = 0.0853, wR <sub>2</sub> = 0.2620
Largest diff. peak/hole / e Å <sup>-3</sup>	0.37/-0.34

**Figure A72.** ORTEP diagram and packing diagram in unit shell of Tropicone (**9**)



# Thesis summary

**Title of thesis:** “Syntheses and Biochemical Assessments of Modified Nucleosides, Nucleic Acids and Peptides Containing Tropolone Surrogates”



# Cu-Catalyzed Synthesis of Alkylaminotroponyl Sulfones as *Pseudomonas aeruginosa* Quorum Sensing Inhibitors Targeting *lasI/R* QS Circuitry

Sagarika Meher,<sup>[a, c]</sup> Supriya Kumari,<sup>[a, b]</sup> Manjusha Dixit,<sup>\*, [b, c]</sup> and Nagendra K. Sharma<sup>\*, [a, c]</sup>

**Abstract:** The scarcity of novel bioactive molecules against multidrug-resistant (MDR) bacterial strains like *Pseudomonas aeruginosa* is alarming. This bacterial virulence is regulated via Quorum sensing (QS), a cell-cell communication process. Disabling QS circuits (*las*, *pqs*, *rhl*) with small molecules has been proposed as a potential strategy to prevent bacterial pathogenicity. This strategy focuses on interruption of bacterial virulence, rather than killing them to tackle the drug resistance problem. Herein, we describe the synthesis of rationally designed Alkylaminotroponyl Sulfone (ATS) deriva-

tives by Cu-catalyzed C(sp<sup>2</sup>)-H functionalization at troponone ring and the screening of their anti-QS activity against *P. aeruginosa*. Importantly, two sulfones (~20 μM) remarkably exhibit the down regulation of the *lasI/R* QS genes. These molecules also inhibit swarming motility, biofilm formation and pyocyanin production, which reduce *P. aeruginosa* virulence in cells. Hence, ATS derivatives could be considered as potential therapeutic candidates for the treatment of *P. aeruginosa* infections.

## Introduction

Bacterial infections have remained a primary cause of concern throughout history.<sup>[1]</sup> Persistent use of antibiotics as monotherapy or in combination has definitely reduced mortality but at the same time is the leading cause of redundant emergence of antibiotic-resistant bacteria pathogenic strains.<sup>[2]</sup> Drug designing strategies must be changed in order to find a sustainable solution to counteract the emerging multidrug resistance issue.<sup>[3]</sup> One such multidrug-resistant and highly adaptable bacterium responsible for nosocomial infections is *Pseudomonas aeruginosa* (PA).<sup>[4]</sup> The bacterium is a well-known causative agent of cystic fibrosis and airway infections. Various reports suggest that the emergence of multidrug-resistant PA is higher than that of novel antibiotics produced for treating the same. It has been reported as the prime reason for hospital-acquired infection in European countries.<sup>[5]</sup> Biofilm formation, Pyocyanin secretion, and protease production are a few important virulent factors possessed by the bacterium.<sup>[6]</sup> Ability to form biofilm is an added advantage for this bacterium that reduces the efficacy of any drug by limiting its penetration potential inside the cell. These virulent factors, as well as their capacity to conquer antibiotics, are controlled by the complex

cell to cell chemical signaling system known as quorum sensing (QS).<sup>[7,8]</sup> The *lasI/R* QS circuit regulates the expression of virulent factors.<sup>[9]</sup> Elastase a protease encoded by *lasB* gene under QS regulon is the most virulent factor. It is responsible for disrupting the tight junctions between host epithelial cells. Pyocyanin production increases oxidative stress and alters the mitochondrial electron transport system of the host.<sup>[10]</sup> Therefore, to control bacterial infections, drug-designing strategies should be advanced, aiming the inhibition of the virulence factors against designing the complete bactericidal drugs. However, the development process might be a reason of concern owing to its safety issues against human uses.

In the literature, sulfone derivatives are bioactive molecules that serve as not only popular antibiotics but also potential drug candidates for the treatment of AIDS/HIV infection and Alzheimer's disease (Figure 1a).<sup>[11]</sup> Tropolone, a non-benzenoid aromatic molecule, is constituent of many troponoid natural products, which exhibit diverse biological activities such as antibacterial, anti-inflammatory, antitumor, and antiviral activity.<sup>[12,13]</sup> For example, the naturally occurring Thujaplicin and synthetic analogue tropolonyl-naphthalenyl urea are potent antibiotics (Figure 1b/c). Thus we rationally designed troponyl-sulfones by synergizing sulfones and troponyl moieties in a single scaffold for exploring their efficacy on PA (Figure 1d). Herein, we planned to synthesize troponyl-sulfone derivatives

- [a] S. Meher, Dr. S. Kumari, Dr. N. K. Sharma  
School of Chemical Sciences; National Institute of Science Education and Research (NISER), Jatani, 752050 Bhubaneswar, Odisha (India)  
E-mail: nagendra@niser.ac.in
- [b] Dr. S. Kumari, Dr. M. Dixit  
School of Biological Sciences; National Institute of Science Education and Research (NISER), Jatani, 752050 Bhubaneswar, Odisha (India)  
E-mail: manjusha@niser.ac.in
- [c] S. Meher, Dr. M. Dixit, Dr. N. K. Sharma  
Homi Bhabha National Institute (HBNI), Training School Complex, Anushaktinagar, 400094 Mumbai (India)
- Supporting information for this article is available on the WWW under <https://doi.org/10.1002/asia.202200866>

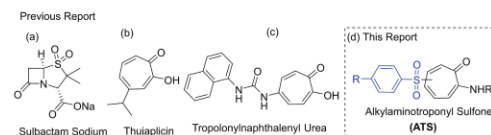


**Figure 1.** Antibiotic and anti-quorum sensing compounds (reported and this report) – (a–c) previous reports; (d) This report.

# Tropolone-Conjugated DNA: A Fluorescent Thymidine Analogue Exhibits Solvatochromism, Enzymatic Incorporation into DNA and HeLa Cell Internalization

Sagarika Meher,<sup>†</sup> Chandrasekhar Reddy Gade,<sup>†</sup> and Nagendra K. Sharma<sup>\*,[a, b]</sup>

Tropolone is a non-benzenoid aromatic scaffold with unique photophysical and metal-chelating properties. Recently, it has been conjugated with DNA, and the photophysical properties of this conjugate have been explored. Tropolonyl-deoxyuridine (tr-dU) is a synthetic fluorescent DNA nucleoside analogue that exhibits pH-dependent emissions. However, its solvent-dependent fluorescence properties are unexplored owing to its poor solubility in most organic solvents. It would be interesting to

incorporate it into DNA primer enzymatically. This report describes the solvent-dependent fluorescence properties of the silyl-derivative, and enzymatic incorporation of its triphosphate analogue. For practical use, its cell-internalization and cytotoxicity are also explored. tr-dU nucleoside was found to be a potential analogue to design DNA probes and can be explored for various therapeutic applications in the future.

## Introduction

2'-Deoxyribose nucleic acid (DNA) is the genetic material of the living organism. It is synthesized through polymerase chain reactions using the building block deoxyribonucleoside triphosphate (dNTP).<sup>[1]</sup> Recently, structurally modified DNA has been synthesized to meet desired functional properties, including fluorescence properties.<sup>[2]</sup> The native DNA is a nonfluorescent molecule but it can become fluorescent by the extension of  $\pi$ -conjugation at nucleobases or by the chemical ligation of selective chromophores/fluorescent dyes at nucleobases.<sup>[3]</sup> There are two major sites of DNA for attaching the chromophores/dyes/fluorophores which are the sugar unit and nucleobase rings. The fluorophore-conjugated nucleobases have emerged as powerful synthetic tools to improve fluorescence efficiency.<sup>[3c,4]</sup> The attachment of chromophores/fluorophores through the linker at the functional group (amine/azide/alkyne) of DNA has become attractive and economical method for labeling DNA.<sup>[5]</sup> The addition of chromophore directly at nucleobases, by maintaining coplanarity, is a major concern to retain the canonical base pairing ability by hydrogen bonding.<sup>[6]</sup> Synthetic fluorescent nucleobases preserve or do not preserve the W–C hydrogen base pairing. The C-nucleosides containing

naphthalene, phenanthrene, pyrene, stilbene, and coumarin fluorogenic aromatic scaffold are known not to preserve W–C hydrogen bonding.<sup>[7]</sup> The introduction of the appropriate electron-withdrawing group (EWG) on a purine ring and electron-donating groups (EDG) on a pyrimidine ring induce the fluorescence character of nucleobases with preserving the W–C hydrogen bonding.<sup>[3c,8]</sup> Recently, Hock and co-workers have prepared functional DNA by appending alkyne linker at nucleobase for sensing and cross-linking which are helpful for studying the protein-DNA binding modulation and transcription.<sup>[8b,9]</sup> Saito and co-workers have coupled an aryl residue at deoxyguanosine through ethynyl linker for exploring the base-discriminating fluorescent (BDF) and environmentally sensitive fluorescent (ESF) probes.<sup>[10]</sup> Bag and co-workers have attached the aromatic scaffold at the nucleobases through propenyl(methyl) amino group and aromatic scaffold, which are microenvironment-sensitive fluorescent nucleobase analogs.<sup>[11]</sup> Tor and co-workers have reported the fluorescent ring fused-cytosine analogs such as pyrrole fused cytosine (pC) and thiophenyl-pC.<sup>[12]</sup> Wilhelmson and co-workers have appended a phenyl scaffold at the cytidine pyrimidine ring through a sulfur-containing six-membered heterocyclic ring to make fluorescent analogs.<sup>[13]</sup> Srivatsan and co-workers have developed microenvironment-sensitive hetero bicyclic pyrimidine fluorescent RNA analogs.<sup>[14]</sup> Kool and co-workers have synthesized various fluorescent DNA analogs using different organic fluorophores directly at sugar rings for labeling the DNA.<sup>[7a]</sup> Most of the chromophores are derived from the benzenoid aromatic scaffolds. In the repertoire of functional DNA synthesis, the non-benzenoid moiety conjugated DNA analogs are not well explored. Tropolone is non-benzenoid aromatic scaffold and its related derivatives are constituents of tropenoid natural products (Figure 1).<sup>[15]</sup> Tropolone has unique intramolecular hydrogen bonding, photophysical properties, and metal chelating ability, strongly with  $\text{Cu}^{2+}$ / $\text{Ni}^{2+}$ / $\text{Zn}^{2+}$  ions.<sup>[16]</sup> Re-

[a] S. Meher,<sup>†</sup> Dr. C. R. Gade,<sup>†</sup> Dr. N. K. Sharma  
School of Chemical Sciences  
National Institute of Science Education and  
Research (NISER) Bhubaneswar  
Jatani 752050, Odisha (India)  
E-mail: nagendra@niser.ac.in

[b] S. Meher,<sup>†</sup> Dr. C. R. Gade,<sup>†</sup> Dr. N. K. Sharma  
Homi Bhabha National Institute (HBNI)  
Training School Complex  
Anushaktinagar, Mumbai, 400094 (India)

[<sup>†</sup>] These authors contributed equally to this work.

Supporting information for this article is available on the WWW under  
https://doi.org/10.1002/cbic.202200732





# Instability of Amide Bond with Trifluoroacetic Acid (20%): Synthesis, Conformational Analysis, and Mechanistic Insights into Cleavable Amide Bond Comprising $\beta$ -Troponylhydrazino Acid

Nihar Ranjan Dalabehera,<sup>§</sup> Sagarika Meher,<sup>§</sup> Bibhuti Bhusana Palai,<sup>§</sup> and Nagendra K. Sharma\*



Cite This: *ACS Omega* 2020, 5, 26141–26152



Read Online

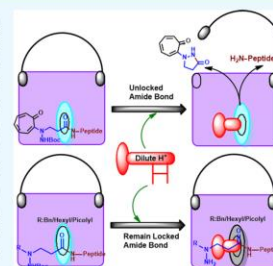
ACCESS |

Metrics & More

Article Recommendations

Supporting Information

**ABSTRACT:** The instability of an amide bond with dilute trifluoroacetic acid (TFA) is a rare chemical event. The native amide bonds are stable even in the neat TFA, which is one of the reagents that releases the peptides from the solid support in the solid-supported peptide synthesis method. In the repertoire of unnatural peptidomimetics,  $\alpha$ -/ $\beta$ -hydrazino acids and their peptides are explored for the synthesis of *N*-amino peptide derivatives, and their amide bonds are stable in TFA (~100%) as natural amide bonds. This report describes the synthesis of a  $\beta$ -hydrazino acid analogue as  $\beta$ -troponylhydrazino acid, containing a nonbenzenoid natural troponyl scaffold. The structural and conformational studies of their hybrid di-/tripeptides with the natural amino acid show that the 2-aminotroponyl residue is involved in hydrogen bonding. Surprisingly, the amide bond of  $\beta$ -troponylhydrazino peptides is cleavable with TFA (~20%) through the formation of a new heterocyclic molecule *N*-troponylpyrazolidinone or troponylpyrazolidinone. Troponone and related compounds are excellent biocompatible chromophores. Hence,  $\beta$ -troponylhydrazino acid could be employed for tuning the peptide structure and considered a promising chromophoric acid-sensitive protecting group of a free amine of amino acids/peptides. It could be applied for the estimation of the free amine group functionality by a UV–vis spectrophotometer.



## INTRODUCTION

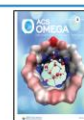
Natural amide bonds are pretty stable, with an estimated half-life of around ~350–600 years for spontaneous hydrolysis at neutral pH and room temperature (RT).<sup>1,2</sup> The natural amide bonds are resonance-stabilized. The carbonyl group of the natural amide is inert toward the nucleophilic addition reaction.<sup>3,4</sup> The cleavage/hydrolysis of amide bonds could be achieved under extreme conditions as the heating under strongly acidic or basic conditions. However, the cyclic amides (lactams) are more cleavable as compared to the linear amides because of ring-strained amides.<sup>5–7</sup> A large number of ring-strained lactams are synthesized and their poor stability is reported even under mild conditions because of the resonance decoupling through N–C=O torsion, which induces the strong electrophilicity at the C=O group as ketonic carbonyl.<sup>8</sup> The cleavage of an amide bond without metal ions becomes a center point of discussion. Brown and co-workers have shown that the resonance decoupling enhances the hydrolysis rate in the strained amide bond because of the direct nucleophilic attack.<sup>3,9</sup> For instance, the twisted amide of 1-aza-2-admantanone derivatives is a highly strained lactam ring and readily cleavable under mild conditions.<sup>10</sup> This twisted amide also shows the dual reactivities such as (i) nucleophilic character of amine and (ii) electrophilicity of the carbonyl. The hydrolysis of linear amide bonds is also possible by decoupling the N–C=O resonance stability within the structurally modified amide bonds. However, the sequence-specific amide

is cleaved/hydrolyzed with enzymes such as proteases. The zinc metal-dependent peptidase cleaves the specific amide bond through zinc ion mediation. These results encourage the synthetic chemists for the development of artificial peptidases.<sup>11</sup> Mashima and co-workers have explored the role of zinc ions in the cleavage of amides bearing  $\beta$ -hydroxyethyl using Lewis acid Zn(OTf)<sub>2</sub>.<sup>12</sup> Recently, the activation of specific amide bonds has been explored using a metal catalyst. For example, Garg, Houk, and co-workers have shown the conversion of an amide functional group into an ester group by cleaving the C–N bond of amide with the Ni-catalyst.<sup>13</sup> The cleavage of the amide bond under near-physiological conditions is still challenging. Booker-Milburn and co-workers have reported the solvolysis of acyclic synthetic amide bonds at RT under neutral conditions via the formation of ketene intermediates.<sup>14</sup> They have shown that an electron-withdrawing group, at the  $\alpha$ -position, of amide carbonyl enhances the protonation of sterically hindered amide amine and facilitates the formation of ketene by cleaving the C–N bond of amide. In a recent report, the cleavage of the terminal

Received: August 5, 2020

Accepted: September 17, 2020

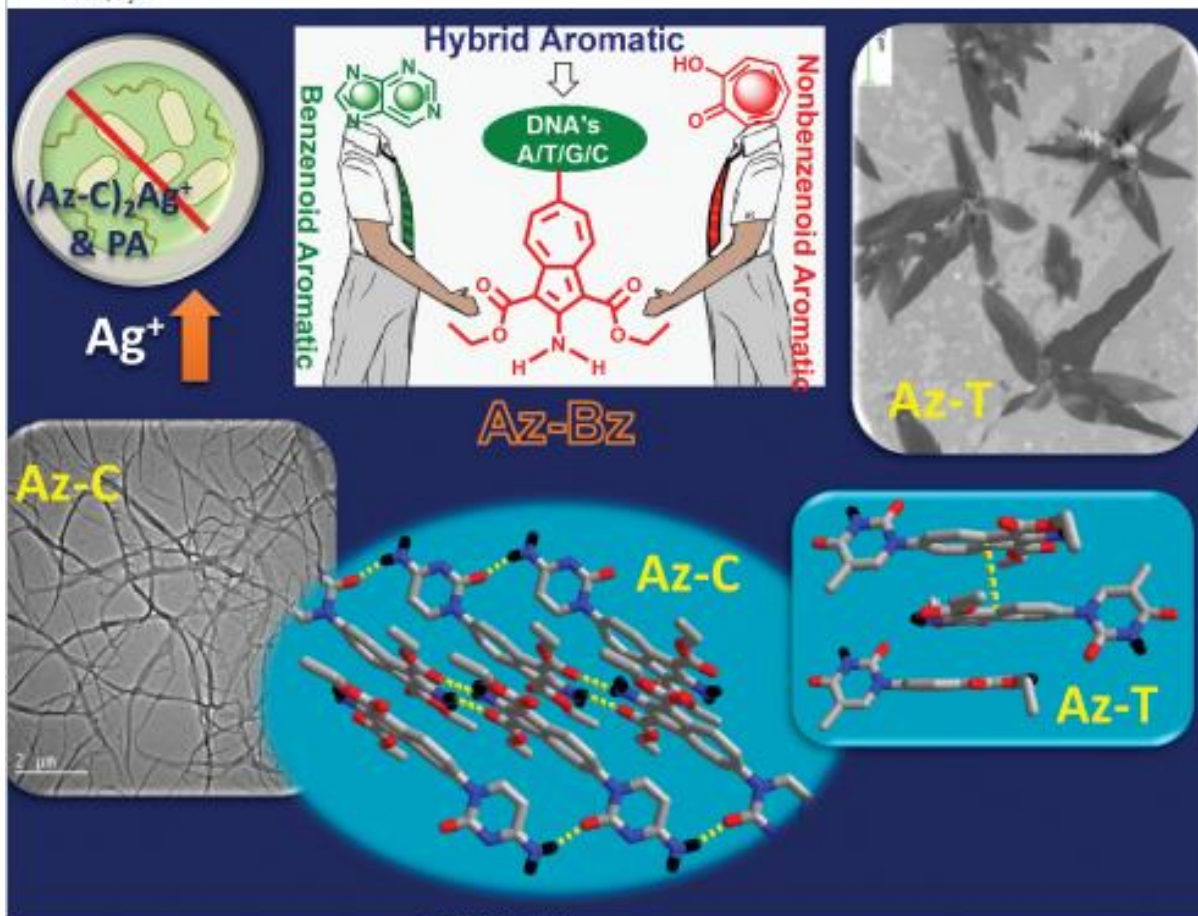
Published: October 1, 2020



# NJC

New Journal of Chemistry  
rsc.li/njc

A journal for new directions in chemistry



ISSN 1444-0546

 ROYAL SOCIETY  
OF CHEMISTRY

COMMUNICATION  
Sagarika Meher and Nagendra K. Sharma  
Azulene tethered *N*-aryl nucleobases: synthesis, morphology  
and biochemical evaluations

